

NASA
Technical Memorandum 109040, Volume 4

ATCOM
TR-93-A-012 , Volume 4

11/22
205043
P-423

Investigation of the Aerodynamic Environment for an Advanced Lightweight Rotor in Forward Flight

*Volume 4: Laser Velocimeter Wake Data,
Advance Ratio of 0.37*

*W. Derry Mace
Lockheed Engineering and Sciences Co.
Hampton, Virginia*

*Joe W. Elliott
Aeroflightdynamics Directorate
JRPO
NASA-Langley Research Center
Hampton, Virginia*

*Martin A. Peryea, Albert G. Brand and Tom L. Wood
Bell Helicopter Textron Inc.
Fort Worth, Texas*

November 1993

(NASA-TM-109040-Vol-4)
INVESTIGATION OF THE AERODYNAMIC
ENVIRONMENT FOR AN ADVANCED
LIGHTWEIGHT ROTOR IN FORWARD
FLIGHT. VOLUME 4: LASER VELOCIMETER
WAKE DATA, ADVANCE RATIO OF 0.037
(Diskette Supplement) (NASA)
423 p

N94-26483

Unclass

10/02 0205048
G3



National Aeronautics and
Space Administration

Langley Research Center
Hampton, Virginia 23681-0001



Summary

An Advanced Lightweight Rotor (ALR) model was tested in high speed forward flight in the 14- by 22-Foot Subsonic Tunnel at the NASA Langley Research Center. The pressure instrumented rotor, provided by Bell Helicopter, was a four-bladed, Mach-scaled, bearingless, soft-in-plane design. Rotor performance data were acquired from Bell's Powered Force Model (PFM) test stand, and the blade airloads were obtained using 92 unsteady pressure transducers. A two-component laser velocimeter was used to obtain azimuthally dependent velocities in the inflow region and in the wake of the rotor. The laser velocimeter acquired wake data are presented in this report without analysis. To facilitate the use of the data, they are also provided on a 1.4 Megabyte 3.5-inch floppy disk in Microsoft MS-DOS format.

Introduction

Investigators have worked on various phases of identifying the wake structure and how it relates to blade airloads (references 1-4). A key element of these studies has been the establishment of the wake geometry, whether defined from flow visualization or other measurements. Comparisons of available rotor performance test data with various analyses show improved correlations at high advance ratio when a free wake model is used in the analysis. Harris (reference 5) noted that the free wake analysis model included in CAMRAD (reference 6) predicts substantial induced drag for a rotor operating at high advance ratio and thrust, particularly over the aft portion of the rotor disk. Understanding the physical processes responsible for the high induced drag requires detailed information concerning the unsteady blade airloads and the surrounding unsteady flow field. Extensive measurements (references 7-9) have documented the induced inflow variations for a model rotor in forward flight. Blade surface pressure measurements have also been obtained in separate efforts, such as the works indicated by Hooper in reference 10, or more recently the pressure instrumented model rotor test at the German-Dutch Wind Tunnel DNW (reference 11). Such measurements serve as a needed vehicle for the validation of existing and emerging aerodynamic computer prediction codes, but comprehensive measurements of the rotor blade loads and rotor flow field nevertheless remain relatively sparse. In particular, a complete simultaneous measurement of inflow velocities, wake velocities, and blade pressures from a single test configuration in forward flight has not been available. Better insight into the validity of the free-wake blade load computations could be gained by combining experimental measurements of blade airloads with flow field velocity data for a single rotocraft configuration. Variations of the rotor tip speed could serve to address questions that have been raised regarding the impact of tip speed on the rotor wake structure (reference 12).

A joint government/industry test program was initiated which concentrated on four flight conditions. The purpose of the test was to investigate the aerodynamic environment of a rotor operating at high advance ratio, high thrust, and with a significant degree of propulsive force. Data concerning flow field velocities and blade pressures for two tip speeds and two thrust coefficients were acquired. The data base provided by this volume includes the velocity measurements acquired in the wake of the rotor for three of the four flight conditions tested. There were no velocity data acquired in the wake of the rotor for the flight condition with a thrust coefficient of 0.0064 and hover tip speed of 603 ft/sec. The induced inflow velocities are reported in Volumes 1-3 of this report, while the induced inflow velocities and blade pressure measurements at an advance ratio of 0.37, thrust coefficient of 0.0081 and hover tip speed of 710 ft/sec are contained in reference 13. References 14 and 15 provide the first analyses utilizing portions of this data base.

Notation

A rotor disk area, πR^2 , ft²

A_0 constant term in Fourier series of blade feathering (collective) at $r/R = 0.7125$, deg

A_1	coefficient of cosine term in Fourier series of blade feathering at $r/R = 0.7125$, deg
B_1	coefficient of sine term in Fourier series of blade feathering at $r/R = 0.7125$, deg
b	number of blades
C_X	rotor propulsive force coefficient, uncorrected, $X/\rho AV_{tip}^2$
C_{Xc}	rotor propulsive force coefficient, corrected for hub tare, $C_X + 0.0001198$
C_T	rotor thrust coefficient, $T/\rho AV_{tip}^2$
c	rotor blade chord, in
EI	bending stiffness, lb-in ²
GJ	torsional stiffness, lb-in ²
P	rotor power, ft-lb/sec
P	local static pressure, lb/in ²
P_∞	free stream pressure, lb/in ²
q	dynamic pressure, lb/ft ²
r	local radius of a rotor blade cross section, ft
R	rotor radius, ft
T	thrust produced by the rotor, perpendicular to the tip path plane, lb
U	streamwise component of velocity, positive downstream, ft/sec
U_∞	free stream velocity, positive downstream, ft/sec
u_i	induced component of velocity parallel to the tip path plane, positive downstream, ft/sec
v	vertical component of velocity, positive up, ft/sec
V_{local}	flow velocity relative to blade, $\Omega r + U_\infty \sin\psi$, ft/sec
V_{tip}	rotor blade tip velocity, ΩR , ft/sec
v_i	induced component of velocity normal to the tip path plane, positive up, ft/sec
X	rotor propulsive force, positive forward (wind axis), lb
x/c	chordwise position, percent

y/c	vertical distance from the chord line, percent
x	distance from the rotor center of rotation, measured along the x coordinate axis, positive downstream, in
y	distance from the rotor center of rotation, measured along the y coordinate axis, positive to right, in
z	distance from the rotor center of rotation, measured along the z coordinate axis, positive up, in

Symbols

α	angle between tip path plane and free stream velocity, positive nose up, deg
μ_∞	rotor advance ratio, $U_\infty \cos \alpha / V_{tip}$
σ	standard deviation
Ω	rotor rotational speed, radians/sec
ψ	rotor azimuth measured from downstream position, positive counterclockwise as viewed from above, deg
ρ	air density, slug/ft ³
σ	rotor solidity, $bc/\pi R$
θ	blade pitch angle at specified azimuth, positive nose up, $r/R = 0.7125$, $\theta = A_0 - A_1 \cos \psi - B_1 \sin \psi$, deg
\bar{x}	mean values

Experimental Apparatus

The experiment was conducted in the NASA Langley Research Center 14- by 22-Foot Subsonic Tunnel using Bell Helicopter Textron's Powered Force Model (PFM), a pressure-instrumented Advanced Lightweight Rotor (ALR) and a two-component laser velocimeter (LV).

The 14- by 22-Foot Subsonic Tunnel is an atmospheric, closed-circuit wind tunnel of conventional design with enhancements for the testing of powered and high-lift configurations (reference 16). The tunnel is pictured in figure 1 and is shown schematically in figure 2. This investigation was conducted with the walls and ceilings raised leaving a solid floor and a flow collector at the rear of the test section. The maximum

tunnel velocity in this configuration is approximately 170 knots. This configuration was selected because it provided the LV system with unrestricted optical access to the test section.

Powered Force Model

Bell Helicopter Textron's Powered Force Model (PFM) is a general purpose rotor test stand designed to test Mach-scaled rotors. Figure 3 shows the PFM installed in the forward part of the test section. The PFM can accept rotors from 4 to 10 feet in diameter and operate at a maximum of 3000 RPM. As shown in figure 4, the PFM is comprised of an input quill assembly, pitch change mechanism, yaw change mechanism, test stand dynamic isolator unit, a five component rotor balance and swash plate for blade pitch controls. The input quill accepts two variable frequency electric motors rated at 75 HP each. Rotor pitch rotation takes place about the input quill axis by a pitch change actuator mechanism. Yaw rotation of the rotor pylon occurs above the input quill along the drive shaft axis. The test stand isolator consists of four rubber dampers that can be adjusted or locked-out depending on the rotor frequency requirements.

The non-metric fairing, shown in figure 5, was designed to minimize test stand aerodynamic interference with the rotor. The cross-sectional shape utilizes a NACA 0033 airfoil shape. The five component balance can resolve the rotor forces into conventional forces and moments. Mast torque is measured by a separate strain gauge located below the rotor hub attachment point. The rotor mast is driven through a flex-coupling designed to eliminate transmission of extraneous loads into the balance. The rotor cyclic and collective control are mounted above the rotor balance.

Advanced Lightweight Rotor System

The Mach-scaled Advanced Lightweight Rotor is a four-bladed, bearingless, soft-inplane design. Two stacked fiberglass flex-beam yokes and four composite rotor blades with integral cuffs and elastomeric shear dampers comprise the rotor system. The rotor characteristics are summarized below and airfoil coordinates are summarized in table 1.

ALR and Blade Characteristics

Hub Type	Flex Beam
Number of Blades	4
Root cut-out, inches	9.00
Geometric pitch-flap angle, deg	51.71
Twist Linear, deg	-8.0
Radius, inches	48.00
Airfoil chord, inches	3.720
Geometric solidity, σ	0.098674
Weight (per blade), lb	1.699
Flapping Inertia, slug-ft ²	0.2151
Lead/Lag damping, in-lb/deg/sec	182.4

The airfoil coordinates shown in table 1 are defined at a specific radius or over a range on the blade. Linear interpolation was used to transition between subsequent values given in the table. The blade twist

distribution is shown in figure 6 and the blade structural properties are tabulated in table 2.

The PFM data acquisition system uses an HP3852A Data Acquisition and Control Unit that receives and stores data from several sources, including the test control computer, the Rotor Synchronized Digitizer (RSD) and NASA's Static Data Acquisition System. The PFM data acquisition system is shown schematically in figure 7. The RSD is a 32 channel sample and hold analog to digital converter. The sampling is triggered by an optical shaft angle encoder that is also used by the LV system.

Laser Velocimeter (LV) System

The LV system used in this investigation was designed to measure the instantaneous components of velocity in the longitudinal (streamwise) and vertical directions as described in reference 17. The system is comprised of four subsystems: optics, traverse, data acquisition, and seeding. The optics subsystem, shown in figure 8, operates in backscatter mode and at high power (4 watts in all lines) in order to accommodate the long focal lengths needed to scan the wide test section. The transmitting and receiving optics packages are augmented by a zoom lens system consisting of a 3-in. clear aperture negative lens and a 12-in. clear aperture positive lens. Bragg cells in each optical path provide a directional measurement capability. The velocity measurements are made at a point in space where the four beams cross, called the sample volume. The length of the sample volume (transverse to the flow direction) increases as the sample volume is moved away from the optics assembly. Over the 10 to 20 foot focal length the sample volume is less than 1 cm long with a nearly constant diameter of 0.2 mm.

The traverse subsystem provides five degrees of freedom in positioning the sample volume and is controlled by the same computer that is used for data acquisition. Translation of the sample volume in the horizontal and vertical directions is accomplished by displacing the entire optics platform. Translation along the lateral axis is accomplished by displacing the negative lens location in the zoom lens assembly, thus refocusing the sample volume along the axis of optical transmission. The other two degrees of freedom, pan and tilt, are implemented by rotating the final mirror about its vertical and horizontal axis in order to change the direction of optical transmission. The total inclusive range of the traversing system is 7 feet vertically, 6 feet streamwise, 16.5 feet laterally, and 7 degrees in both pan and tilt. Measurements can be made outside of this envelope by repositioning the optics platform, which is mounted on wheels to facilitate such relocations. For this study, the traversing system was positioned to the left of the test section when looking downstream as shown earlier in figure 3.

The LV data acquisition subsystem, shown schematically in figure 9, interfaces with the optical signal processing equipment to receive two channels of raw LV data and up to five channels of auxiliary data. In this investigation, the tunnel and model parameters were passed from the 14- by 22-foot Tunnel Static Data Acquisition System (SDAS) and Bell's Model Data Acquisition System (MDAS). Two of the auxiliary channels (one each for the U and V components) measured the azimuthal position of the rotor shaft. The system converts the raw LV data to engineering units and determines the statistical characteristics of the data so that the preliminary test results can be evaluated during the acquisition process. The raw data which is acquired from the buffer interface device and the 64 parameters which are acquired from the SDAS and MDAS are written to magnetic tape for later analysis. Another function performed by the data system is to interface with and control the five degree-of-freedom traversing subsystem.

The seeding subsystem, shown schematically in figure 10, is a solid particle, liquid-dispensing system (reference 18). Solid polystyrene latex microspheres are suspended in 100 proof Ethanol and dispensed into the tunnel flow. Polystyrene particles are used because of their low density, high reflectivity and precise particle size. The particles used in this investigation were 1.7 microns in diameter with a standard deviation of 0.0239 microns. The particle mixture is pumped to an array of nozzles where compressed air is used to atomize the mixture. These nozzles are mounted on a frame in the settling chamber of the tunnel as shown in figure 11. The position of the frame is remotely controlled by the laser operator during

the data acquisition process. The low vapor pressure of the mixture allows it to evaporate as it travels the 85 feet from the settling chamber to the test section. This process provides isolated single particles in the flow field whose velocities are measured as they pass through the sample volume. The local fluid velocity is inferred from the seed particle velocity.

Error Analysis

The overall LV system error is obtained by summing the error of all of the components that contribute to an error in the velocity measurement. The error sources are summarized in table 3 and are defined in references 19 and 20. They result in a velocity bias error of -0.32 to 0.84 percent and a random error of 0.37 percent. Taking the square root of the sum of the squares of these values yields a total system error of 0.49 to 0.92 percent of the measured velocity.

Test Procedures

Wake Velocities

The wake measurement locations were proposed during pre-test evaluations of the wake geometry, as defined in reference 21, and were finalized after flow visualization. A top view of the wake measurement locations and the predicted location of the rotor and tip vortices at $\psi = 0$ is shown in figure 12. Each circle represents a vertical line of measurement stations positioned to capture a tip vortex at a specified time (rotor azimuth angle). The vertical spacing between wake measurement points at a given location in figure 12 is 1.03 inches. The wake measurement stations are summarized in figures 13 - 15. The measured component of velocity is shown in vector form for points in the y/R cross-sectional planes for the instant when the rotor azimuth is zero degrees. These velocities are in the tip-path-plane axis system, i.e., they have been rotated from the horizontal by the tip-path-plane angle, α . The marker symbol in these figures represent predicted locations of tip vortices in the corresponding cross-section. The inset depicts the top view, showing the predicted wake geometry in relation to the measured locations. Generally, the measurement locations were chosen so that the blade passage effects would be minimal when the vortex was at the measurement site.

The LV data acquisition process consisted of placing the sample volume at the location to be measured and acquiring up to 16384 (16K) individual velocity measurements for both the U and V components. During data acquisition, conditional sampling techniques were employed to measure the azimuth of the rotor. Each of the velocity measurements were thus permanently identified with a known rotor azimuth angle so that the data could be cycle averaged. At the conclusion of this process, the measurement location was changed and the acquisition process repeated.

Data Reduction

Velocity Measurements

Each velocity measurement has associated with it an encoder signal indicating the position of the blades when the measurement was made. This information was used to sort the velocities into 128 bins, each 2.81 degrees wide, encompassing the 360 degrees of blade rotation. This sorting process was required to

present the data in a format of a single rotor revolution. The velocity value assigned to each of the 128 azimuthal intervals used in the azimuth dependent reconstruction is the arithmetic mean of all velocity measurements which occurred within the specified azimuthal interval.

Experimental Results

Rotor Performance

The nominal rotor performance during the wake measurement process is presented in table 4 for the three flight conditions tested. The values for the uncorrected propulsive force shown in table 4 include the effects of the hub. The hub tares were not measured in this test, but the results obtained in an earlier investigation conducted at 163 knots were used to correct the propulsive force on this test. The correction consisted of adding 0.0001198 to the uncorrected propulsive force.

Wake Velocity Measurements

The mean and standard deviation of the two components of the measured wake velocities are given in tables 5 - 7. Also included are the number of measurements comprising the statistical values for each case. Shown in figures 16 through 204 are the time dependent velocity data. These figures show the measured velocity versus azimuth at the top of the figure, the number of measurements that went into determining the mean for each bin in the center, and an order ratio analysis of the time dependent data at the bottom of each figure. The velocity data are presented in the tip-path-plane coordinate system. The plotted data presented in figures 16 through 204 are also contained on 3.5 inch floppy disks in Microsoft MS-DOS format (see pocket inside rear cover). The details of the data format and file structure are located in the file "README.DOC".

The figure numbers associated with each flight condition are given below.

$C_T = 0.0081 ; V_{tip} = 710 \text{ ft/sec}$ Figures 16 - 89

$C_T = 0.0081 ; V_{tip} = 603 \text{ ft/sec}$ Figures 90 - 162

$C_T = 0.0064 ; V_{tip} = 710 \text{ ft/sec}$ Figures 163 - 204

Concluding Remarks

An Advanced Lightweight Rotor (ALR) model was tested in high speed forward flight, $\mu=0.37$, at the 14-foot by 22-Foot Subsonic Tunnel at the NASA Langley Research Center. The pressure instrumented rotor, provided by Bell Helicopter, was a four-bladed, Mach-scaled, bearingless, soft-in-plane design. Rotor performance data were acquired from Bell's Powered Force Model (PFM) test stand, and the blade

airloads were obtained using 92 unsteady pressure transducers. A two-component laser velocimeter was used to obtain azimuthally dependent velocities in the inflow region and in the wake of the rotor. The laser velocimeter acquired wake data are presented in this report without analysis. To facilitate the use of the data, they are also provided on a 1.4 Megabyte 3.5-inch floppy disk in Microsoft MS-DOS format.

References

1. Landgrebe, A.J.; and Johnson, B.V.: Measurement of Model Helicopter Rotor Flow Velocities with a Laser Doppler Velocimeter. *Journal of the American Helicopter Society*, Volume 19, July 1974, pp. 39-43.
2. Biggers, James C.; Chu, Sing; and Orloff, Kenneth L.: Laser Velocimeter Measurements of Rotor Blade Loads and Tip Vortex Rollup. Pre-Print No. 900, 31st Annual Forum of the American Helicopter Society, Washington, D.C., May 1975.
3. Tangler, James L.: Schlieren and Noise Studies of Rotors in Forward Flight. Pre-Print 77.33-05, 33rd Annual Forum of the American Helicopter Society, Washington D.C., May 1977.
4. Biggers, James C.; Lee, Albert; and Orloff, Kenneth L.: Measurement of Helicopter Rotor Tip Vortices. Pre-Print 77.33-06, 33rd Annual Forum of the American Helicopter Society, Washington, D.C., May 1977.
5. Harris, F.D.: Rotary Wing Aerodynamics-Historical Perspective and Important Issues. Presented at the AHS National Specialists Meeting on Aerodynamics and Aeroacoustics, Arlington, TX, February 25-27, 1987.
6. Johnson, W.: A Comprehensive Analytical Model of Rotorcraft Aerodynamics and Dynamics. NASA TM-81182, June 1980.
7. Elliott, J.W.; Althoff, S.L.; and Sailey, R.H.: Inflow Measurements Made With a Laser Velocimeter on a Helicopter Model in Forward Flight, Volume I- Rectangular Planform Blades at an Advance Ratio of 0.15. NASA TM-100541, April 1988.
8. Elliott, J.W.; Althoff, S.L.; and Sailey, R.H.: Inflow Measurements Made With a Laser Velocimeter on a Helicopter Model in Forward Flight, Volume II- Rectangular Planform Blades at an Advance Ratio of 0.23. NASA TM-100542, April 1988.
9. Elliott, J.W.; Althoff, S.L.; and Sailey, R.H.: Inflow Measurements Made With a Laser Velocimeter on a Helicopter Model in Forward Flight, Volume III- Rectangular Planform Blades at an Advance Ratio of 0.30. NASA TM-100543, April 1988.
10. Hooper, W.E.: The Vibratory Airloading of Helicopter Rotors. *Vertica*, Volume 8, 1984. Also: paper No. 46, Ninth Annual European Rotorcraft Forum, September 13-15, 1983.
11. Lorber, P.F.: Aerodynamic Results of a Pressure Instrumented Model Rotor Test at the DNW. Presented at the 46th Annual Forum of the American Helicopter Society, Washington, D.C., May 1990.
12. Althoff, S.L.: Effect of Tip Speed on Rotor Inflow. *Journal of the American Helicopter Society*, Volume 34, No. 4, October 1989.
13. Elliott, J.W.; Peryea, M.A.; Brand, A.G.; and Wood, T.L.: Induced Inflow Velocity and Blade Surface Pressure Measurements for a Helicopter in Forward Flight, Volume 1- Advance Ratio of 0.37, Thrust Coefficient of 0.0081 and Hover Tip Speed of 710 Ft/Sec. NASA TM-104224, April 1992.

14. Wood, T.L.; Brand, A.G.; and Elliott, J.W.: An Experimental Investigation of Rotor Blade Airloads and Wake Structure at High Advance Ratio. Presented at the 46th Annual Forum of the American Helicopter Society, Washington, D.C., May 21-23, 1990.
15. Yen, G.J.; Yuce, M.; Chao C.F.; and Schillings, J.: Validation of Vibratory Airloads and Application to Helicopter Response. Journal of the American Helicopter Society, Volume 35, No. 4, pp. 63-71, October 1990.
16. Applin, Z. T.: Flow Improvements in the Circuit of the Langley 4- by 7-Meter Tunnel. NASA TM-85662, December 1983.
17. Sellers, W.L.; and Elliott, J.W.: Applications of a Laser Velocimeter in the Langley 4- by 7-Meter Tunnel. Proceedings on the Workshop on Flow Visualization and Laser Velocimetry for Wind Tunnels, NASA CP-2243, March 1982, pp. 288-298.
18. Elliott, J.E.; and Nichols, C.E.: Seeding Systems for Use With a Laser Velocimeter in Large Scale Wind Tunnels. NASA CP-2393, March 1985, pp. 93-103.
19. Young, W.H.; Meyers, J.F.; and Hepner, T.E.: Laser Velocimeter Systems Analysis Applied to a Flow Survey Above a Stalled Wing. NASA TN D-8408, August 1977.
20. Dring, R.P.: Sizing Criteria for Laser Anemometry Particles. Journal of Fluid Engineering, Volume 104, March 1982, pp. 15-17.
21. Peryea, M.: Test Plan for the 1/5 Scale Pressure Instrumented ALR Rotor/Laser Velocimeter Wind Tunnel Test at NASA Langley. Bell Helicopter Textron Inc. Report No. 699-199-014, May 1989.

Table 1.- ALR Rotor Airfoil Coordinates

Station 10.7 inches		Thickness 22%	
<u>Upper Coordinates</u>		<u>Lower Coordinates</u>	
x/c	y/c	x/c	y/c
0.000000	0.000000	0.000000	0.000000
0.001220	0.012950	0.003140	0.011900
0.006200	0.025980	0.010650	0.023150
0.014570	0.038320	0.021860	0.033650
0.025980	0.049900	0.036200	0.043390
0.039990	0.060680	0.053170	0.052320
0.056350	0.070600	0.072420	0.060500
0.074710	0.079640	0.093690	0.067870
0.094860	0.087820	0.116660	0.074490
0.116540	0.095100	0.141170	0.080330
0.139590	0.101490	0.166930	0.085400
0.163810	0.107020	0.193760	0.089680
0.189030	0.111640	0.221380	0.093180
0.215040	0.115390	0.249580	0.095860
0.241580	0.118210	0.278120	0.097760
0.268450	0.120130	0.306870	0.098810
0.295570	0.121120	0.335870	0.099060
0.322910	0.121190	0.365250	0.098490
0.350590	0.120360	0.395300	0.097130
0.378760	0.118620	0.426570	0.094970
0.407610	0.116000	0.459690	0.091990
0.437330	0.112500	0.495590	0.088090
0.468080	0.108110	0.535620	0.083270
0.499980	0.103170	0.580850	0.077380
0.533000	0.098000	0.631770	0.070480
0.567030	0.092460	0.689310	0.062420
0.602170	0.086510	0.747400	0.054100
0.638900	0.080040	0.795870	0.046940
0.679610	0.072570	0.838160	0.040040
0.736040	0.061700	0.870240	0.034030
0.781000	0.052620	0.893380	0.029290
0.819440	0.044540	0.912620	0.025080
0.864810	0.034660	0.929830	0.021090
0.892040	0.028540	0.945600	0.017240
0.911860	0.024090	0.960300	0.013500
0.929350	0.020090	0.974180	0.009760
0.945260	0.016420	0.987380	0.006000
0.960080	0.012810	1.000000	0.002090
0.974060	0.009370		
0.987310	0.005670		
1.000000	0.002090		

Table 1. - Continued

Station 15.70 to 36.70 inches		Thickness 10 %	
<u>Upper Coordinates</u>		<u>Lower Coordinates</u>	
x/c	y/c	x/c	y/c
0.000000	0.000000	0.000000	0.000000
0.000490	0.004200	0.000150	0.001950
0.002890	0.010640	0.002290	0.007350
0.007080	0.016980	0.006780	0.011990
0.012840	0.023070	0.013280	0.015870
0.019850	0.028860	0.021360	0.019150
0.027950	0.034230	0.030760	0.021840
0.036960	0.039160	0.041290	0.023960
0.046740	0.043610	0.052830	0.025550
0.057240	0.047580	0.065300	0.026630
0.068410	0.051090	0.078880	0.027300
0.080230	0.054150	0.093900	0.027580
0.092760	0.056820	0.111230	0.027550
0.106040	0.059110	0.134510	0.027230
0.135280	0.062810	0.160910	0.026800
0.168990	0.065510	0.183280	0.026610
0.208730	0.067580	0.205070	0.026610
0.231160	0.068450	0.227670	0.026790
0.254970	0.069190	0.252350	0.027160
0.279130	0.069810	0.281730	0.027750
0.302810	0.070280	0.320600	0.028590
0.325590	0.070560	0.352370	0.029230
0.347420	0.070670	0.379770	0.029670
0.368450	0.070600	0.405350	0.029960
0.388890	0.070310	0.429860	0.030120
0.428520	0.069130	0.453700	0.030110
0.467480	0.067080	0.500750	0.029630
0.479280	0.066280	0.524590	0.029150
0.499170	0.064720	0.549160	0.028500
0.519100	0.062920	0.575060	0.027680
0.544020	0.060380	0.603240	0.026670
0.573880	0.056970	0.635430	0.025390
0.593790	0.054490	0.675830	0.023720
0.633630	0.049080	0.718460	0.021910
0.673460	0.043120	0.751940	0.020450
0.708180	0.037630	0.780510	0.019100
0.777400	0.026830	0.806450	0.017770
0.816630	0.021270	0.831000	0.016370
0.836320	0.018670	0.855010	0.014860
0.875820	0.013820	0.879280	0.013170
0.895650	0.011560	0.901560	0.011490
0.915490	0.009430	0.918490	0.010150
0.930390	0.007920	0.932090	0.009010
0.945280	0.006480	0.944000	0.007970
0.965130	0.004690	0.954830	0.006990
0.975060	0.003850	0.974320	0.005040
0.985040	0.003050	0.983290	0.004030
0.995020	0.002270	0.991850	0.002980
1.000000	0.001880	1.000000	0.001880

Table 1.- Continued

Station 43.70 inches		Thickness 8 %	
<u>Upper Coordinates</u>		<u>Lower Coordinates</u>	
x/c	y/c	x/c	y/c
0.000000	0.000000	0.000000	0.000000
0.001600	0.005040	0.000350	0.004690
0.004760	0.009670	0.002990	0.008460
0.009410	0.013880	0.007710	0.011370
0.015390	0.017760	0.014130	0.013780
0.022590	0.021370	0.022200	0.015820
0.030880	0.024760	0.031950	0.017620
0.040110	0.027920	0.043460	0.019280
0.050140	0.030830	0.056690	0.020880
0.060830	0.033500	0.071380	0.022400
0.072090	0.035910	0.087120	0.023810
0.083880	0.038080	0.103610	0.025110
0.096180	0.040000	0.120770	0.026280
0.109000	0.041690	0.138580	0.027340
0.122380	0.043170	0.157120	0.028290
0.136330	0.044460	0.176430	0.029140
0.150870	0.045550	0.196530	0.029910
0.166010	0.046470	0.217360	0.030580
0.181760	0.047220	0.238860	0.031170
0.198080	0.047800	0.260930	0.031660
0.232300	0.048510	0.283480	0.032080
0.268340	0.048610	0.306440	0.032400
0.306060	0.048130	0.329770	0.032640
0.345650	0.047100	0.353430	0.032800
0.387590	0.045530	0.377390	0.032870
0.432470	0.043420	0.425930	0.032770
0.480990	0.040770	0.474680	0.032340
0.533810	0.037570	0.522640	0.031590
0.591580	0.033810	0.568960	0.030540
0.655500	0.029420	0.613430	0.029150
0.690490	0.026950	0.656520	0.027410
0.728250	0.024300	0.699080	0.025270
0.769570	0.021410	0.742450	0.022660
0.811070	0.018460	0.788840	0.019450
0.846730	0.015870	0.843600	0.015320
0.878030	0.013540	0.876000	0.012790
0.901390	0.011770	0.900990	0.010800
0.921140	0.010180	0.914890	0.009680
0.940890	0.008440	0.935550	0.007970
0.960620	0.006510	0.952510	0.006490
0.980330	0.004340	0.960180	0.005790
1.000000	0.001880	0.981150	0.003700
		1.000000	0.001880

Table 1.- Concluded

Station 45.90 to 48.00 inches		Thickness 6 %	
<u>Upper Coordinates</u>		<u>Lower Coordinates</u>	
x/c	y/c	x/c	y/c
0.000000	0.000000	0.000000	0.000000
0.000380	0.002760	0.000220	0.001690
0.002360	0.007150	0.002420	0.005210
0.006010	0.011000	0.006750	0.007860
0.011120	0.014330	0.012950	0.009870
0.017550	0.017260	0.020880	0.011600
0.025200	0.019890	0.030660	0.013130
0.043670	0.024410	0.042320	0.014560
0.065310	0.027990	0.070230	0.017190
0.089390	0.030630	0.101880	0.019370
0.116100	0.032420	0.137100	0.021150
0.146610	0.033560	0.176300	0.022630
0.183180	0.034250	0.218970	0.023810
0.227410	0.034630	0.264430	0.024720
0.274670	0.034730	0.311780	0.025340
0.320940	0.034520	0.359630	0.025680
0.367390	0.033990	0.407270	0.025710
0.415380	0.033130	0.455250	0.025450
0.465380	0.031940	0.504860	0.024890
0.517010	0.030450	0.556950	0.024030
0.569690	0.028680	0.610330	0.022910
0.622850	0.026660	0.662610	0.021580
0.675790	0.024400	0.713070	0.020040
0.727890	0.021950	0.761690	0.018290
0.778480	0.019300	0.807940	0.016330
0.826160	0.016540	0.850920	0.014190
0.848350	0.015150	0.871010	0.013040
0.869380	0.013740	0.889940	0.011860
0.889260	0.012310	0.905580	0.010800
0.905400	0.011070	0.927930	0.009100
0.917610	0.010080	0.945640	0.007580
0.927360	0.009250	0.961000	0.006130
0.937110	0.008380	0.968120	0.005420
0.949700	0.007210	0.974930	0.004700
0.962280	0.005970	0.981510	0.003990
0.968570	0.005330	0.987860	0.003290
0.974860	0.004670	0.994020	0.002580
0.981150	0.003990	1.000000	0.001880
0.987430	0.003310		
0.993720	0.002600		
1.000000	0.001880		

Table 2.- ALR Blade Structural Properties

RADIAL STATION (IN)	WT/IN (LB/IN)	EI*10 ⁻⁶ (LBF-IN ²)		CENTER OF GRAVITY OFFSET (IN)		GJ*10 ⁻⁶ (LBF-IN ²)	SHEAR CENTER OFFSET (IN)		NEUTRAL AXIS CENTER OFFSET (IN)	
		BEAM	CHORD	BEAM	CHORD		BEAM	CHORD	BEAM	CHORD
0.900	0.2818	2.7579	7.027	0.000	0.000	0.149	0.000	0.000	0.000	0.000
1.500	0.0244	0.0089	0.390	0.000	0.000	0.001	0.000	0.000	0.000	0.000
1.900	0.0179	0.0045	0.297	0.000	0.000	0.002	0.000	0.000	0.000	0.000
2.300	0.0252	0.0037	0.254	0.000	0.000	0.002	0.000	0.000	0.000	0.000
2.700	0.6237	0.0035	0.212	0.000	0.000	0.002	0.000	0.000	0.000	0.000
3.200	0.0144	0.0039	0.169	0.000	0.000	0.001	0.000	0.000	0.000	0.000
5.200	0.0080	0.0036	0.063	0.000	0.000	0.000	0.000	0.000	0.000	0.000
6.530	0.0065	0.0044	0.031	0.000	0.000	0.000	0.000	0.000	0.000	0.000
7.862	0.0054	0.0051	0.013	0.000	0.000	0.000	0.000	0.000	0.000	0.000
8.119	0.0090	0.0072	0.009	0.000	0.000	0.001	0.000	0.000	0.000	0.000
9.000	0.3164	0.0115	0.053	0.000	0.000	0.002	0.000	0.000	0.000	0.000
10.700	0.0625	0.1363	1.220	0.012	0.225	0.146	0.008	-0.122	-0.010	0.127
12.900	0.0260	0.0521	0.823	0.020	0.272	0.038	0.004	0.043	-0.017	0.110
14.050	0.0211	0.0287	0.677	0.015	0.274	0.016	0.012	0.056	-0.011	0.077
16.040	0.0251	0.0225	0.627	0.020	0.169	0.013	0.014	0.062	-0.011	0.052
18.030	0.0245	0.0210	0.570	0.022	0.148	0.012	0.011	0.015	-0.014	0.011
20.020	0.0239	0.0196	0.513	0.022	0.137	0.011	0.011	-0.022	-0.014	-0.020
22.010	0.0233	0.0182	0.457	0.022	0.116	0.010	0.012	-0.069	-0.014	-0.062
24.000	0.0227	0.0167	0.400	0.021	0.095	0.009	0.012	-0.116	-0.014	-0.103
26.000	0.0253	0.0148	0.358	0.030	-0.149	0.009	0.008	-0.141	-0.014	-0.149
26.900	0.0237	0.0114	0.322	0.032	-0.137	0.008	0.011	-0.116	-0.016	-0.141
28.750	0.0235	0.0111	0.319	0.032	-0.122	0.008	0.013	-0.107	-0.017	-0.133
30.600	0.0235	0.0111	0.319	0.032	-0.102	0.008	0.013	-0.087	-0.017	-0.113
32.450	0.0235	0.0111	0.319	0.032	-0.082	0.008	0.013	-0.067	-0.017	-0.093
34.300	0.0235	0.0111	0.319	0.032	-0.062	0.008	0.013	-0.047	-0.017	-0.073
36.200	0.0233	0.0108	0.320	0.033	-0.045	0.008	0.010	-0.047	-0.019	-0.067
38.100	0.0228	0.0103	0.321	0.035	0.000	0.007	0.003	-0.036	-0.022	-0.044
39.320	0.0222	0.0095	0.320	0.038	0.025	0.007	-0.006	-0.037	-0.027	-0.035
40.000	0.0289	0.0087	0.321	0.041	-0.089	0.007	-0.014	-0.008	-0.031	-0.033
42.000	0.0350	0.0077	0.320	0.044	-0.170	0.006	-0.024	0.027	-0.036	-0.017
43.800	0.0321	0.0060	0.312	0.050	-0.122	0.005	-0.039	0.046	-0.045	0.023
45.600	0.0284	0.0039	0.301	0.056	-0.066	0.004	-0.052	0.073	-0.054	0.067
48.000	0.0268	0.0030	0.296	0.059	-0.020	0.003	-0.058	0.107	-0.059	0.109

Table 3.- Laser Velocimeter System Error Summary

Error Source	Bias Percent	Random Percent
Cross Beam Angle Measurement	± 0.48	None
Divergent Fringes	A	A
Time Jitter	N/A	N/A
Clock Synchronization	0.26	± 0.26
Quantization	A	± 0.26
Velocity Bias	B	B
Bragg Bias	B	B
Velocity Gradient	B	B
Particle Lag	± 0.10	B
Total , %	-0.32 to 0.84	0.37
SYSTEM ERROR , %		0.49 to 0.92

A - Not Measured

B - Negligible

N/A - Not Applicable

Table 4.- Nominal Rotor Parameters During LV Measurements

Parameters	Flight Conditions		
Rotor Thrust, C_T , non-dimensional	0.0081	0.0081	0.0064
Tip Speed, V_{tip} , ft/sec	710.91	605.17	708.85
Tip Path Plane Angle of Attack, α , deg	-5.879	-5.817	-5.824
Collective Angle, A_0 , deg	14.03	13.24	11.31
Lateral Feathering, A_1 , deg	-0.86	-2.14	-0.57
Longitudinal Feathering, B_1 , deg	11.31	10.94	9.05
Blade Coning Angle, deg	2.69	2.69	1.45
Blade Lag Angle, (mean), deg	1.0	1.0	0.75
Advance Ratio, μ_∞ , non-dimensional	0.37	0.37	0.37
Uncorrected Propulsive Force, C_X	0.000574	0.000559	0.000319
Corrected Propulsive Force, C_{Xc}	0.000694	0.000679	0.000438
Rotor Power, C_P , non-dimensional	0.000633	0.000610	0.000439
Tunnel Velocity, V , knots	155.86	132.46	155.35
Tip Mach Number, M_{tip} , non-dimensional	0.617	0.525	0.617

Table 5.- Wake Velocity Summary

 $C_T = 0.0081$ $V_{tip} = 710 \text{ fps}$

x/R	y/R	z, in	\bar{u}_i , fps	σ_u	Number	\bar{v}_i , fps	σ_v	Number
-0.45	-0.60	1.65	-7.80	9.17	11636	9.90	11.80	7092
-0.45	-0.60	0.62	-9.50	15.22	13077	8.60	18.30	14045
-0.45	-0.60	-2.47	-8.80	15.82	13475	22.20	10.28	5630
-0.45	-0.60	-3.50	-18.80	14.63	13365	7.10	21.90	14530
-0.45	-0.60	-4.53	-23.40	13.87	13143	8.10	15.97	11788
0.80	-0.60	-0.27	21.80	16.02	15332	-14.60	16.42	15074
0.80	-0.60	-1.30	21.10	18.39	15571	-15.80	17.57	15214
0.80	-0.60	-2.33	24.80	14.31	15471	-15.80	17.67	15046
0.80	-0.60	-3.36	25.00	15.95	10516	-14.10	13.76	14942
0.80	-0.60	-4.39	21.70	7.58	16018	-17.20	6.52	15684
0.80	-0.60	-5.42	20.80	9.72	16078	-17.40	7.47	15950
0.80	-0.60	-6.45	23.10	8.35	15992	-16.20	5.62	15884
0.90	-0.20	-0.27	-25.70	4.29	12932	10.90	14.59	13654
0.90	-0.20	-1.30	-27.10	5.75	12994	11.60	11.51	13467
0.90	-0.20	-2.33	-26.60	6.73	12676	11.30	9.13	12994
0.90	-0.20	-3.36	-25.50	8.50	12632	8.00	6.49	12996
0.90	-0.20	-4.39	-24.00	8.21	12377	4.20	5.19	12885
0.90	-0.20	-5.42	-22.70	8.97	12417	2.20	5.04	12775
0.90	-0.20	-6.45	-21.70	9.18	12633	1.00	4.85	12654
1.10	-0.20	8.85	-12.00	10.56	12976	-15.40	11.35	14205
1.10	-0.20	7.82	-10.70	14.07	12871	-15.10	20.88	13930
1.10	-0.20	6.79	-3.50	12.59	12740	-16.60	23.22	13965
1.10	-0.20	5.76	1.30	10.90	12627	-16.90	14.54	14085
1.10	-0.20	4.73	3.60	8.54	13067	-16.60	13.19	14627
1.10	-0.20	3.70	1.00	6.43	13142	-14.00	14.08	14563
1.10	-0.20	2.67	-6.70	8.36	13196	-11.20	15.64	14465
1.50	-0.20	8.37	-4.90	6.26	9617	-12.10	8.94	13701
1.50	-0.20	7.34	-5.00	9.42	9805	-12.70	13.11	14078
1.50	-0.20	6.31	-3.50	10.36	9979	-14.20	19.29	14140

Table 5.- Continued.

x/R	y/R	z, in	\bar{u}_i , fps	σ_u	Number	\bar{v}_i , fps	σ_v	Number
1.50	-0.20	5.28	1.80	7.88	10314	-15.20	18.90	14224
1.50	-0.20	4.25	1.10	7.12	10529	-15.00	16.90	14577
1.50	-0.20	3.22	0.50	7.23	10787	-13.80	15.78	14650
1.50	-0.20	2.19	-0.40	7.94	10773	-13.20	15.40	14815
1.50	-0.20	-1.23	-13.60	7.53	12081	-4.30	9.93	13820
1.50	-0.20	-2.26	-12.60	4.94	10837	-3.50	7.44	13784
1.50	-0.20	-3.20	-16.30	5.67	10017	-2.30	6.55	13755
1.50	-0.20	-4.32	-17.20	7.04	9703	-3.10	6.76	13386
1.50	-0.20	-5.35	-18.50	6.94	9624	-2.80	6.51	13349
1.50	-0.20	-6.38	-16.90	6.72	9659	-2.40	5.89	13308
1.50	-0.20	-7.41	-16.70	6.43	9663	-2.90	5.82	13345
-0.27	0.20	0.21	-37.90	10.61	13953	3.80	11.52	15095
-0.27	0.20	-1.85	-36.40	9.39	13547	4.80	11.13	14828
-0.27	0.20	-2.88	-36.60	3.83	12612	10.70	4.36	11801
-0.27	0.20	-3.91	-38.20	3.20	12734	11.50	4.65	14026
-0.27	0.20	-4.94	-38.50	2.63	12855	12.70	4.12	14680
-0.27	0.20	-5.97	-37.10	2.40	12975	13.90	3.23	14430
0.70	0.20	-4.11	-13.70	4.65	12255	-34.70	4.02	14586
0.70	0.20	-5.14	-10.50	2.86	12567	-31.40	3.86	14306
0.70	0.20	-6.17	-16.40	2.19	11933	-24.80	3.31	12853
0.70	0.20	-7.20	-15.60	1.59	11358	-20.80	1.35	10632
0.70	0.20	-8.23	-14.40	1.26	11348	-18.00	0.95	10636
0.70	0.20	-9.26	-13.70	1.14	11345	-15.50	0.80	10849
0.70	0.20	-10.29	-12.00	0.99	11313	-13.10	0.63	10606
1.10	0.20	-6.51	-12.20	2.73	12141	-34.10	3.20	14854
1.10	0.20	-7.54	-12.60	2.09	12100	-31.30	2.75	14667
1.10	0.20	-8.57	-14.00	2.66	11666	-28.00	2.60	14289
1.10	0.20	-9.60	-13.70	2.10	11517	-25.30	1.91	14062
1.10	0.20	-10.63	-11.60	1.91	11482	-23.40	1.78	13984
1.10	0.20	-11.66	-10.90	1.44	11663	-21.30	1.57	13916
1.10	0.20	-12.64	-9.90	1.27	11866	-18.80	1.25	14040

Table 5.- Concluded.

x/R	y/R	z, in	\bar{u}_i , fps	σ_u	Number	\bar{v}_i , fps	σ_v	Number
1.50	0.20	6.93	-12.80	4.47	12109	-22.40	5.27	14525
1.50	0.20	5.90	-12.80	6.67	12685	-23.40	7.80	14691
1.50	0.20	4.87	-13.20	8.90	12730	-25.30	12.29	14938
1.50	0.20	3.84	-7.80	7.63	12791	-28.40	15.00	14952
1.50	0.20	2.81	-3.80	7.61	12816	-31.40	12.14	14989
1.50	0.20	1.78	-3.80	5.98	12713	-33.30	8.85	14825
1.50	0.20	0.75	-2.50	5.36	12749	-34.50	7.12	14893
1.50	0.20	-7.40	-12.30	3.17	12878	-40.90	2.21	15414
1.50	0.20	-8.50	-12.10	1.94	12599	-40.80	2.23	15256
1.50	0.20	-9.53	-13.50	3.27	12921	-40.90	2.31	15671
1.50	0.20	-10.56	-13.20	1.94	11693	-32.90	2.20	14157
1.50	0.20	-11.59	-12.60	1.95	11570	-31.20	1.94	13971
1.50	0.20	-12.62	-10.20	1.80	11303	-27.30	1.15	13452
1.50	0.20	-13.56	-10.80	1.81	11529	-27.30	1.20	13735

Table 6.- Wake Velocity Summary

 $C_T = 0.0081$ $V_{tip} = 603$ fps

x/R	y/R	z, in	\bar{u}_i , fps	σ_u	Number	\bar{v}_i , fps	σ_v	Number
-0.45	-0.60	1.65	-5.7	9.97	12125	7.3	11.75	11795
-0.45	-0.60	0.62	-7.9	13.13	12270	8.0	14.56	11486
-0.45	-0.60	-2.00	-9.3	7.64	11571	6.8	12.20	12554
-0.45	-0.60	-2.47	-13.0	9.97	11525	4.7	15.37	11795
-0.45	-0.60	-3.50	-17.8	9.80	11427	7.3	10.88	10875
-0.45	-0.60	-4.53	-17.0	7.73	10198	8.7	8.70	10386
0.80	-0.60	-0.27	2.6	3.40	9839	-3.7	19.71	13258
0.80	-0.60	-1.30	-2.6	9.04	11979	-4.4	17.92	11827
0.80	-0.60	-2.33	-3.8	8.55	11684	-4.2	14.53	11497
0.80	-0.60	-3.36	-3.4	7.21	11437	-3.5	12.40	11004
0.80	-0.60	-4.39	-2.8	6.47	11620	-3.1	10.53	11202
0.80	-0.60	-5.42	-4.8	6.31	11871	-2.2	8.72	11204
0.80	-0.60	-6.45	-5.2	5.34	11670	-1.0	6.73	10825
0.90	-0.20	-0.27	-19.9	5.12	12190	10.8	14.32	11130
0.90	-0.20	-1.30	-22.6	5.33	12264	13.3	12.58	10625
0.90	-0.20	-2.33	-24.7	7.24	11974	13.7	9.23	10388
0.90	-0.20	-3.36	-24.5	7.69	11745	11.6	5.85	10077
0.90	-0.20	-4.39	-25.6	8.70	11911	8.7	3.56	10399
0.90	-0.20	-5.42	-24.1	9.60	12103	6.2	2.71	10689
0.90	-0.20	-6.45	-21.7	9.57	12201	4.2	3.53	10762
1.10	-0.20	8.85	-4.8	6.20	11846	-12.5	6.43	11451
1.10	-0.20	7.82	-6.2	8.76	11879	-12.9	10.08	11497
1.10	-0.20	6.79	-3.2	8.52	11283	-11.9	13.92	10011
1.10	-0.20	5.76	1.1	8.73	11089	-13.3	14.17	10324
1.10	-0.20	4.73	4.5	7.87	11580	-14.8	13.91	12547
1.10	-0.20	3.70	8.6	6.70	12475	-13.1	14.59	13428
1.10	-0.20	2.67	3.3	7.77	12330	-10.1	14.52	13335
1.50	-0.20	8.37	-10.1	7.65	11920	-12.0	8.60	10683
1.50	-0.20	7.34	-9.2	11.29	12087	-12.2	12.54	11425

Table 6.- Continued.

x/R	y/R	z, in	\bar{u}_i , fps	σ_u	Number	\bar{v}_i , fps	σ_v	Number
1.50	-0.20	6.31	-8.0	12.44	12005	-12.5	18.05	11324
1.50	-0.20	5.28	-3.6	7.86	12003	-19.4	13.62	10490
1.50	-0.20	4.25	0.0	7.72	12010	-14.9	19.15	11949
1.50	-0.20	3.22	0.5	8.95	12058	-14.5	15.64	12796
1.50	-0.20	2.19	-0.8	9.83	12193	-12.9	14.36	13102
1.50	-0.20	-1.23	-20.0	8.28	11810	-0.8	7.03	11135
1.50	-0.20	-2.26	-25.3	6.47	11694	0.7	5.62	10998
1.50	-0.20	-3.29	-28.5	5.52	11571	1.0	4.91	10711
1.50	-0.20	-4.32	-33.4	8.04	11290	0.1	5.80	10661
1.50	-0.20	-5.35	-30.2	9.06	11221	-0.7	5.44	10489
1.50	-0.20	-6.38	-31.4	10.37	11342	0.3	4.89	10435
1.50	-0.20	-7.41	-28.1	9.63	10960	-0.6	5.00	10390
-0.27	0.20	0.21	-2.1	6.54	11501	2.8	9.84	11741
-0.27	0.20	-1.85	-27.6	8.95	11890	4.0	7.38	12261
-0.27	0.20	-2.88	-31.9	2.94	11498	7.5	3.52	11622
-0.27	0.20	-3.91	-30.8	2.01	11366	9.2	2.12	11351
-0.27	0.20	-4.94	-29.5	1.76	11175	10.2	1.45	10997
-0.27	0.20	-5.97	-28.5	1.39	11104	11.0	1.00	10973
0.70	0.20	-6.17	-11.5	2.35	11791	-20.1	2.09	11864
0.70	0.20	-7.20	-11.2	1.37	11878	-17.3	1.18	11771
0.70	0.20	-8.23	-10.1	1.11	11659	-14.1	0.88	11448
0.70	0.20	-9.26	-9.2	0.94	11707	-12.4	0.69	11700
0.70	0.20	-10.29	-8.1	0.89	11719	-10.2	0.62	11557
1.10	0.20	-6.51	-7.6	3.08	11930	-35.9	2.28	14119
1.10	0.20	-7.54	-7.3	3.32	12303	-34.6	3.09	14238
1.10	0.20	-8.57	-9.8	2.10	11115	-27.1	2.15	11918
1.10	0.20	-9.60	-9.2	1.71	11265	-24.0	1.47	11638
1.10	0.20	-10.63	-8.3	1.50	11116	-21.9	1.29	11520
1.10	0.20	-11.66	-7.8	1.26	11172	-20.1	1.18	11586
1.10	0.20	-12.64	-7.1	0.96	11062	-18.5	1.03	11632
1.50	0.20	6.93	-11.0	4.05	12106	-21.7	4.99	12190

Table 6.- Concluded.

x/R	y/R	z, in	\bar{u}_i , fps	σ_u	Number	\bar{v}_i , fps	σ_v	Number
1.50	0.20	5.90	-11.5	5.83	12019	-22.2	7.28	11866
1.50	0.20	4.87	-10.9	9.03	11812	-23.5	10.60	12210
1.50	0.20	3.84	-7.4	7.65	11721	-23.6	14.46	11908
1.50	0.20	2.81	-3.3	6.21	11624	-26.5	12.31	11886
1.50	0.20	1.78	-0.8	6.59	11686	-31.0	11.01	12496
1.50	0.20	0.75	0.1	5.82	11668	-32.3	7.77	12697
1.50	0.20	-7.47	-9.7	2.59	12218	-36.3	1.85	13695
1.50	0.20	-8.50	-9.7	2.14	12095	-36.5	1.71	13389
1.50	0.20	-9.53	-10.3	2.52	12204	-36.1	2.57	13736
1.50	0.20	-10.56	-11.1	2.97	11785	-33.2	3.10	13123
1.50	0.20	-11.59	-11.6	2.13	11352	-28.8	1.94	11840
1.50	0.20	-12.62	-10.5	1.61	11222	-26.0	1.37	11630
1.50	0.20	-13.56	-10.3	1.49	11282	-25.1	1.19	11745

Table 7.- Wake Velocity Summary

 $C_T = 0.0064$ $V_{tip} = 710$ fps

x/R	y/R	z, in	\bar{u}_i , fps	σ_u	Number	\bar{v}_i , fps	σ_v	Number
1.10	-0.20	8.85	-4.90	4.28	13189	-8.10	4.22	14106
1.10	-0.20	7.82	-3.40	6.40	13214	-7.60	5.51	13905
1.10	-0.20	6.79	-6.10	7.92	12431	-6.90	11.24	12473
1.10	-0.20	5.76	-2.70	8.30	12554	-9.10	10.47	13641
1.10	-0.20	4.73	0.30	7.74	12710	-8.70	9.19	14175
1.10	-0.20	3.70	0.60	8.06	12935	-8.60	9.70	14174
1.10	-0.20	2.67	-5.20	8.51	12866	-4.20	11.42	13951
0.90	-0.20	-0.27	-17.20	5.46	12261	17.10	14.07	13202
0.90	-0.20	-1.30	-19.50	7.18	12877	18.10	11.26	12926
0.90	-0.20	-2.36	-20.30	8.71	12713	16.00	7.84	12770
0.90	-0.20	-3.36	-19.80	9.25	12663	13.20	4.91	12649
0.90	-0.20	-4.39	-13.30	8.25	12236	9.60	3.16	12264
0.90	-0.20	-5.42	-12.90	9.04	12260	7.30	3.40	12130
0.90	-0.20	-6.45	-12.70	8.71	12421	5.60	3.96	12413
1.50	-0.20	8.37	-12.60	5.28	12427	-9.80	5.82	11583
1.50	-0.20	7.34	-12.20	8.38	12555	-9.50	9.07	12119
1.50	-0.20	6.31	-9.50	7.58	12466	-9.50	13.75	12170
1.50	-0.20	5.28	-5.90	6.44	12826	-11.10	13.85	12878
1.50	-0.20	4.25	-5.10	5.75	12804	-10.60	11.18	13091
1.50	-0.20	3.22	-5.10	7.36	12817	-10.40	11.07	13573
1.50	-0.20	2.19	-8.10	10.45	12607	-8.70	11.30	13208
1.50	-0.20	-1.23	-20.20	6.45	12730	17.00	14.99	13575
1.50	-0.20	-2.26	-20.60	7.99	12643	18.80	15.06	13400
1.50	-0.20	-3.29	-28.30	8.77	12452	2.00	7.50	12669
1.50	-0.20	-4.32	-32.20	11.05	12436	1.40	7.21	12810
1.50	-0.20	-5.35	-32.10	12.00	12275	1.20	5.88	12713
1.50	-0.20	-6.38	-34.40	13.63	12390	2.30	6.17	12530
1.50	-0.20	-7.41	-31.30	12.97	12342	0.60	5.74	12604
1.50	0.20	6.93	-11.00	2.96	12942	-19.70	3.65	13186

Table 7.- Concluded.

x/R	y/R	z, in	\bar{u}_i , fps	σ_u	Number	\bar{v}_i , fps	σ_v	Number
1.50	0.20	5.90	-11.90	4.99	12834	-20.40	5.49	13260
1.50	0.20	4.87	-10.50	5.14	12822	-21.90	8.92	13588
1.50	0.20	3.84	-8.60	4.52	12835	-24.50	7.39	13736
1.50	0.20	2.81	-6.50	4.92	12738	-26.10	5.06	13929
1.50	0.20	1.78	-5.50	4.89	12720	-27.90	4.51	14025
1.50	0.20	0.75	-4.80	4.55	12784	-29.30	4.02	14181
1.50	0.20	-7.47	-10.70	2.40	12485	-36.30	2.44	14523
1.50	0.20	-8.50	-11.80	3.26	12754	-35.30	2.73	14776
1.50	0.20	-9.53	-13.00	2.25	12614	-33.50	2.26	14674
1.50	0.20	-10.56	-11.60	1.74	11836	-27.70	1.31	11326
1.50	0.20	-11.59	-10.90	1.54	11779	-26.40	1.30	11250
1.50	0.20	-12.62	-10.80	1.48	11907	-25.40	1.31	11309
1.50	0.20	-13.56	-10.80	1.33	12099	-23.70	1.11	11004

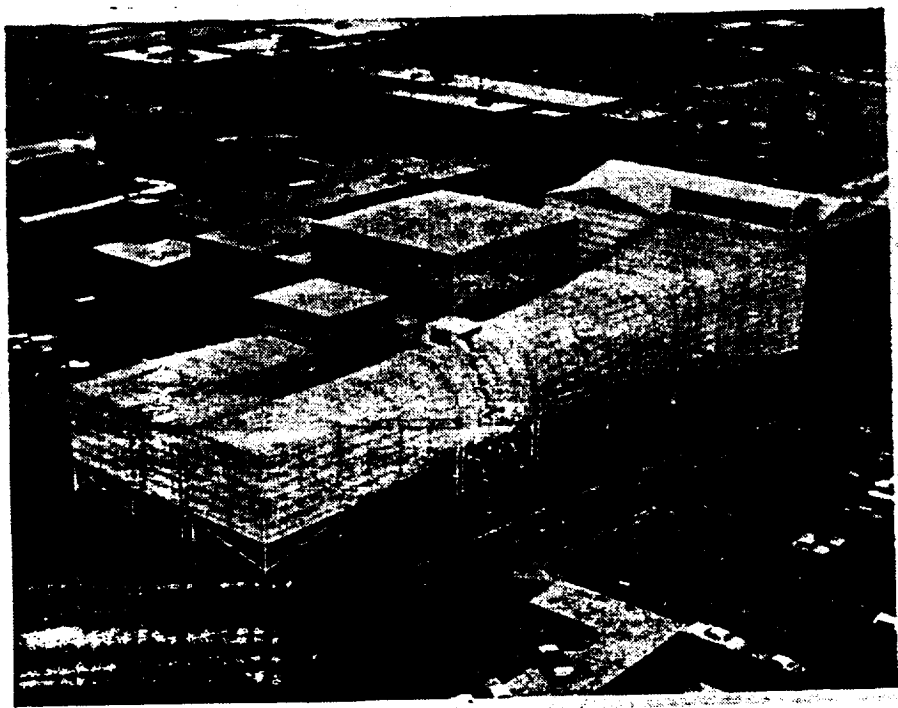


Figure 1.- NASA Langley 14- X 22- Foot Subsonic Wind Tunnel.

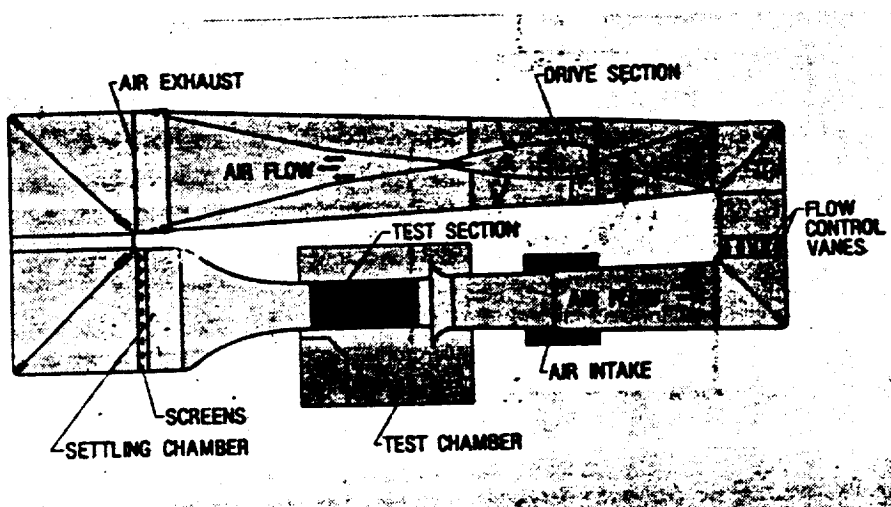


Figure 2.- Schematic view of wind tunnel.

ORIGINAL PAGE IS
OF POOR QUALITY

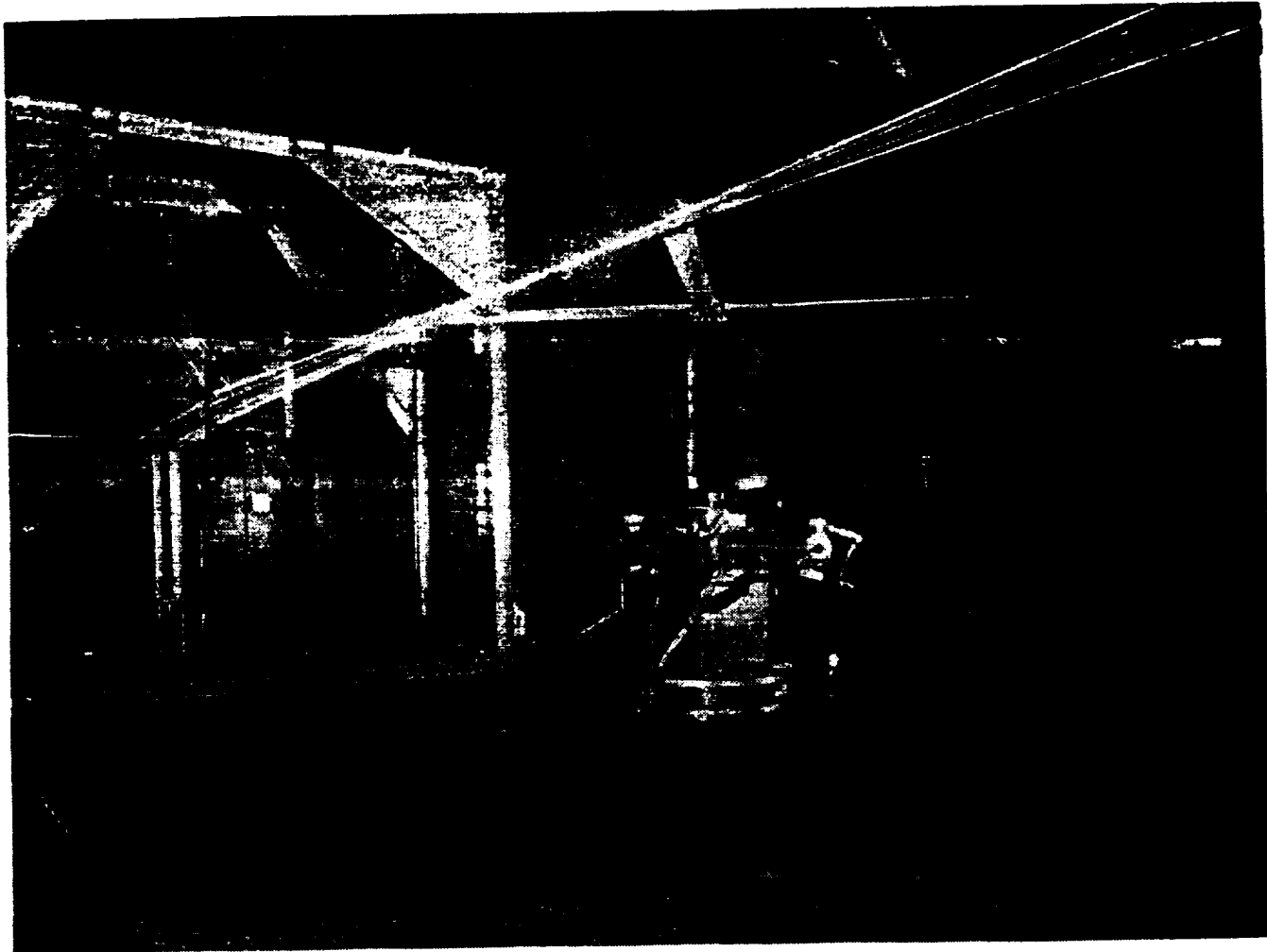


Figure 3.- PFM Test Stand and ALR installed in the test section with the LV and Traversing Platform in the background.

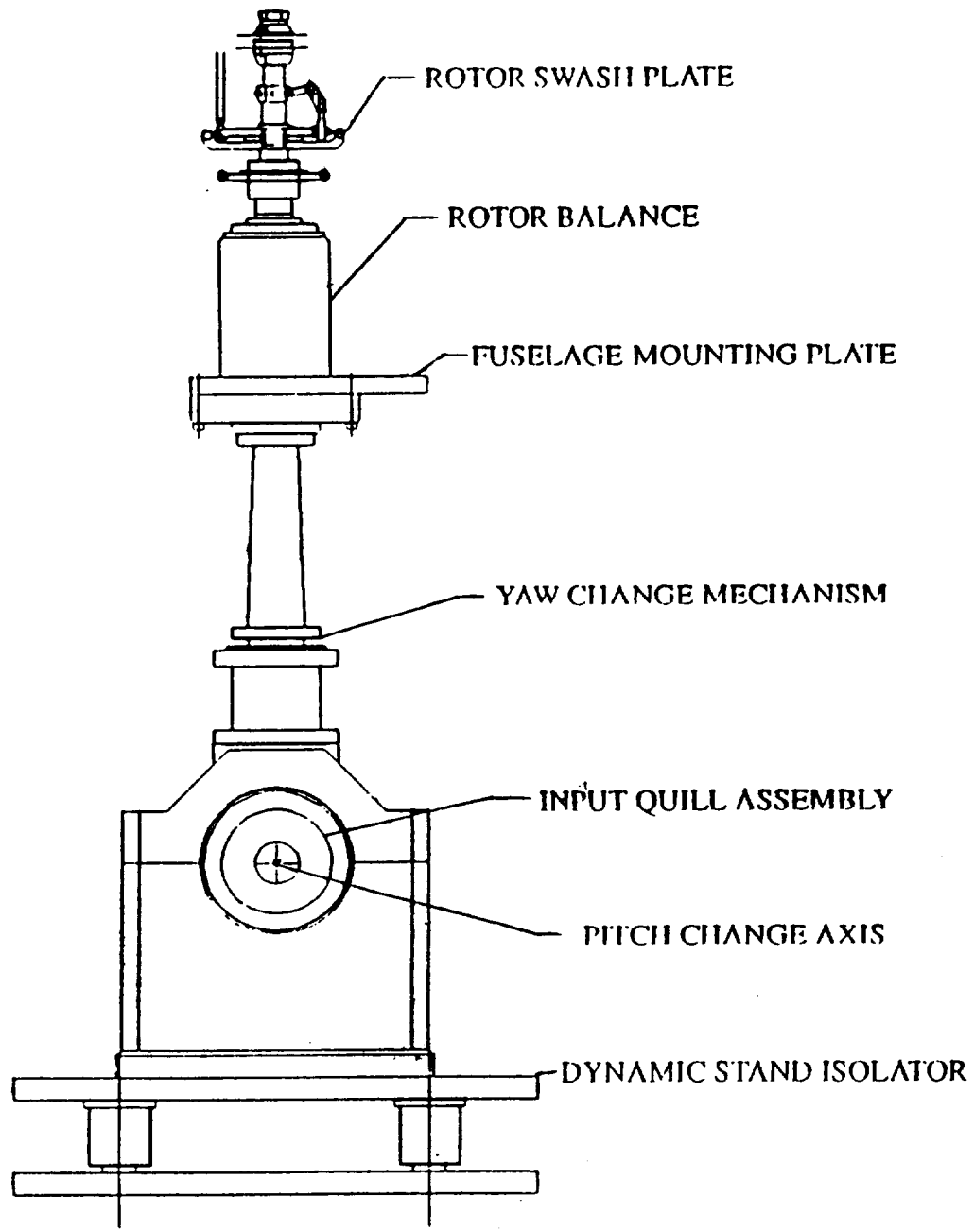


Figure 4.- BHTI Powered Force Model (PFM).

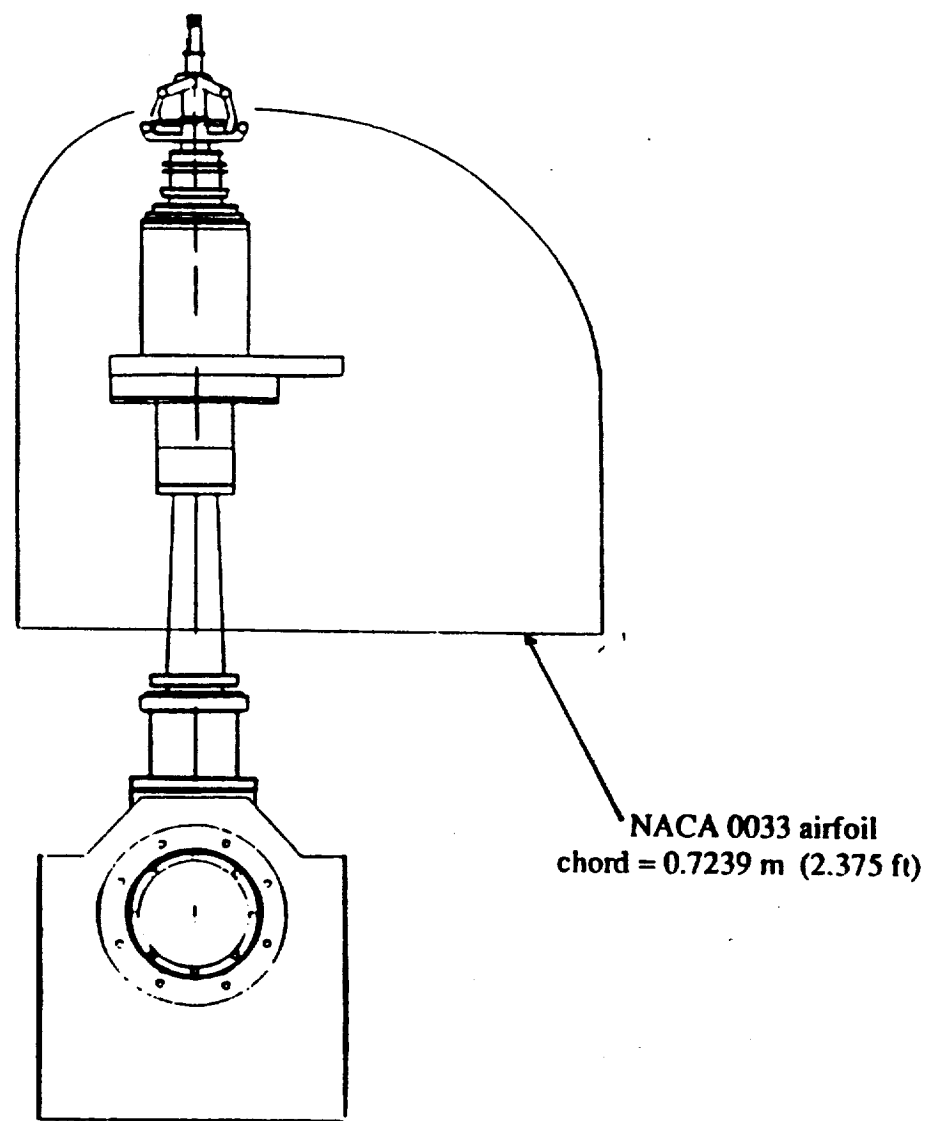


Figure 5.- PFM rotor test stand fairing.

ALR ROTOR BLADE TWIST DISTRIBUTION

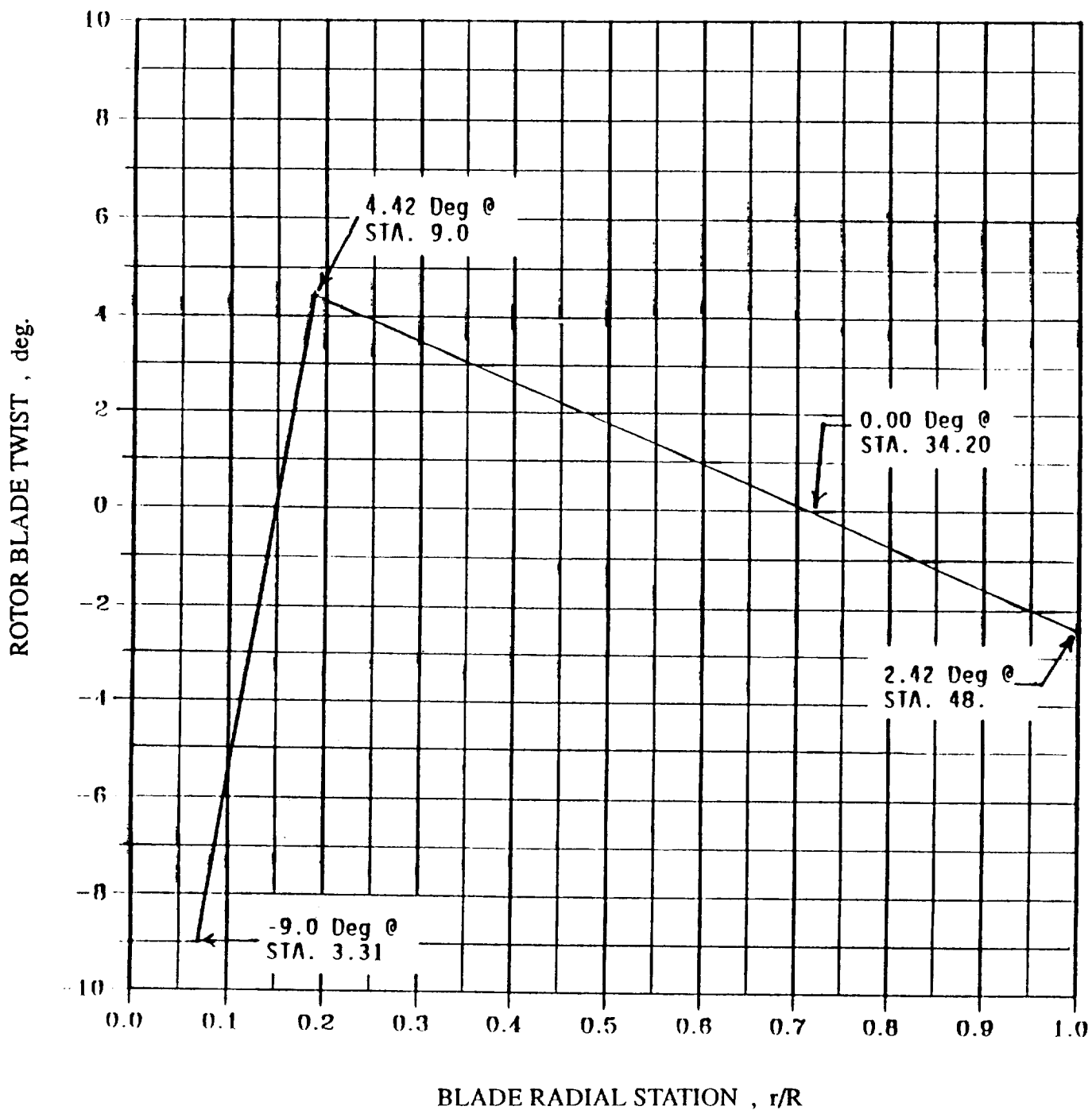


Figure 6.- ALR rotor blade twist characteristics.

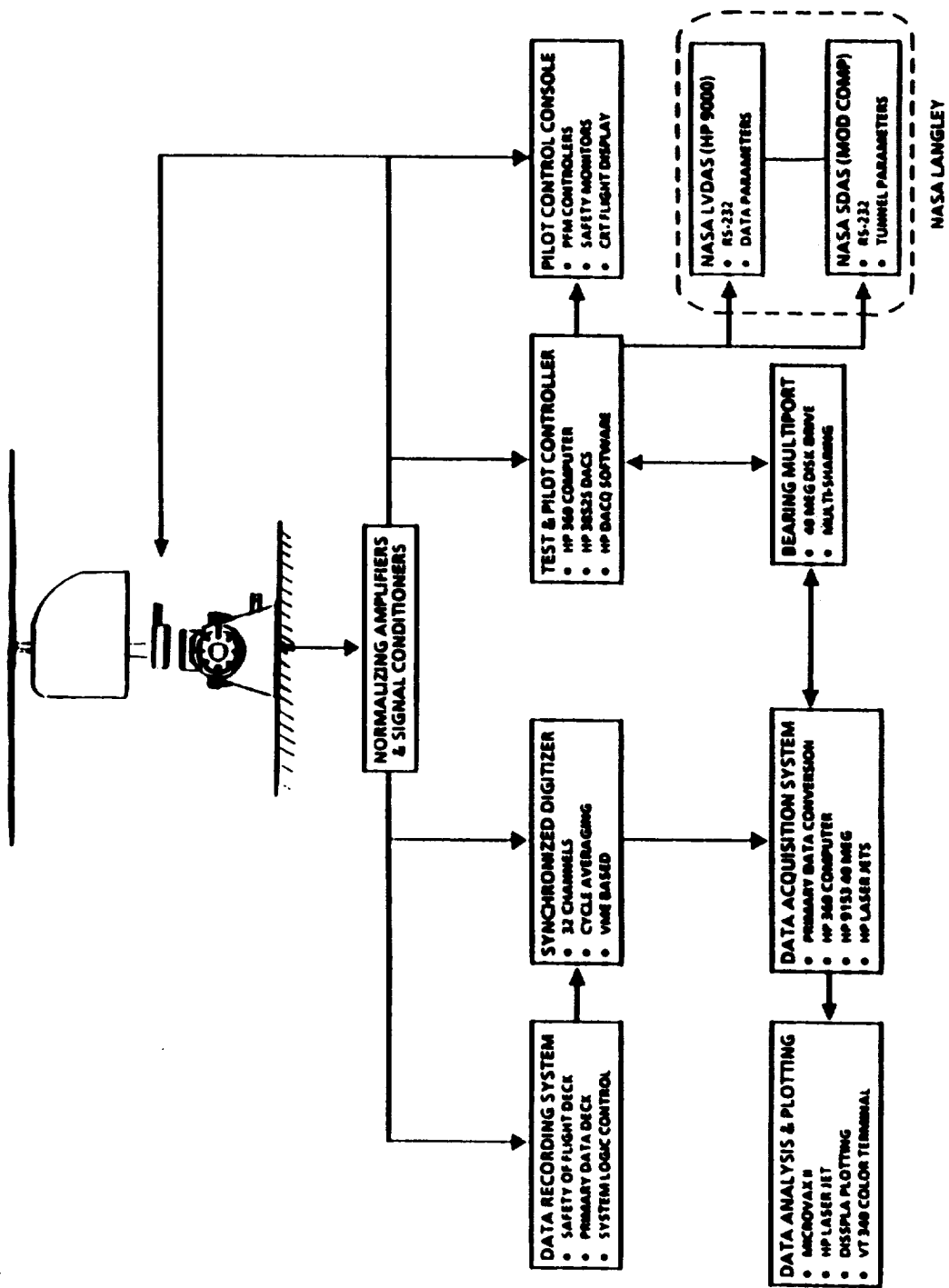


Figure 7.- PFM model data acquisition system.

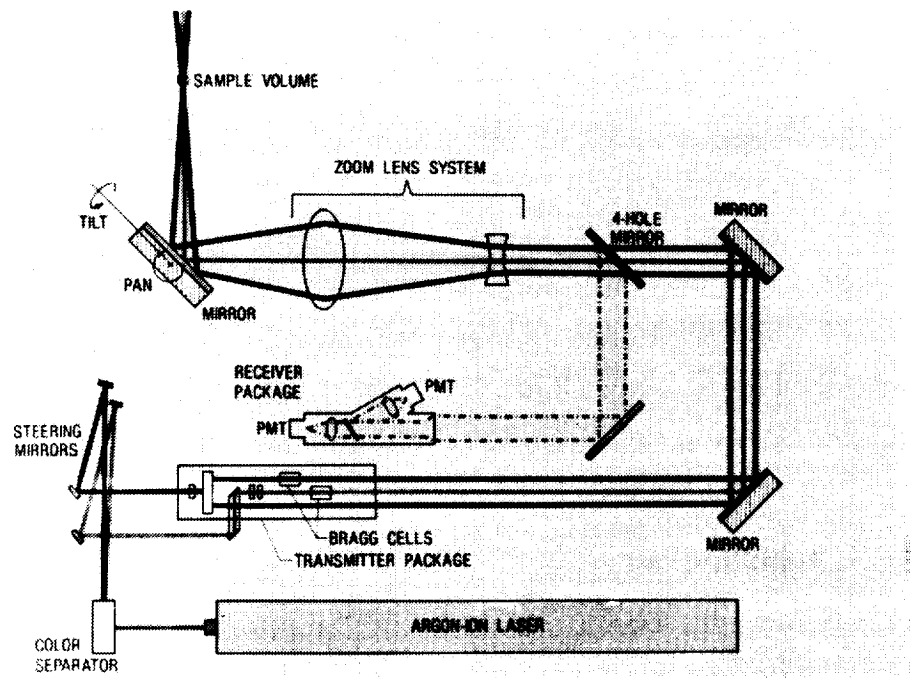


Figure 8.- Schematic diagram of LV optics subsystem.

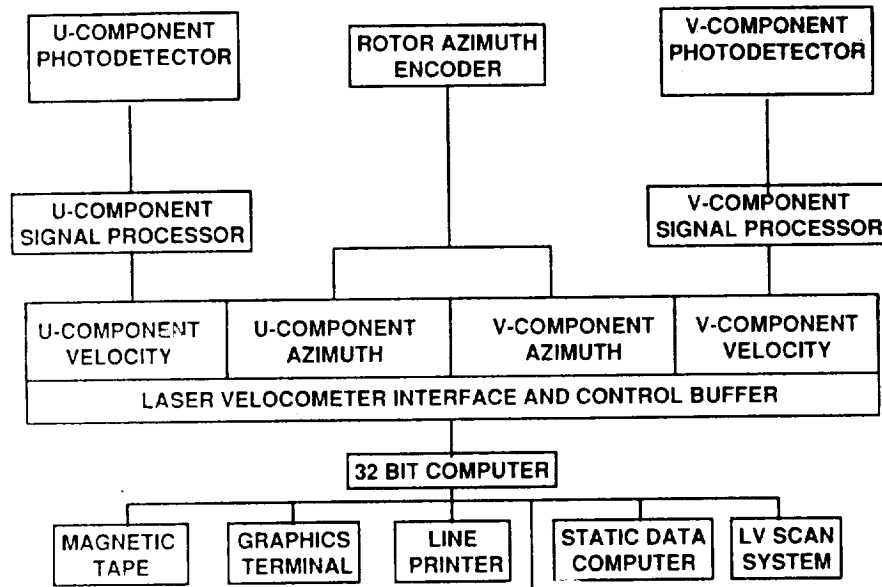


Figure 9.- Schematic diagram of LV data acquisition and control subsystem.

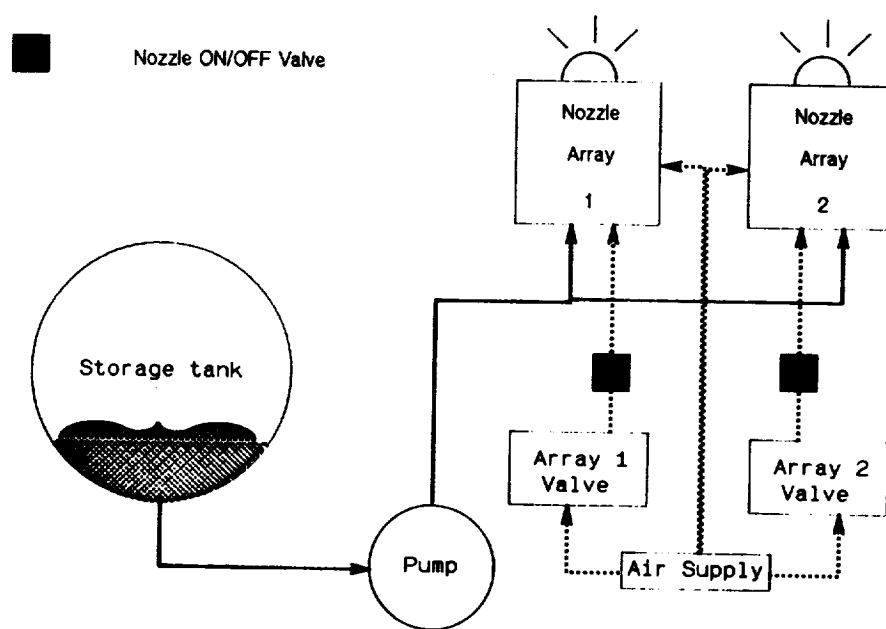


Figure 10.- Schematic of LV seeding subsystem.

ORIGINAL PAGE
BLACK AND WHITE PHOTOGRAPH

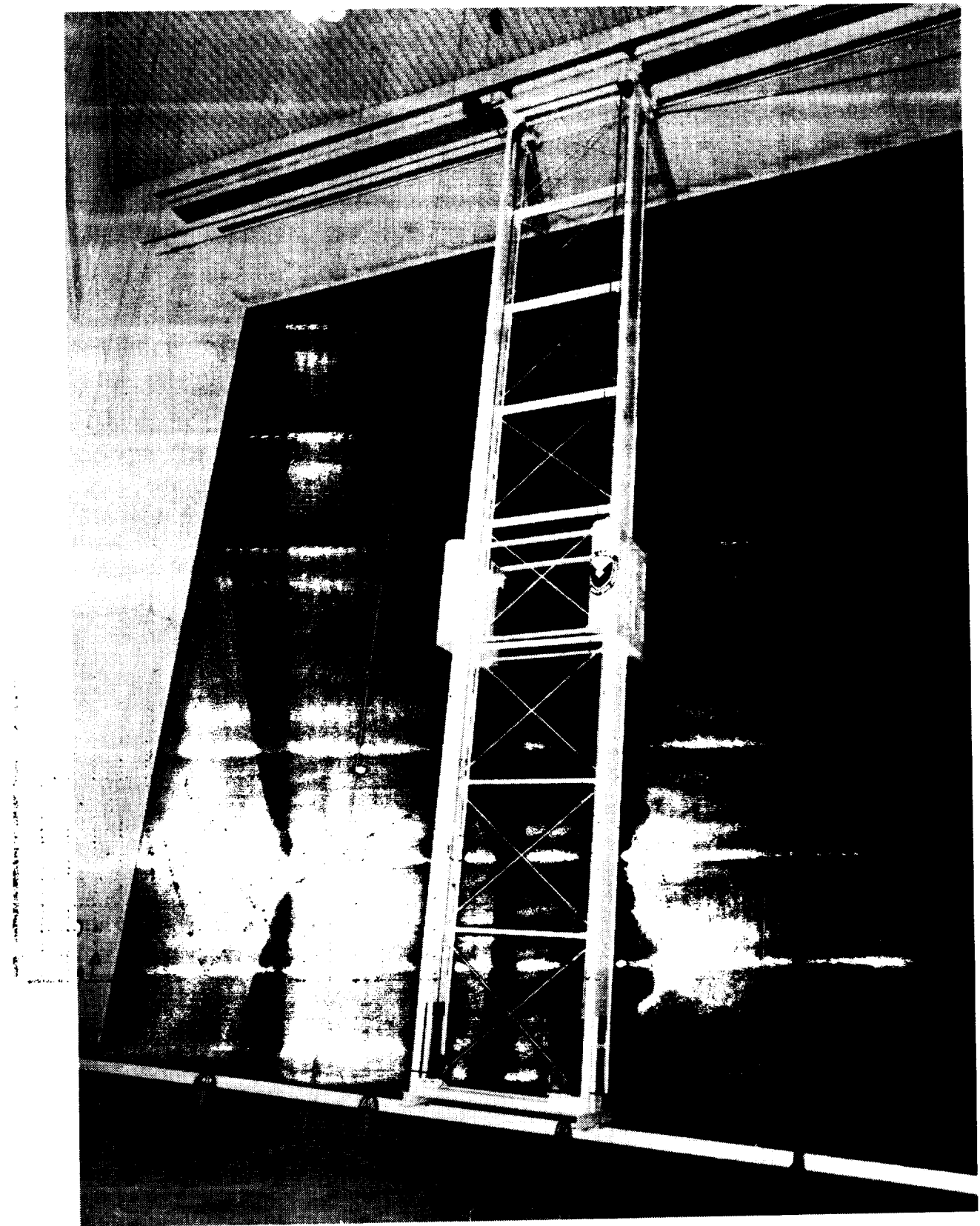
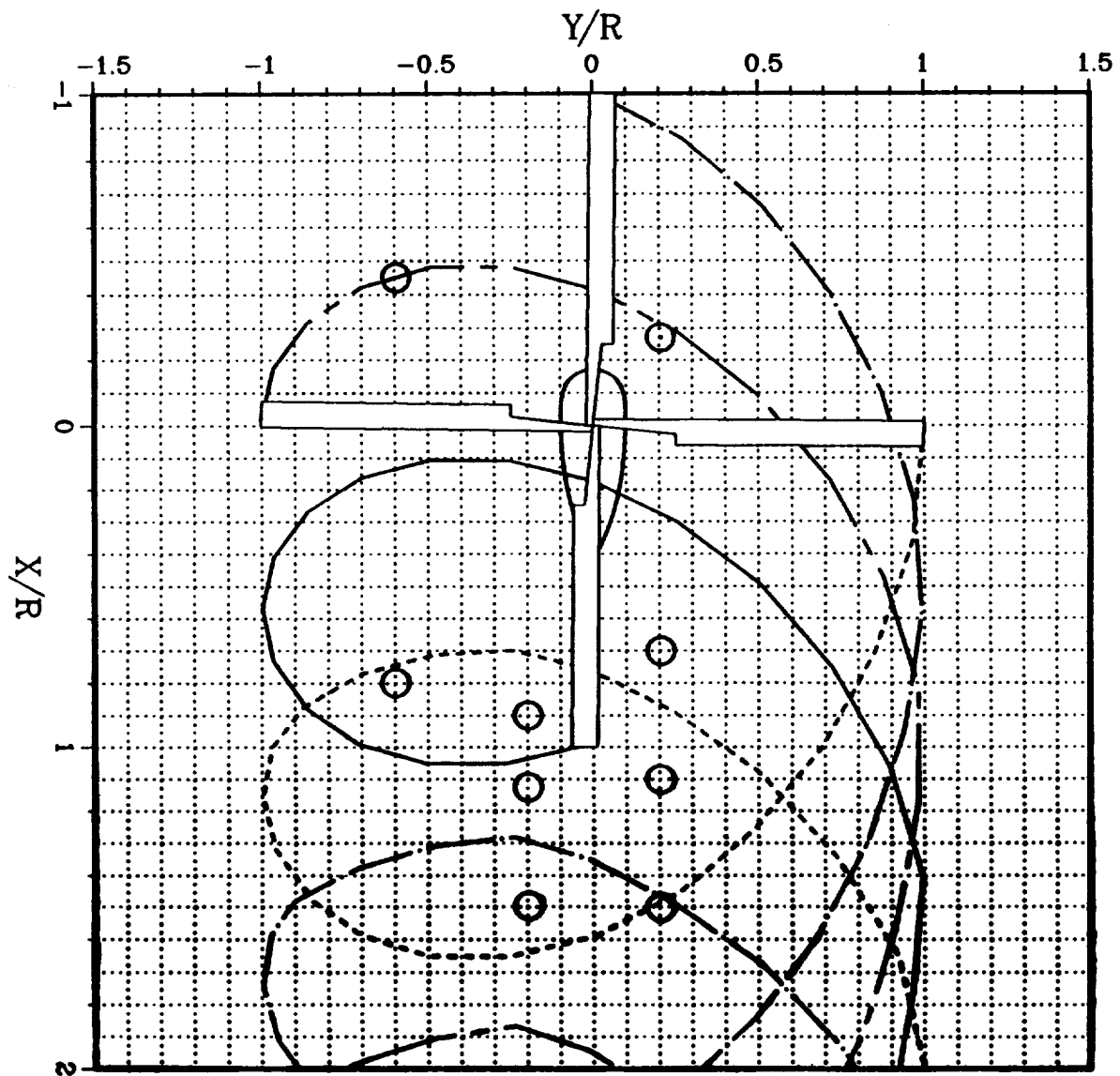
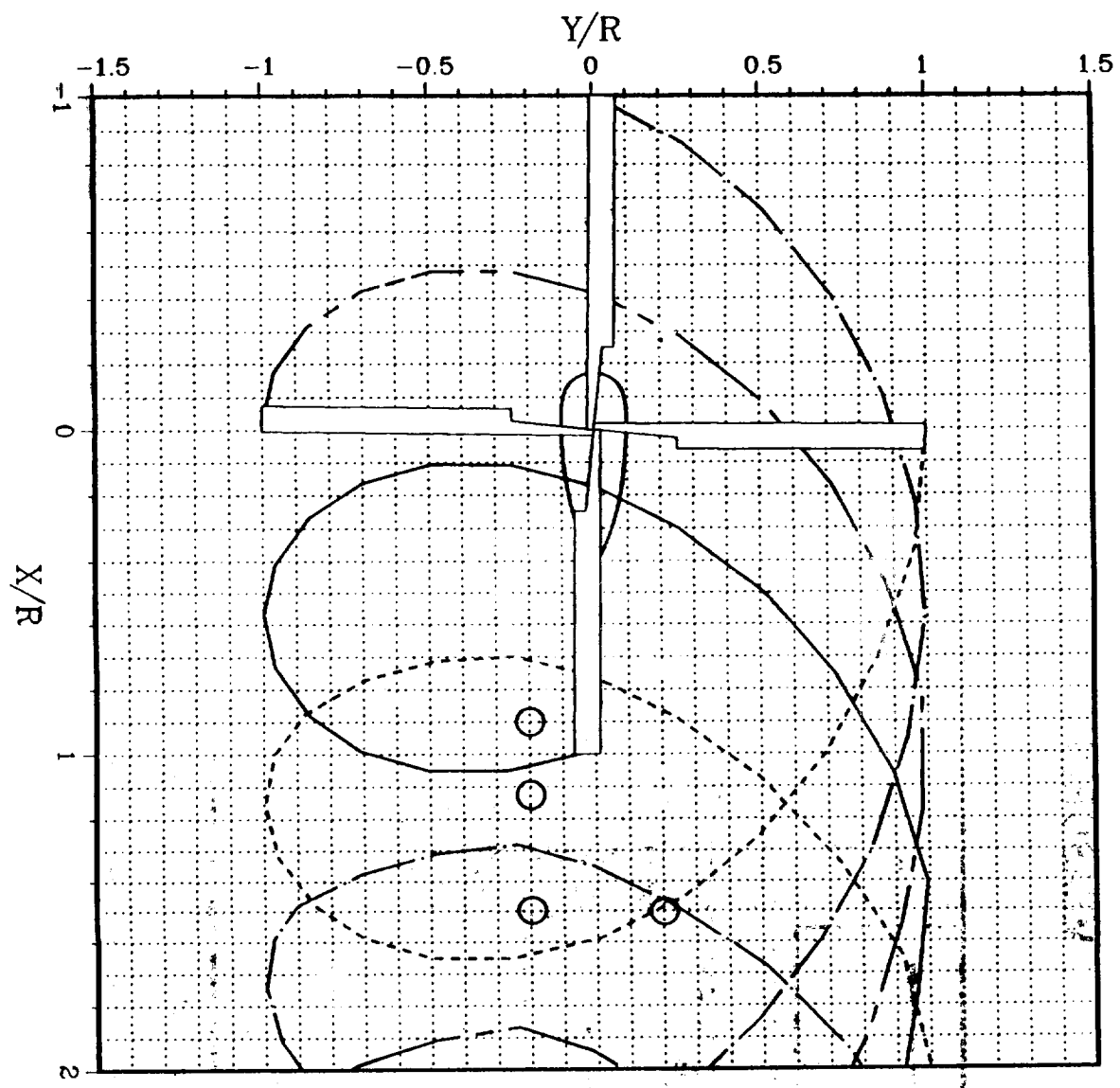


Figure 11.- Traverse assembly for LV seeding subsystem shown in the settling chamber of the tunnel.



(a) $C_T = 0.0081$, $V_{tip} = 710$ ft/sec and $C_T = 0.0081$, $V_{tip} = 603$ ft/sec

Figure 12.- Location of the wake measurement points.



(b) $C_T = 0.0064$, $V_{tip} = 710$ ft/sec

Figure 12.- Concluded.

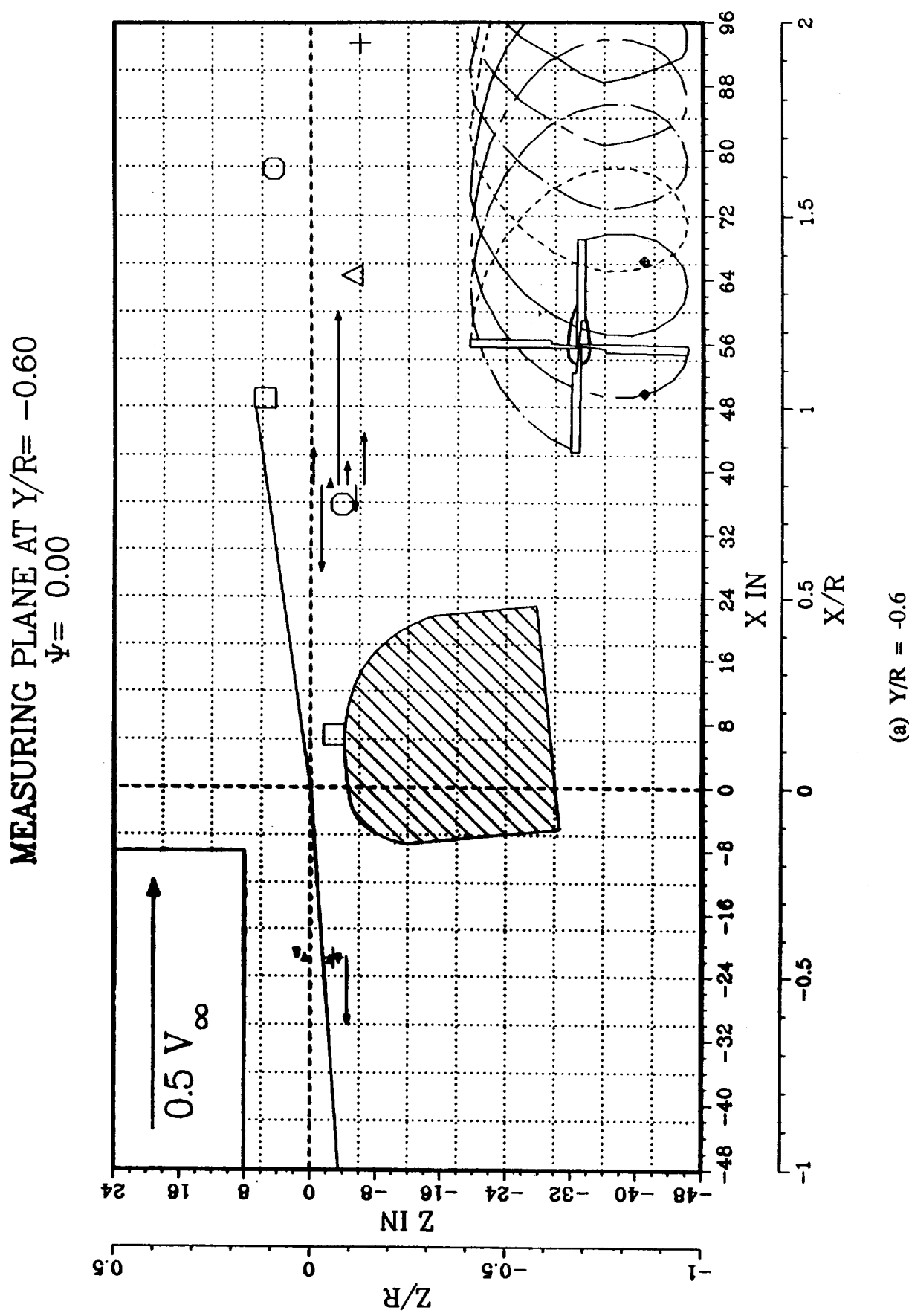
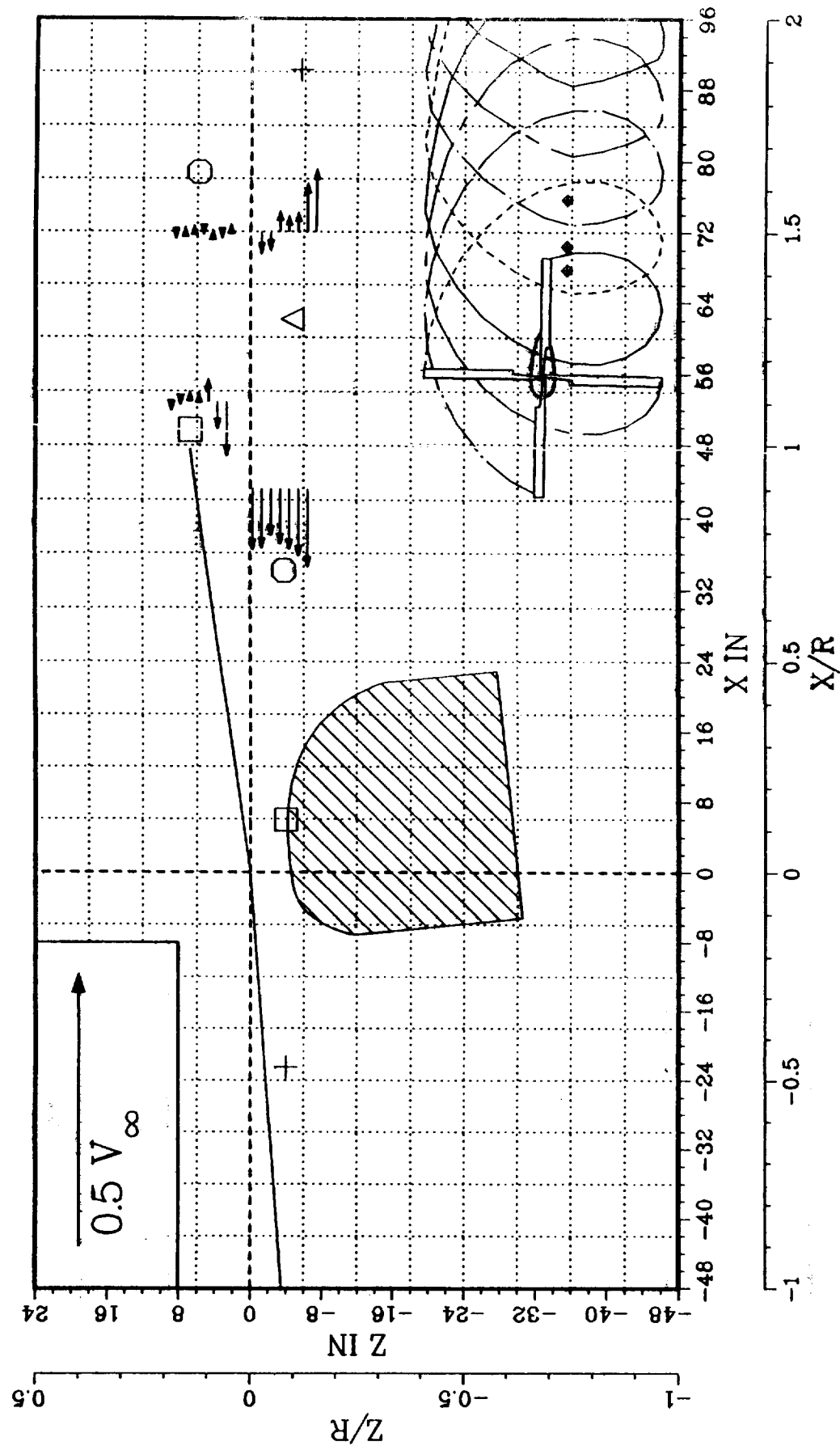


Figure 13.- Wake measurements at $V_{\text{tip}} = 710 \text{ fps}$; $C_T = 0.0081$

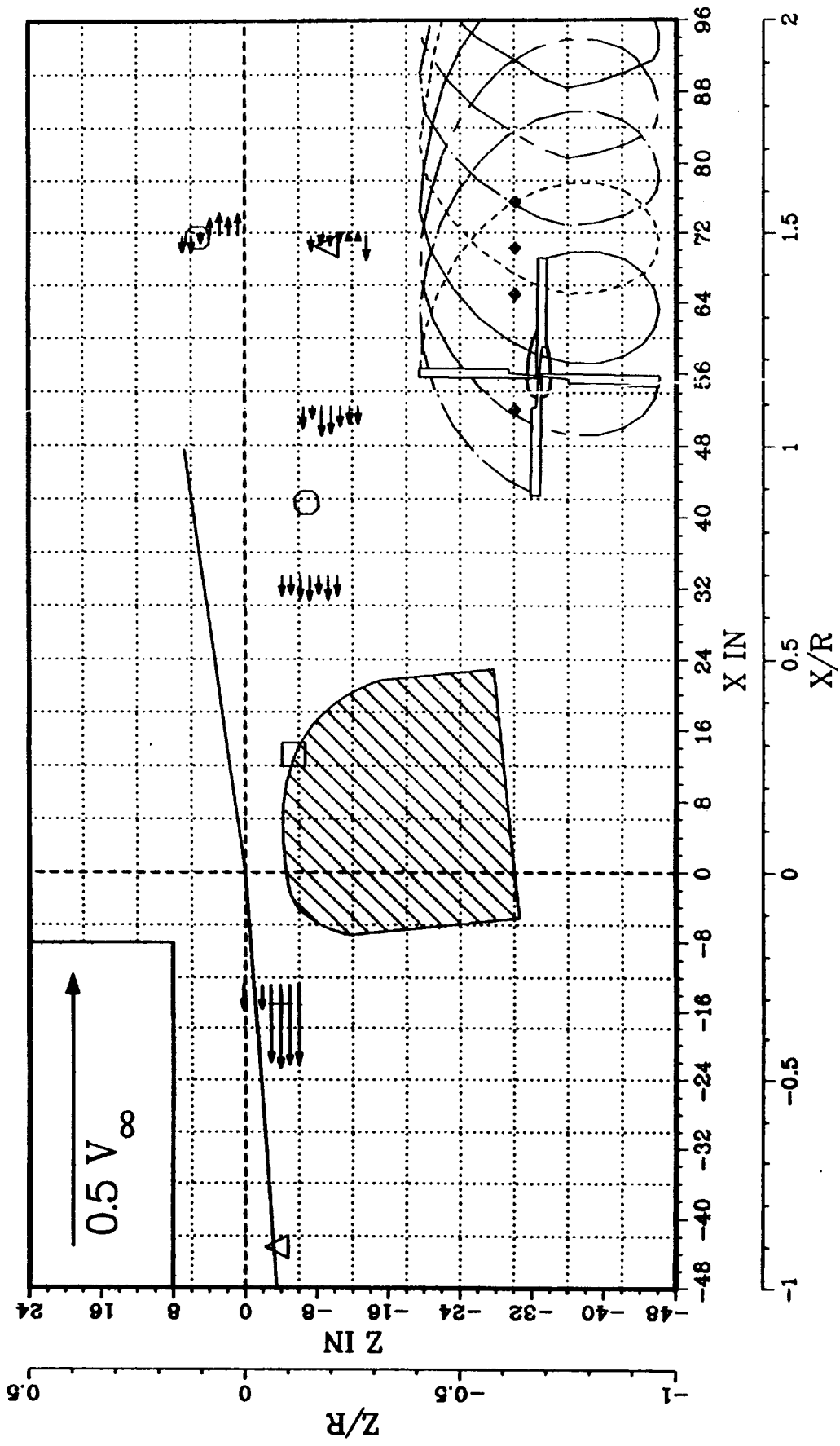
MEASURING PLANE AT $Y/R = -0.20$
 $\Psi = 0.00$



(b) $Y/R = -0.2$

Figure 13.- Continued.

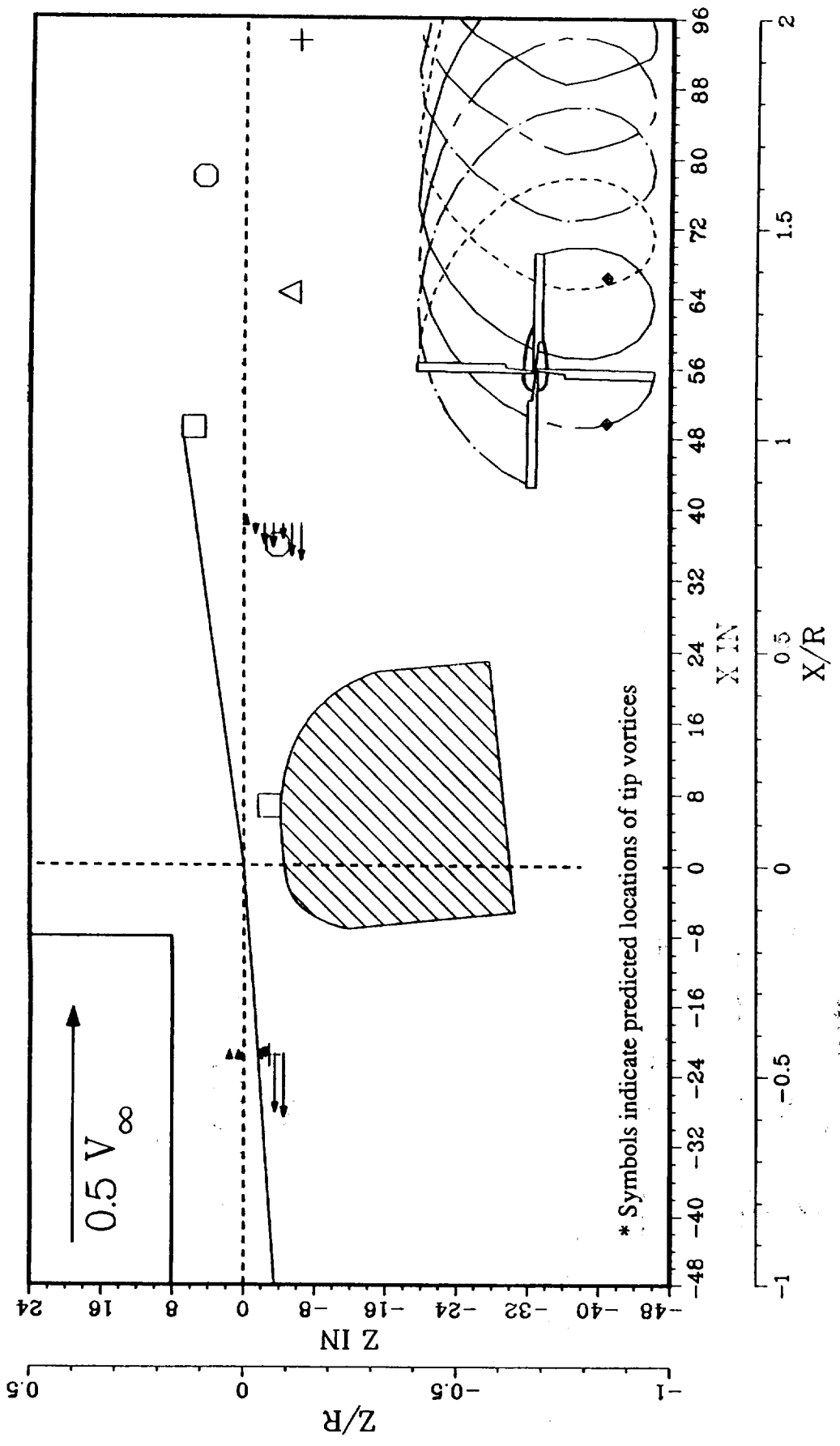
MEASURING PLANE AT $Y/R = 0.20$
 $\Psi = 0.00$



(c) $Y/R = 0.2$

Figure 13.- Concluded.

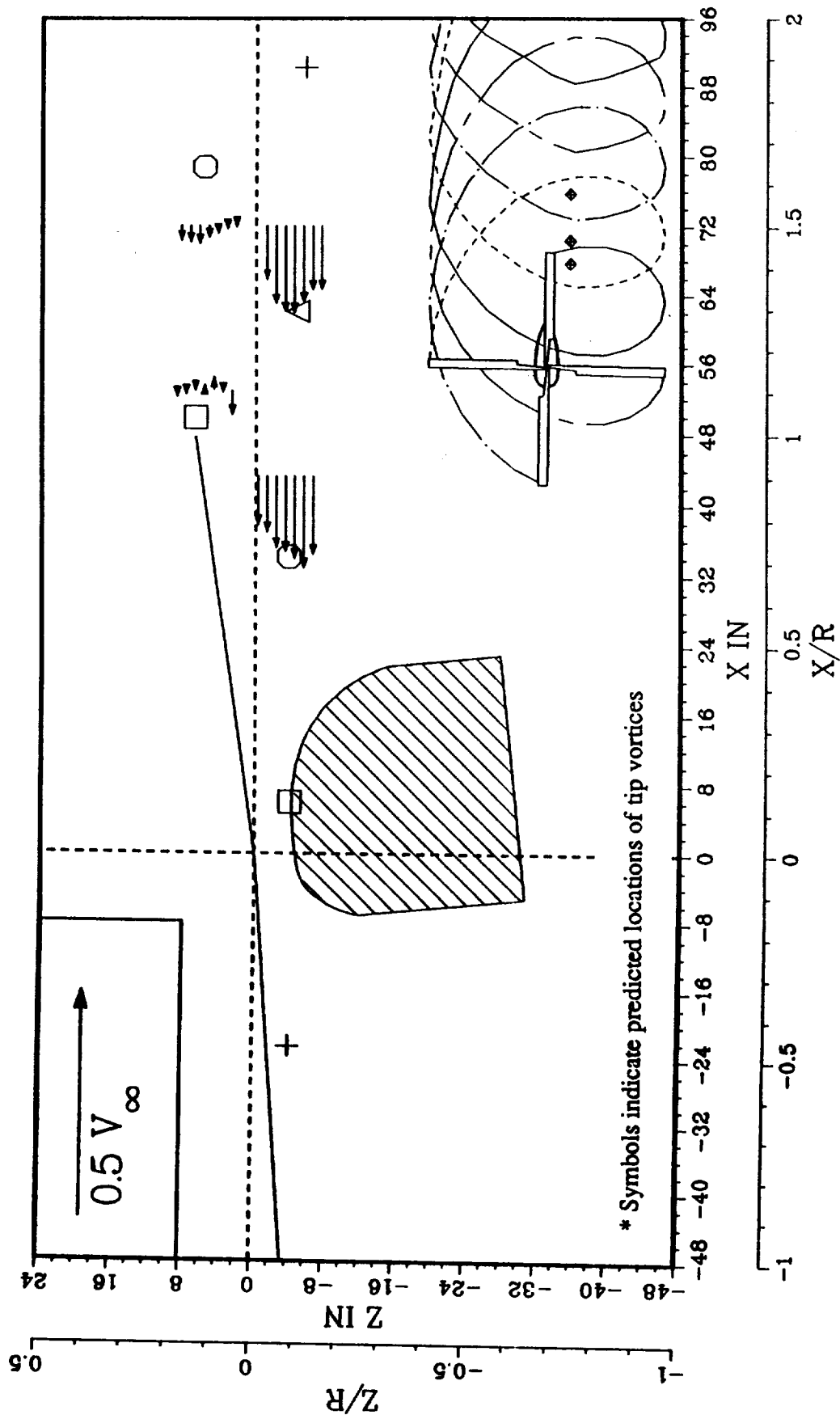
MEASURING PLANE AT $Y/R = -0.60$
 $\Psi = 0.00$



(a) $Y/R = -0.6$

Figure 14.- Wake measurements at $V_{\text{tip}} = 603 \text{ fps} ; C_T = 0.0081$

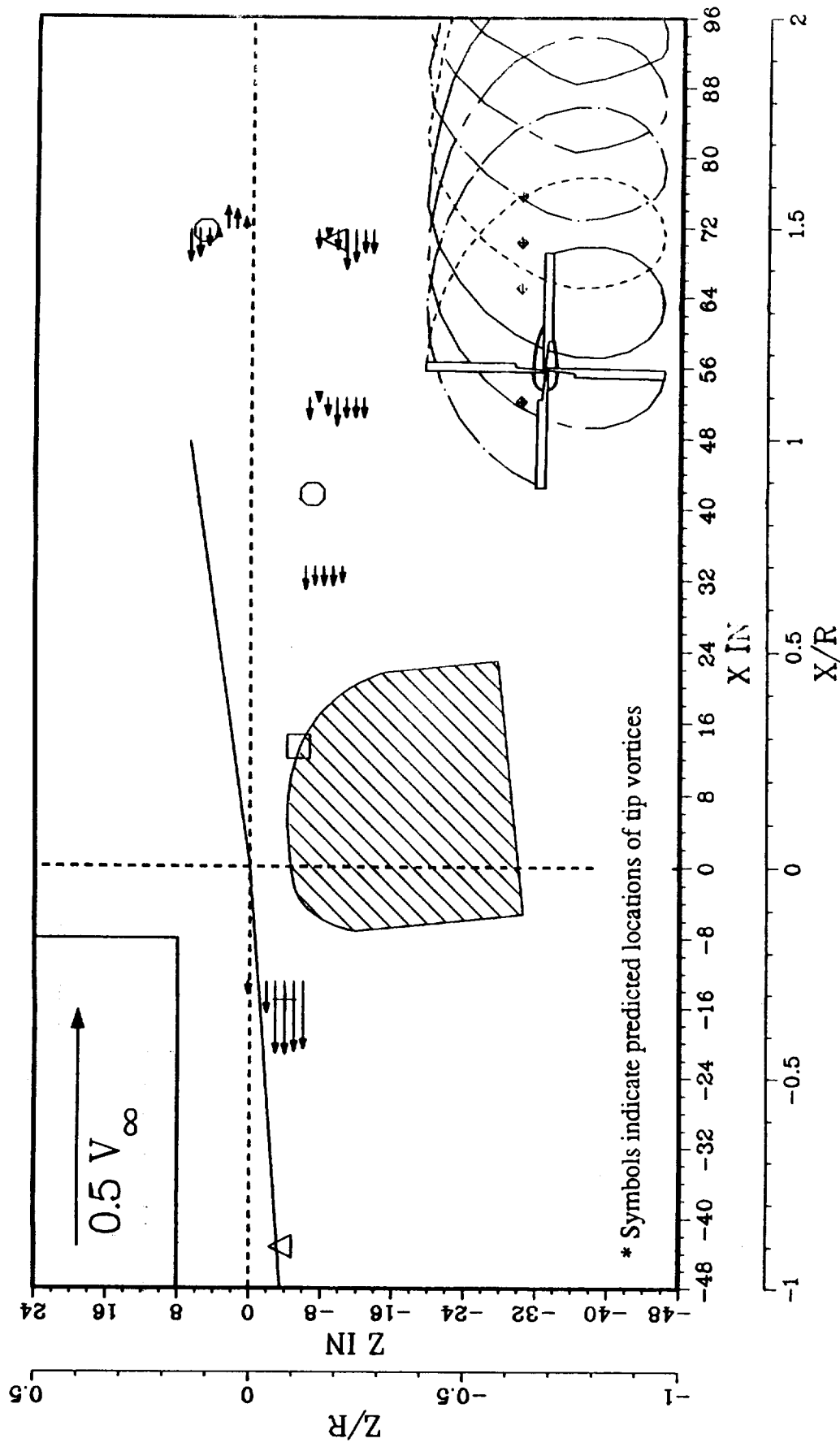
MEASURING PLANE AT $Y/R = -0.20$
 $\Psi = 0.00$



(b) $Y/R = -0.2$

Figure 14.- Continued.

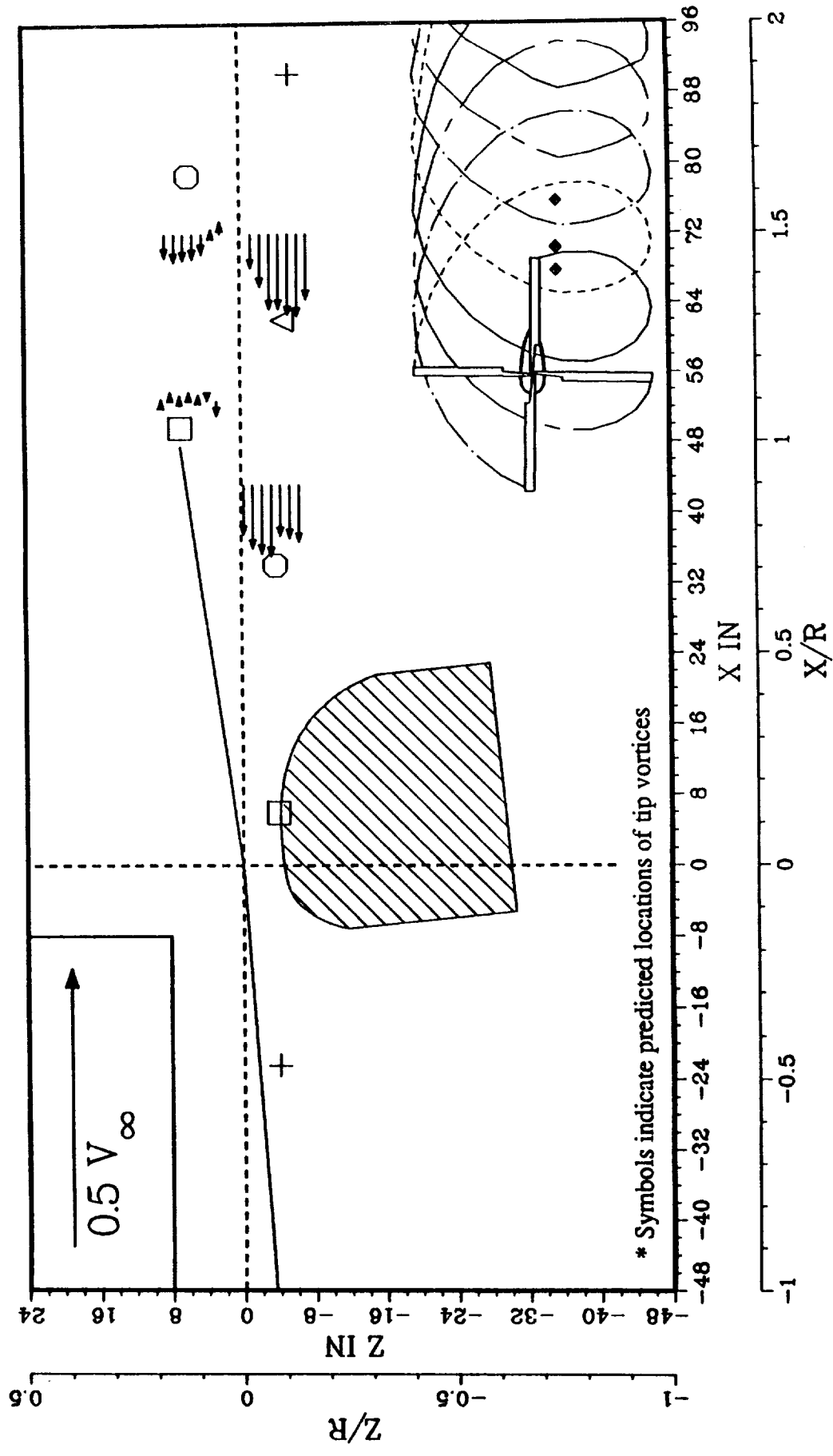
MEASURING PLANE AT $Y/R = 0.20$
 $\Psi = 0.00$



(c) $Y/R = 0.2$

Figure 14.- Concluded.

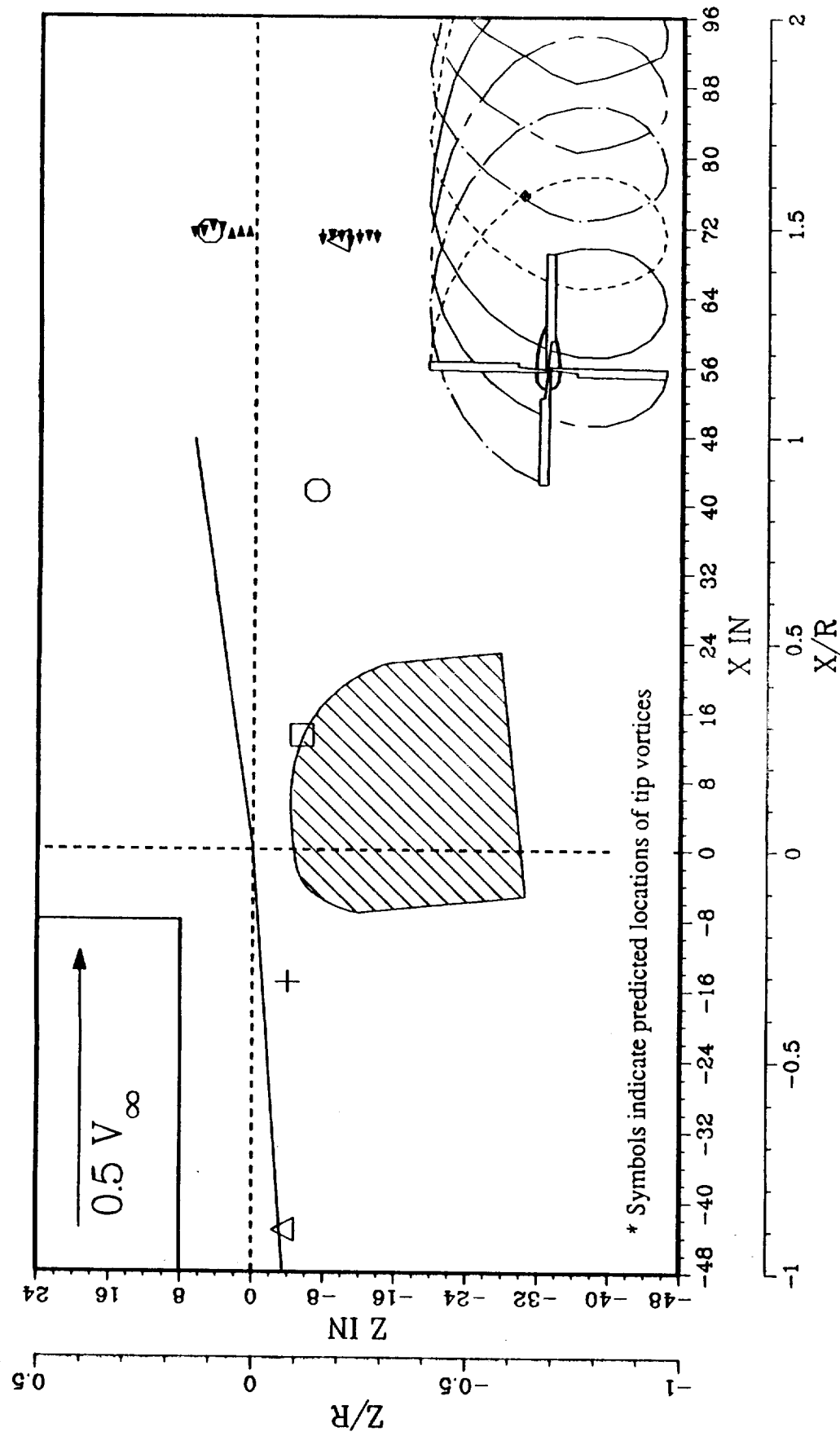
MEASURING PLANE AT $Y/R = -0.20$
 $\Psi = 0.00$



(a) $Y/R = -0.2$

Figure 15.- Wake measurements at $V_{\text{tip}} = 710 \text{ fpm}$; $C_T = 0.0064$.

MEASURING PLANE AT $Y/R = 0.20$
 $\Psi = 0.00$



(b) $Y/R = 0.2$

Figure 15.- Concluded.

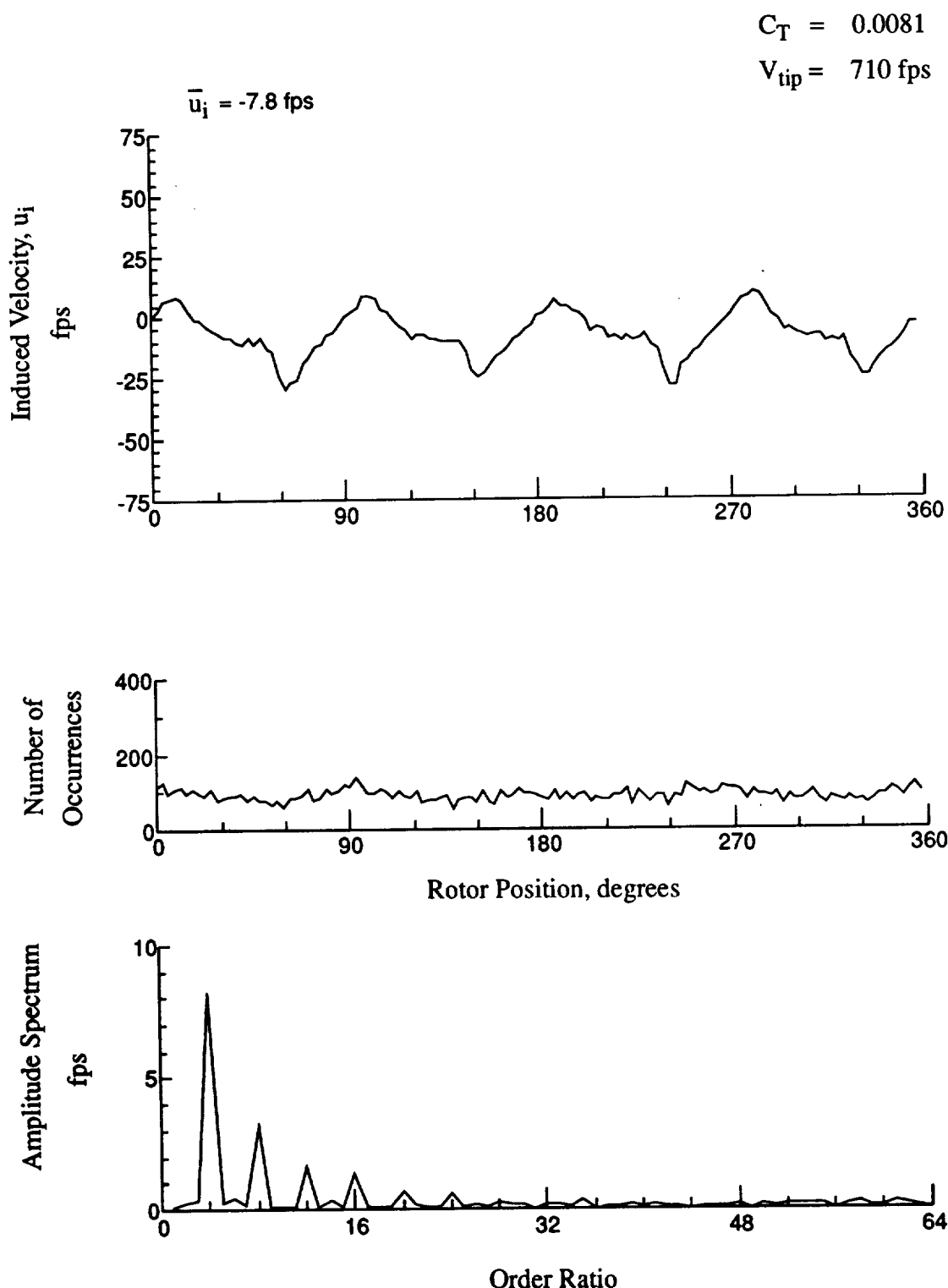


Figure 16.- Wake Measurements at
 $x/R = -0.45$, $y/R = -0.60$, $z = 1.65 \text{ in.}$

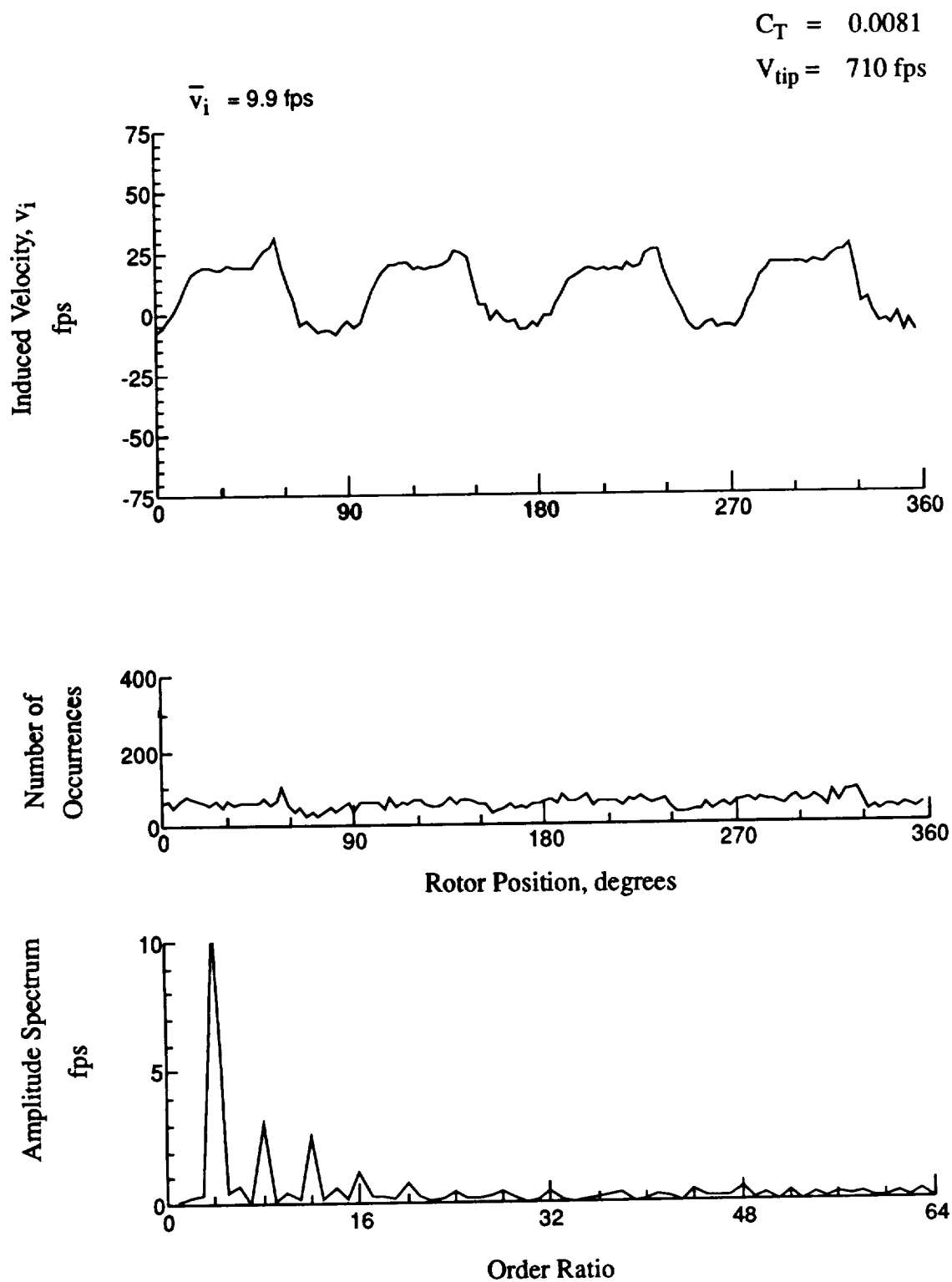


Figure 16.- Concluded.
 $x/R = -0.45$, $y/R = -0.60$, $z = 1.65 \text{ in.}$

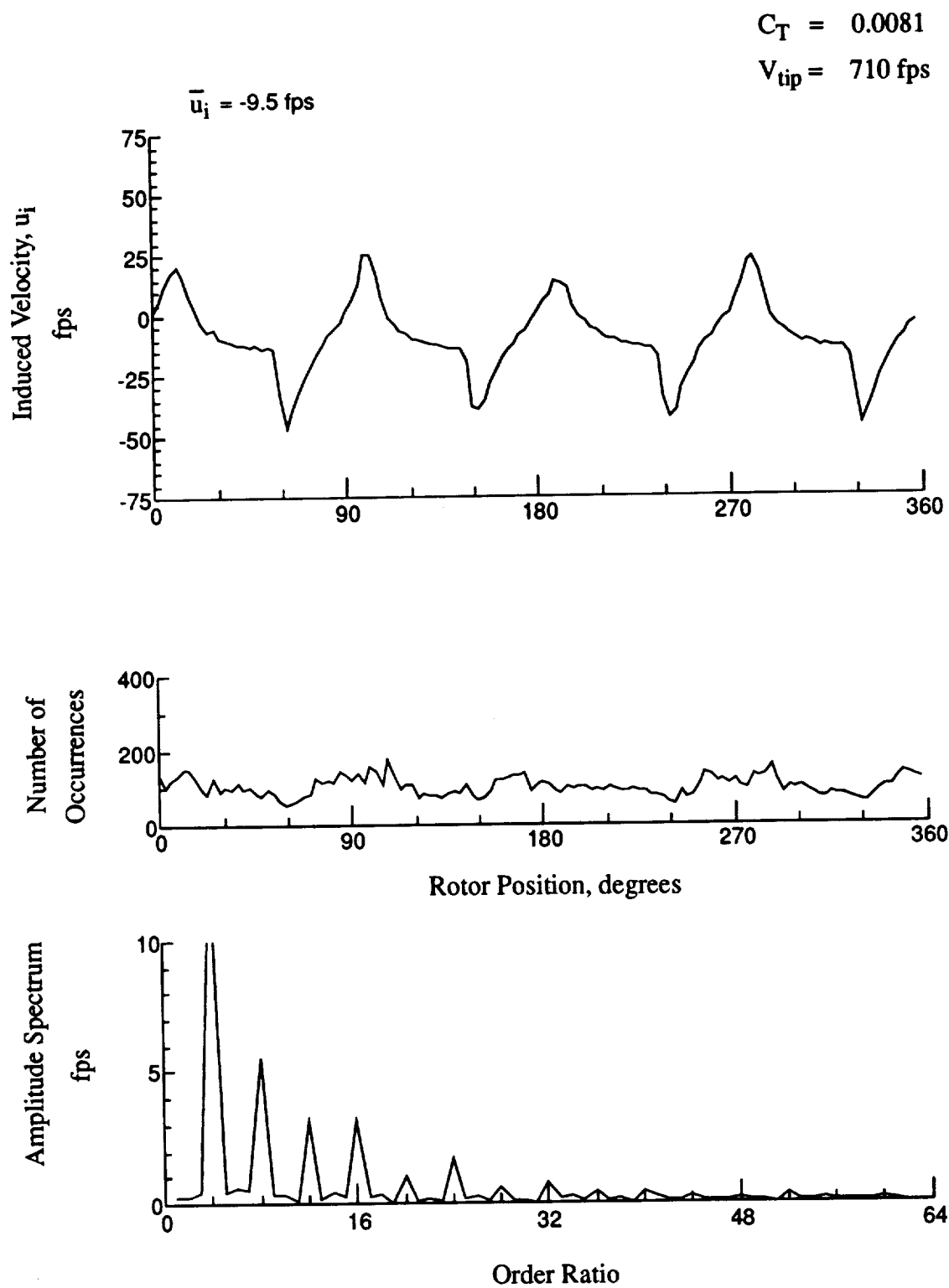


Figure 17.- Wake Measurements at
 $x/R = -0.45$, $y/R = -0.60$, $z = 0.62$ in.

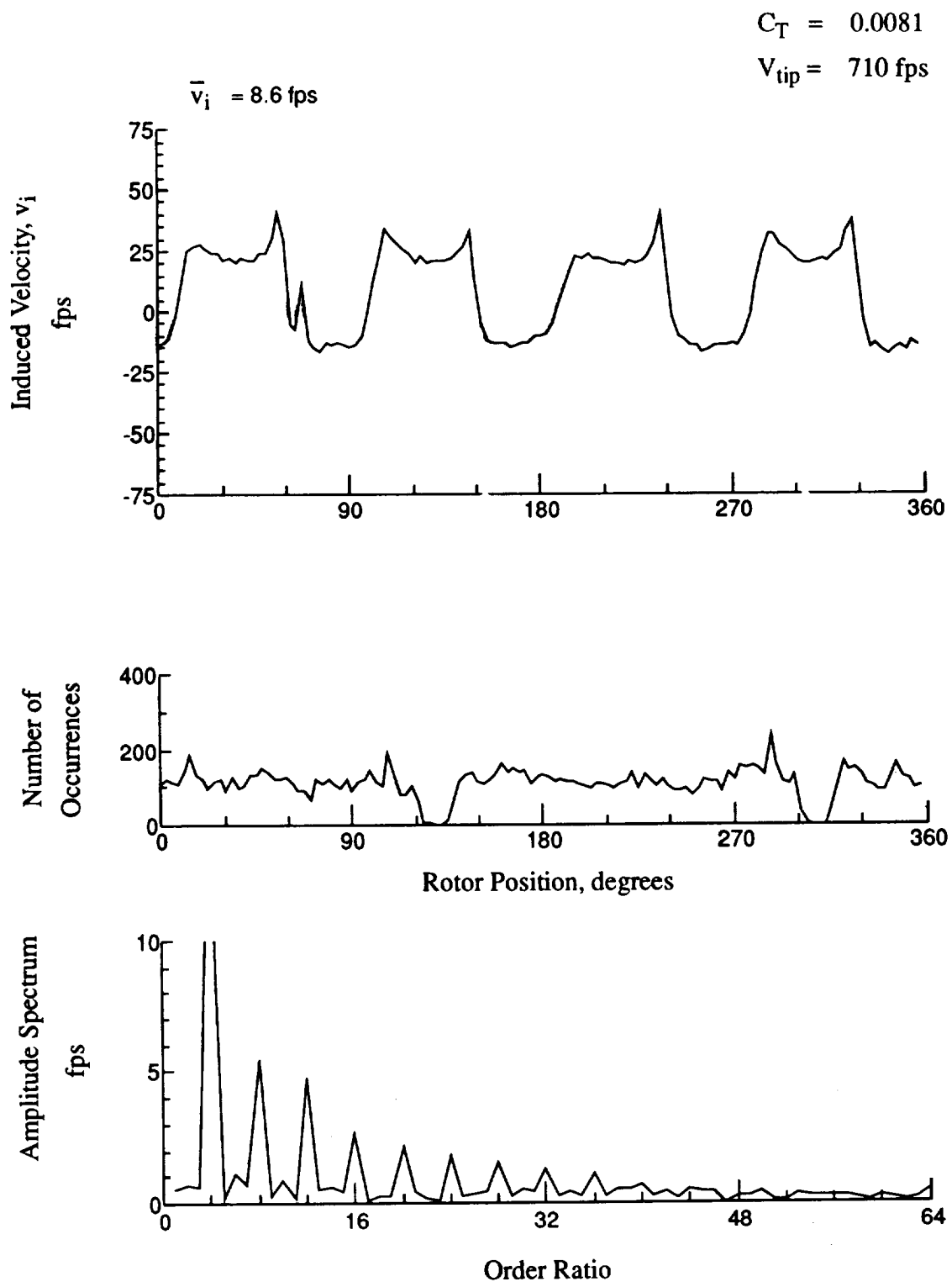


Figure 17.- Concluded.
 $x/R = -0.45$, $y/R = -0.60$, $z = 0.62 \text{ in.}$

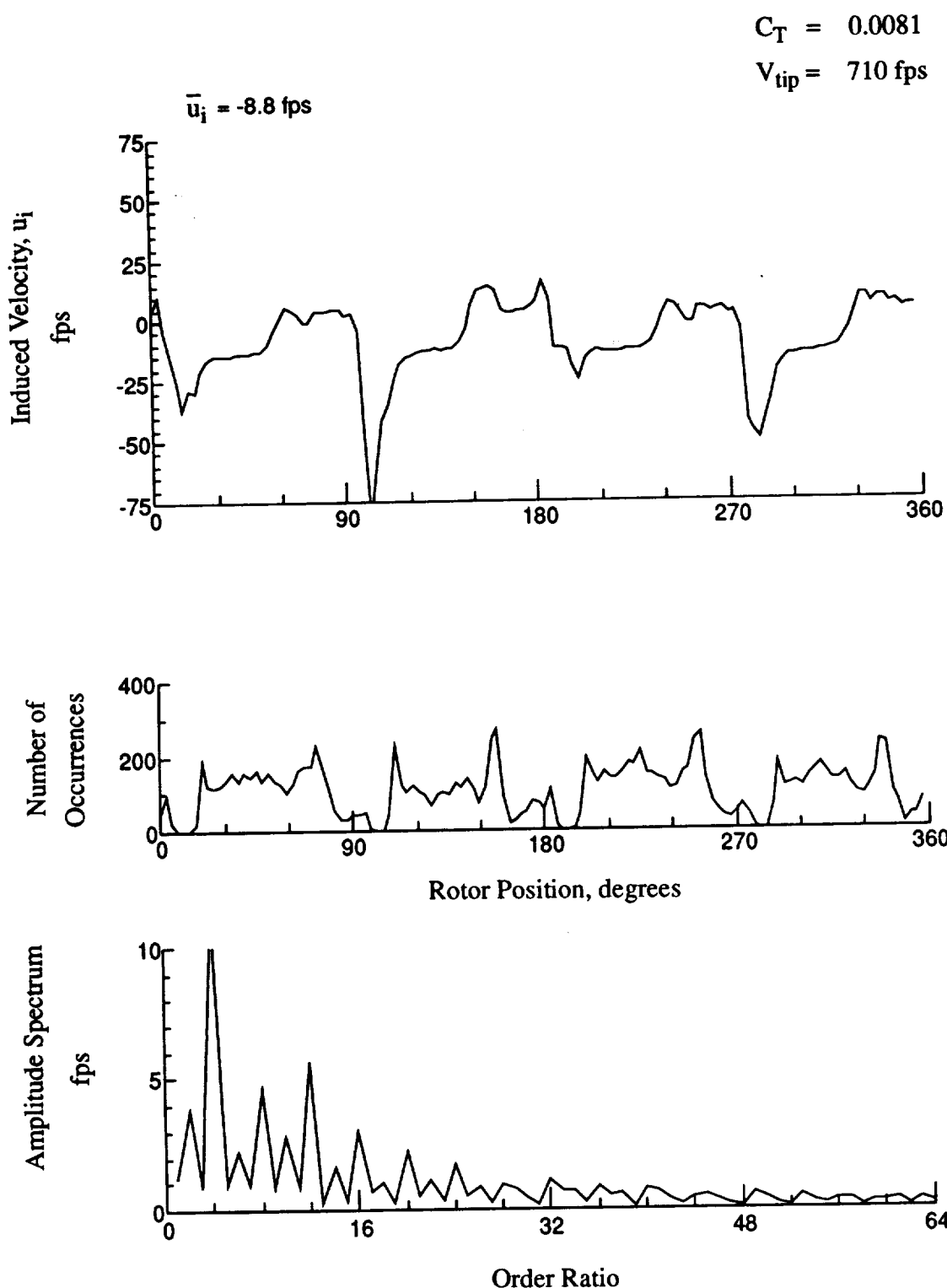


Figure 18.- Wake Measurements at
 $x/R = -0.45$, $y/R = -0.60$, $z = -2.47 \text{ in.}$

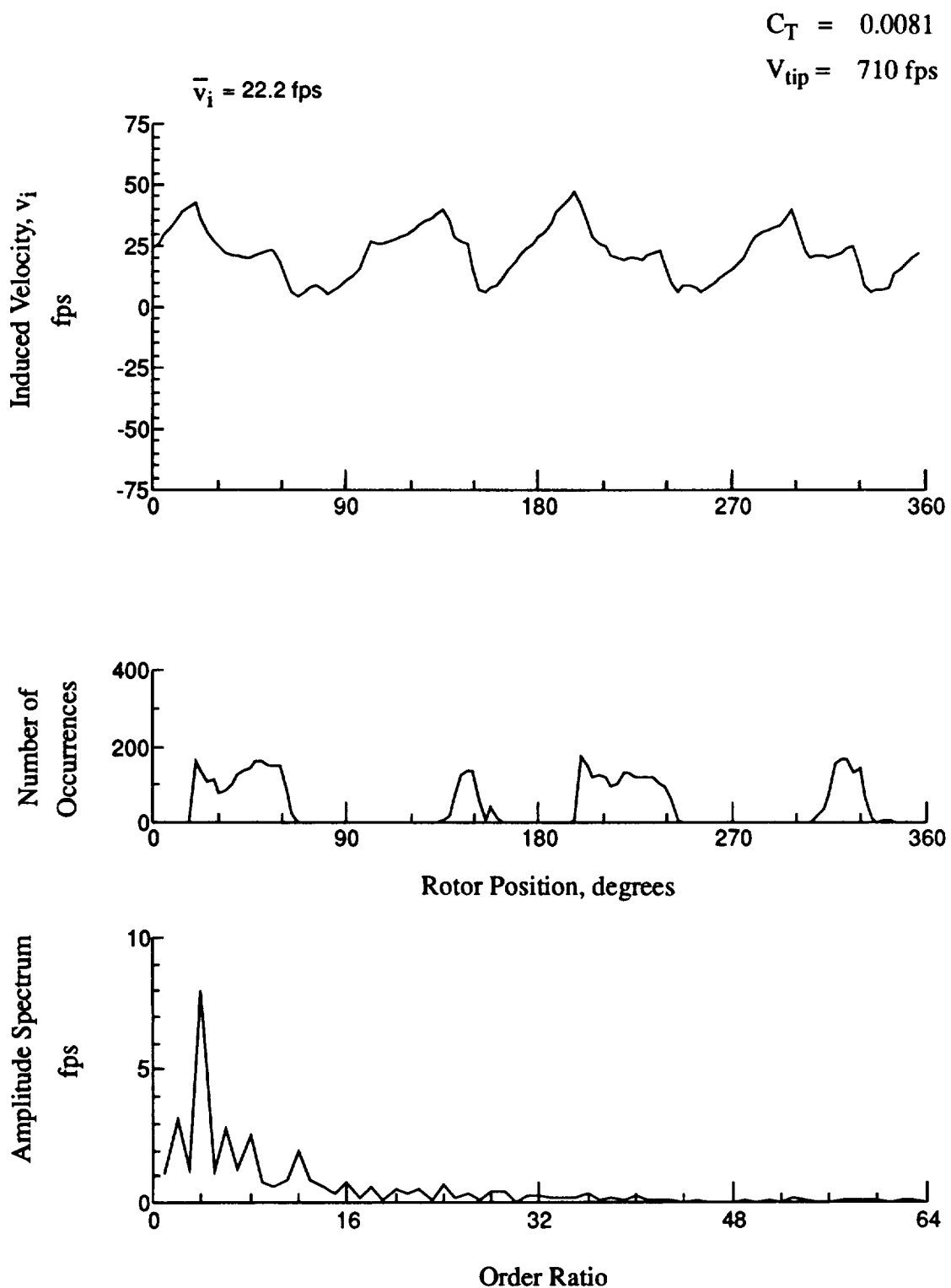


Figure 18.- Concluded.
 $x/R = -0.45$, $y/R = -0.60$, $z = -2.47 \text{ in.}$

$$C_T = 0.0081$$

$$V_{tip} = 710 \text{ fps}$$

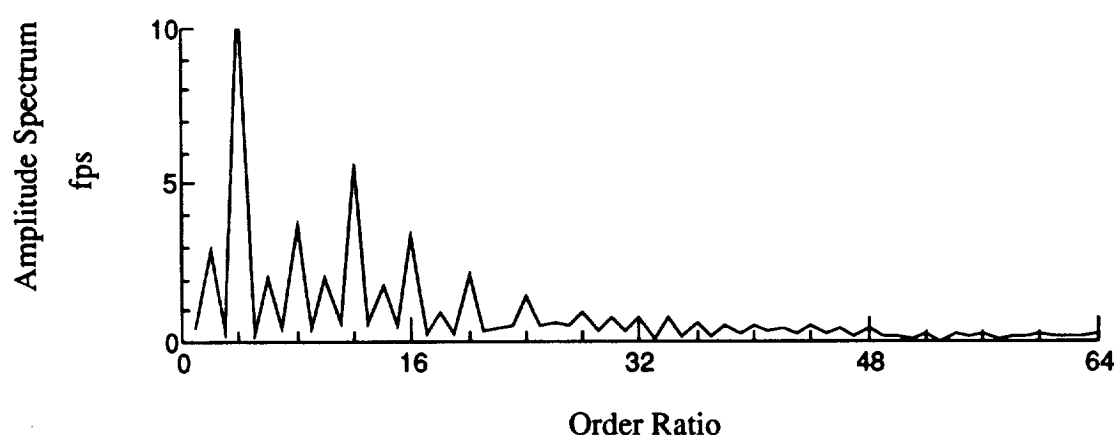
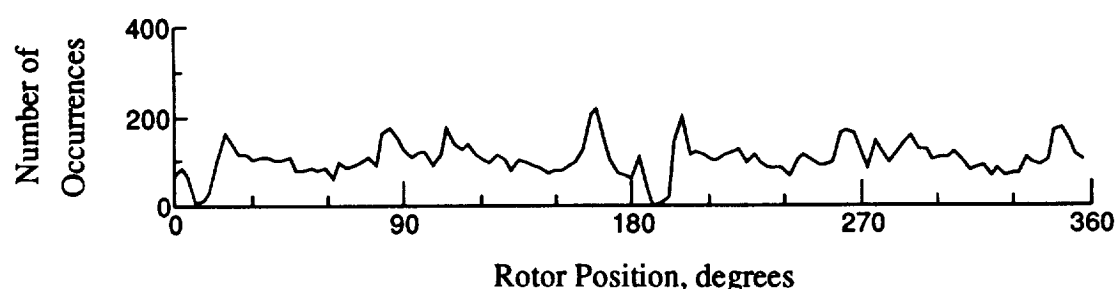
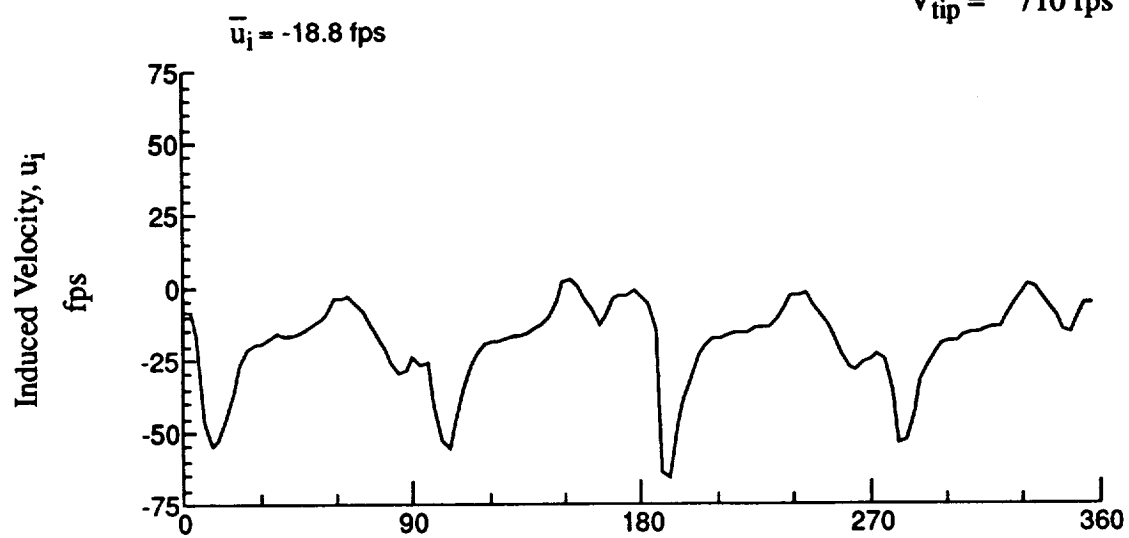


Figure 19.- Wake Measurements at
 $x/R = -0.45$, $y/R = -0.60$, $z = -3.50$ in.

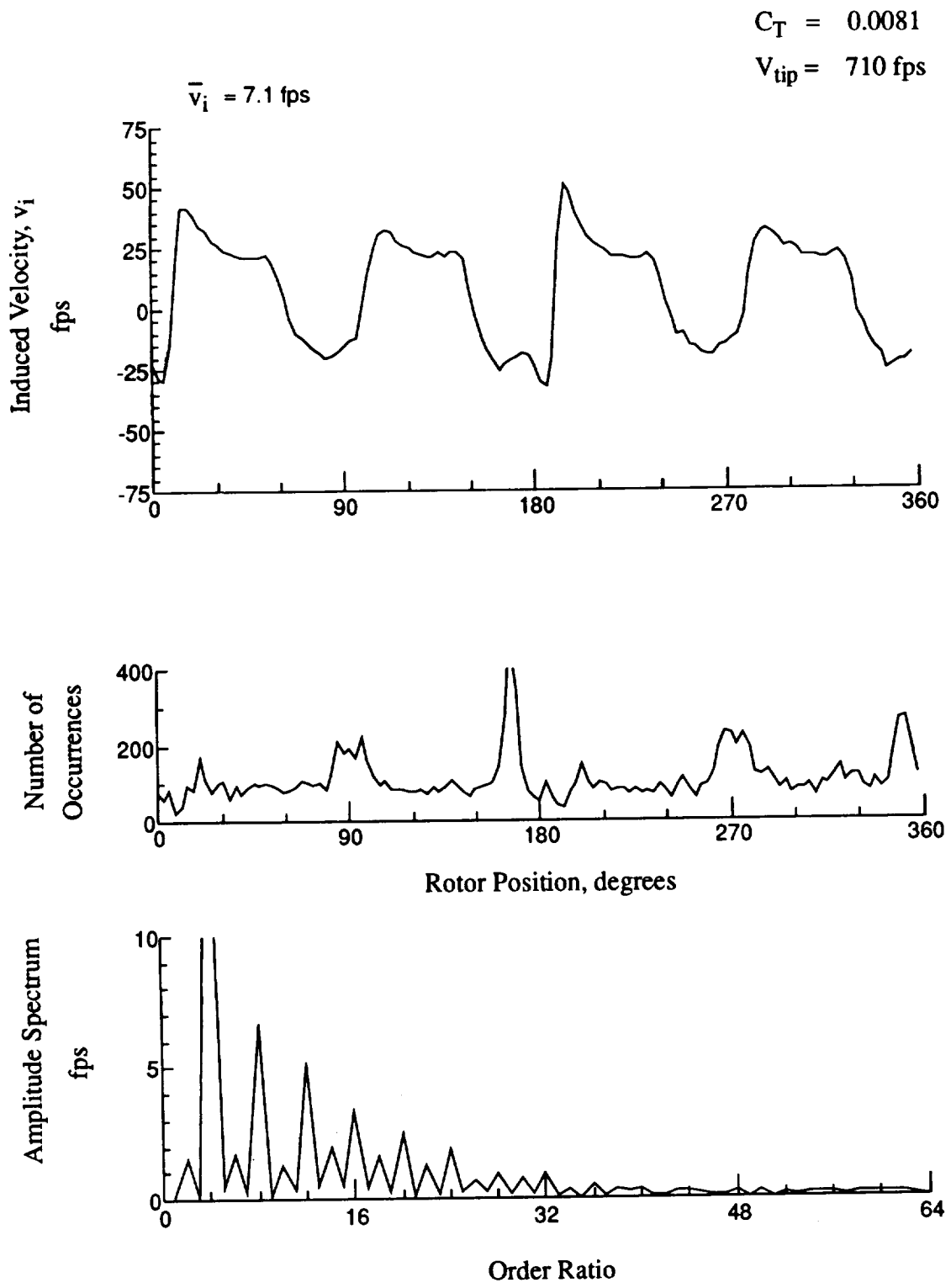


Figure 19.- Concluded.
 $x/R = -0.45$, $y/R = -0.60$, $z = -3.50 \text{ in.}$

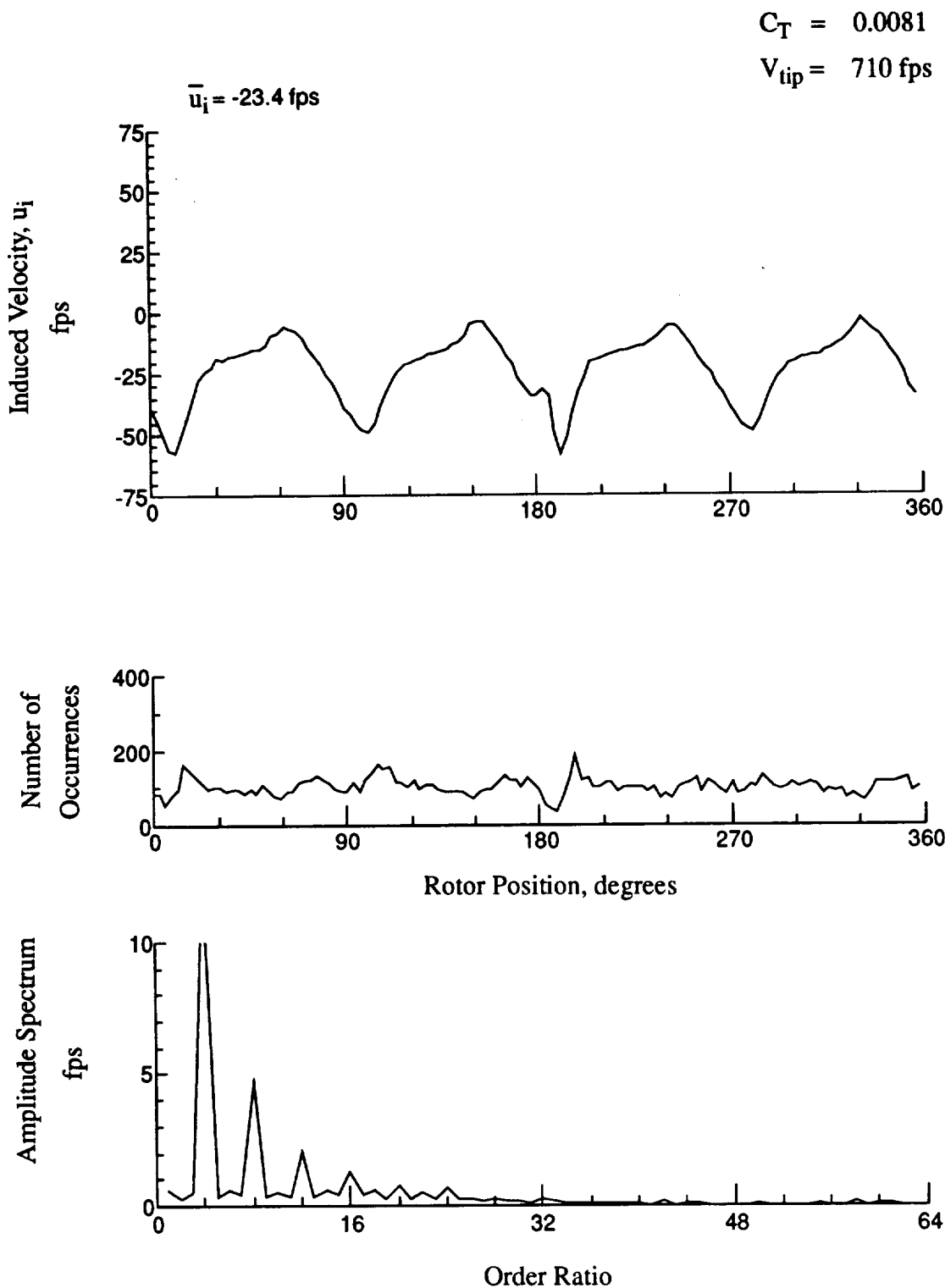


Figure 20.- Wake Measurements at
 $x/R = -0.45$, $y/R = -0.60$, $z = -4.53 \text{ in.}$

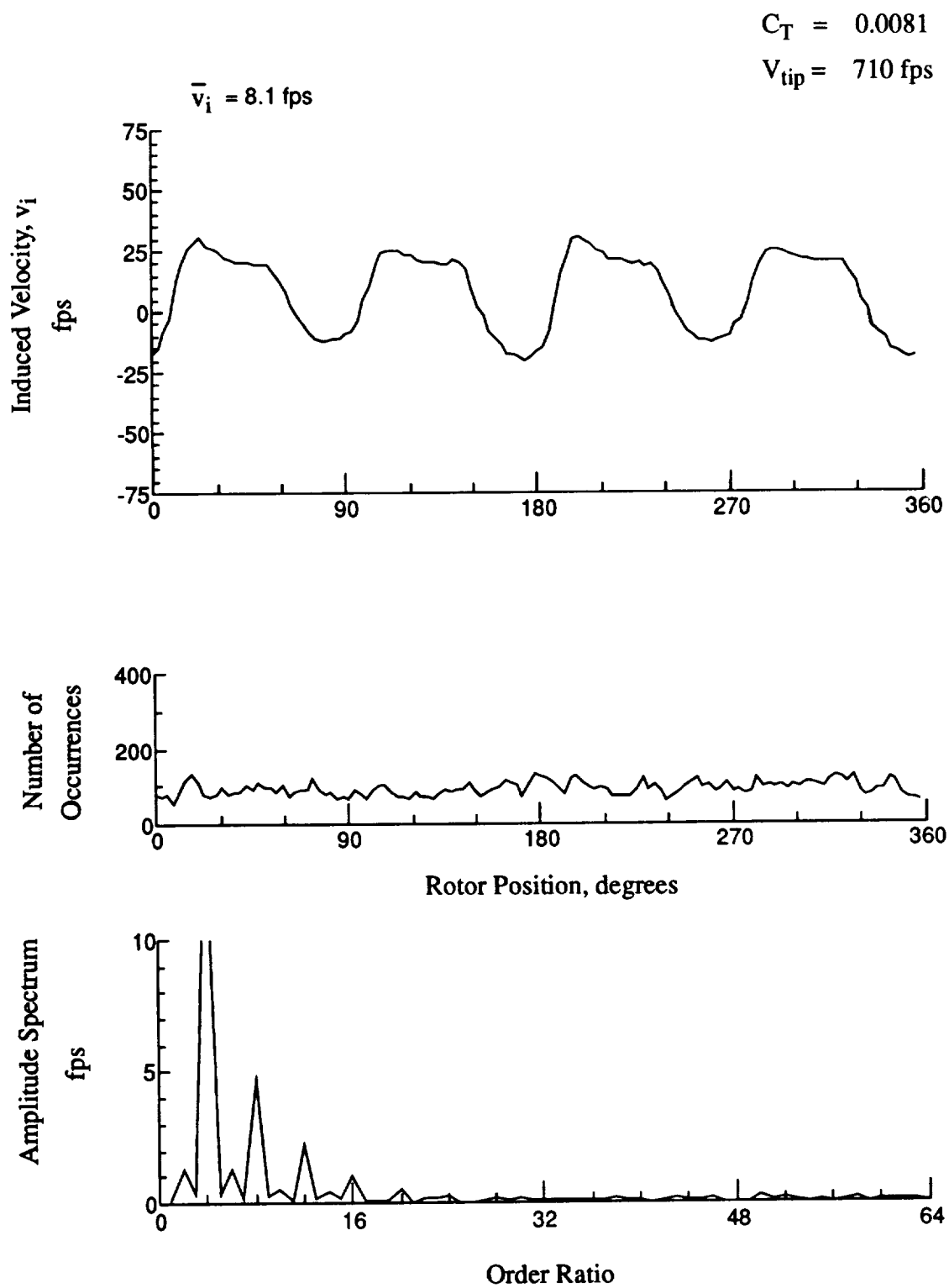


Figure 20.- Concluded.

$x/R = -0.45$, $y/R = -0.60$, $z = -4.53 \text{ in.}$

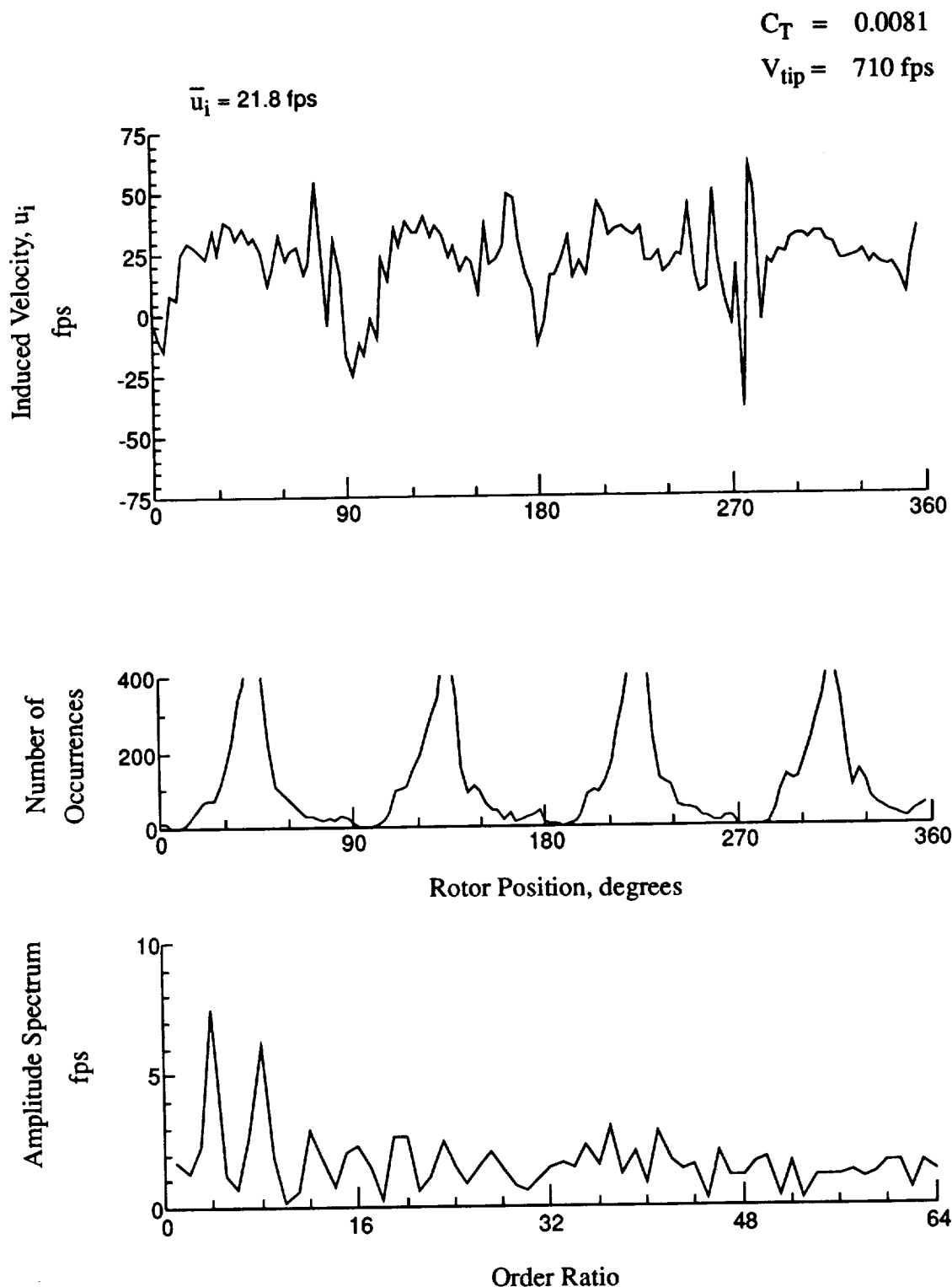


Figure 21.- Wake Measurements at
 $x/R = 0.80$, $y/R = -0.60$, $z = -0.27$ in.

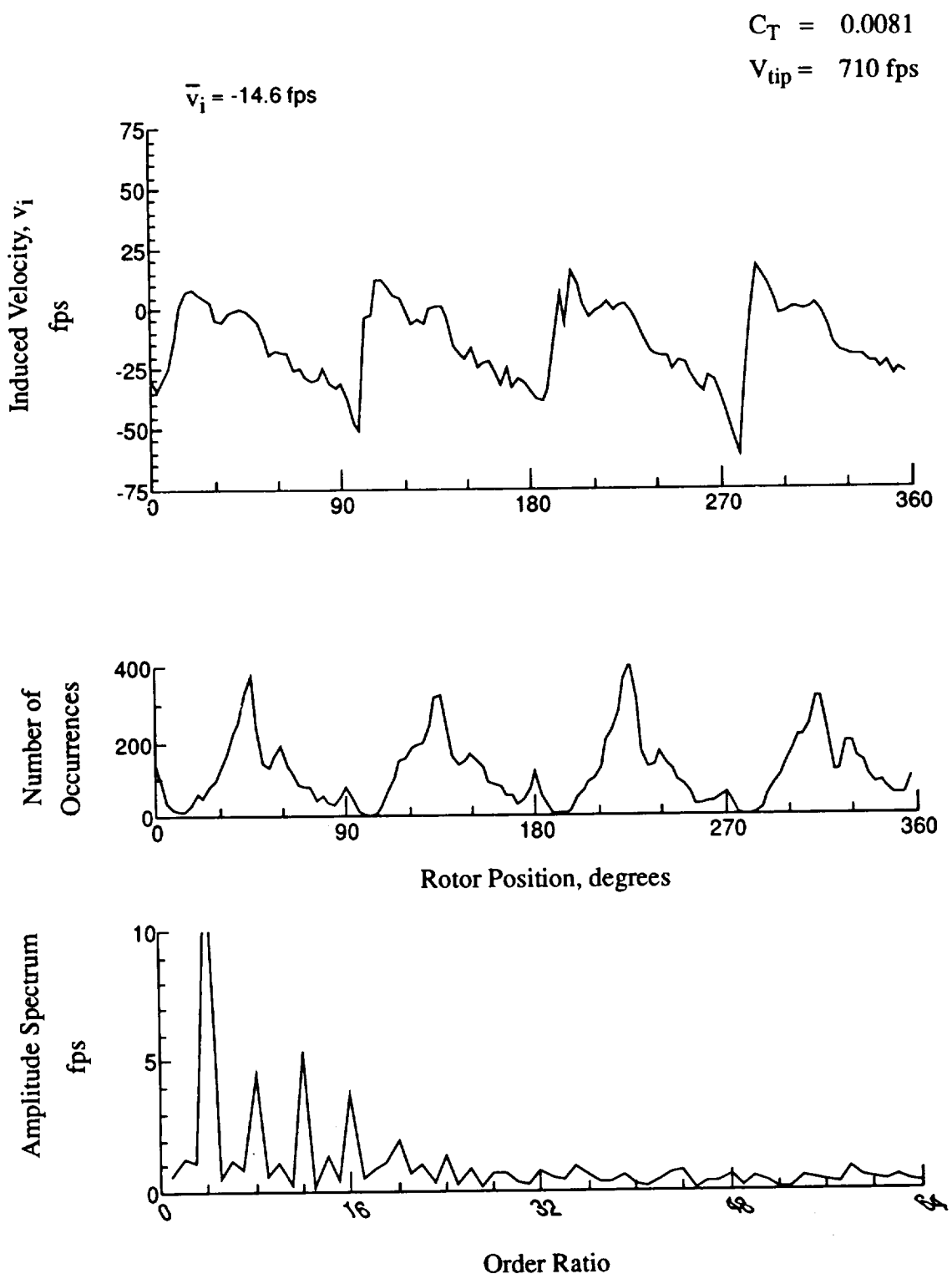


Figure 21.- Concluded.
 $x/R = 0.80$, $y/R = -0.60$, $z = -0.27 \text{ in.}$

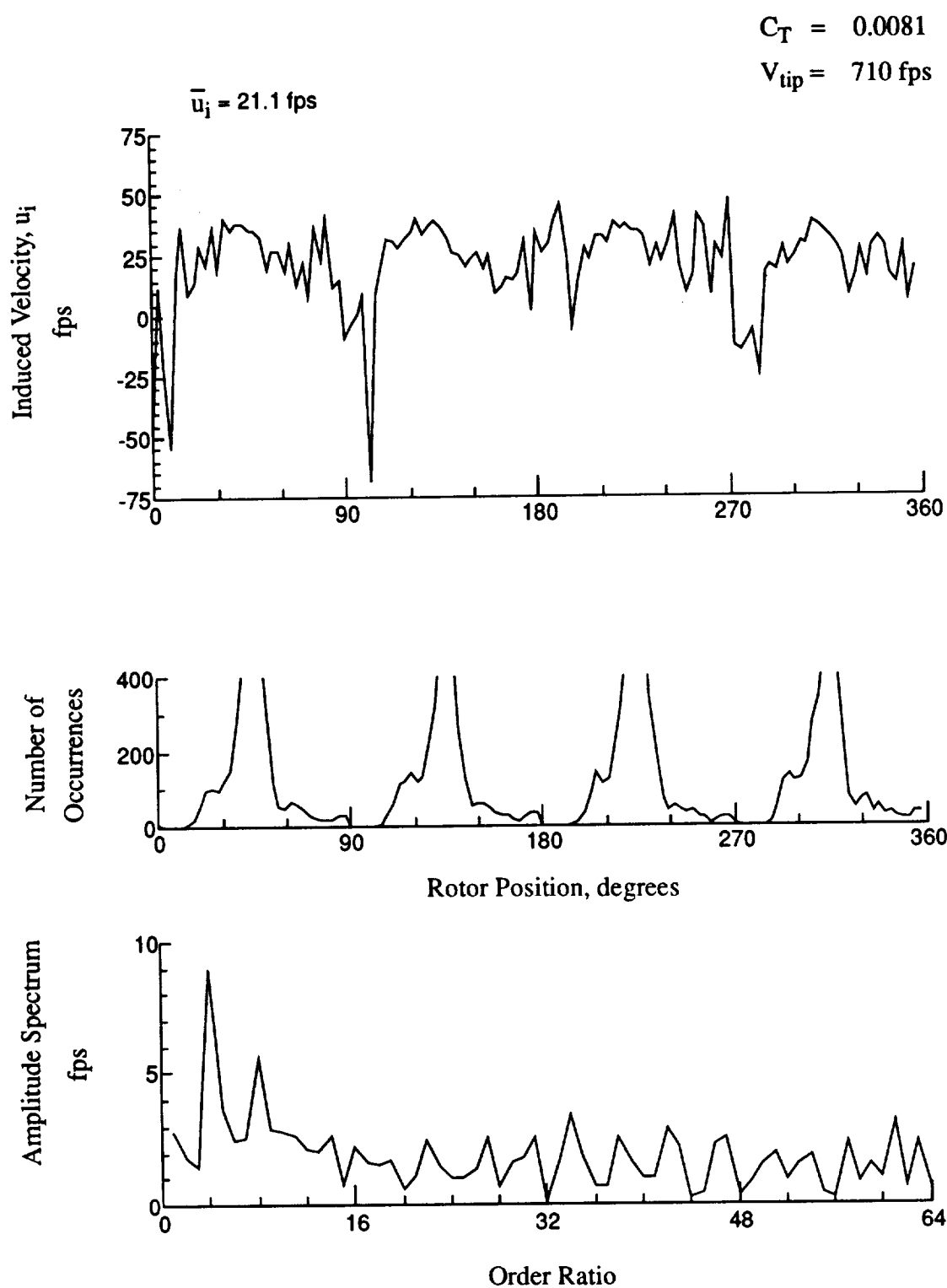


Figure 22.- Wake Measurements at
 $x/R = 0.80$, $y/R = -0.60$, $z = -1.30 \text{ in.}$

$$C_T = 0.0081$$

$$V_{tip} = 710 \text{ fps}$$

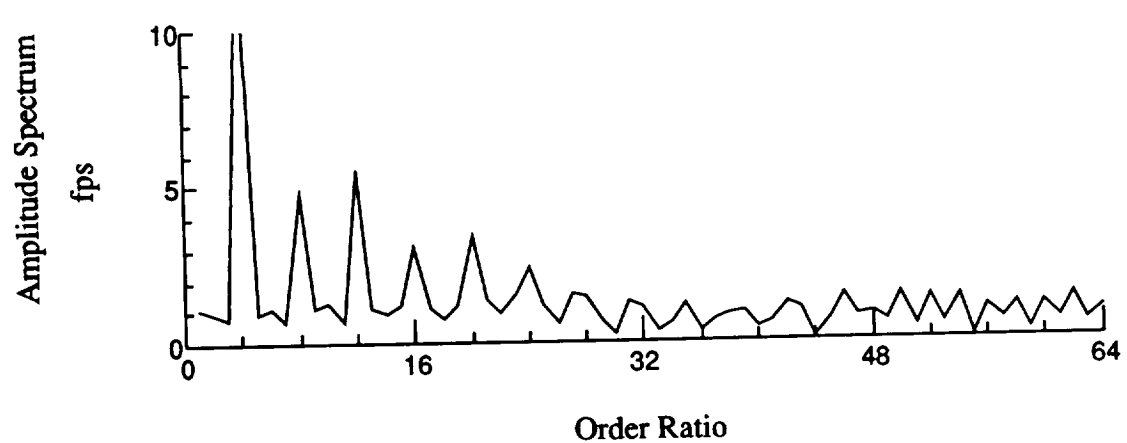
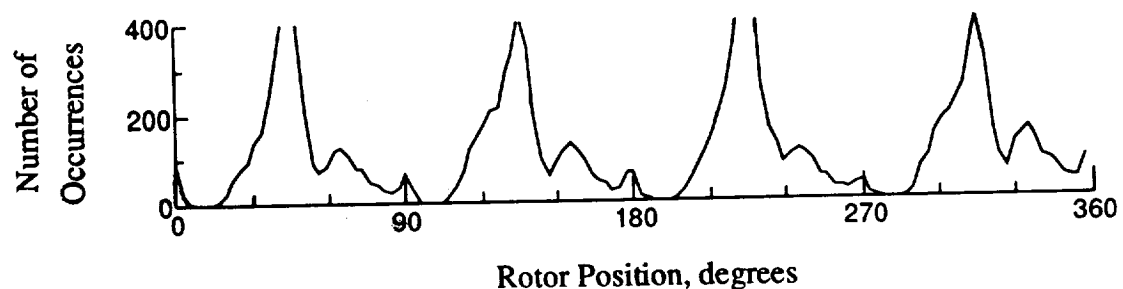
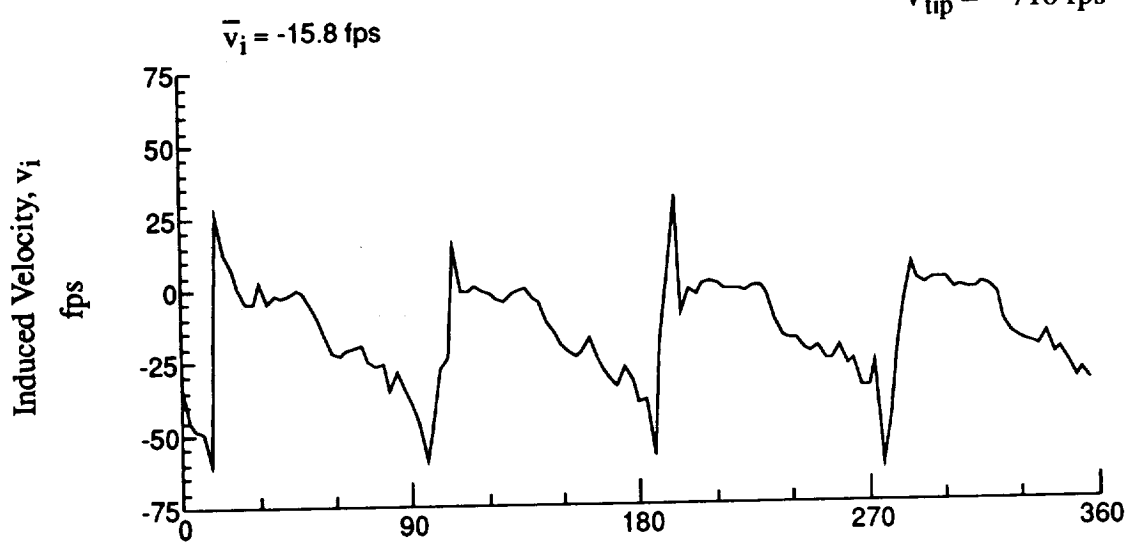


Figure 22.- Concluded.

$x/R = 0.80$, $y/R = -0.60$, $z = -1.30$ in.

$C_T = 0.0081$

$V_{tip} = 710 \text{ fps}$

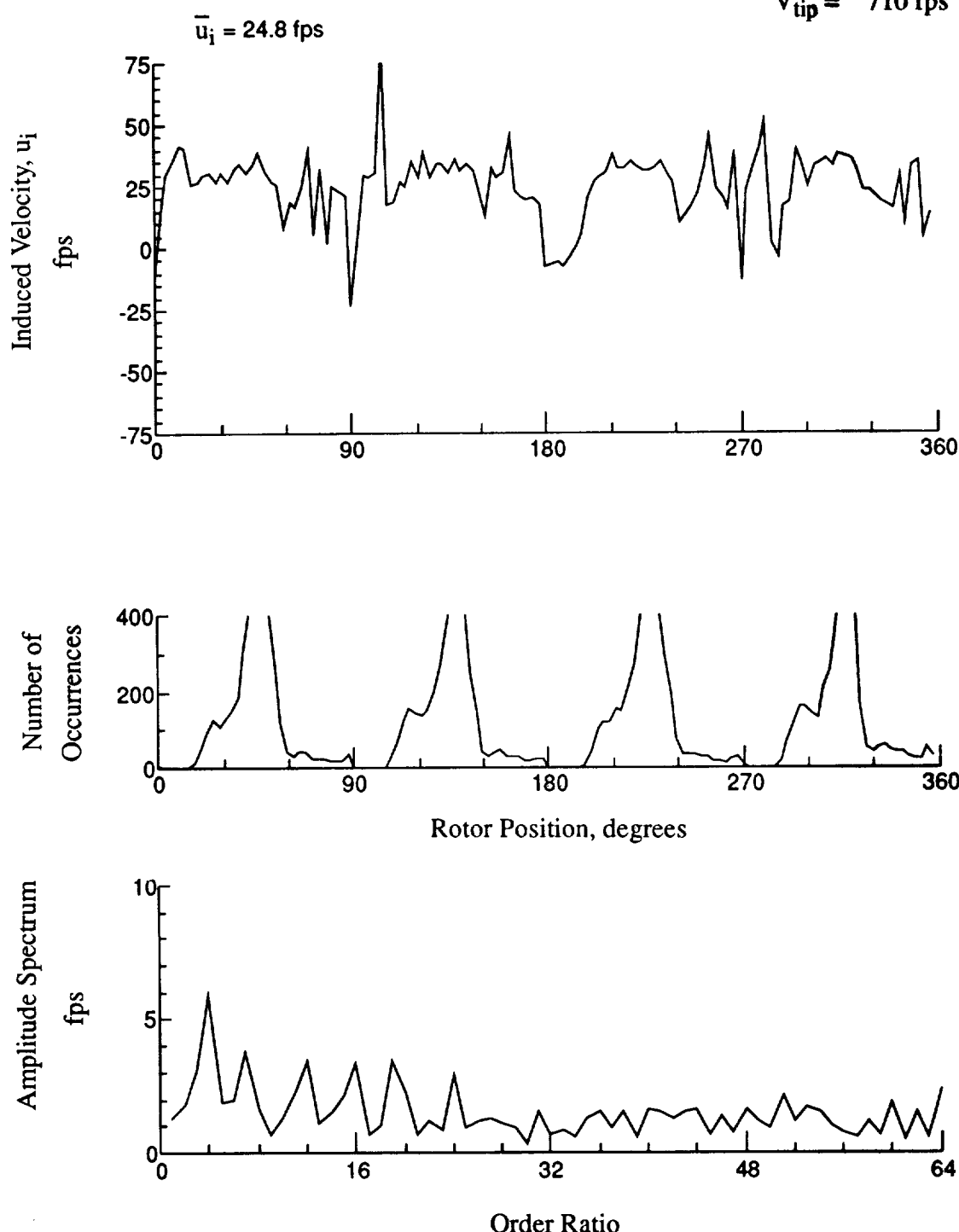


Figure 23.- Wake Measurements at
 $x/R = 0.80$, $y/R = -0.60$, $z = -2.33 \text{ in.}$

$$C_T = 0.0081$$

$$V_{tip} = 710 \text{ fps}$$

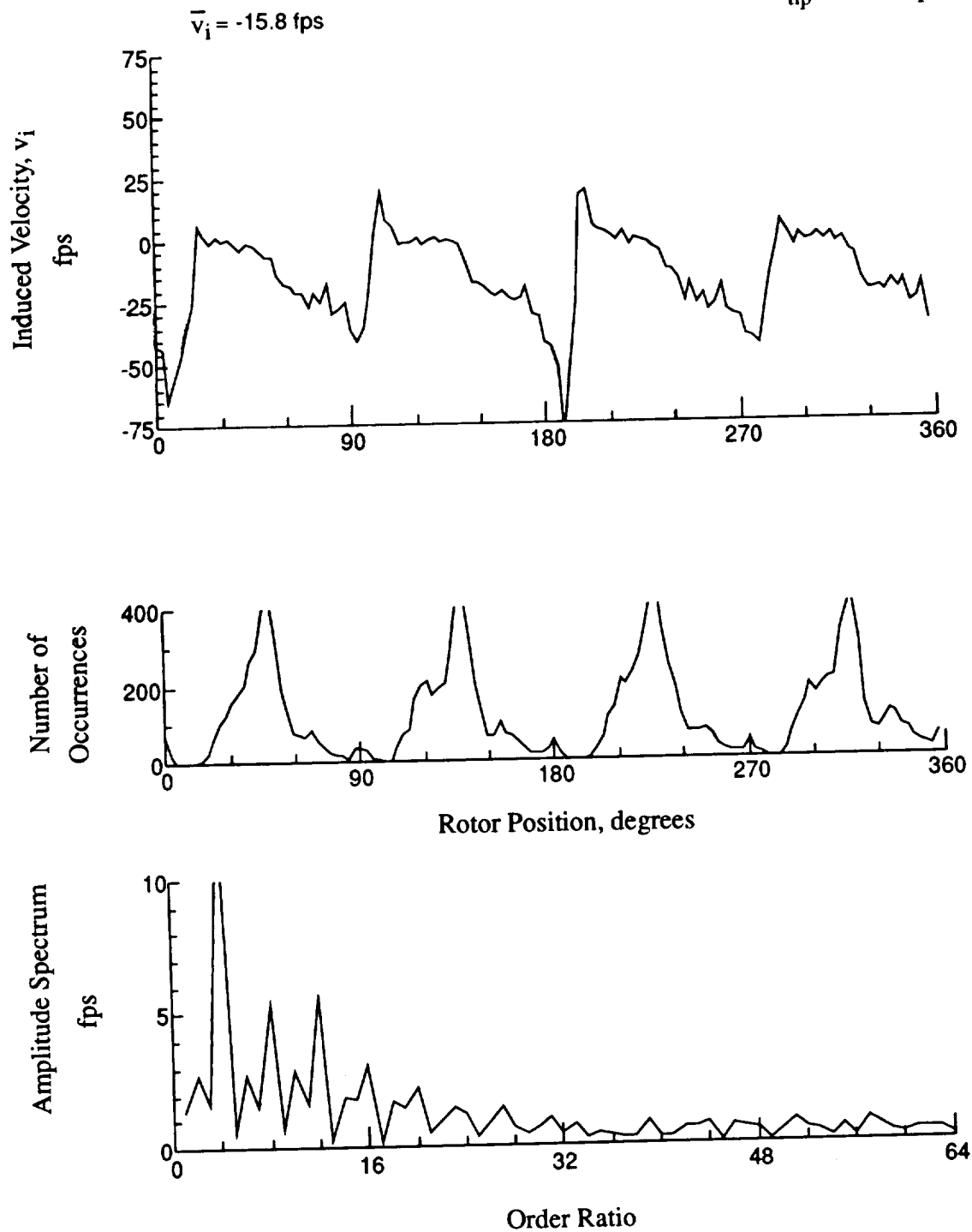


Figure 23.- Concluded.
 $x/R = 0.80$, $y/R = -0.60$, $z = -2.33 \text{ in.}$

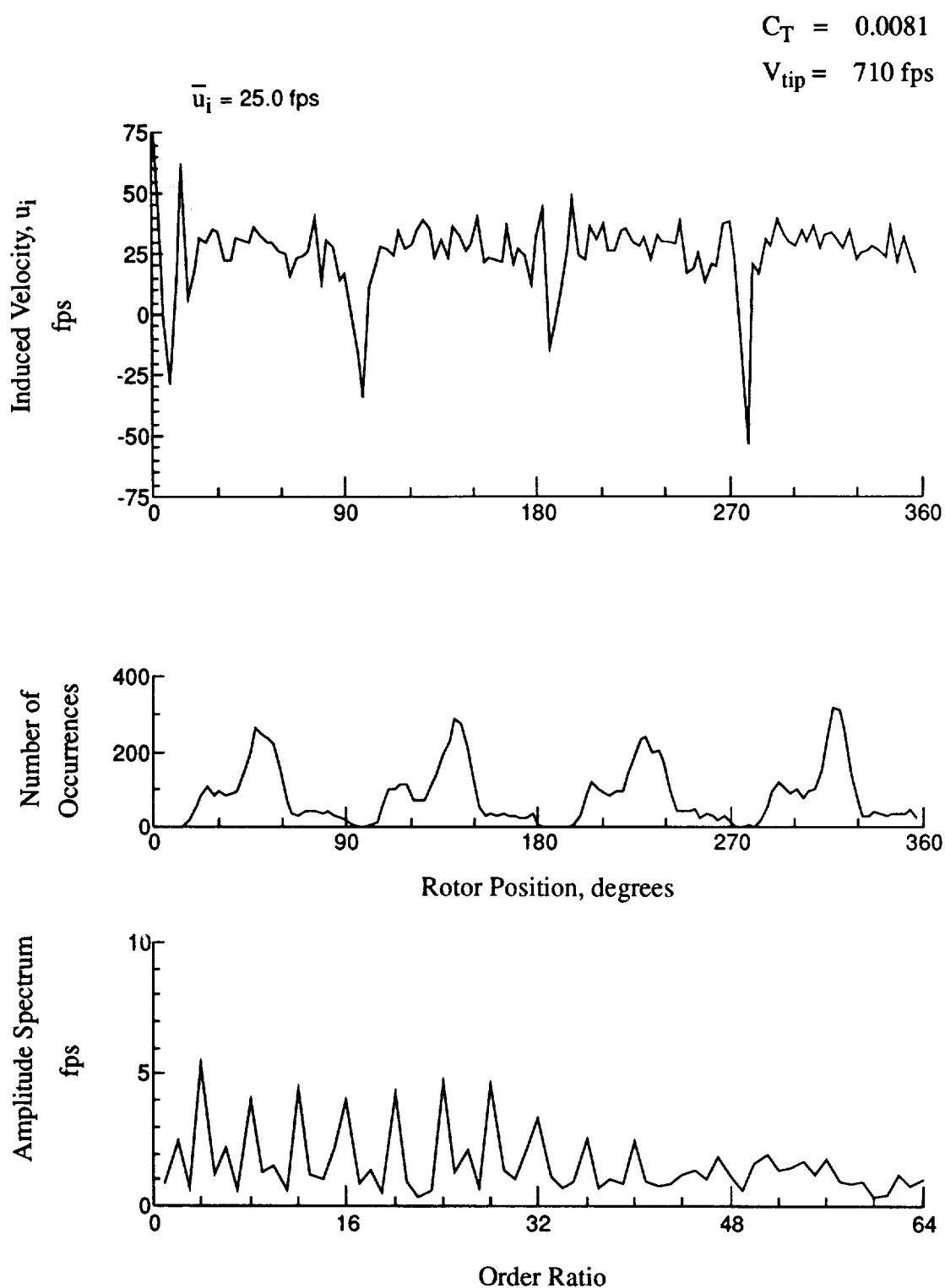


Figure 24.- Wake Measurements at
 $x/R = 0.80$, $y/R = -0.60$, $z = -3.36 \text{ in.}$

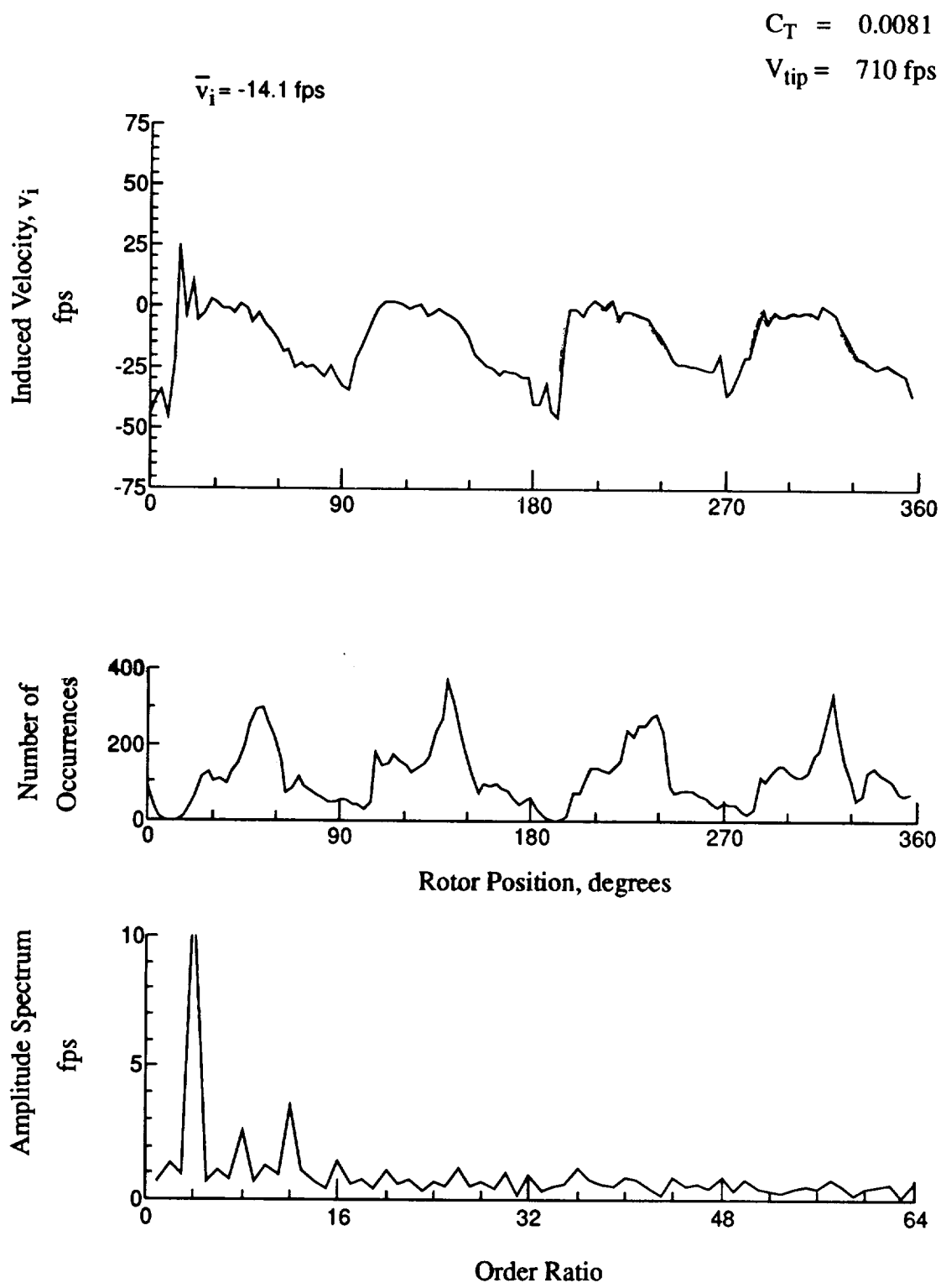


Figure 24.- Concluded.
 $x/R = 0.80$, $y/R = -0.60$, $z = -3.36 \text{ in.}$

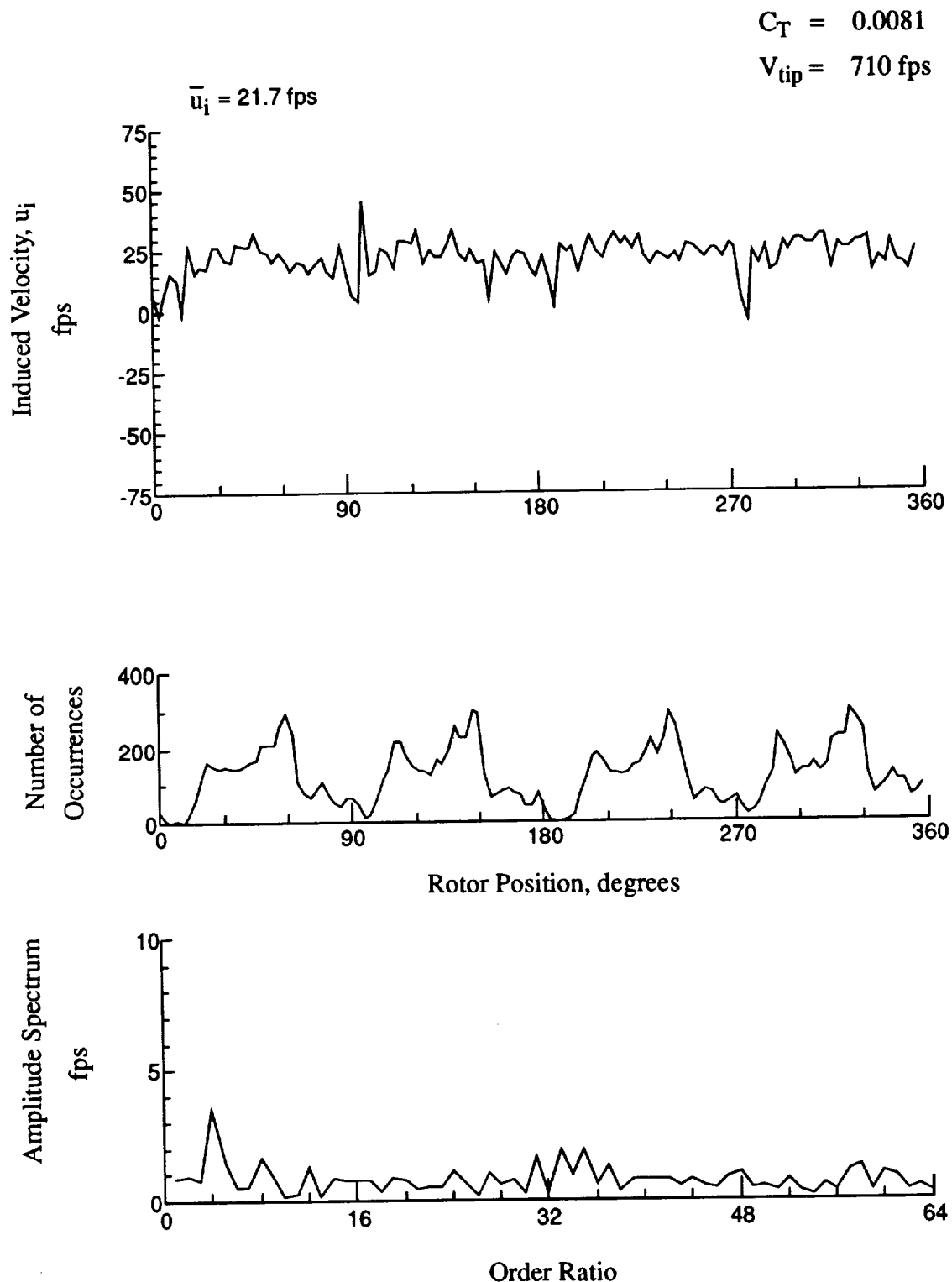


Figure 25.- Wake Measurements at
 $x/R = 0.80$, $y/R = -0.60$, $z = -4.39 \text{ in.}$

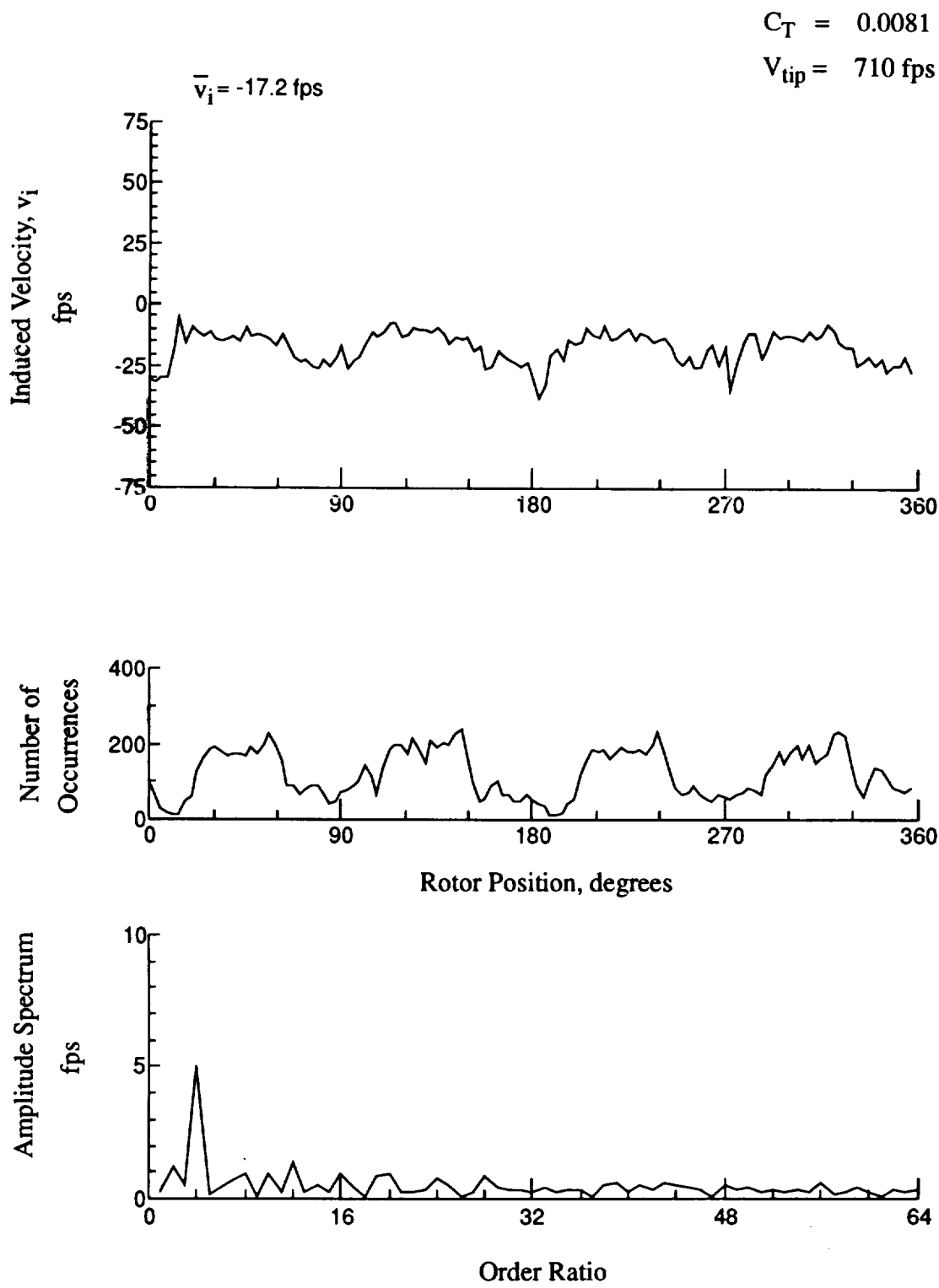


Figure 25.- Concluded.
 $x/R = 0.80$, $y/R = -0.60$, $z = -4.39 \text{ in.}$

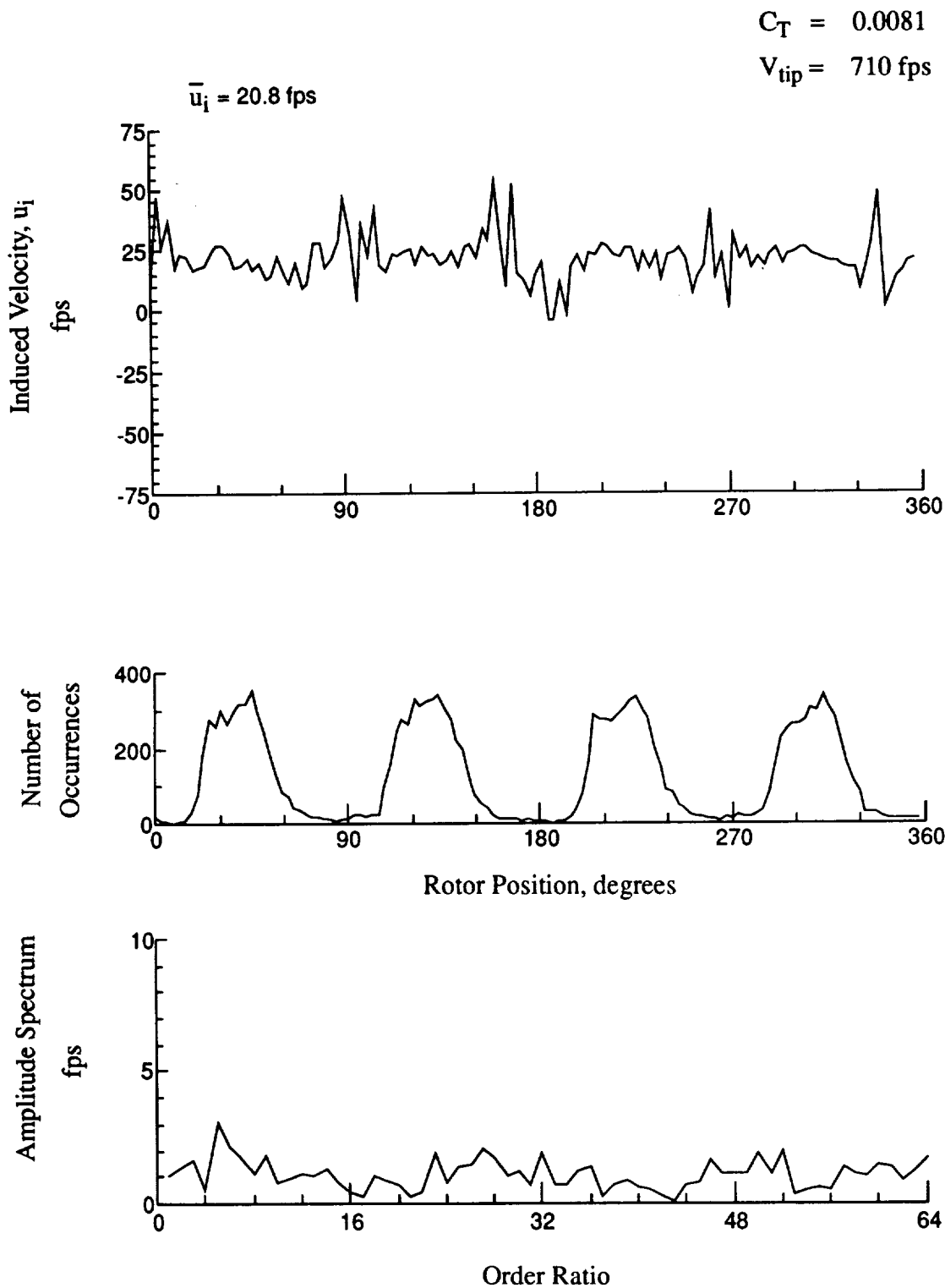


Figure 26.- Wake Measurements at
 $x/R = 0.80$, $y/R = -0.60$, $z = -5.42 \text{ in.}$

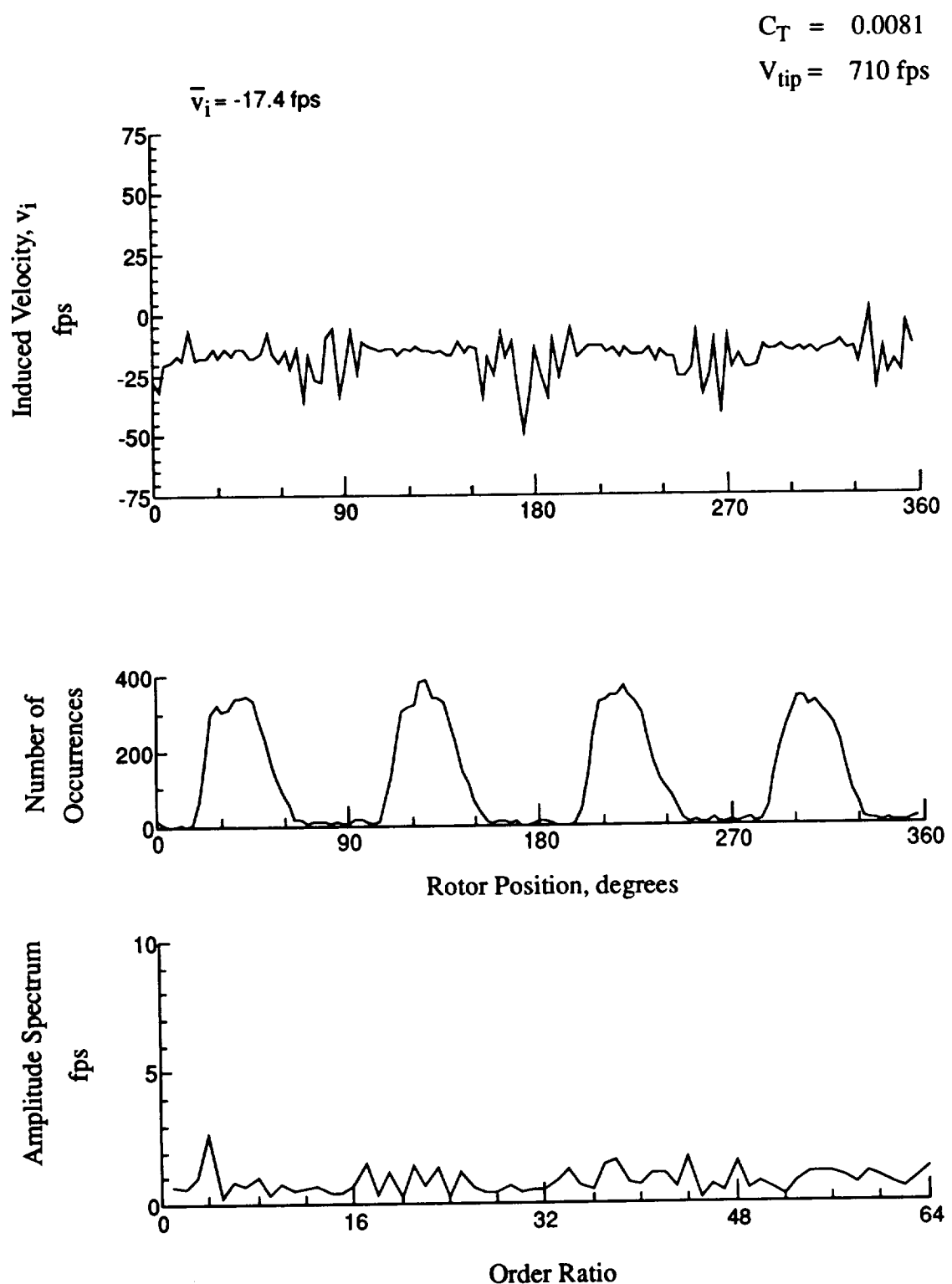


Figure 26.- Concluded.
 $x/R = 0.80$, $y/R = -0.60$, $z = -5.42 \text{ in.}$

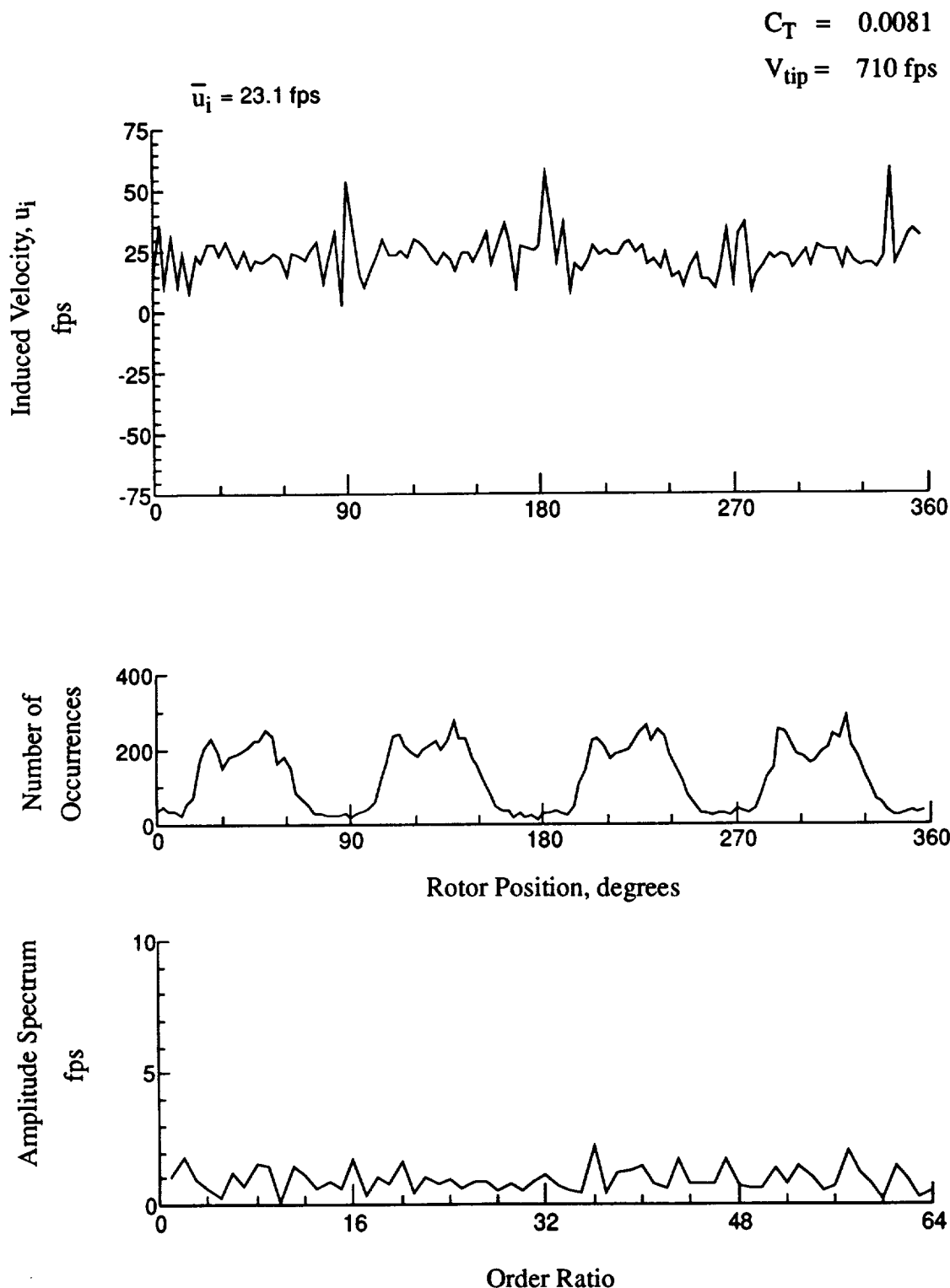


Figure 27.- Wake Measurements at
 $x/R = 0.80$, $y/R = -0.60$, $z = -6.45 \text{ in.}$

$$C_T = 0.0081$$

$$V_{tip} = 710 \text{ fps}$$

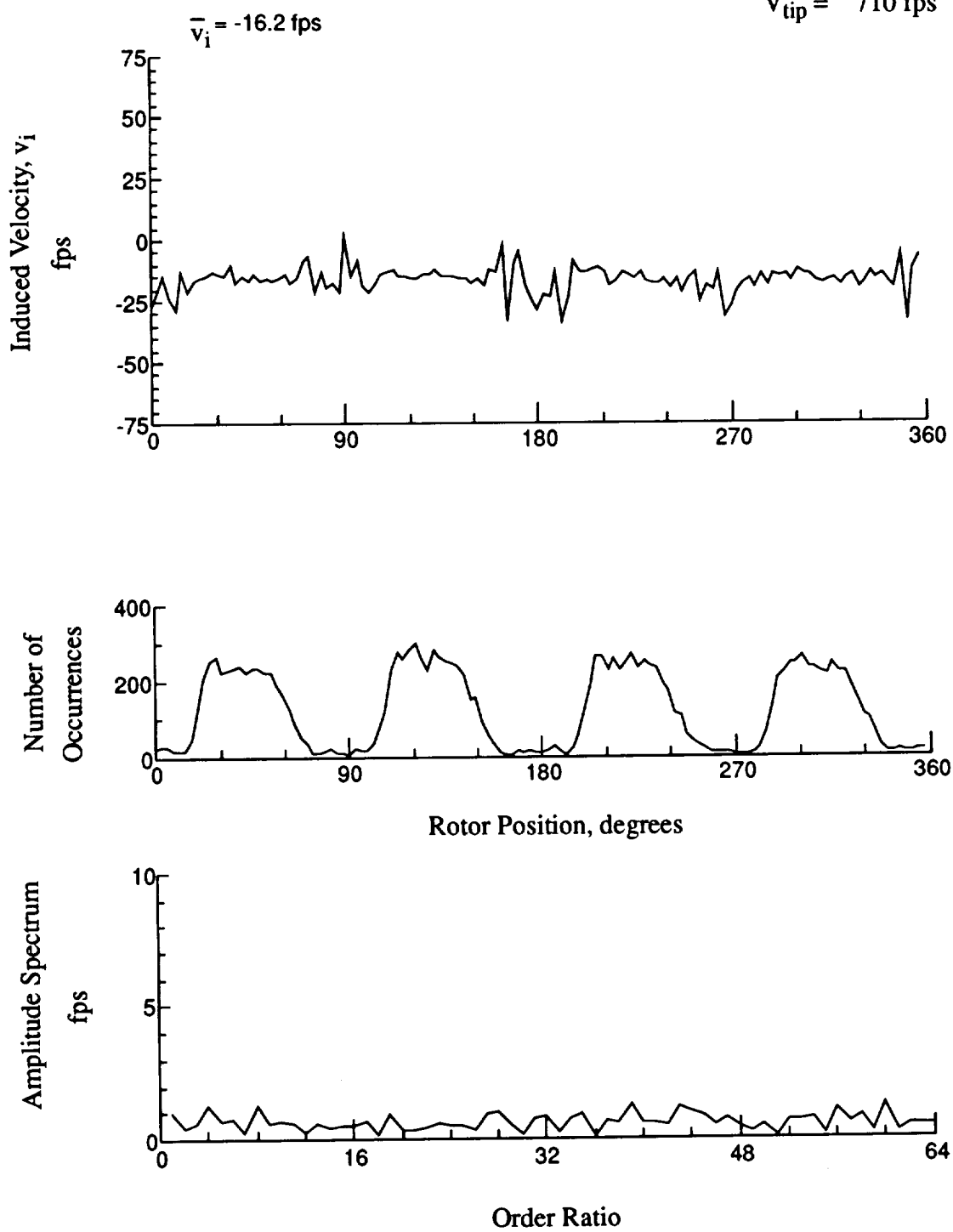
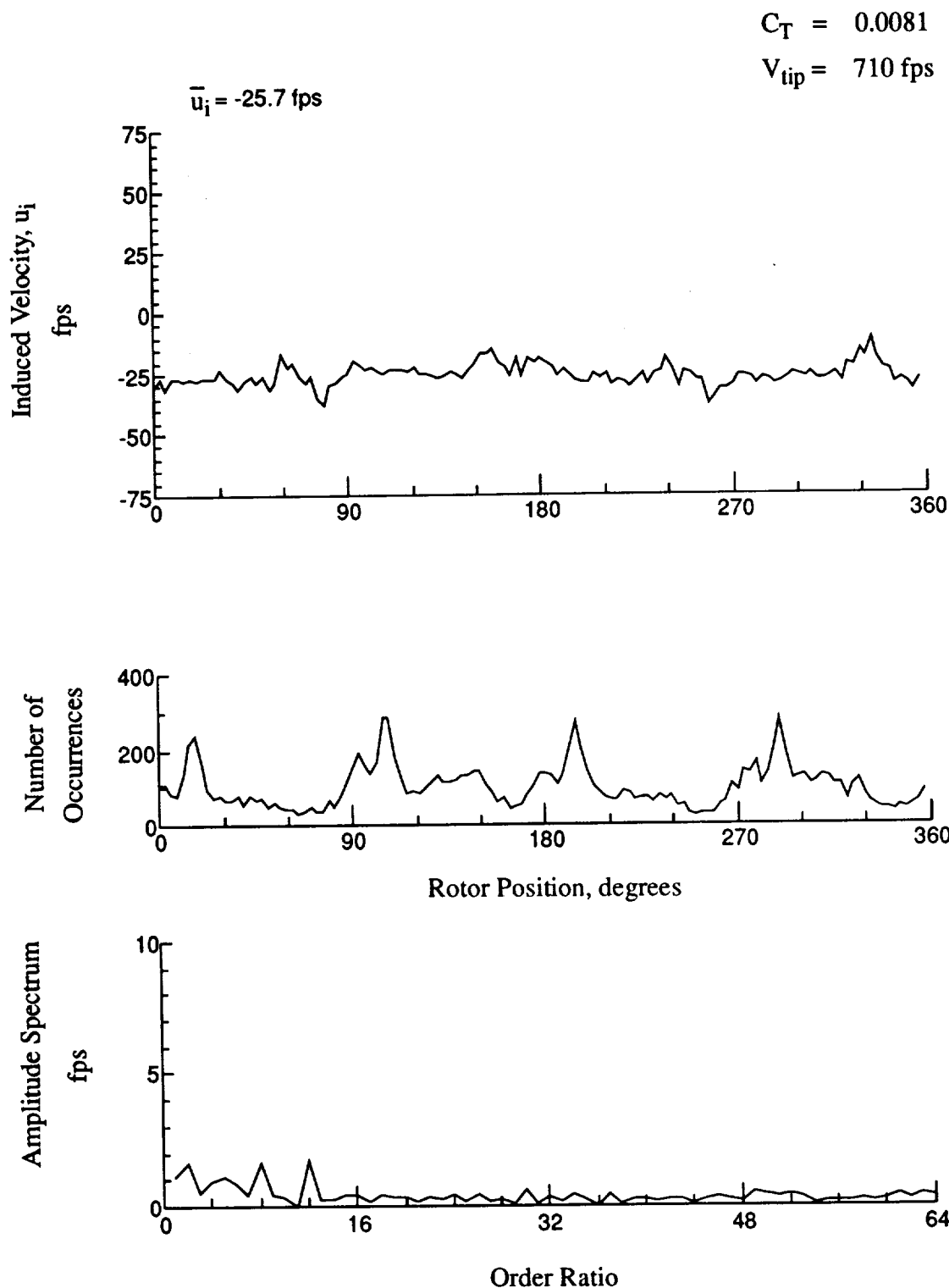


Figure 27.- Concluded.
 $x/R = 0.80$, $y/R = -0.60$, $z = -6.45 \text{ in.}$



**Figure 28.- Wake Measurements at
 $x/R = 0.90$, $y/R = -0.20$, $z = -0.27 \text{ in.}$**

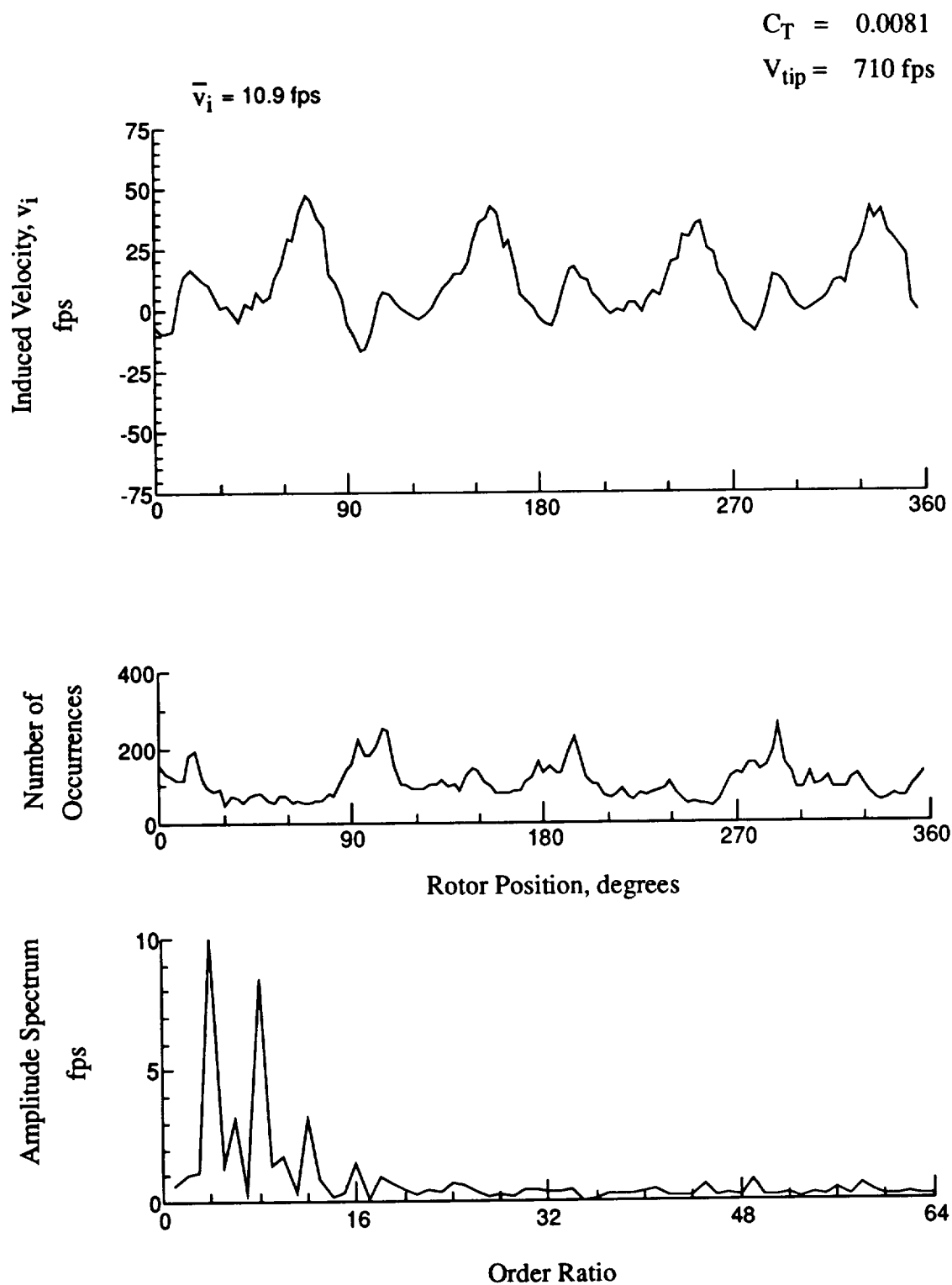


Figure 28.- Concluded.
 $x/R = 0.90$, $y/R = -0.20$, $z = -0.27 \text{ in.}$

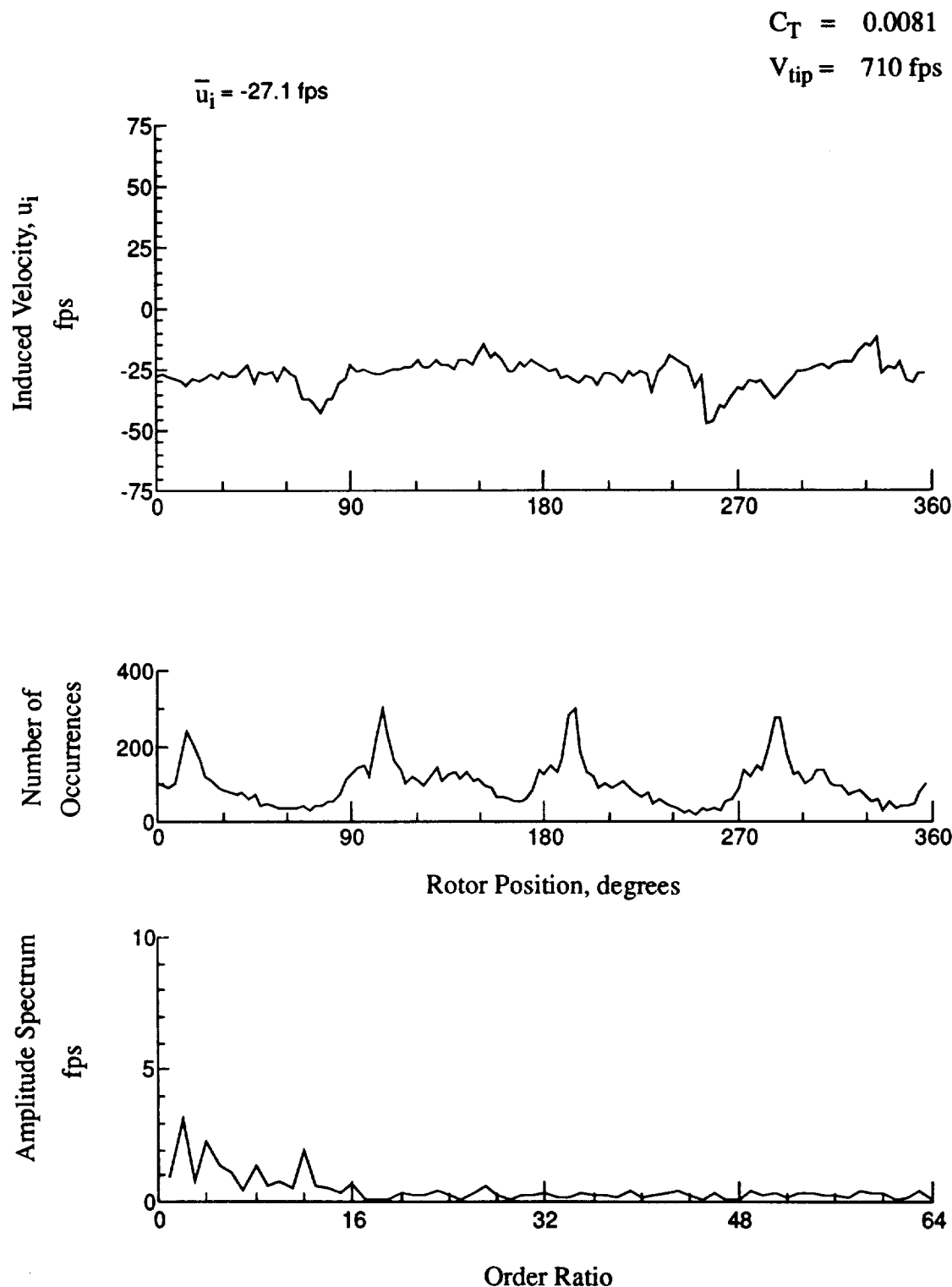


Figure 29.- Wake Measurements at
 $x/R = 0.90$, $y/R = -0.20$, $z = -1.30 \text{ in.}$

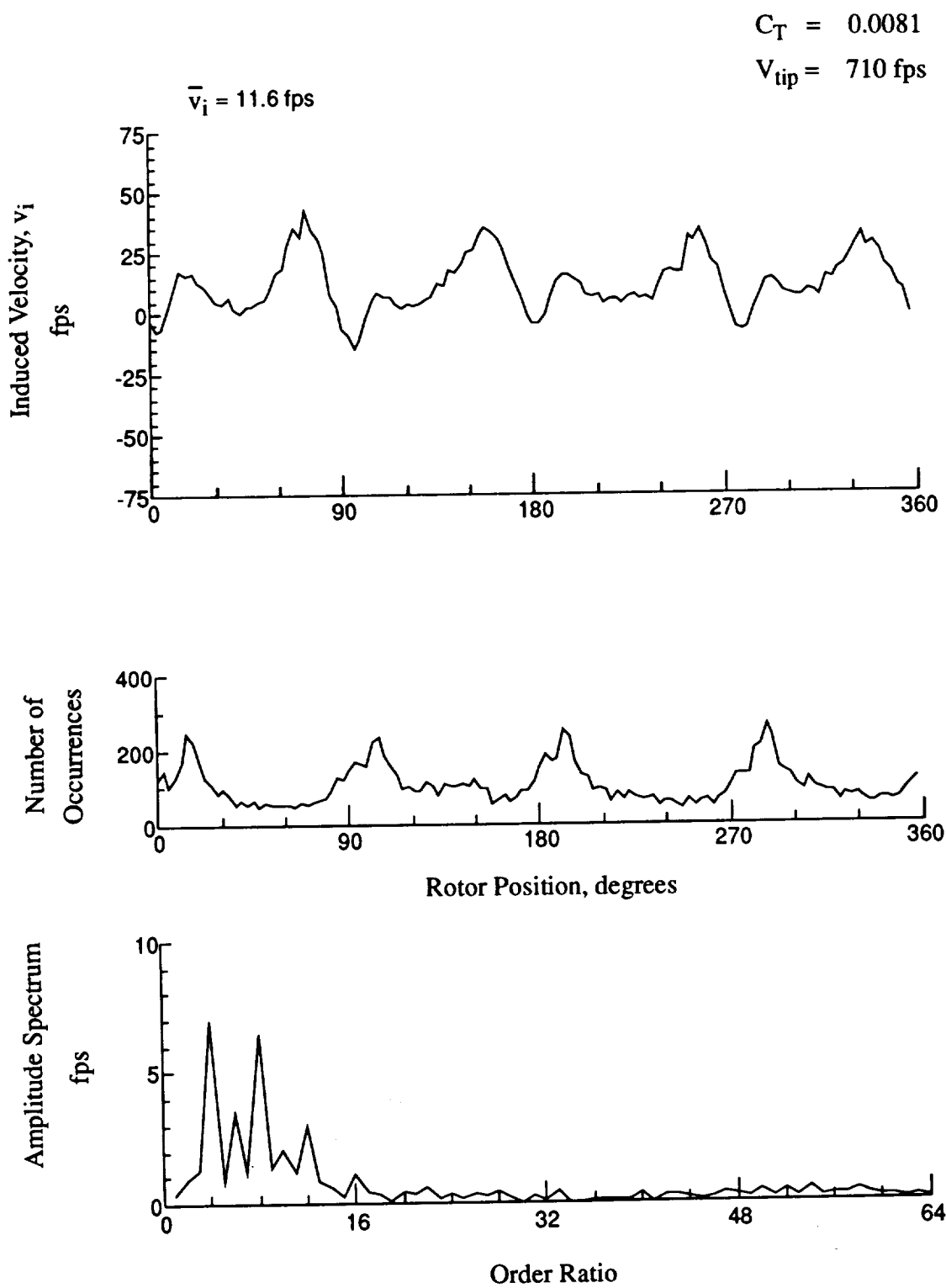
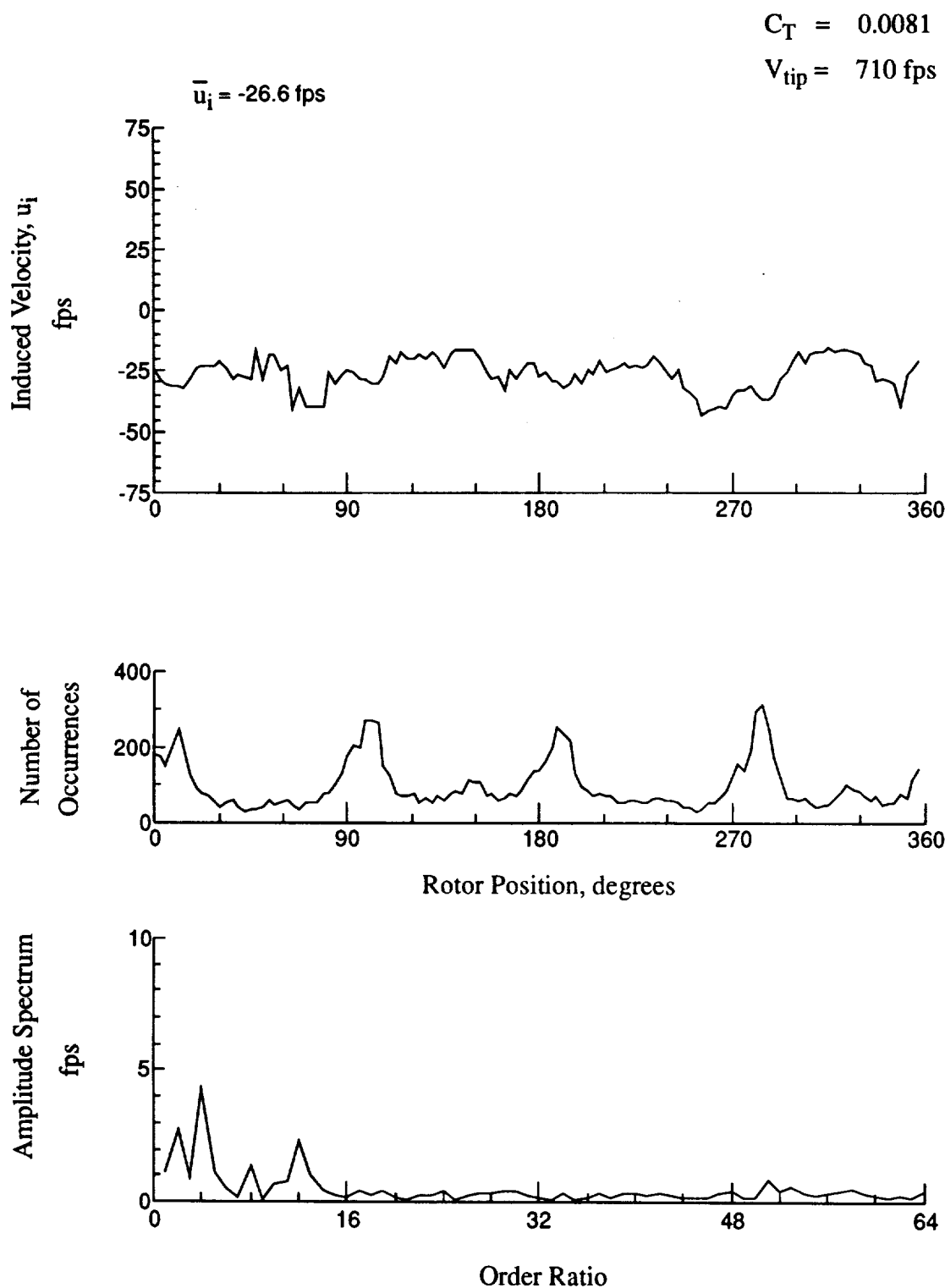


Figure 29.- Concluded.
 $x/R = 0.90$, $y/R = -0.20$, $z = -1.30 \text{ in.}$



**Figure 30.- Wake Measurements at
 $x/R = 0.90$, $y/R = -0.20$, $z = -2.33$ in.**

$$C_T = 0.0081$$

$$V_{tip} = 710 \text{ fps}$$

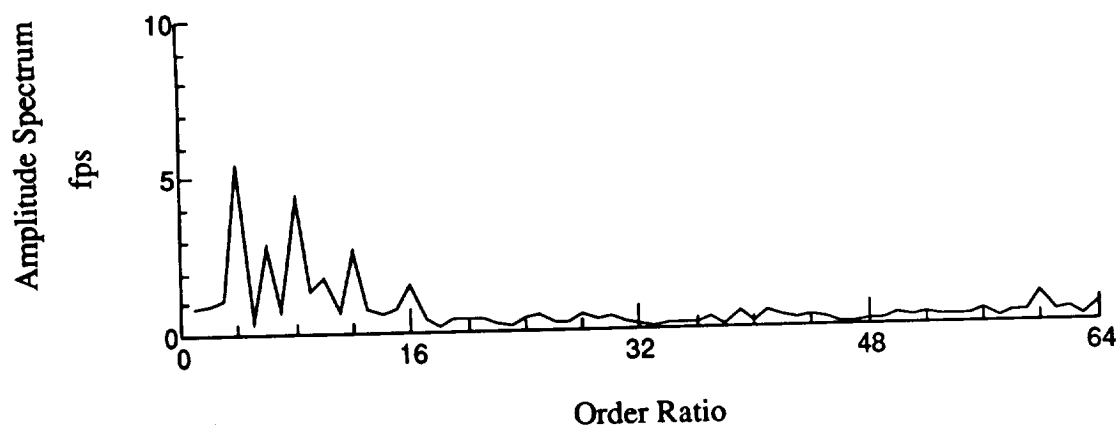
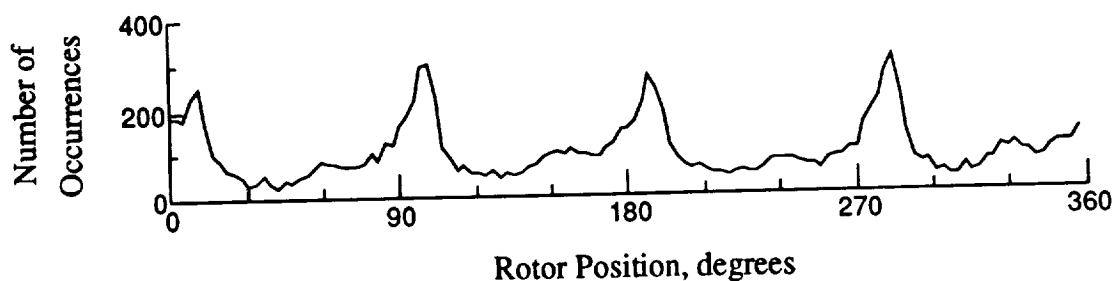
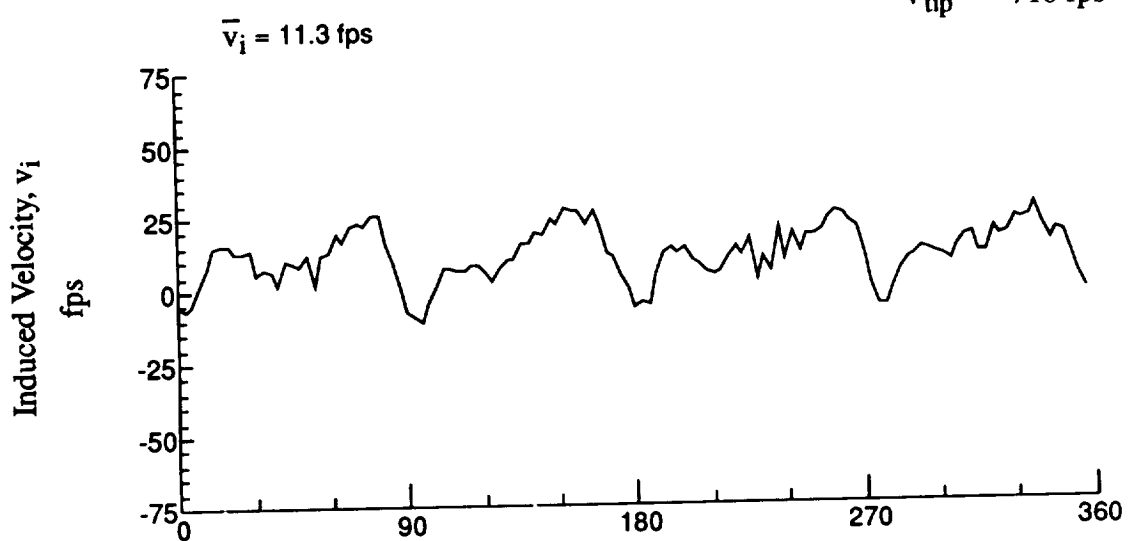
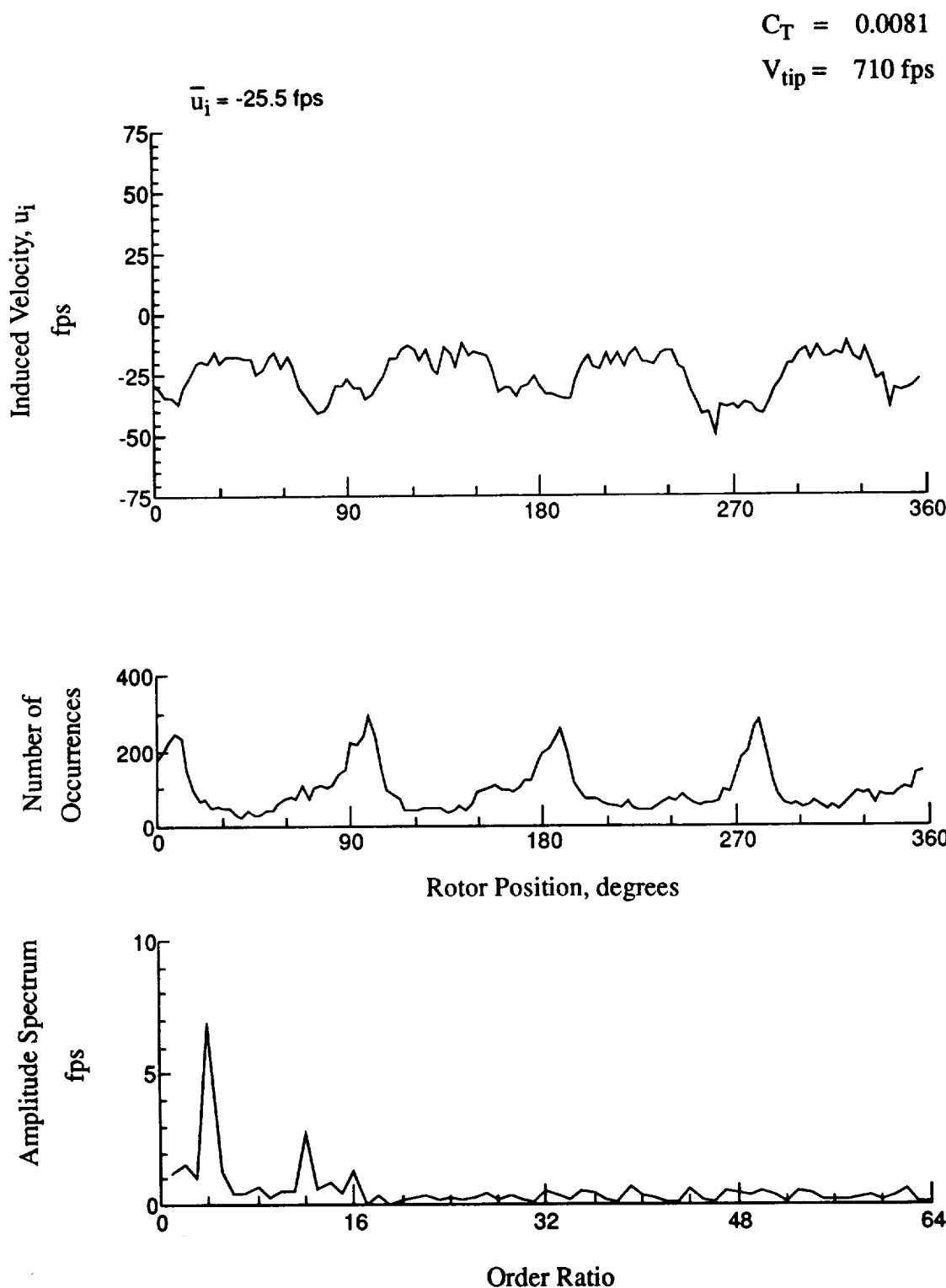


Figure 30.- Concluded.

$x/R = 0.90$, $y/R = -0.20$, $z = -2.33$ in.



**Figure 31.- Wake Measurements at
 $x/R = 0.90$, $y/R = -0.20$, $z = -3.36 \text{ in.}$**

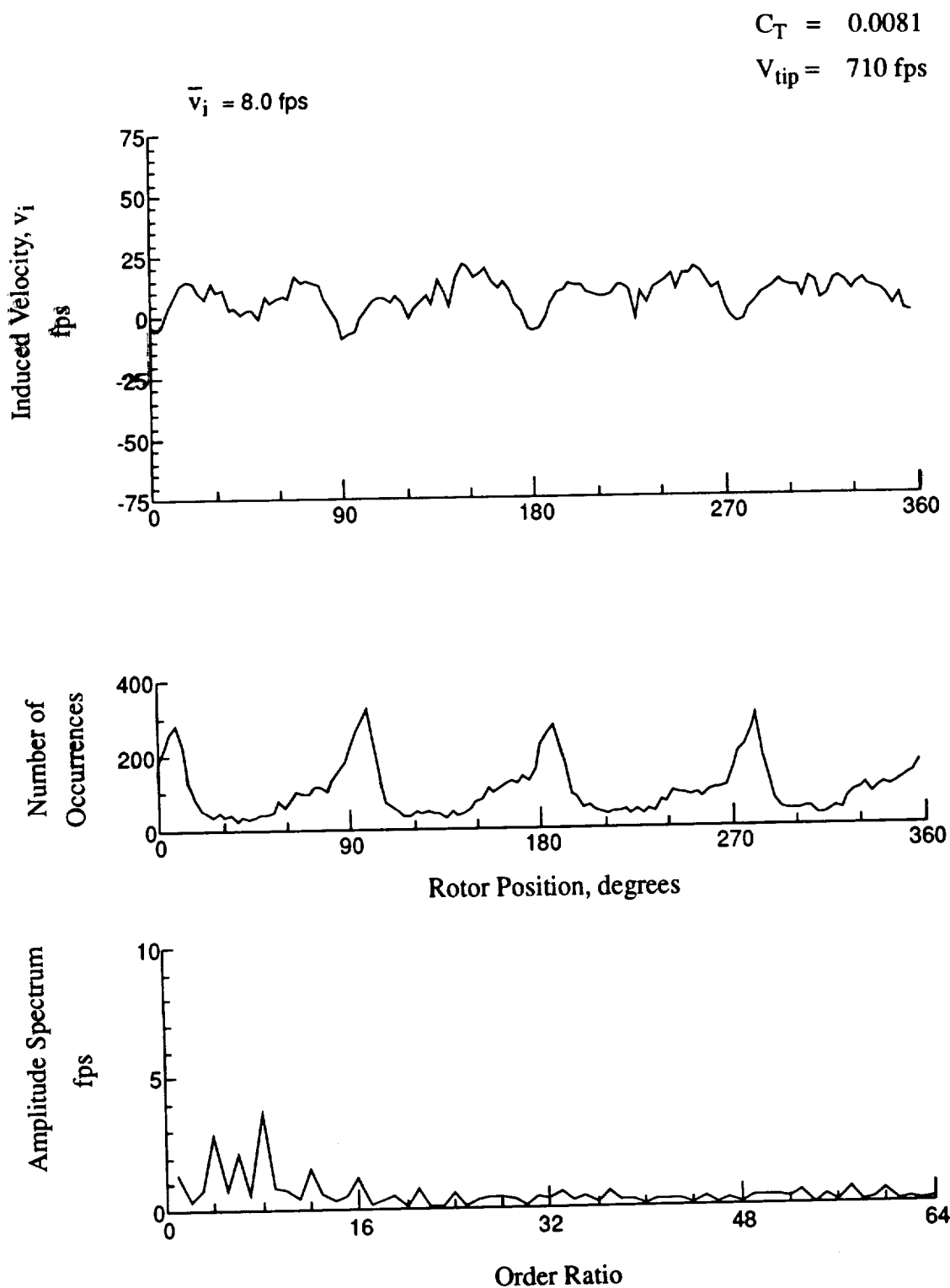
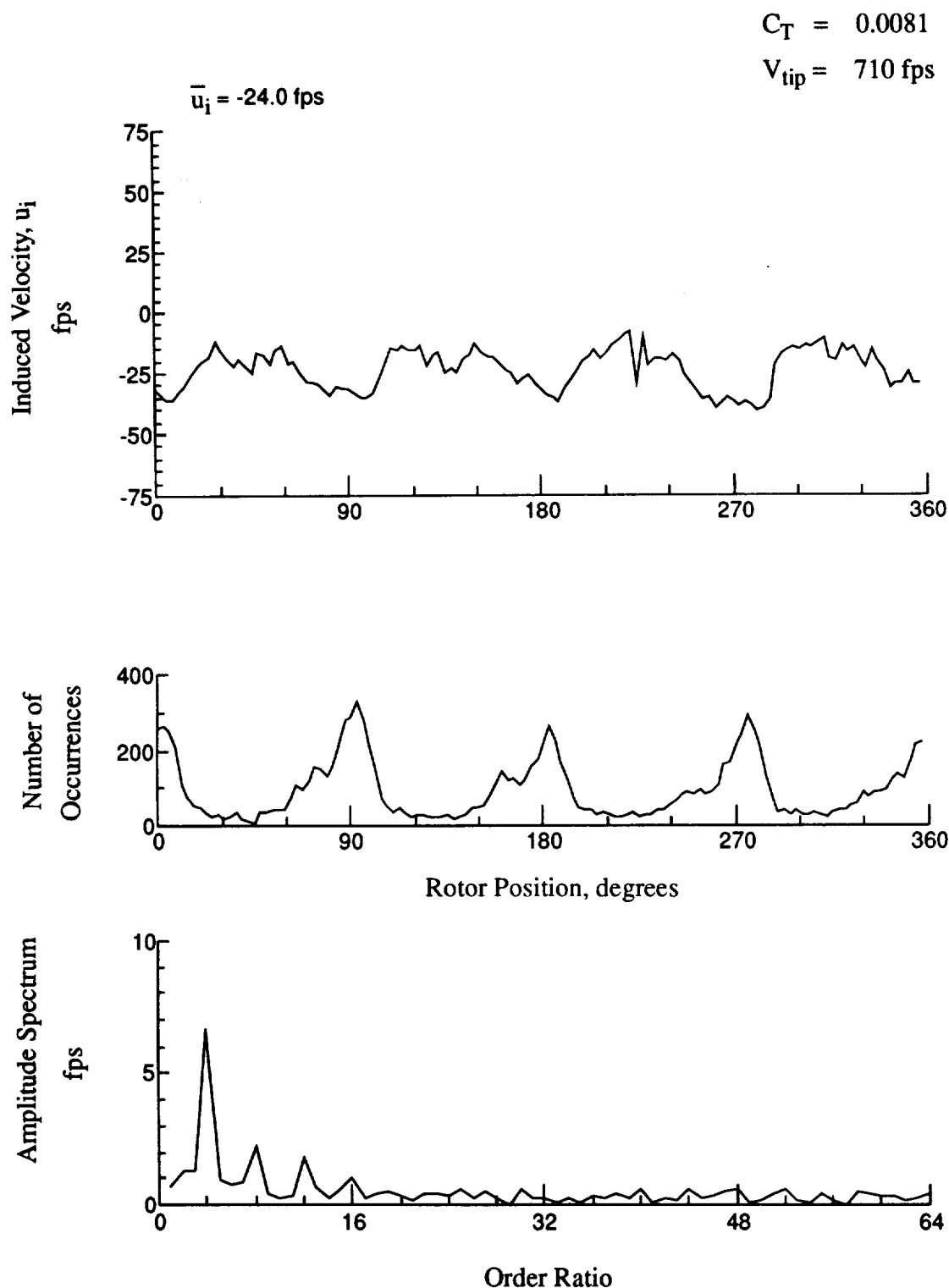


Figure 31.- Concluded.
 $x/R = 0.90$, $y/R = -0.20$, $z = -3.36 \text{ in.}$



**Figure 32.- Wake Measurements at
 $x/R = 0.90$, $y/R = -0.20$, $z = -4.39$ in.**

$$C_T = 0.0081$$

$$V_{tip} = 710 \text{ fps}$$

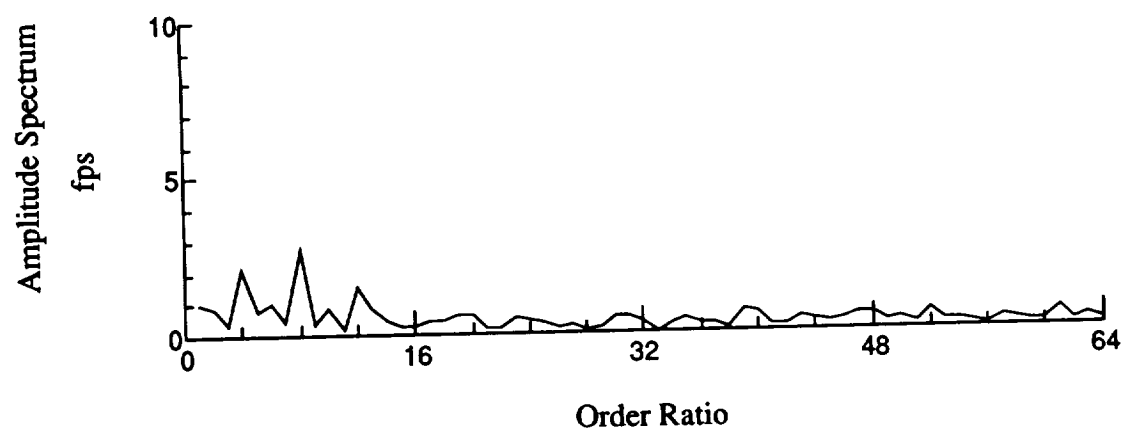
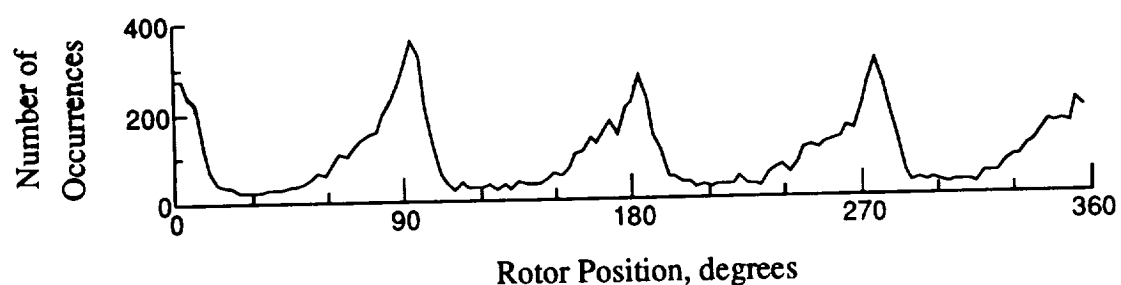
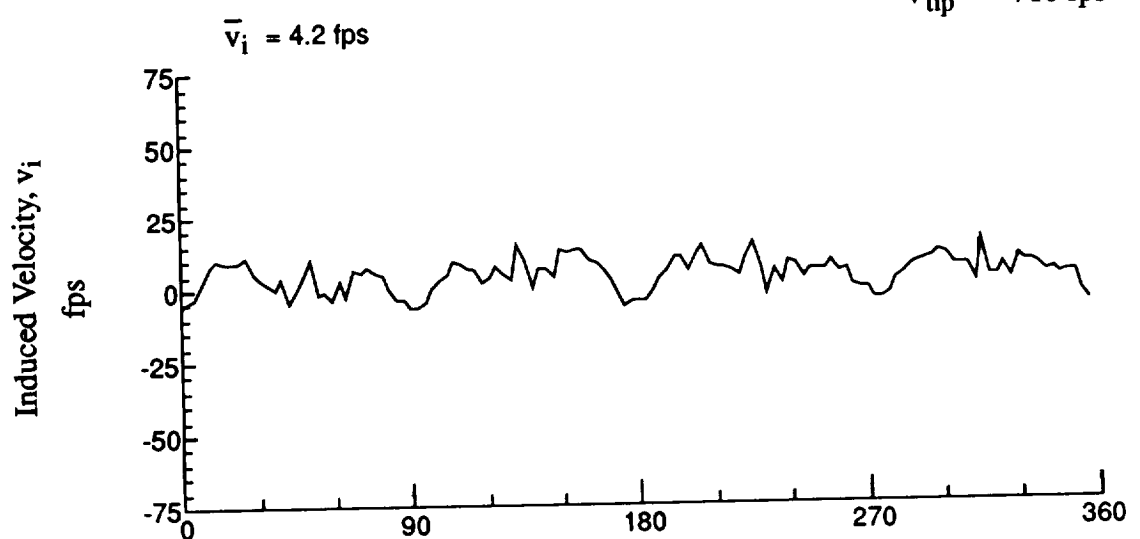


Figure 32.- Concluded.
 $x/R = 0.90$, $y/R = -0.20$, $z = -4.39$ in.

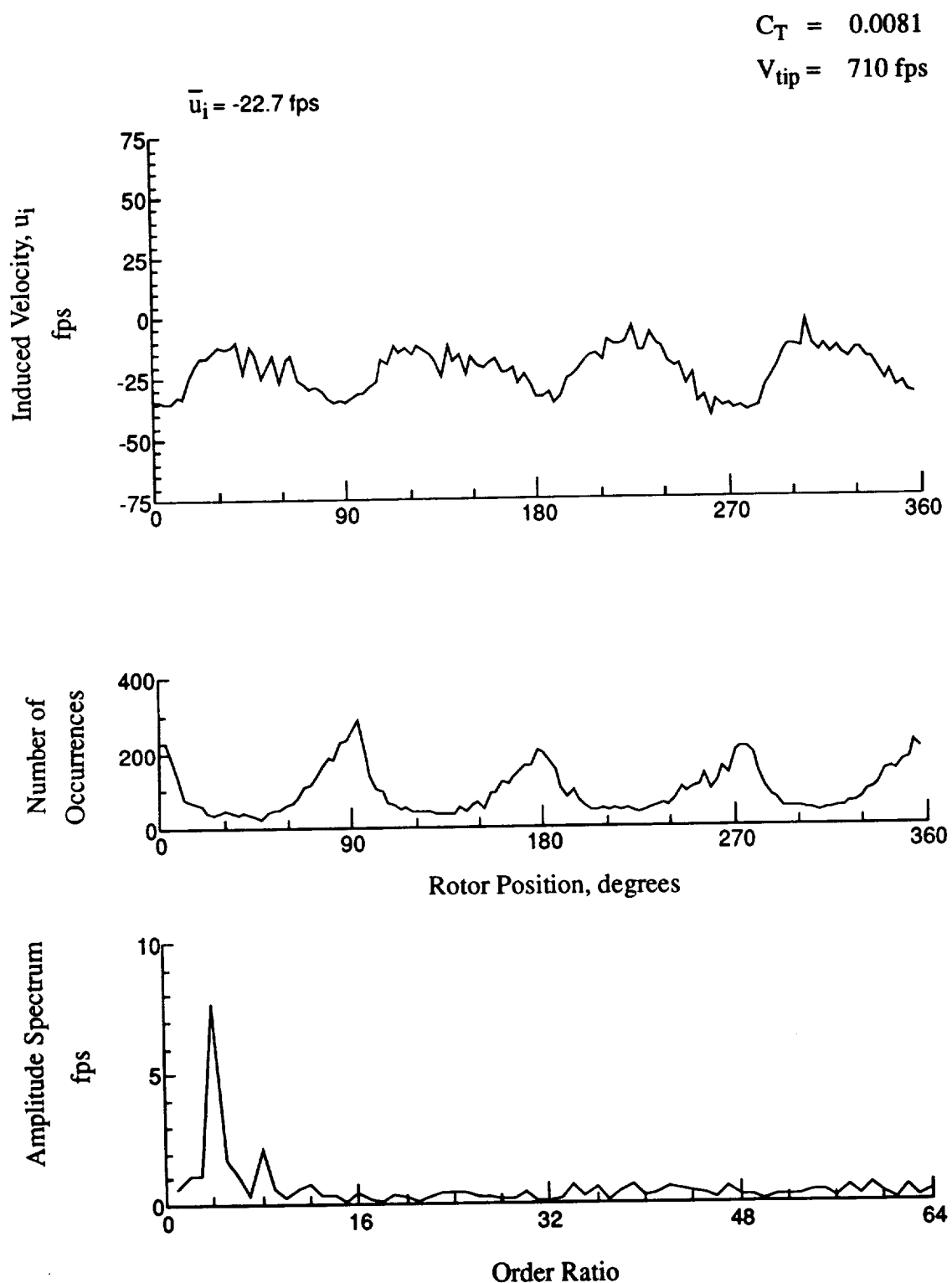


Figure 33.- Wake Measurements at
 $x/R = 0.90$, $y/R = -0.20$, $z = -5.42 \text{ in.}$

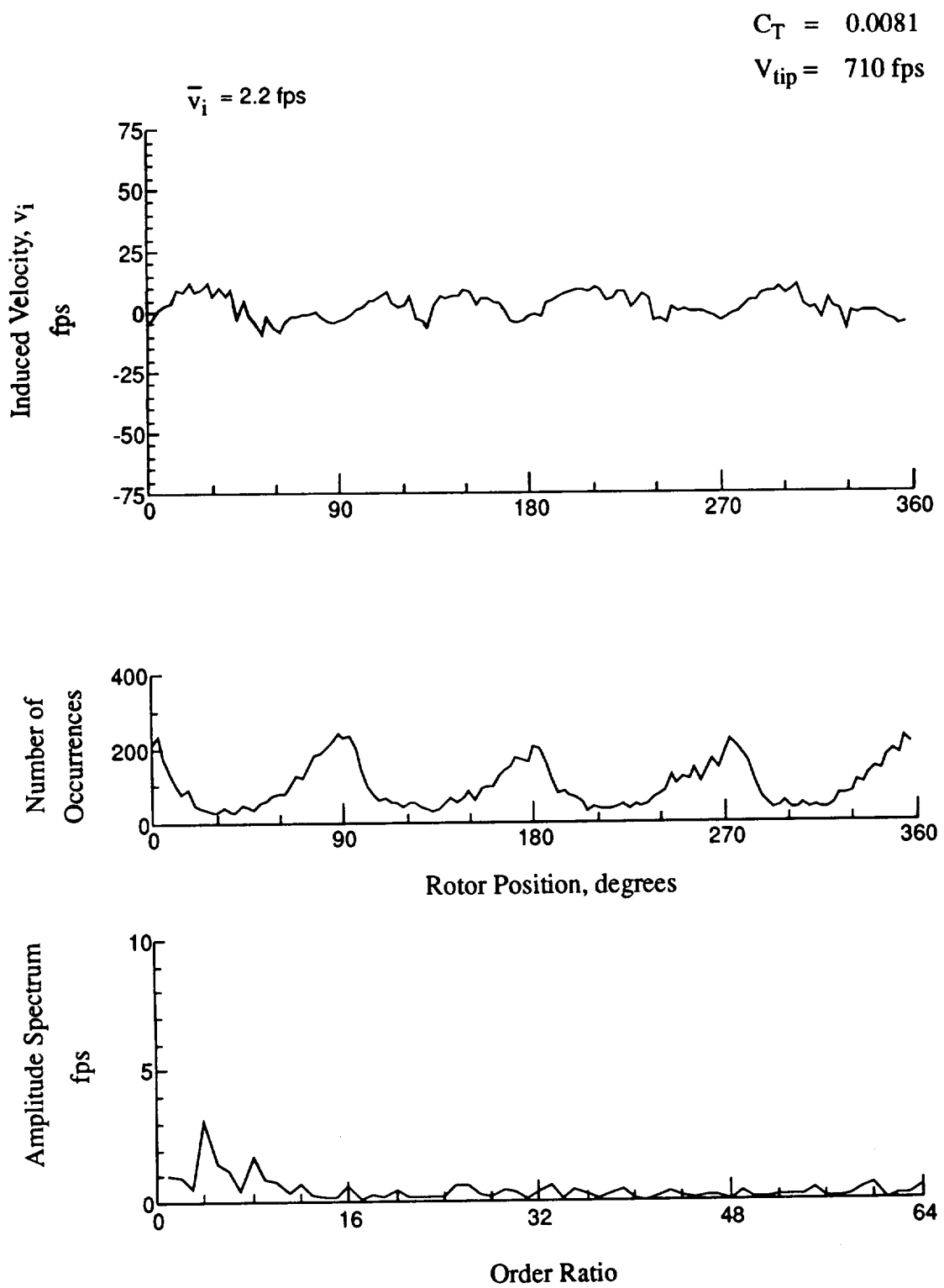
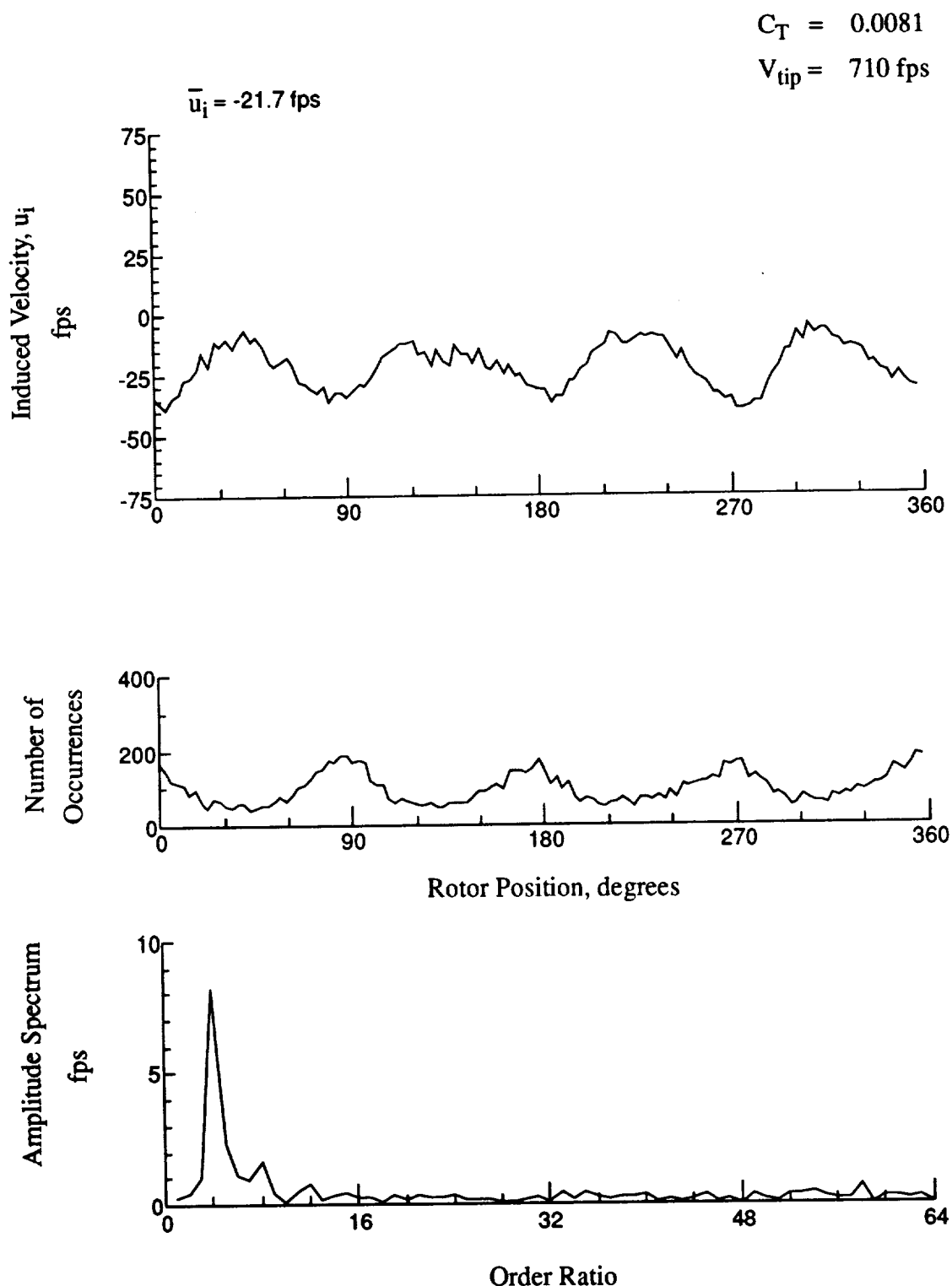


Figure 33.- Concluded.
 $x/R = 0.90$, $y/R = -0.20$, $z = -5.42 \text{ in.}$



**Figure 34.- Wake Measurements at
 $x/R = 0.90$, $y/R = -0.20$, $z = -6.45 \text{ in.}$**

$$C_T = 0.0081$$

$$V_{tip} = 710 \text{ fps}$$

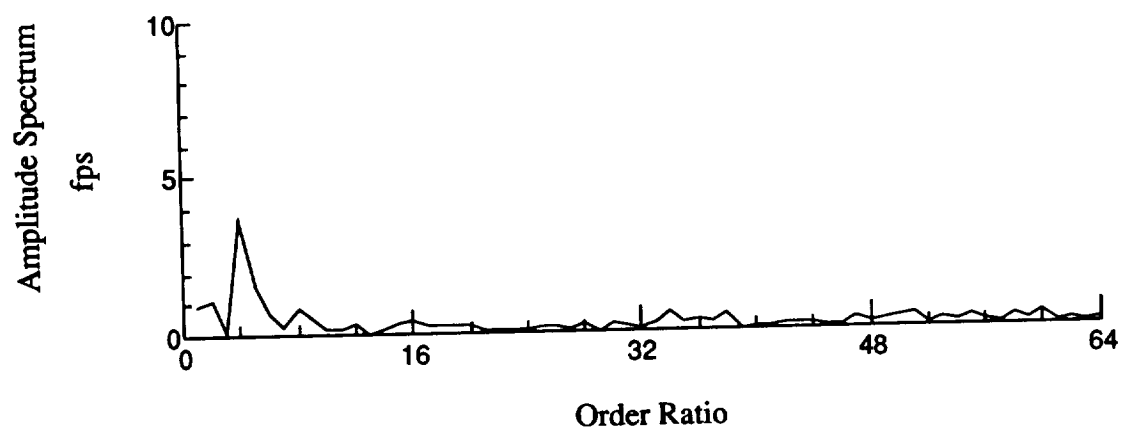
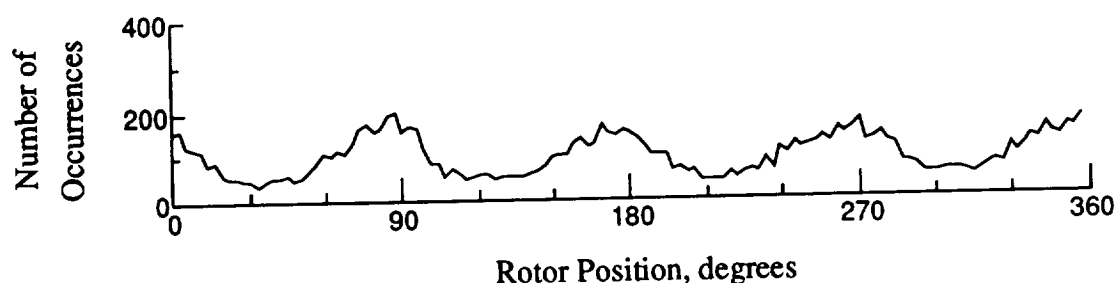
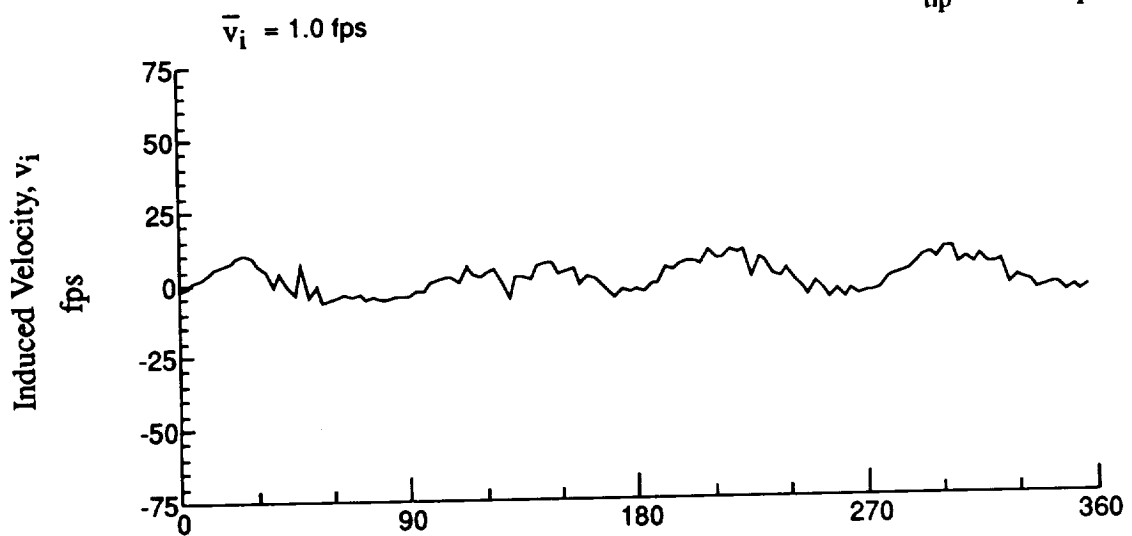


Figure 34.- Concluded.
 $x/R = 0.90$, $y/R = -0.20$, $z = -6.45 \text{ in.}$

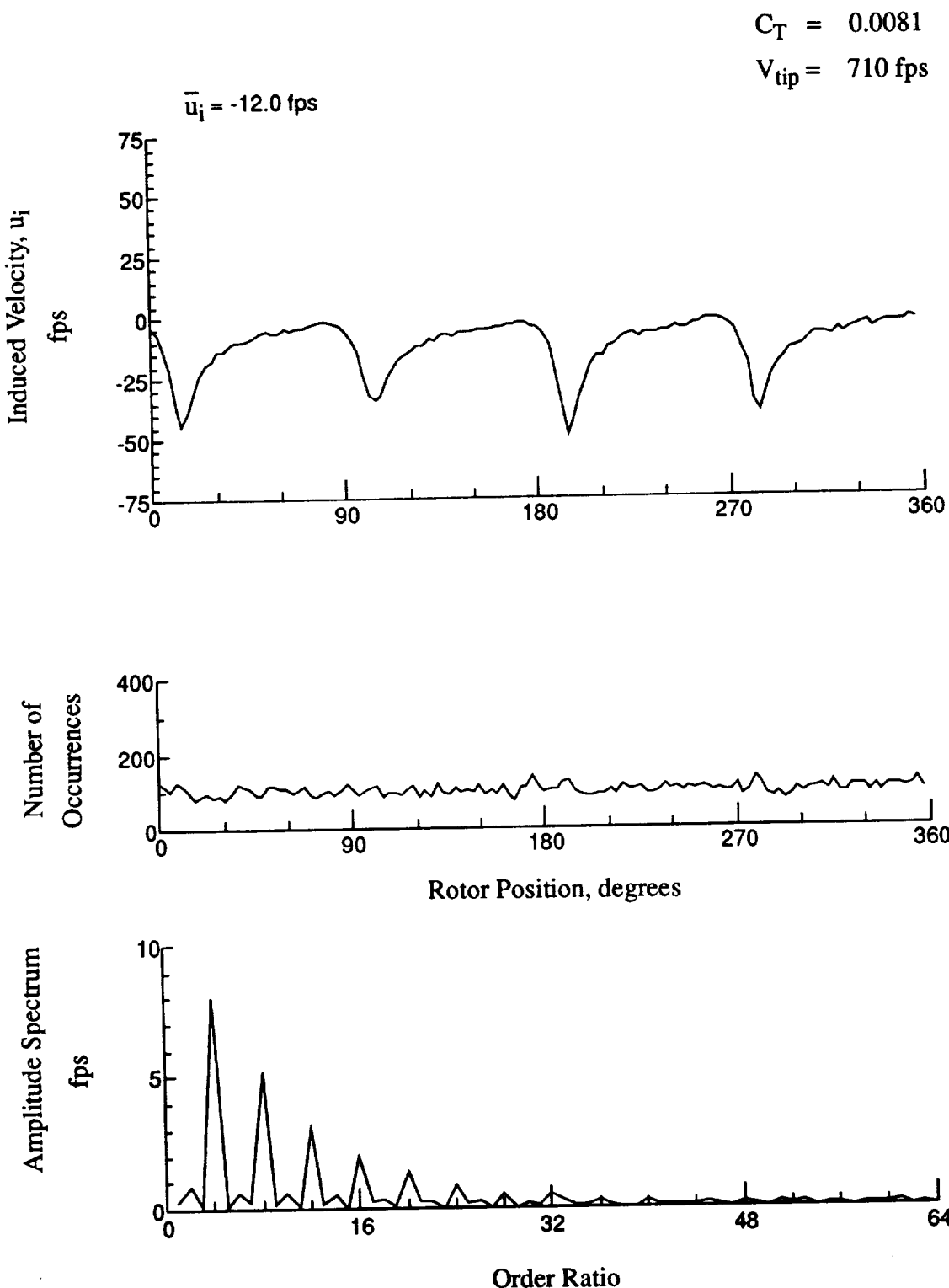


Figure 35.- Wake Measurements at
 $x/R = 1.10$, $y/R = -0.20$, $z = 8.85 \text{ in.}$

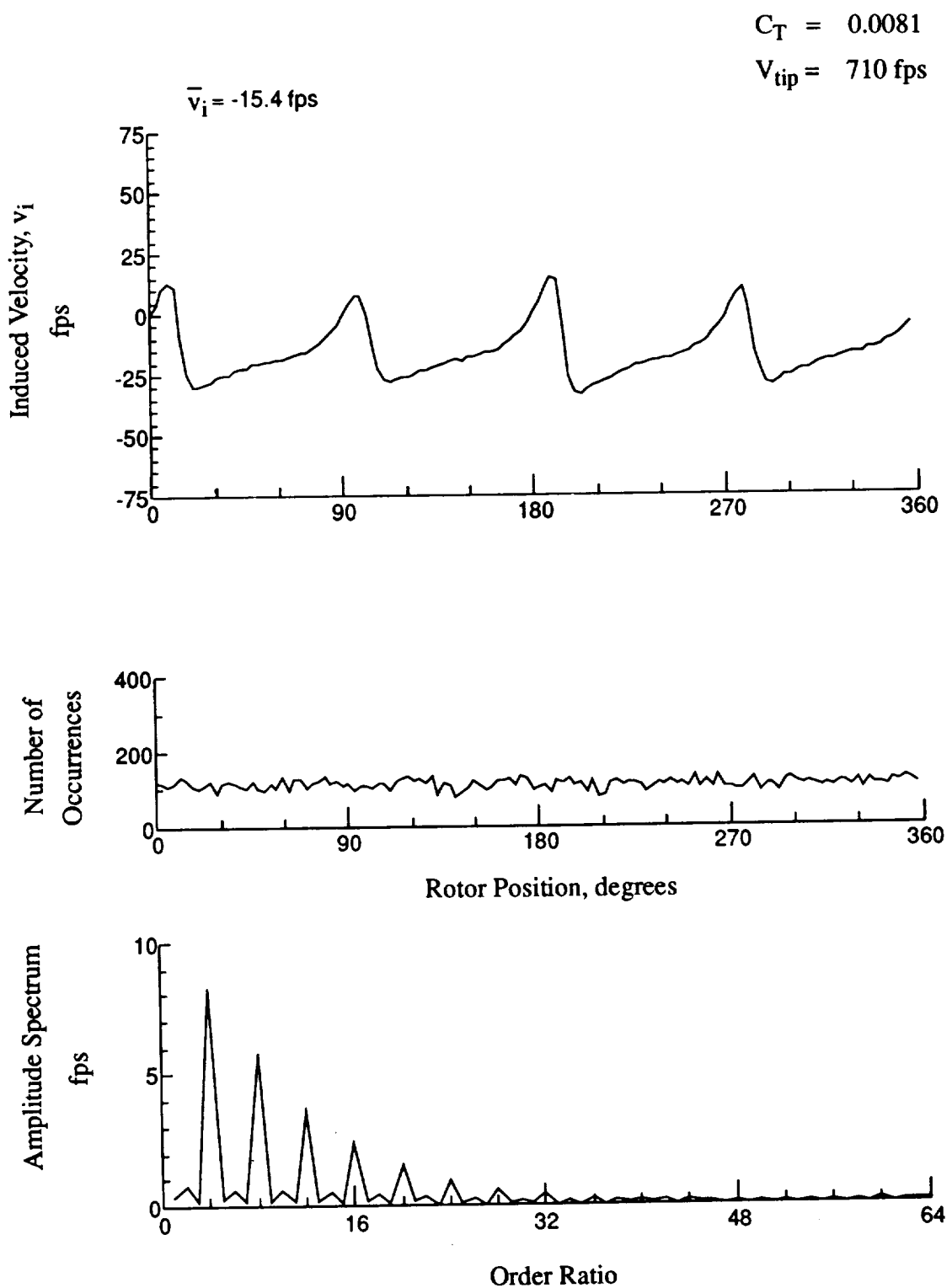
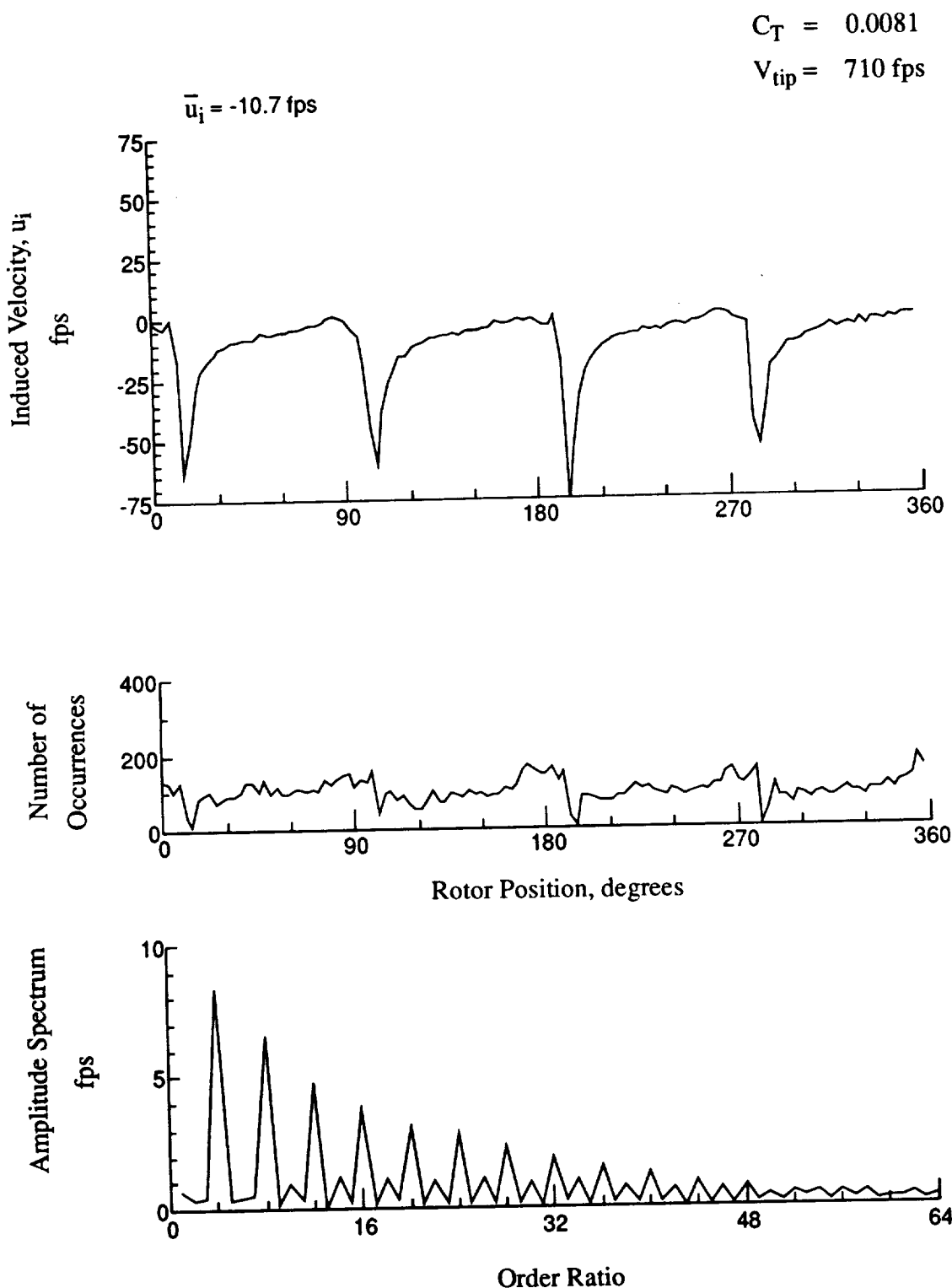


Figure 35.- Concluded.
 $x/R = 1.10$, $y/R = -0.20$, $z = 8.85 \text{ in.}$



**Figure 36.- Wake Measurements at
 $x/R = 1.10$, $y/R = -0.20$, $z = 7.82$ in.**

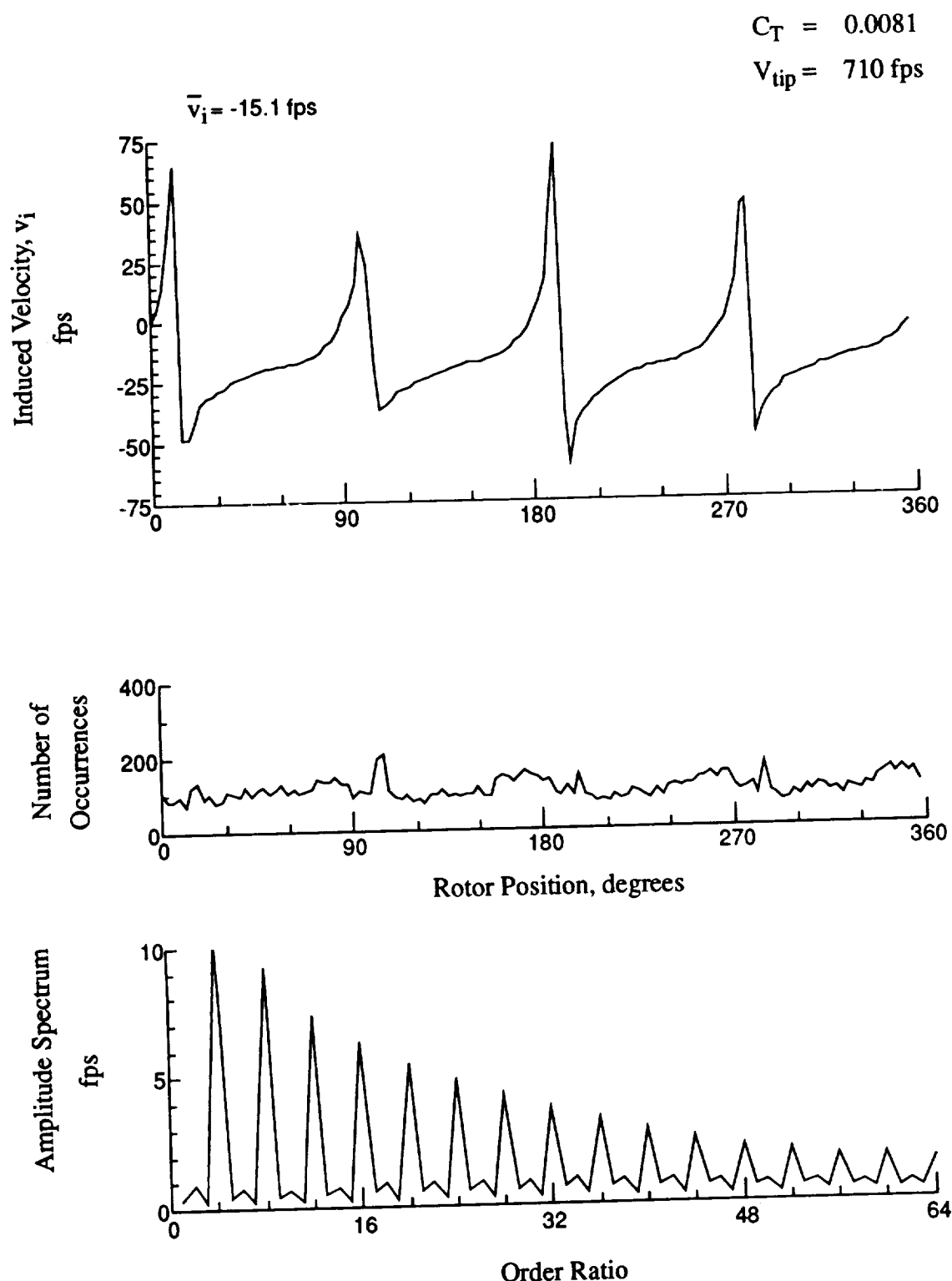


Figure 36.- Concluded.
 $x/R = 1.10$, $y/R = -0.20$, $z = 7.82 \text{ in.}$

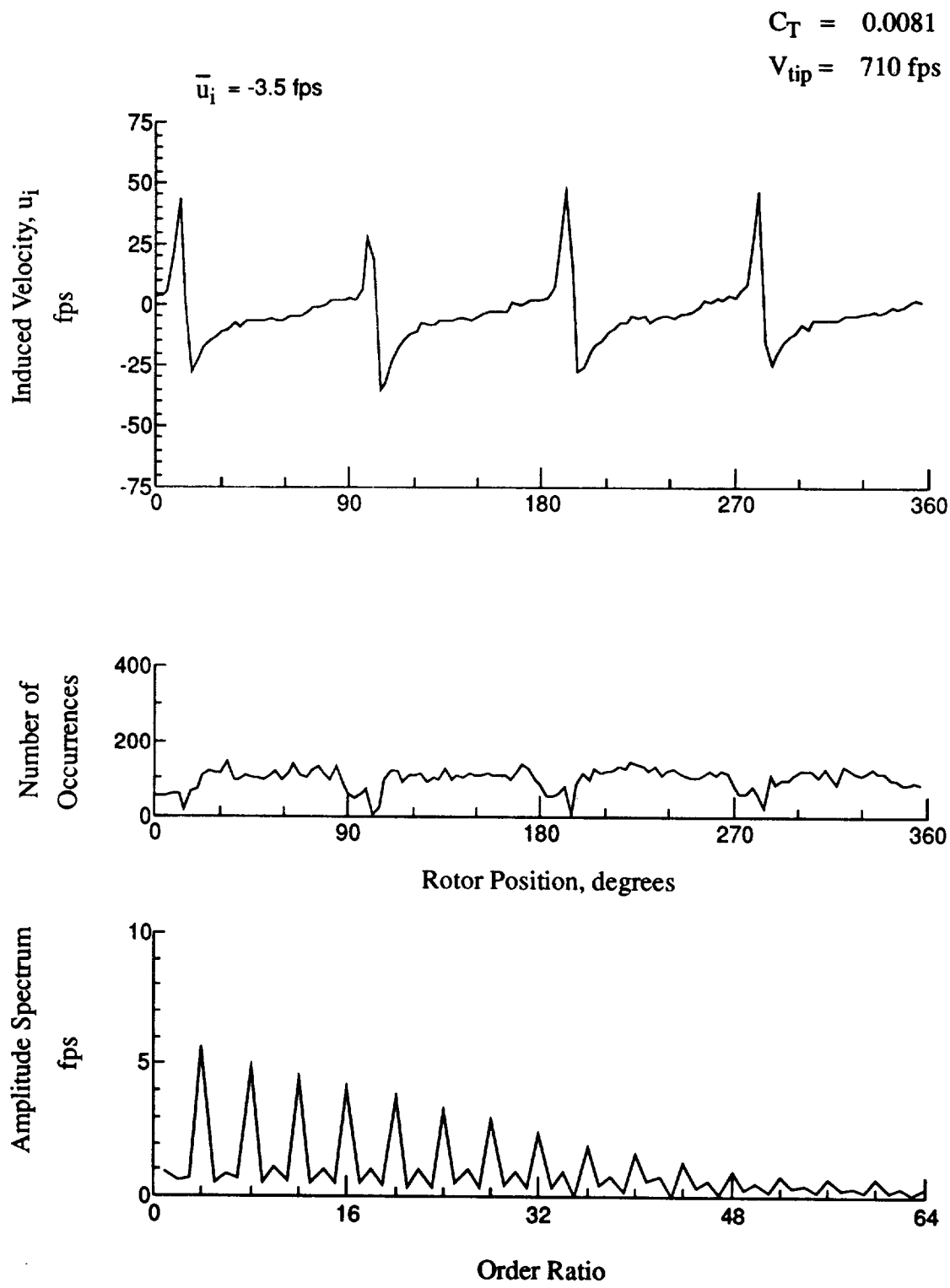


Figure 37.- Wake Measurements at
 $x/R = 1.10$, $y/R = -0.20$, $z = 6.79$ in.

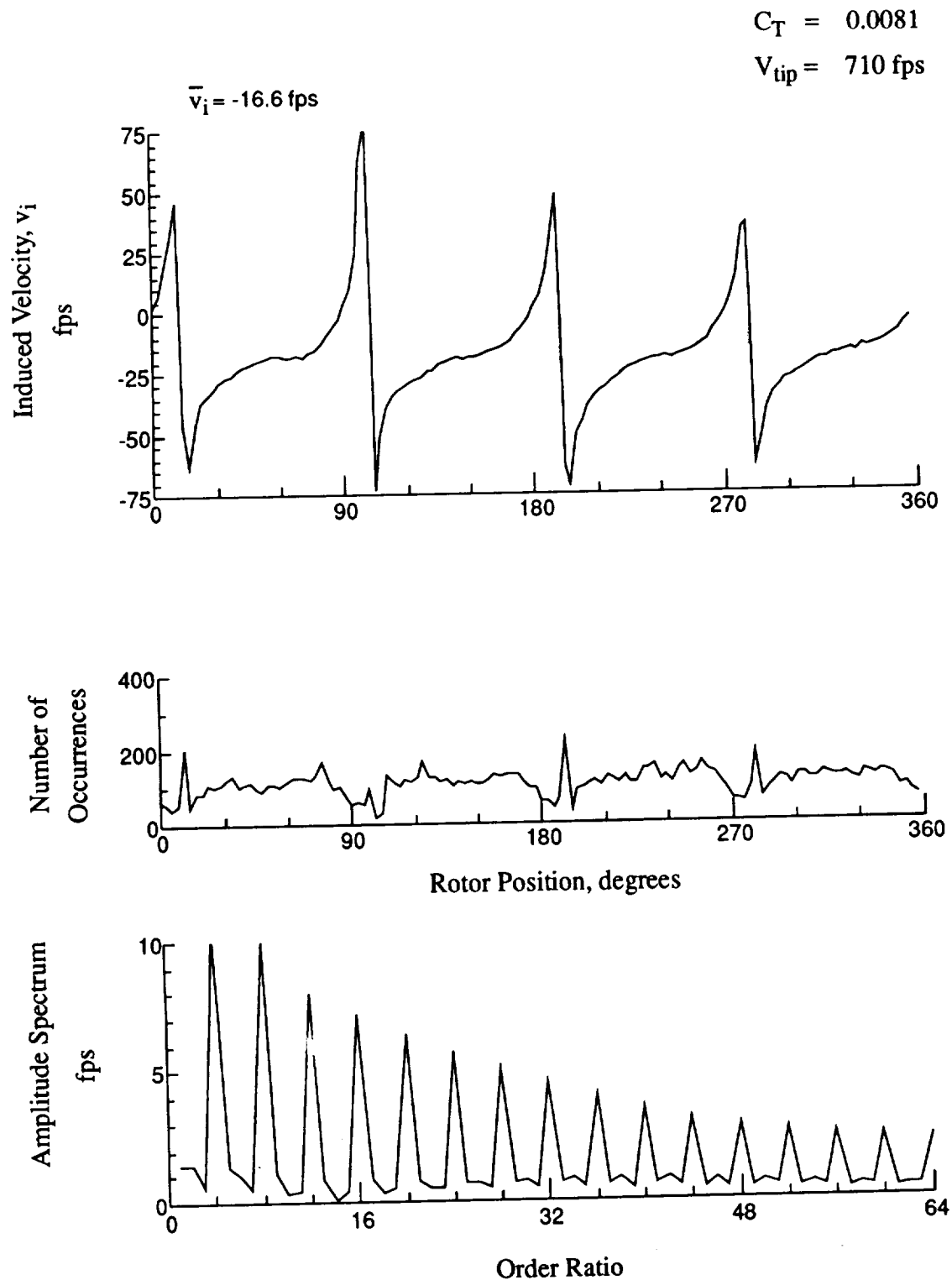
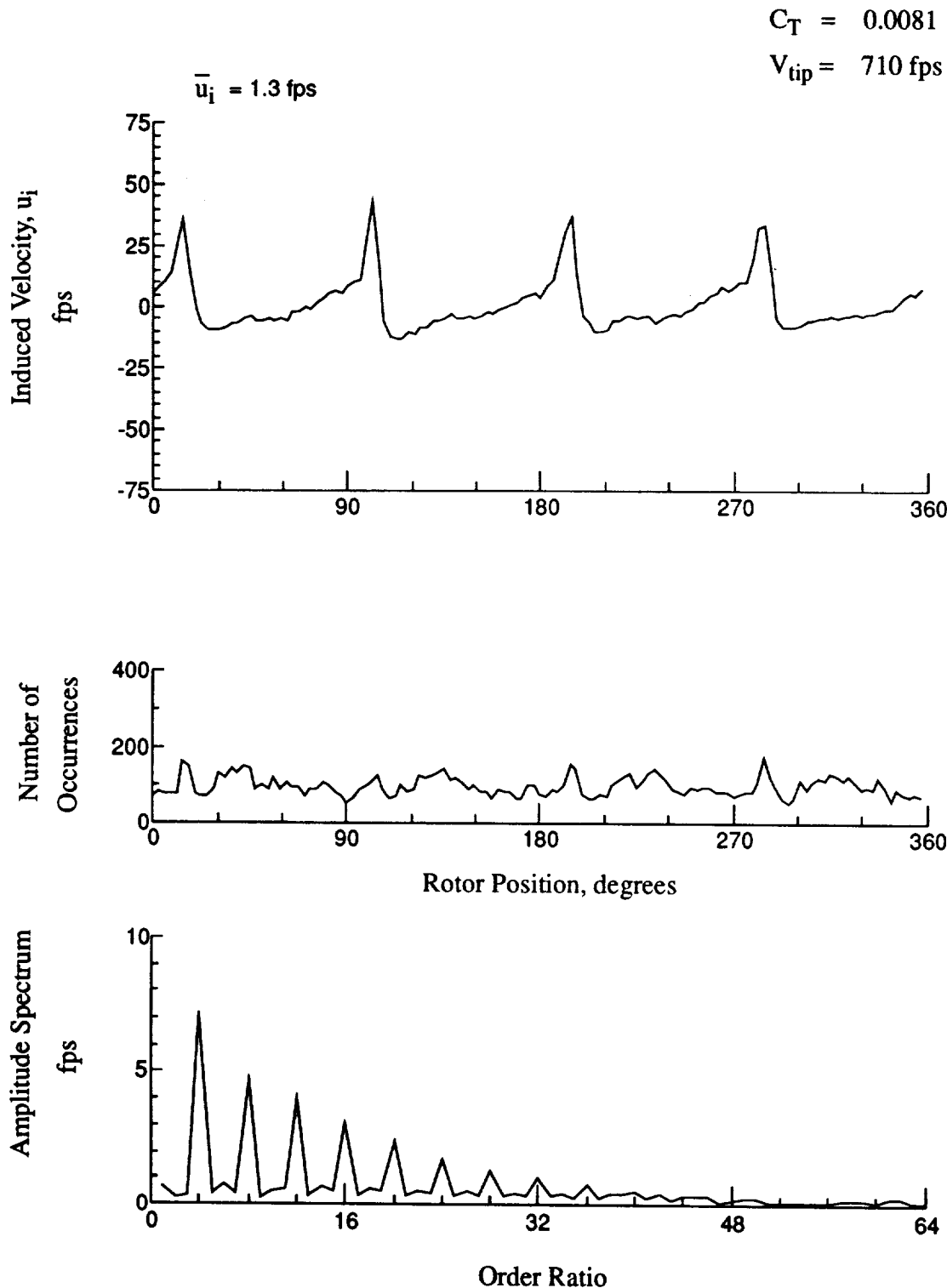


Figure 37.- Concluded.
 $x/R = 1.10$, $y/R = -0.20$, $z = 6.79 \text{ in.}$



**Figure 38.- Wake Measurements at
 $x/R = 1.10$, $y/R = -0.20$, $z = 5.76 \text{ in.}$**

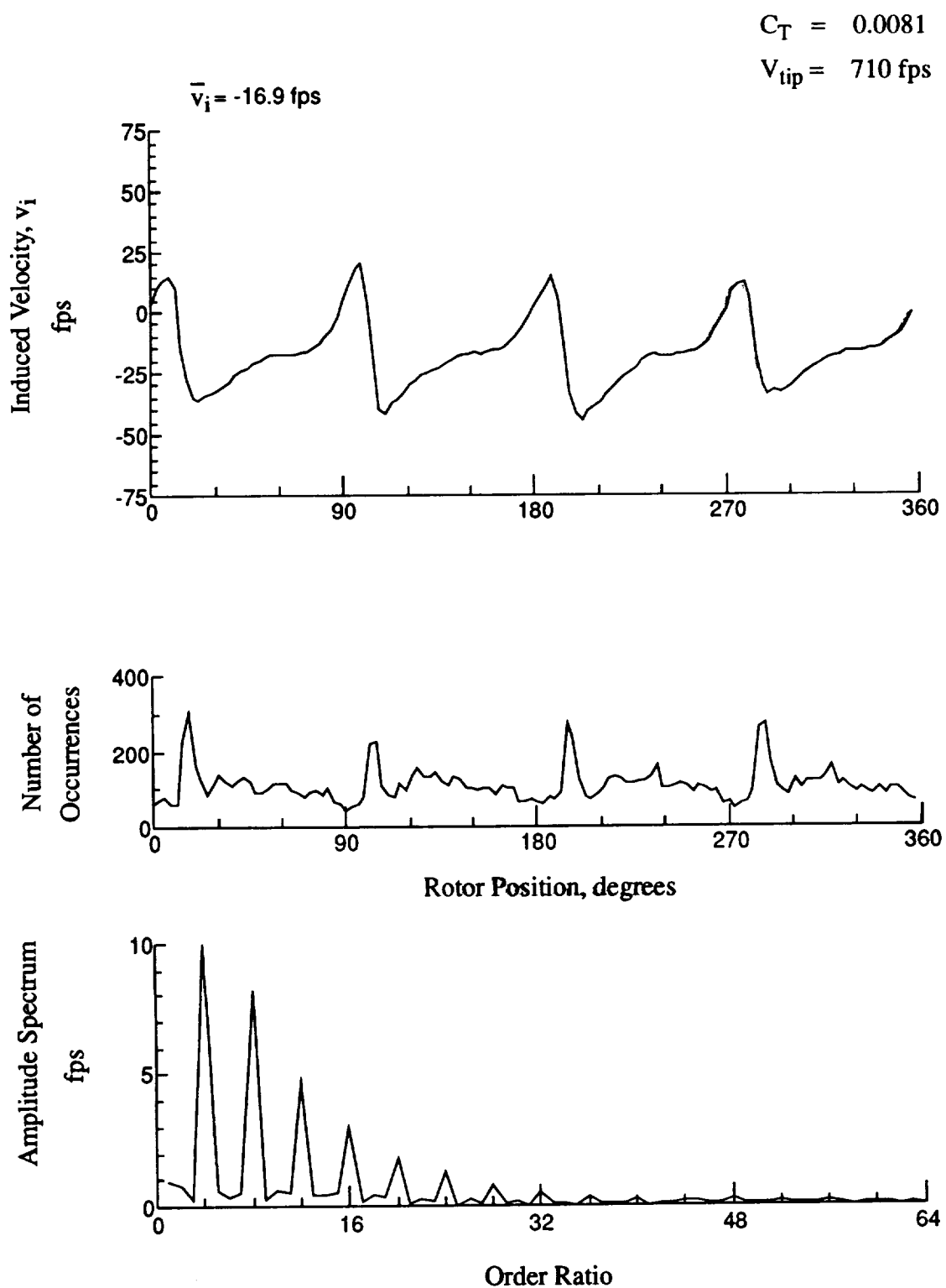
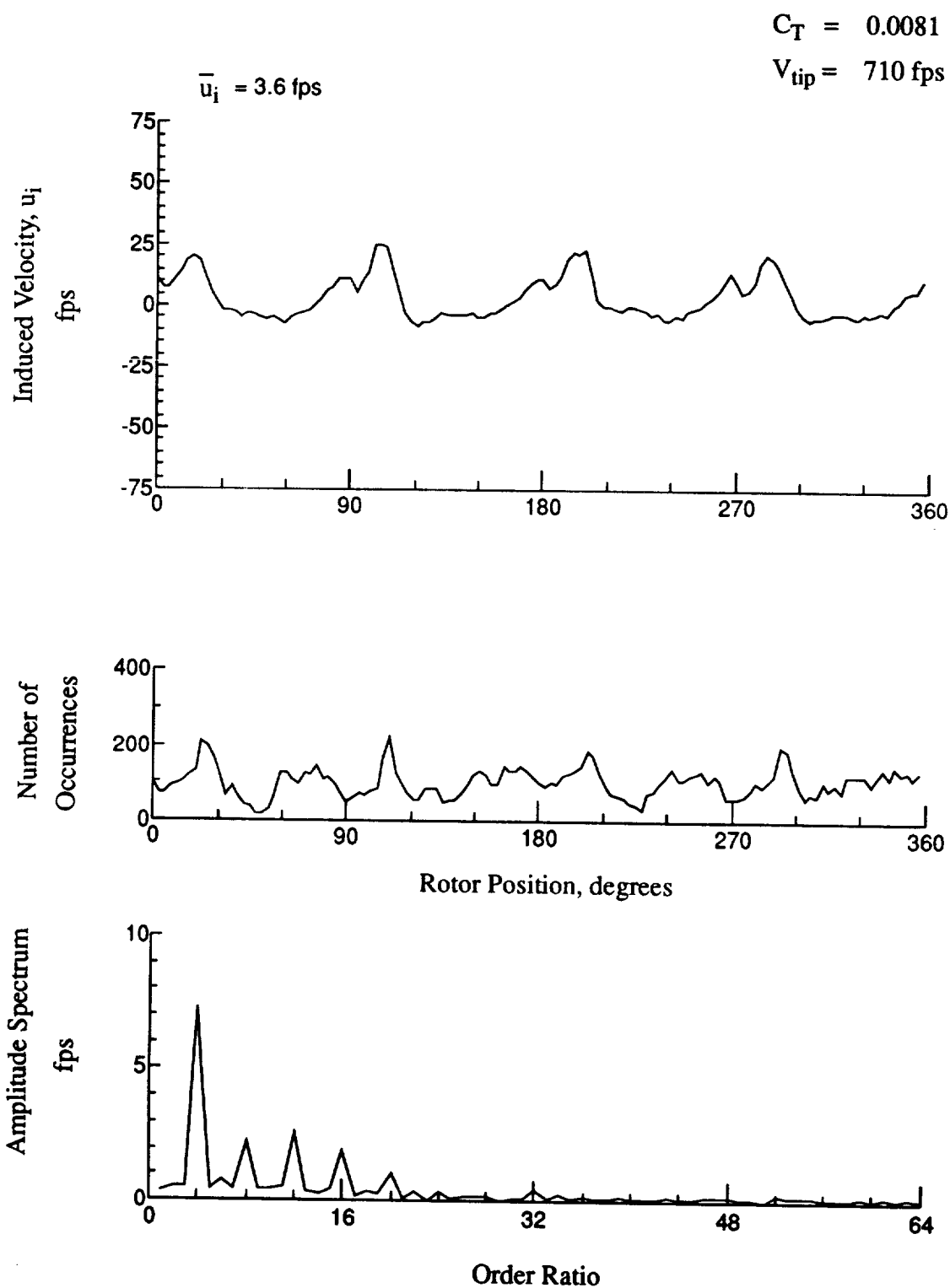


Figure 38.- Concluded.

$x/R = 1.10$, $y/R = -0.20$, $z = 5.76 \text{ in.}$



**Figure 39.- Wake Measurements at
 $x/R = 1.10$, $y/R = -0.20$, $z = 4.73 \text{ in.}$**

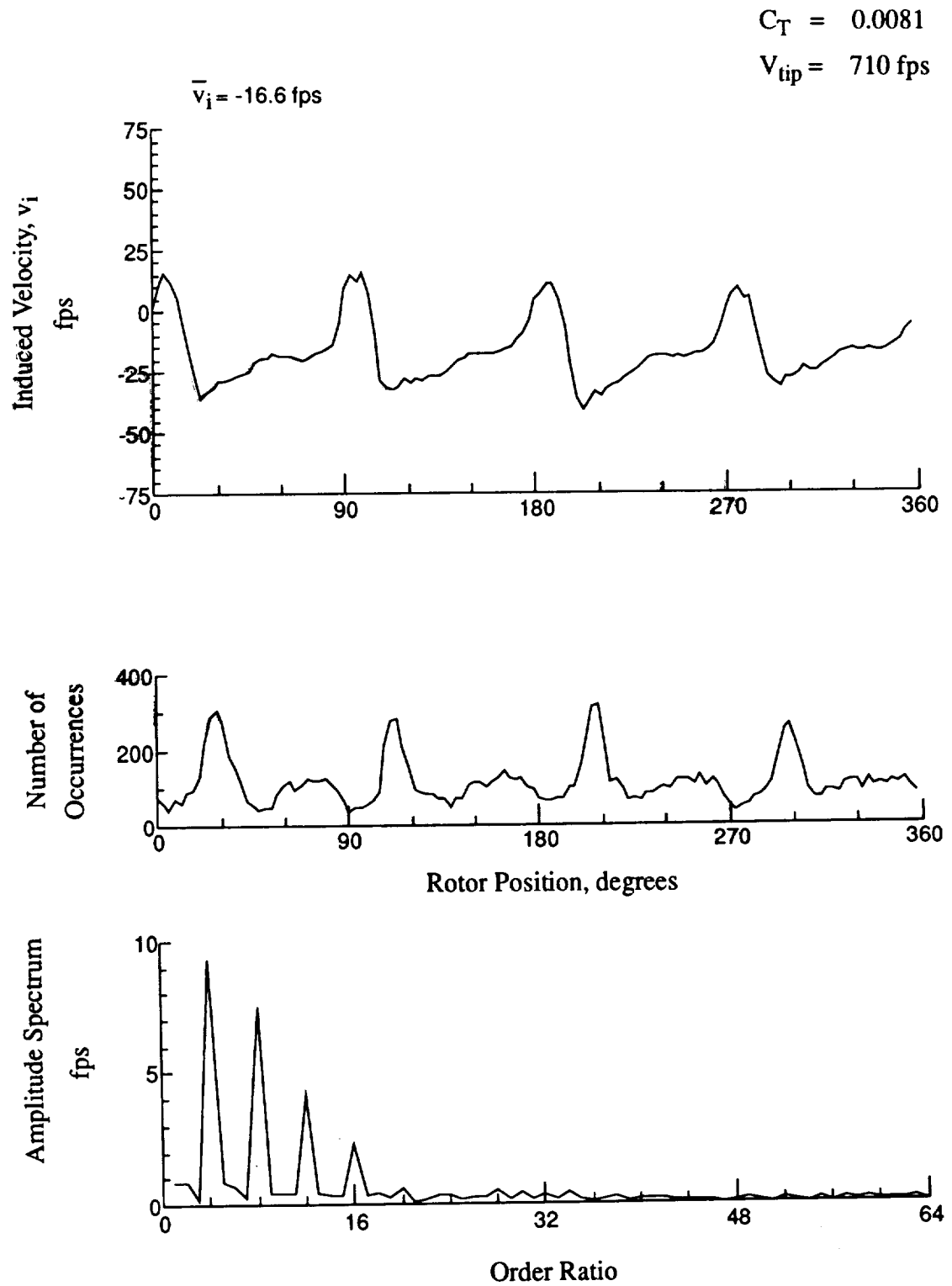
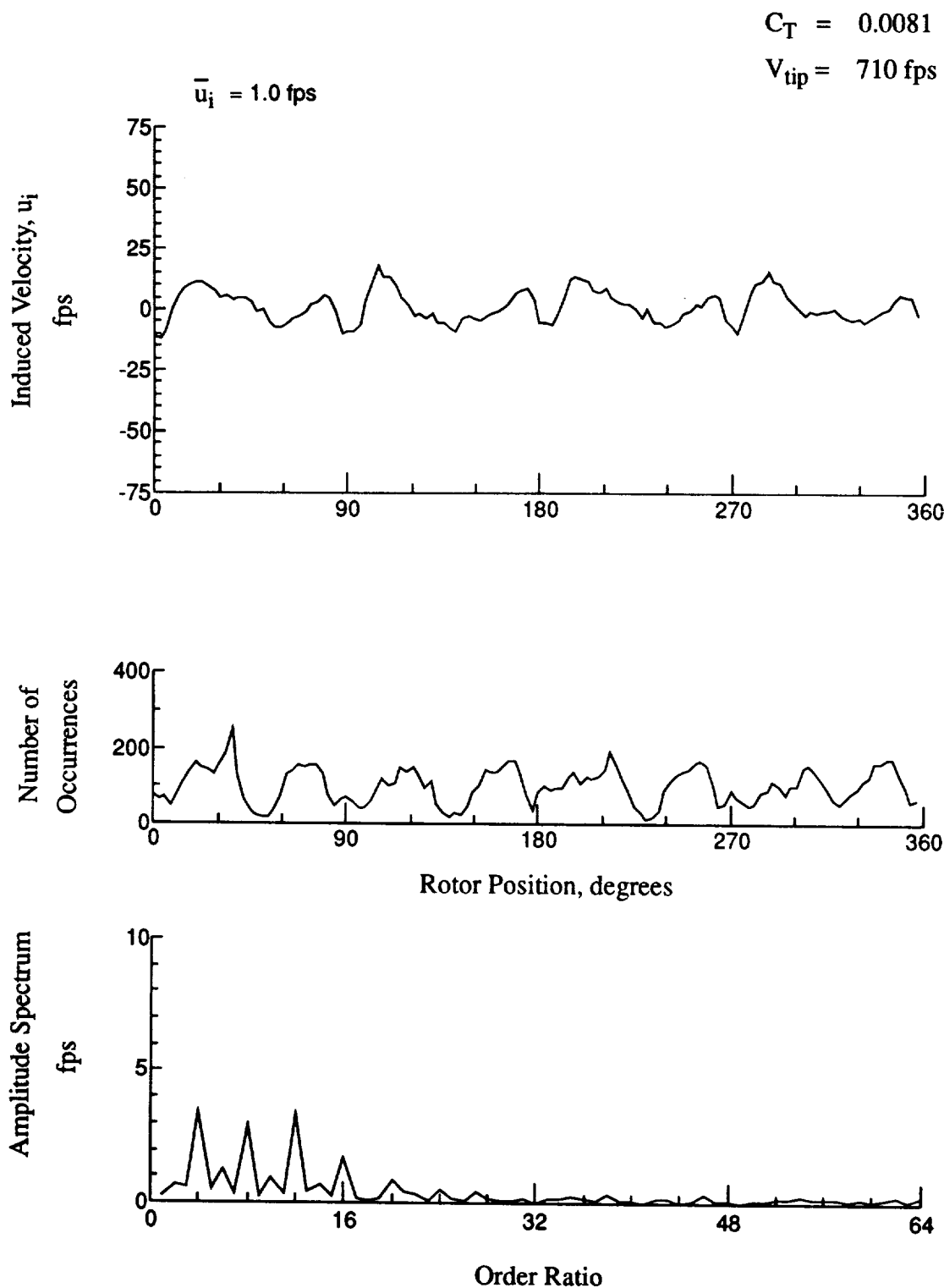


Figure 39.- Concluded.
 $x/R = 1.10$, $y/R = -0.20$, $z = 4.73 \text{ in.}$



**Figure 40.- Wake Measurements at
 $x/R = 1.10$, $y/R = -0.20$, $z = 3.70$ in.**

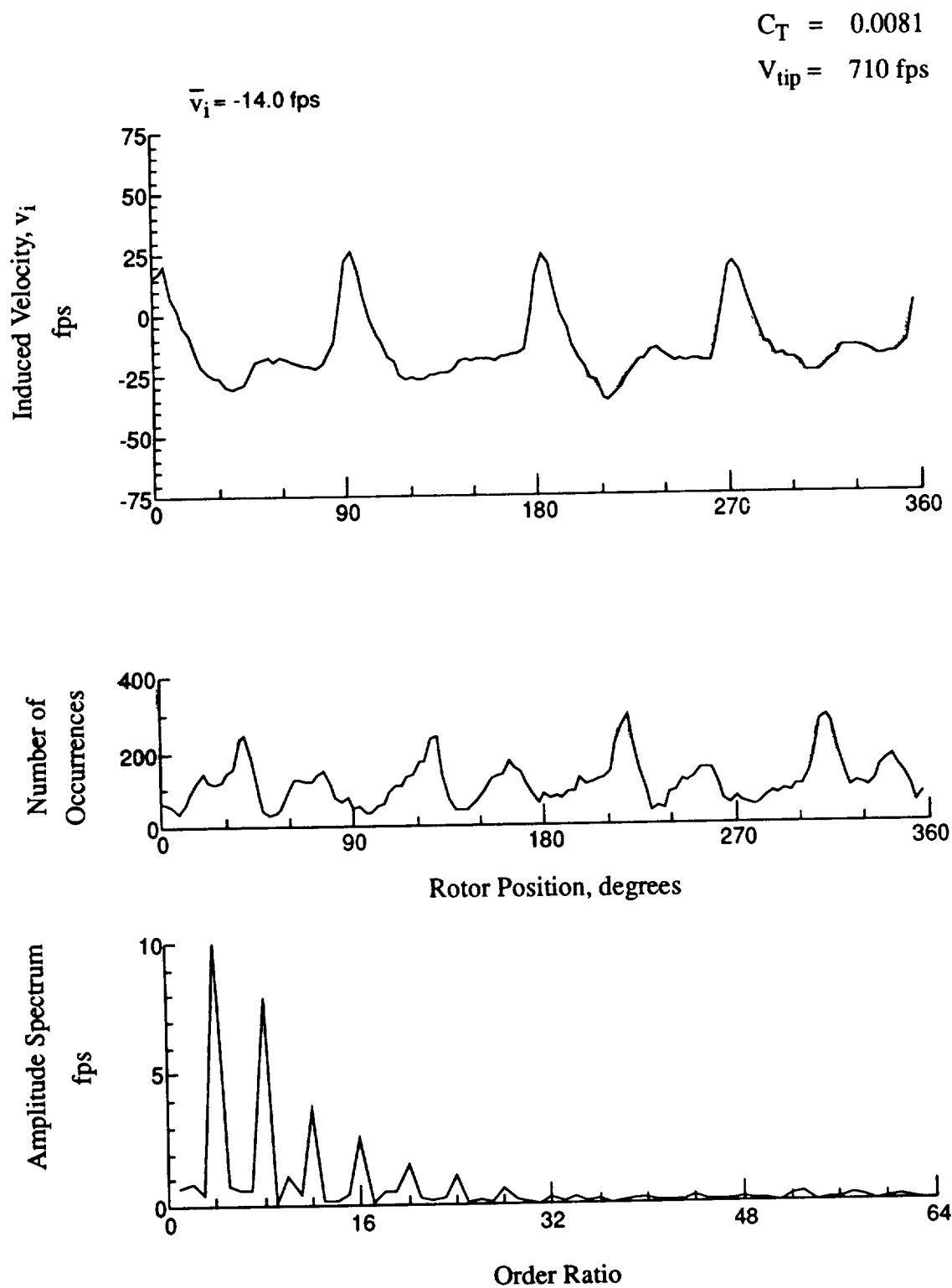
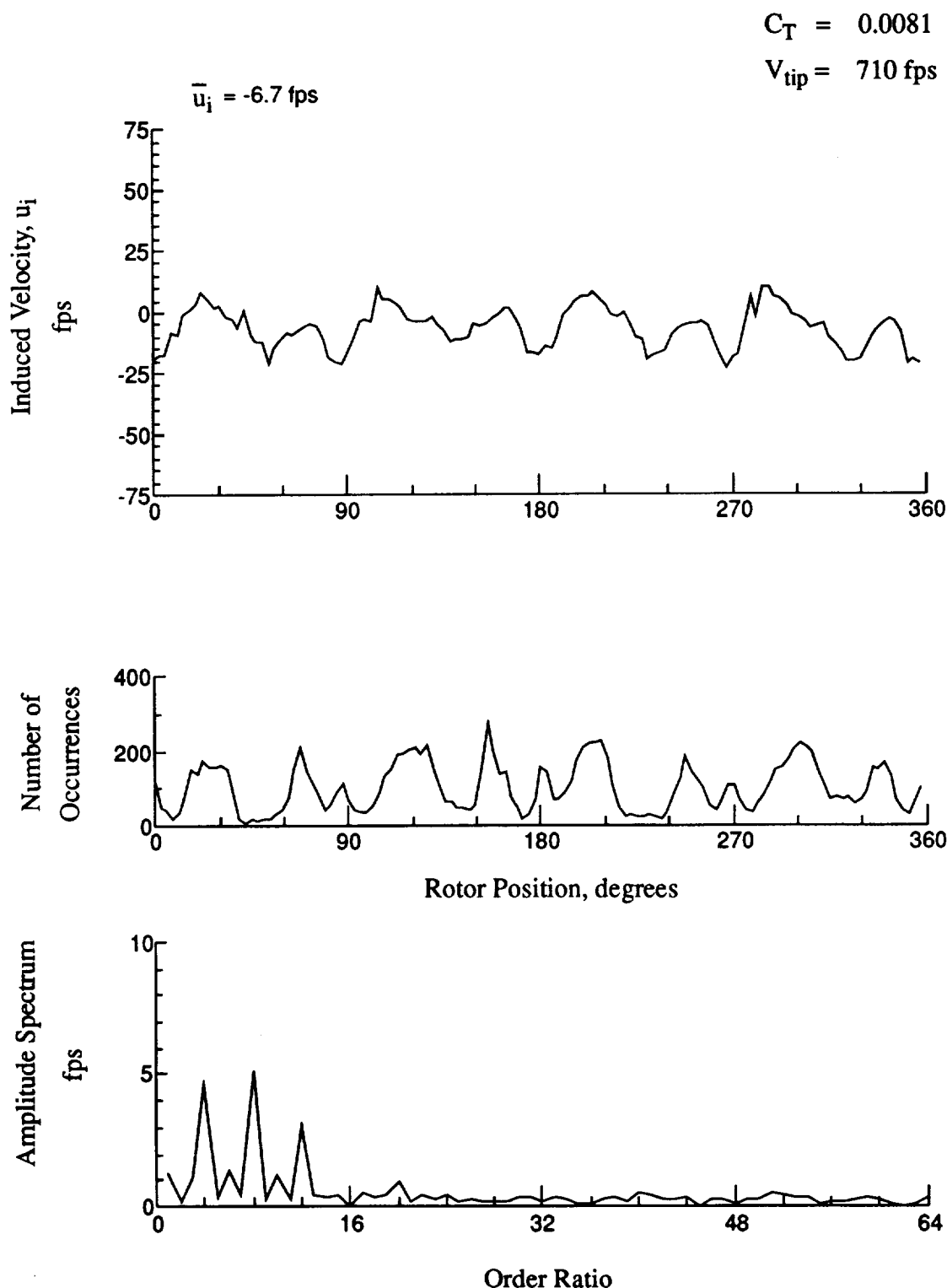


Figure 40.- Concluded.
 $x/R = 1.10$, $y/R = -0.20$, $z = 3.70 \text{ in.}$



**Figure 41.- Wake Measurements at
 $x/R = 1.10$, $y/R = -0.20$, $z = 2.67$ in.**

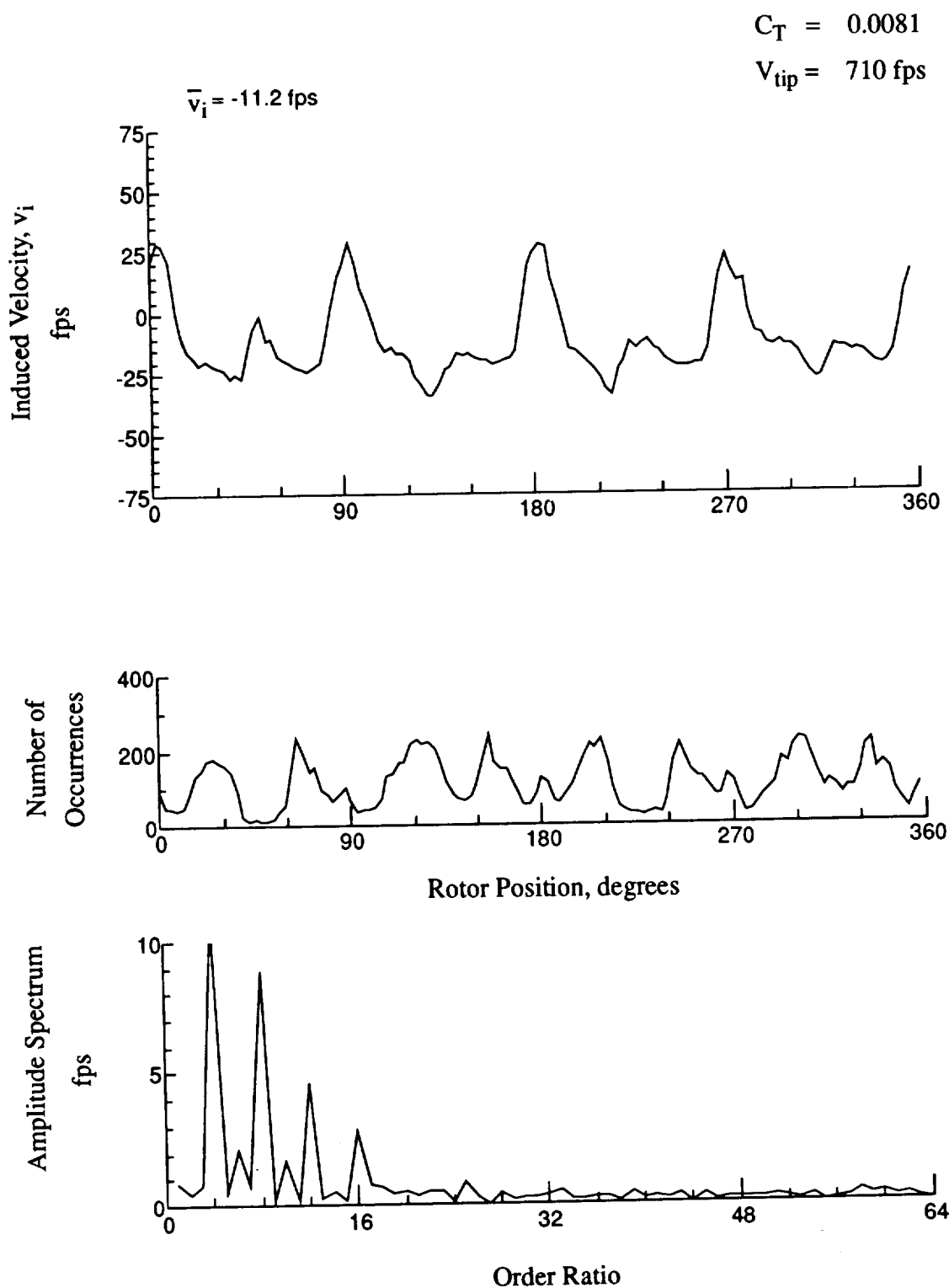
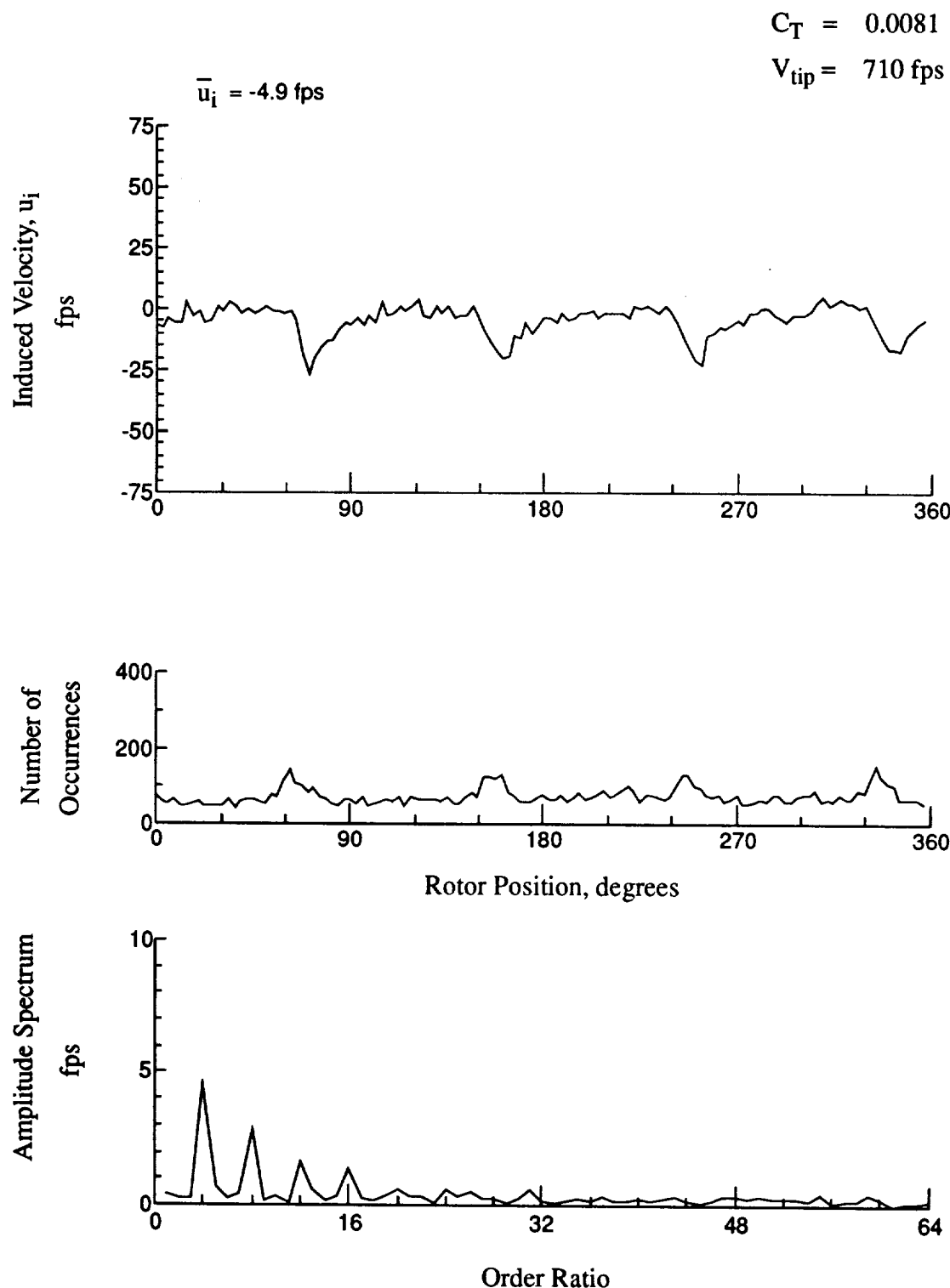


Figure 41.- Concluded.
 $x/R = 1.10$, $y/R = -0.20$, $z = 2.67 \text{ in.}$



**Figure 42.- Wake Measurements at
 $x/R = 1.50$, $y/R = -0.20$, $z = 8.37 \text{ in.}$**

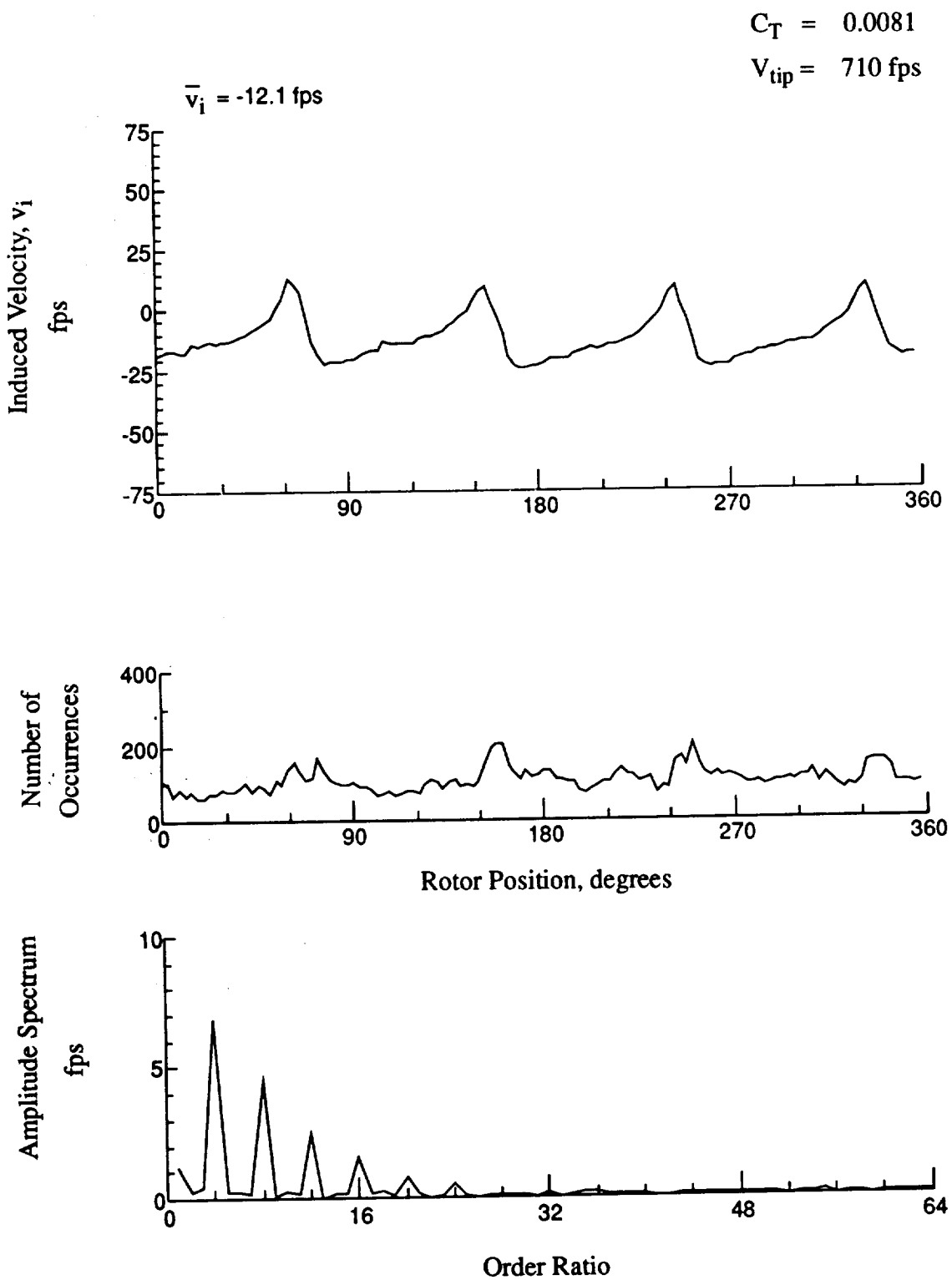


Figure 42.- Concluded.
 $x/R = 1.50$, $y/R = -0.20$, $z = 8.37 \text{ in.}$

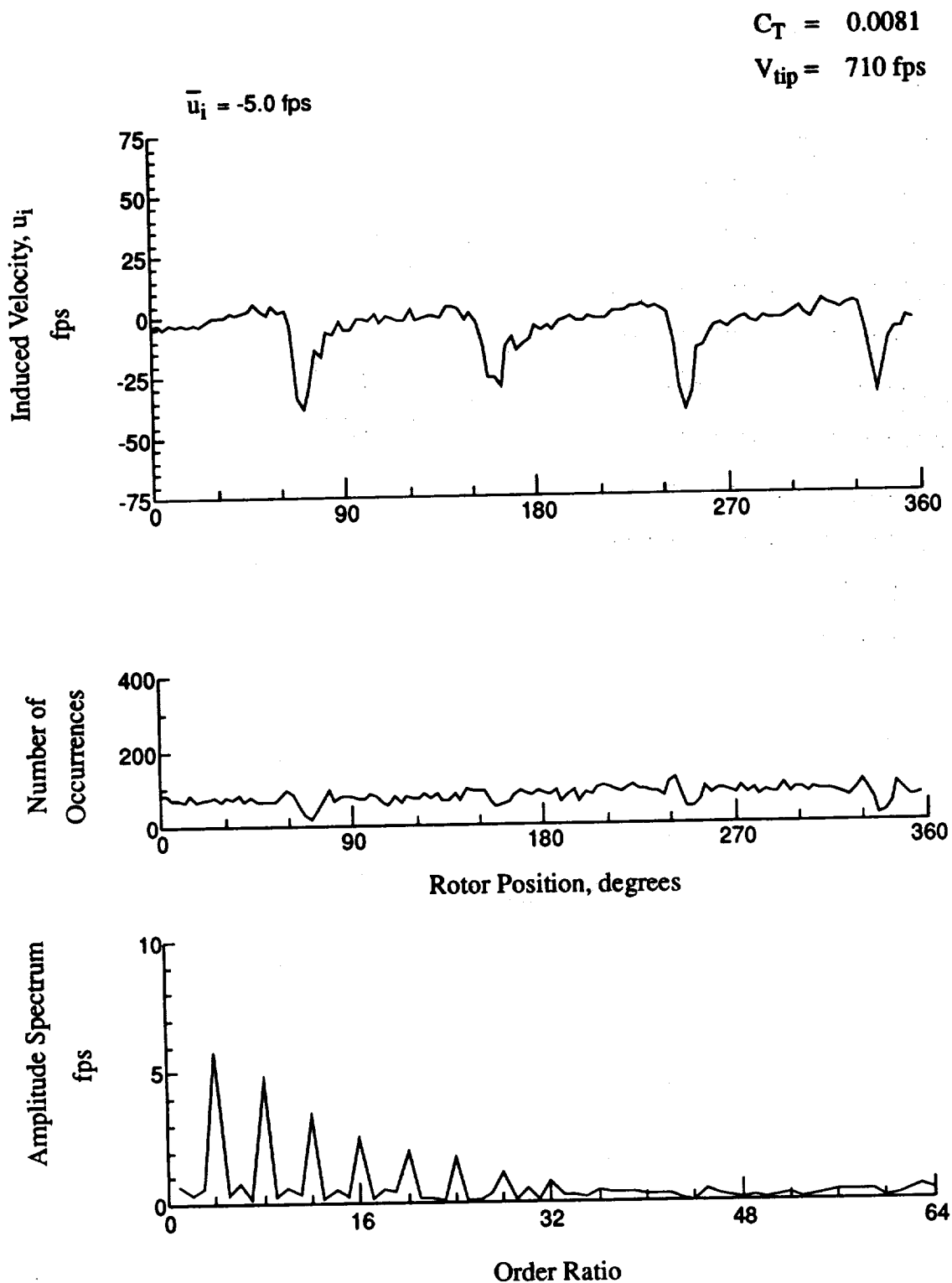


Figure 43.- Wake Measurements at
 $x/R = 1.50$, $y/R = -0.20$, $z = 7.34 \text{ in.}$

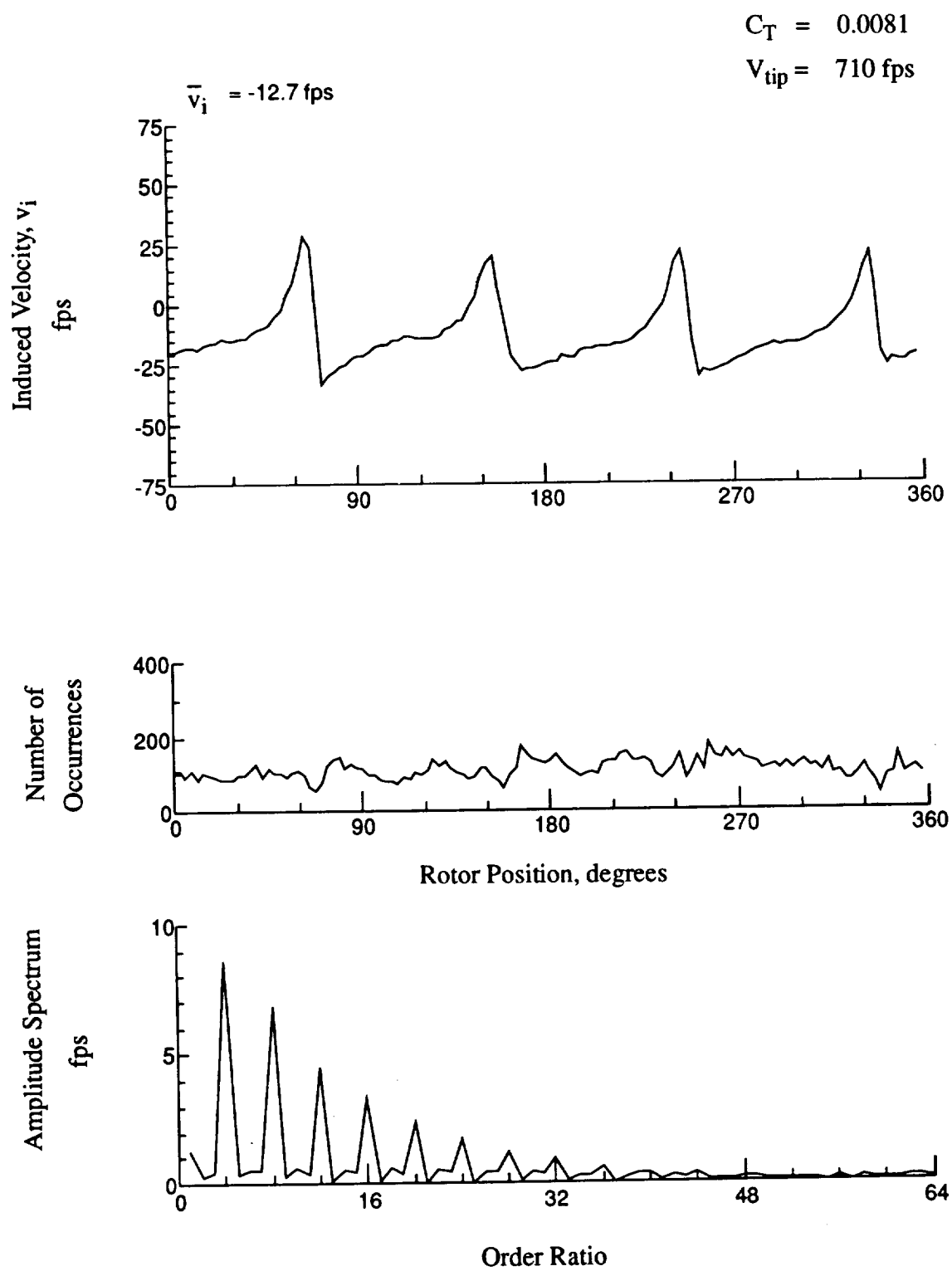


Figure 43.- Concluded.
 $x/R = 1.50$, $y/R = -0.20$, $z = 7.34 \text{ in.}$

$$C_T = 0.0081$$

$$V_{tip} = 710 \text{ fps}$$

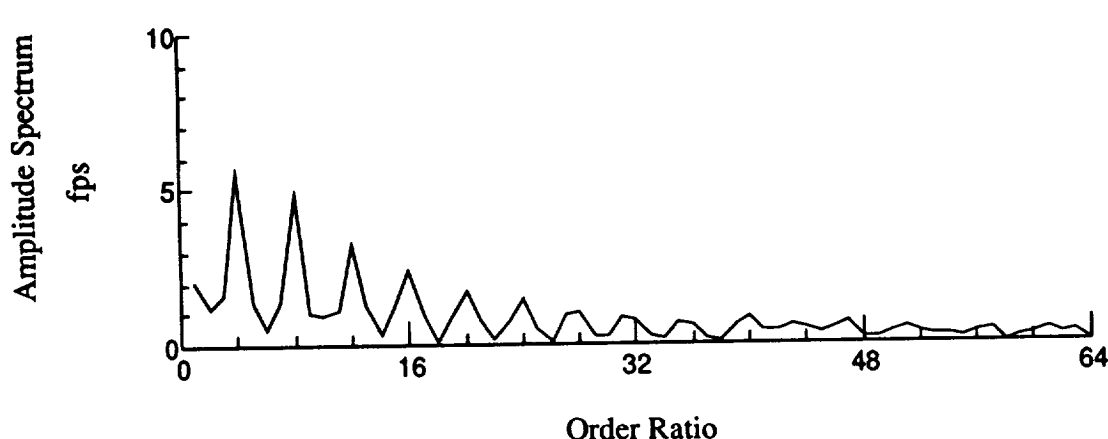
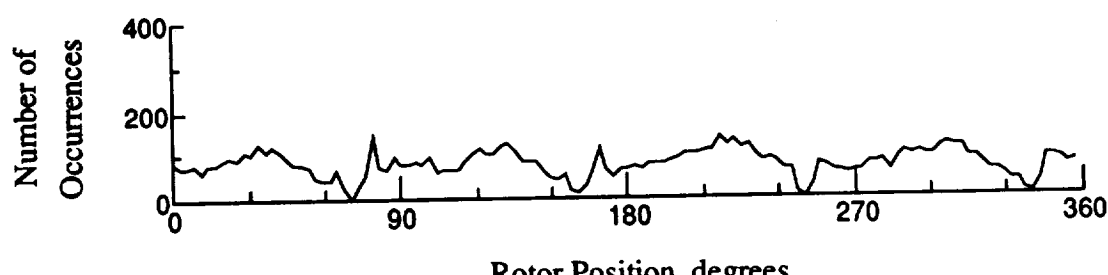
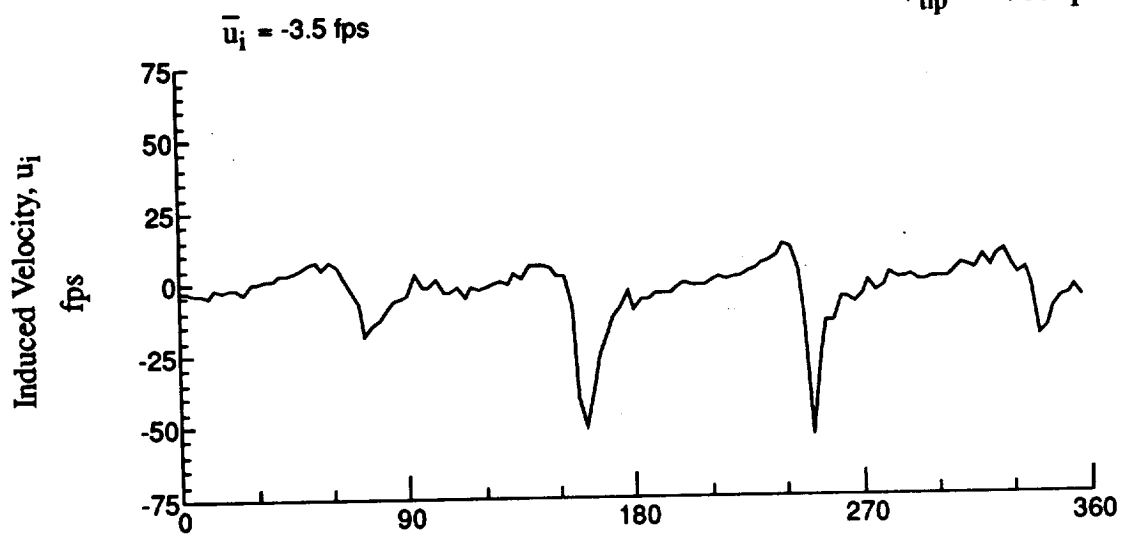


Figure 44.- Wake Measurements at
 $x/R = 1.50$, $y/R = -0.20$, $z = 6.31$ in.

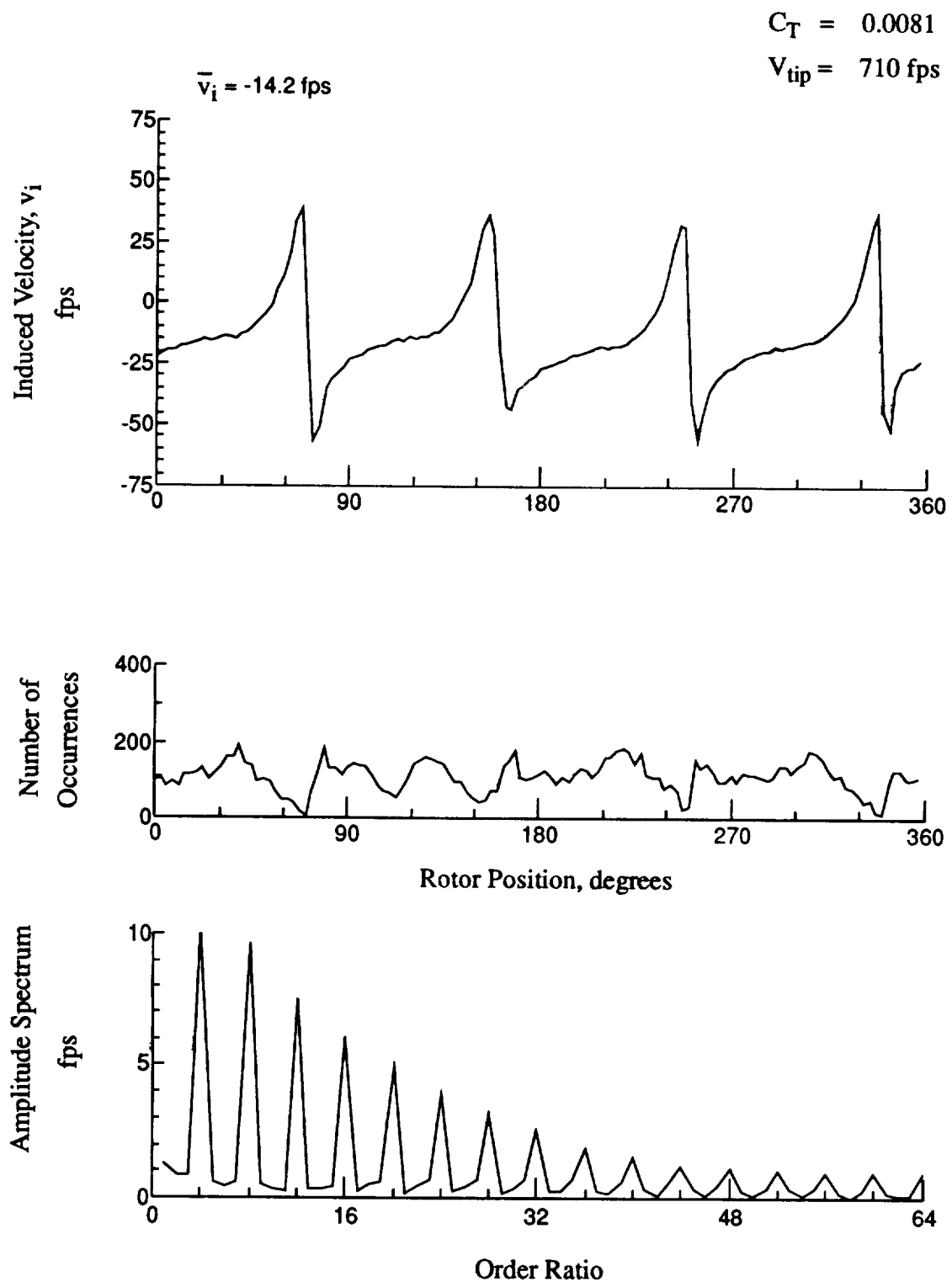


Figure 44.- Concluded.
 $x/R = 1.50$, $y/R = -0.20$, $z = 6.31 \text{ in.}$

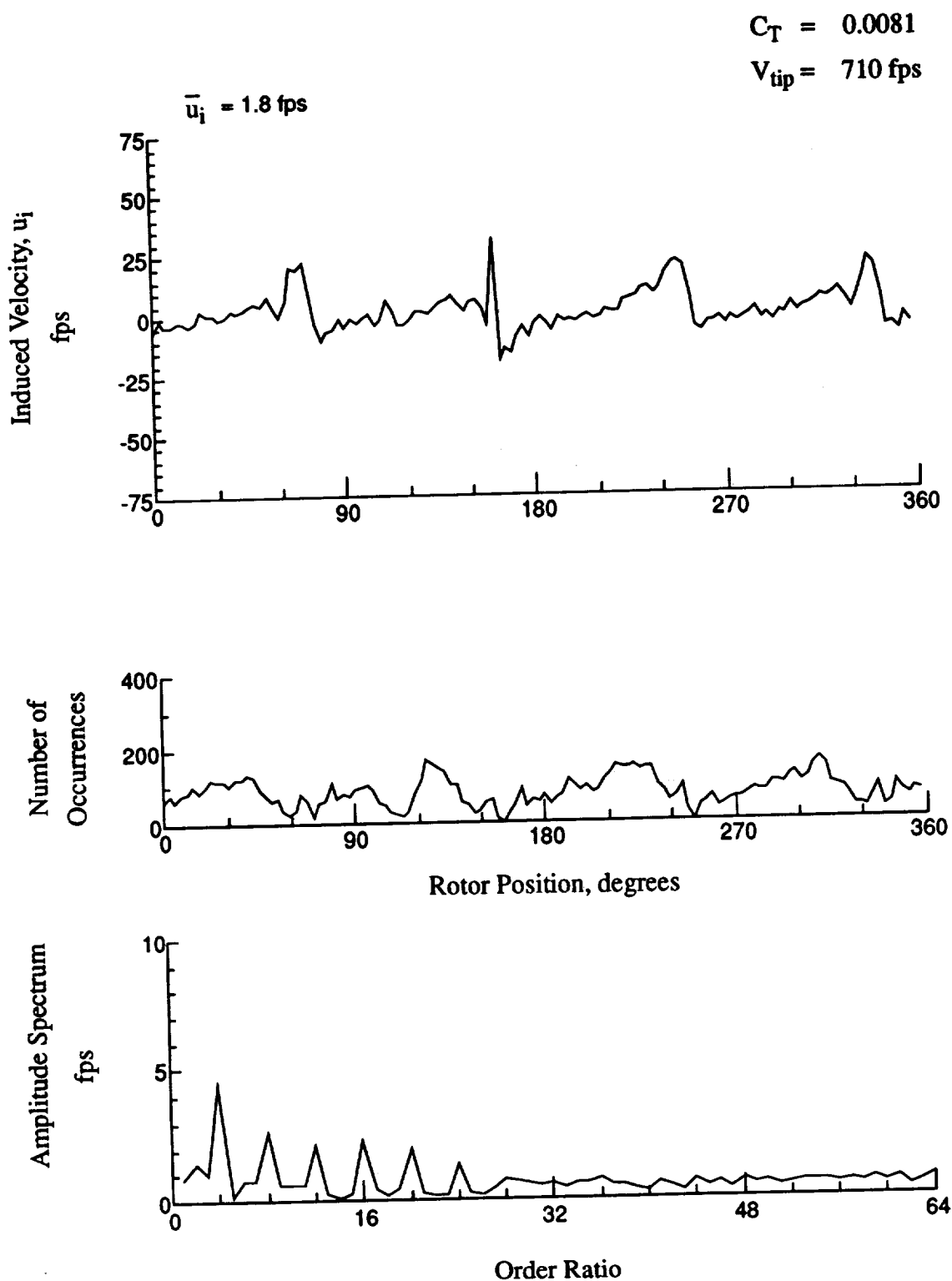


Figure 45.- Wake Measurements at
 $x/R = 1.50$, $y/R = -0.20$, $z = 5.28 \text{ in.}$

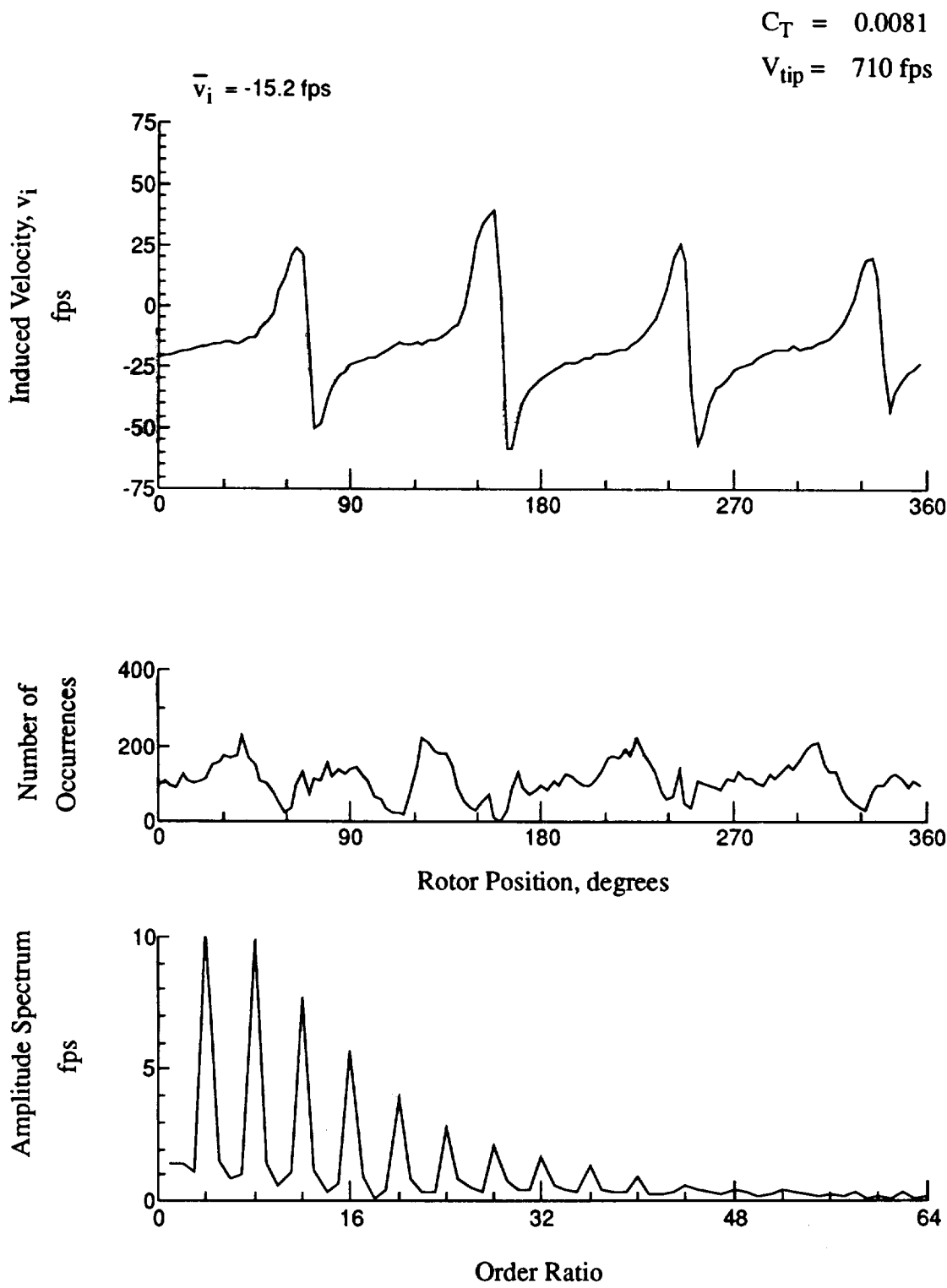


Figure 45.- Concluded.
 $x/R = 1.50$, $y/R = -0.20$, $z = 5.28 \text{ in.}$

$$C_T = 0.0081$$

$$V_{tip} = 710 \text{ fps}$$

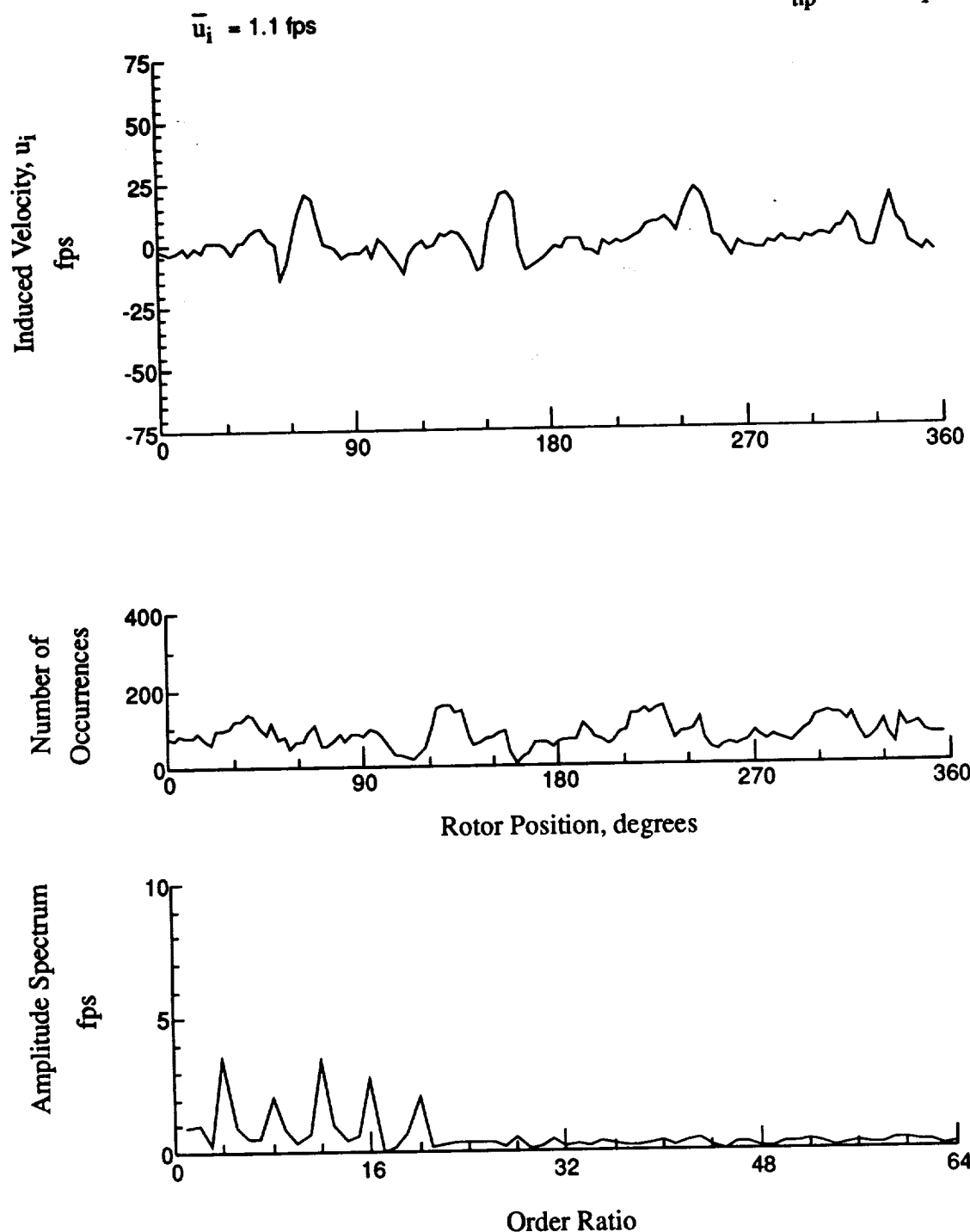


Figure 46.- Wake Measurements at
 $x/R = 1.50$, $y/R = -0.20$, $z = 4.25$ in.

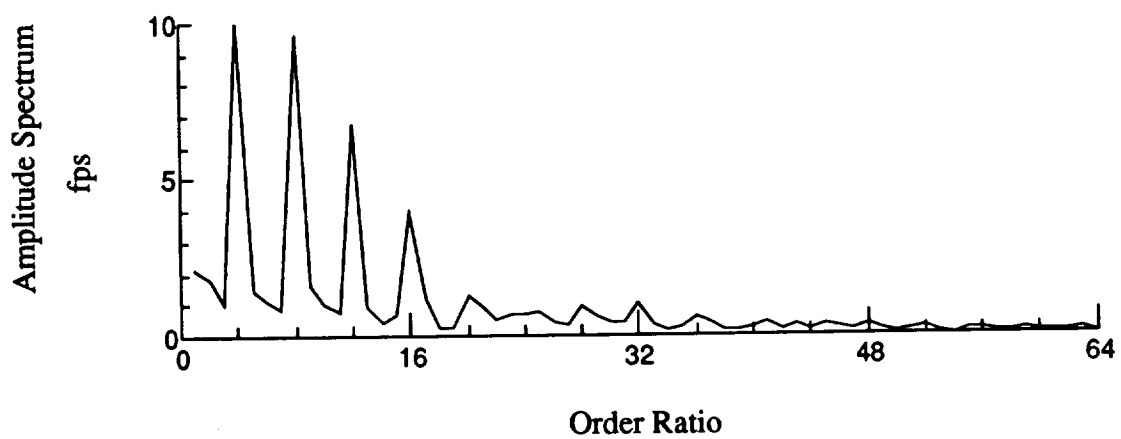
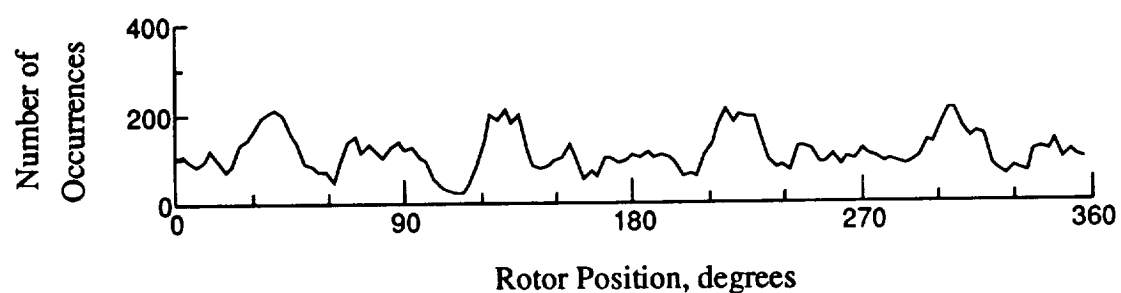
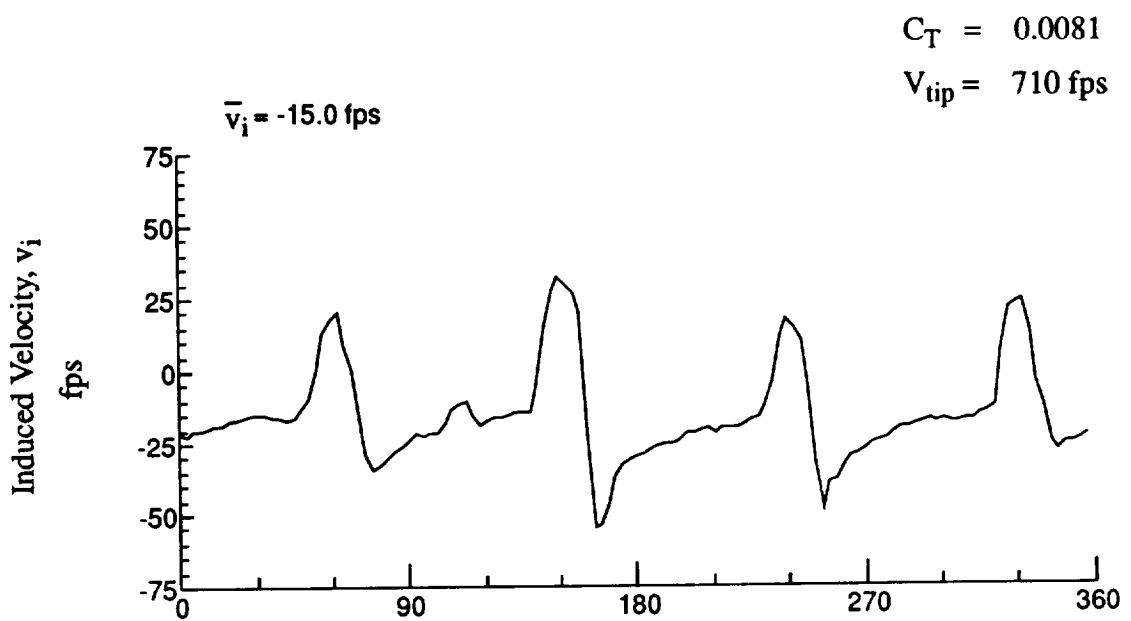


Figure 46.- Concluded.
 $x/R = 1.50$, $y/R = -0.20$, $z = 4.25 \text{ in.}$

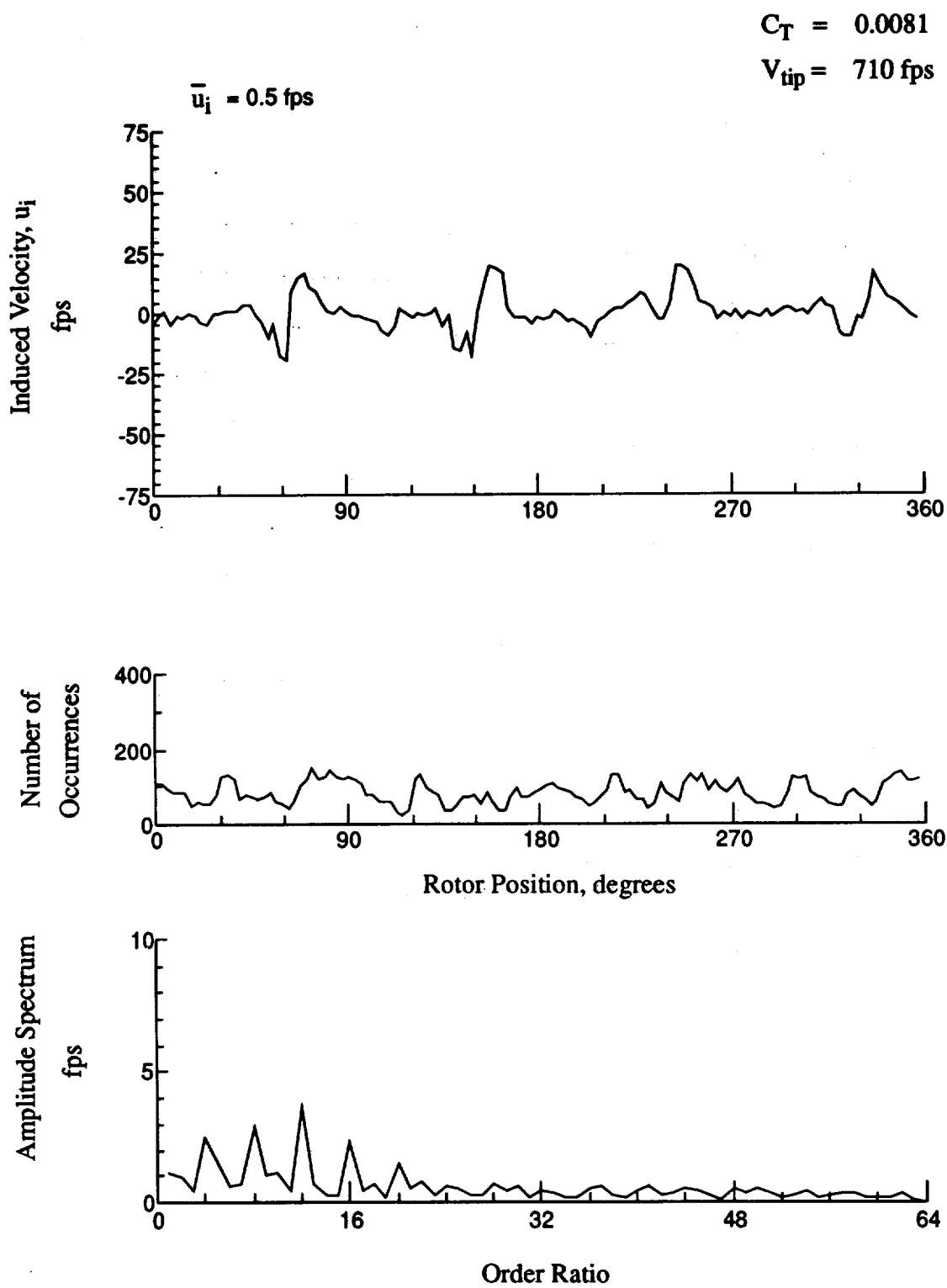


Figure 47.- Wake Measurements at
 $x/R = 1.50$, $y/R = -0.20$, $z = 3.22 \text{ in.}$

$$C_T = 0.0081$$

$$V_{tip} = 710 \text{ fps}$$

$$\bar{v}_i = -13.8 \text{ fps}$$

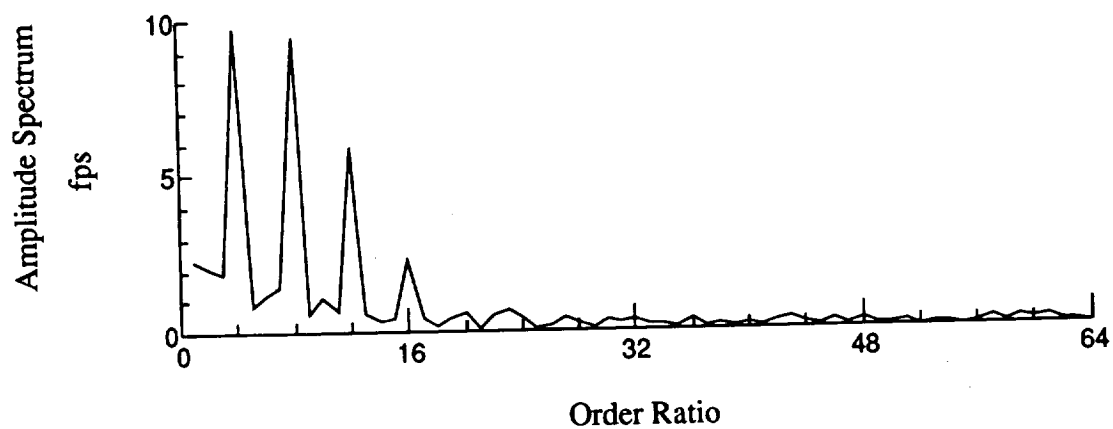
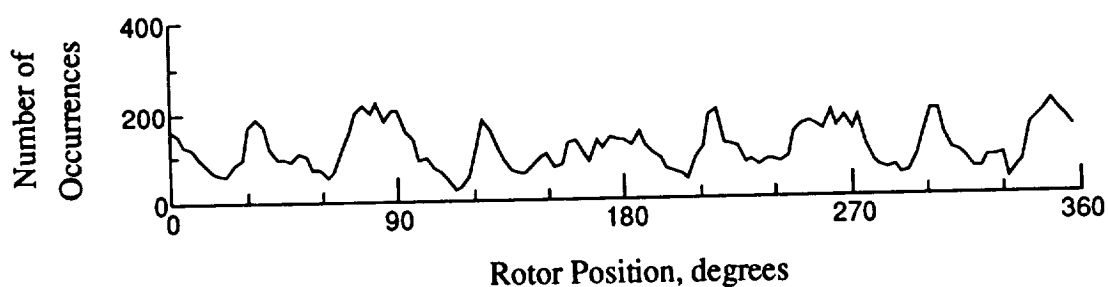
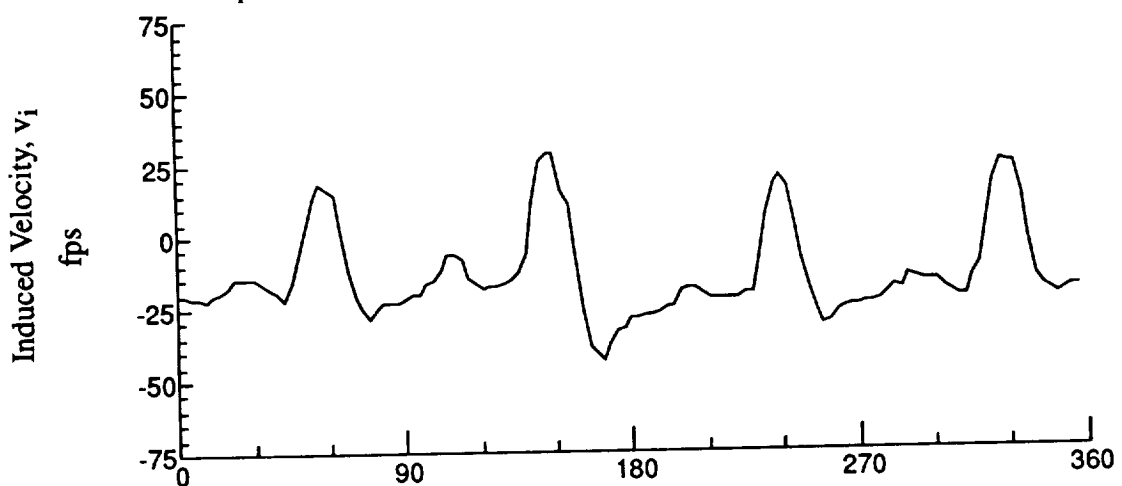


Figure 47.- Concluded.
 $x/R = 1.50$, $y/R = -0.20$, $z = 3.22$ in.

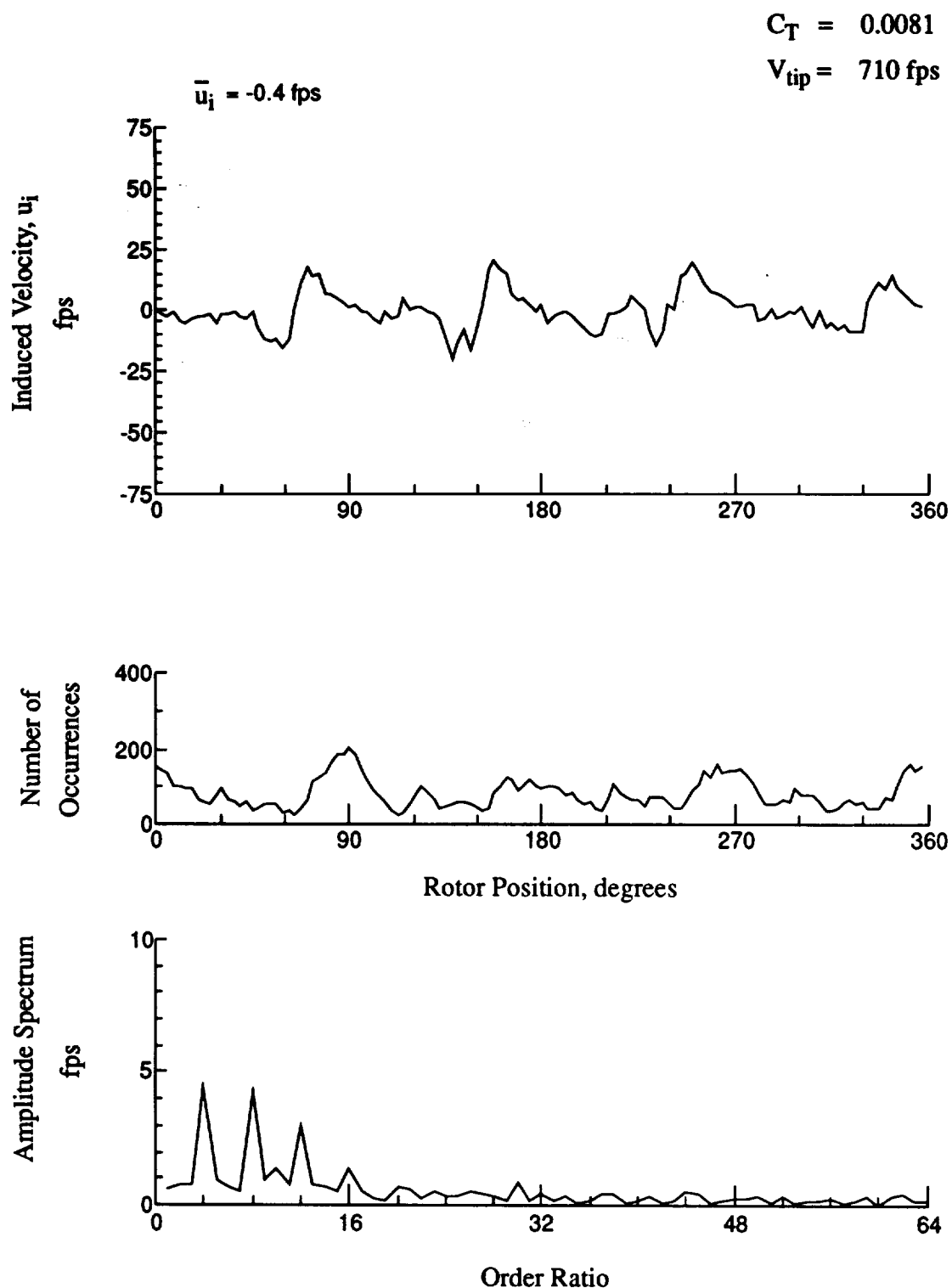


Figure 48.- Wake Measurements at
 $x/R = 1.50$, $y/R = -0.20$, $z = 2.19 \text{ in.}$

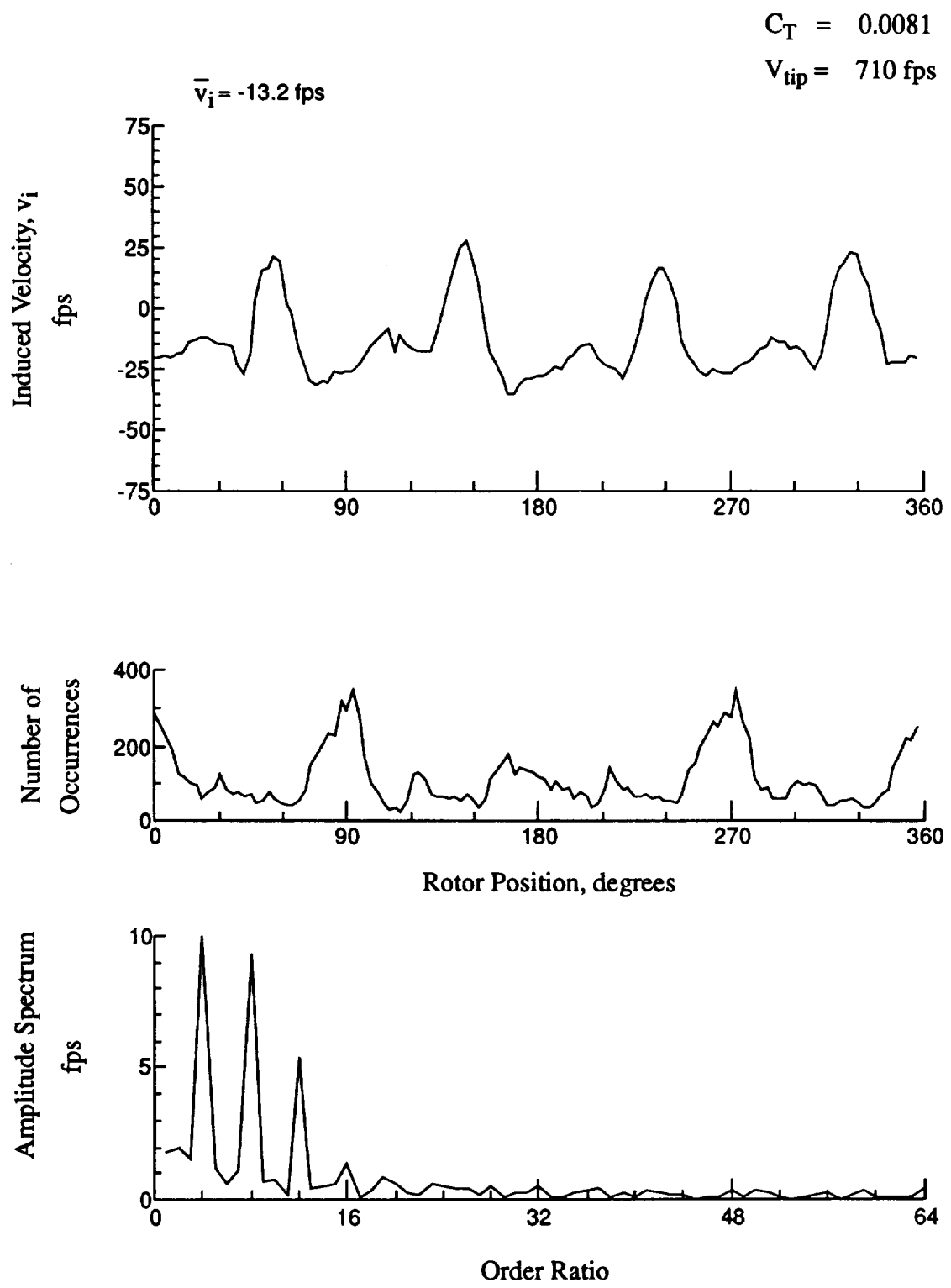


Figure 48.- Concluded.
 $x/R = 1.50$, $y/R = -0.20$, $z = 2.19 \text{ in.}$

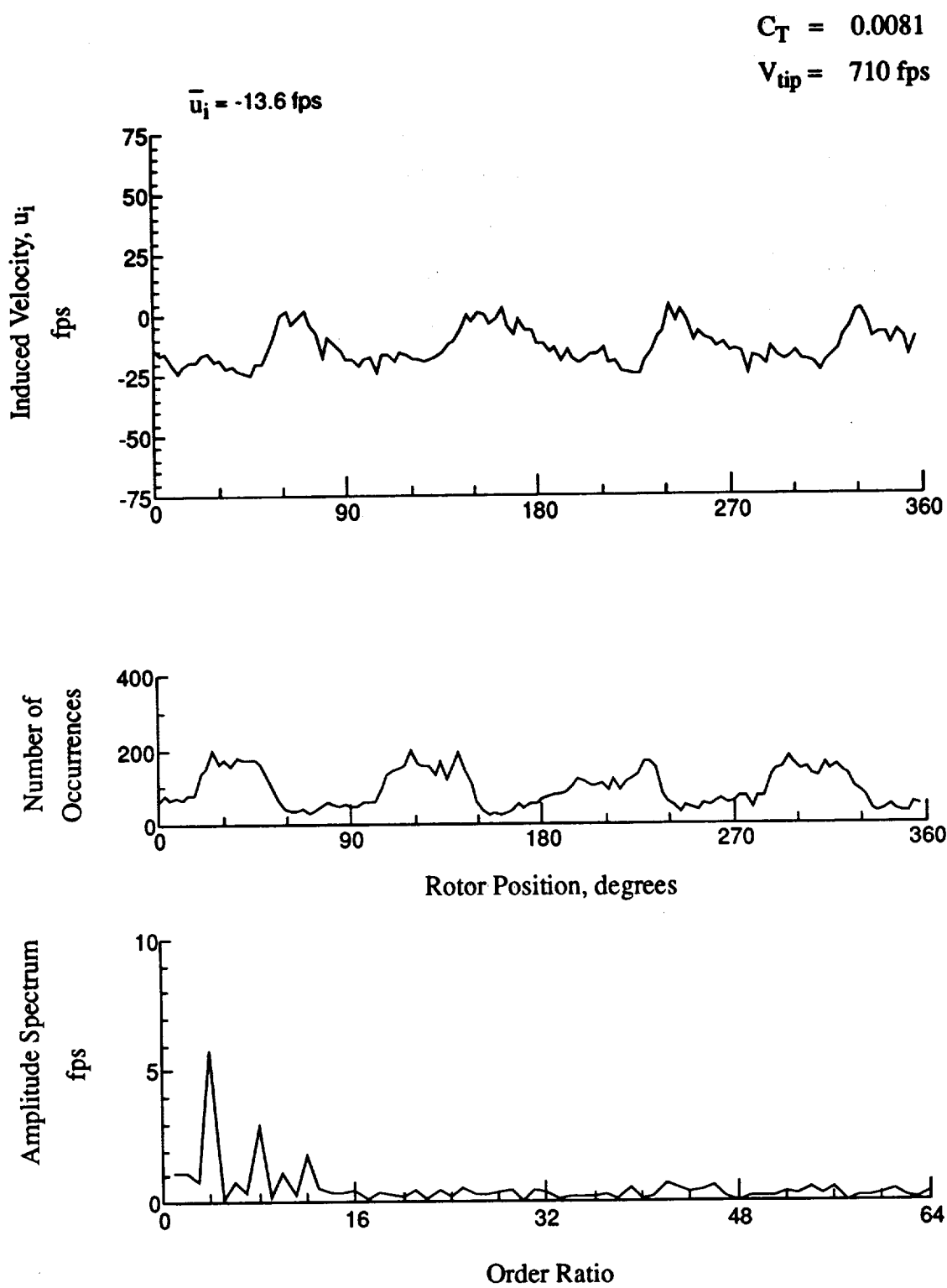


Figure 49.- Wake Measurements at
 $x/R = 1.50$, $y/R = -0.20$, $z = -1.23$ in.

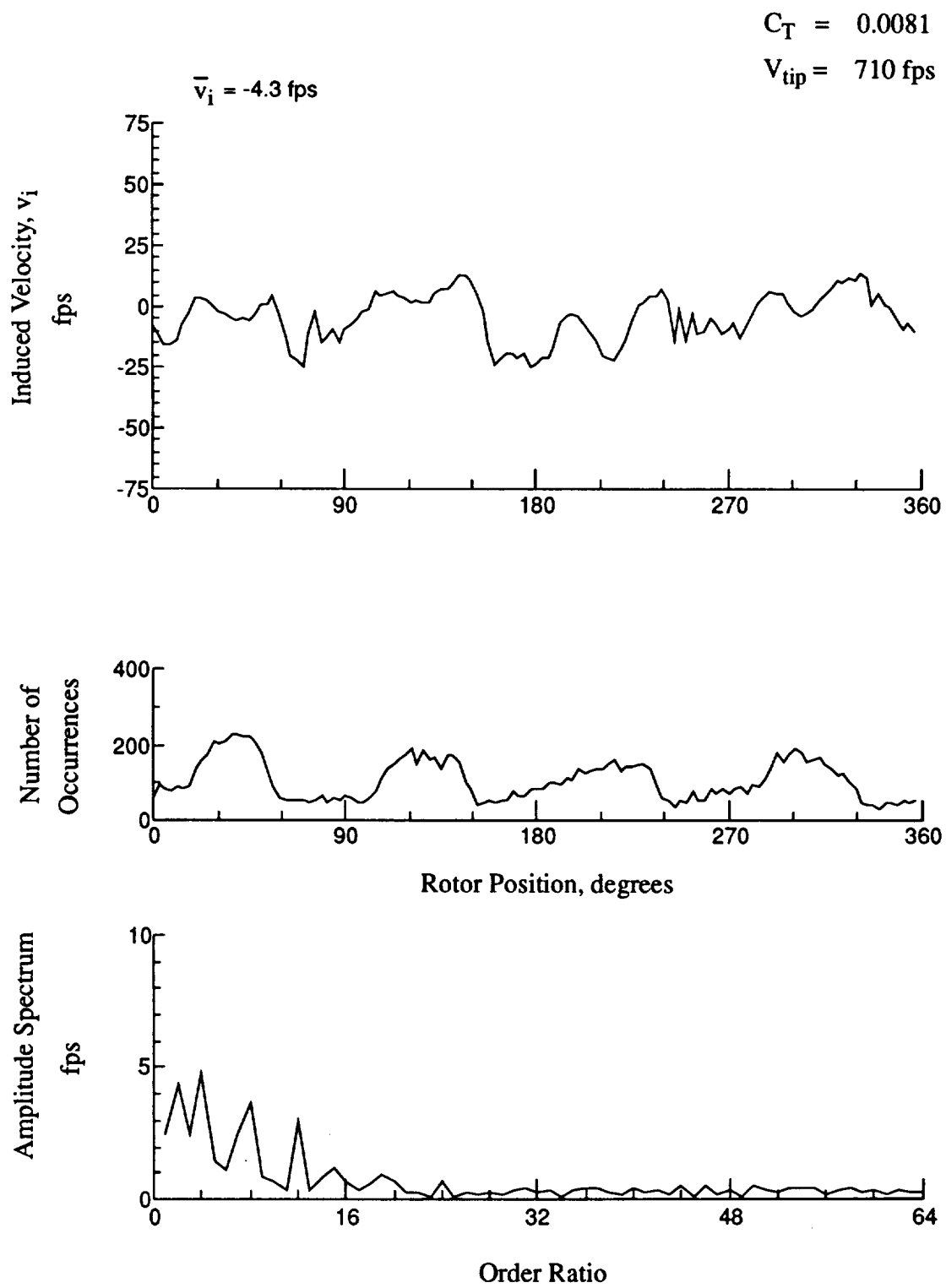


Figure 49.- Concluded.
 $x/R = 1.50$, $y/R = -0.20$, $z = -1.23 \text{ in.}$

$$C_T = 0.0081$$

$$V_{tip} = 710 \text{ fps}$$

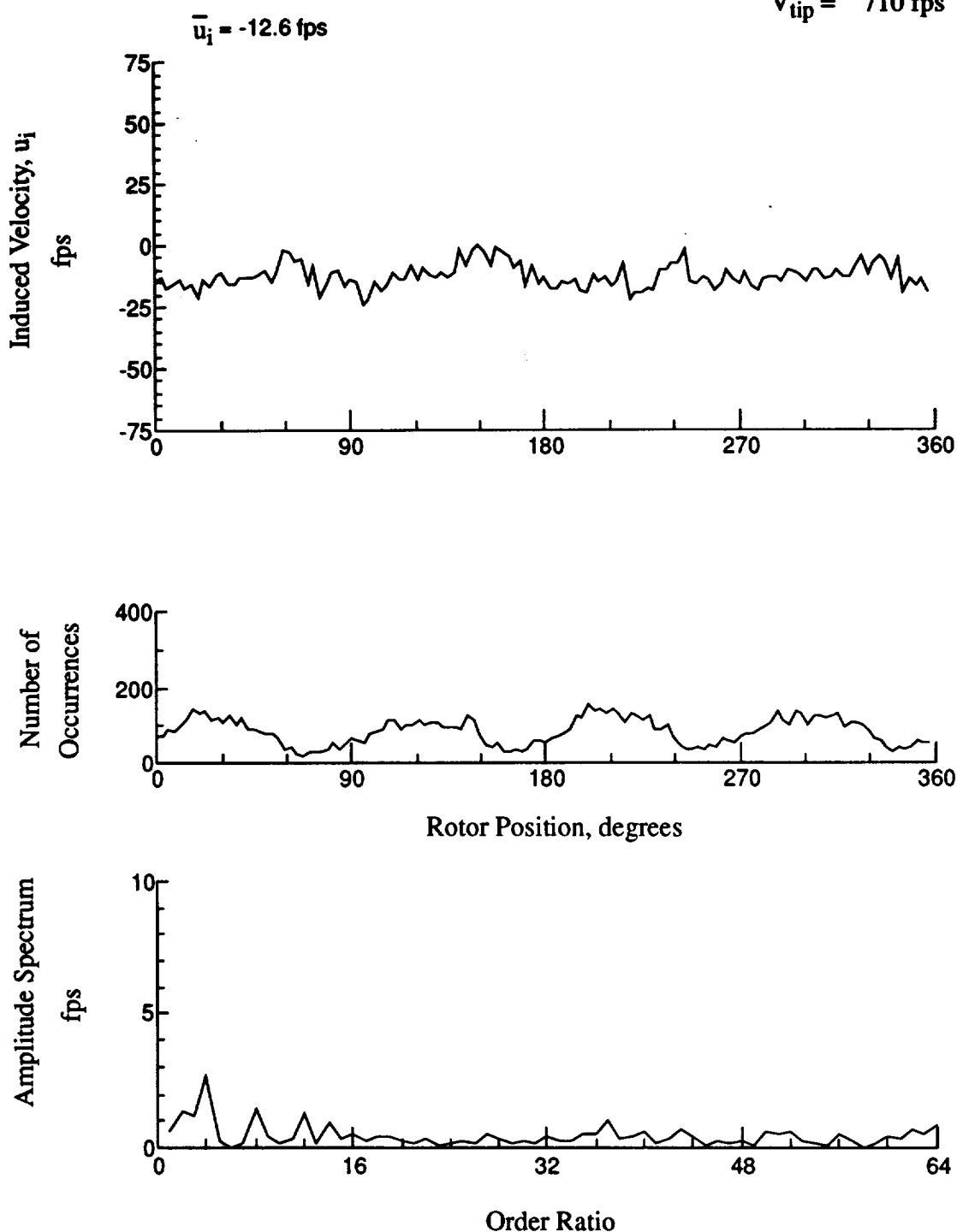


Figure 50.- Wake Measurements at
 $x/R = 1.50$, $y/R = -0.20$, $z = -2.26$ in.

$$C_T = 0.0081$$

$$V_{tip} = 710 \text{ fps}$$

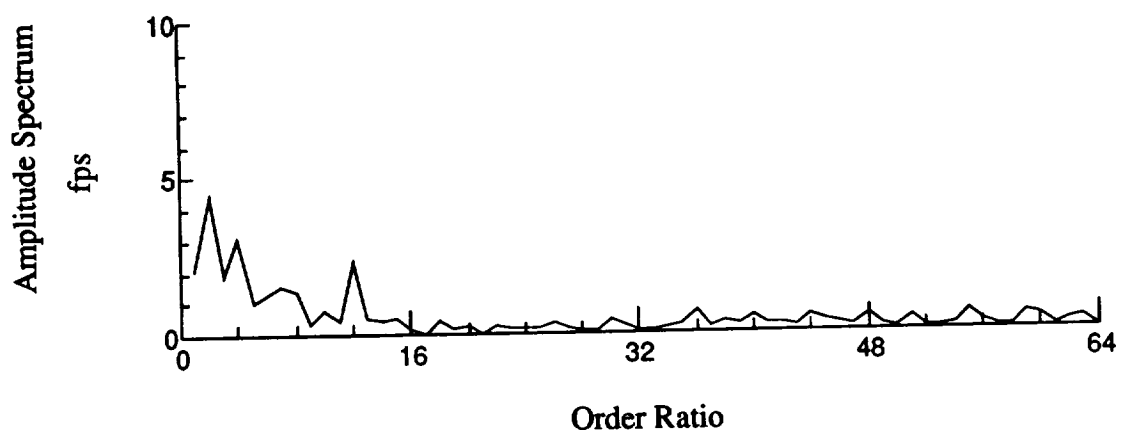
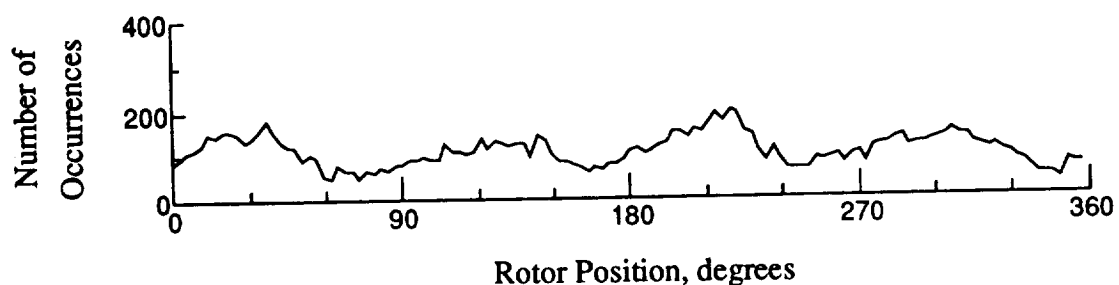
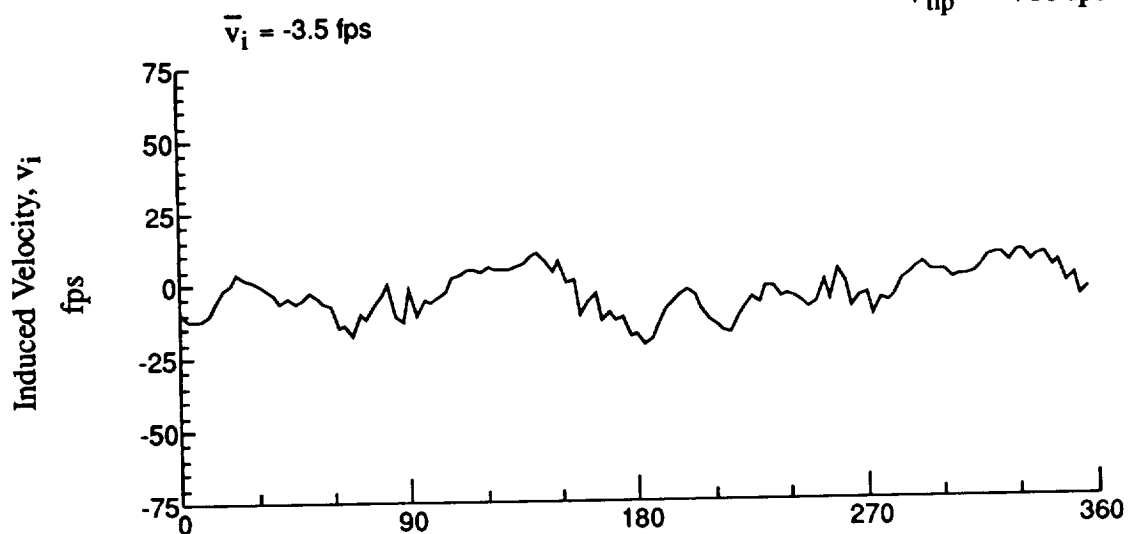


Figure 50.- Concluded.
 $x/R = 1.50$, $y/R = -0.20$, $z = -2.26 \text{ in.}$

$$C_T = 0.0081$$

$$V_{tip} = 710 \text{ fps}$$

$$\bar{u}_i = -16.3 \text{ fps}$$

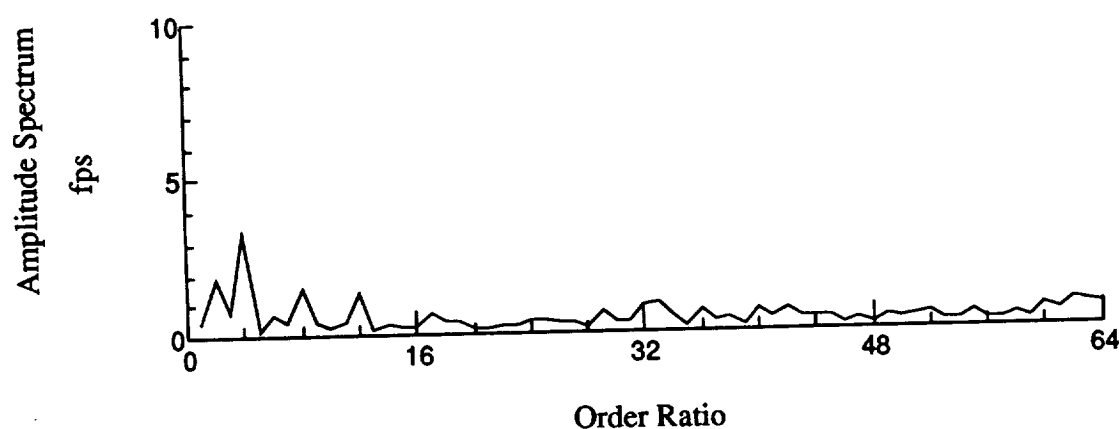
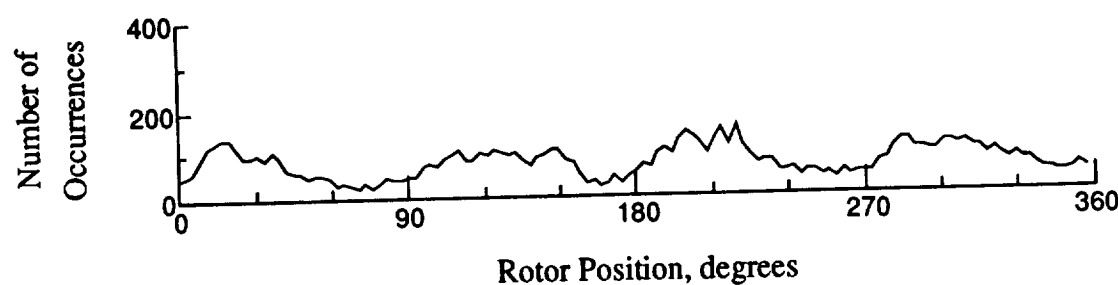
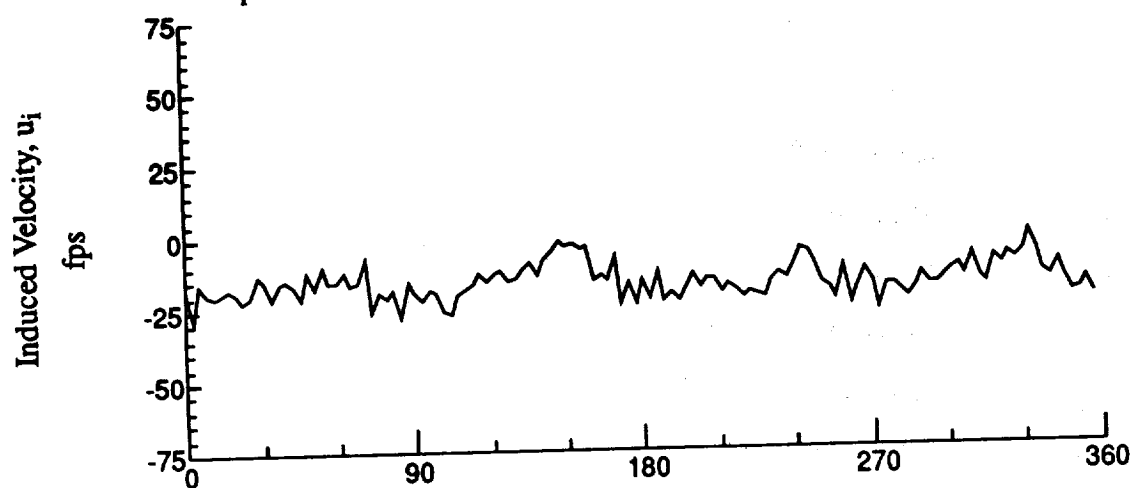


Figure 51.- Wake Measurements at
 $x/R = 1.50$, $y/R = -0.20$, $z = -3.20$ in.

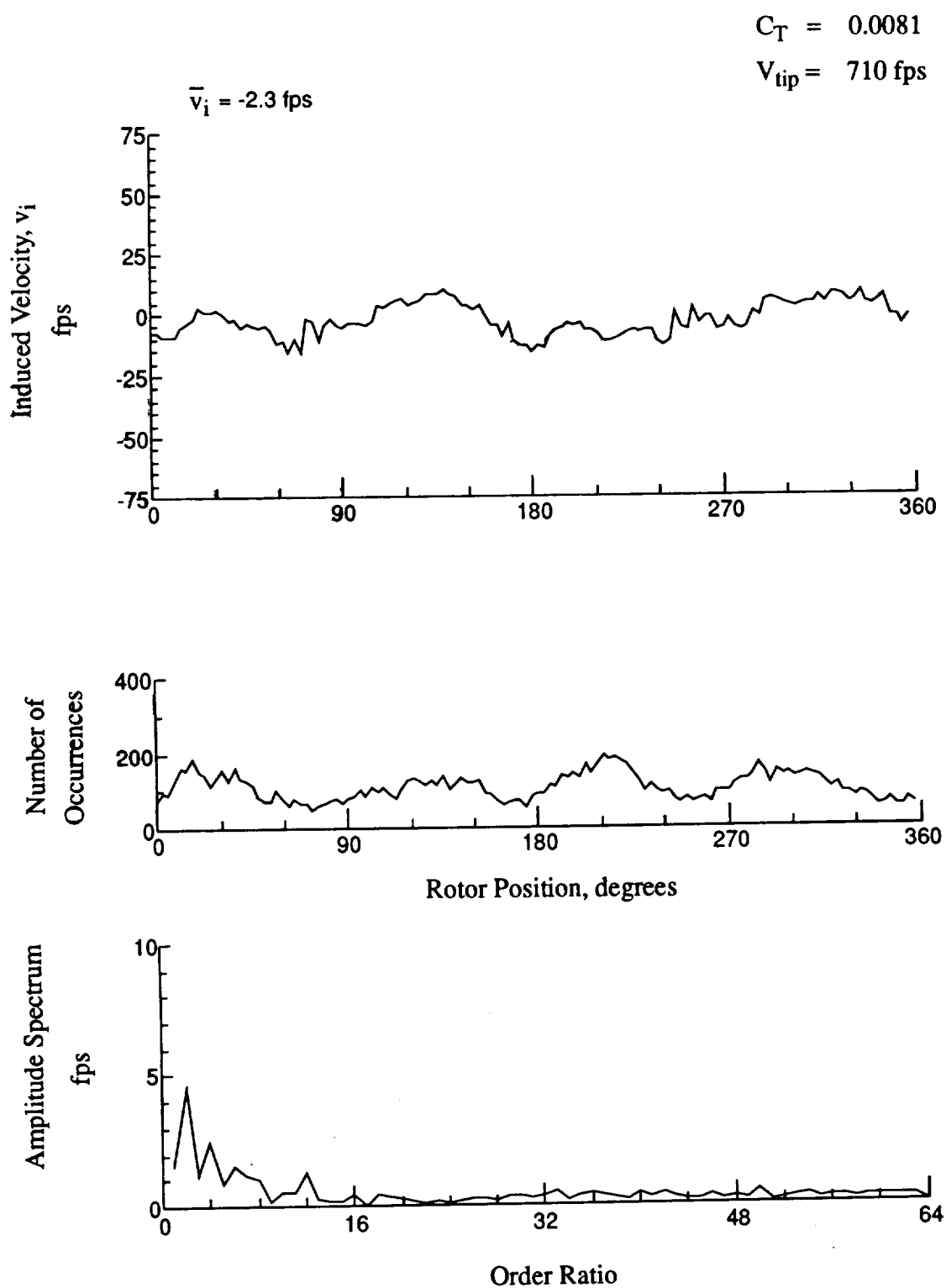


Figure 51.- Concluded.
 $x/R = 1.50$, $y/R = -0.20$, $z = -3.20 \text{ in.}$

$$C_T = 0.0081$$

$$V_{tip} = 710 \text{ fps}$$

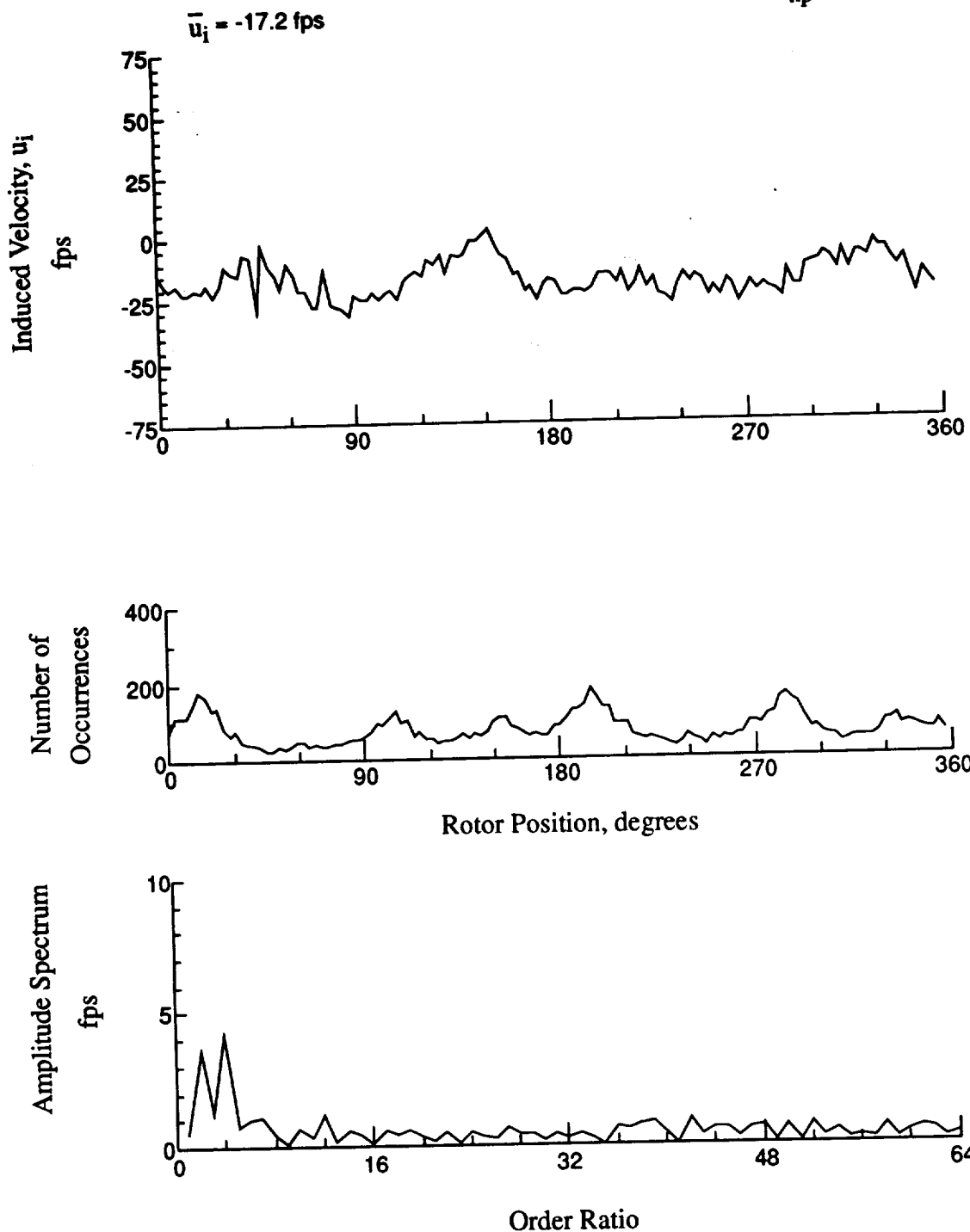


Figure 52.- Wake Measurements at
 $x/R = 1.50$, $y/R = -0.20$, $z = -4.32 \text{ in.}$

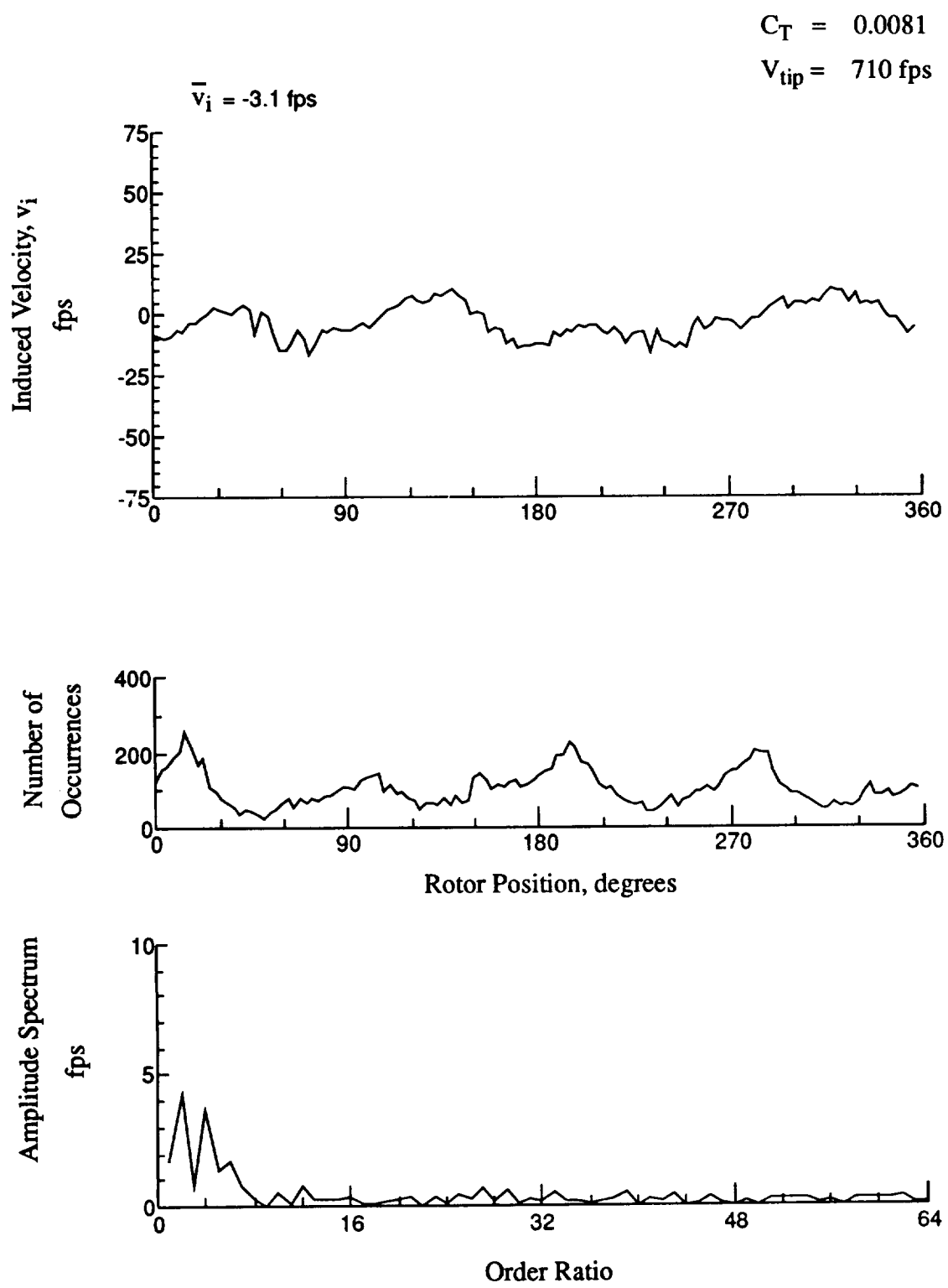
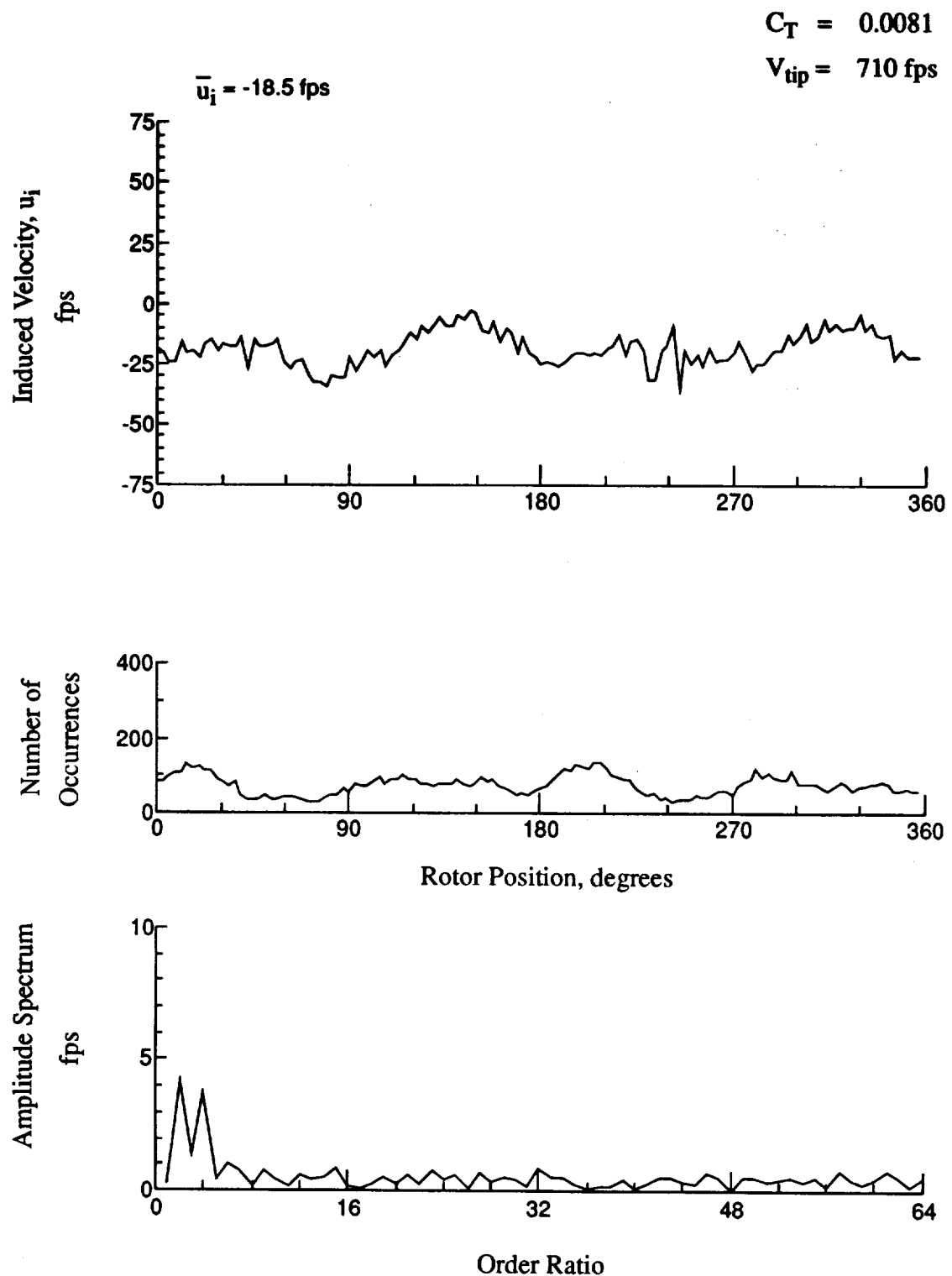


Figure 52.- Concluded.
 $x/R = 1.50$, $y/R = -0.20$, $z = -4.32 \text{ in.}$



**Figure 53.- Wake Measurements at
 $x/R = 1.50$, $y/R = -0.20$, $z = -5.35 \text{ in.}$**

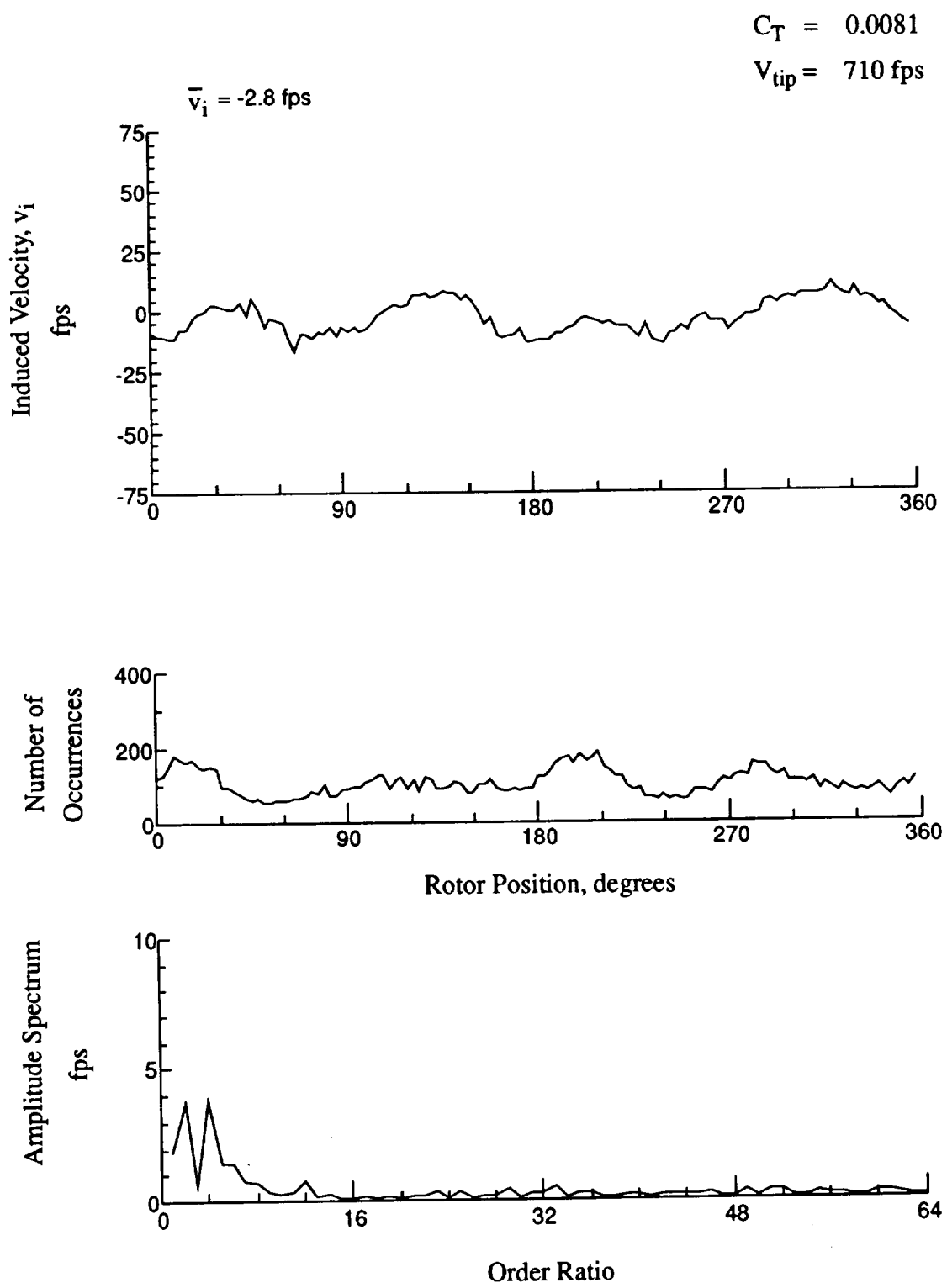


Figure 53.- Concluded.
 $x/R = 1.50$, $y/R = -0.20$, $z = -5.35 \text{ in.}$

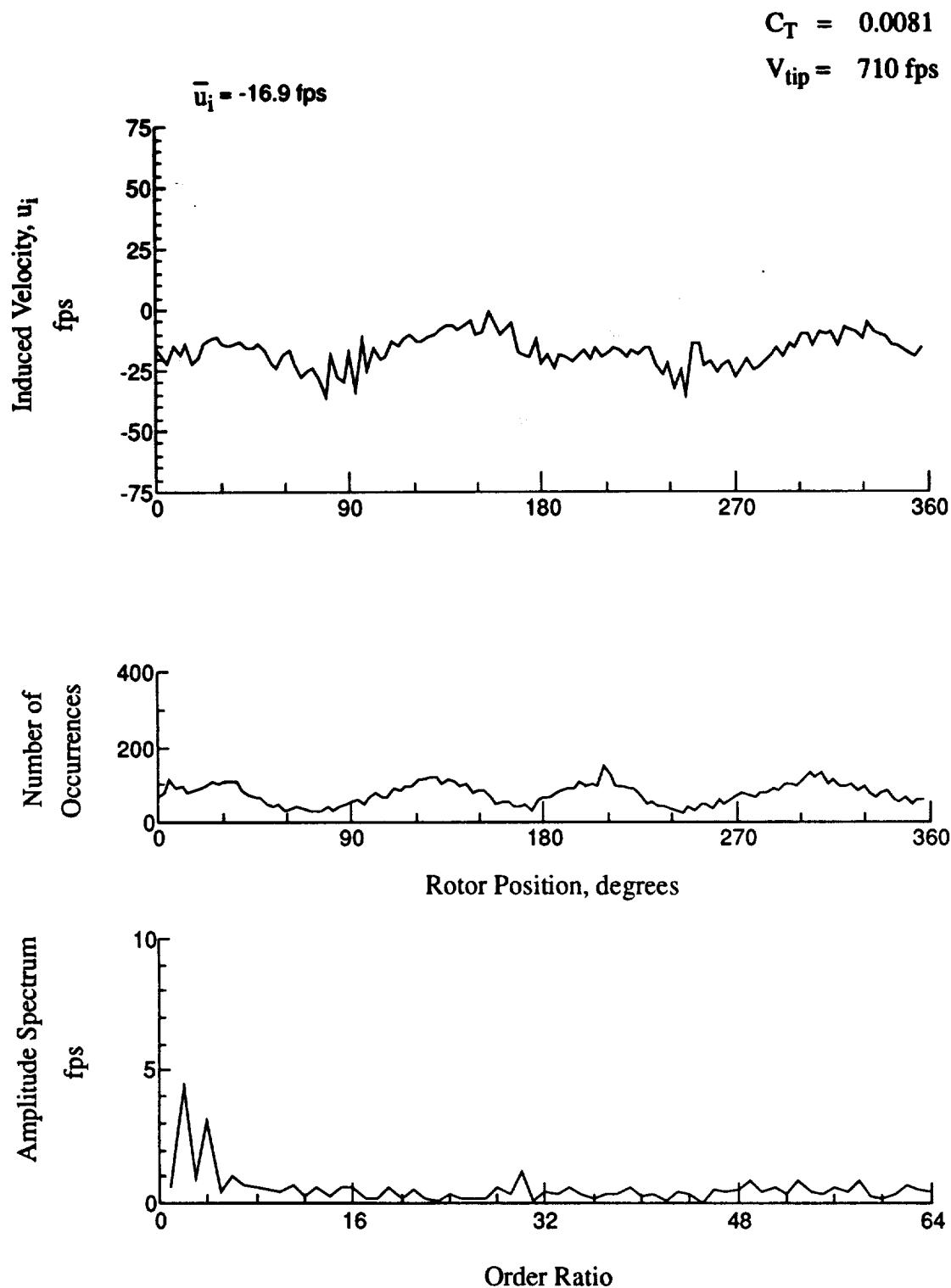


Figure 54.- Wake Measurements at
 $x/R = 1.50$, $y/R = -0.20$, $z = -6.38 \text{ in.}$

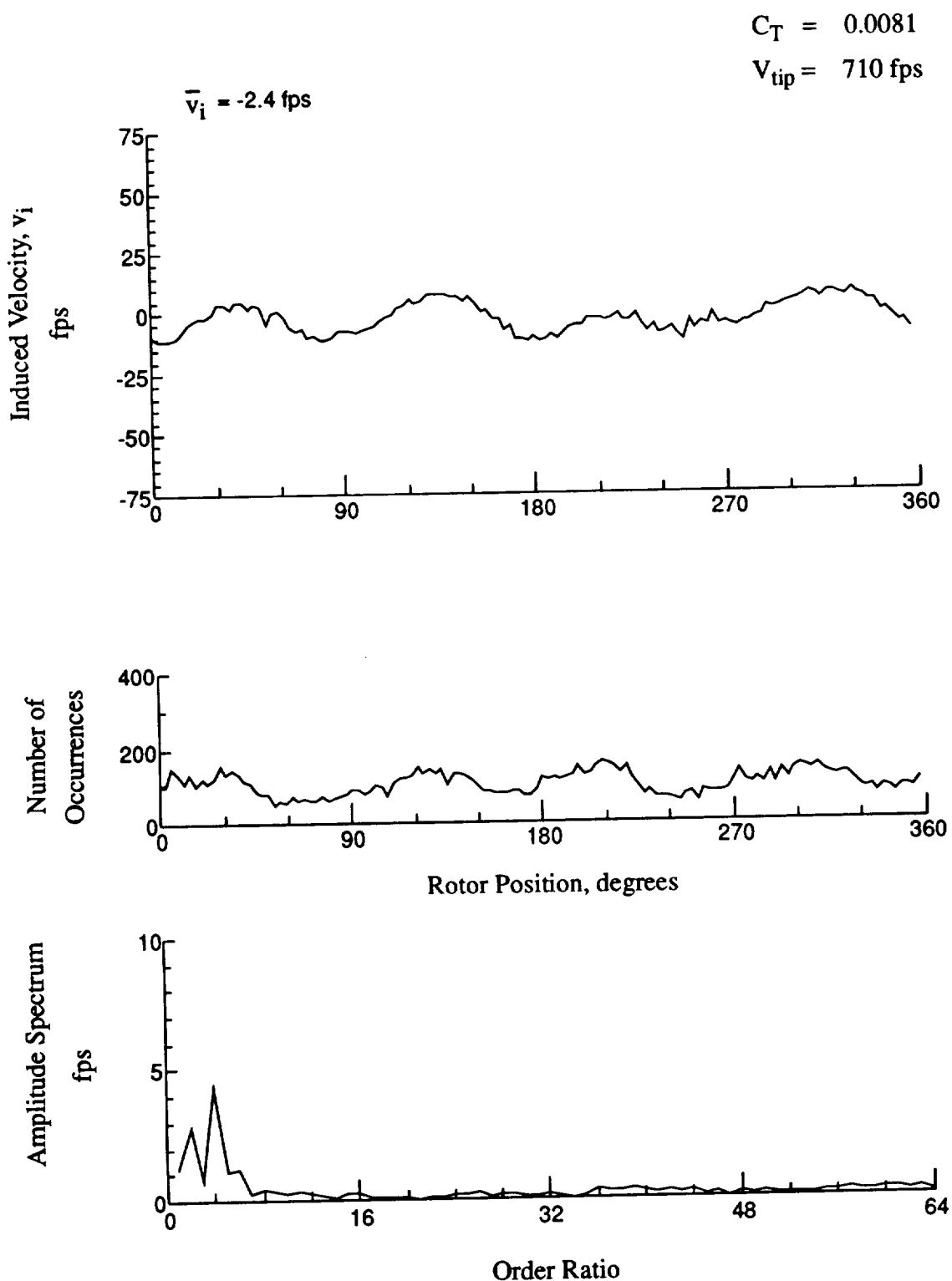


Figure 54.- Concluded.
 $x/R = 1.50$, $y/R = -0.20$, $z = -6.38 \text{ in.}$

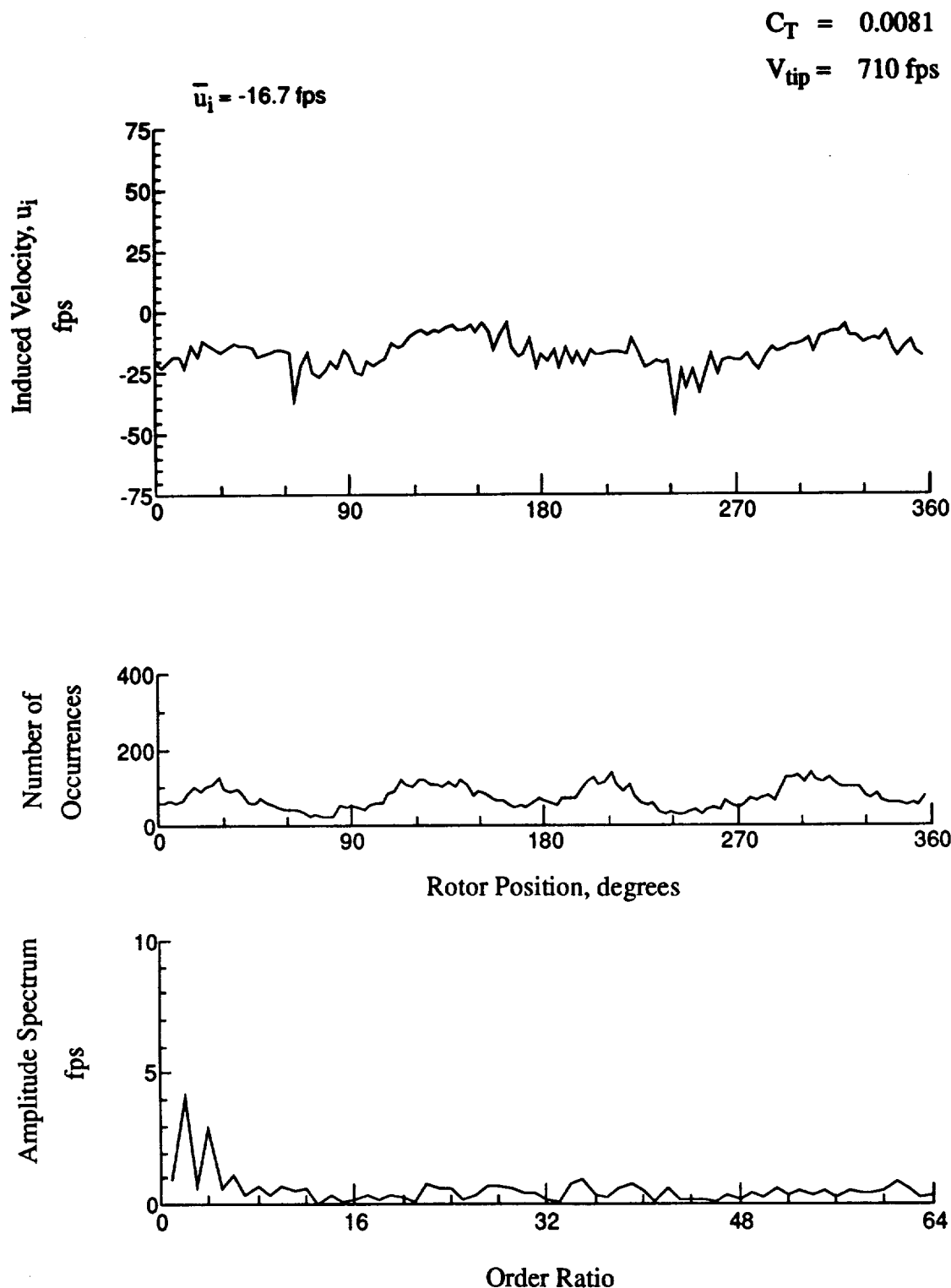


Figure 55.- Wake Measurements at
 $x/R = 1.50$, $y/R = -0.20$, $z = -7.41 \text{ in.}$

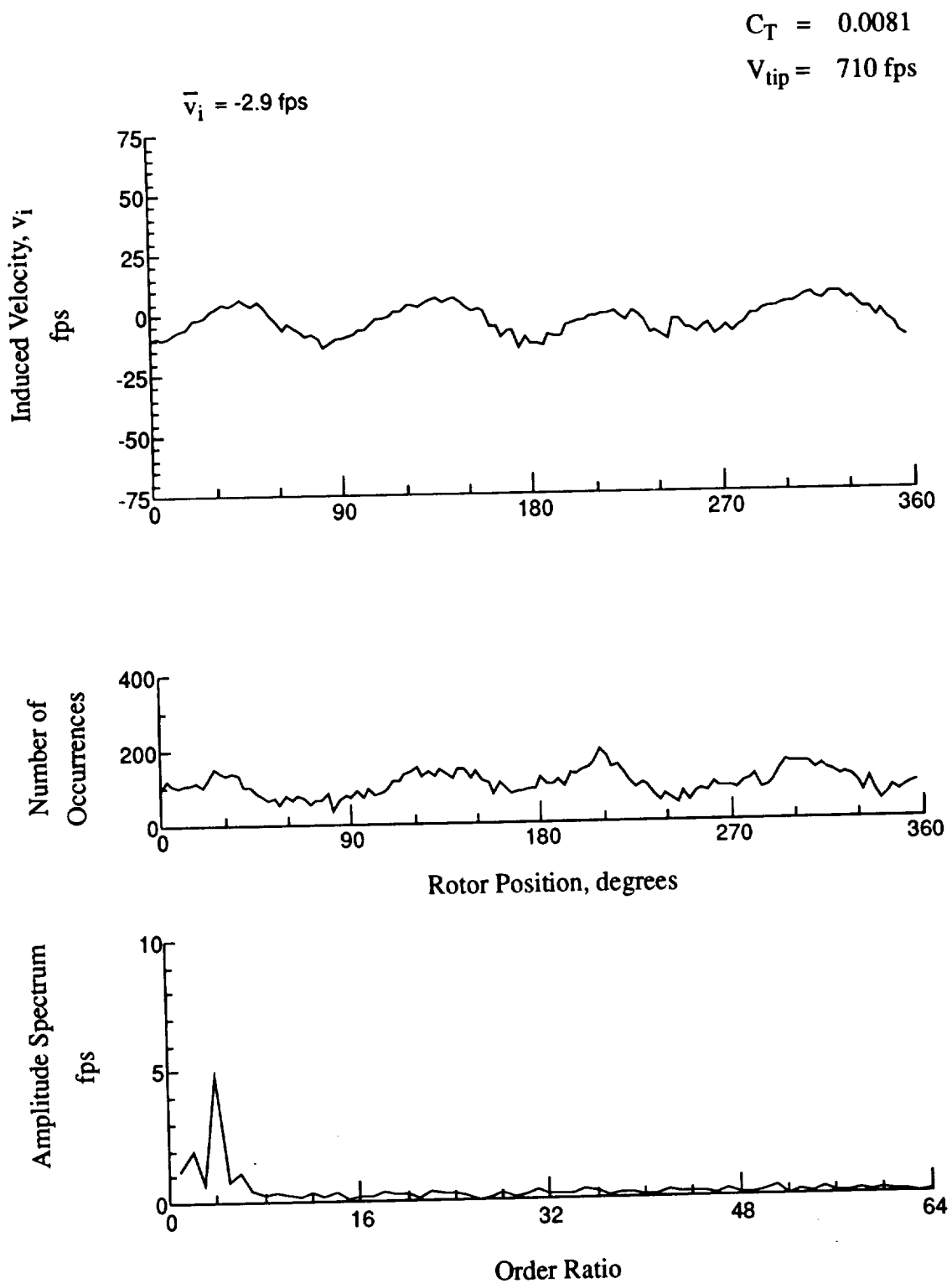


Figure 55.- Concluded.
 $x/R = 1.50$, $y/R = -0.20$, $z = -7.41 \text{ in.}$

$$C_T = 0.0081$$

$$V_{tip} = 710 \text{ fps}$$

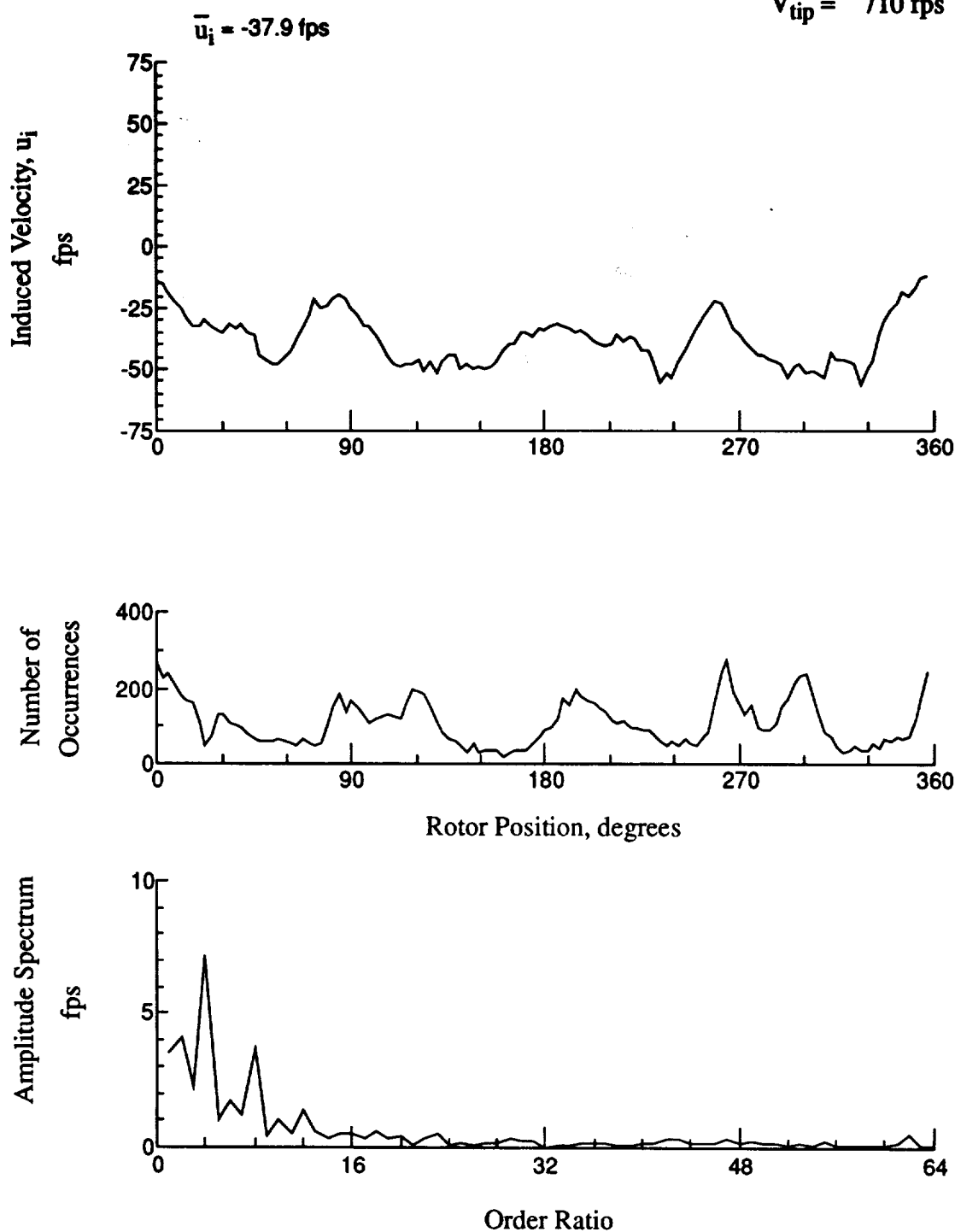


Figure 56.- Wake Measurements at
 $x/R = -0.27$, $y/R = 0.20$, $z = 0.21$ in.

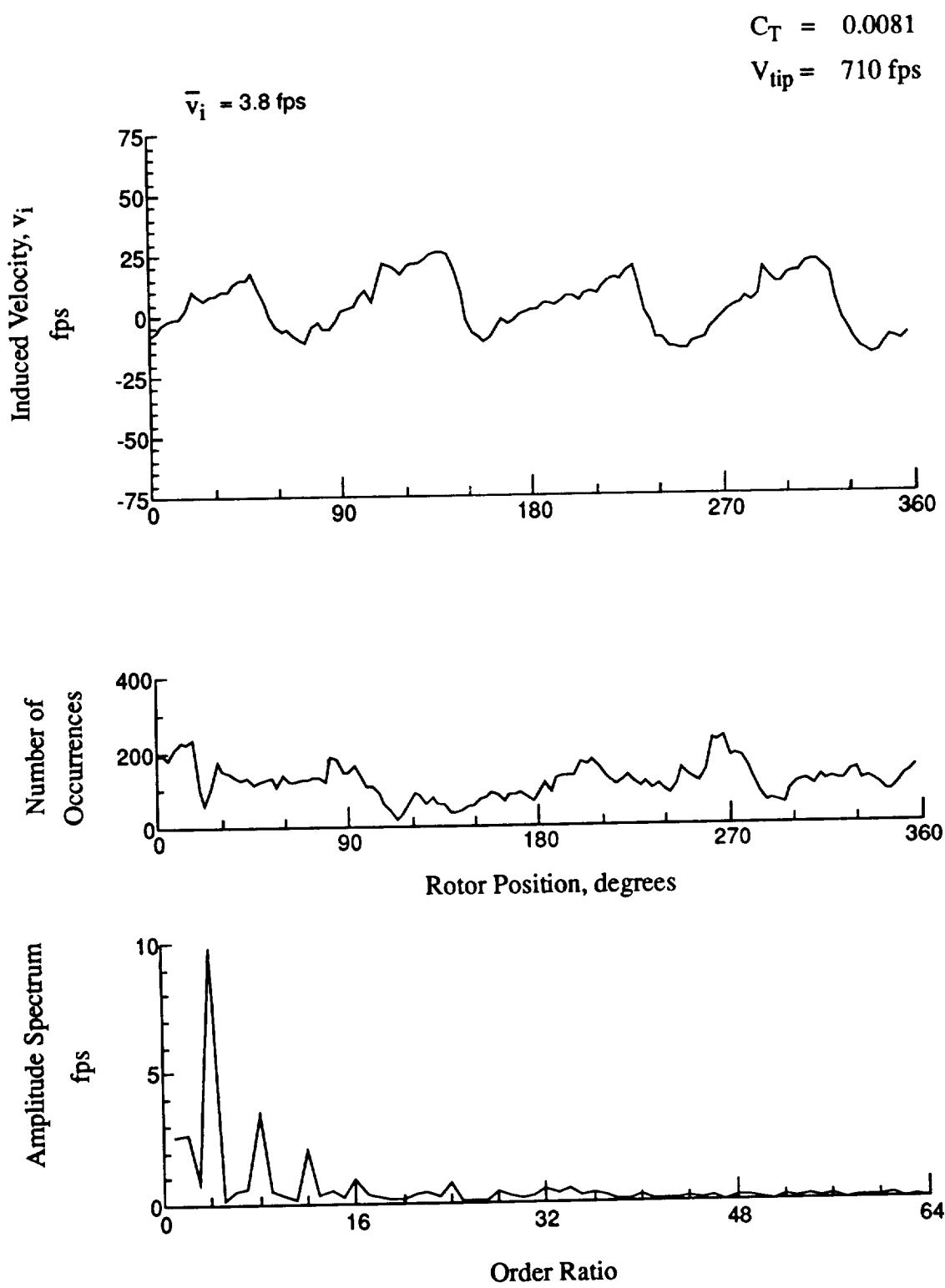


Figure 56.- Concluded.
 $x/R = -0.27$, $y/R = 0.20$, $z = 0.21 \text{ in.}$

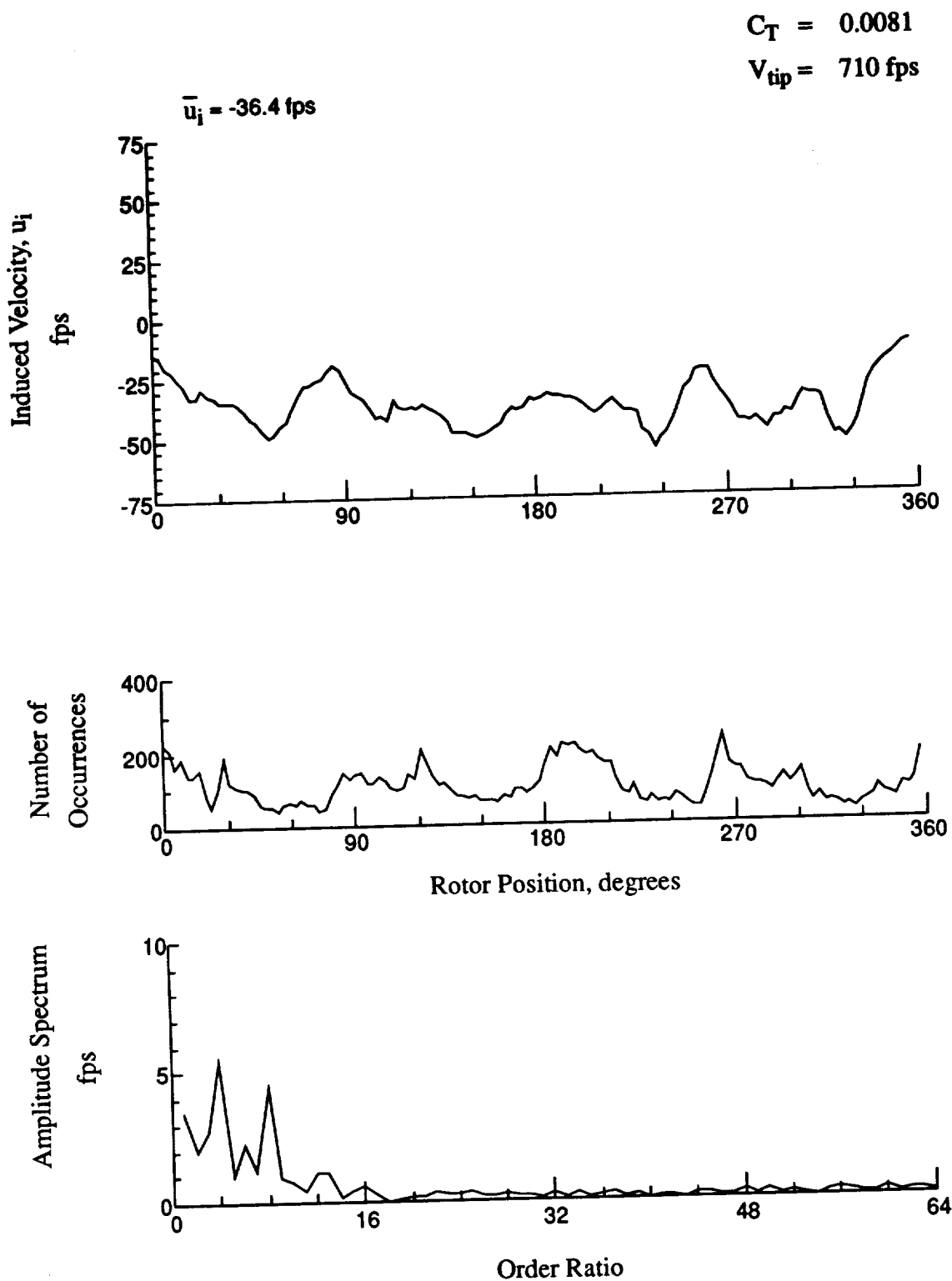


Figure 57.- Wake Measurements at
 $x/R = -0.27$, $y/R = 0.20$, $z = -1.85 \text{ in.}$

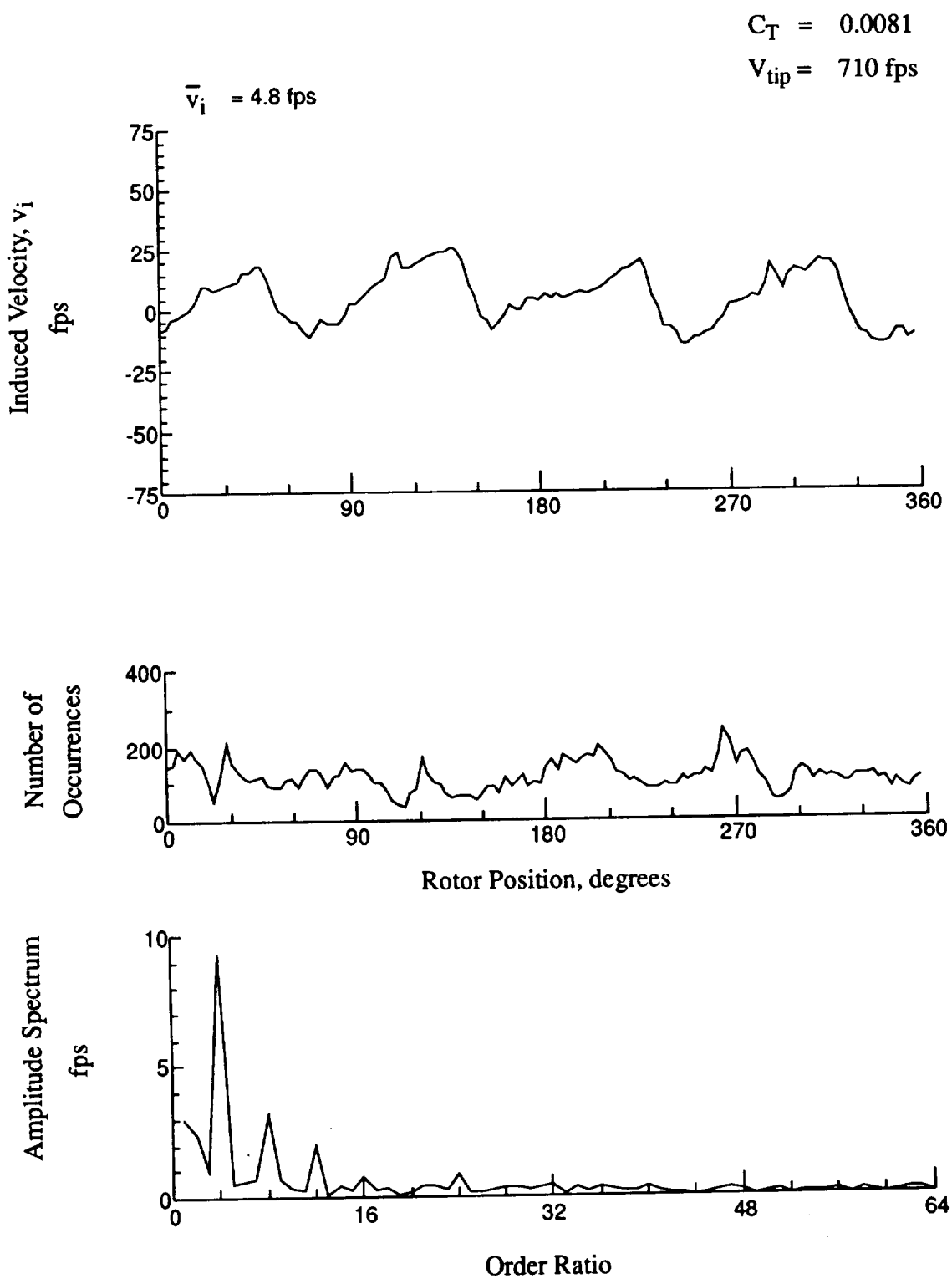


Figure 57.- Concluded.
 $x/R = -0.27$, $y/R = 0.20$, $z = -1.85 \text{ in.}$

$$C_T = 0.0081$$

$$V_{tip} = 710 \text{ fps}$$

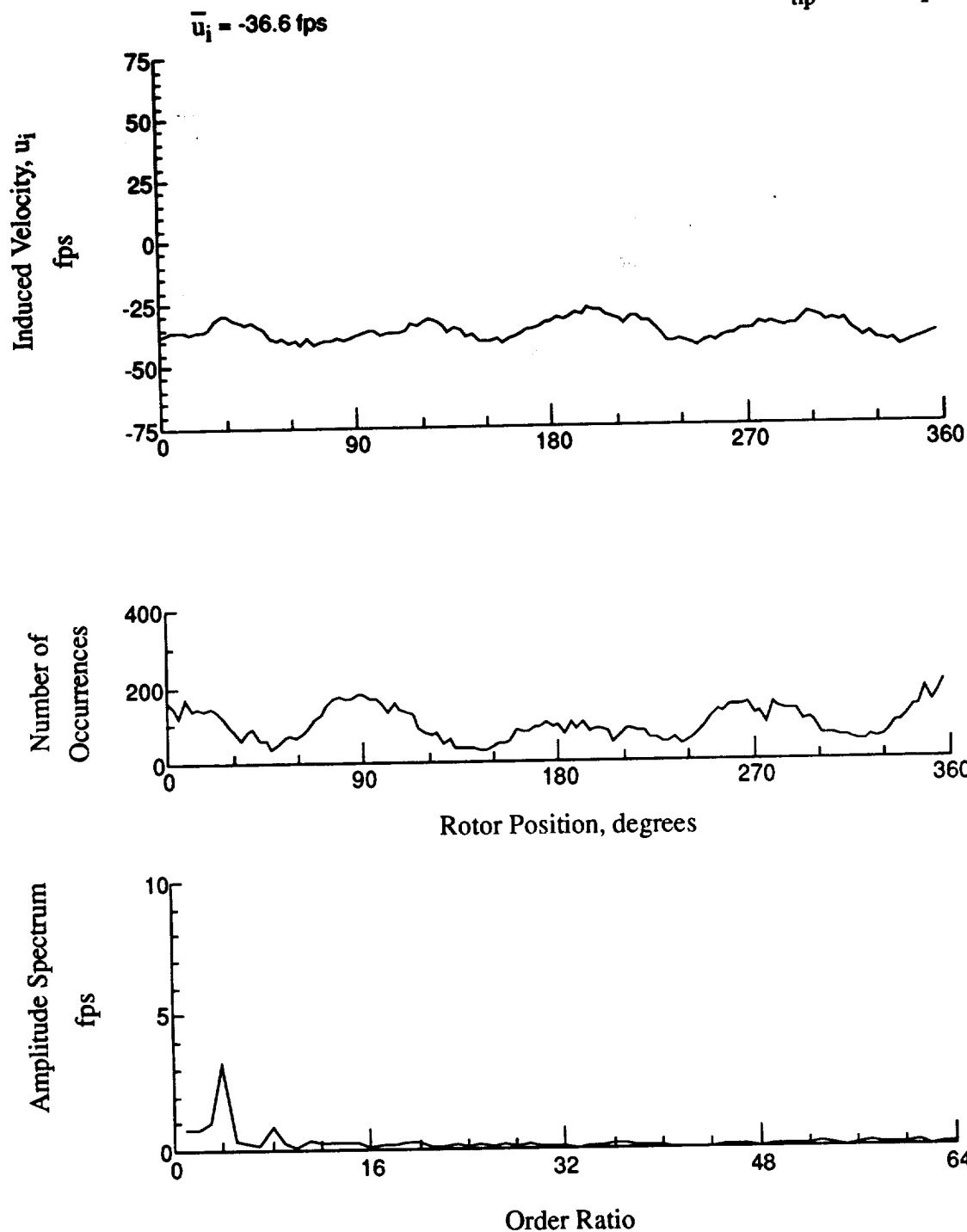


Figure 58.- Wake Measurements at
 $x/R = -0.27$, $y/R = 0.20$, $z = -2.88 \text{ in.}$

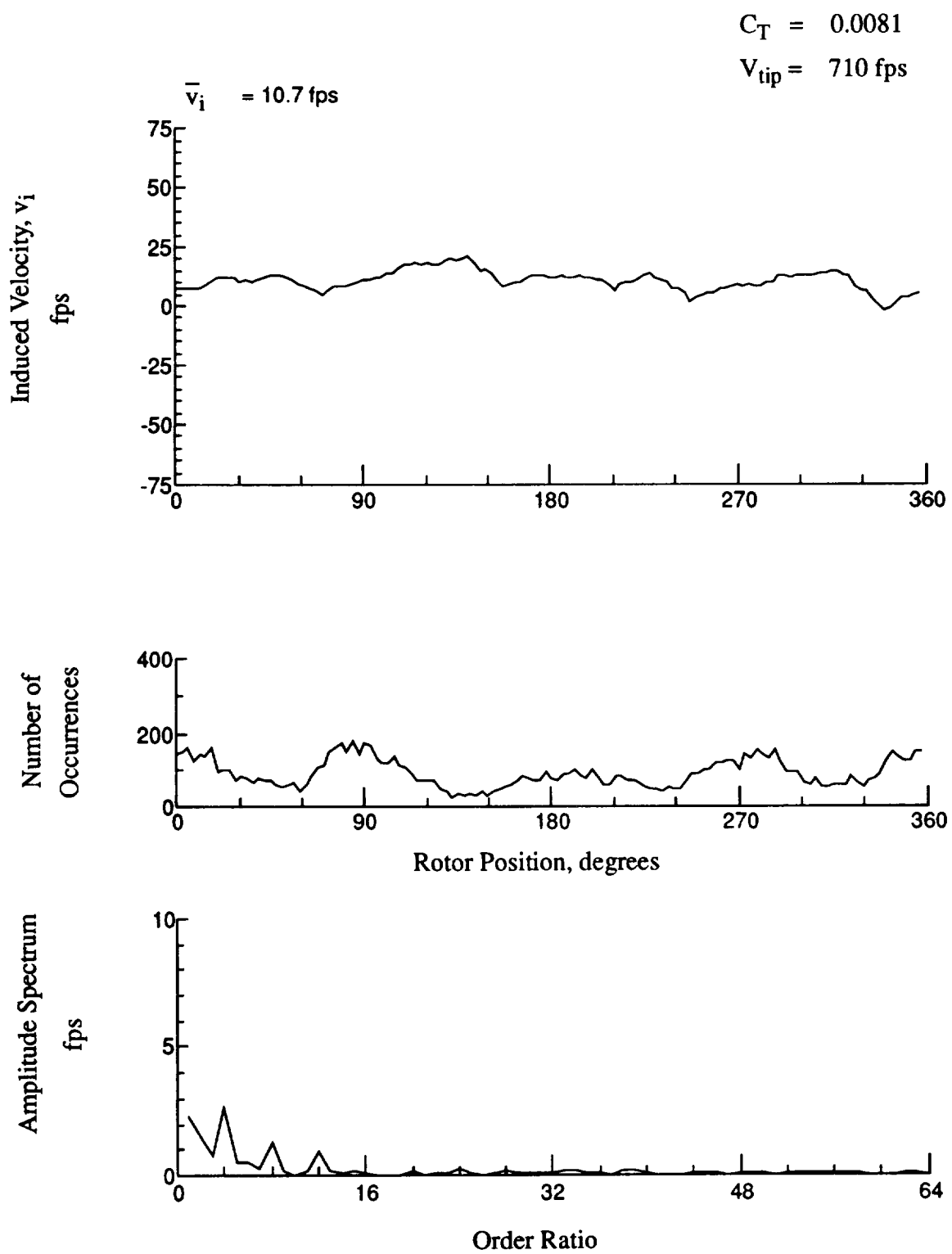


Figure 58.- Concluded.
 $x/R = -0.27$, $y/R = 0.20$, $z = -2.88 \text{ in.}$

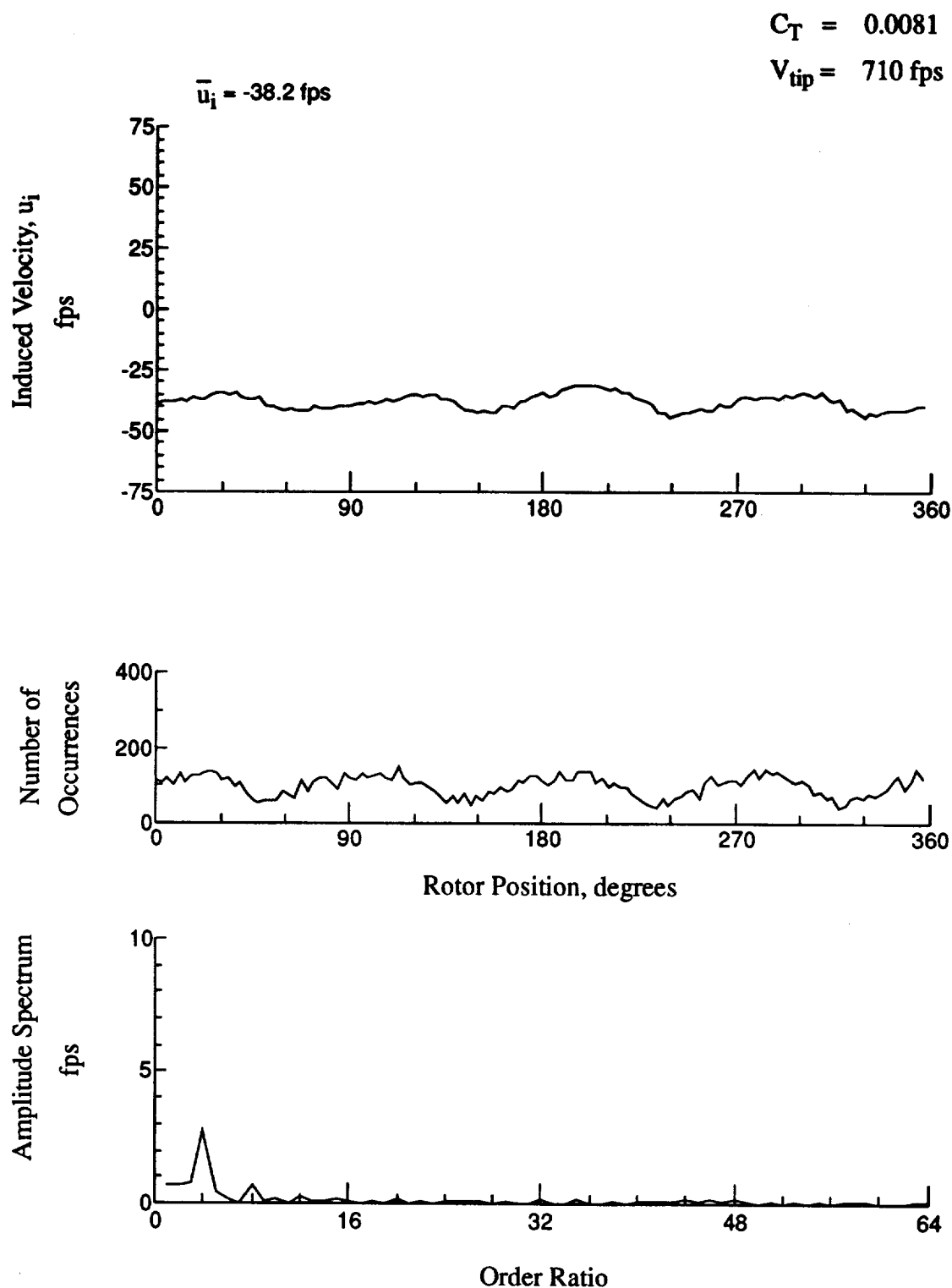


Figure 59.- Wake Measurements at
 $x/R = -0.27$, $y/R = 0.20$, $z = -3.91 \text{ in.}$

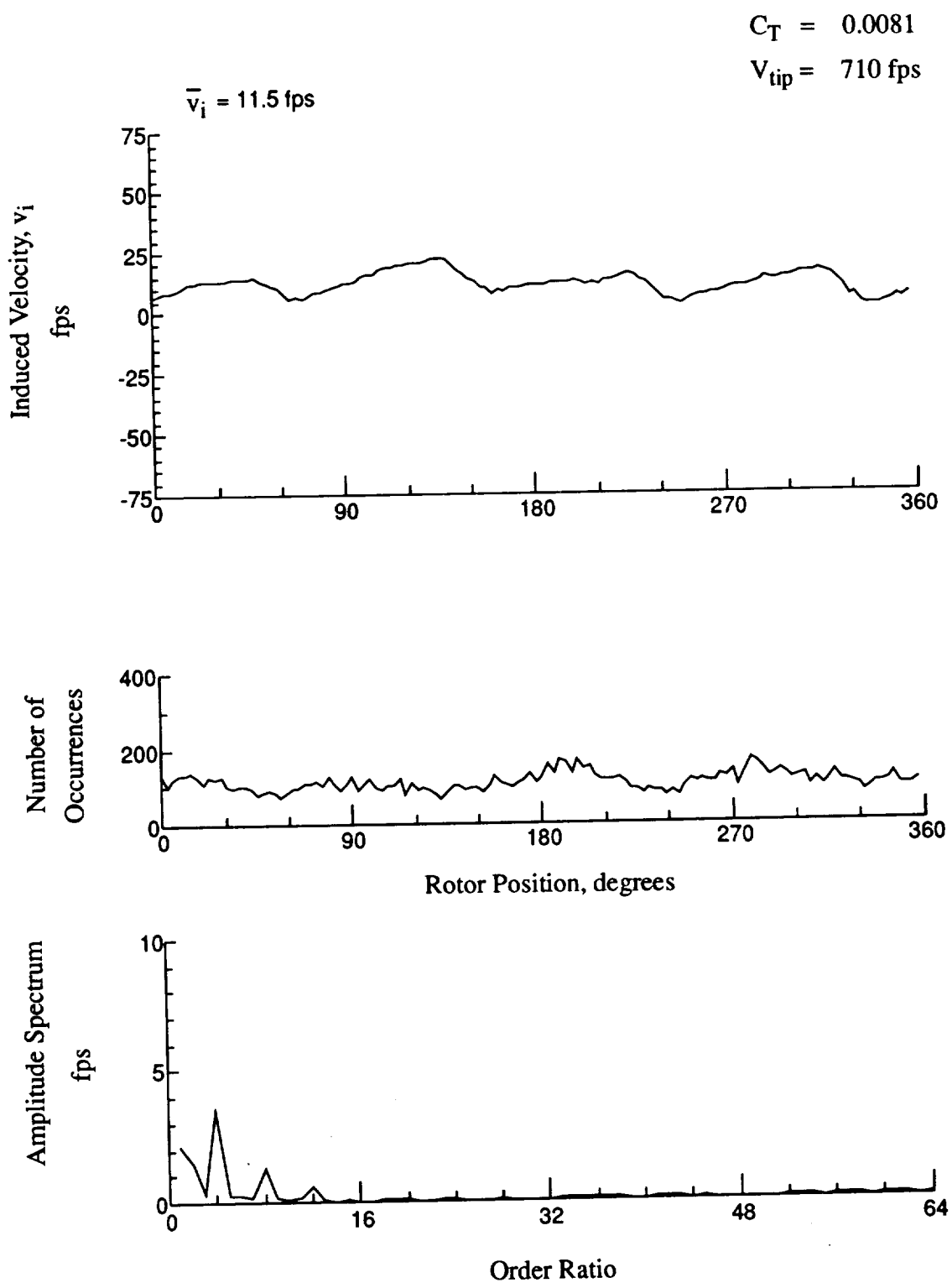


Figure 59.- Concluded.
 $x/R = -0.27$, $y/R = 0.20$, $z = -3.91 \text{ in.}$

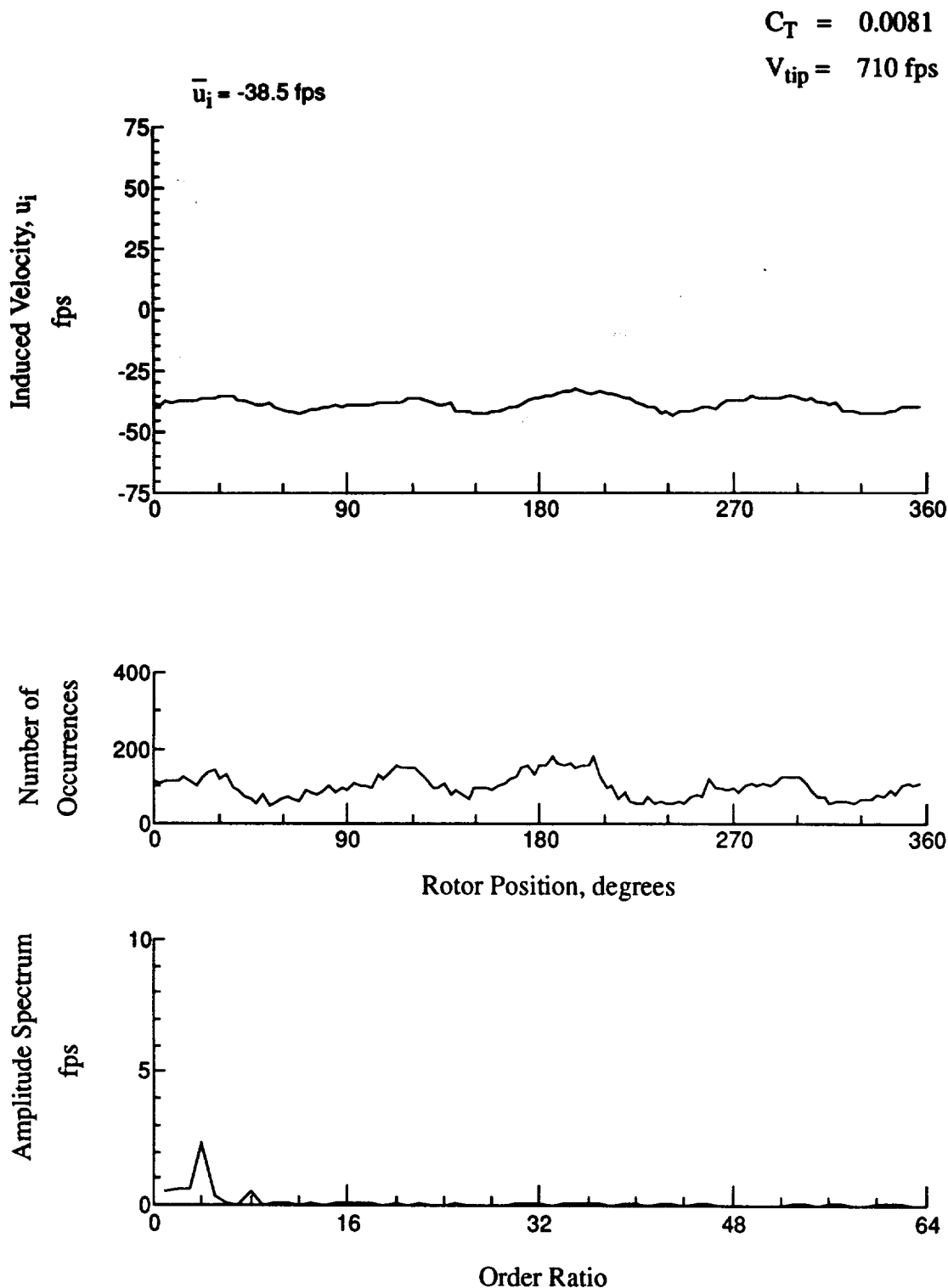


Figure 60.- Wake Measurements at
 $x/R = -0.27$, $y/R = 0.20$, $z = -4.94 \text{ in.}$

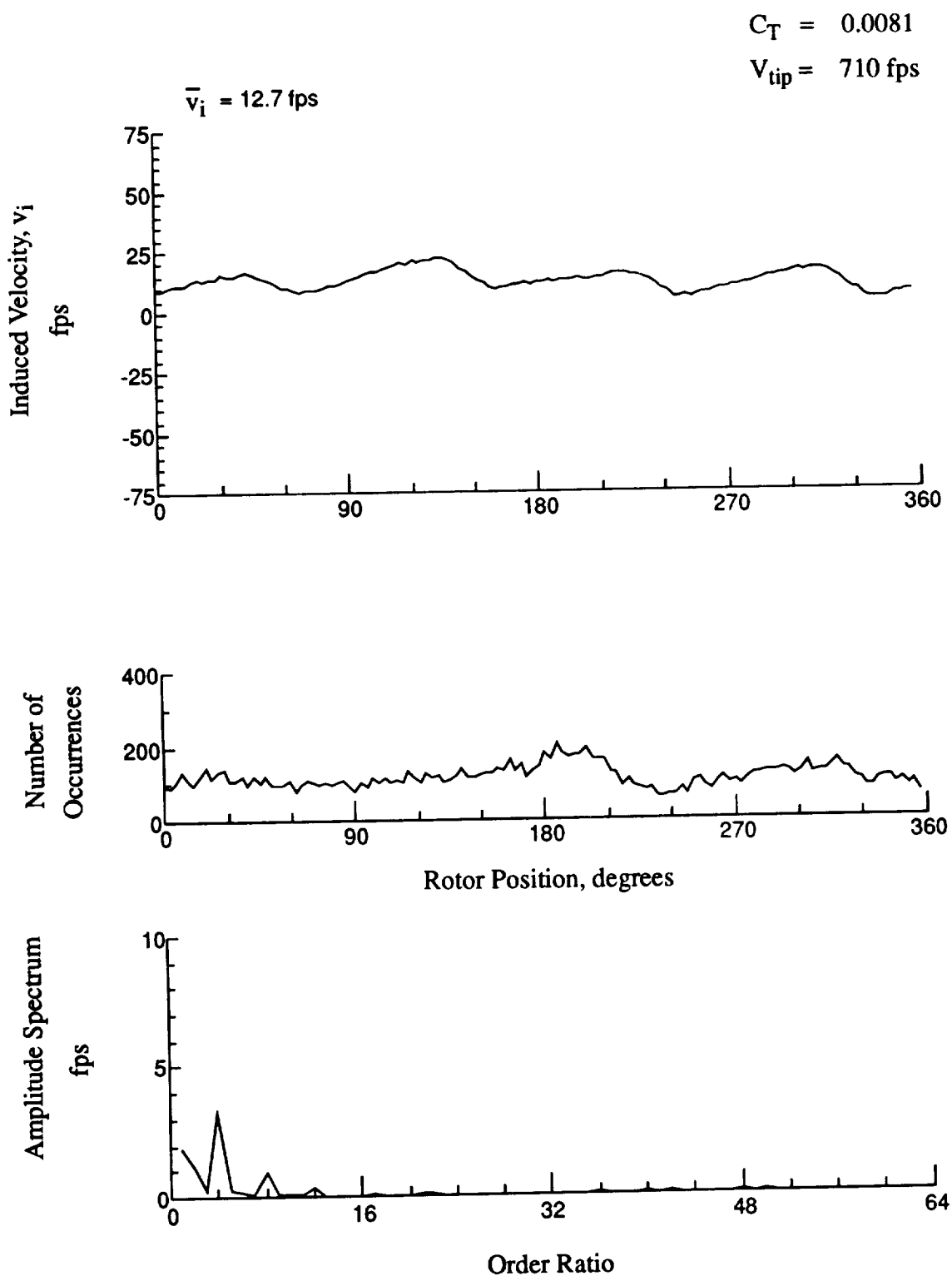


Figure 60.- Concluded.
 $x/R = -0.27$, $y/R = 0.20$, $z = -4.94 \text{ in.}$

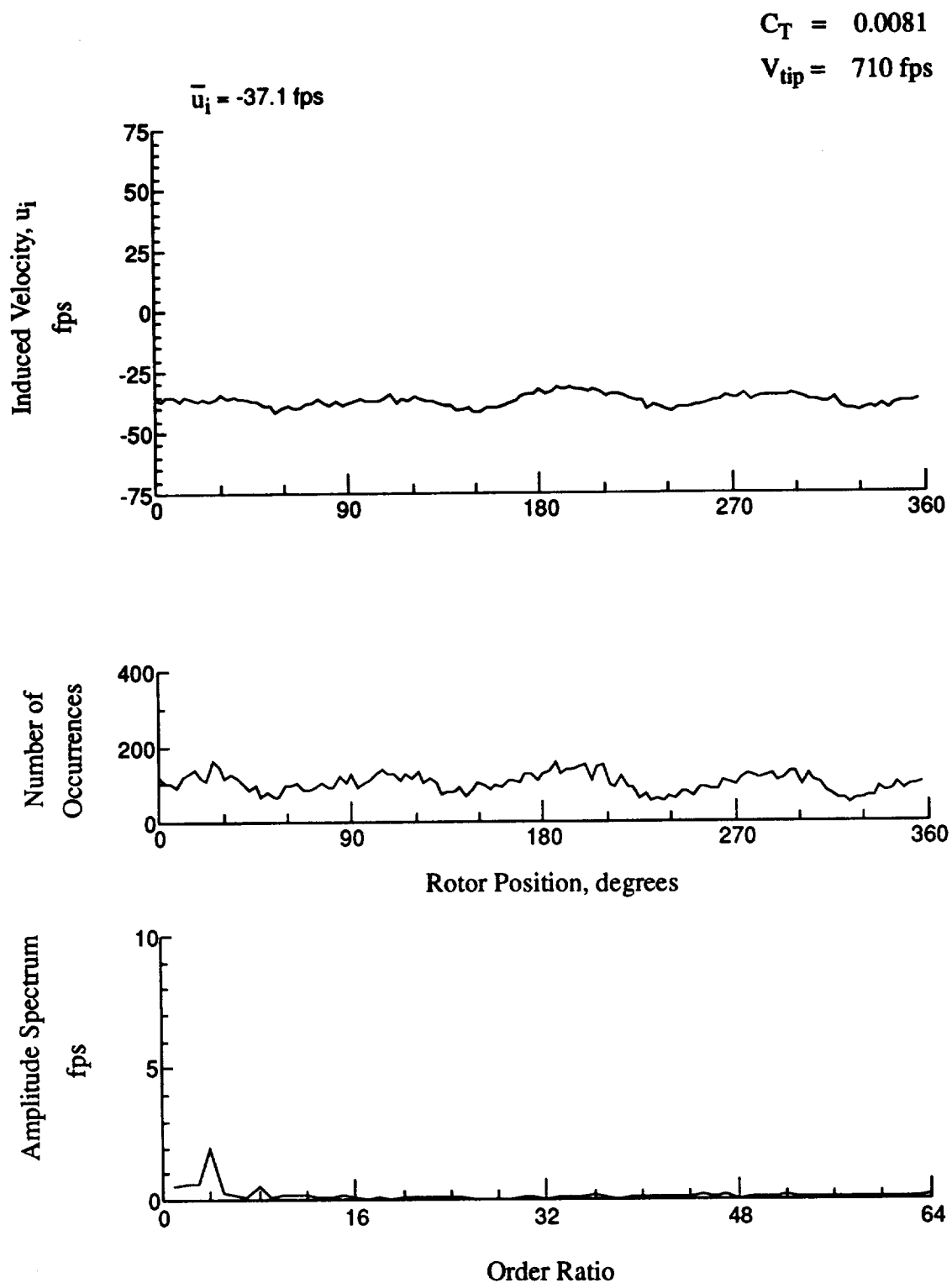


Figure 61.- Wake Measurements at
 $x/R = -0.27$, $y/R = 0.20$, $z = -5.97 \text{ in.}$

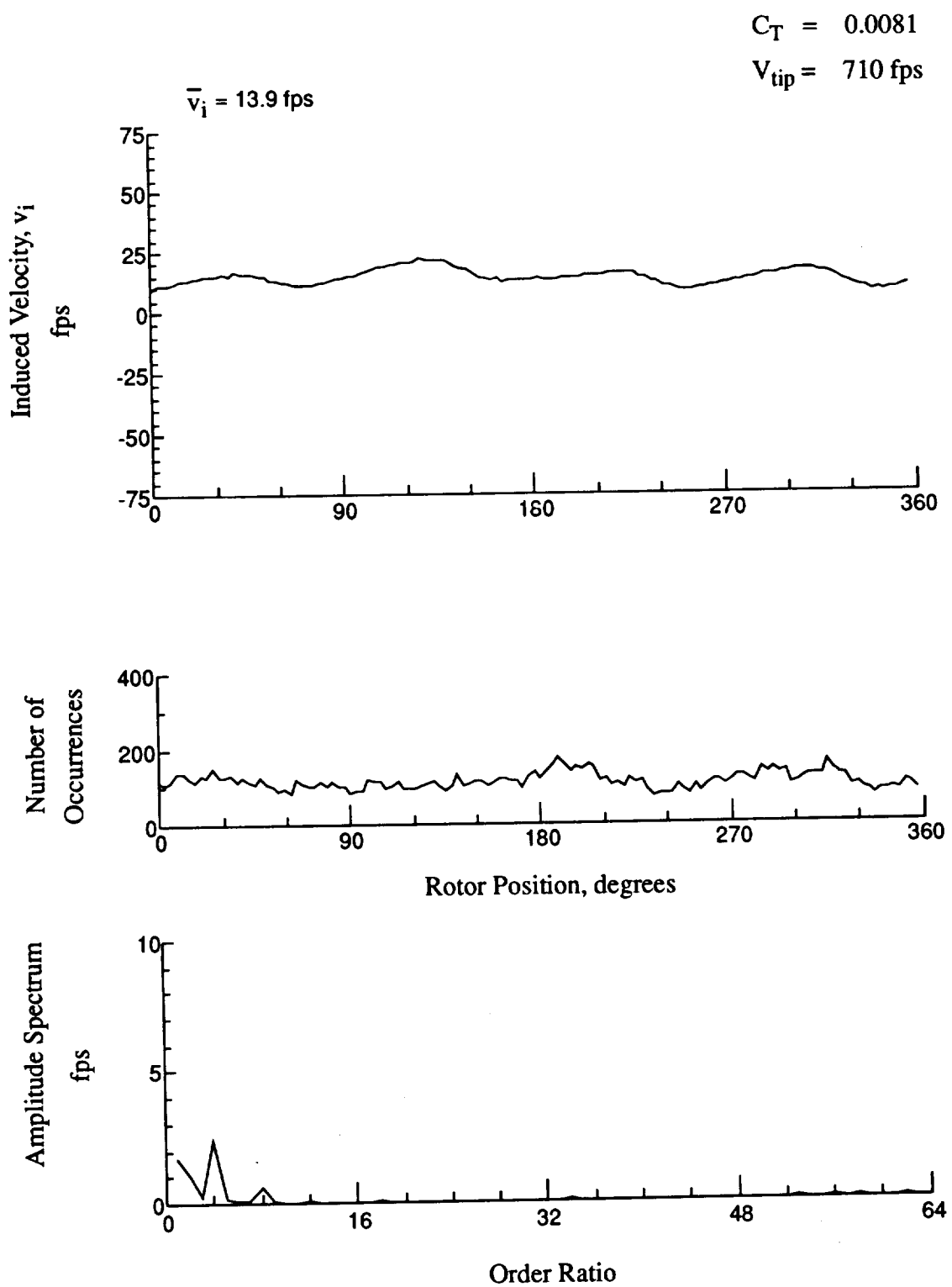


Figure 61.- Concluded.
 $x/R = -0.27$, $y/R = 0.20$, $z = -5.97 \text{ in.}$

$$C_T = 0.0081$$

$$V_{tip} = 710 \text{ fps}$$

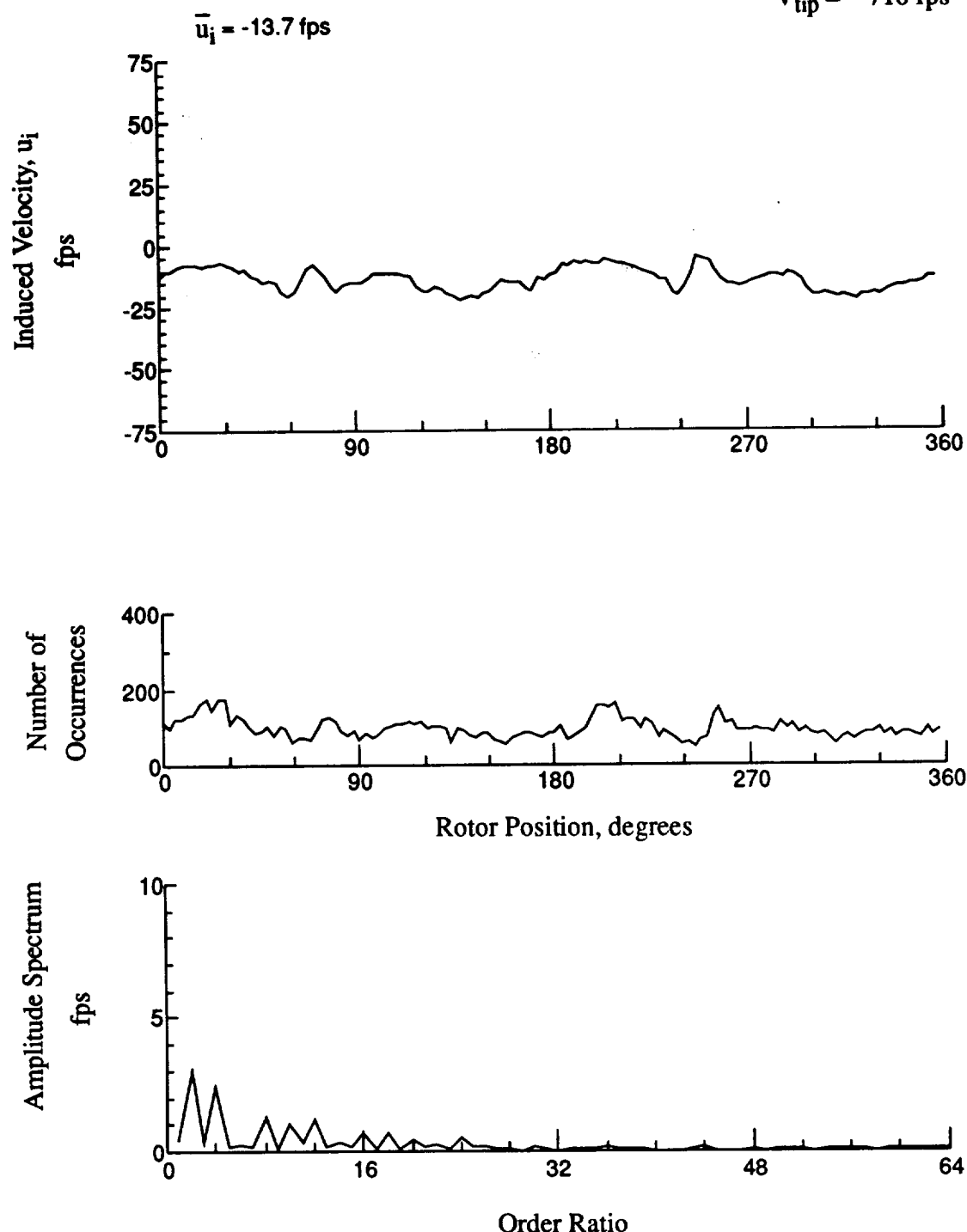


Figure 62.- Wake Measurements at
 $x/R = 0.70$, $y/R = 0.20$, $z = -4.11$ in.

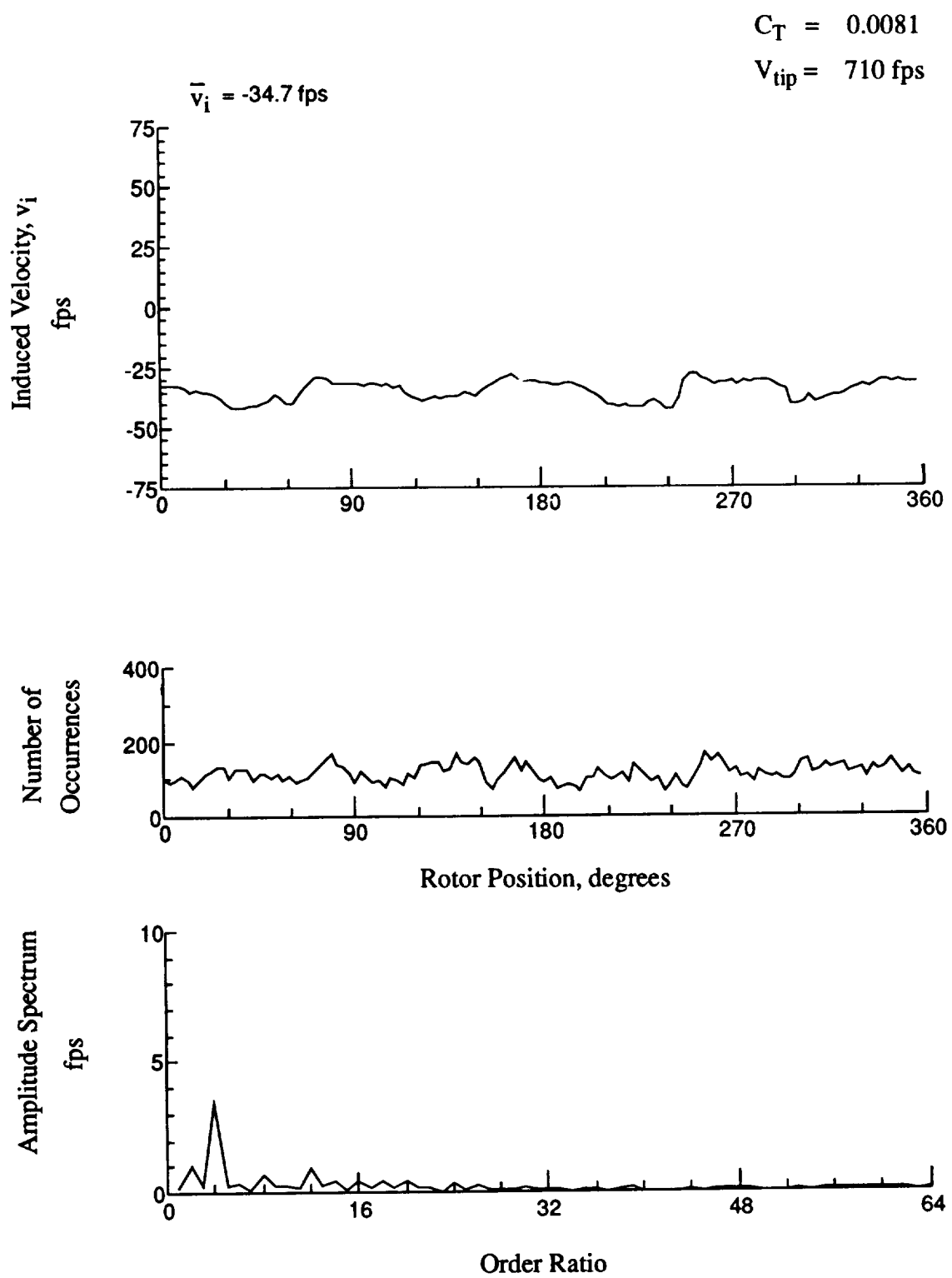


Figure 62.- Concluded.
 $x/R = 0.70$, $y/R = 0.20$, $z = -4.11 \text{ in.}$

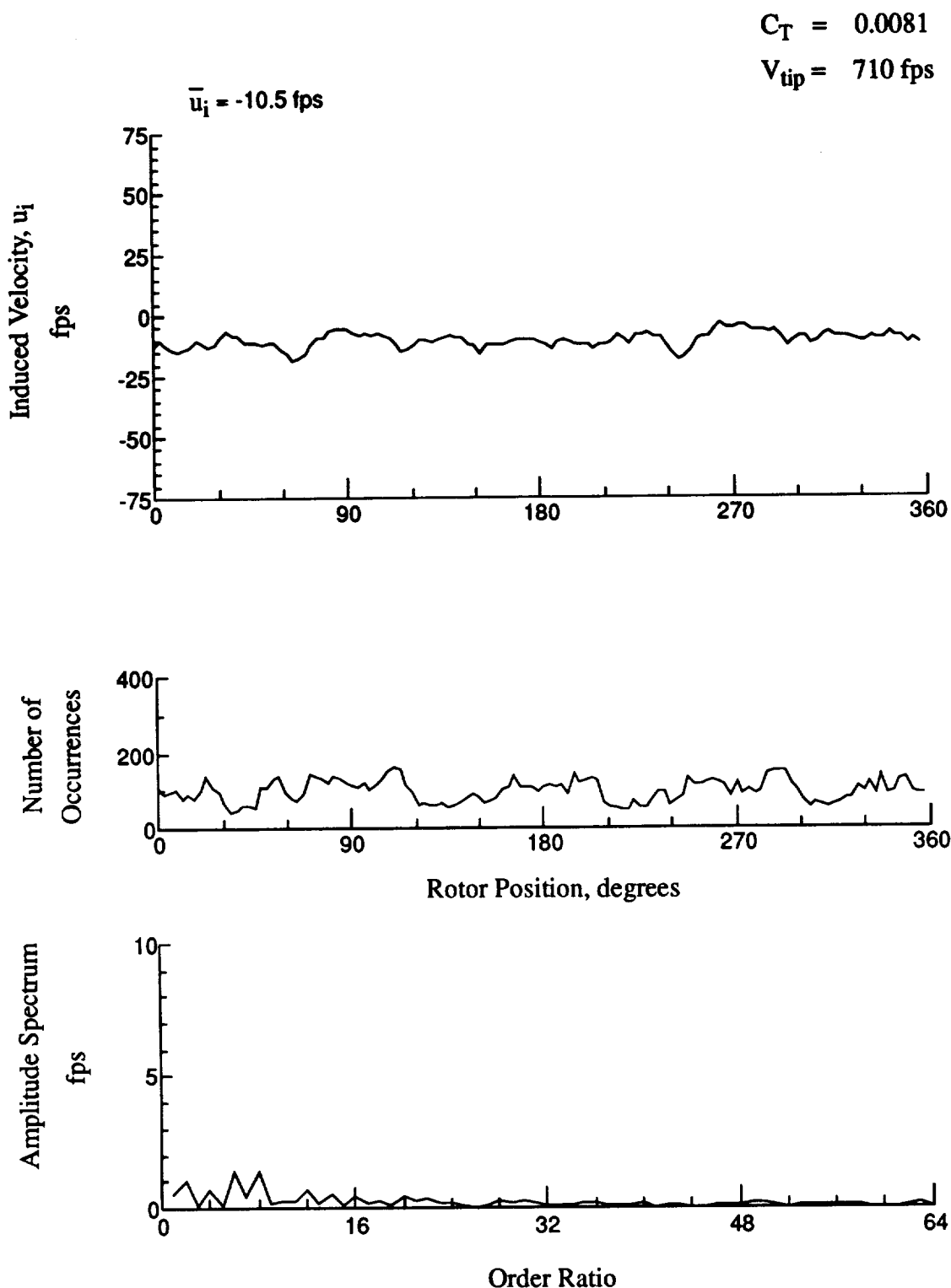


Figure 63.- Wake Measurements at
 $x/R = 0.70$, $y/R = 0.20$, $z = -5.14 \text{ in.}$

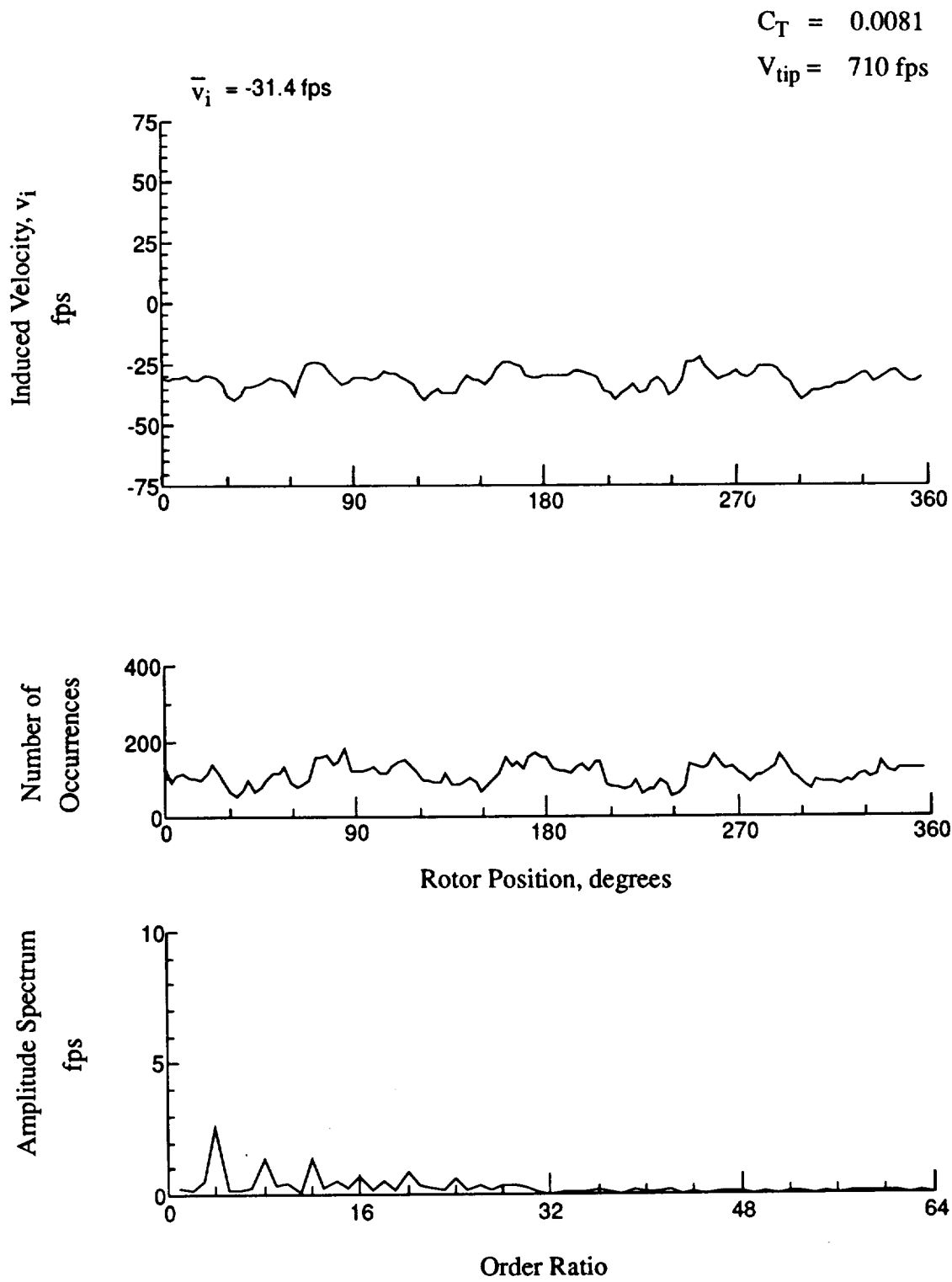


Figure 63.- Concluded.
 $x/R = 0.70$, $y/R = 0.20$, $z = -5.14 \text{ in.}$

$$C_T = 0.0081$$

$$V_{tip} = 710 \text{ fps}$$

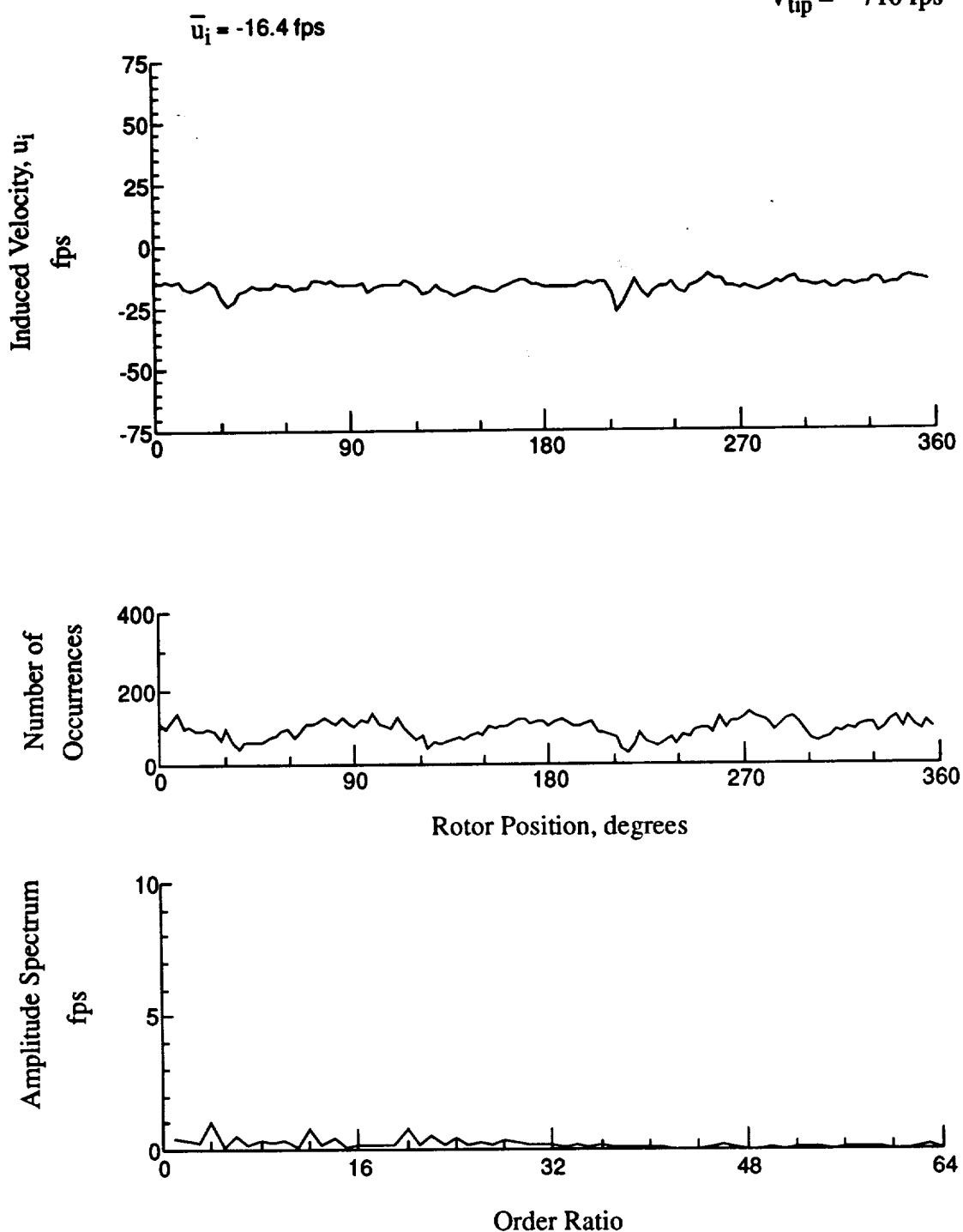


Figure 64.- Wake Measurements at
 $x/R = 0.70$, $y/R = 0.20$, $z = -6.17 \text{ in.}$

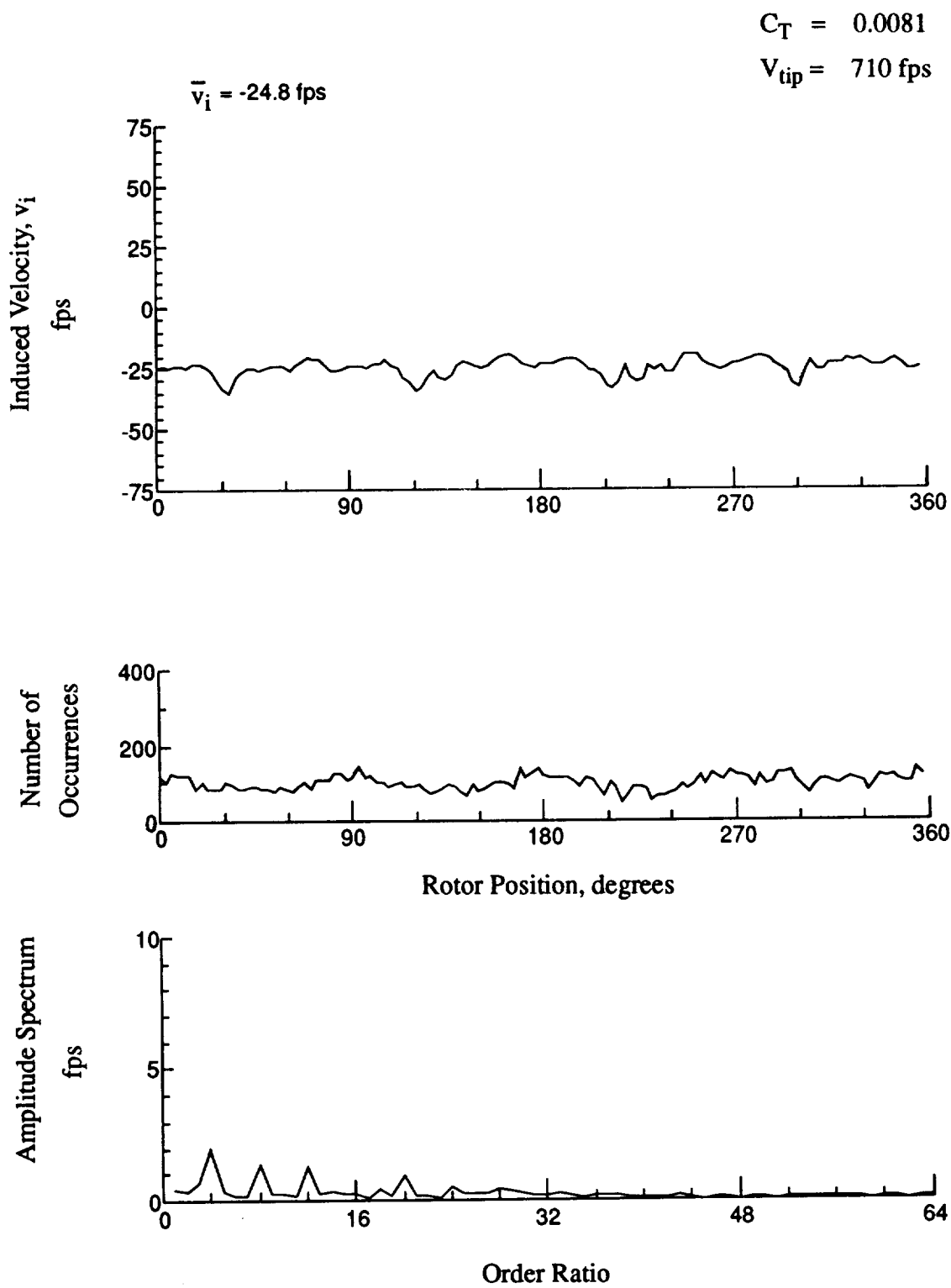


Figure 64.- Concluded.
 $x/R = 0.70$, $y/R = 0.20$, $z = -6.17 \text{ in.}$

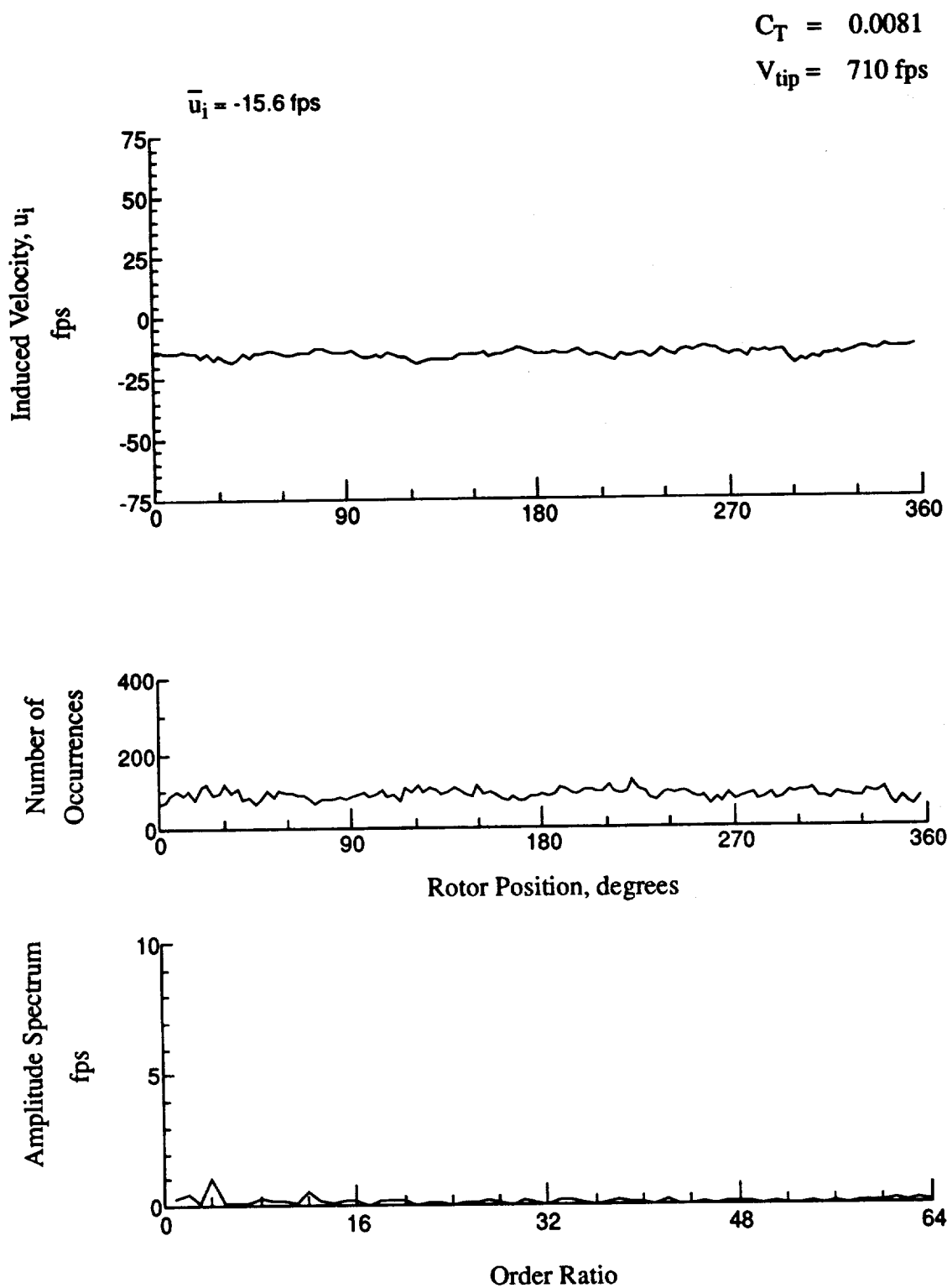


Figure 65.- Wake Measurements at
 $x/R = 0.70$, $y/R = 0.20$, $z = -7.20 \text{ in.}$

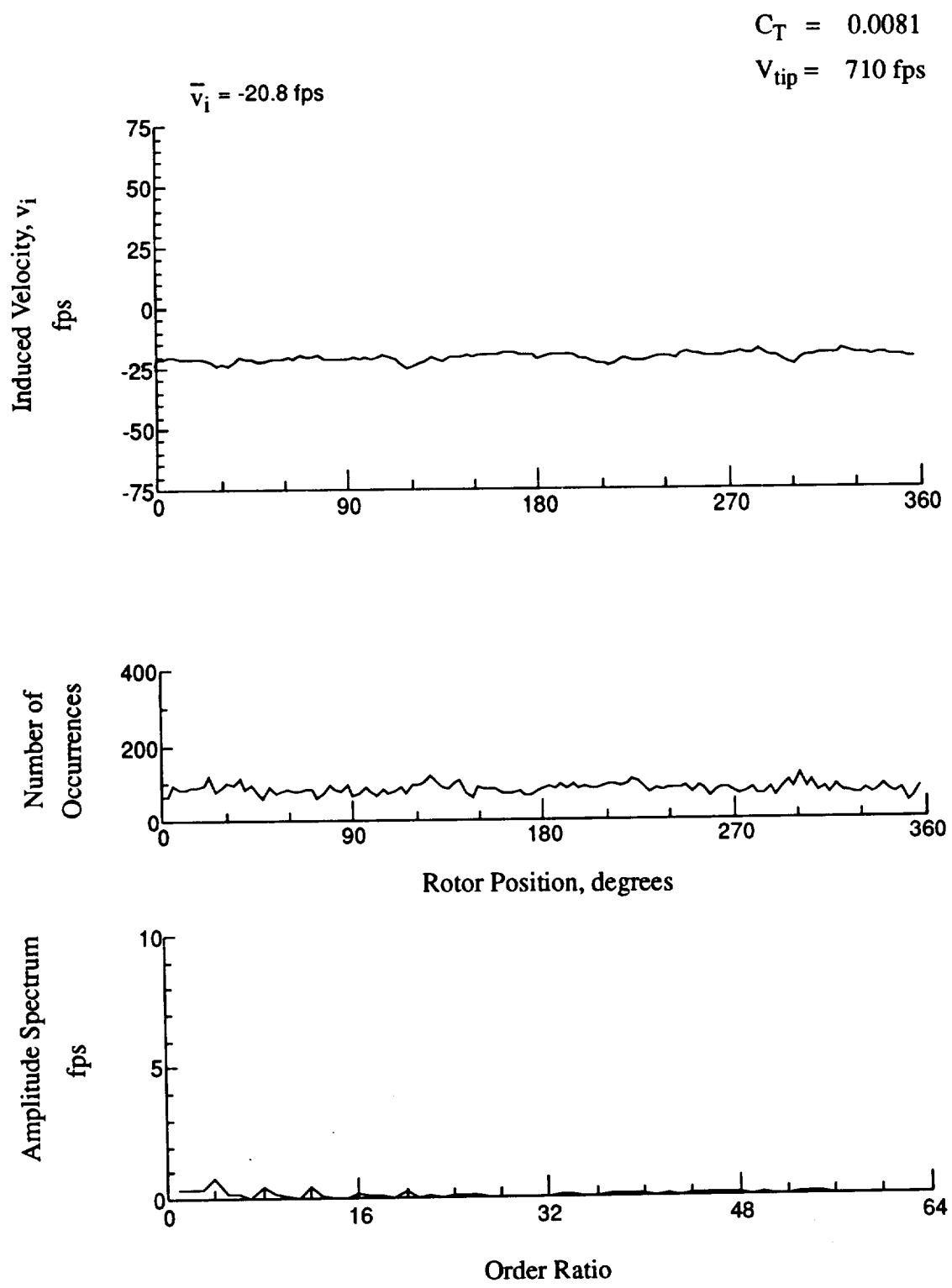


Figure 65.- Concluded.
 $x/R = 0.70$, $y/R = 0.20$, $z = -7.20 \text{ in.}$

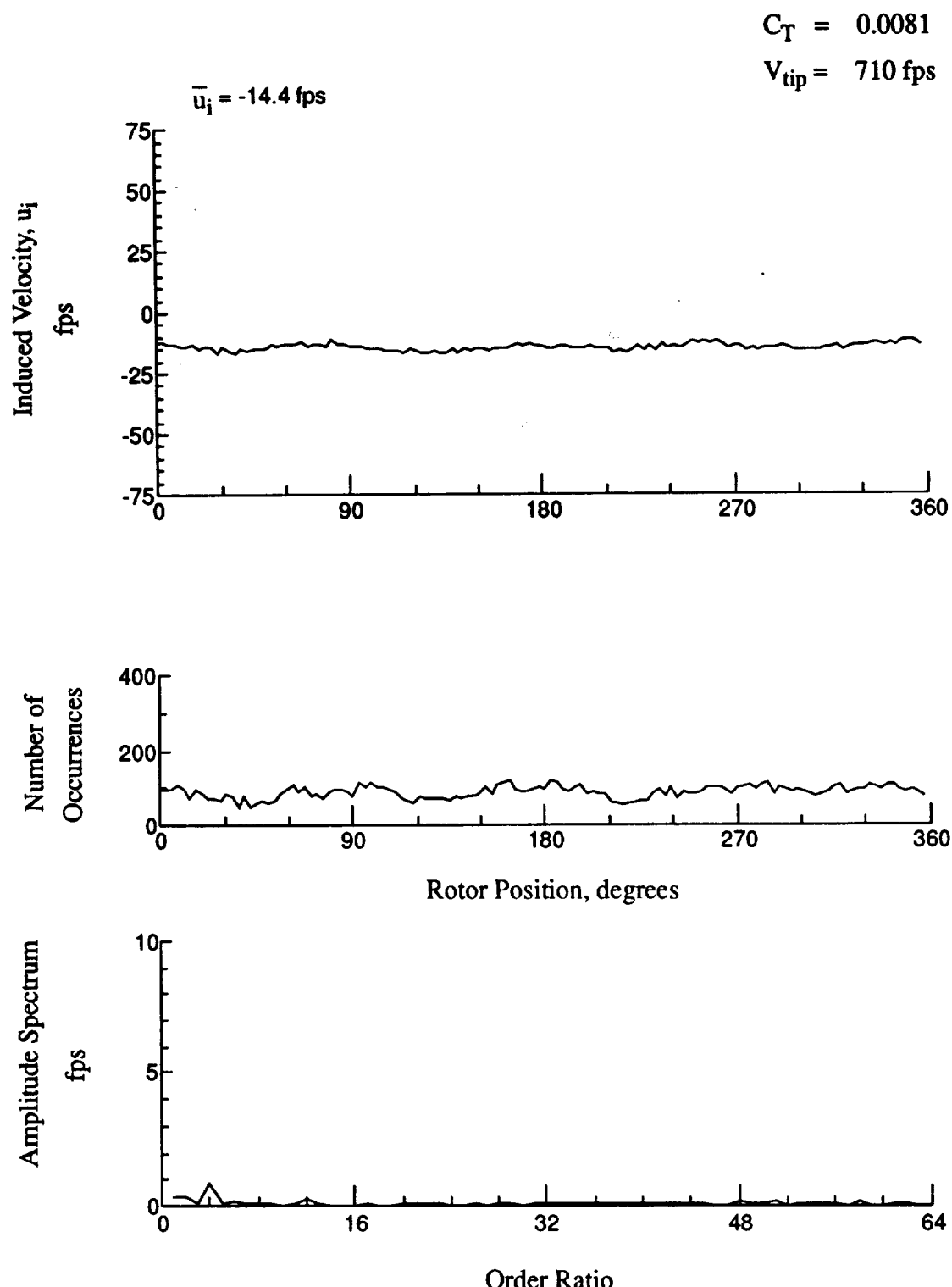


Figure 66.- Wake Measurements at
 $x/R = 0.70$, $y/R = 0.20$, $z = -8.23 \text{ in.}$

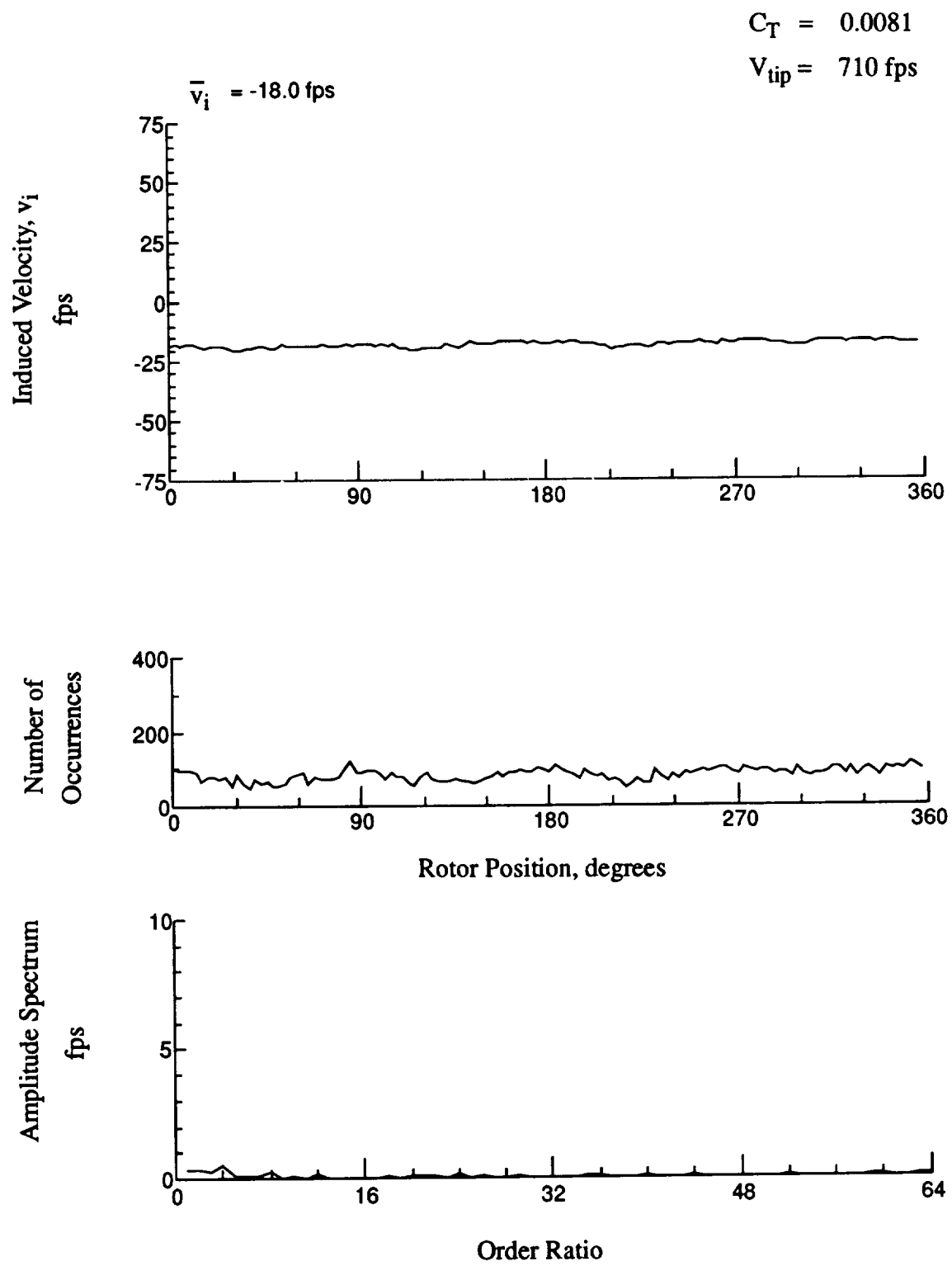


Figure 66.- Concluded.
 $x/R = 0.70$, $y/R = 0.20$, $z = -8.23 \text{ in.}$

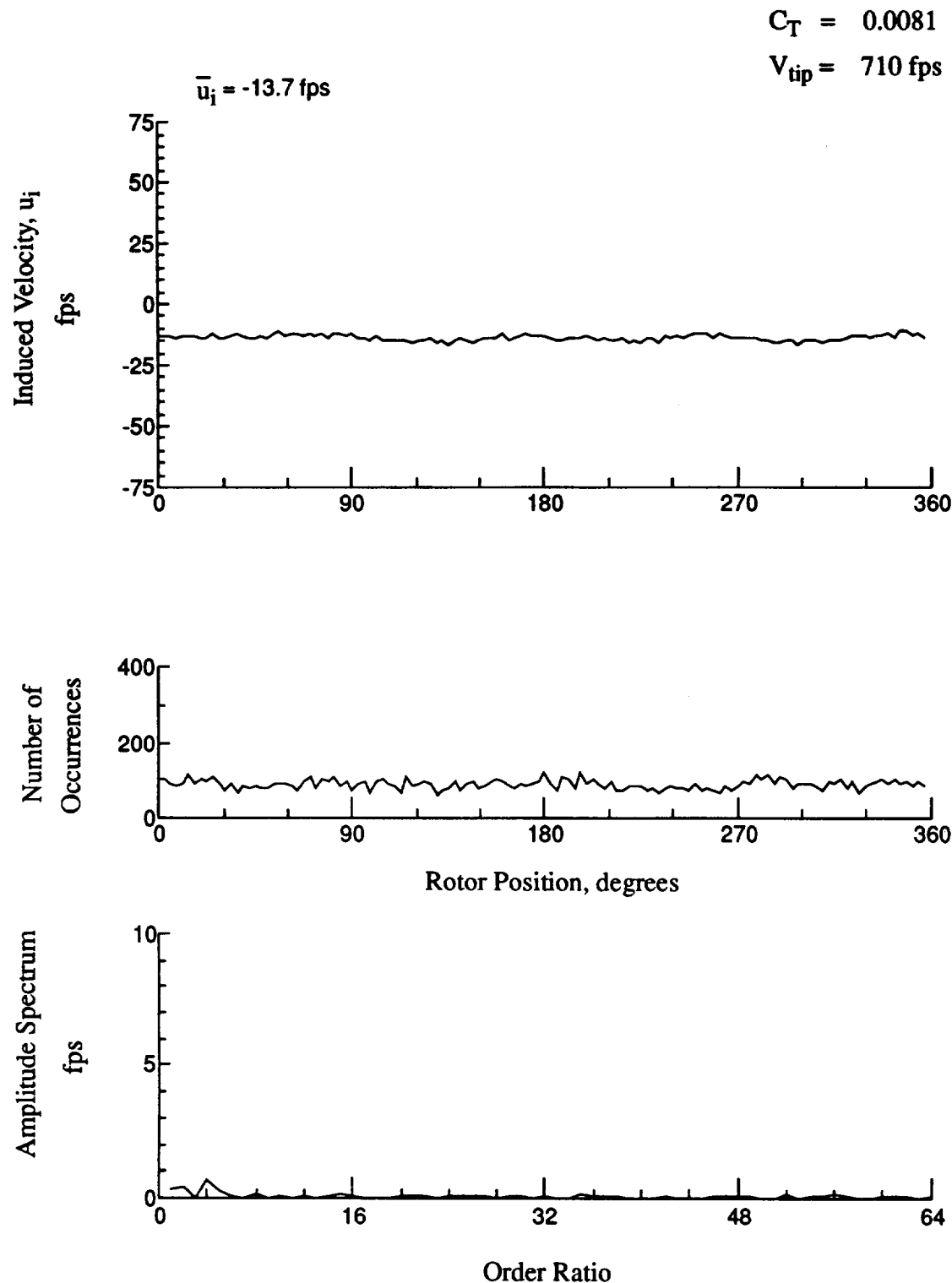


Figure 67.- Wake Measurements at
 $x/R = 0.70$, $y/R = 0.20$, $z = -9.26 \text{ in.}$

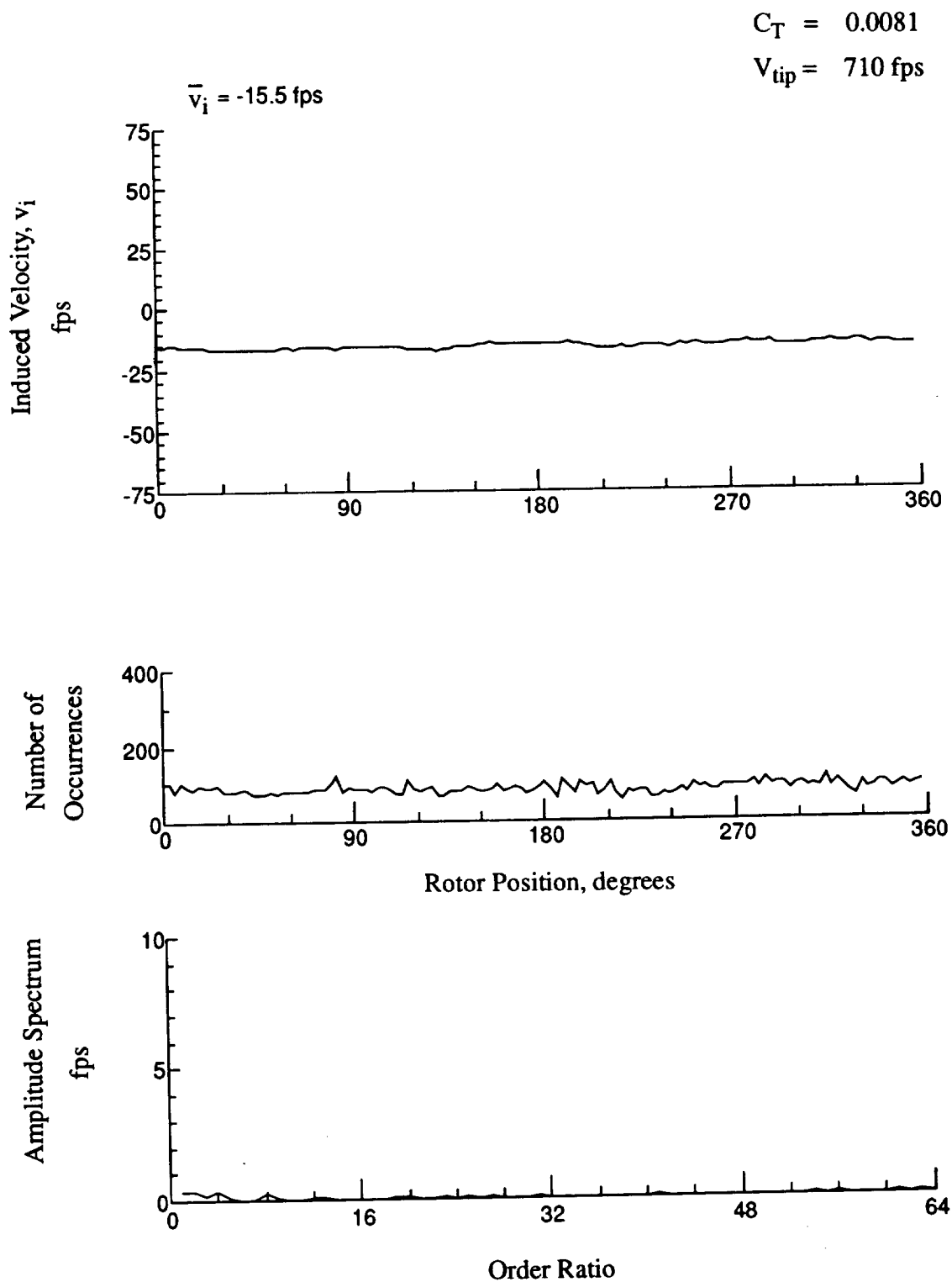


Figure 67.- Concluded.
 $x/R = 0.70$, $y/R = 0.20$, $z = -9.26 \text{ in.}$

$$C_T = 0.0081$$

$$V_{tip} = 710 \text{ fps}$$

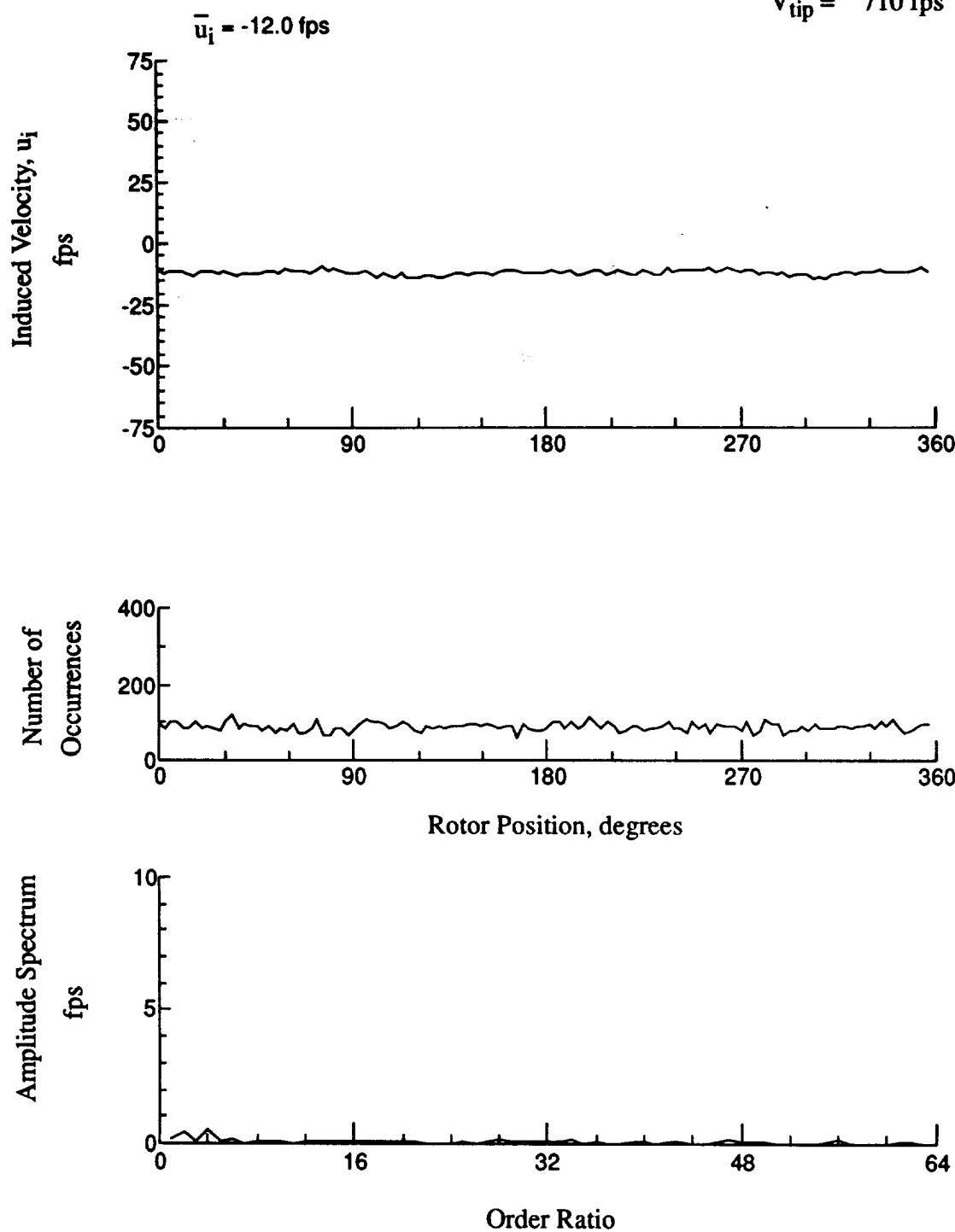


Figure 68.- Wake Measurements at
 $x/R = 0.70$, $y/R = 0.20$, $z = -10.29 \text{ in.}$

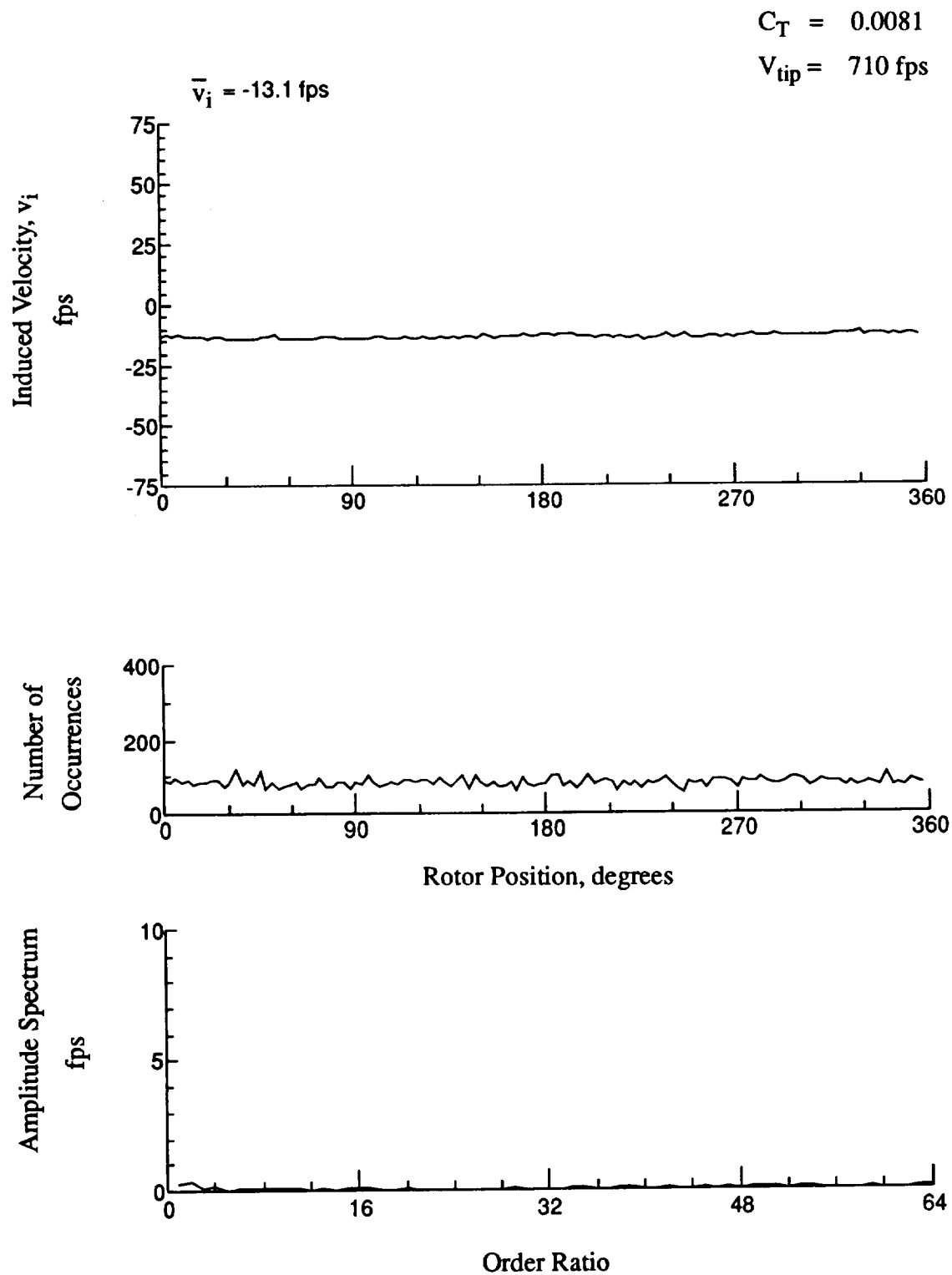


Figure 68.- Concluded.
 $x/R = 0.70$, $y/R = 0.20$, $z = -10.29 \text{ in.}$

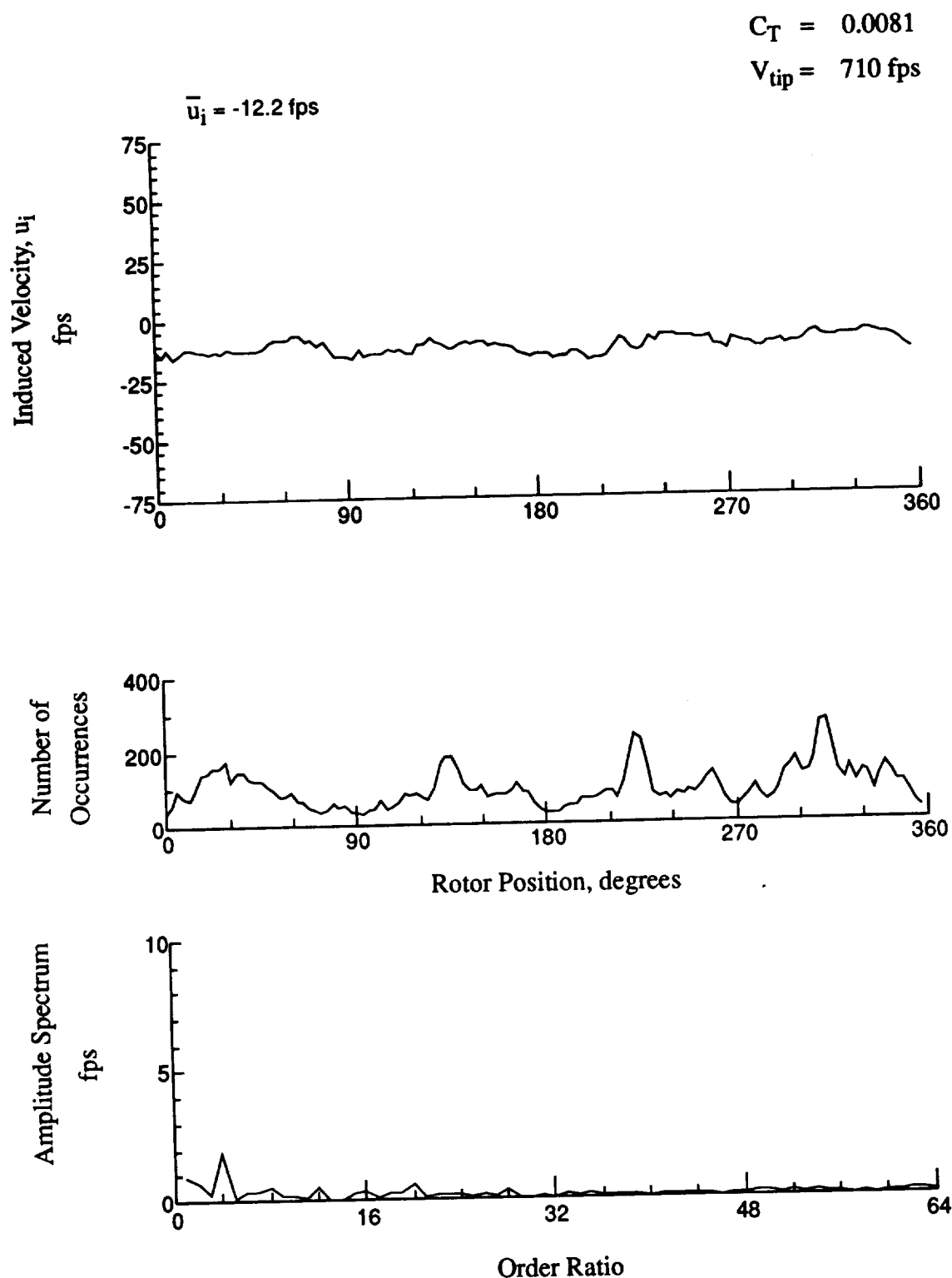


Figure 69.- Wake Measurements at
 $x/R = 1.10$, $y/R = 0.20$, $z = -6.51 \text{ in.}$

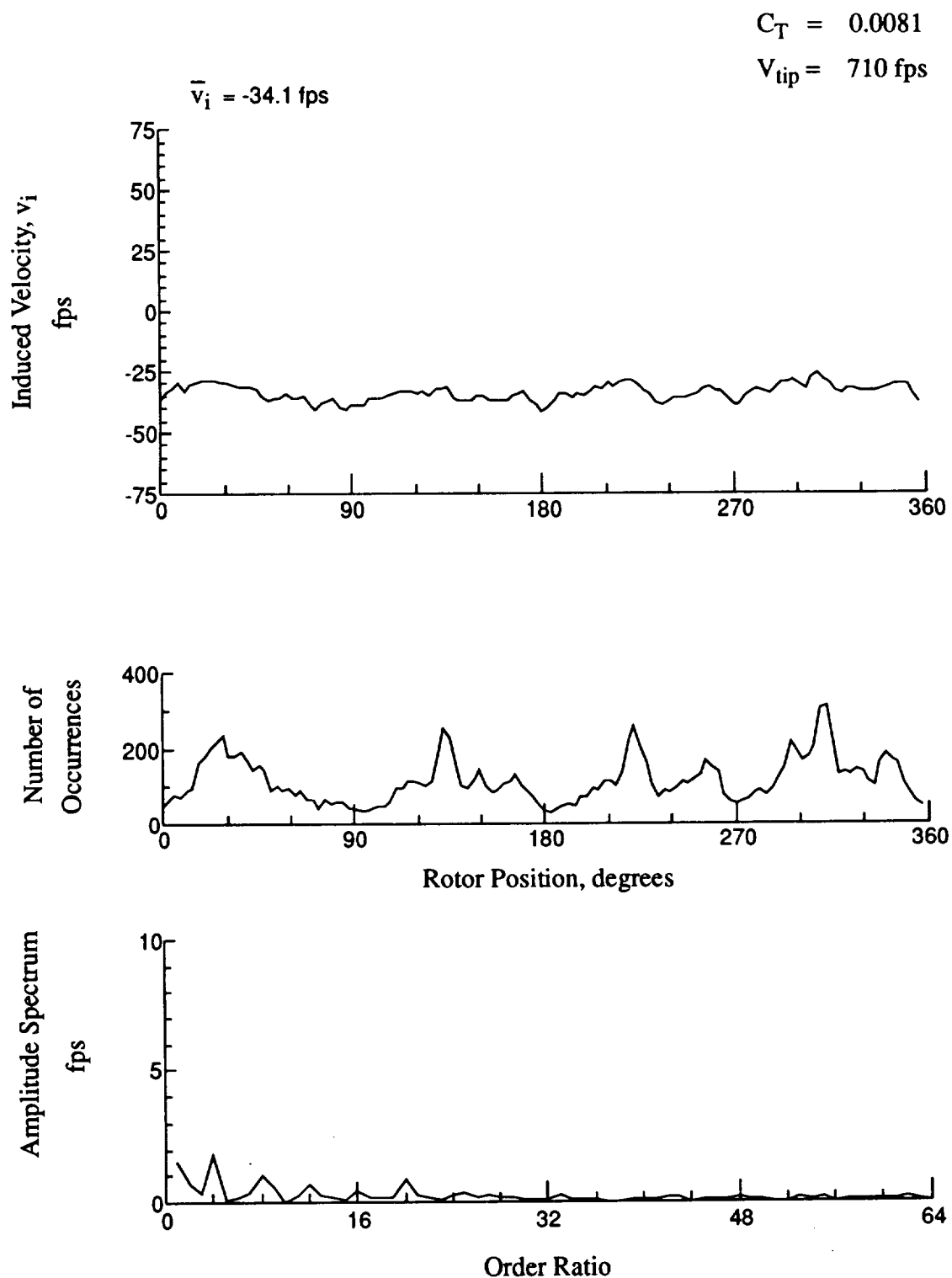


Figure 69.- Concluded.
 $x/R = 1.10$, $y/R = 0.20$, $z = -6.51 \text{ in.}$

$$C_T = 0.0081$$

$$V_{tip} = 710 \text{ fps}$$

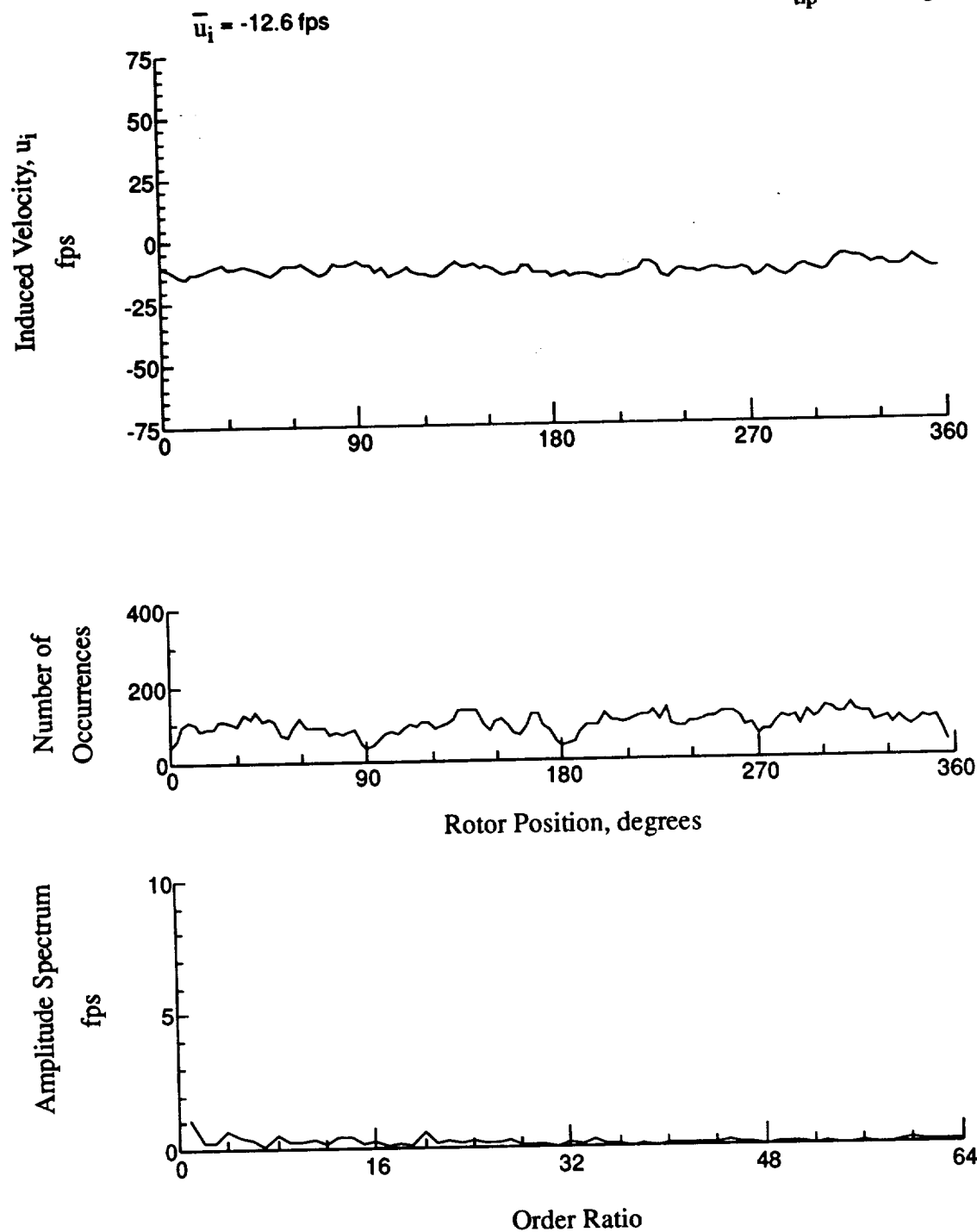


Figure 70.- Wake Measurements at
 $x/R = 1.10$, $y/R = 0.20$, $z = -7.54$ in.

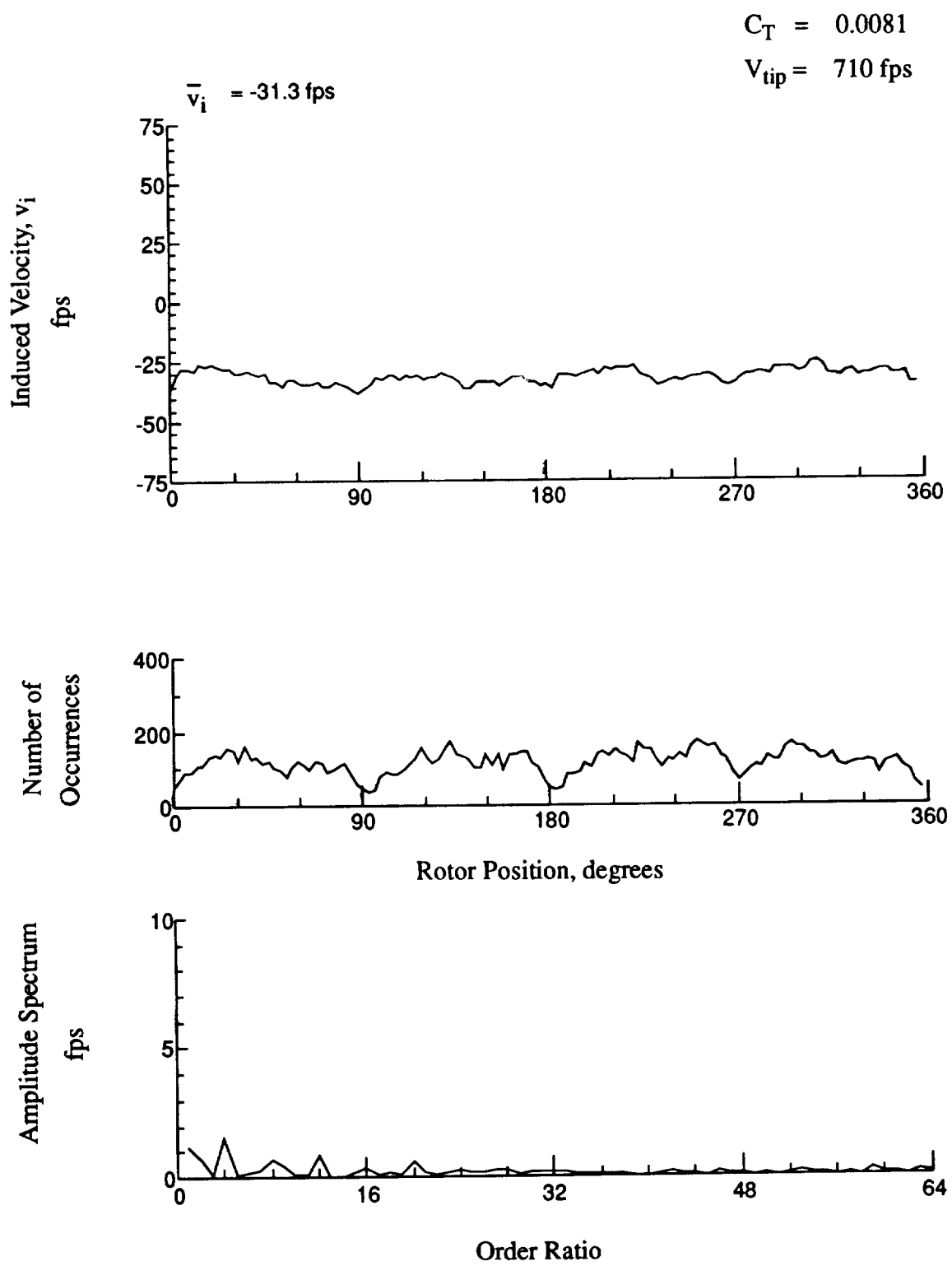
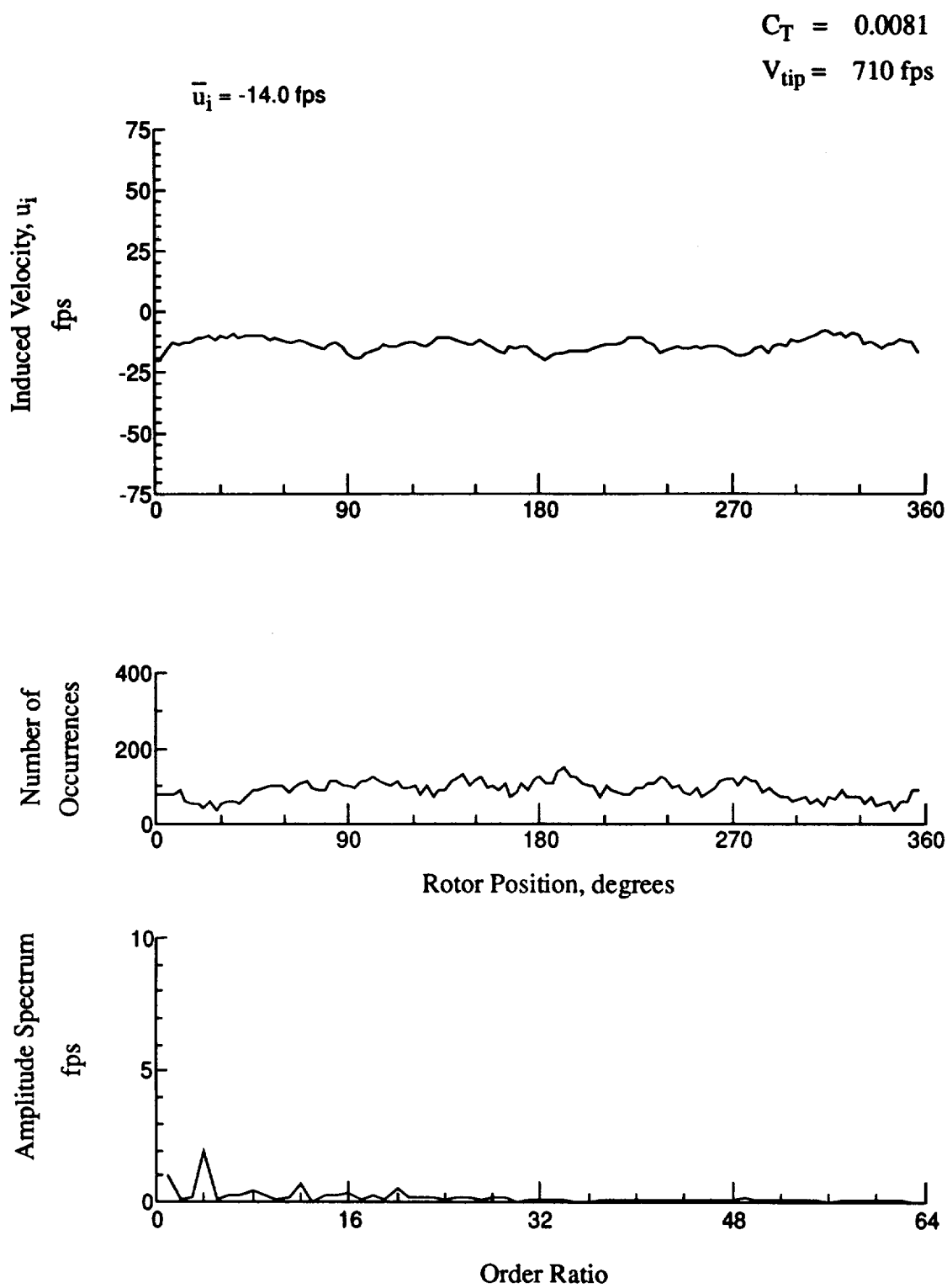


Figure 70.- Concluded.
 $x/R = 1.10$, $y/R = 0.20$, $z = -7.54 \text{ in.}$



**Figure 71.- Wake Measurements at
 $x/R = 1.10$, $y/R = 0.20$, $z = -8.57 \text{ in.}$**

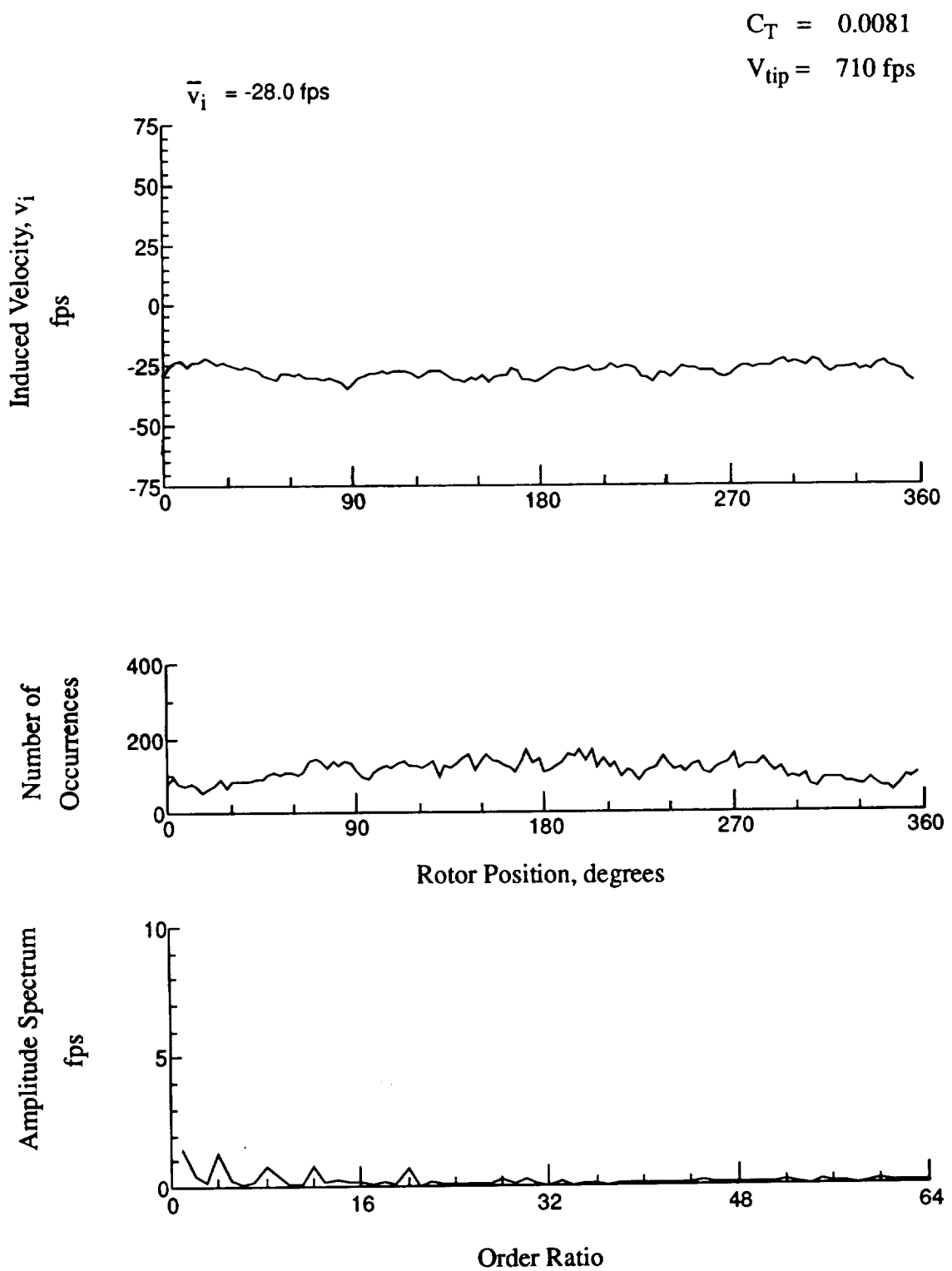


Figure 71.- Concluded.
 $x/R = 1.10$, $y/R = 0.20$, $z = -8.57 \text{ in.}$

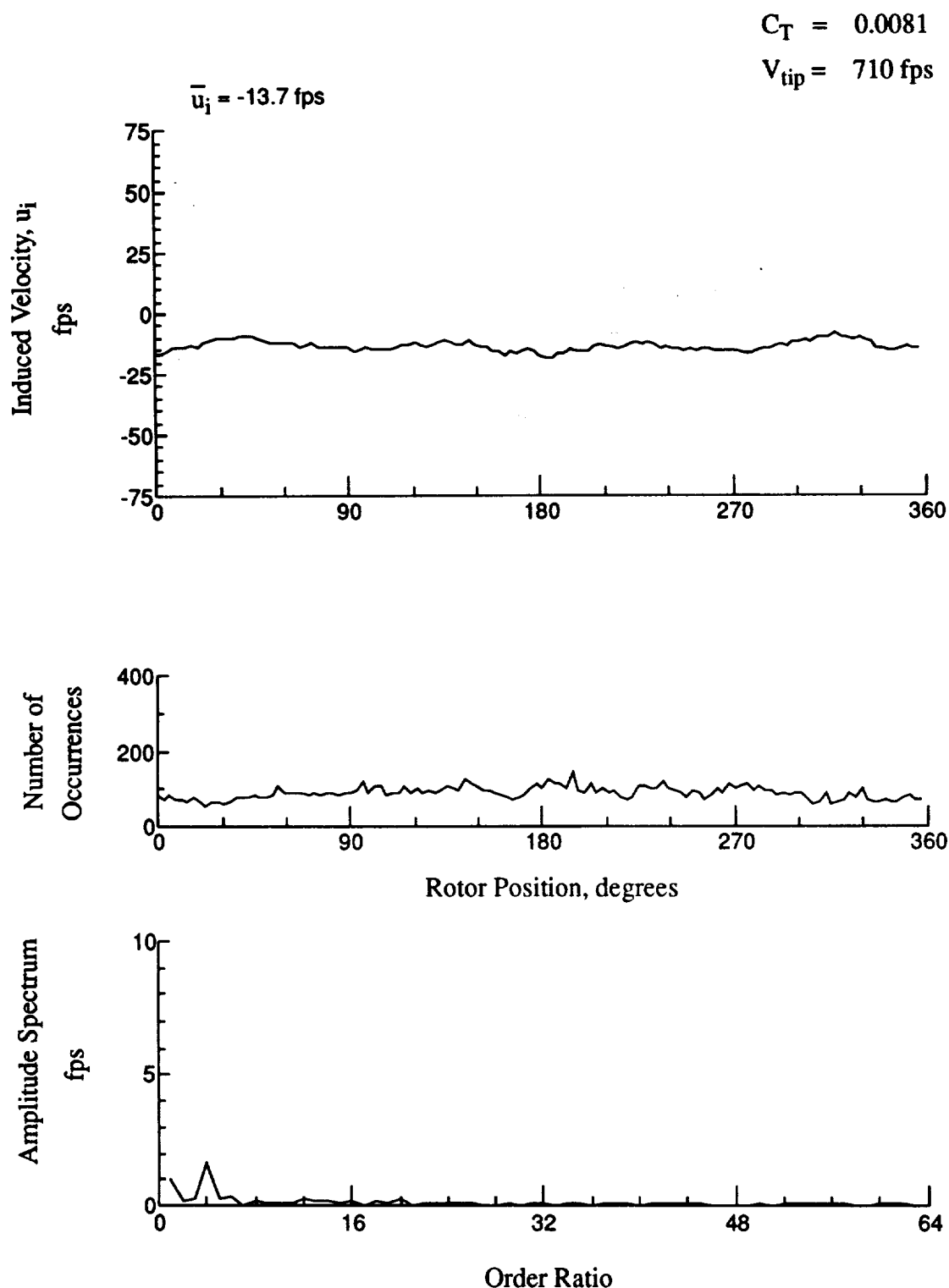


Figure 72.- Wake Measurements at
 $x/R = 1.10$, $y/R = 0.20$, $z = -9.60 \text{ in.}$

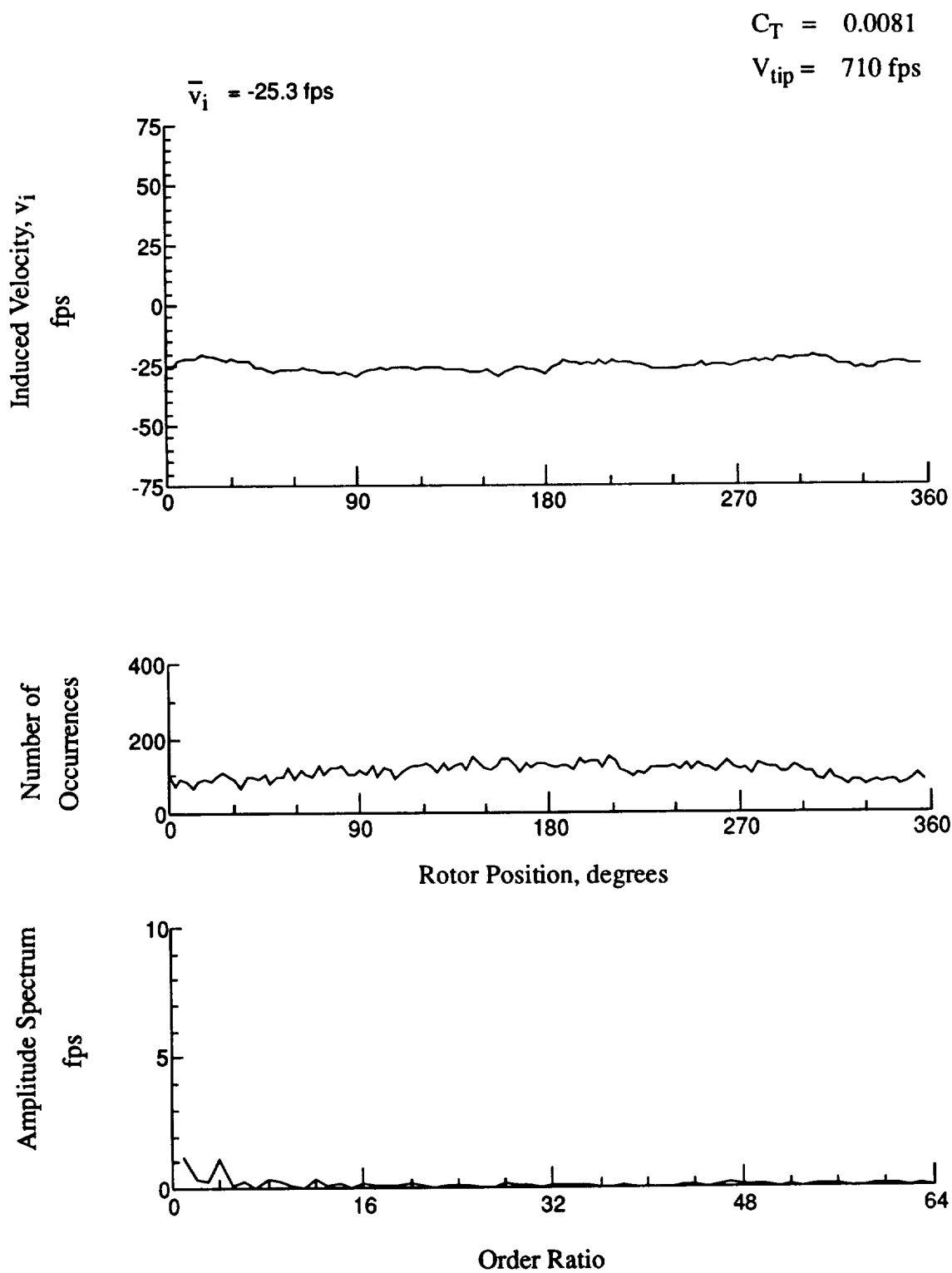


Figure 72.- Concluded.
 $x/R = 1.10$, $y/R = 0.20$, $z = -9.60 \text{ in.}$

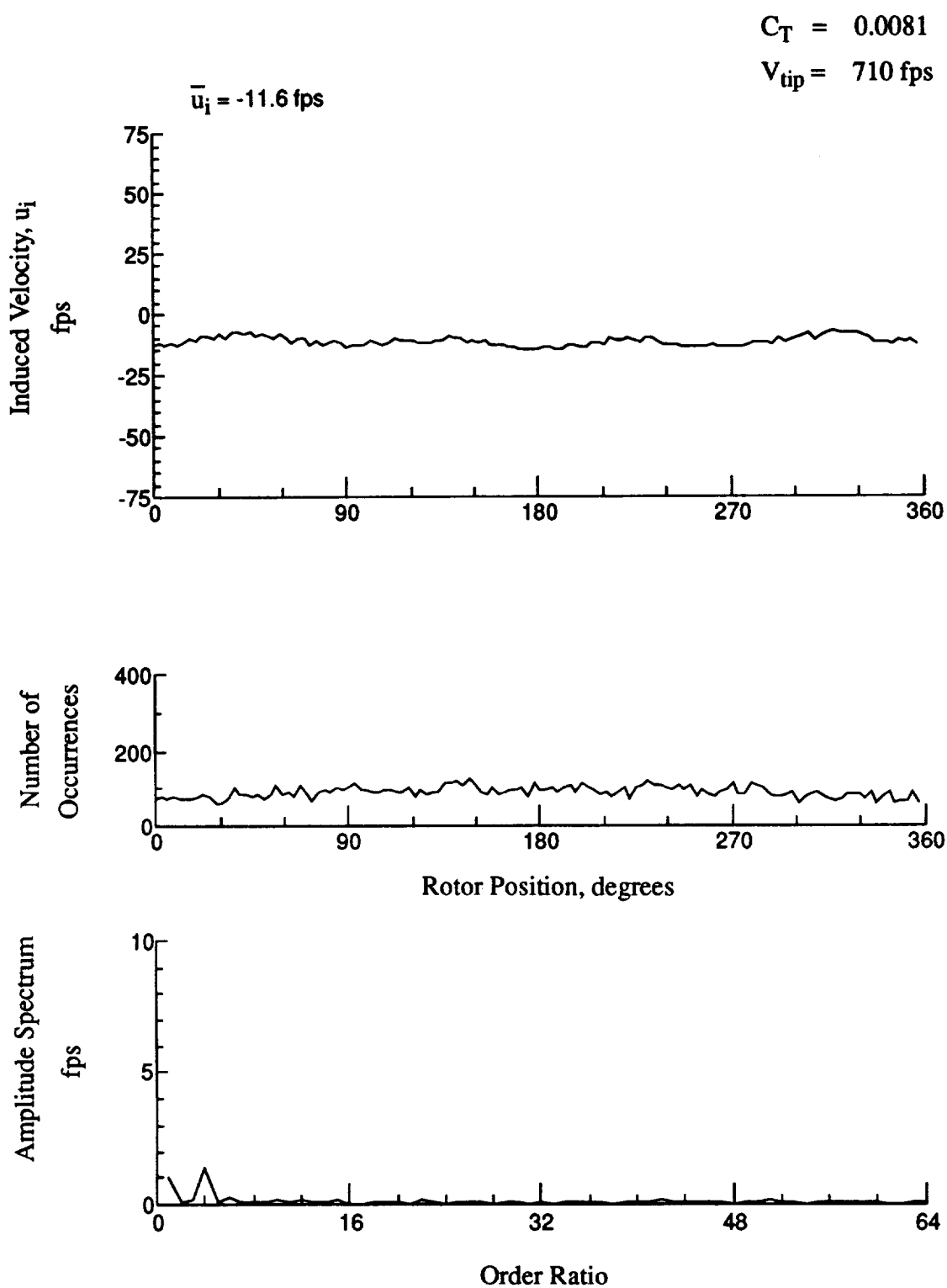


Figure 73.- Wake Measurements at
 $x/R = 1.10$, $y/R = 0.20$, $z = -10.63 \text{ in.}$

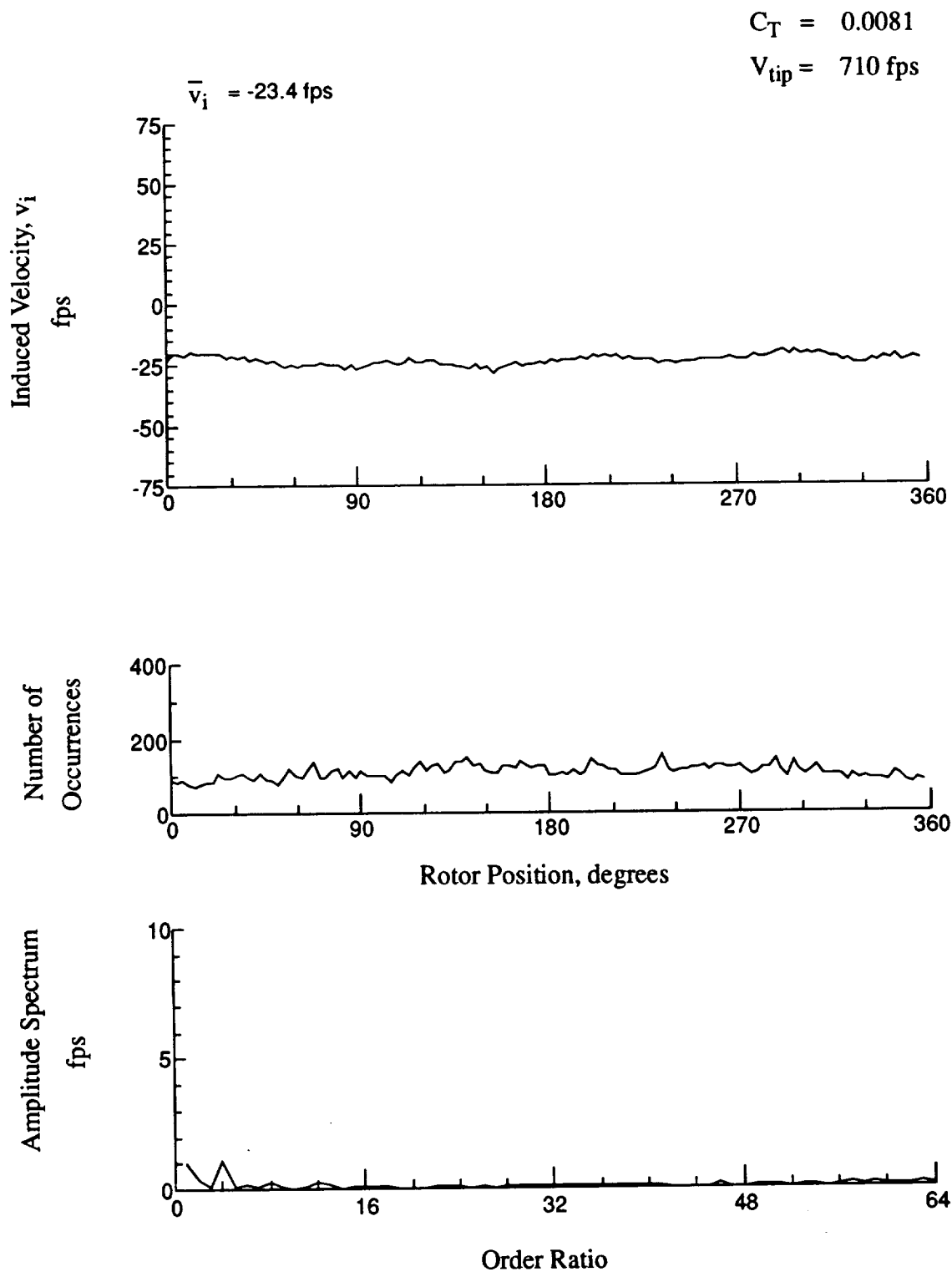
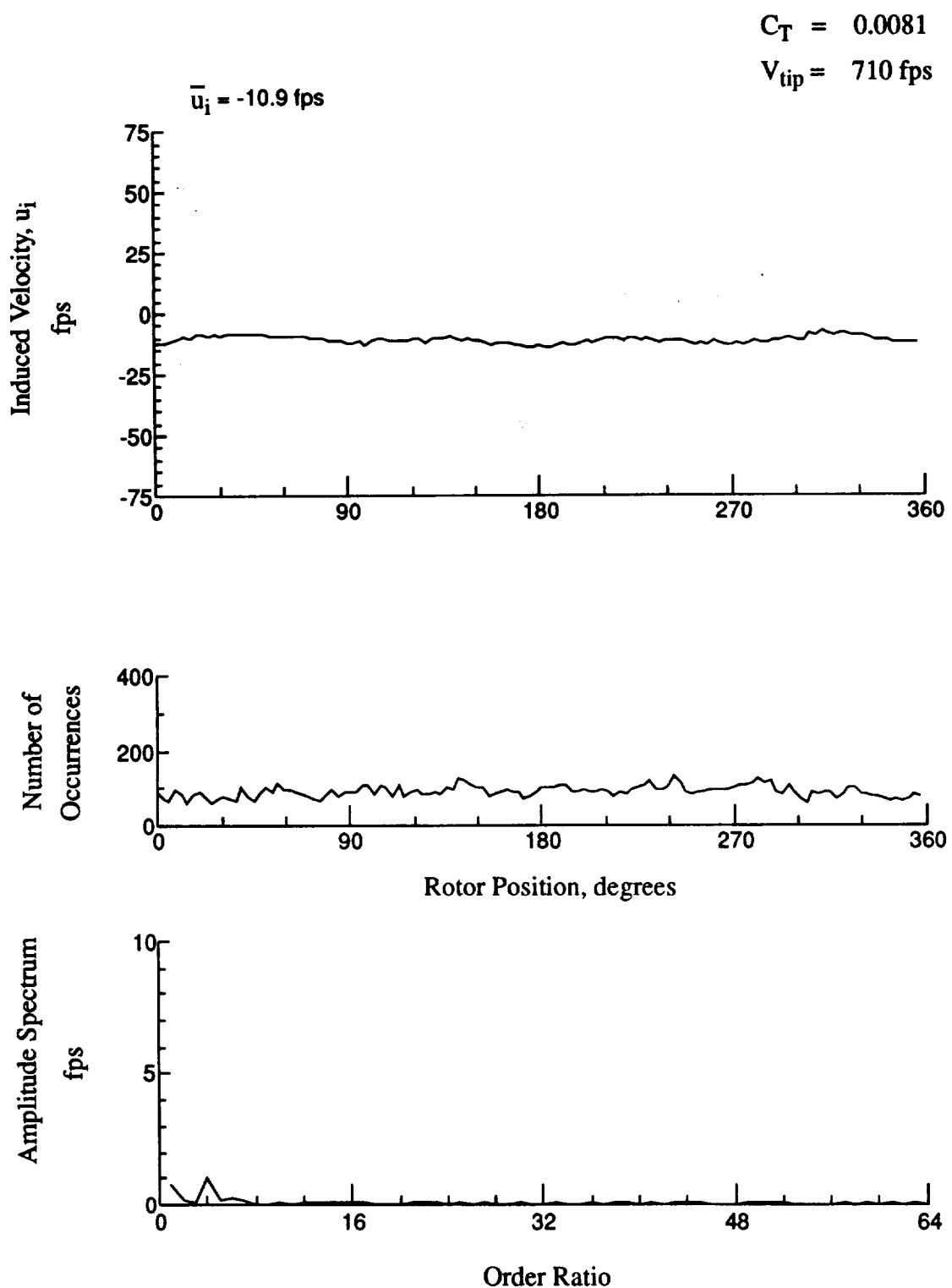


Figure 73.- Concluded.
 $x/R = 1.10$, $y/R = 0.20$, $z = -10.63 \text{ in.}$



**Figure 74.- Wake Measurements at
 $x/R = 1.10$, $y/R = 0.20$, $z = -11.66 \text{ in.}$**

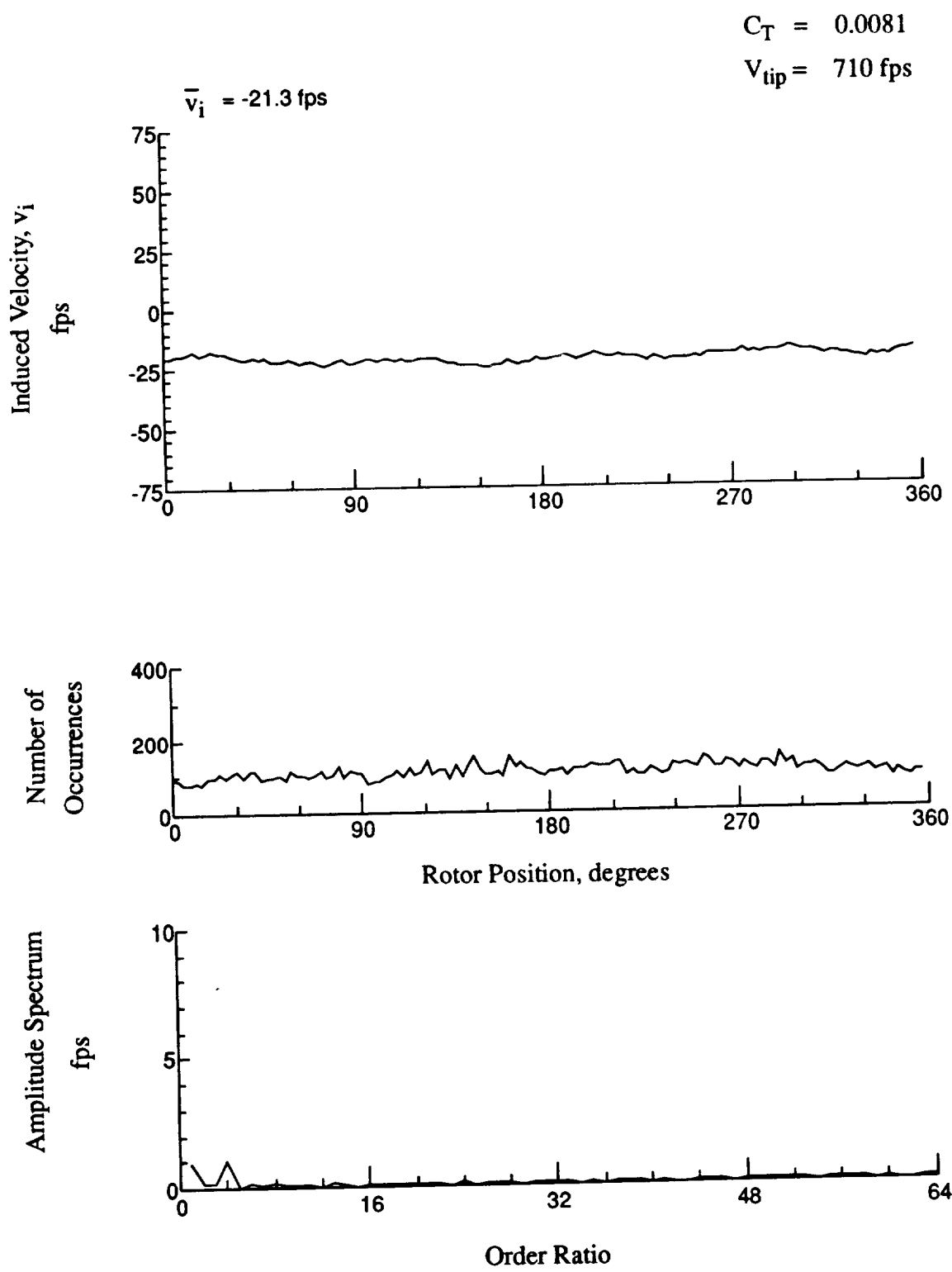


Figure 74.- Concluded.
 $x/R = 1.10$, $y/R = 0.20$, $z = -11.66 \text{ in.}$

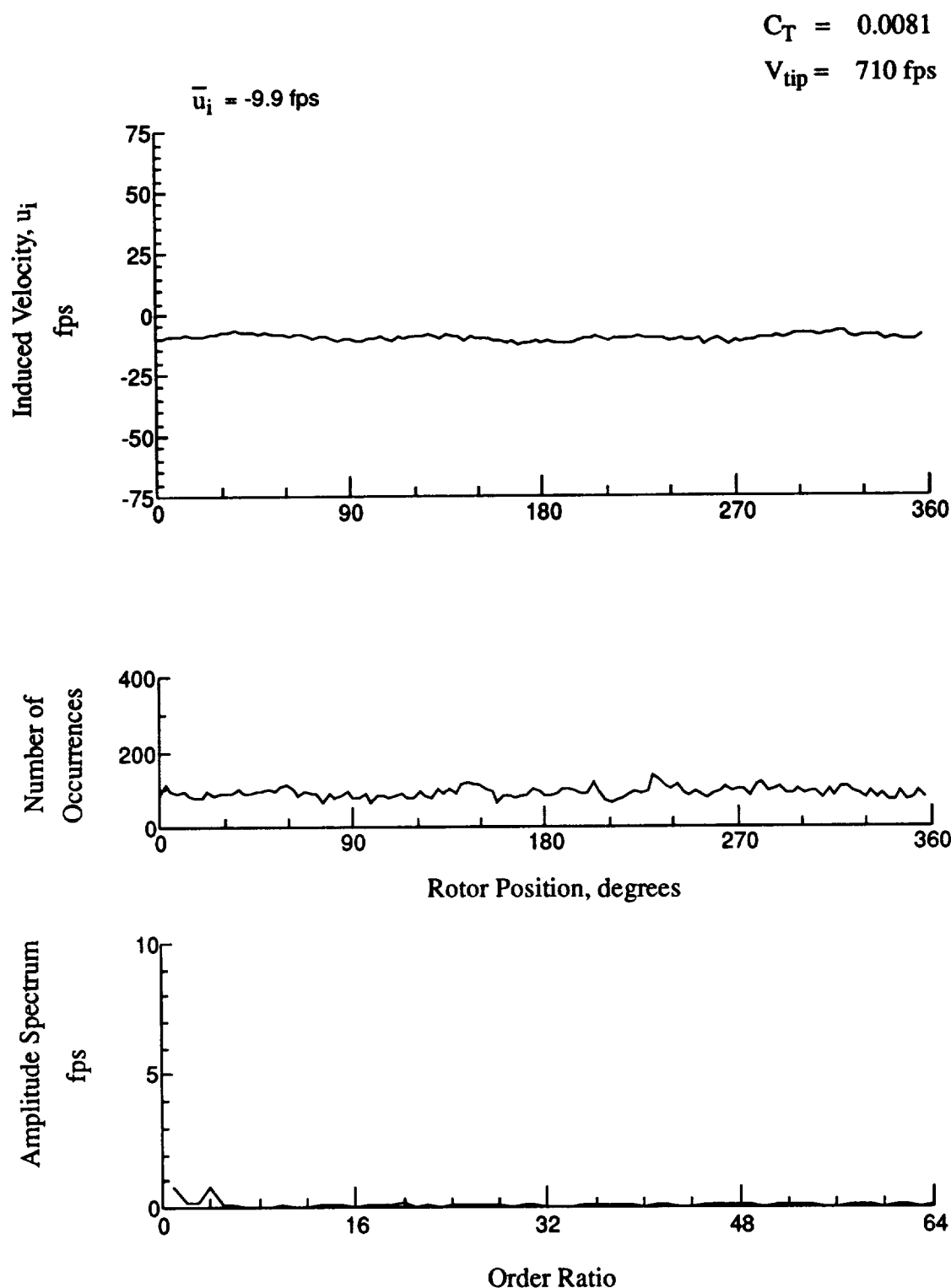


Figure 75.- Wake Measurements at
 $x/R = 1.10$, $y/R = 0.20$, $z = -12.64 \text{ in.}$

$$C_T = 0.0081$$

$$V_{tip} = 710 \text{ fps}$$

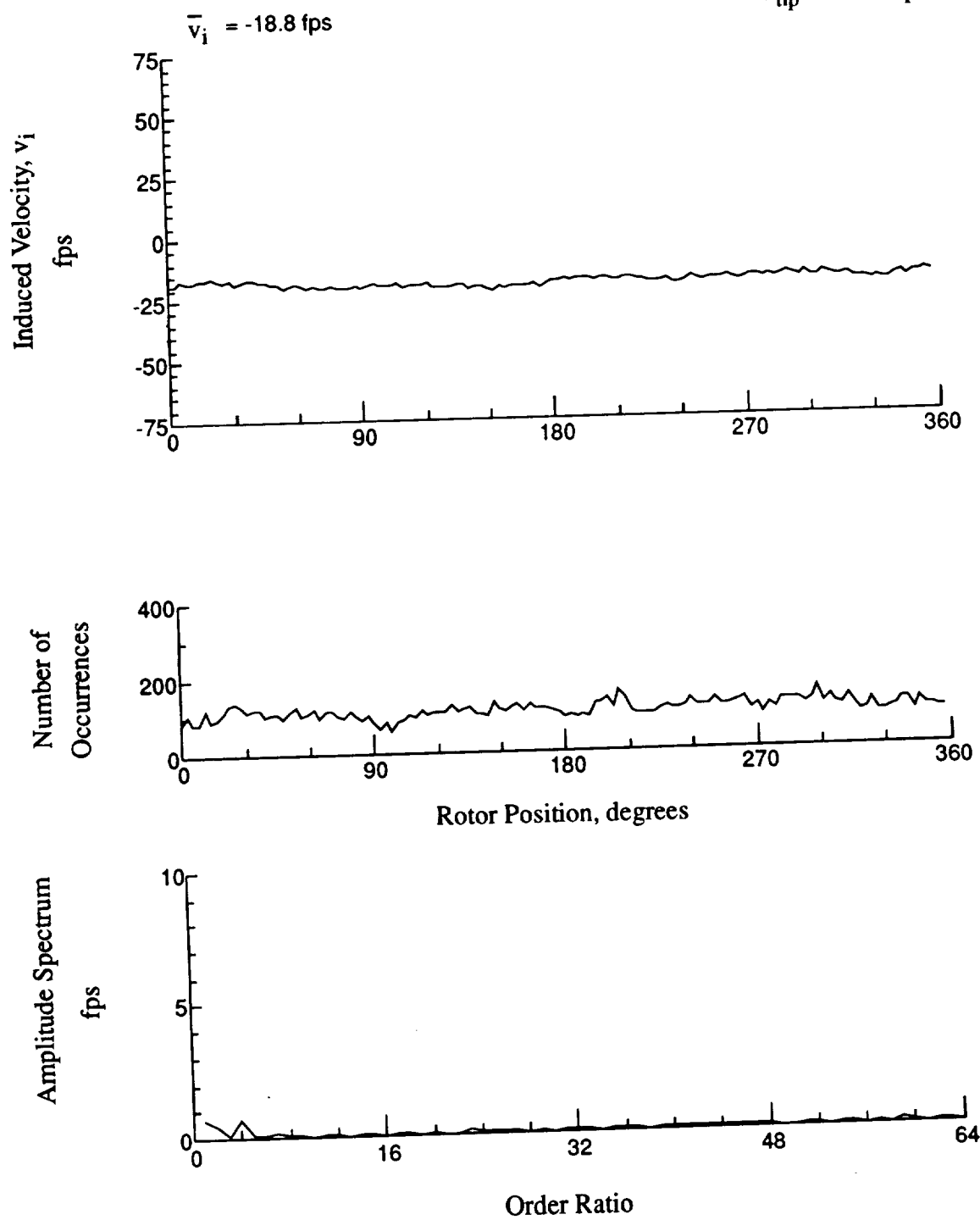


Figure 75.- Concluded.
 $x/R = 1.10$, $y/R = 0.20$, $z = -12.64 \text{ in.}$

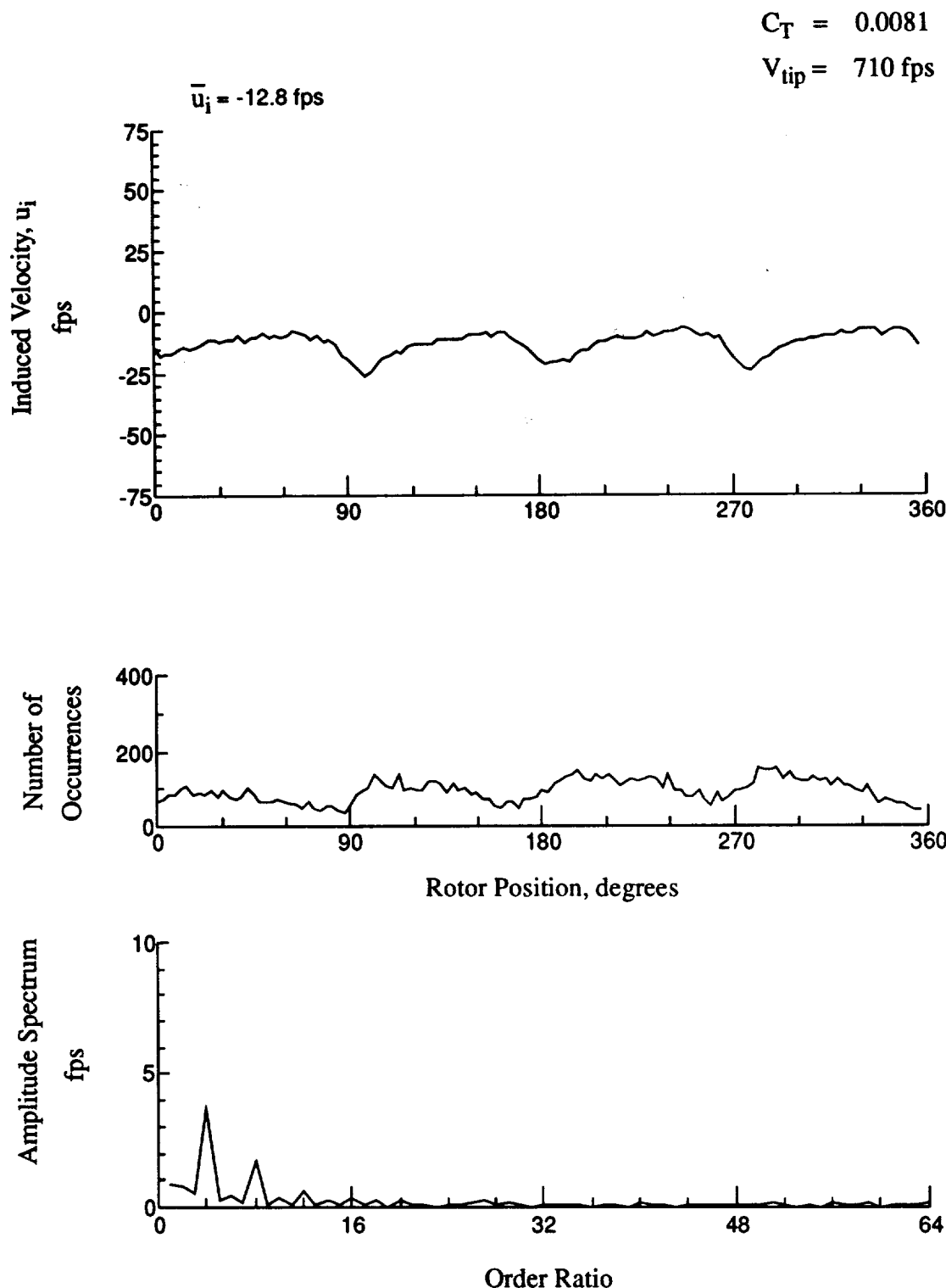


Figure 76.- Wake Measurements at
 $x/R = 1.50$, $y/R = 0.20$, $z = 6.93 \text{ in.}$

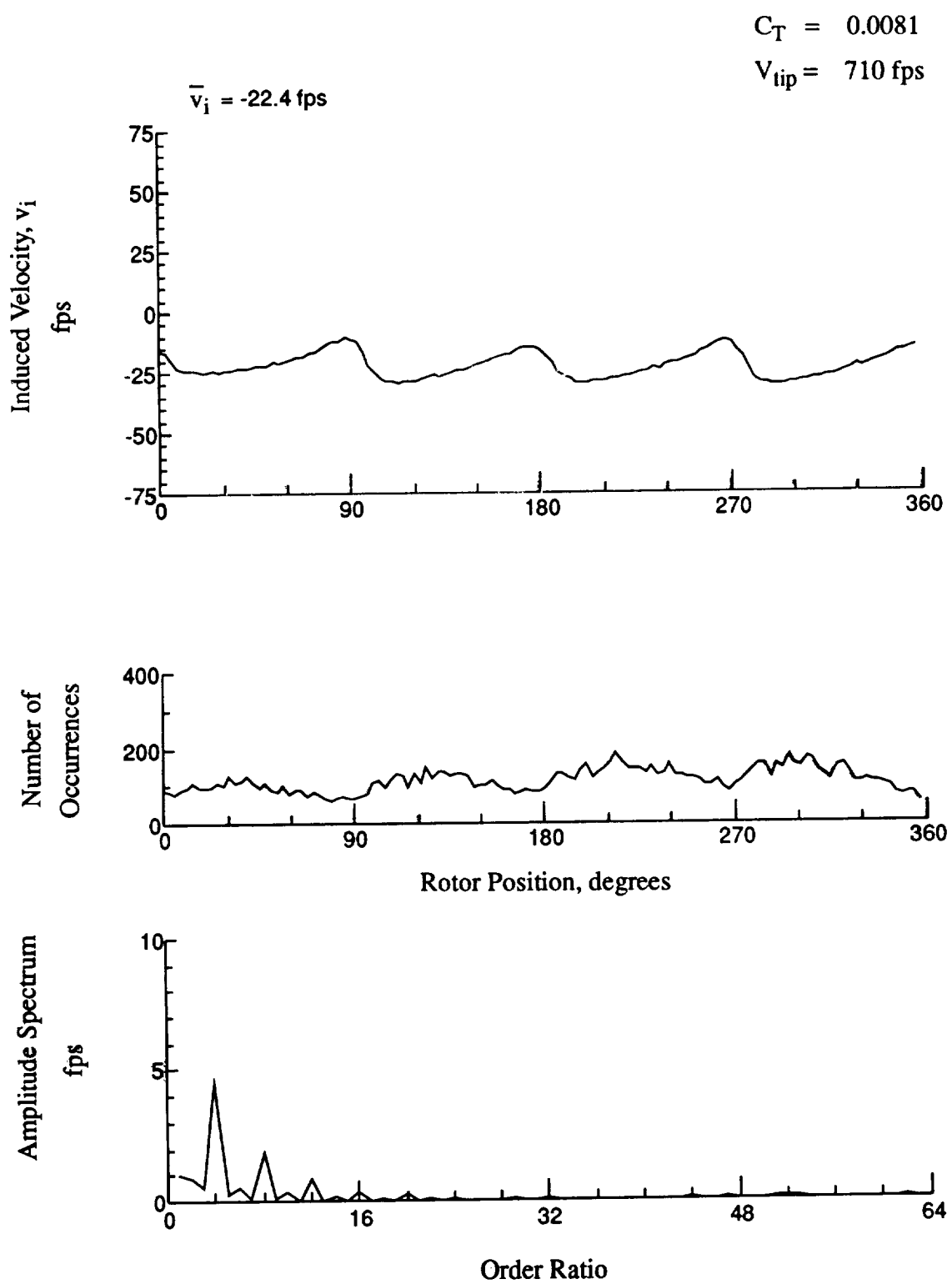


Figure 76.- Concluded.
 $x/R = 1.50$, $y/R = 0.20$, $z = 6.93 \text{ in.}$

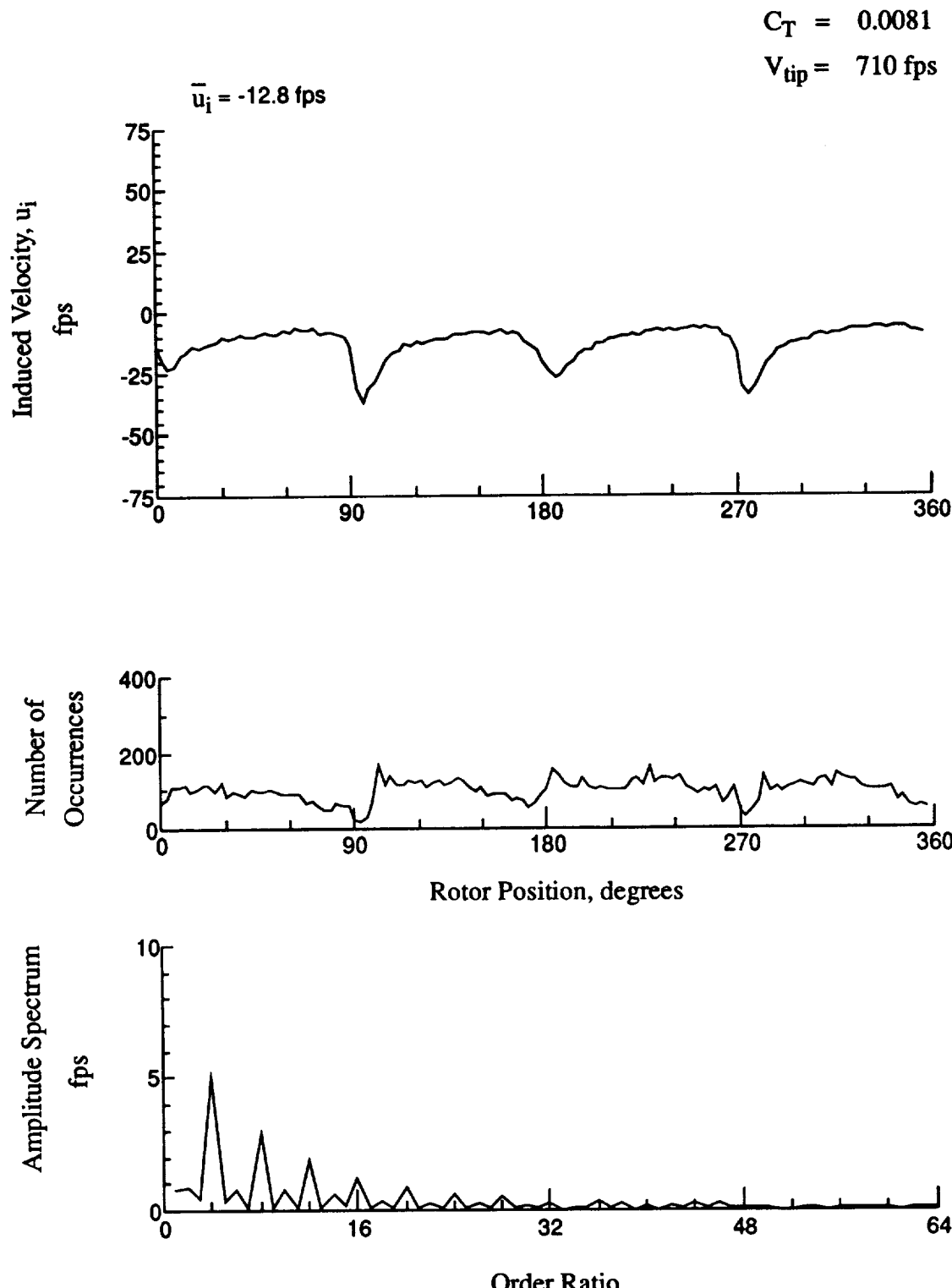


Figure 77.- Wake Measurements at
 $x/R = 1.50$, $y/R = 0.20$, $z = 5.90 \text{ in.}$

$$C_T = 0.0081$$

$$V_{tip} = 710 \text{ fps}$$

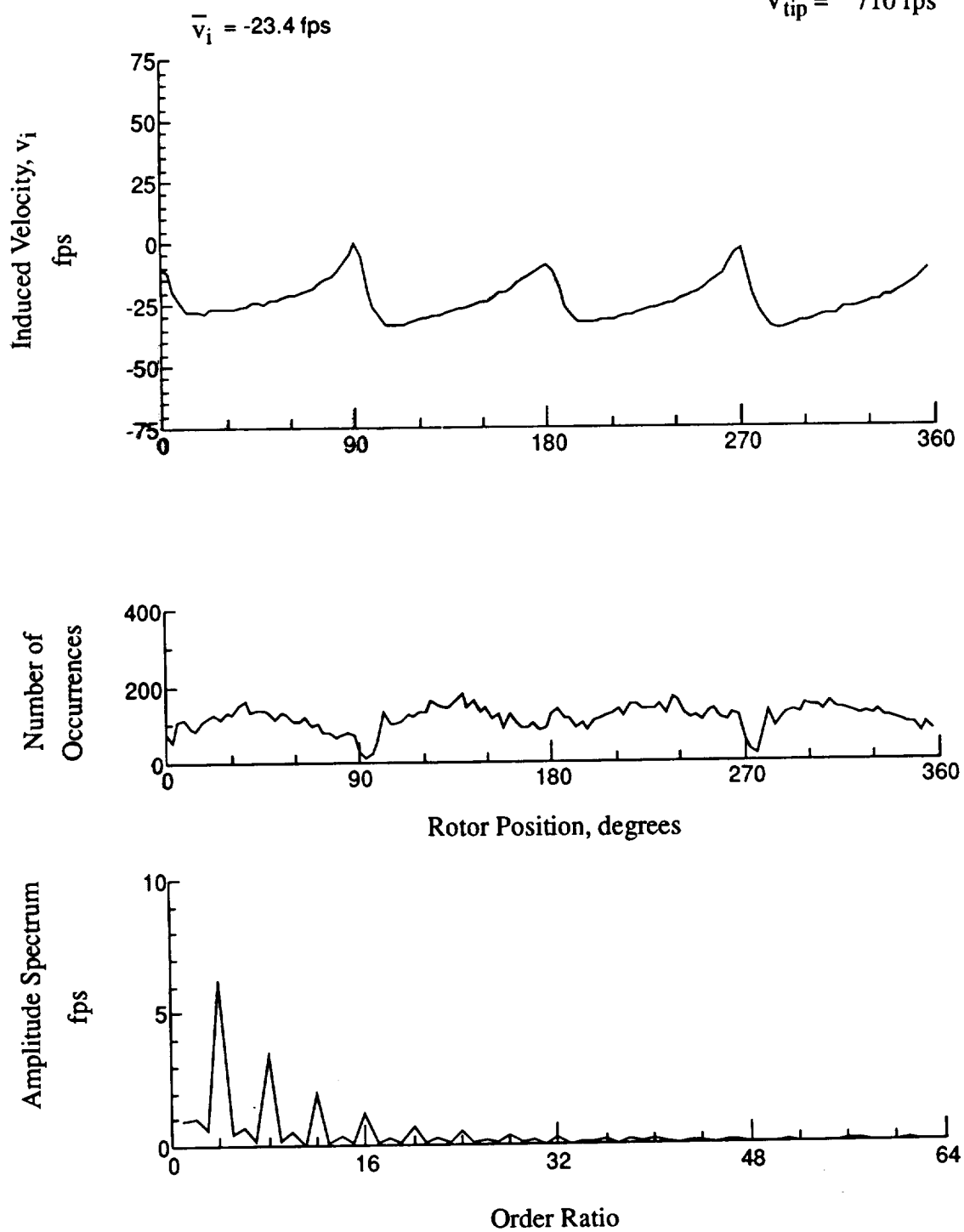


Figure 77.- Concluded.
 $x/R = 1.50$, $y/R = 0.20$, $z = 5.90$ in.

$$C_T = 0.0081$$

$$V_{tip} = 710 \text{ fps}$$

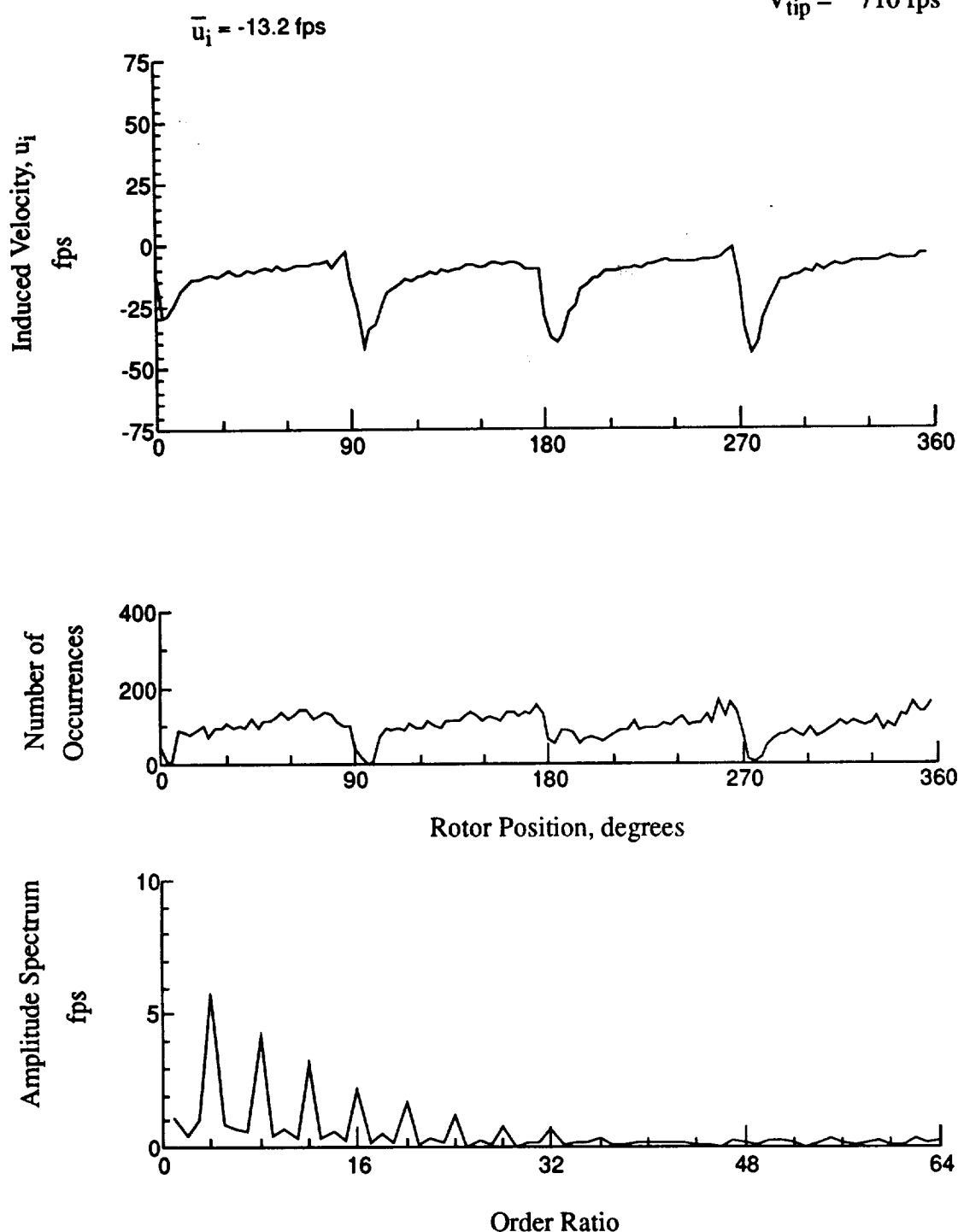


Figure 78.- Wake Measurements at
 $x/R = 1.50$, $y/R = 0.20$, $z = 4.87$ in.

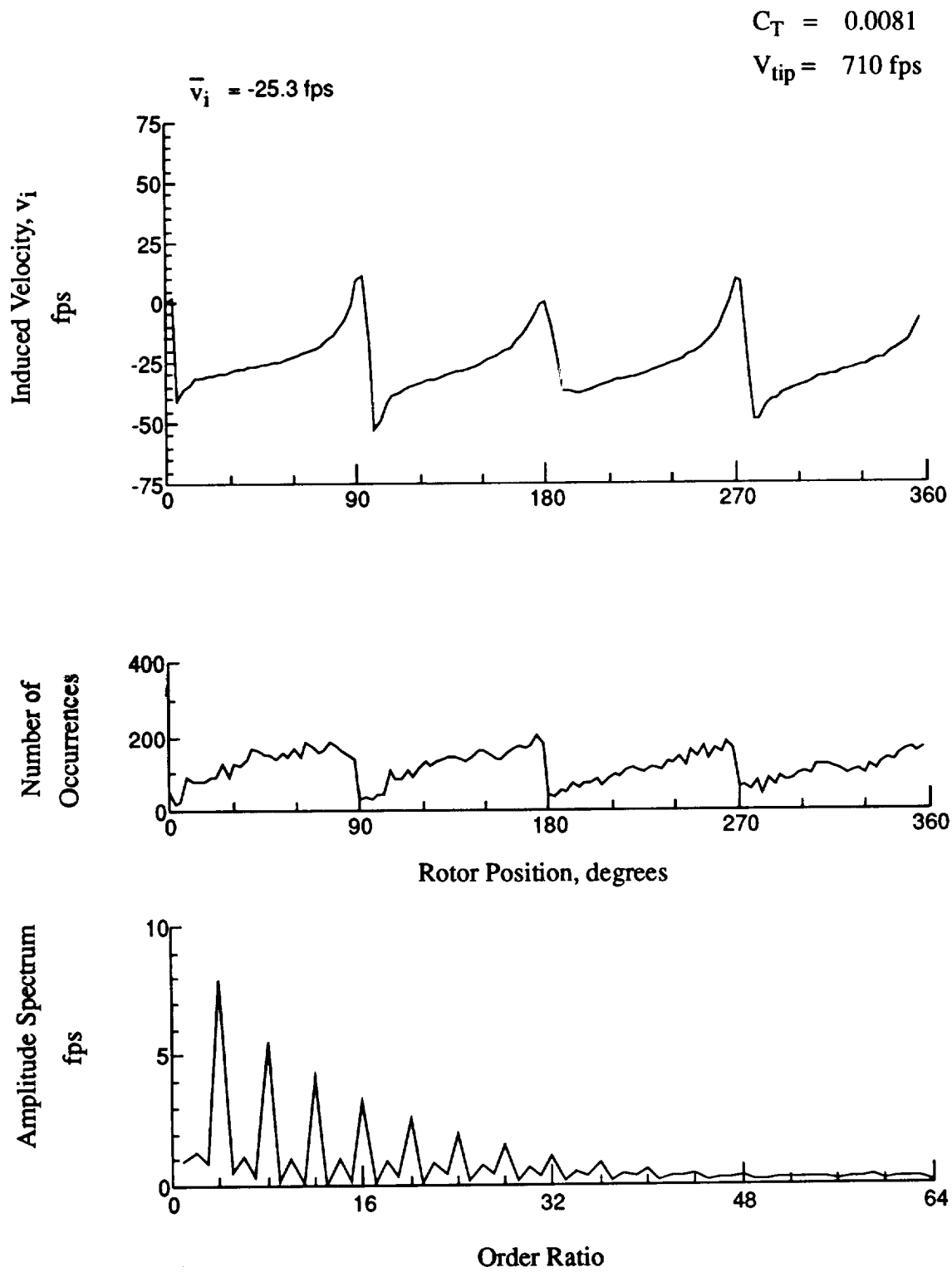
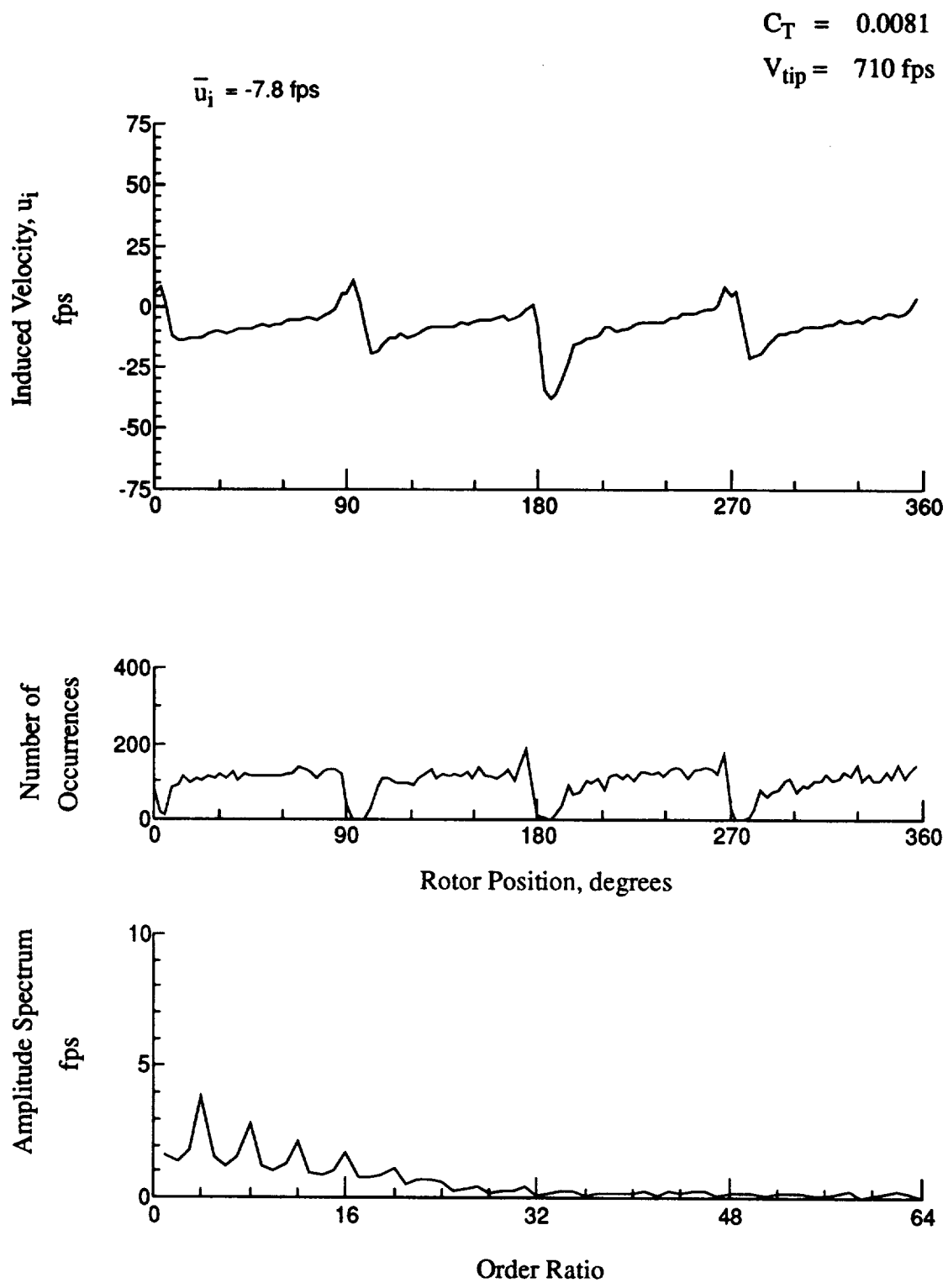


Figure 78.- Concluded.
 $x/R = 1.50$, $y/R = 0.20$, $z = 4.87 \text{ in.}$



**Figure 79.- Wake Measurements at
 $x/R = 1.50$, $y/R = 0.20$, $z = 3.84$ in.**

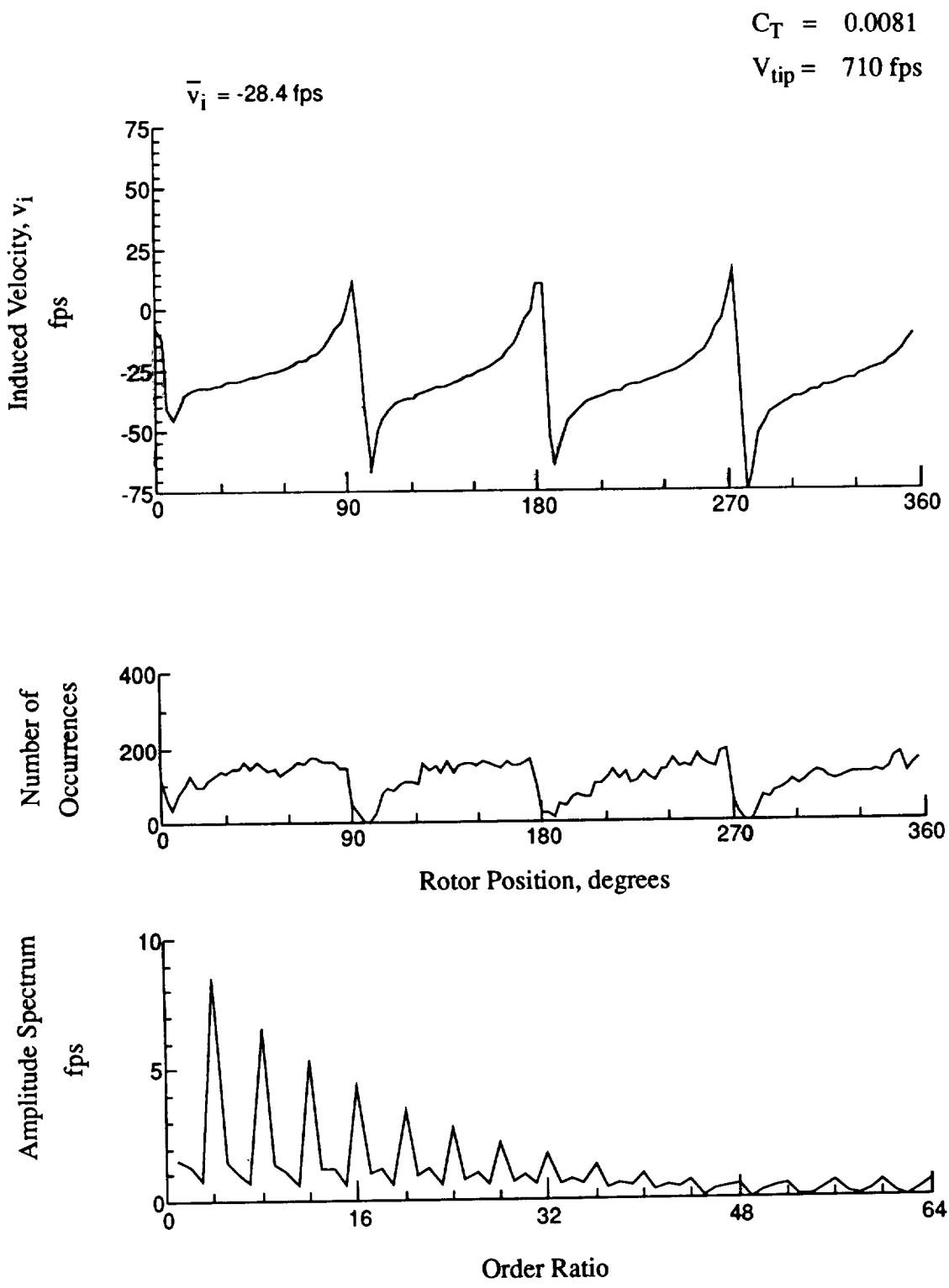


Figure 79.- Concluded.
 $x/R = 1.50$, $y/R = 0.20$, $z = 3.84 \text{ in.}$

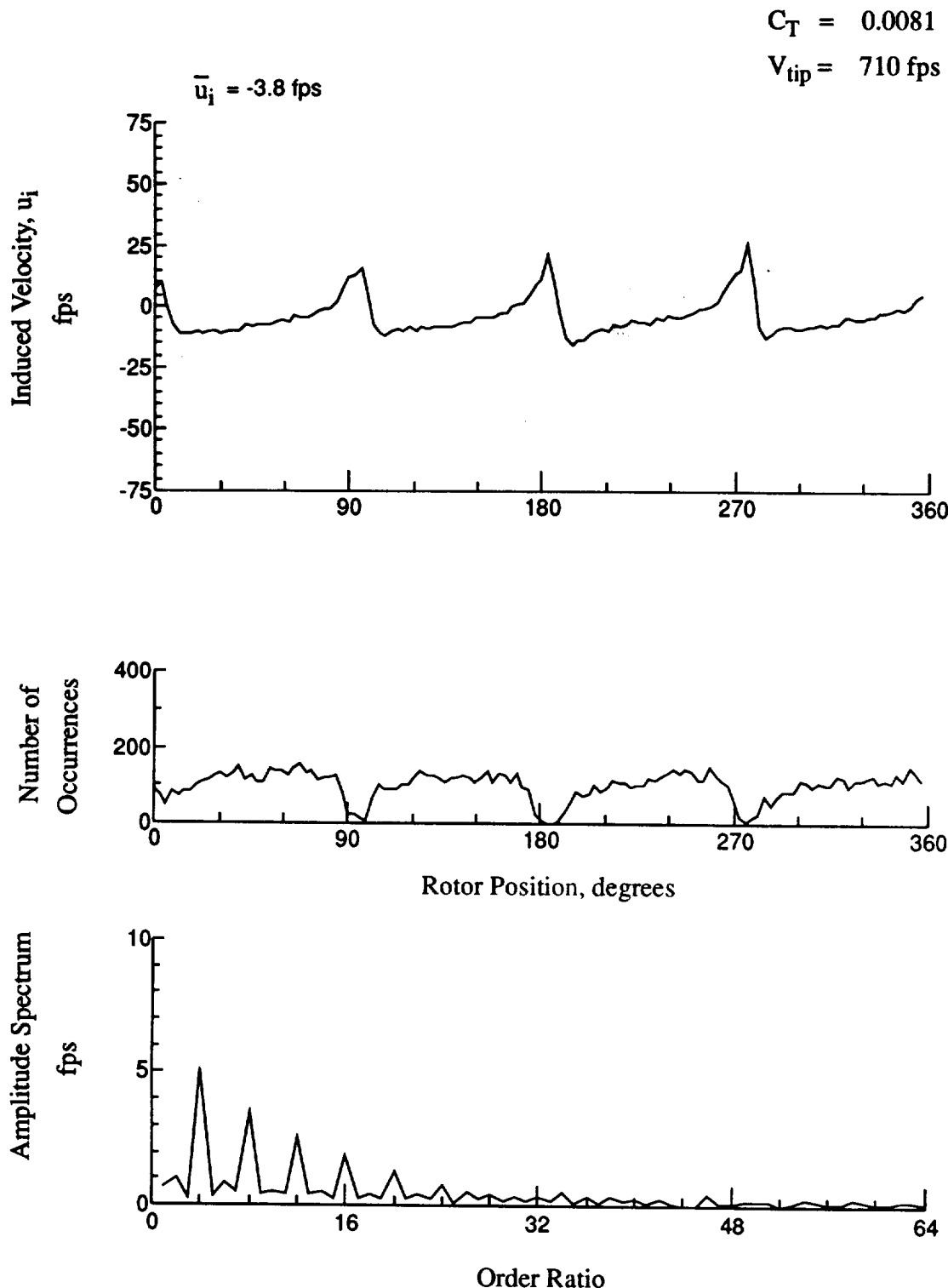


Figure 80.- Wake Measurements at
 $x/R = 1.50$, $y/R = 0.20$, $z = 2.81 \text{ in.}$

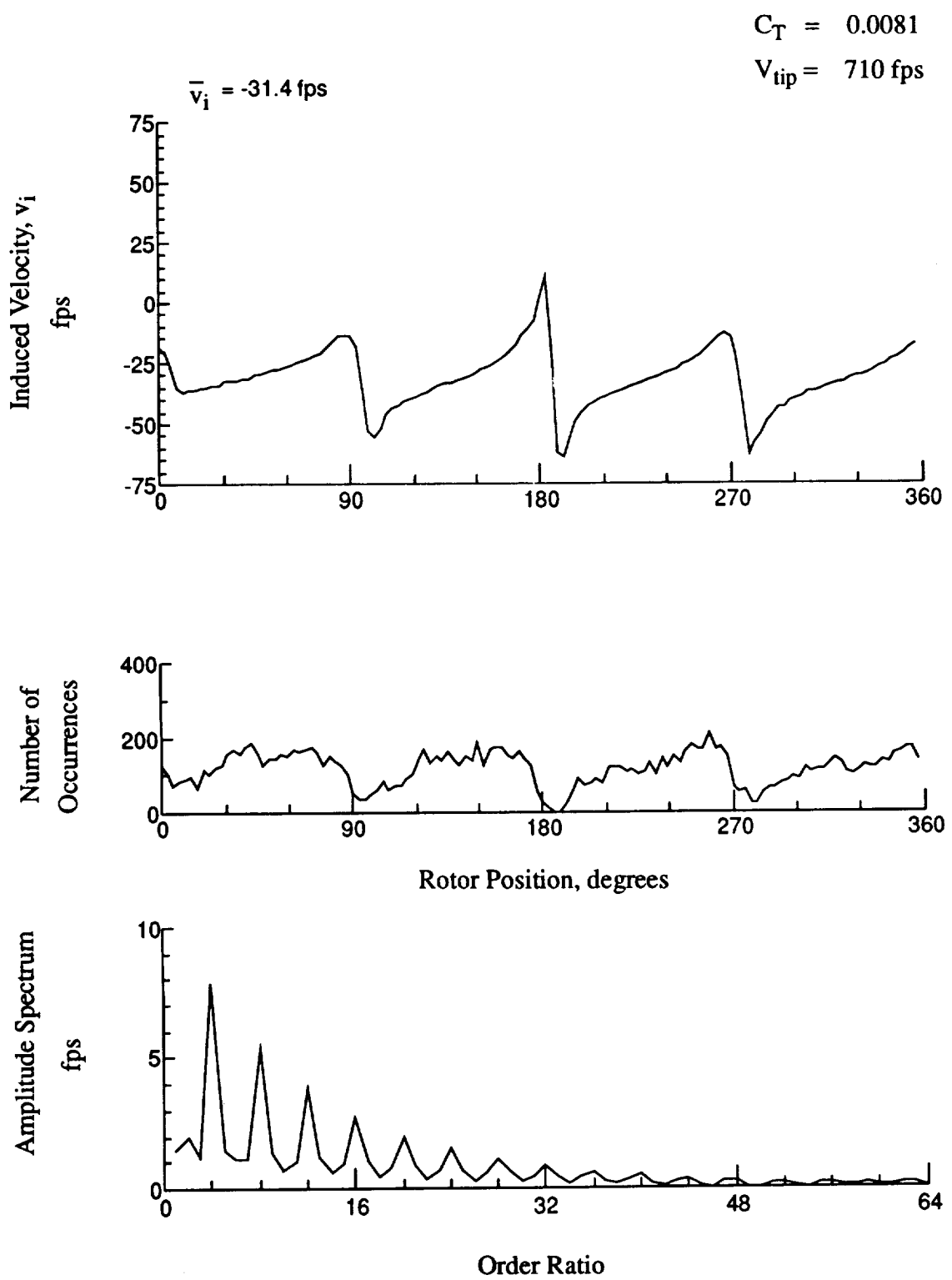
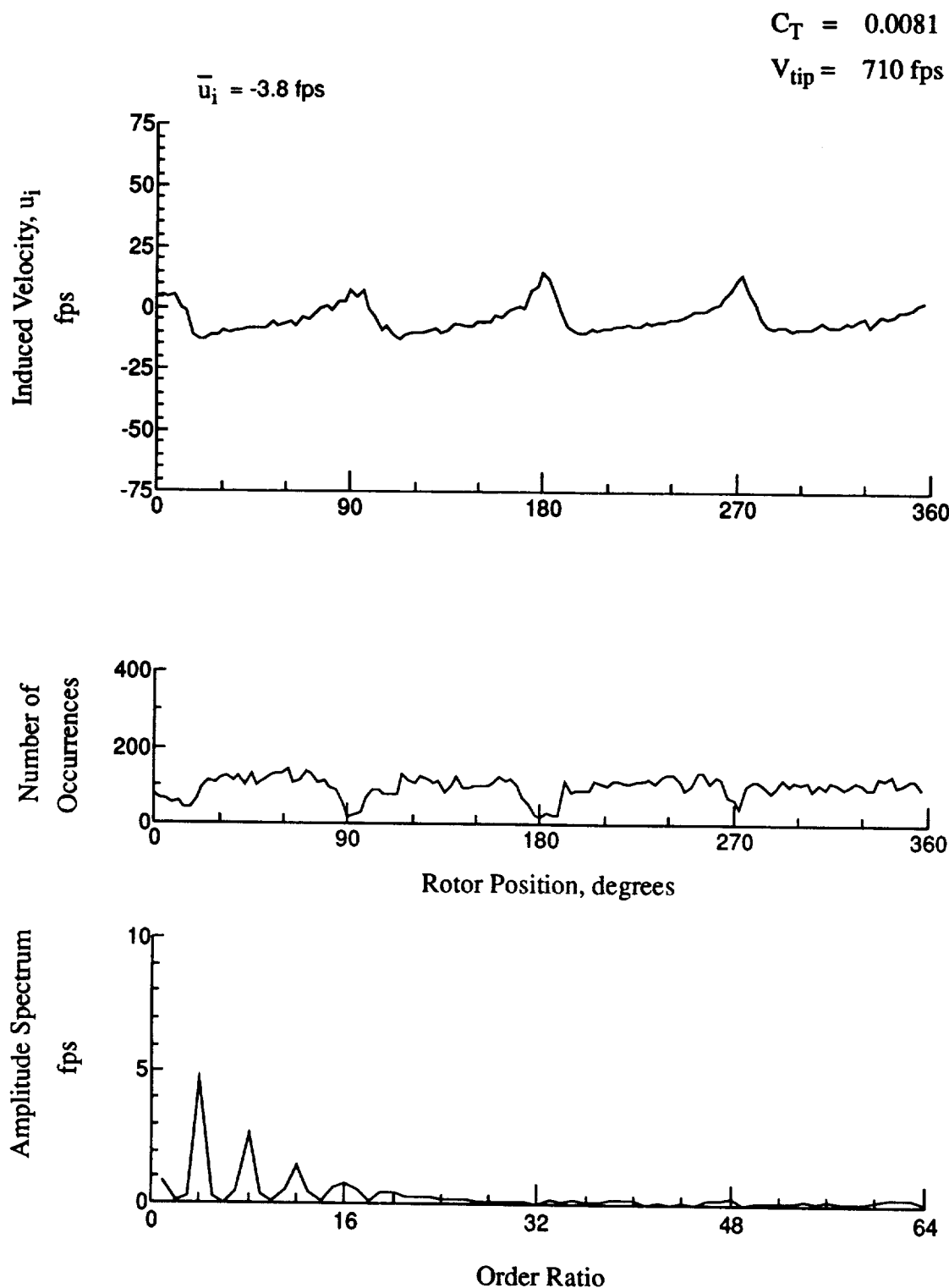


Figure 80.- Concluded.
 $x/R = 1.50$, $y/R = 0.20$, $z = 2.81 \text{ in.}$



**Figure 81.- Wake Measurements at
 $x/R = 1.50$, $y/R = 0.20$, $z = 1.78 \text{ in.}$**

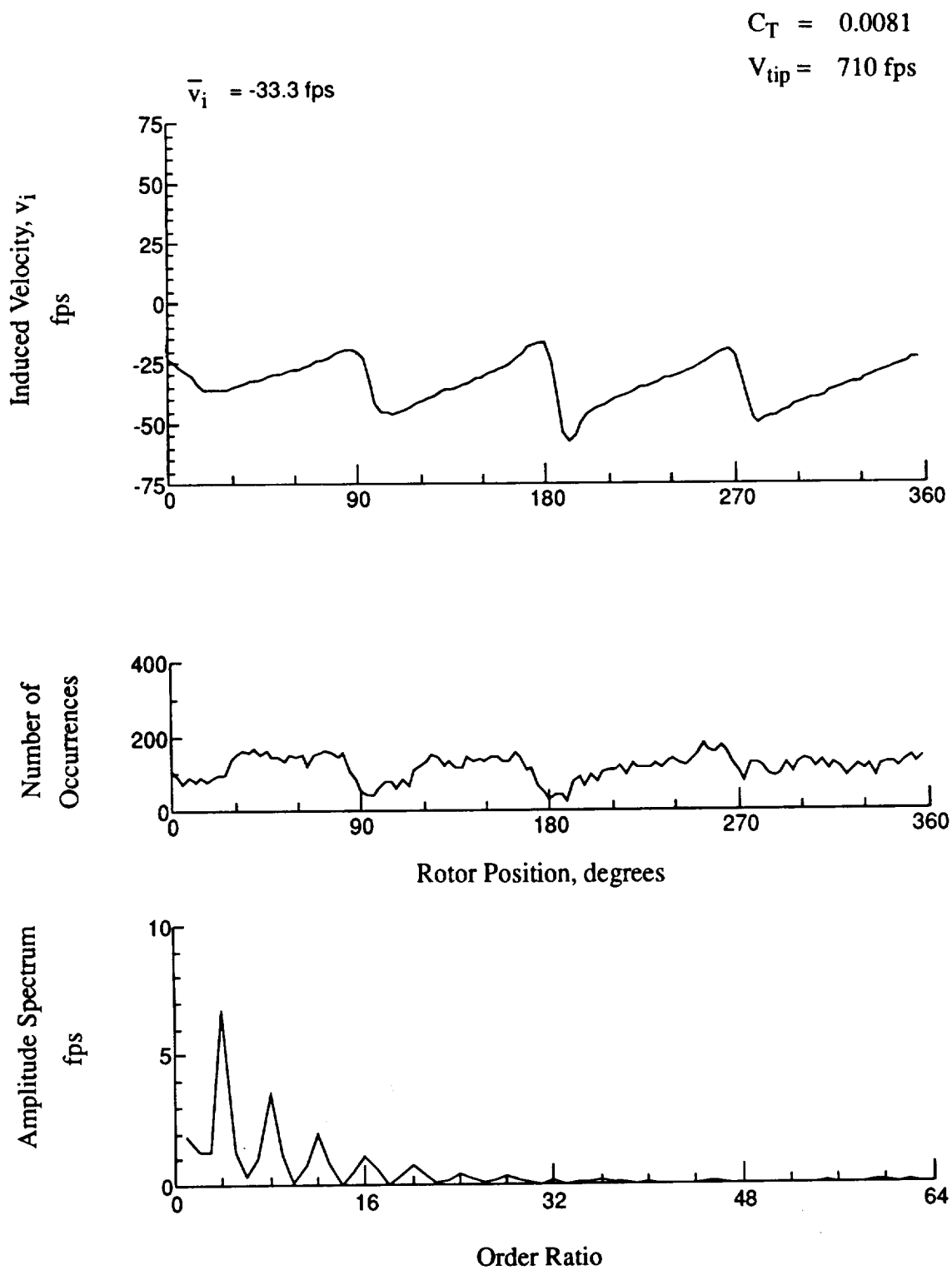
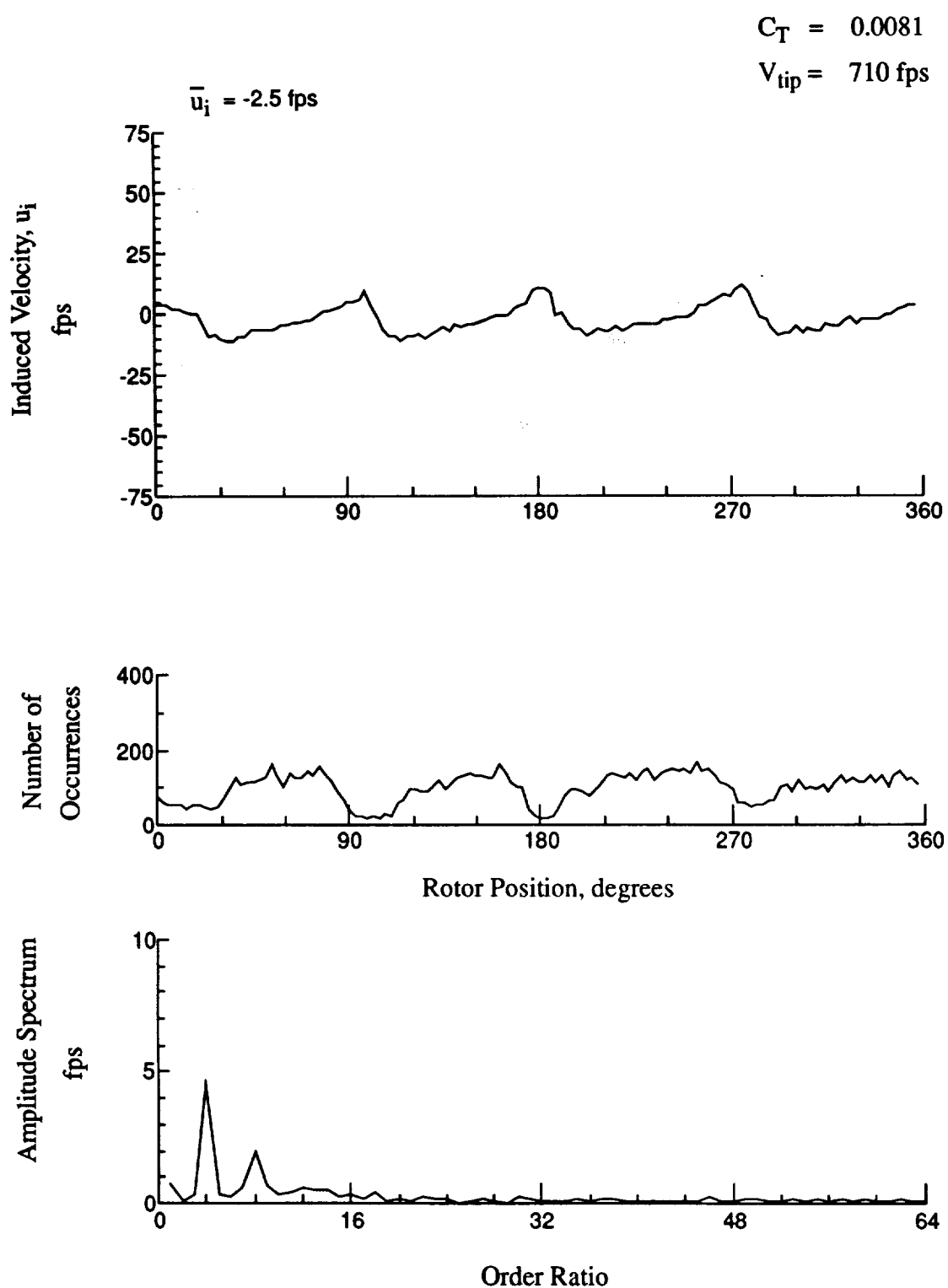


Figure 81.- Concluded.
 $x/R = 1.50$, $y/R = 0.20$, $z = 1.78 \text{ in.}$



**Figure 82.- Wake Measurements at
 $x/R = 1.50$, $y/R = 0.20$, $z = 0.75 \text{ in.}$**

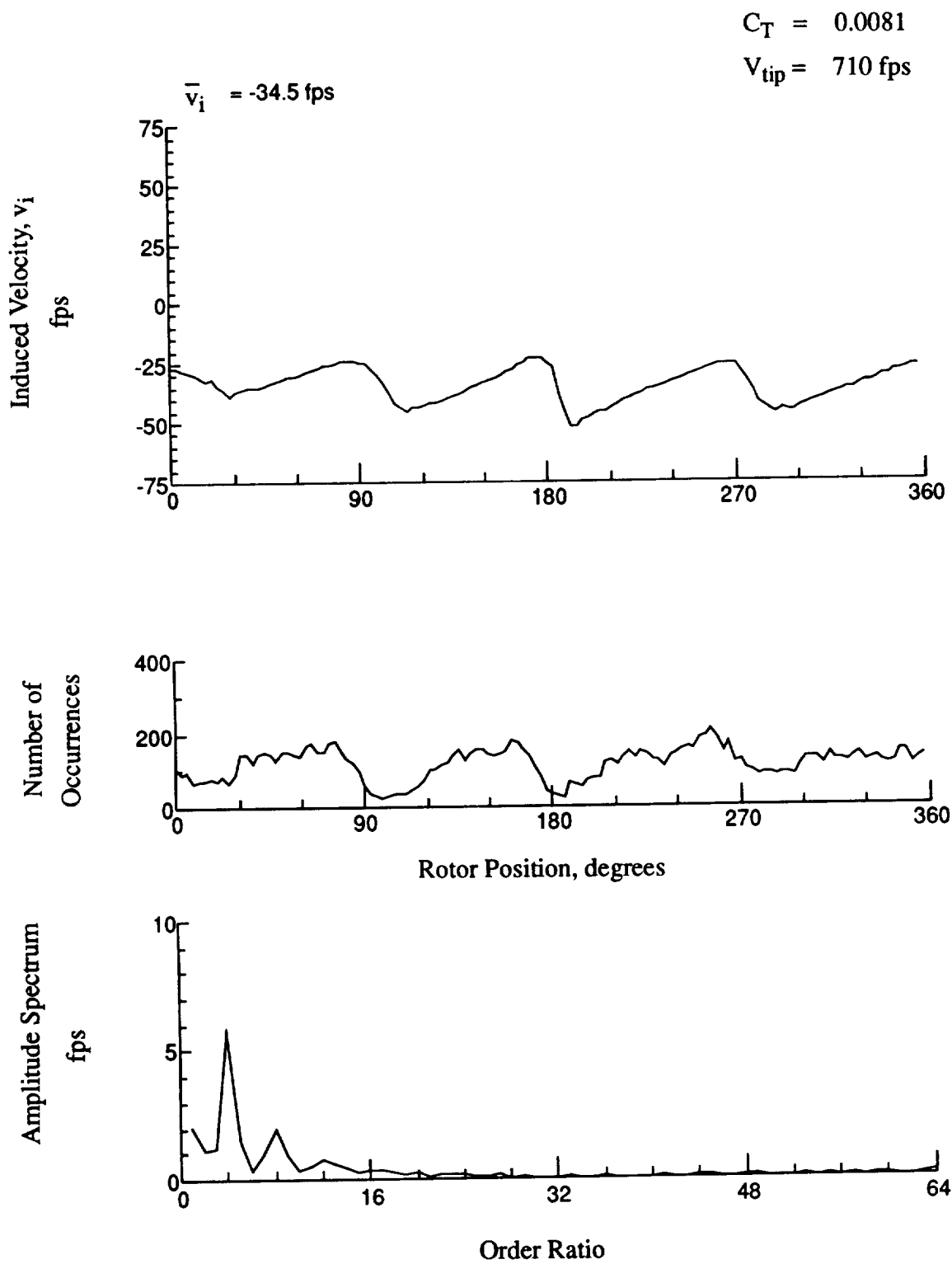
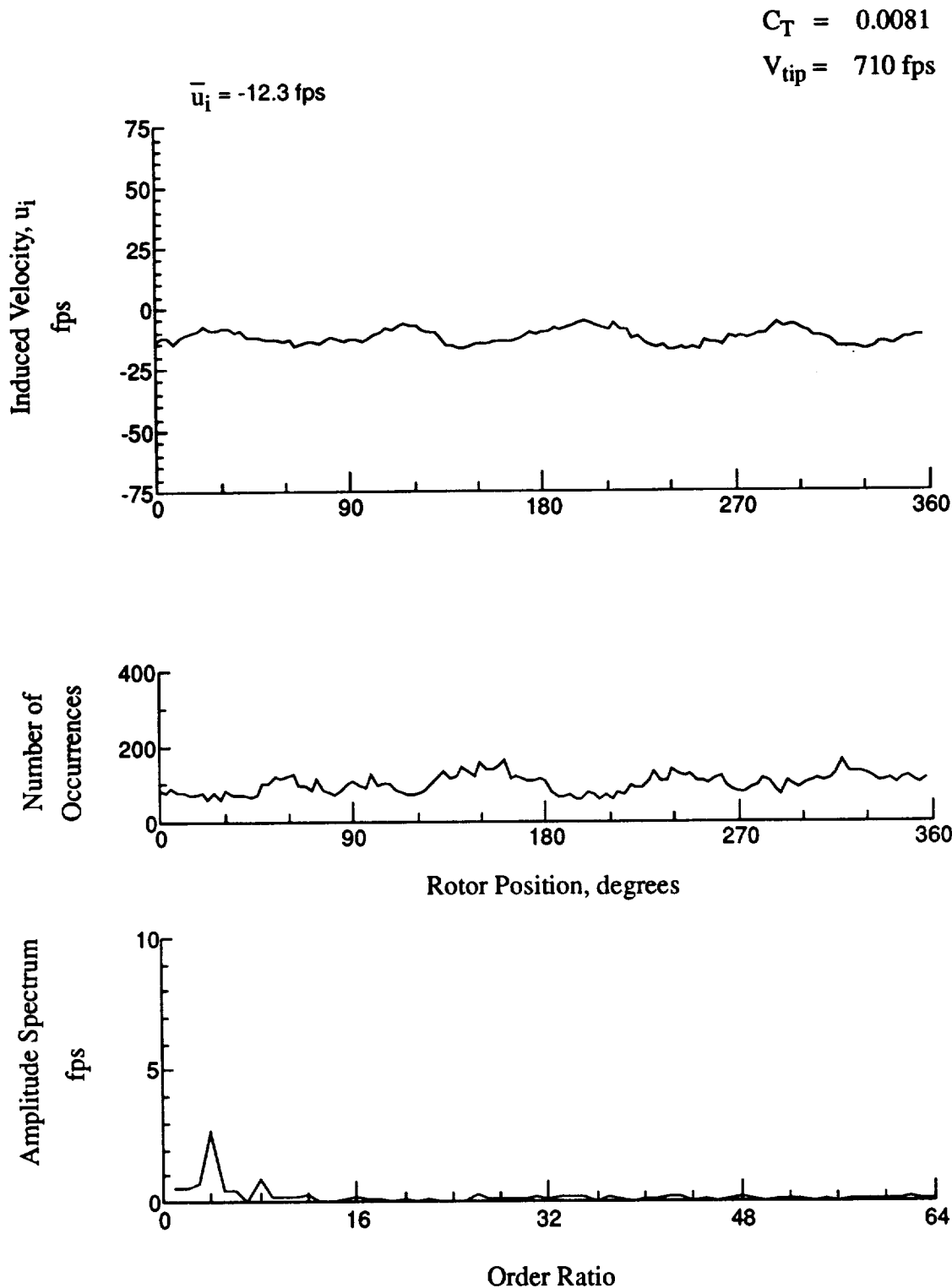


Figure 82.- Concluded.
 $x/R = 1.50$, $y/R = 0.20$, $z = 0.75 \text{ in.}$



**Figure 83.- Wake Measurements at
 $x/R = 1.50$, $y/R = 0.20$, $z = -7.40 \text{ in.}$**

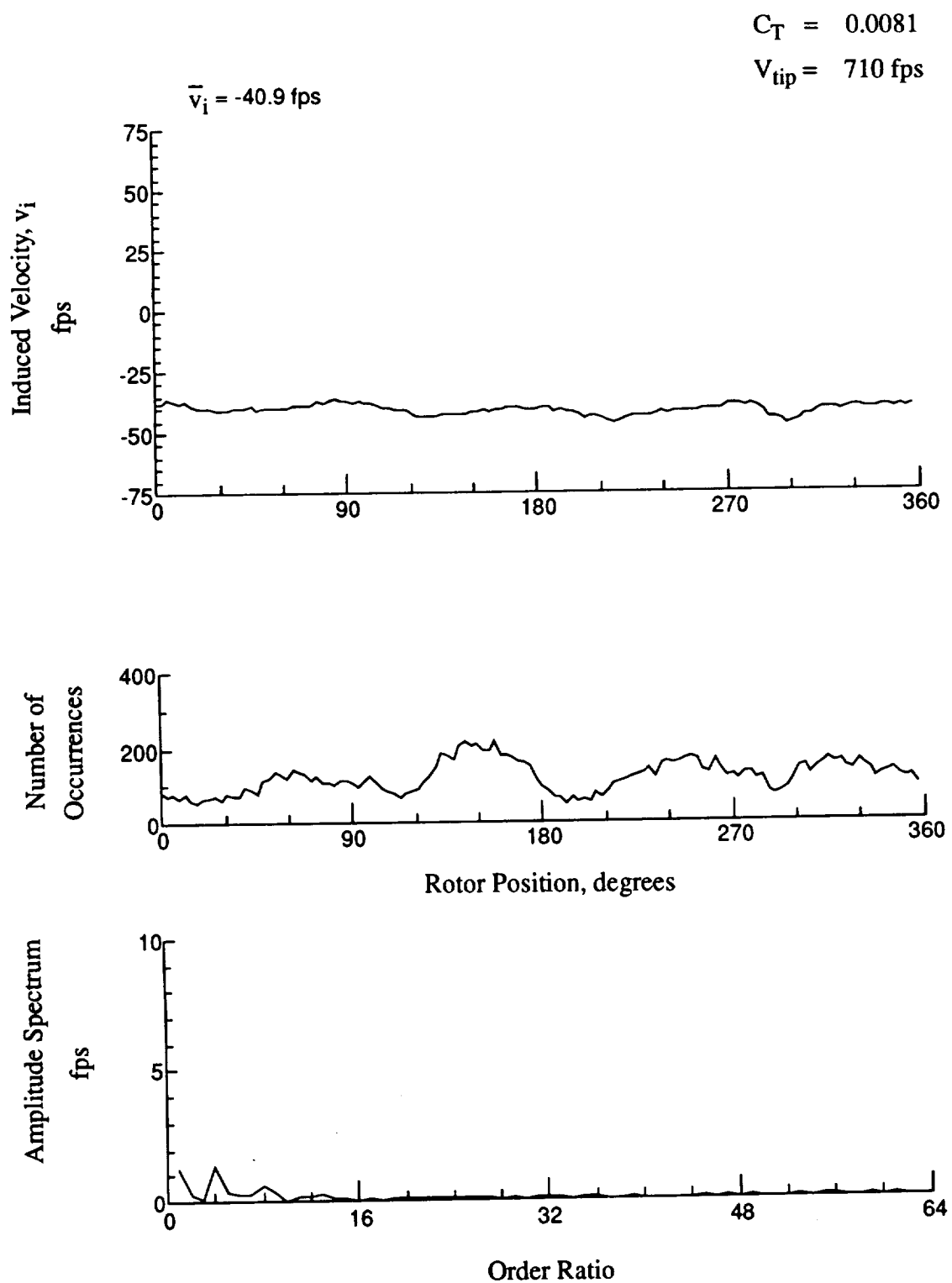


Figure 83.- Concluded.
 $x/R = 1.50$, $y/R = 0.20$, $z = -7.40 \text{ in.}$

$$C_T = 0.0081$$

$$V_{tip} = 710 \text{ fps}$$

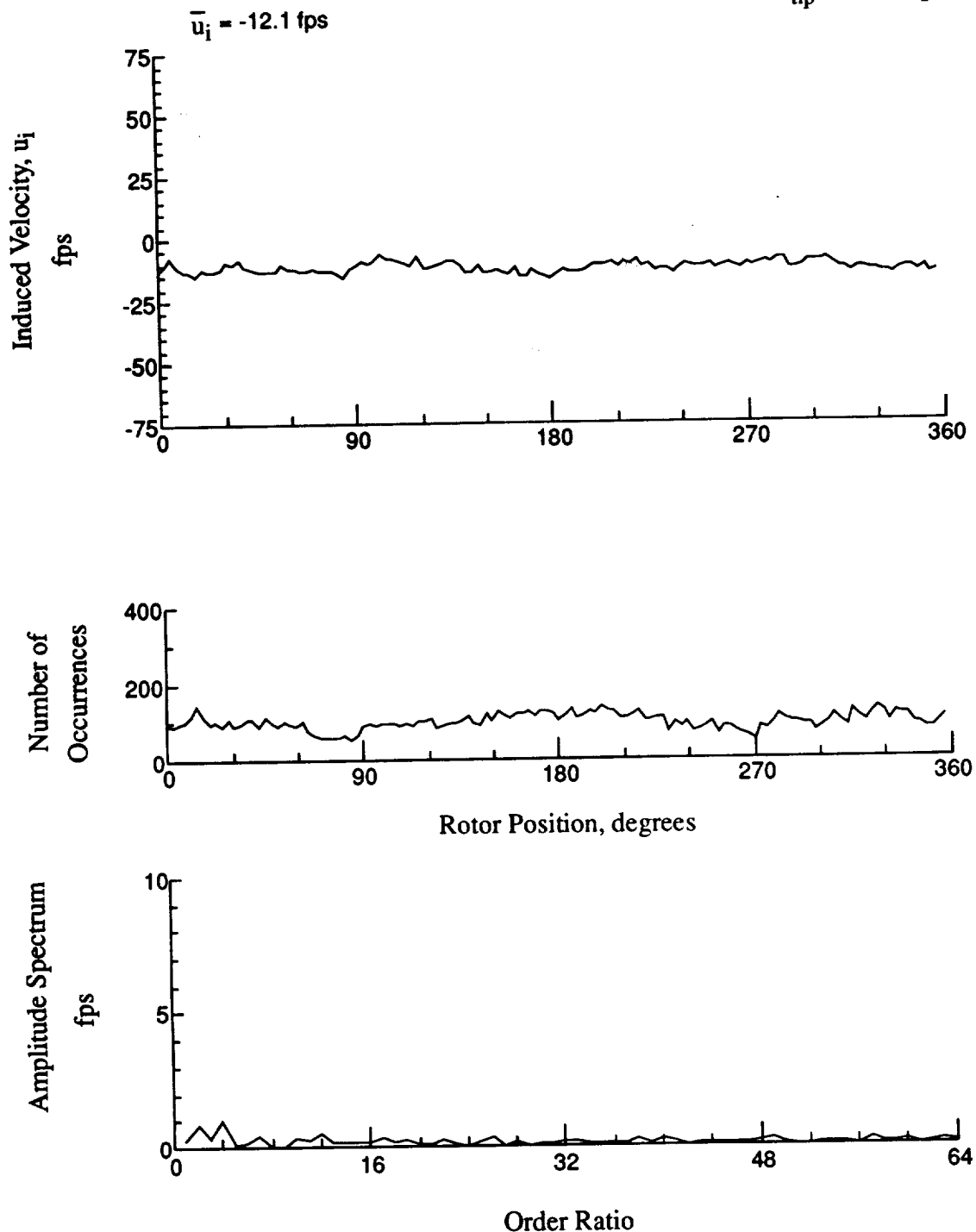


Figure 84.- Wake Measurements at
 $x/R = 1.50$, $y/R = 0.20$, $z = -8.50 \text{ in.}$

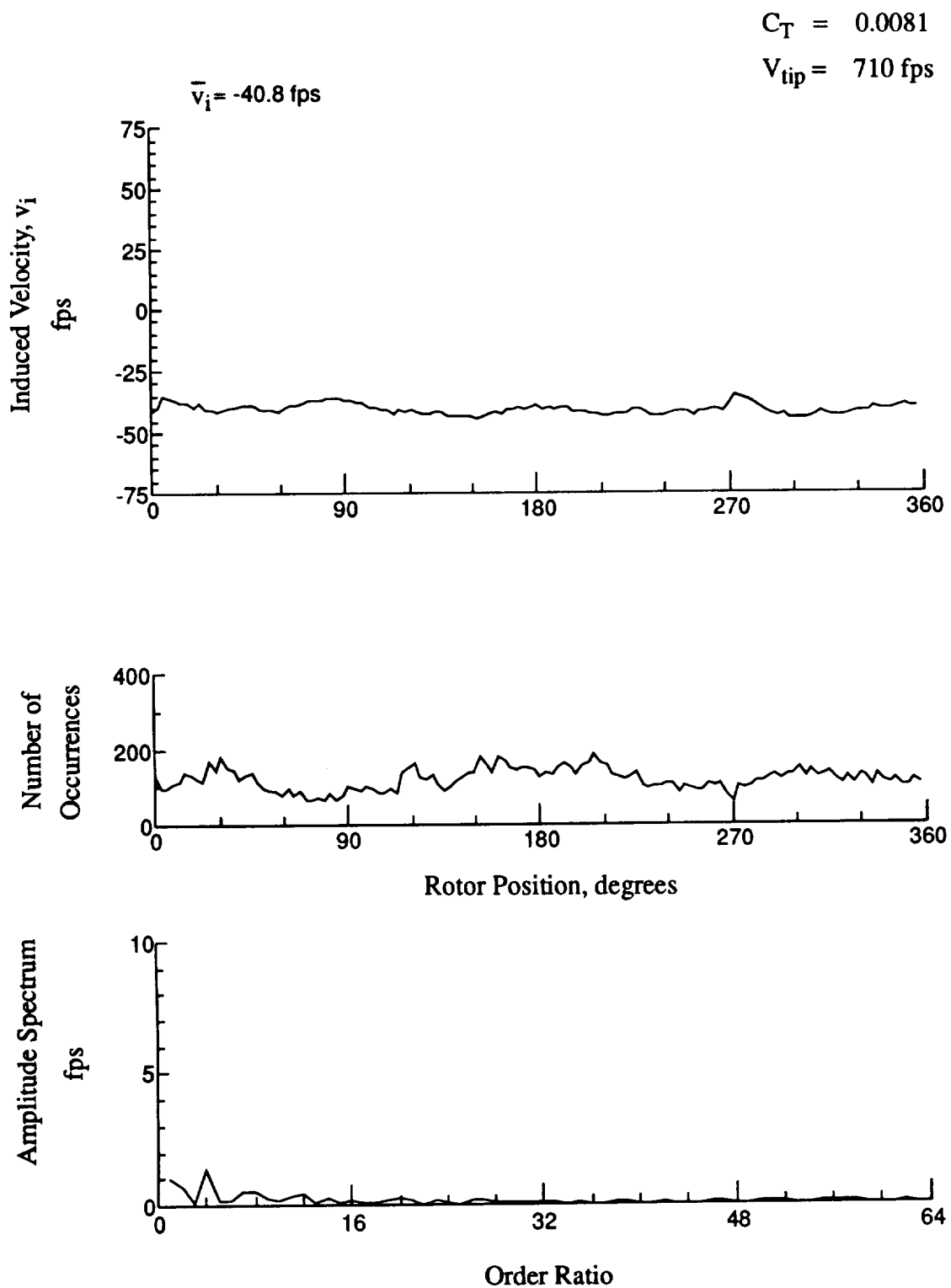
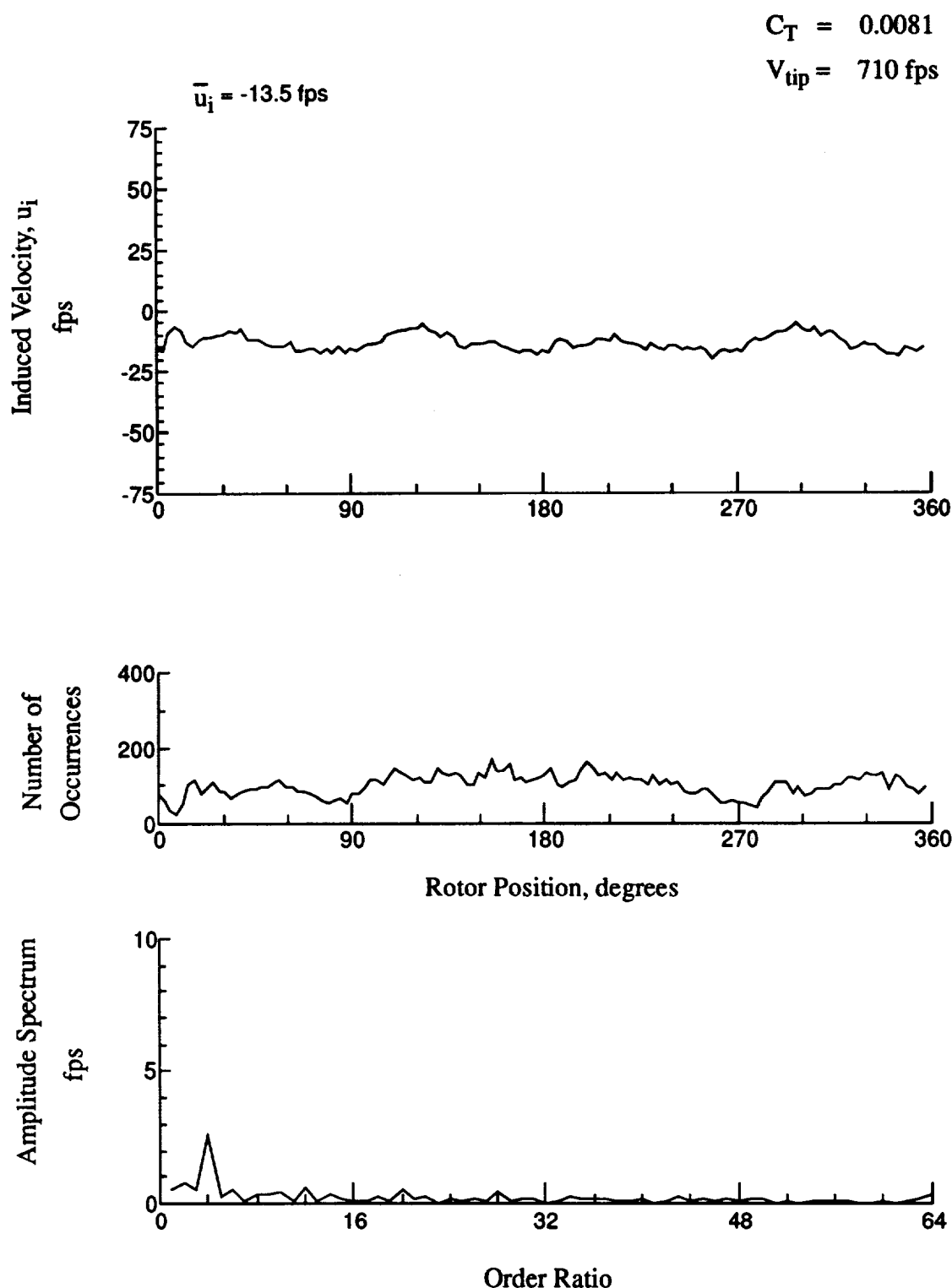


Figure 84.- Concluded.
 $x/R = 1.50$, $y/R = 0.20$, $z = -8.50 \text{ in.}$



**Figure 85.- Wake Measurements at
 $x/R = 1.50$, $y/R = 0.20$, $z = -9.53 \text{ in.}$**

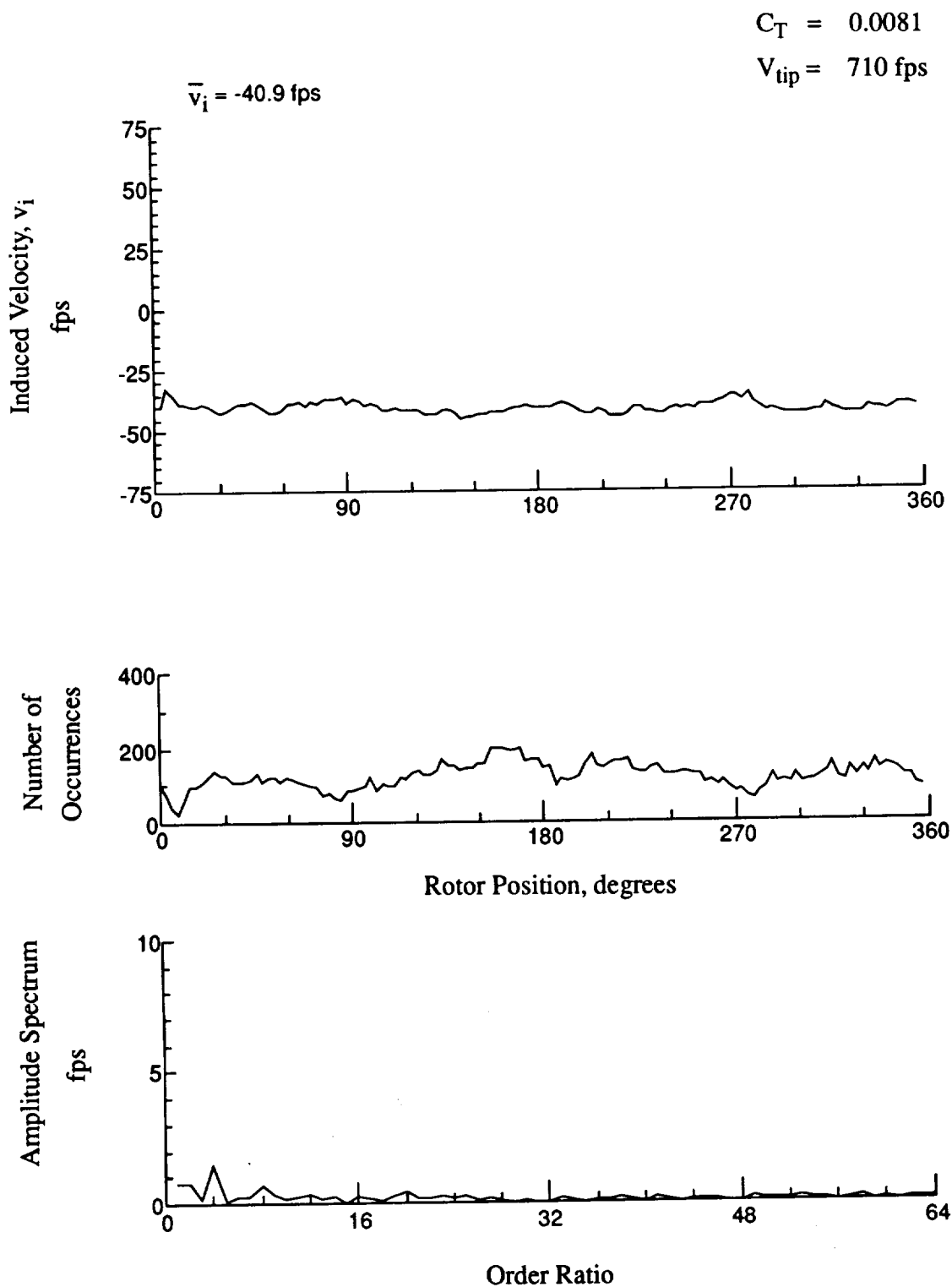


Figure 85.- Concluded.
 $x/R = 1.50$, $y/R = 0.20$, $z = -9.53 \text{ in.}$

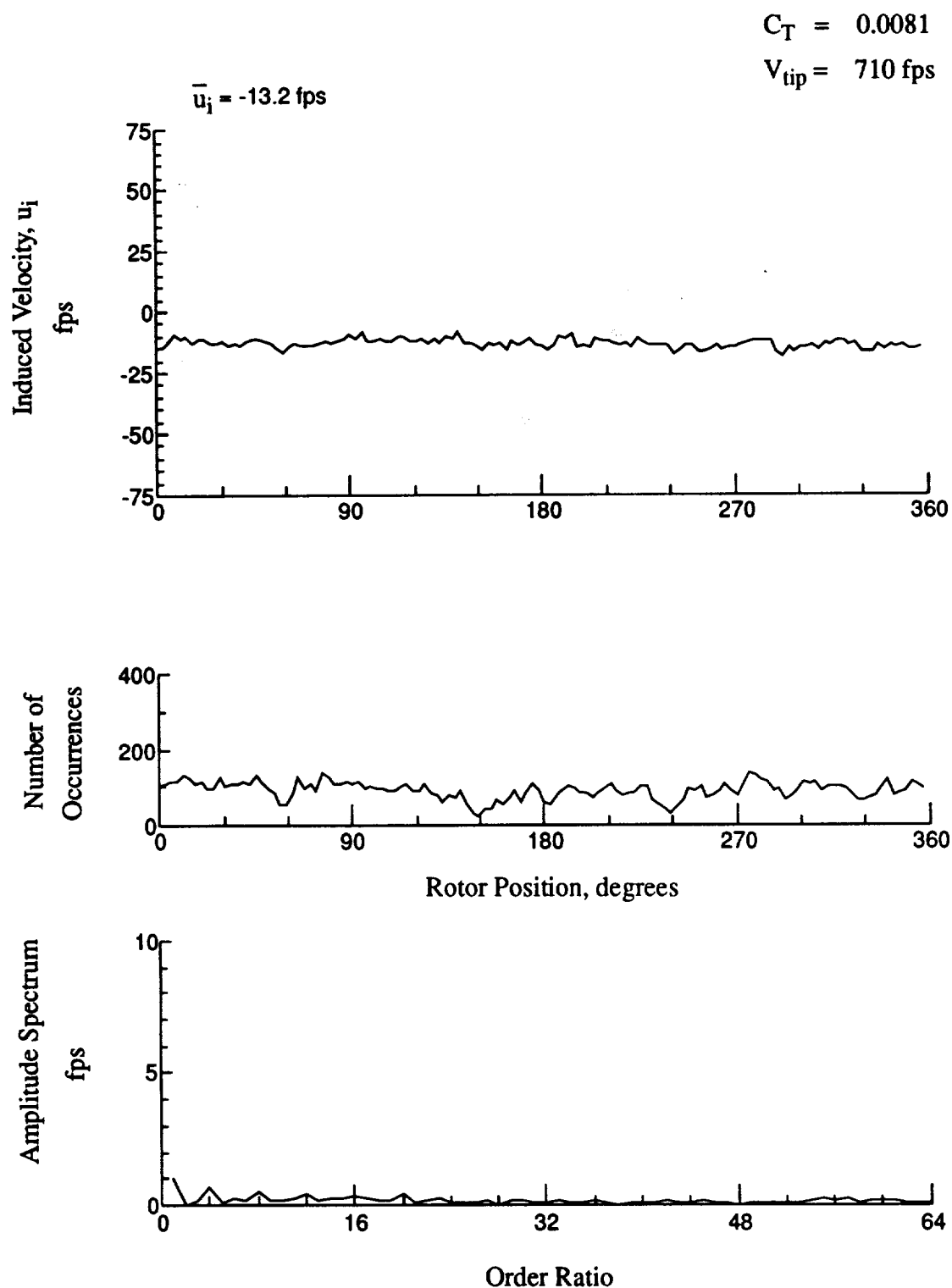


Figure 86.- Wake Measurements at
 $x/R = 1.50$, $y/R = 0.20$, $z = -10.56 \text{ in.}$

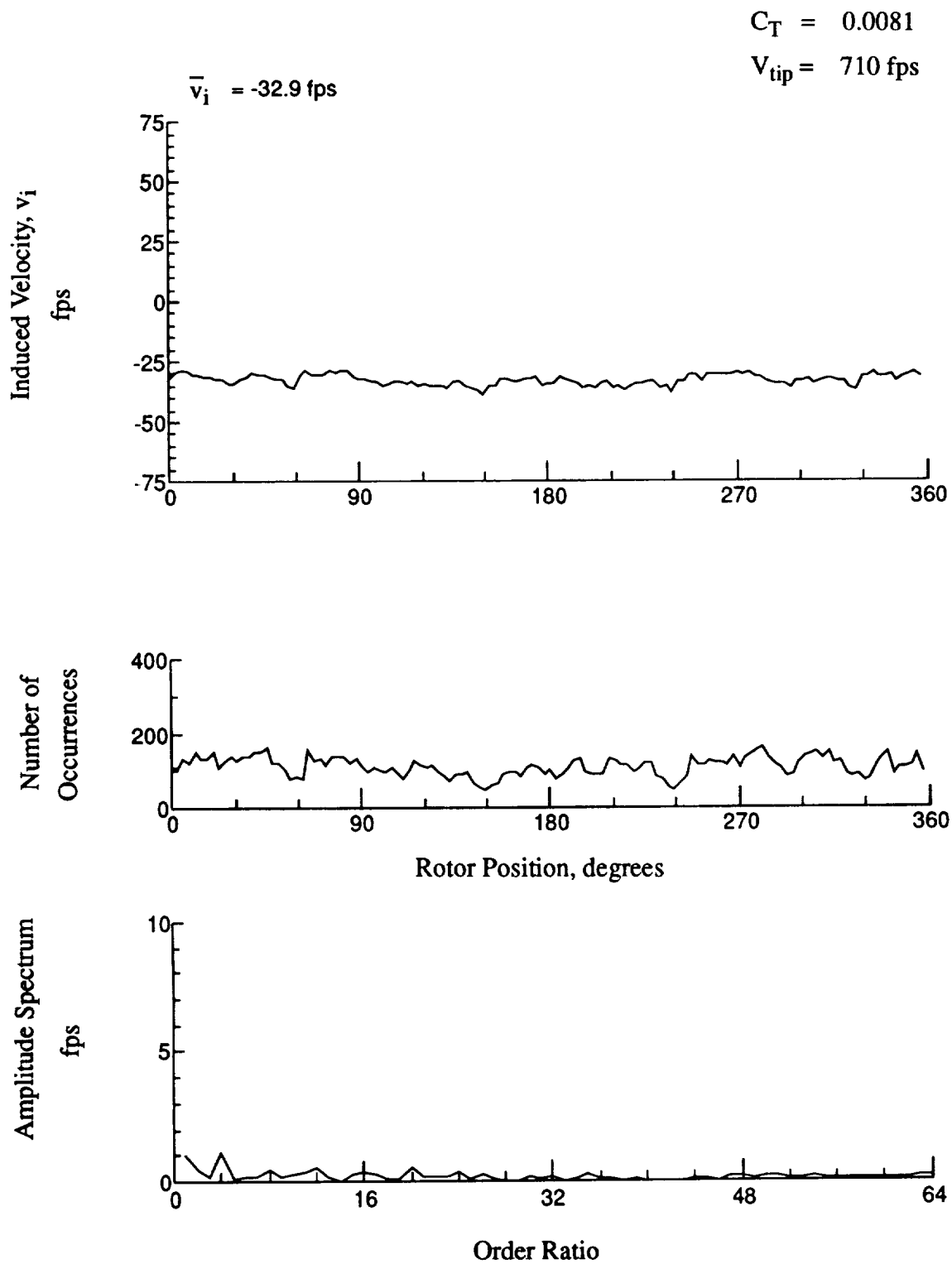


Figure 86.- Concluded.
 $x/R = 1.50$, $y/R = 0.20$, $z = -10.56 \text{ in.}$

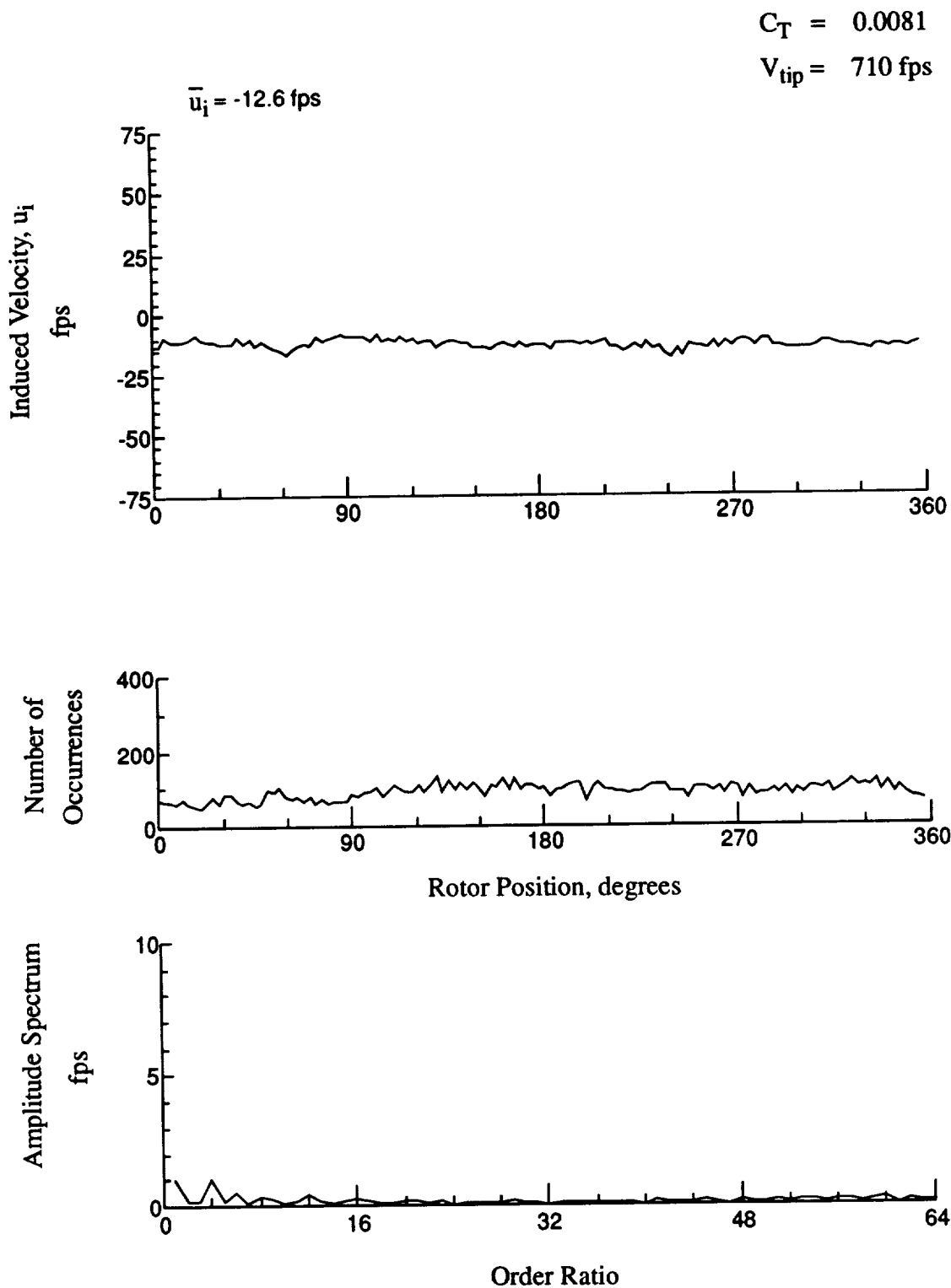


Figure 87.- Wake Measurements at
 $x/R = 1.50$, $y/R = 0.20$, $z = -11.59 \text{ in.}$

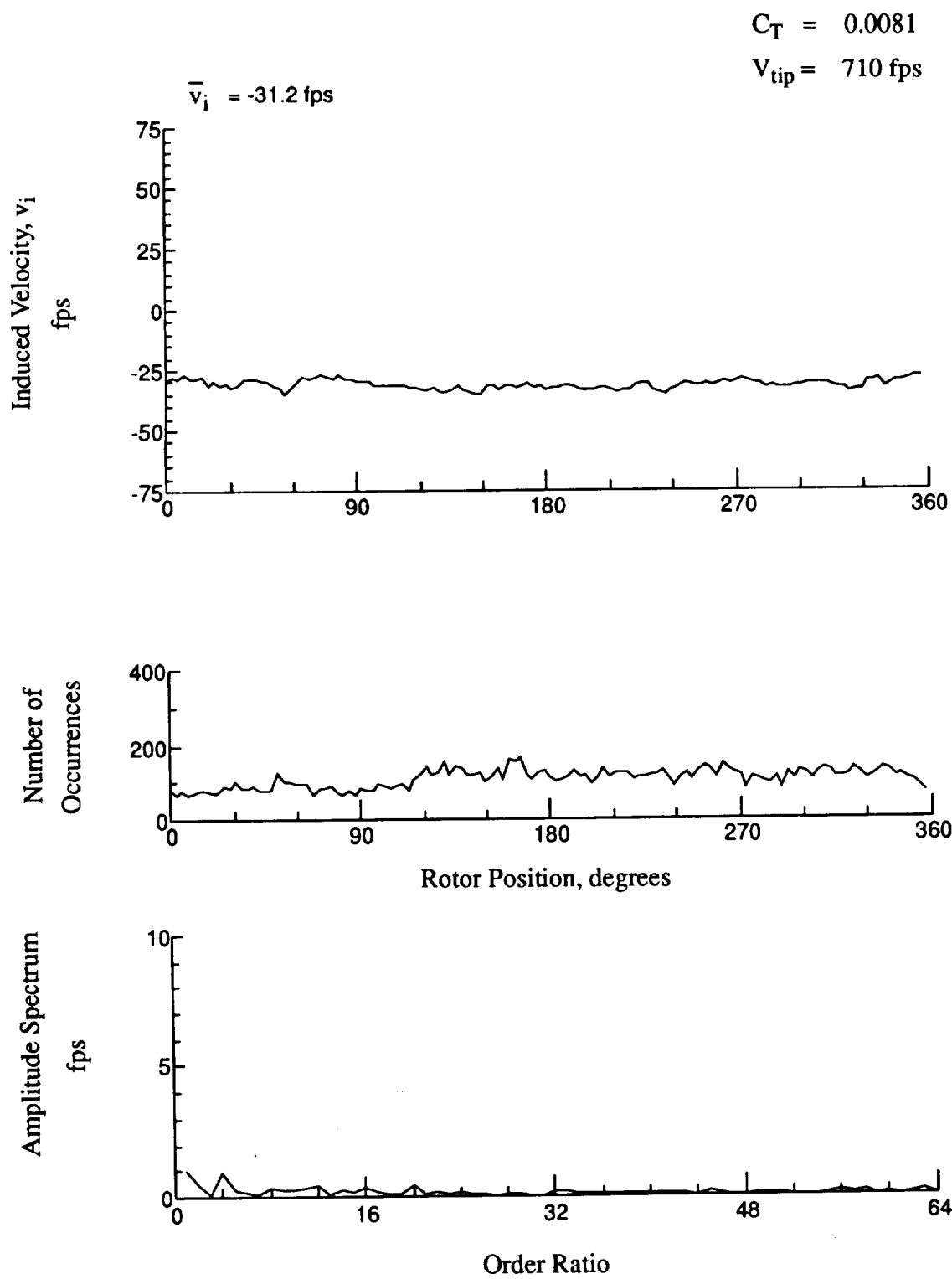


Figure 87.- Concluded.
 $x/R = 1.50$, $y/R = 0.20$, $z = -11.59 \text{ in.}$

$$C_T = 0.0081$$

$$V_{tip} = 710 \text{ fps}$$

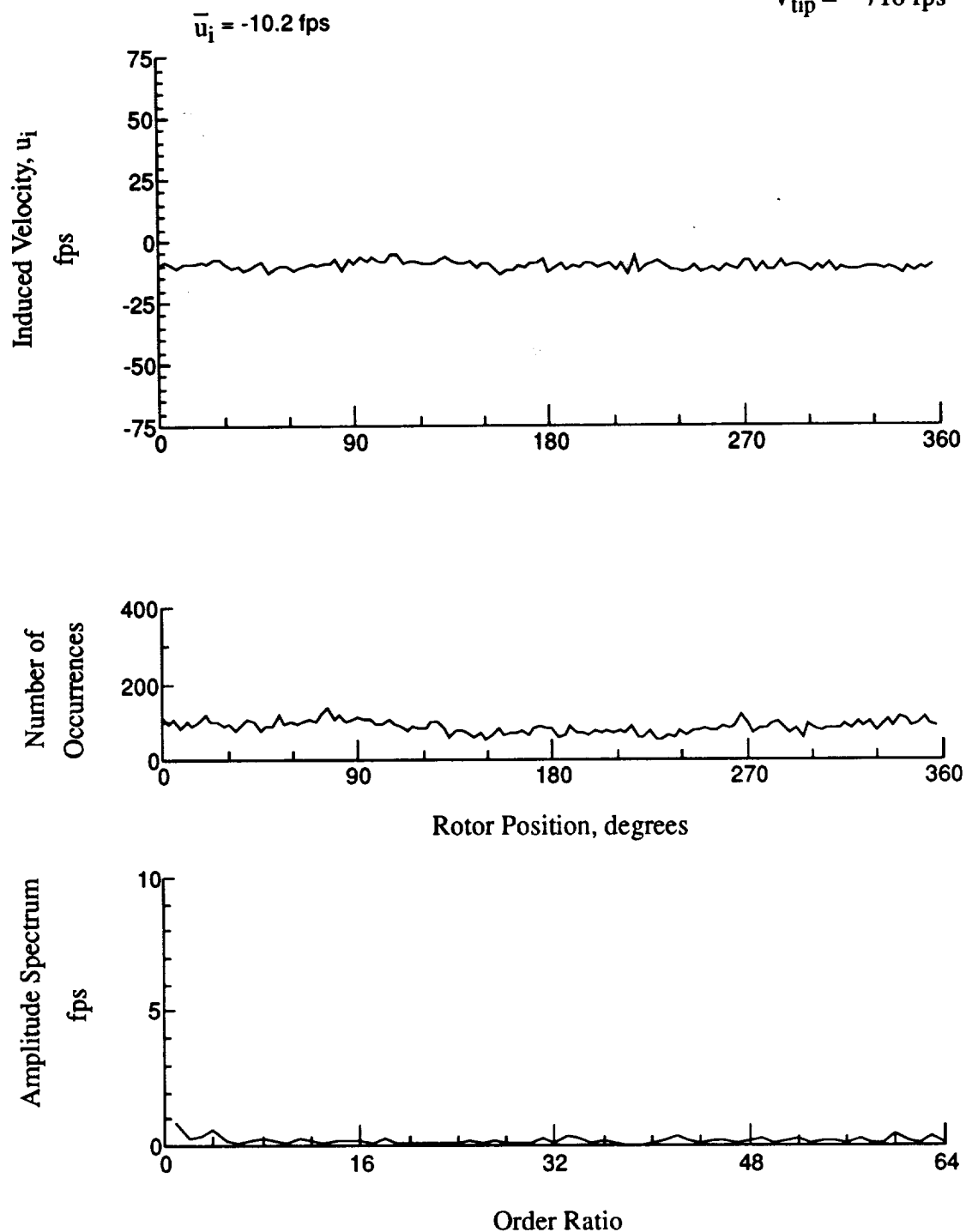


Figure 88.- Wake Measurements at
 $x/R = 1.50$, $y/R = 0.20$, $z = -12.62 \text{ in.}$

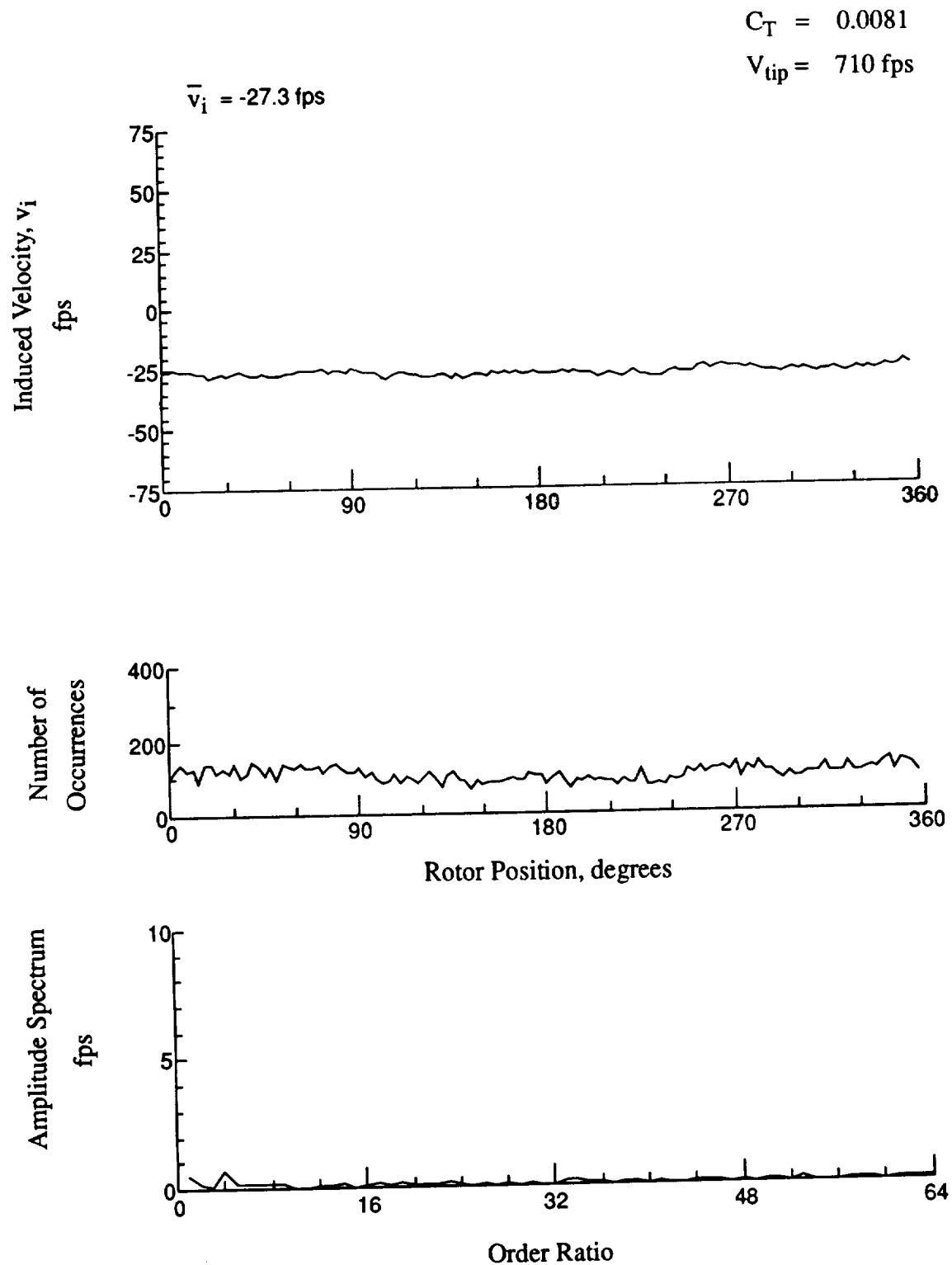


Figure 88.- Concluded.
 $x/R = 1.50$, $y/R = 0.20$, $z = -12.62 \text{ in.}$

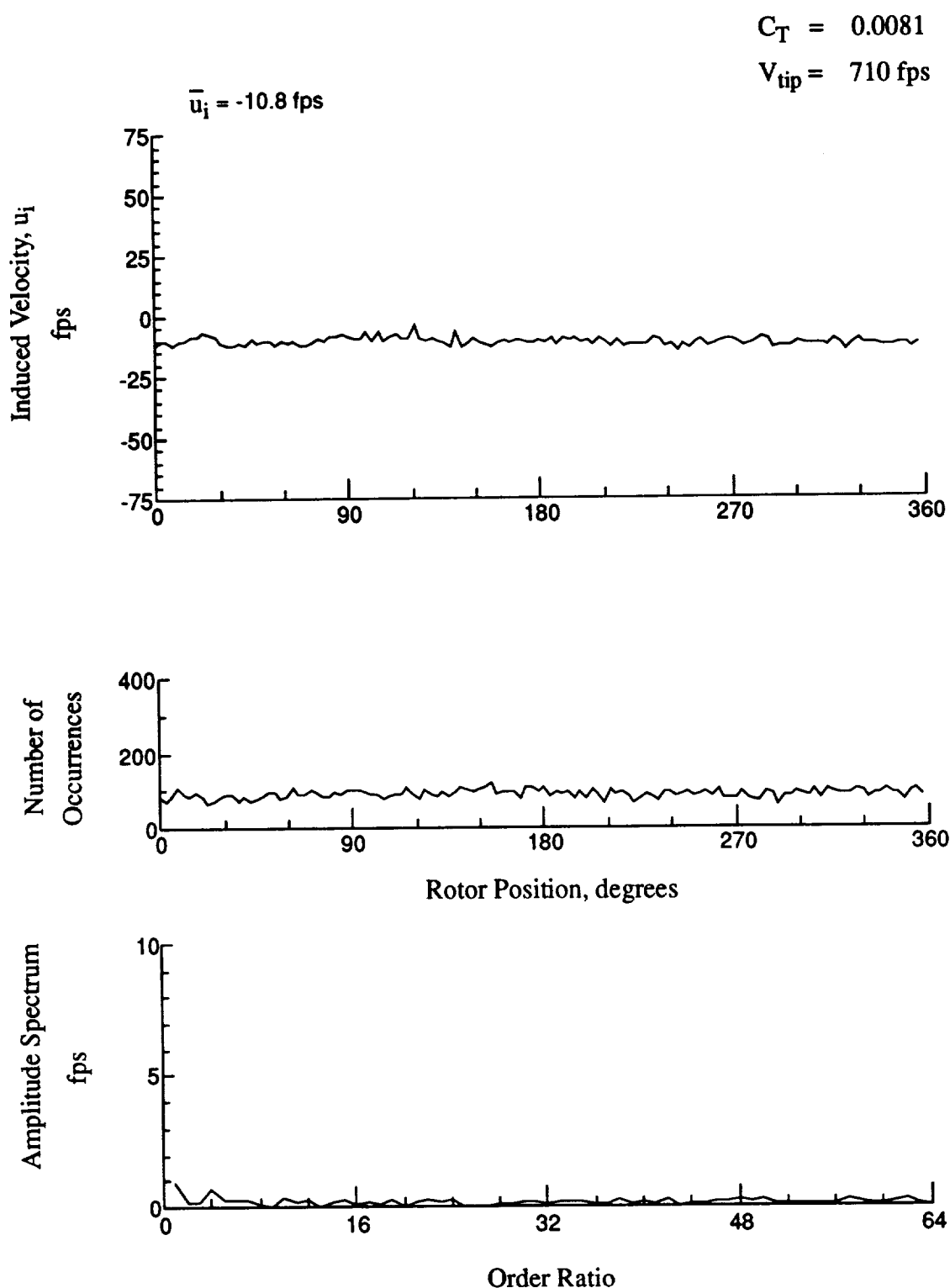


Figure 89.- Wake Measurements at
 $x/R = 1.50$, $y/R = 0.20$, $z = -13.56 \text{ in.}$

$$C_T = 0.0081$$

$$V_{tip} = 710 \text{ fps}$$

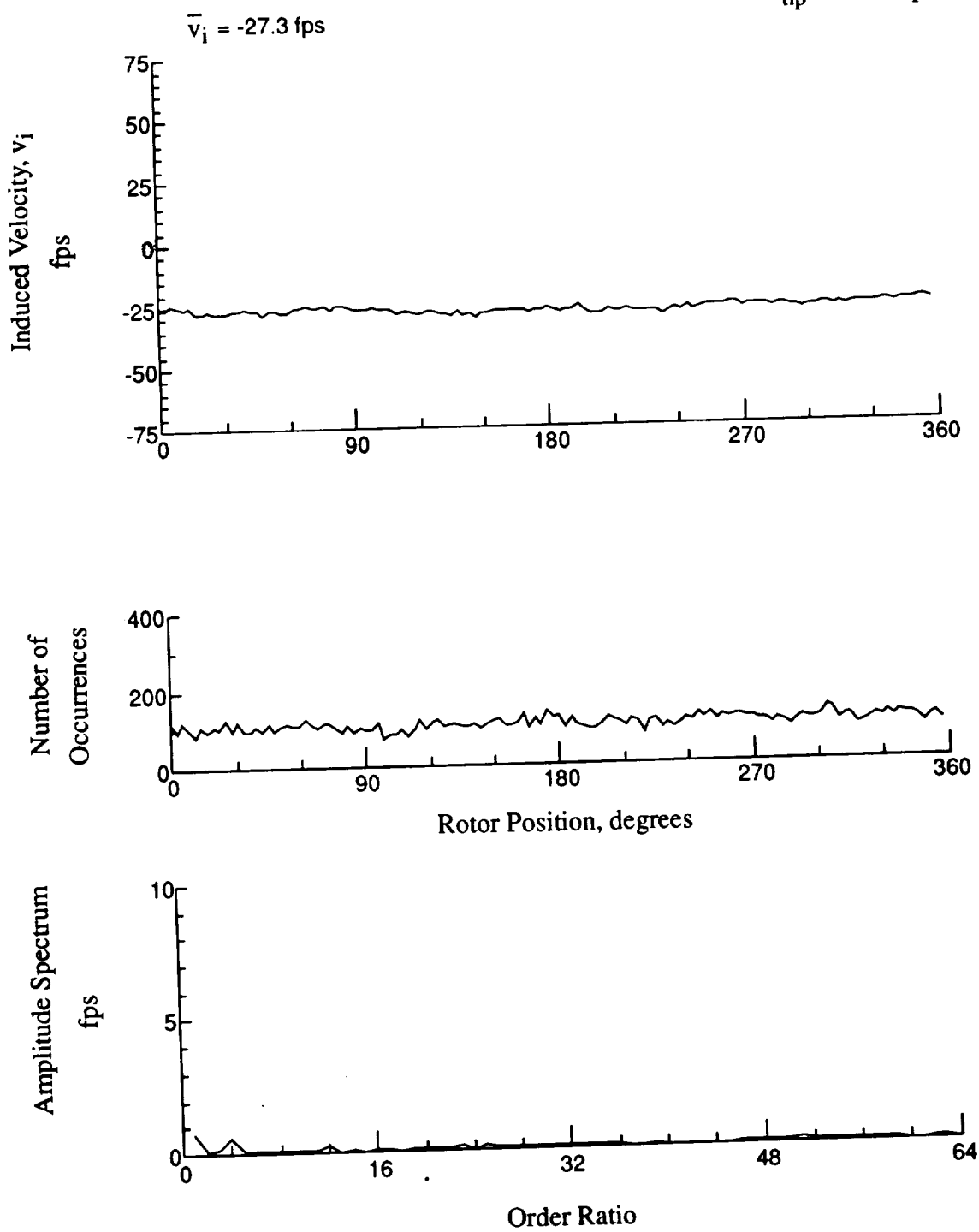


Figure 89.- Concluded.
 $x/R = 1.50$, $y/R = 0.20$, $z = -13.56 \text{ in.}$

$$C_T = 0.0081$$

$$V_{tip} = 603 \text{ fps}$$

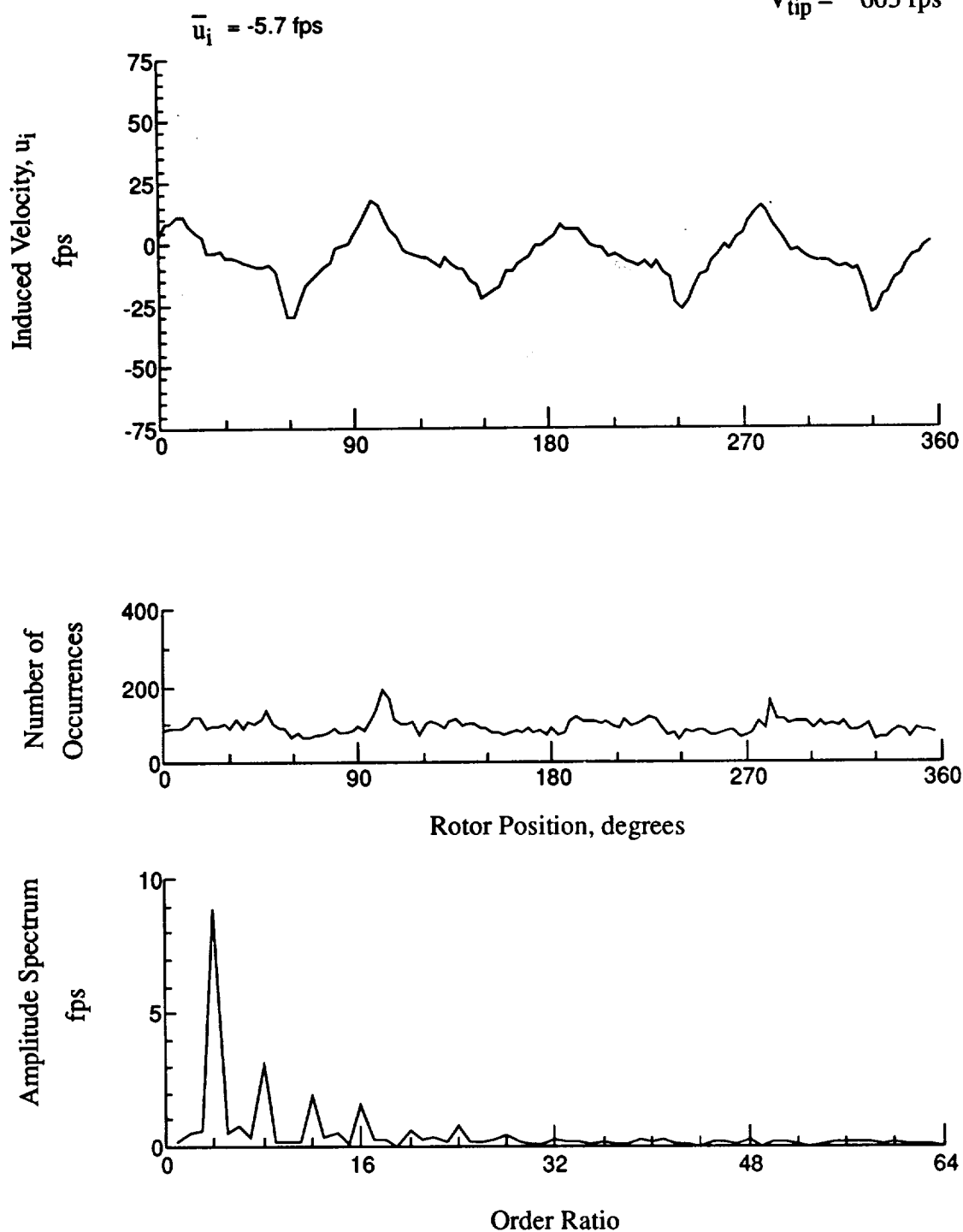


Figure 90.- Wake Measurements at
 $x/R = -0.45$, $y/R = -0.60$, $z = 1.65 \text{ in.}$

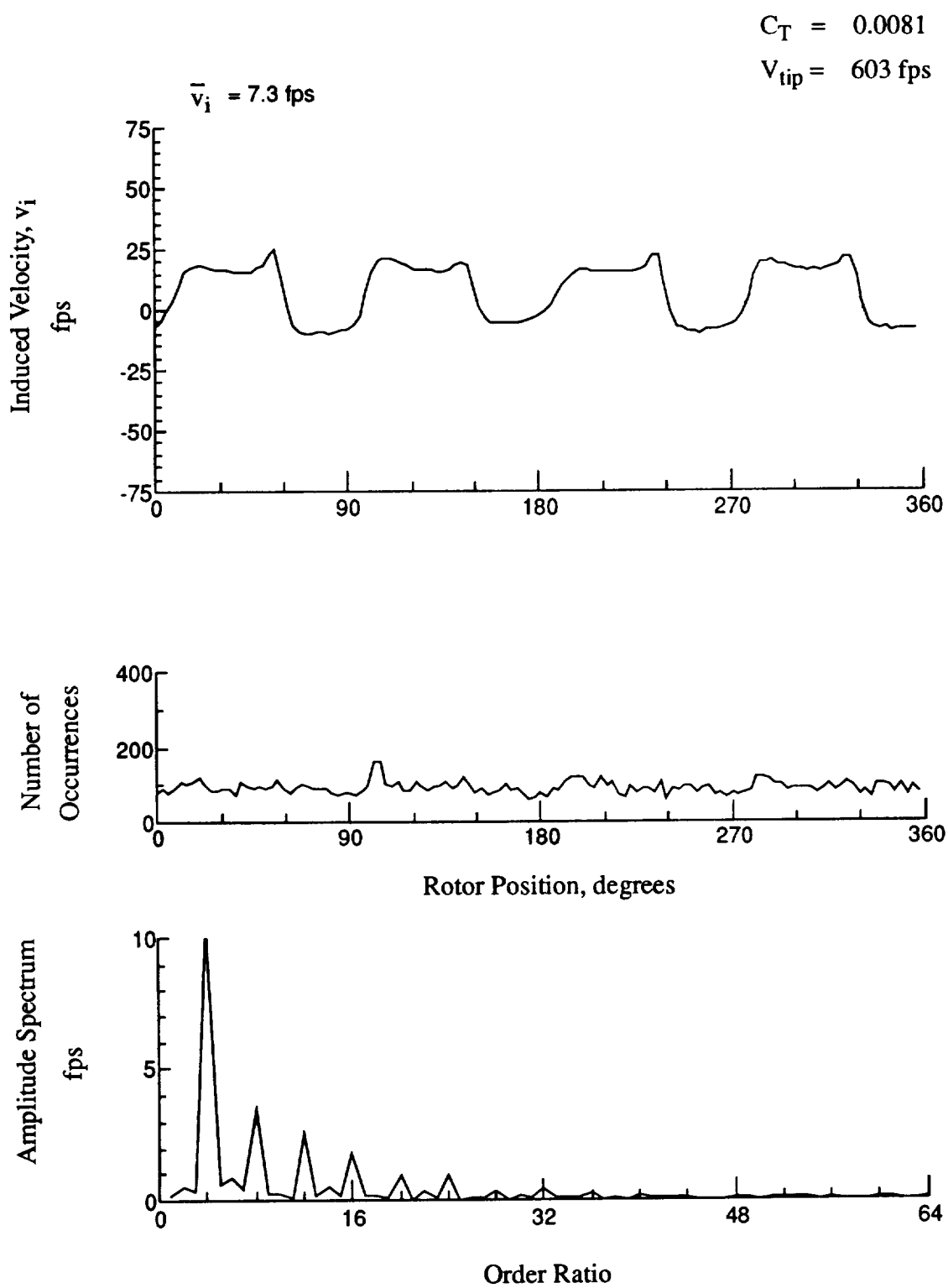


Figure 90.- Concluded.
 $x/R = -0.45$, $y/R = -0.60$, $z = 1.65 \text{ in.}$

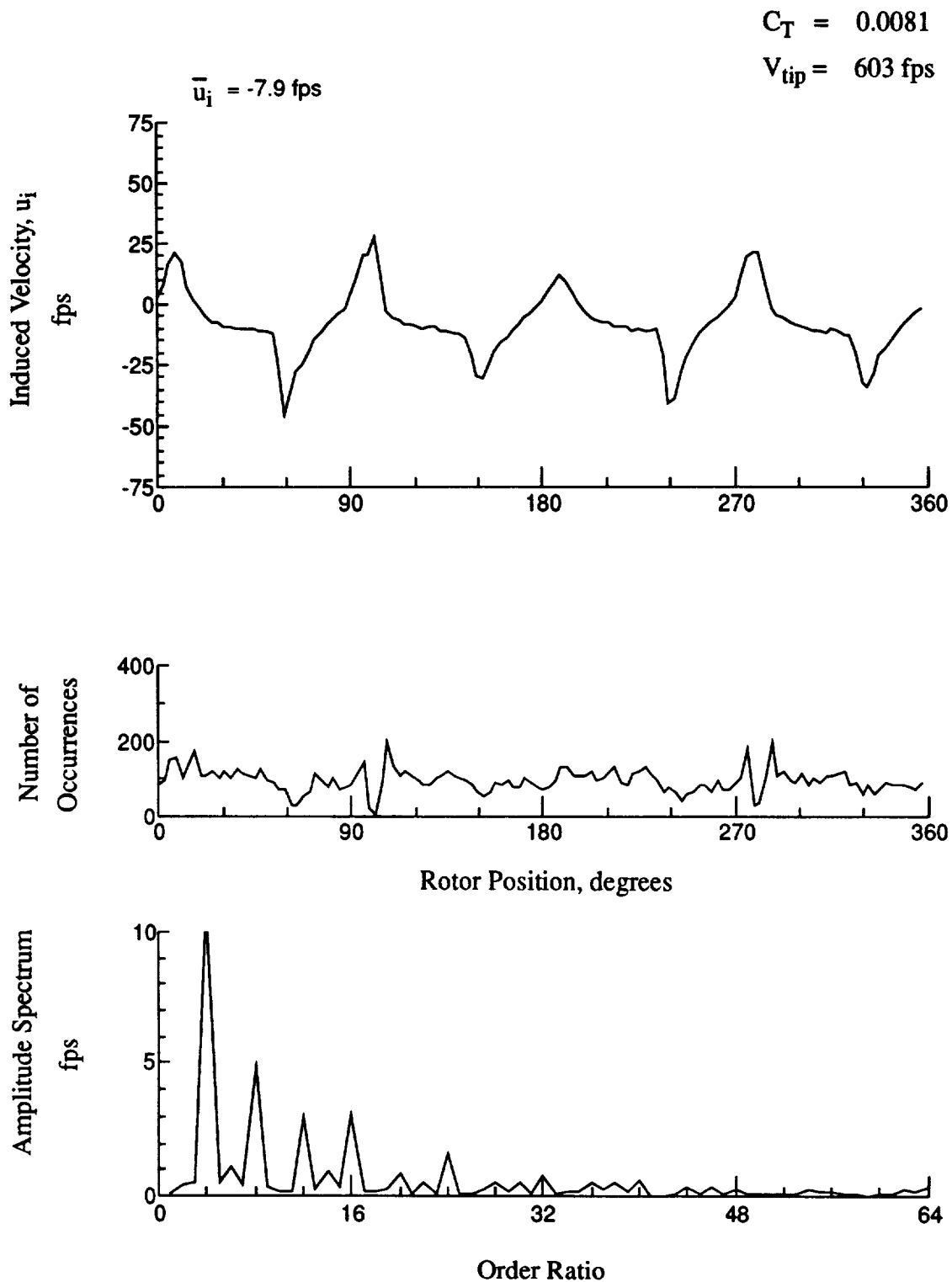


Figure 91.- Wake Measurements at
 $x/R = -0.45$, $y/R = -0.60$, $z = 0.62 \text{ in.}$

$C_T = 0.0081$

$V_{tip} = 603 \text{ fps}$

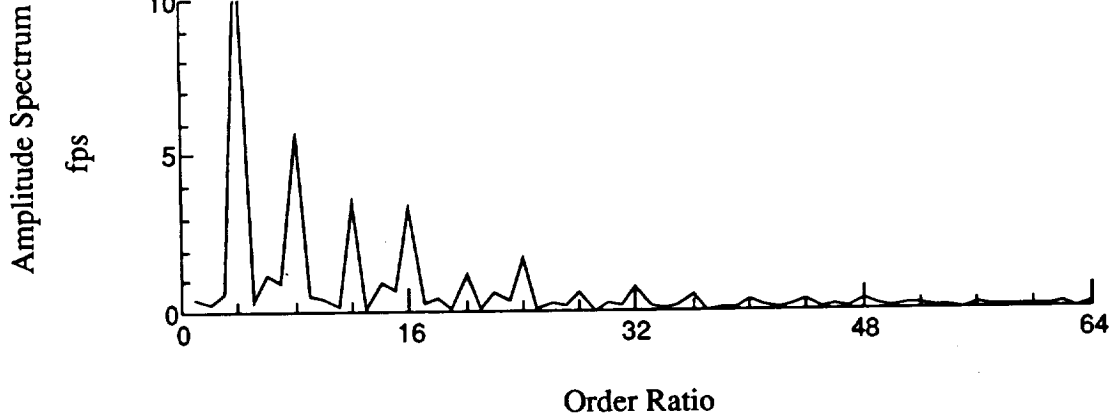
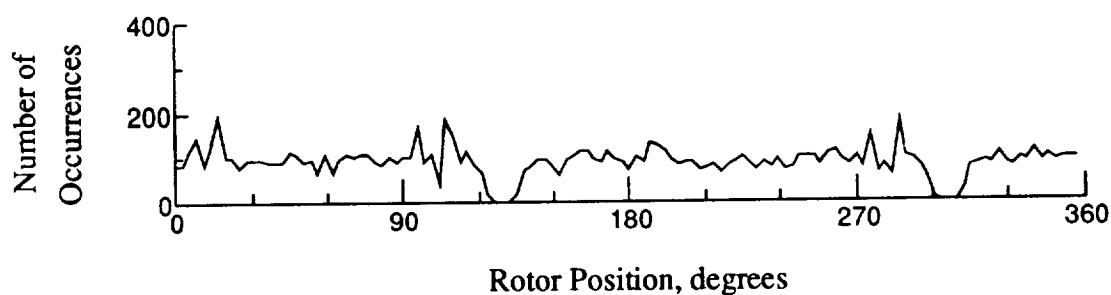
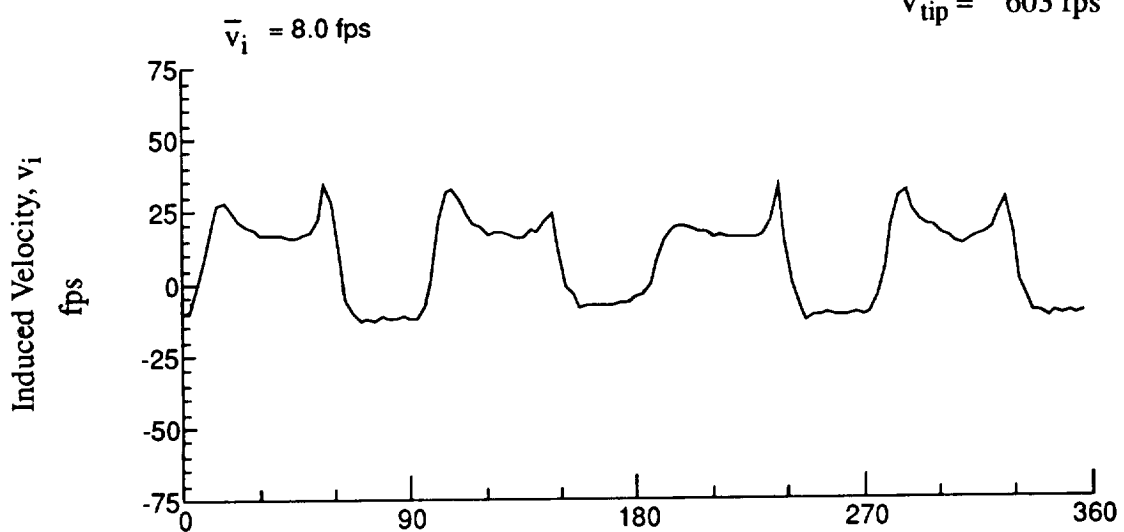


Figure 91.- Concluded.
 $x/R = -0.45$, $y/R = -0.60$, $z = 0.62 \text{ in.}$

$$C_T = 0.0081$$

$$V_{tip} = 603 \text{ fps}$$

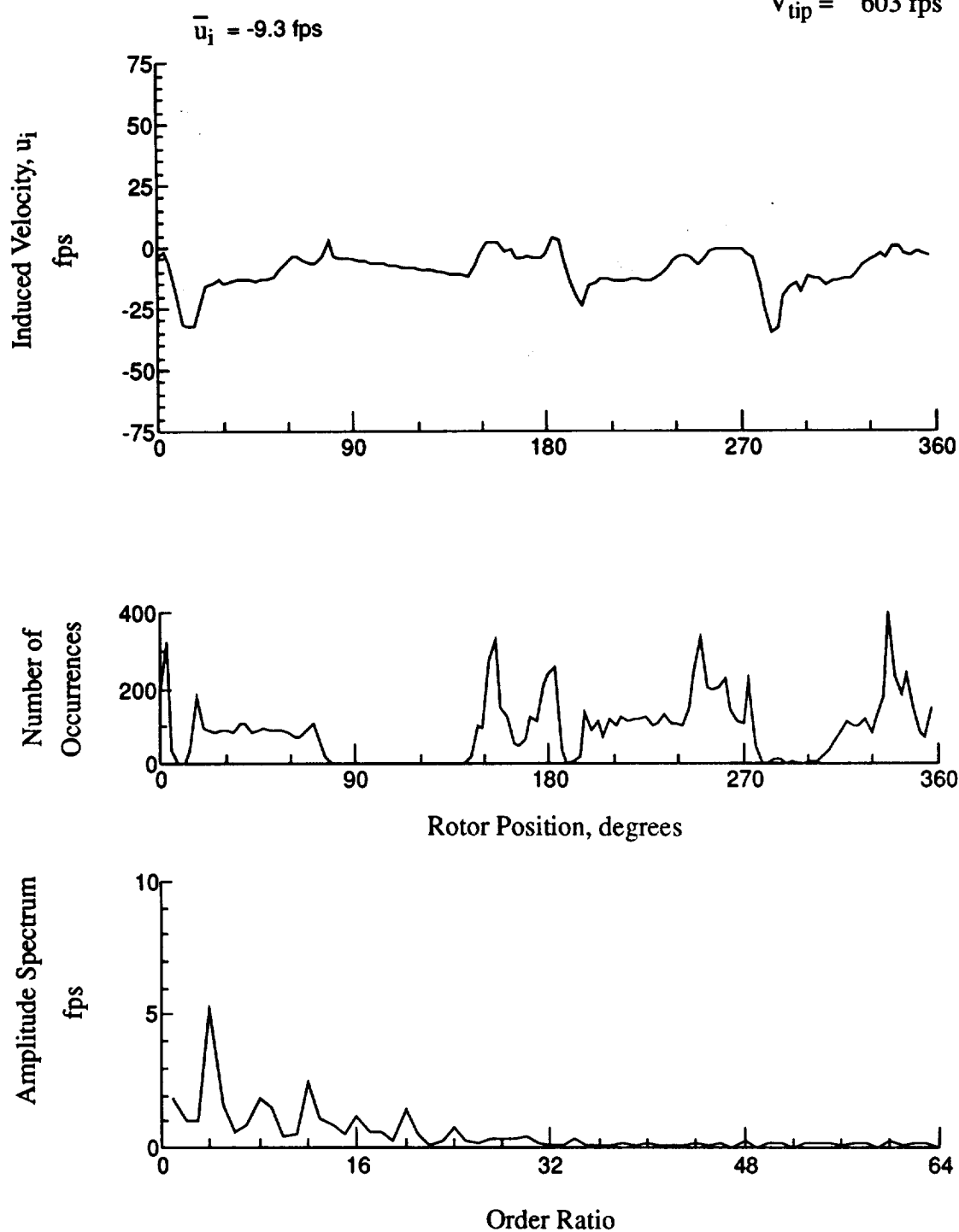


Figure 92.- Wake Measurements at
 $x/R = -0.45$, $y/R = -0.60$, $z = -2.00$ in.

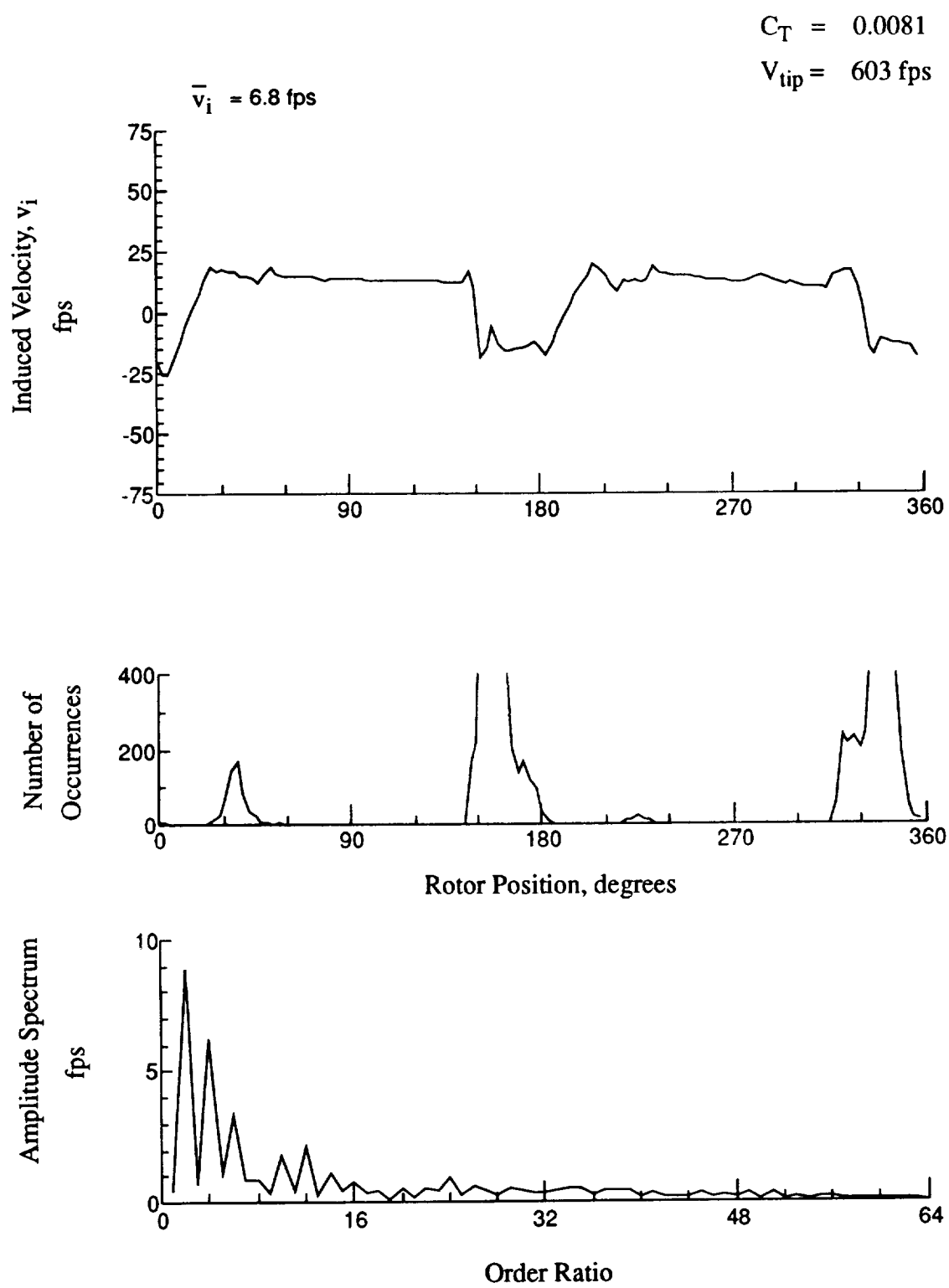


Figure 92.- Concluded.
 $x/R = -0.45$, $y/R = -0.60$, $z = -2.00 \text{ in.}$

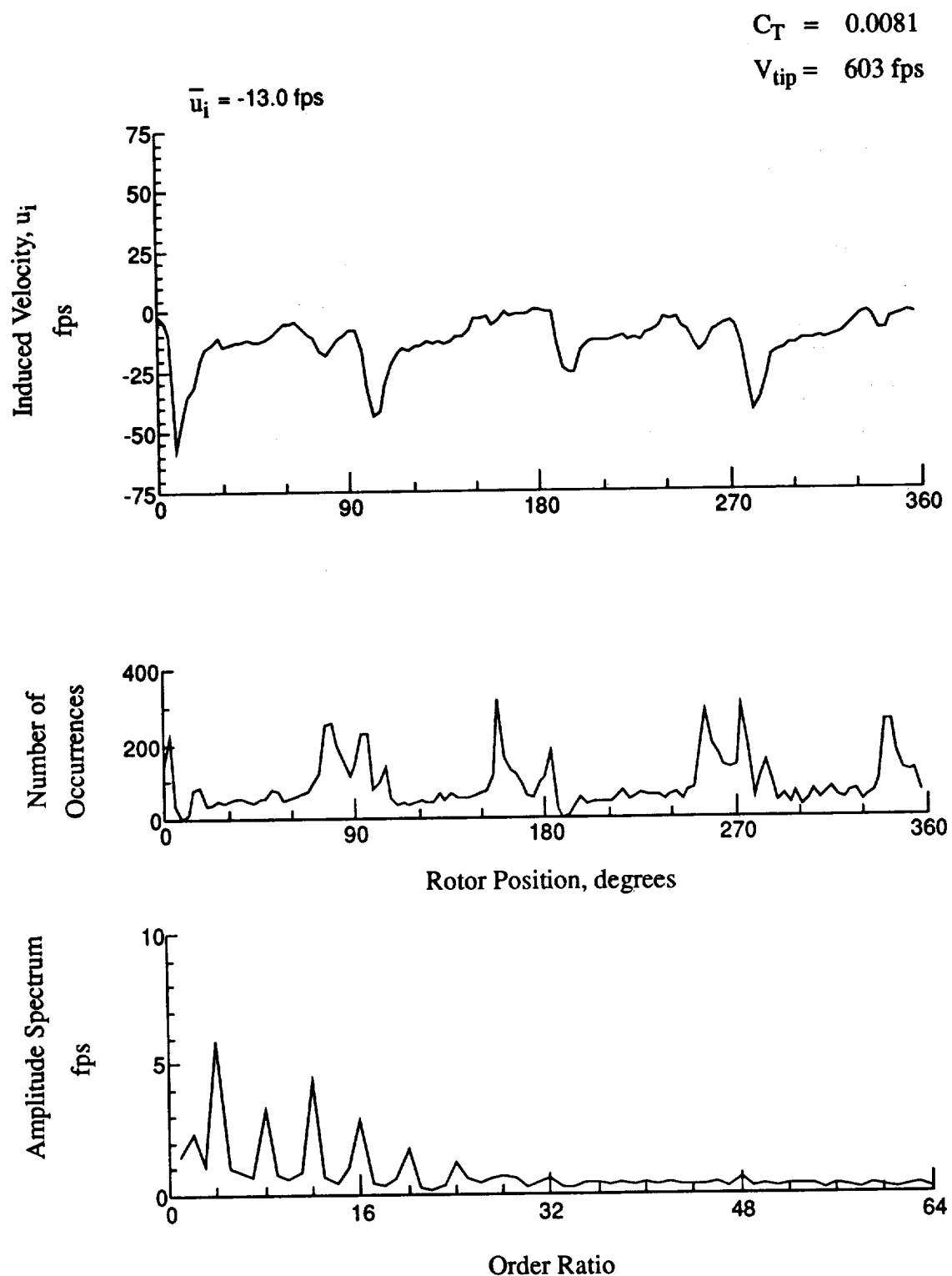


Figure 93.- Wake Measurements at
 $x/R = -0.45$, $y/R = -0.60$, $z = -2.47 \text{ in.}$

$C_T = 0.0081$

$V_{tip} = 603 \text{ fps}$

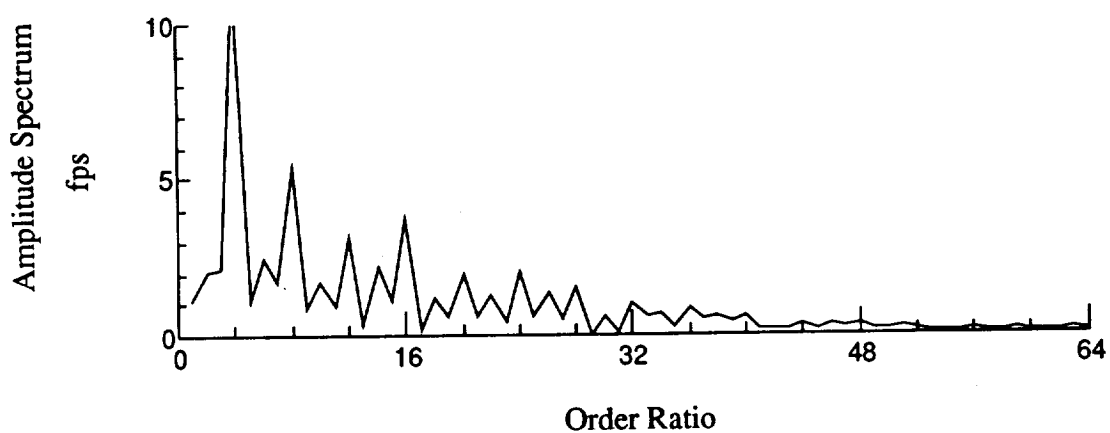
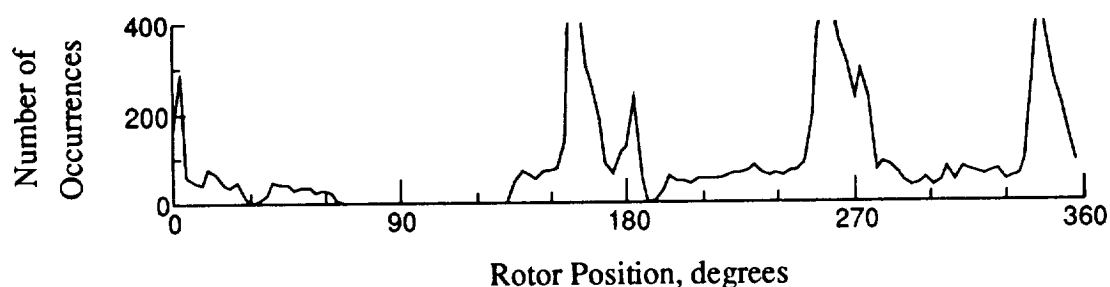
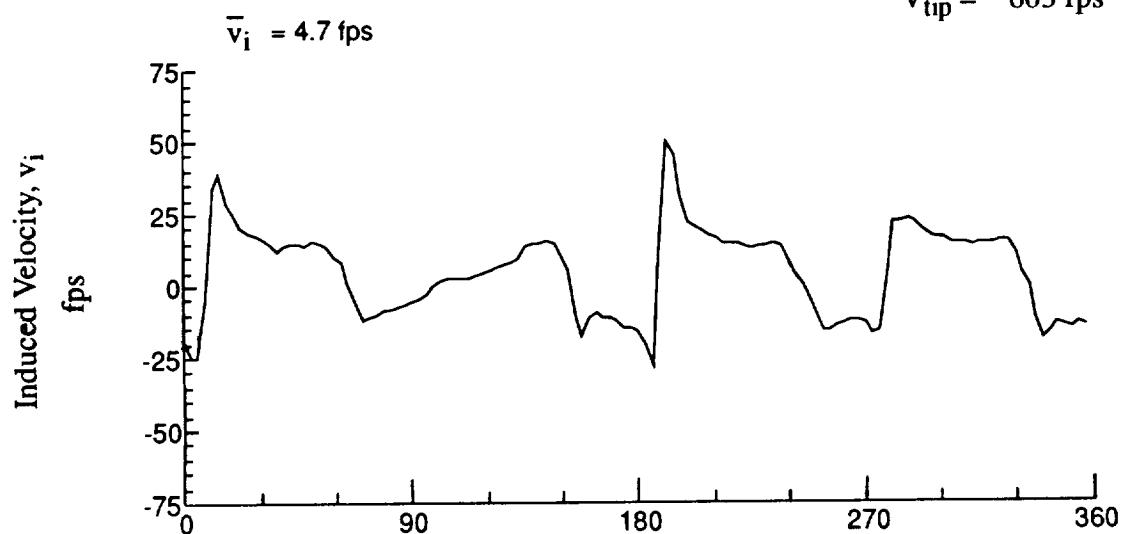


Figure 93.- Concluded.

$x/R = -0.45$, $y/R = -0.60$, $z = -2.47 \text{ in.}$

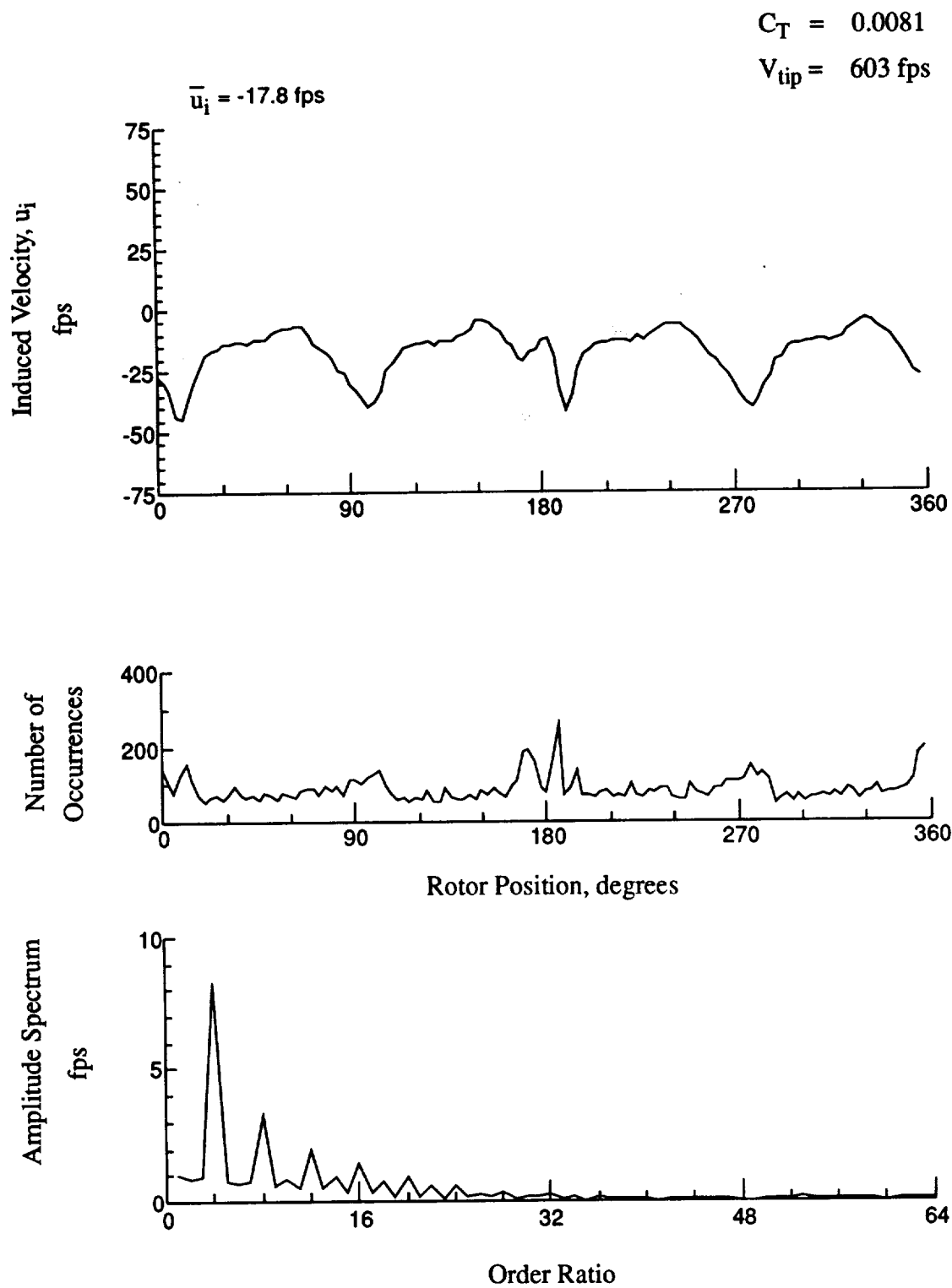


Figure 94.- Wake Measurements at
 $x/R = -0.45$, $y/R = -0.60$, $z = -3.50 \text{ in.}$

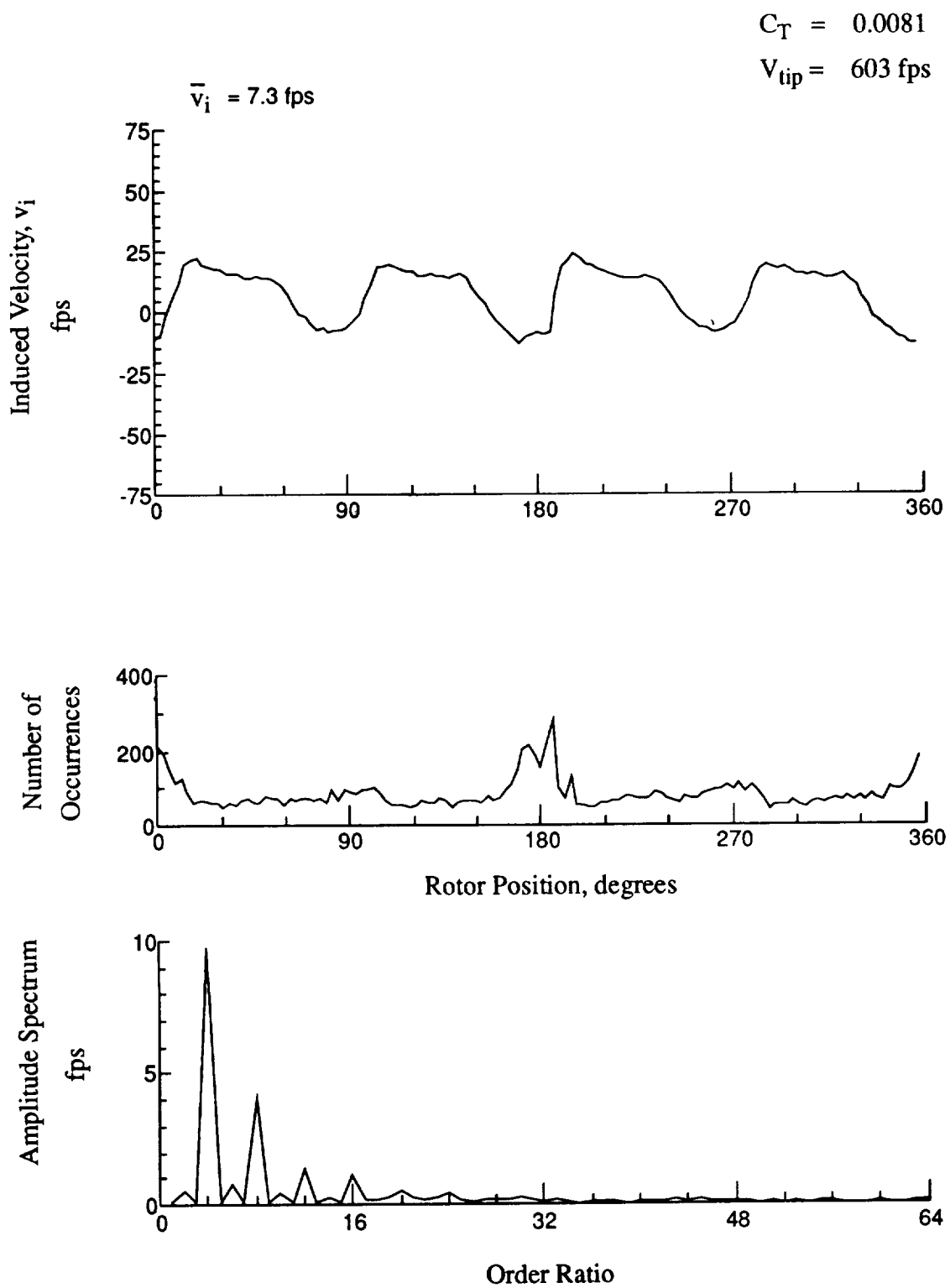


Figure 94.- Concluded.
 $x/R = -0.45$, $y/R = -0.60$, $z = -3.50 \text{ in.}$

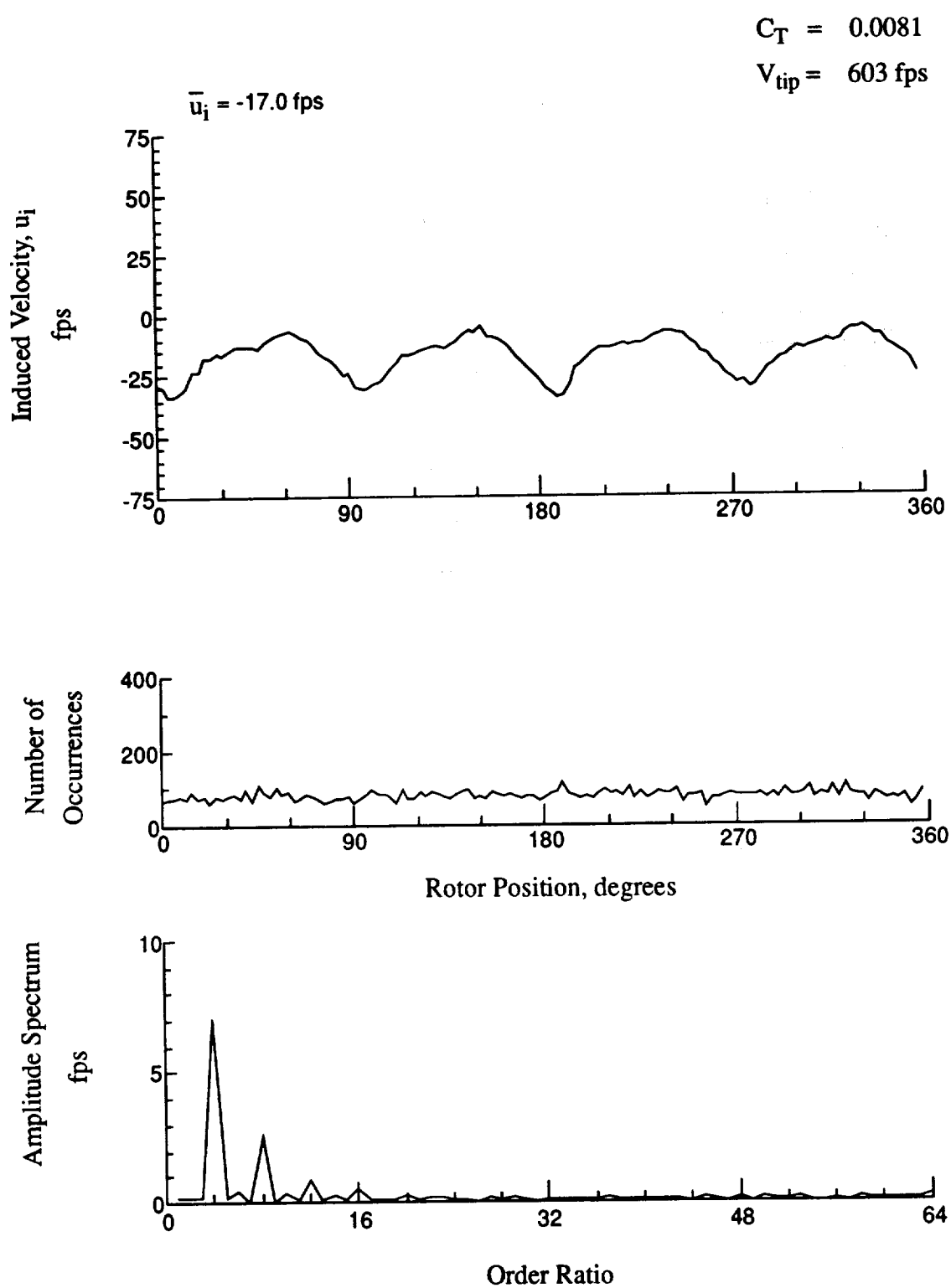


Figure 95.- Wake Measurements at
 $x/R = -0.45$, $y/R = -0.60$, $z = -4.53 \text{ in.}$

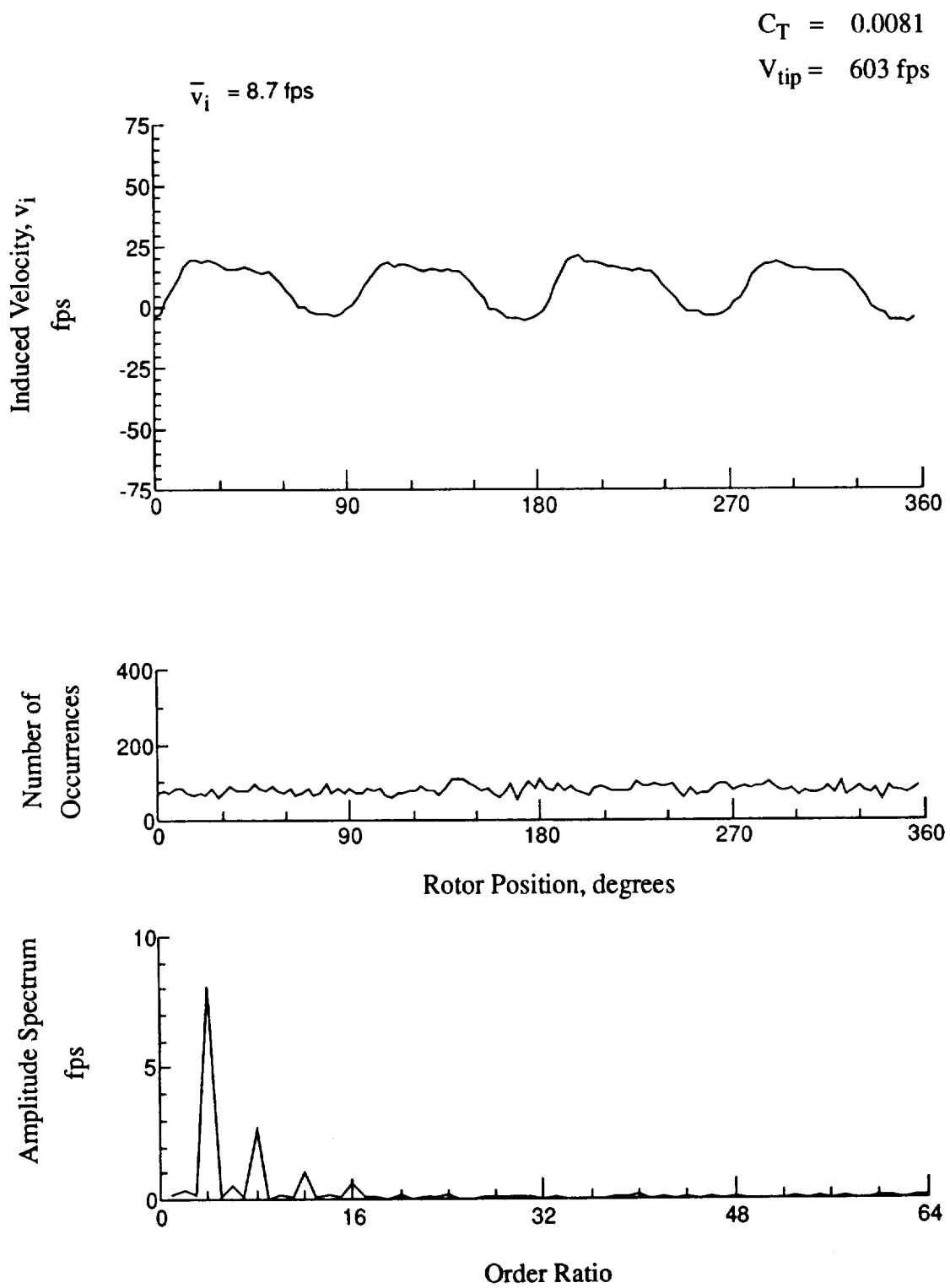


Figure 95.- Concluded.
 $x/R = -0.45$, $y/R = -0.60$, $z = -4.53 \text{ in.}$

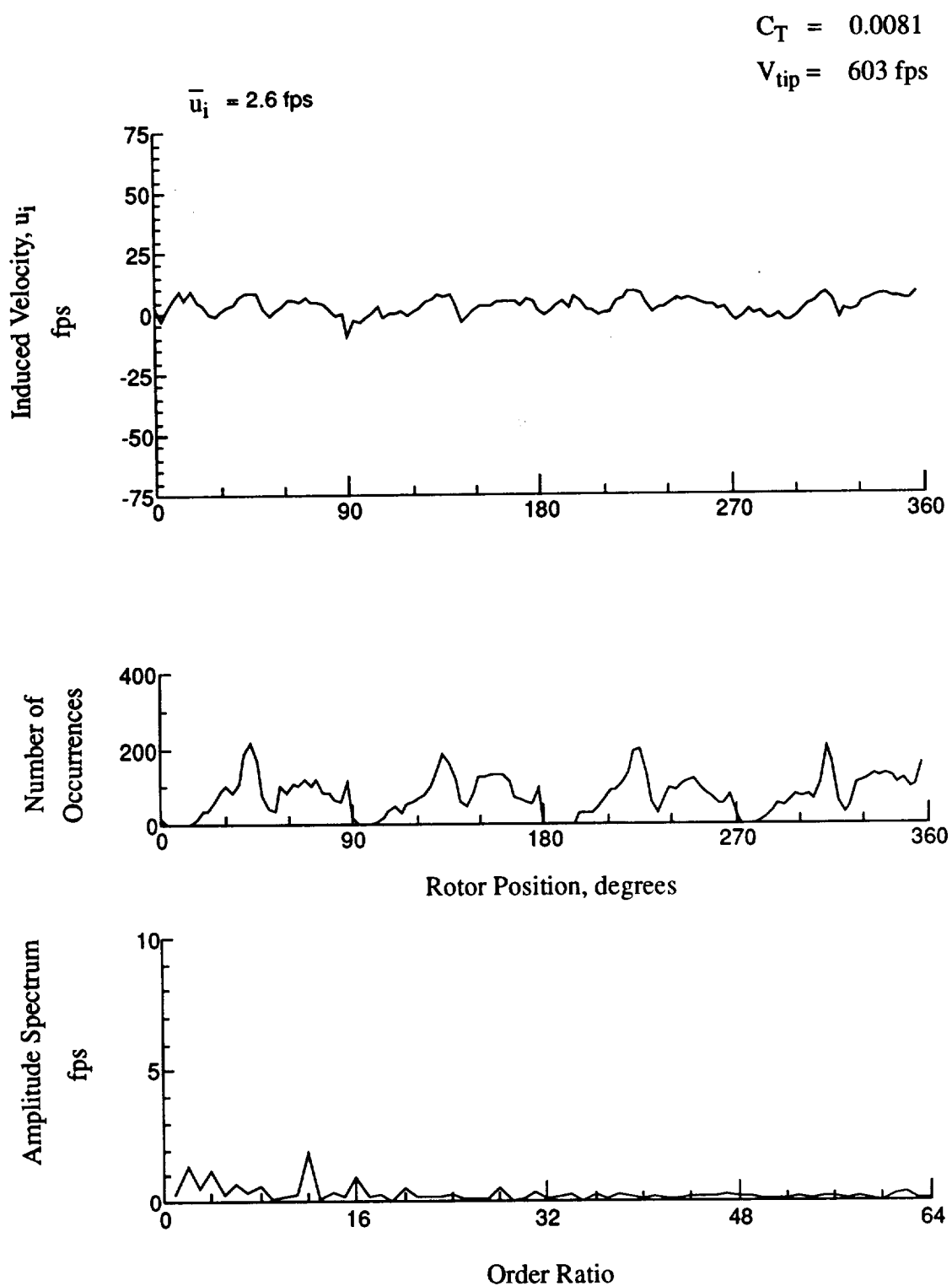


Figure 96.- Wake Measurements at
 $x/R = 0.80$, $y/R = -0.60$, $z = -0.27 \text{ in.}$

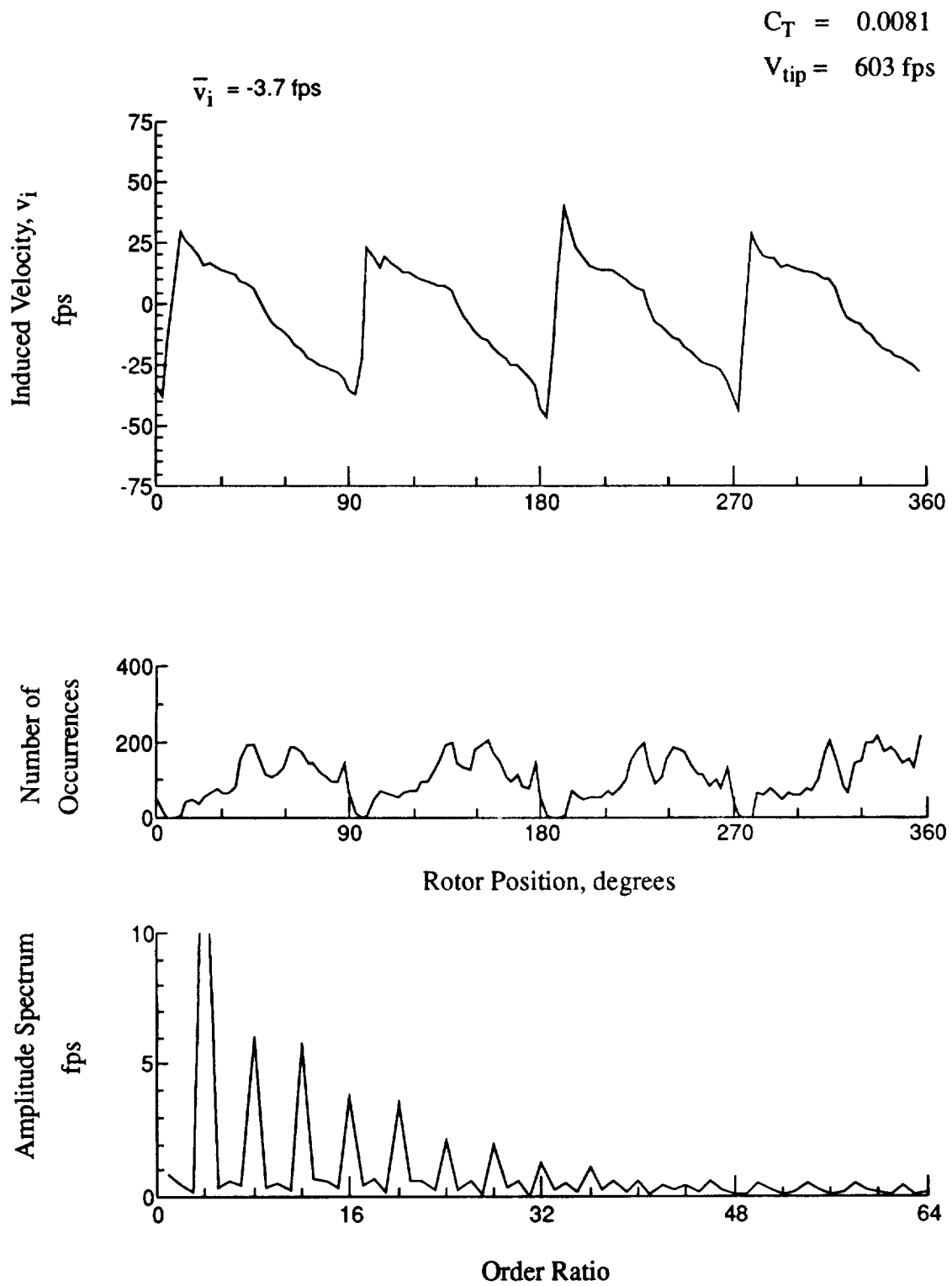


Figure 96.- Concluded.
 $x/R = 0.80$, $y/R = -0.60$, $z = -0.27 \text{ in.}$

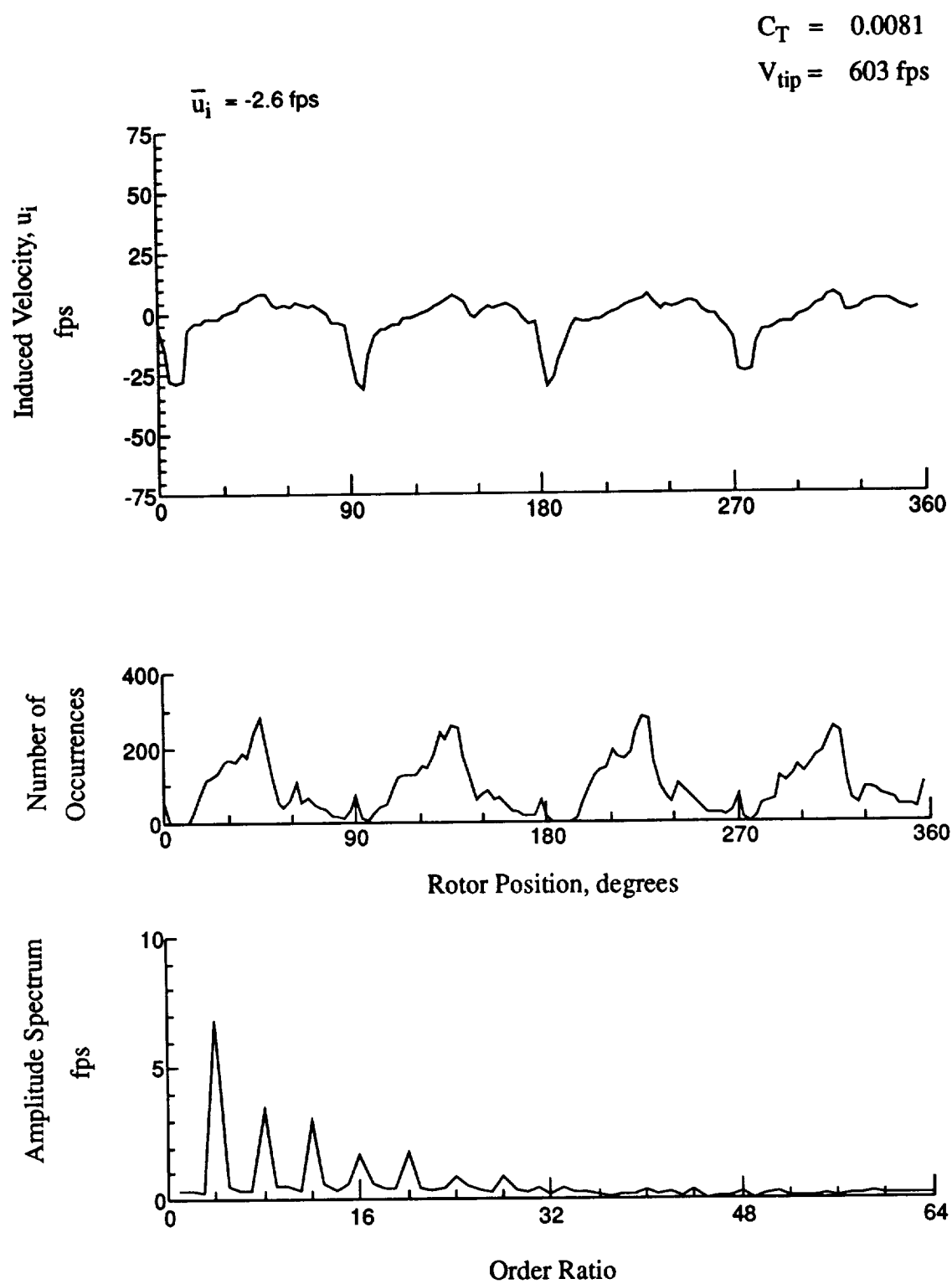


Figure 97.- Wake Measurements at
 $x/R = 0.80$, $y/R = -0.60$, $z = -1.30 \text{ in.}$

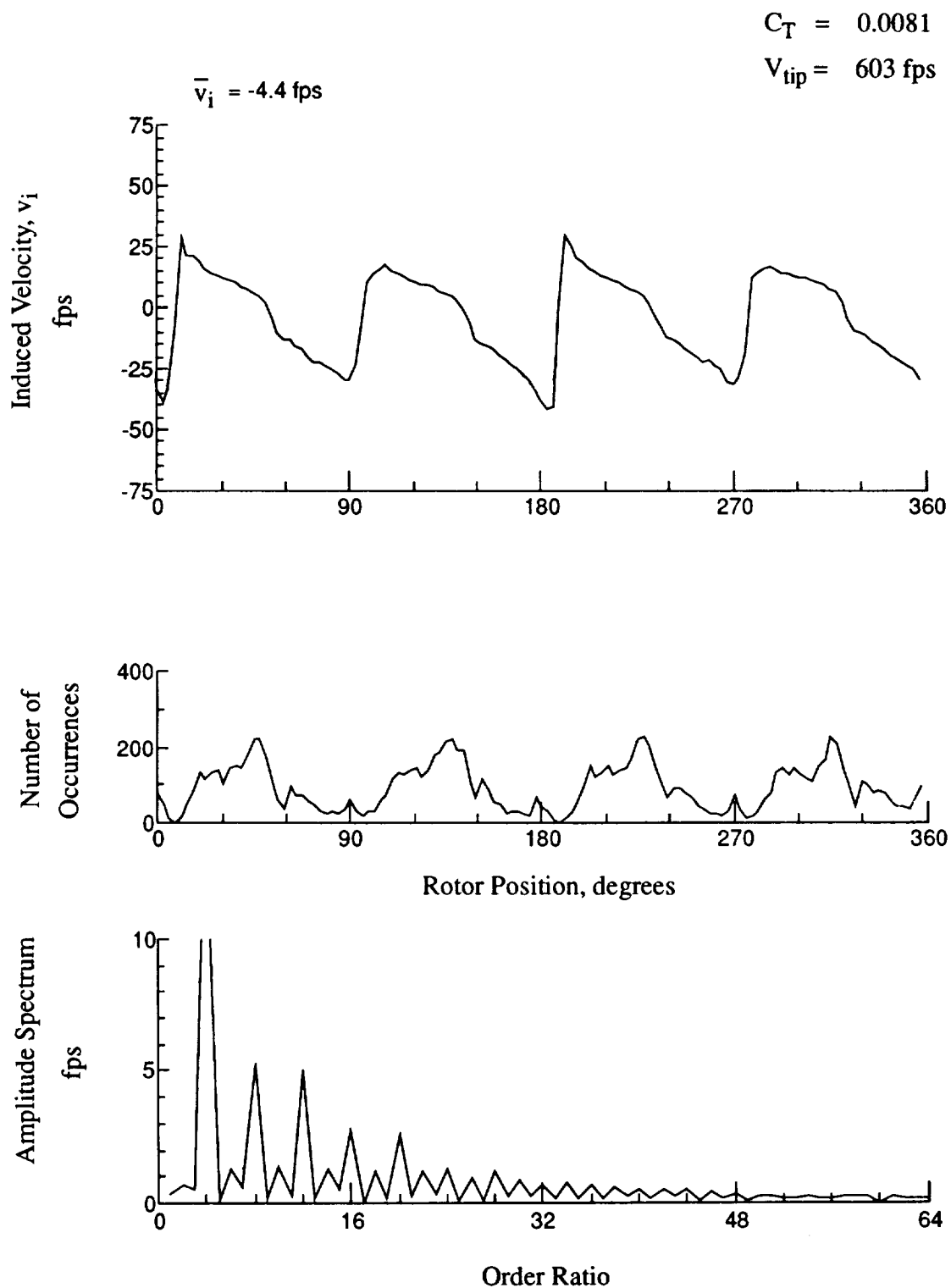


Figure 97.- Concluded.

$x/R = 0.80$, $y/R = -0.60$, $z = -1.30 \text{ in.}$

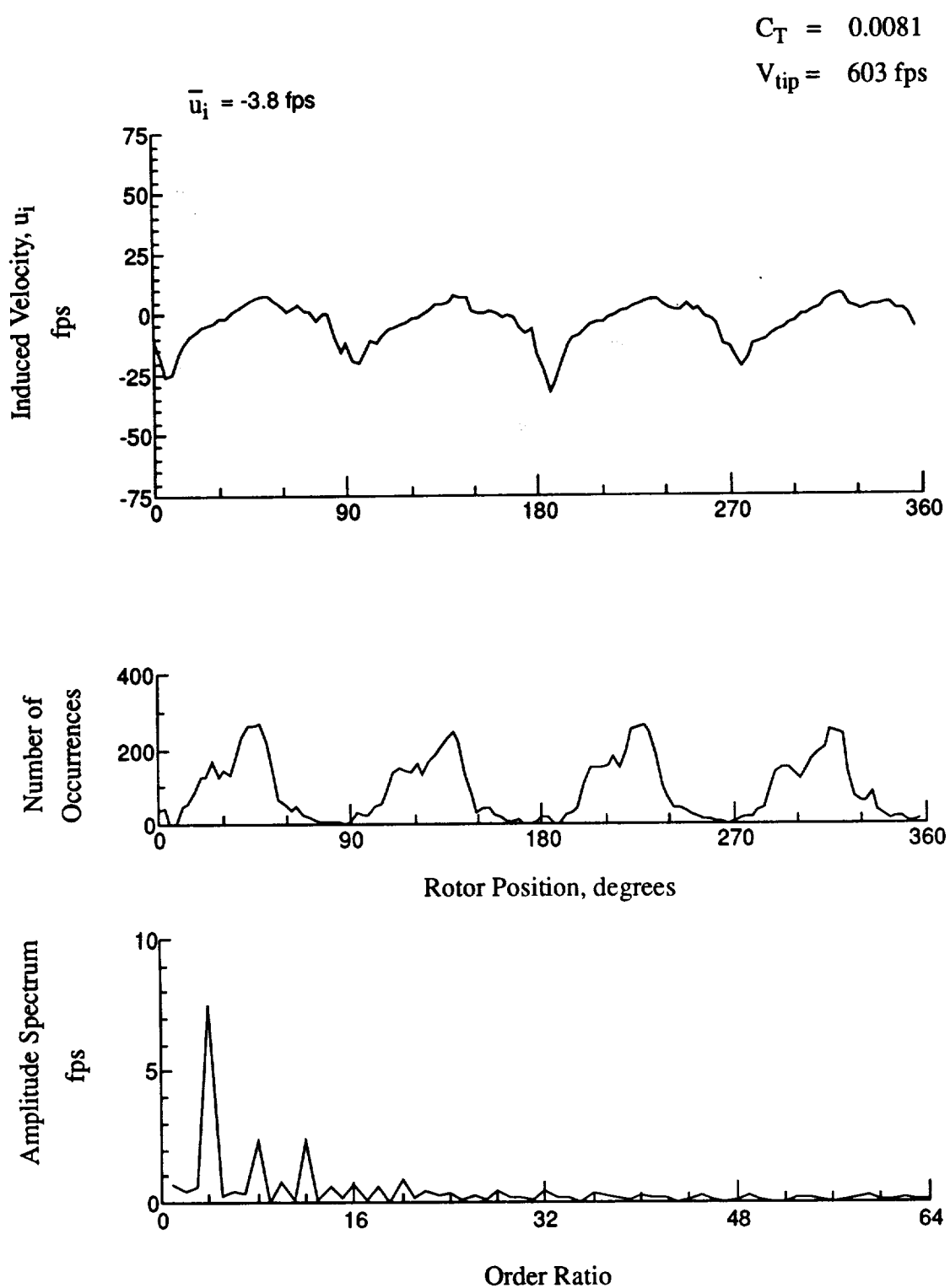


Figure 98.- Wake Measurements at
 $x/R = 0.80$, $y/R = -0.60$, $z = -2.33 \text{ in.}$

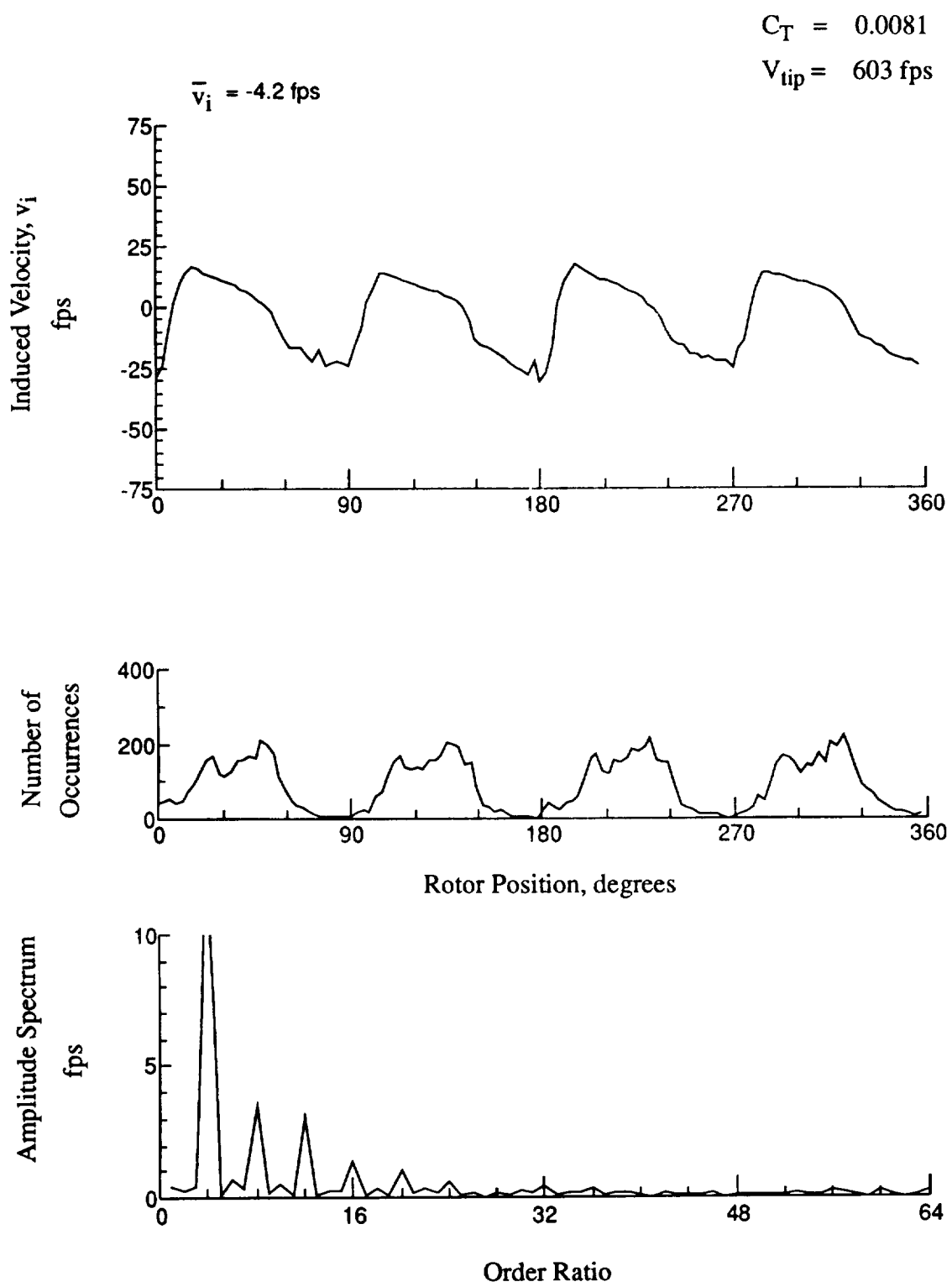


Figure 98.- Concluded.
 $x/R = 0.80$, $y/R = -0.60$, $z = -2.33 \text{ in.}$

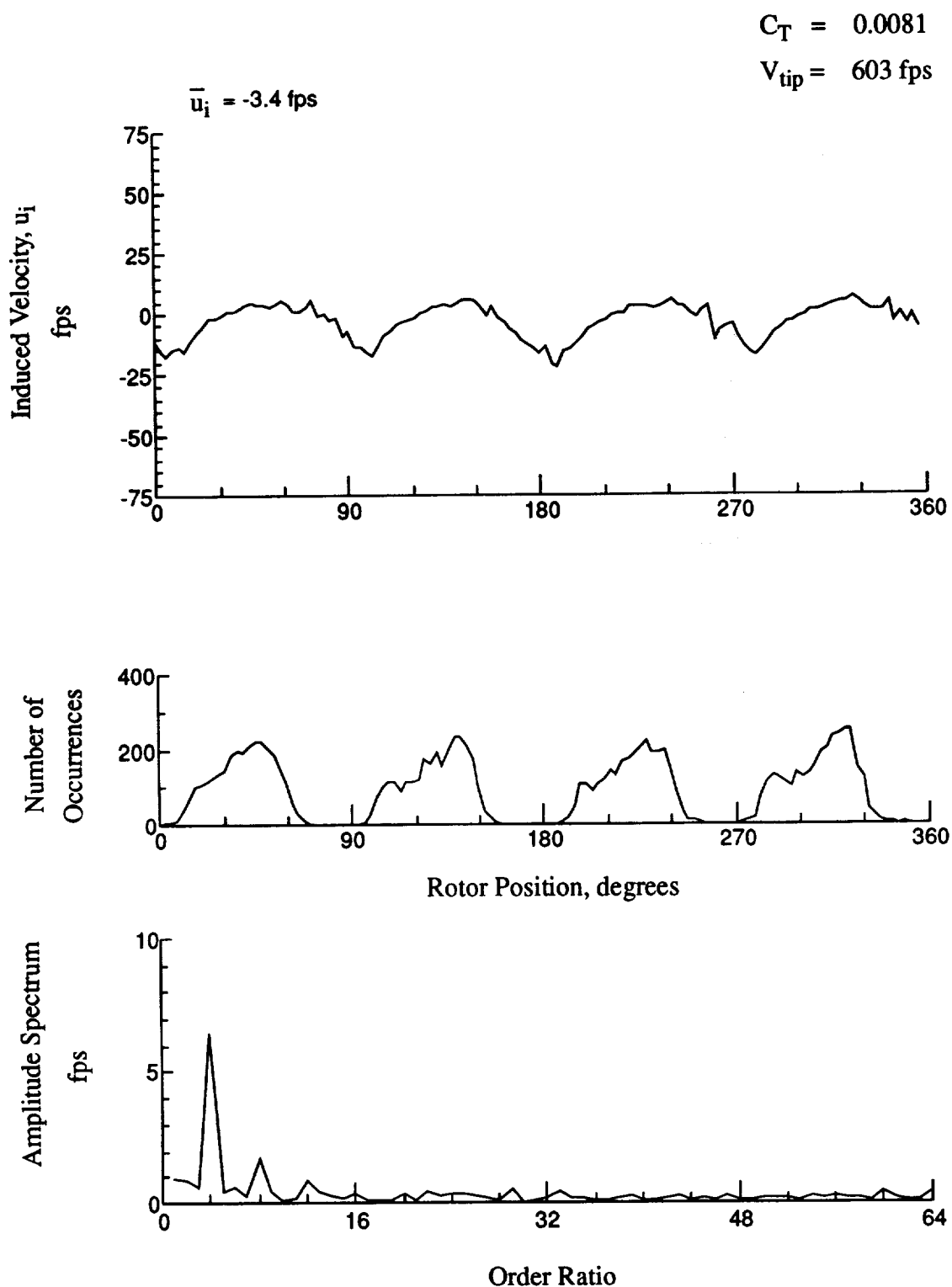


Figure 99.- Wake Measurements at
 $x/R = 0.80$, $y/R = -0.60$, $z = -3.36 \text{ in.}$

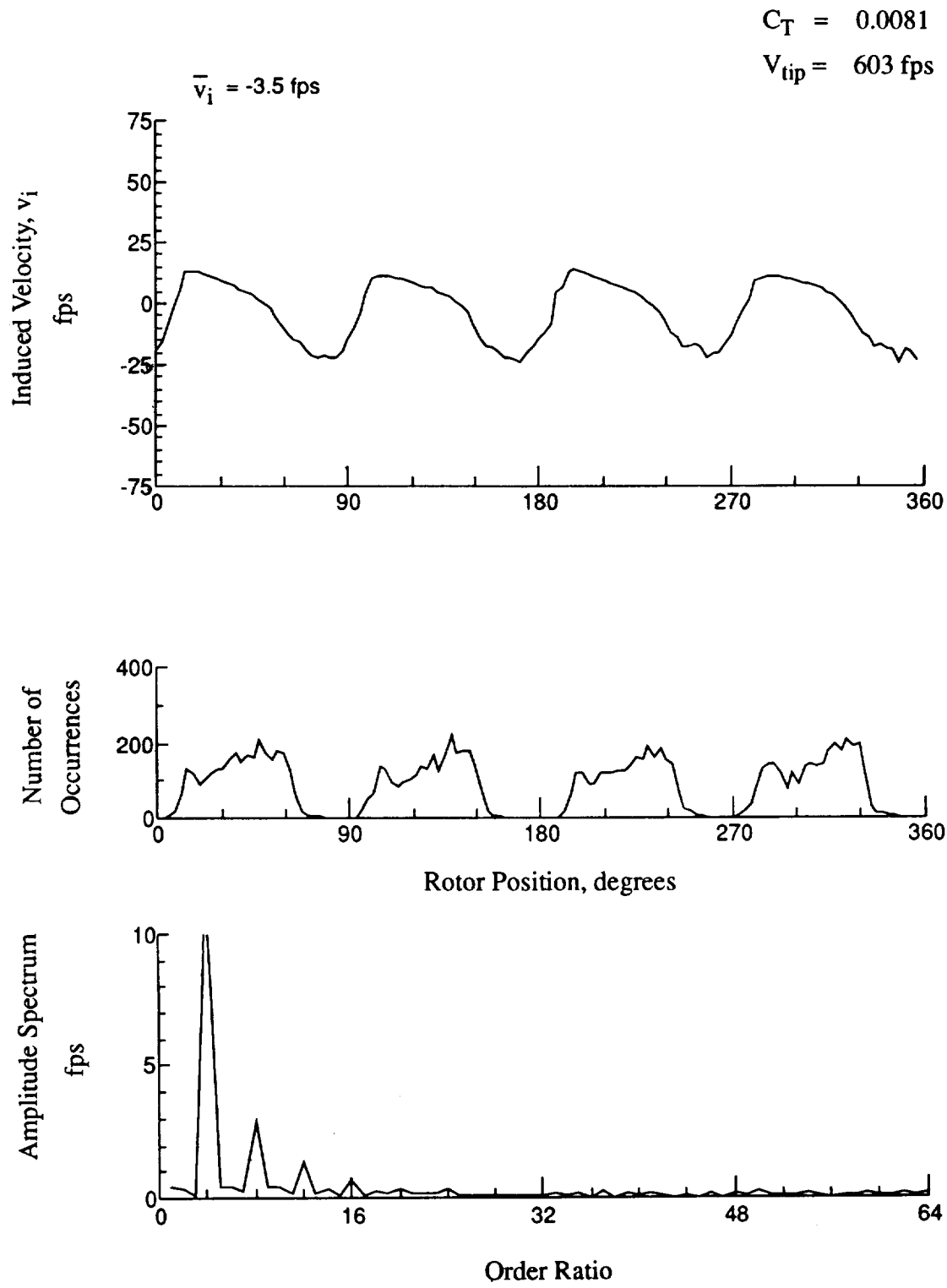


Figure 99.- Concluded.
 $x/R = 0.80$, $y/R = -0.60$, $z = -3.36 \text{ in.}$

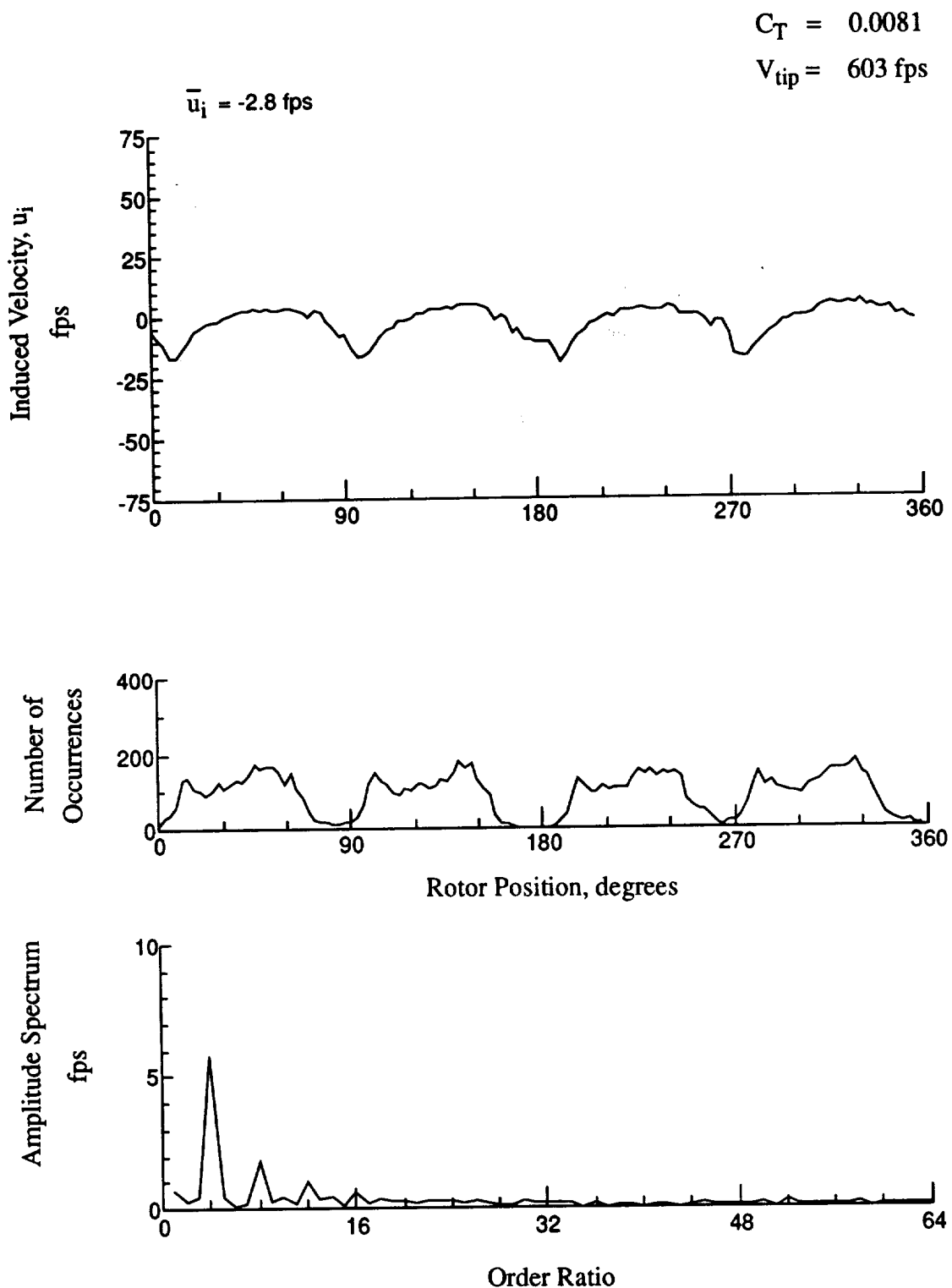


Figure 100.- Wake Measurements at
 $x/R = 0.80$, $y/R = -0.60$, $z = -4.39$ in.

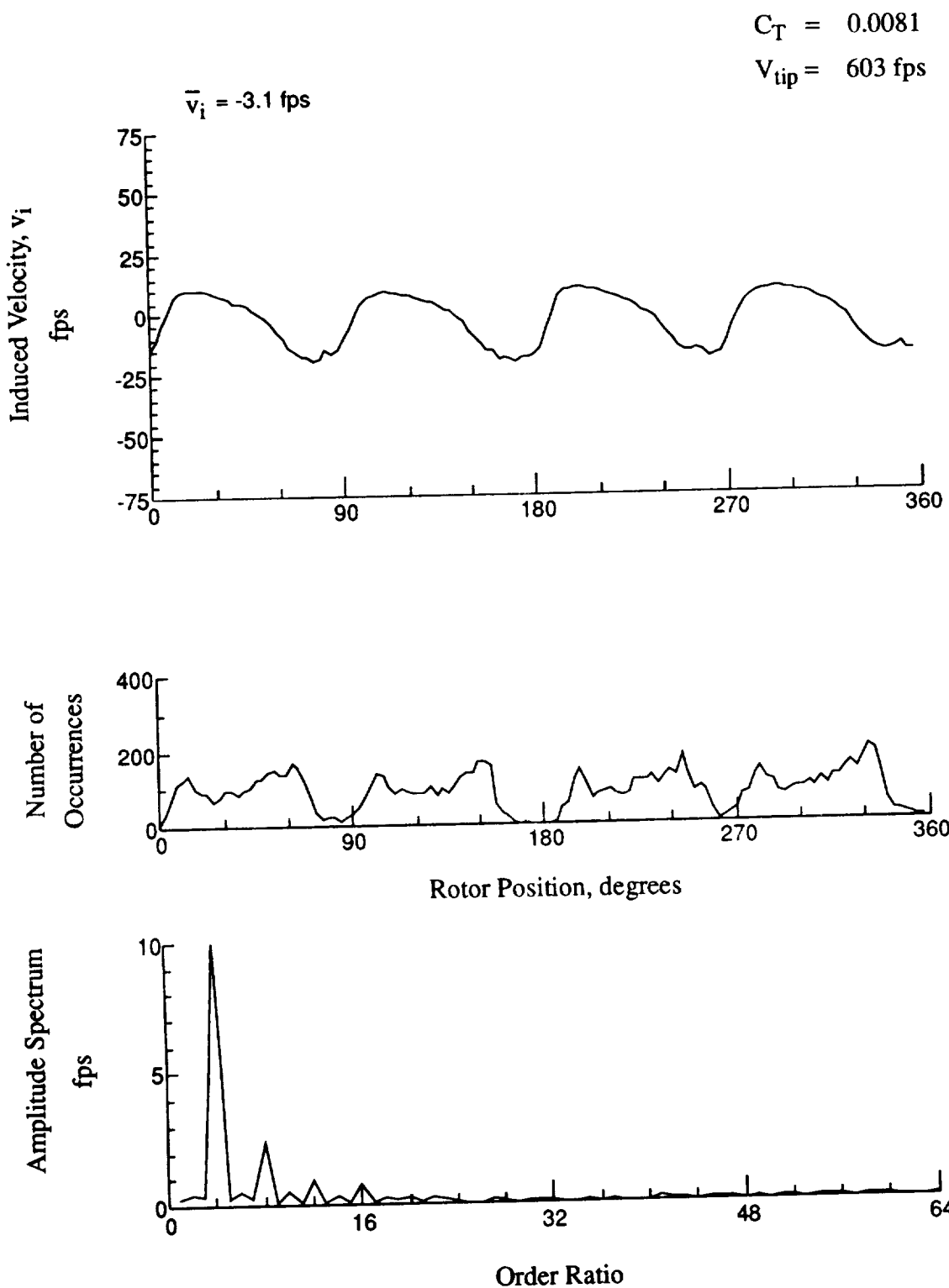


Figure 100.- Concluded.
 $x/R = 0.80$, $y/R = -0.60$, $z = -4.39 \text{ in.}$

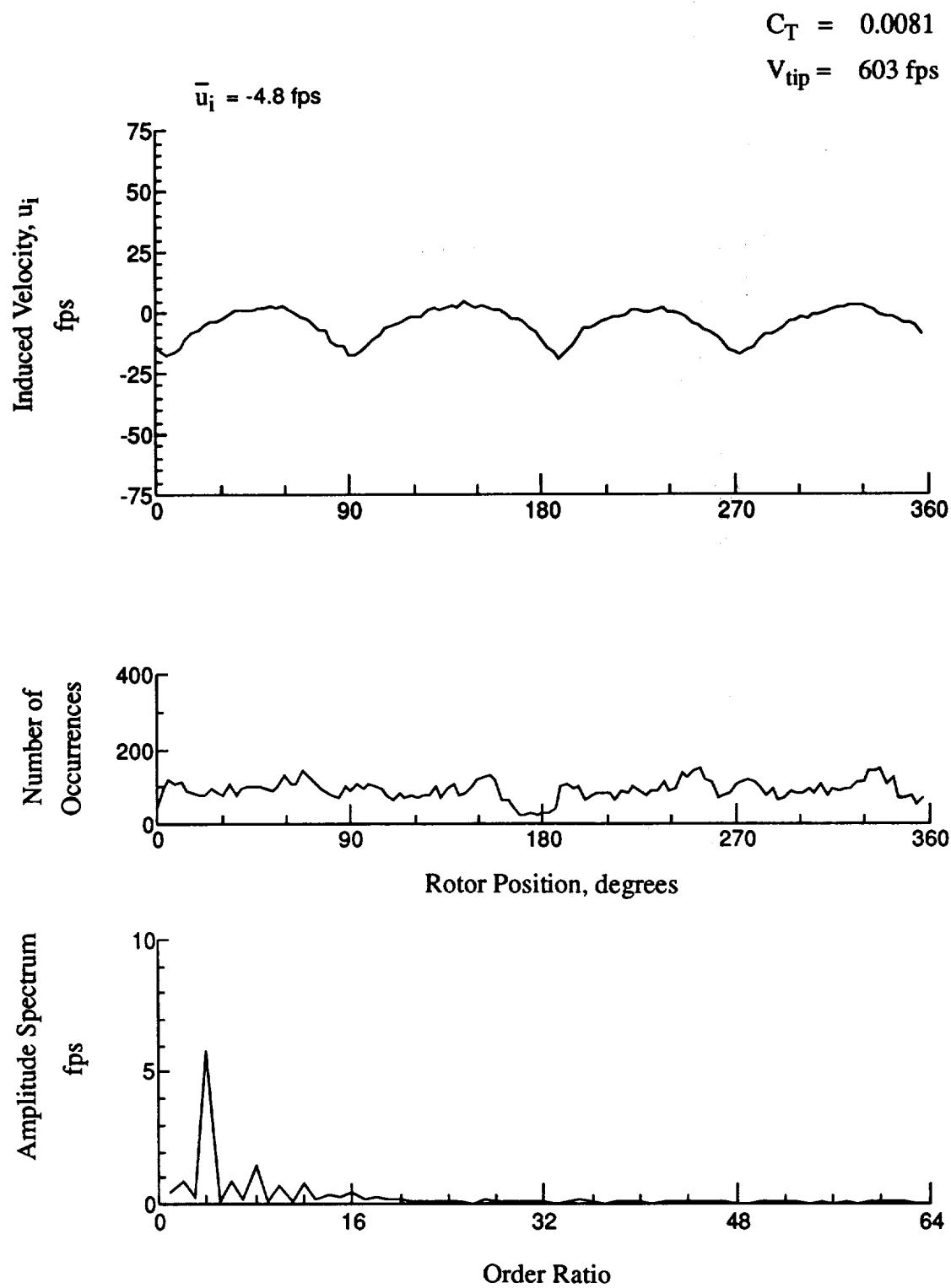


Figure 101.- Wake Measurements at
 $x/R = 0.80$, $y/R = -0.60$, $z = -5.42 \text{ in.}$

$$C_T = 0.0081$$

$$V_{tip} = 603 \text{ fps}$$

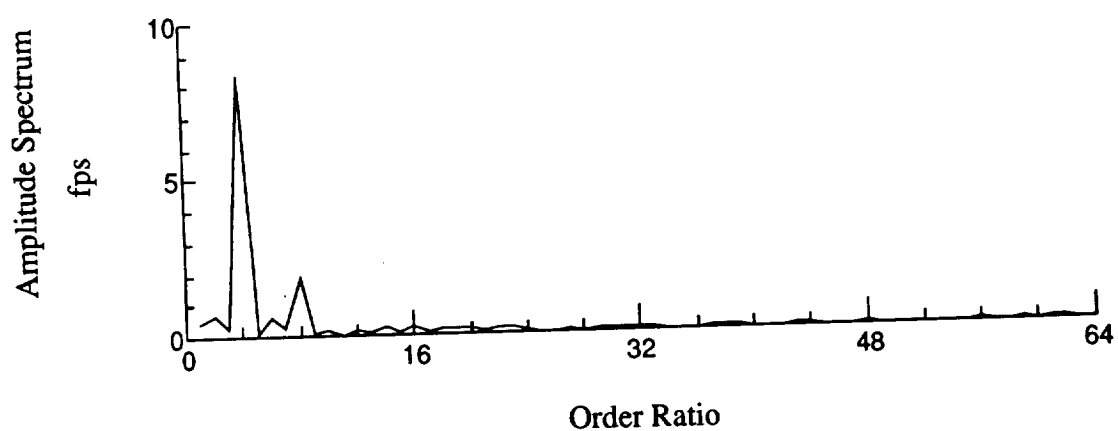
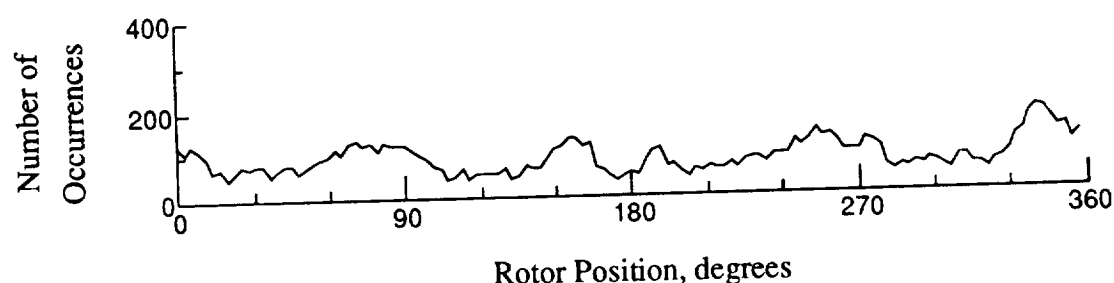
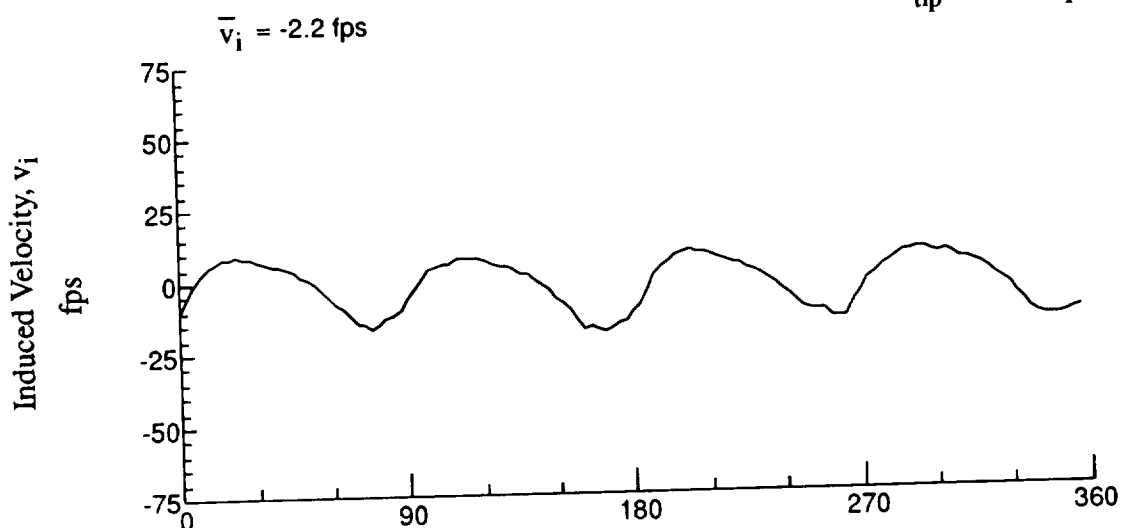


Figure 101.- Concluded.
 $x/R = 0.80$, $y/R = -0.60$, $z = -5.42$ in.

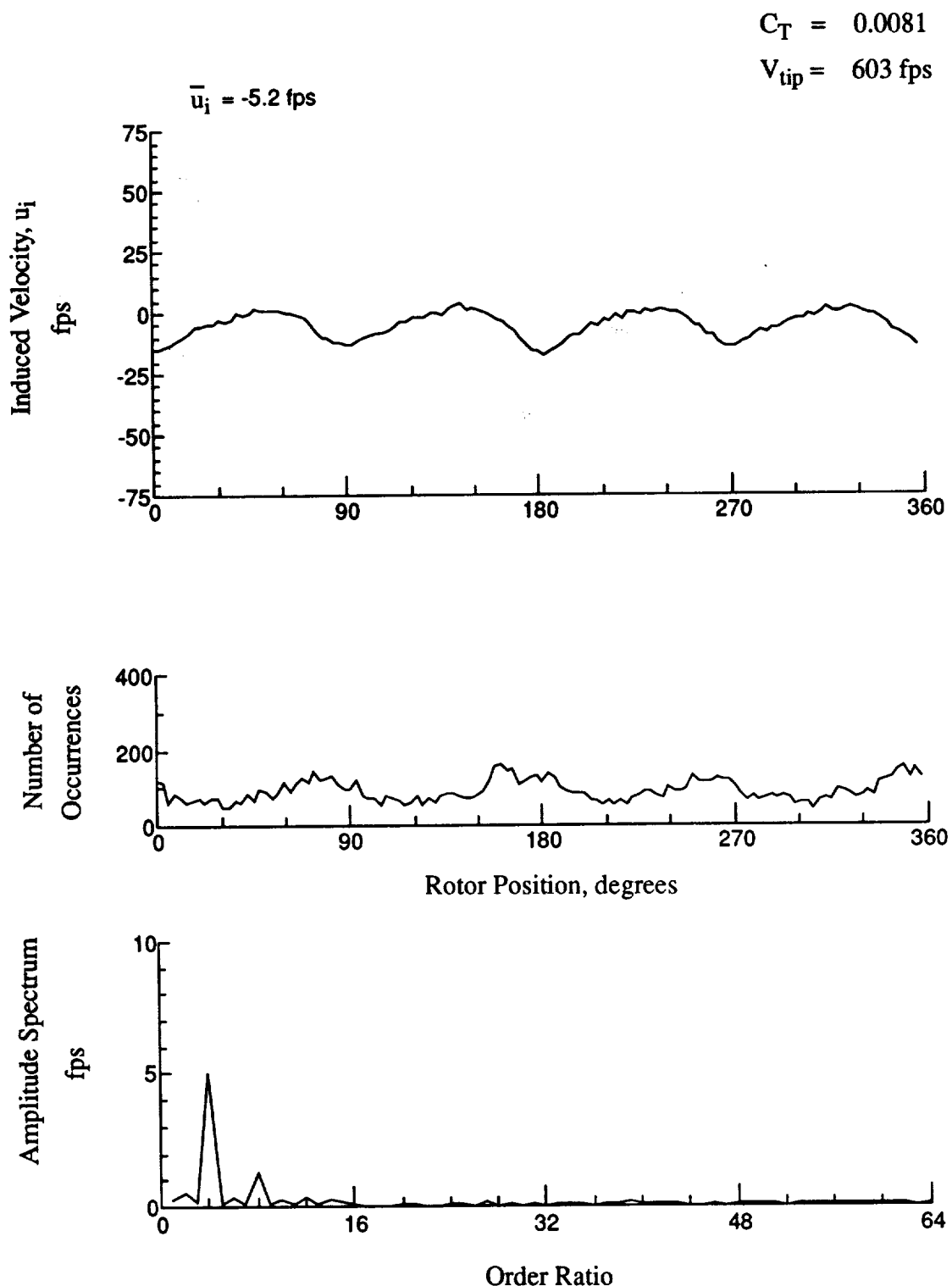


Figure 102.- Wake Measurements at
 $x/R = 0.80$, $y/R = -0.60$, $z = -6.45 \text{ in.}$

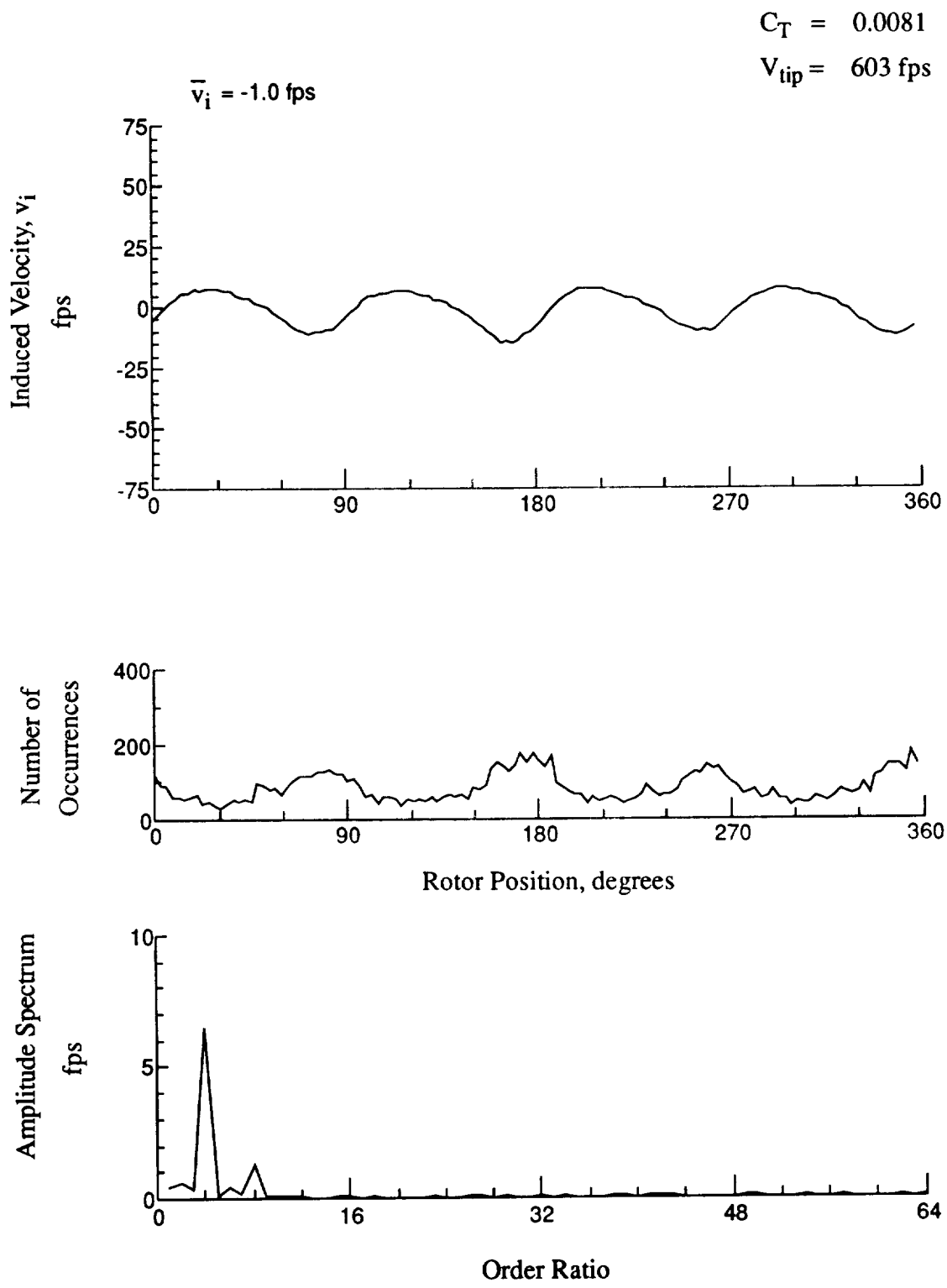


Figure 102.- Concluded.
 $x/R = 0.80$, $y/R = -0.60$, $z = -6.45 \text{ in.}$

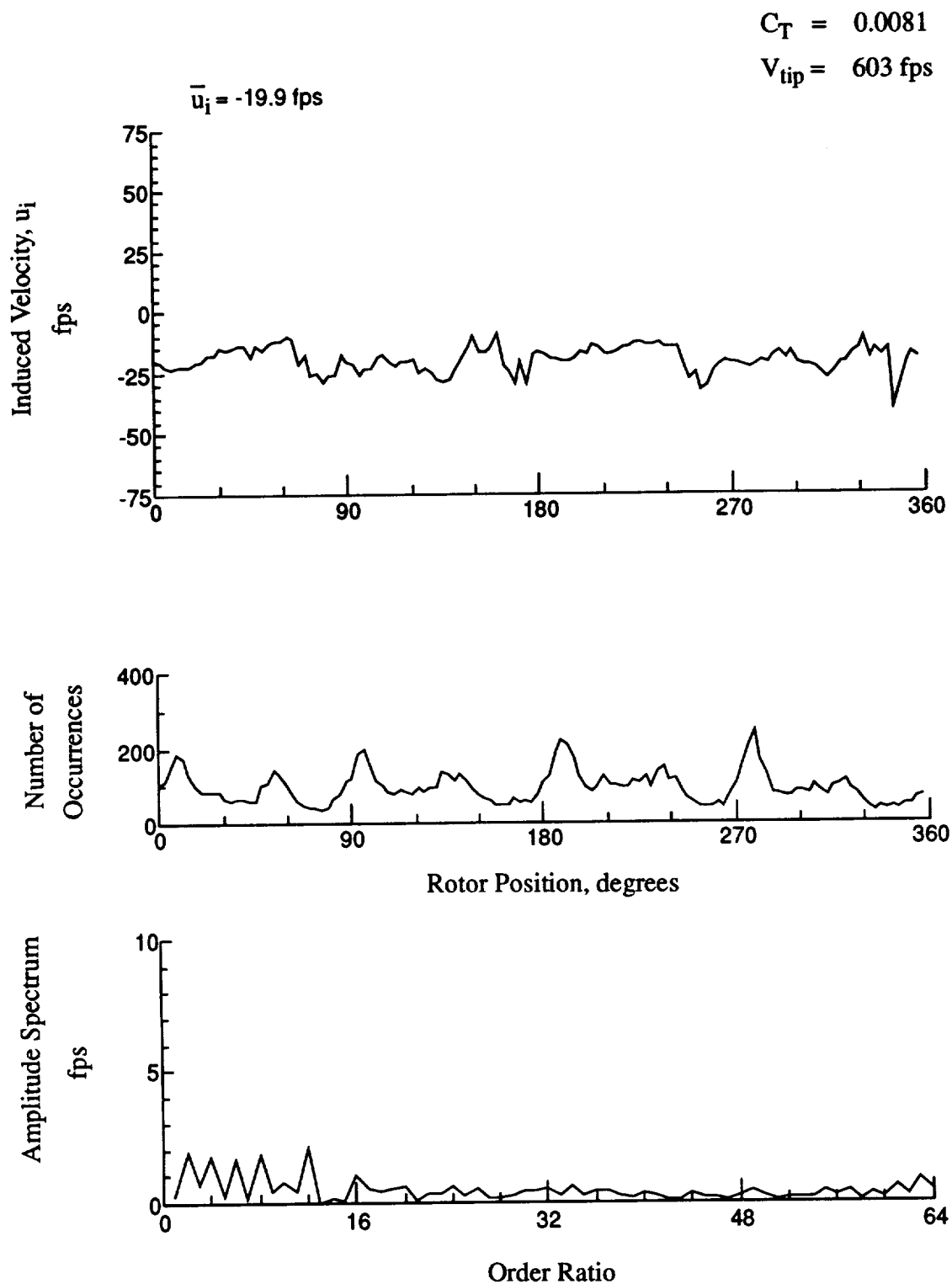


Figure 103.- Wake Measurements at
 $x/R = 0.90$, $y/R = -0.20$, $z = -0.27 \text{ in.}$

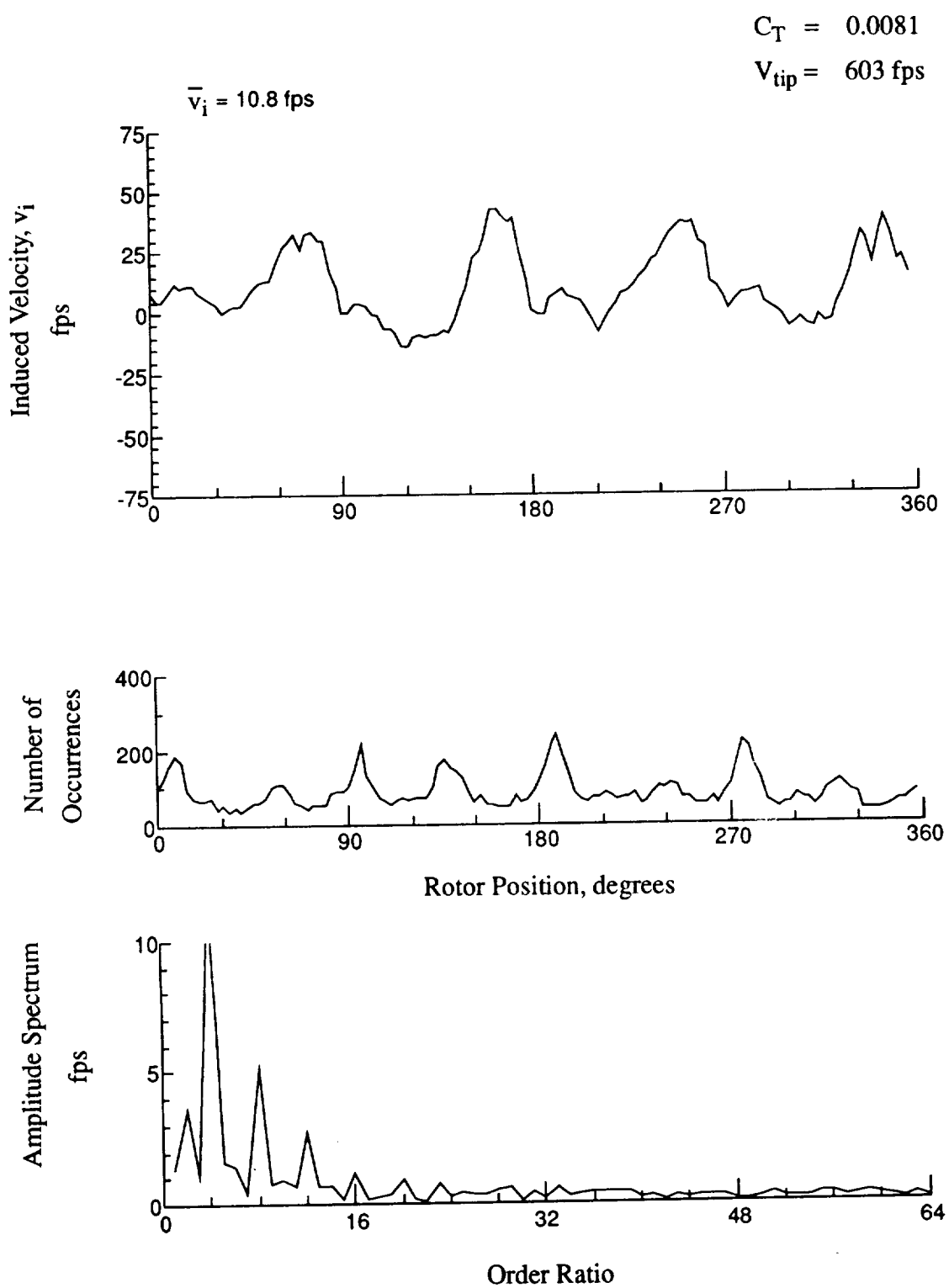


Figure 103.- Concluded.
 $x/R = 0.90$, $y/R = -0.20$, $z = -0.27 \text{ in.}$

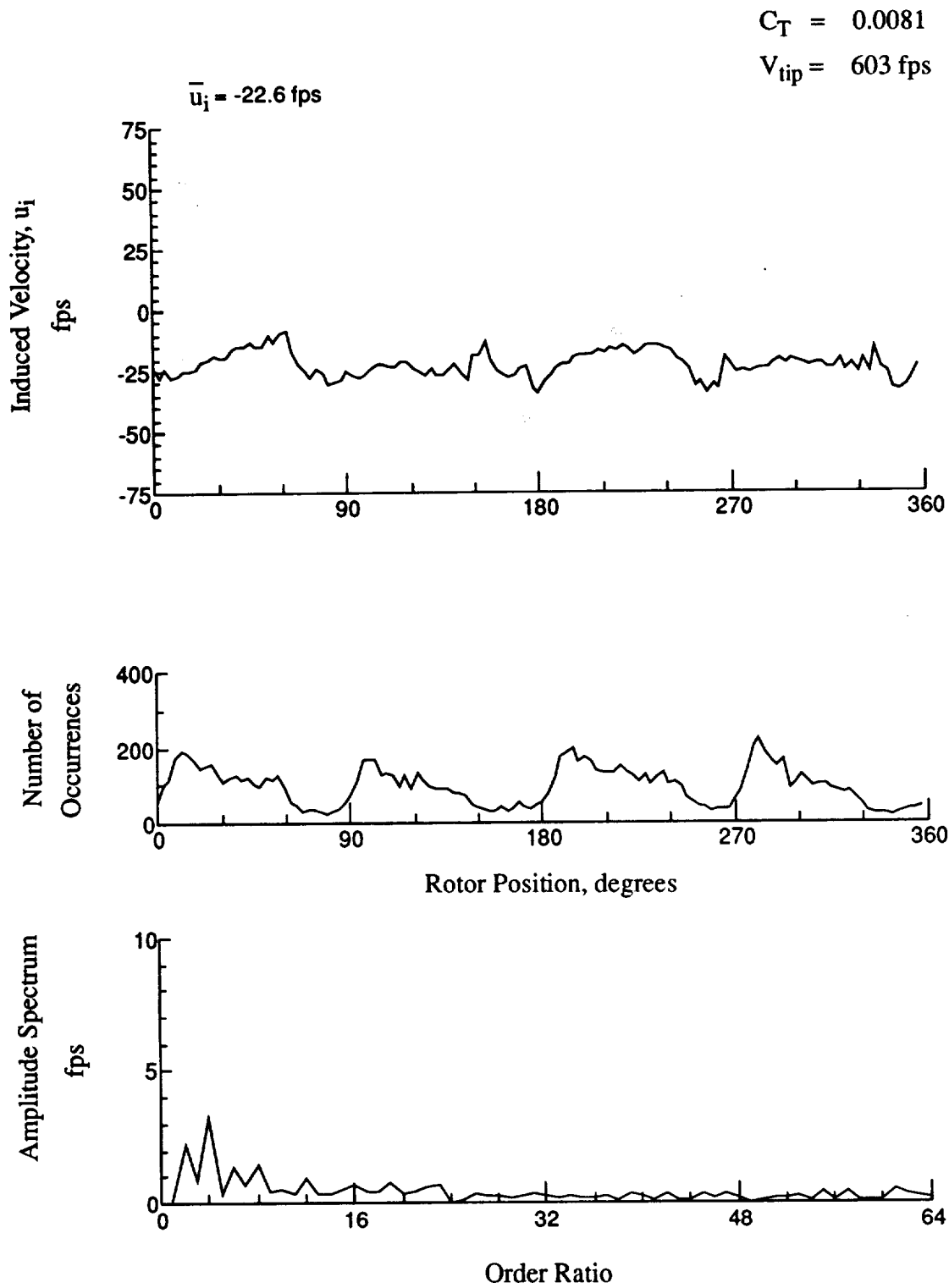


Figure 104.- Wake Measurements at
 $x/R = 0.90$, $y/R = -0.20$, $z = -1.30 \text{ in.}$

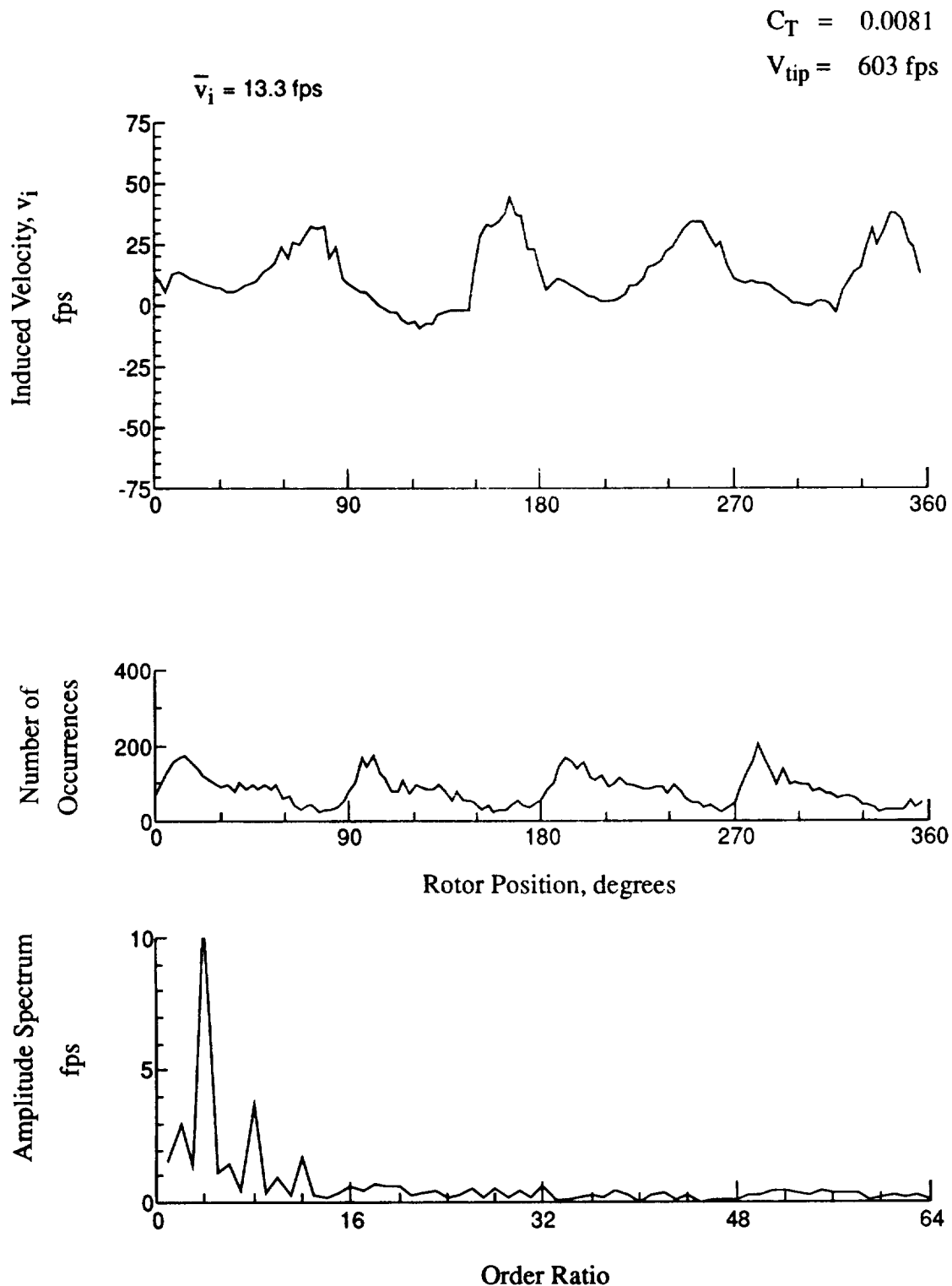
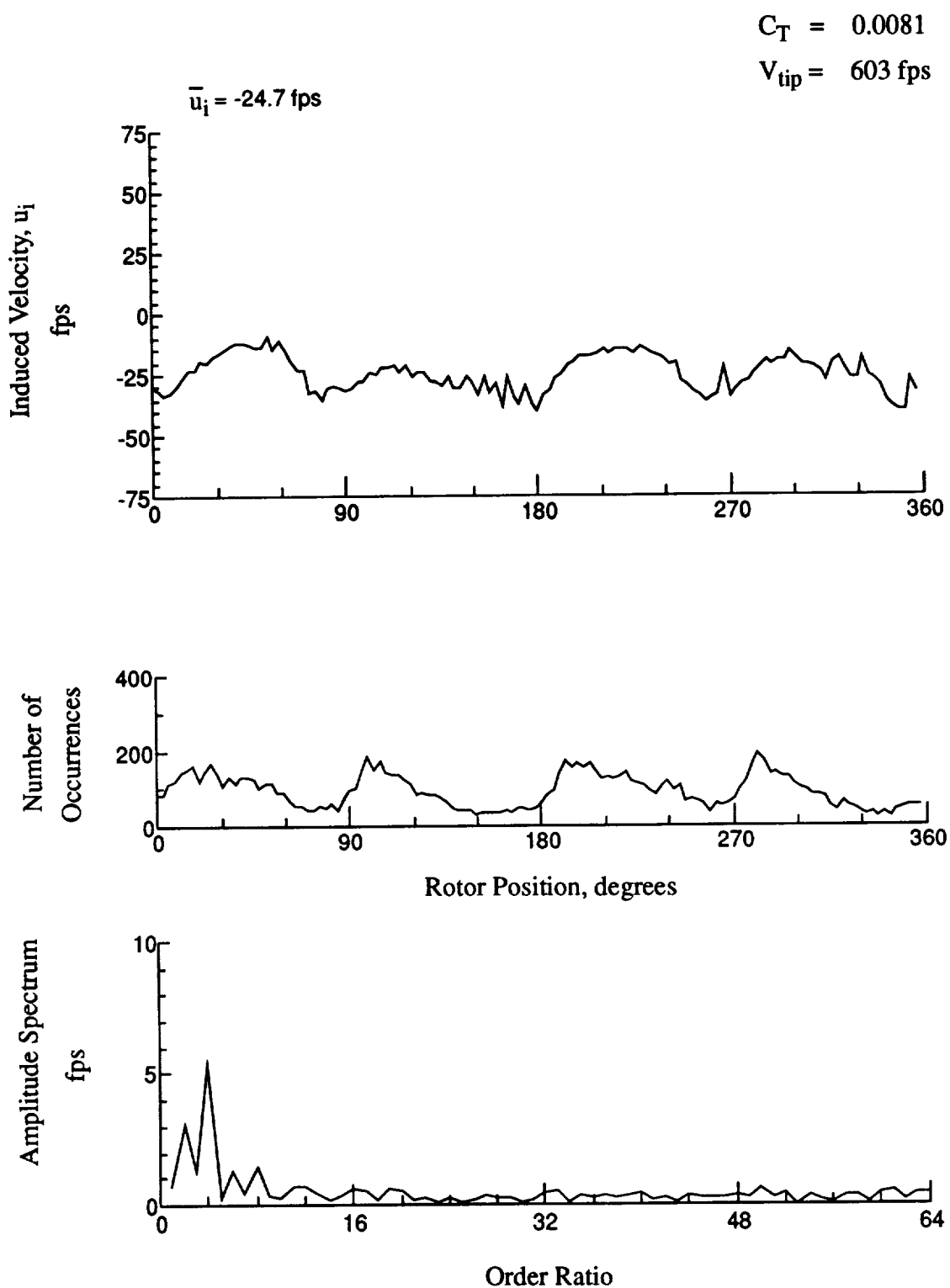


Figure 104.- Concluded.
 $x/R = 0.90$, $y/R = -0.20$, $z = -1.30 \text{ in.}$



**Figure 105.- Wake Measurements at
 $x/R = 0.90$, $y/R = -0.20$, $z = -2.33 \text{ in.}$**

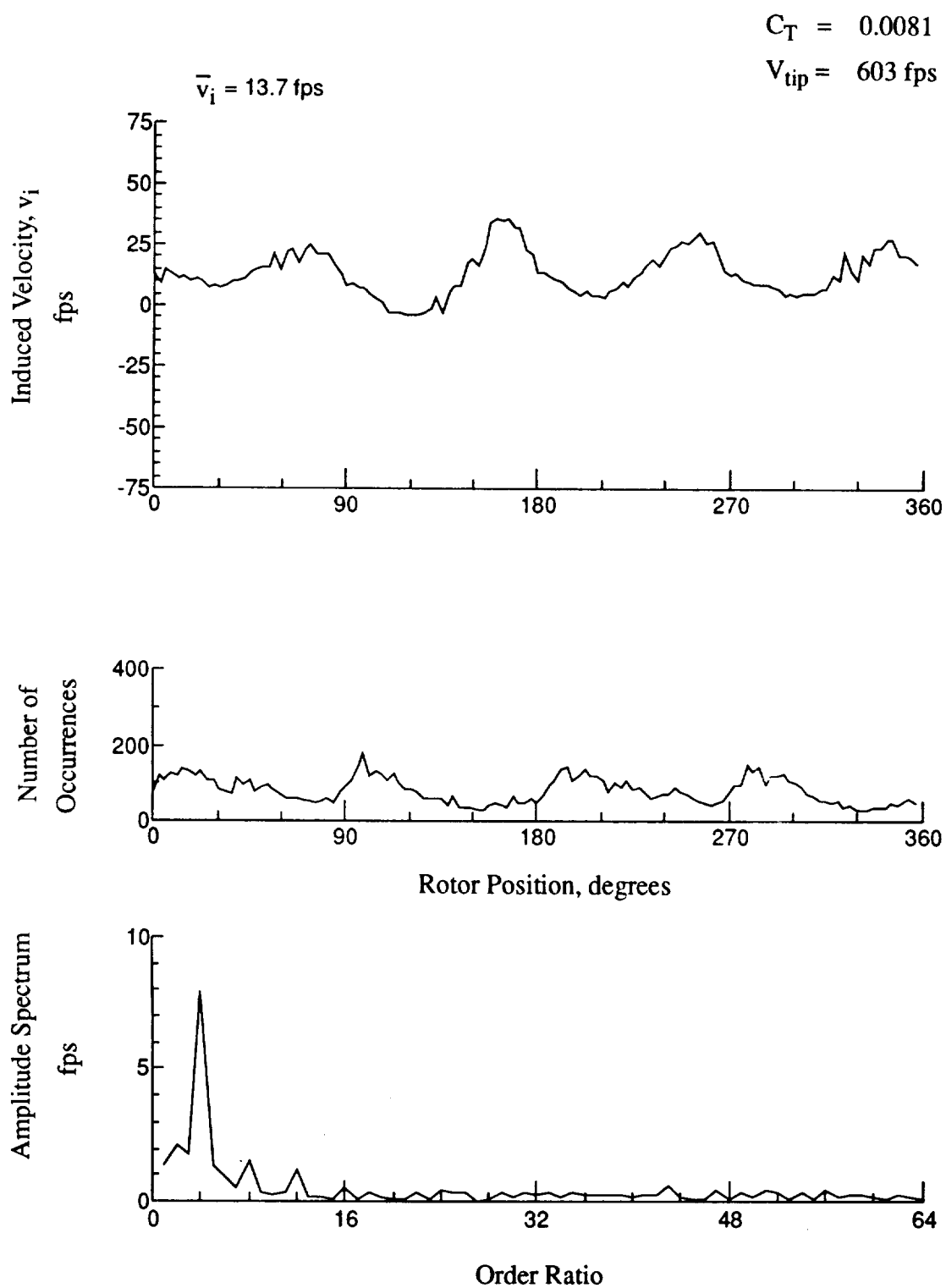


Figure 105.- Concluded.
 $x/R = 0.90$, $y/R = -0.20$, $z = -2.33 \text{ in.}$

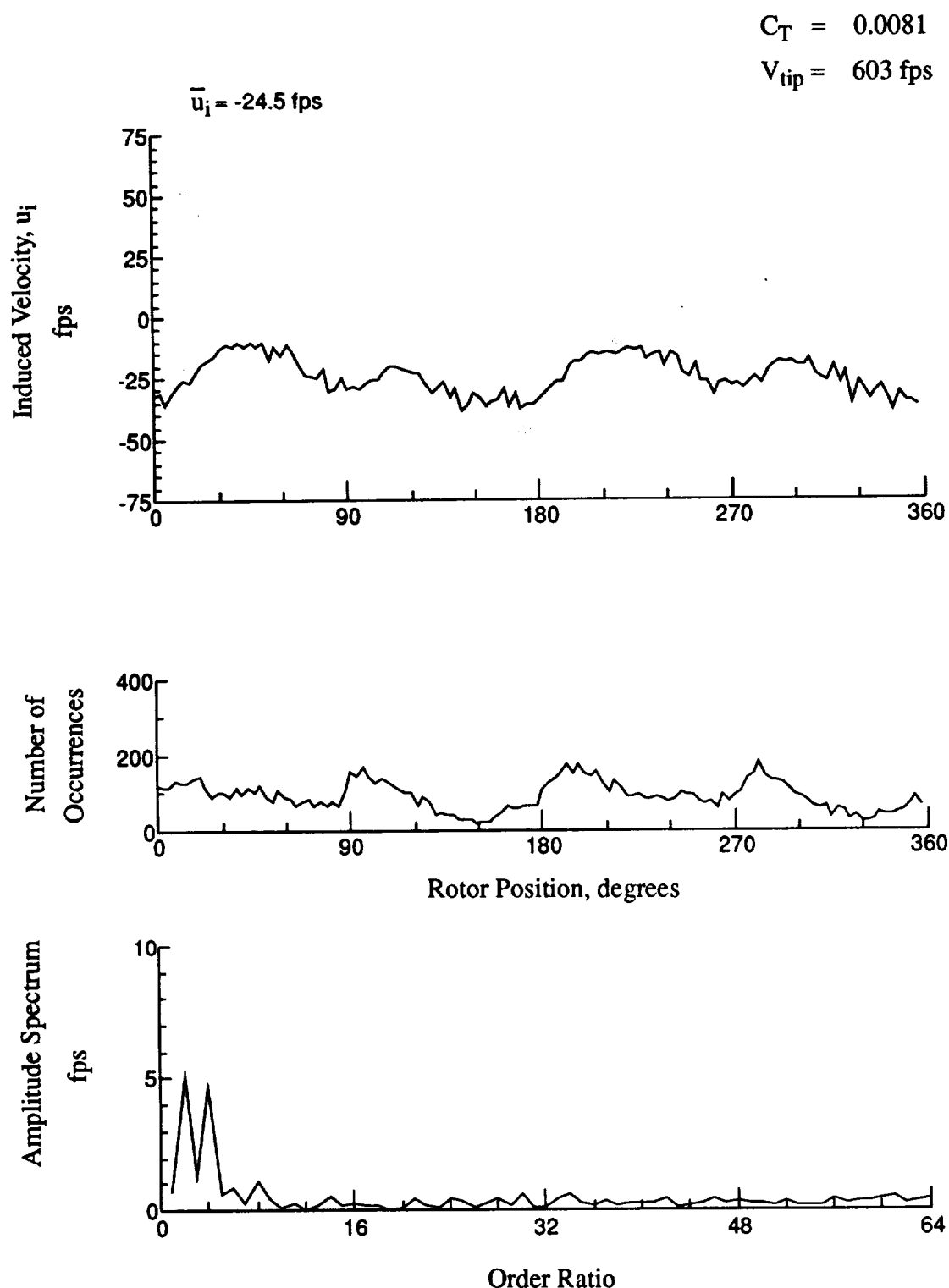


Figure 106.- Wake Measurements at
 $x/R = 0.90$, $y/R = -0.20$, $z = -3.36$ in.

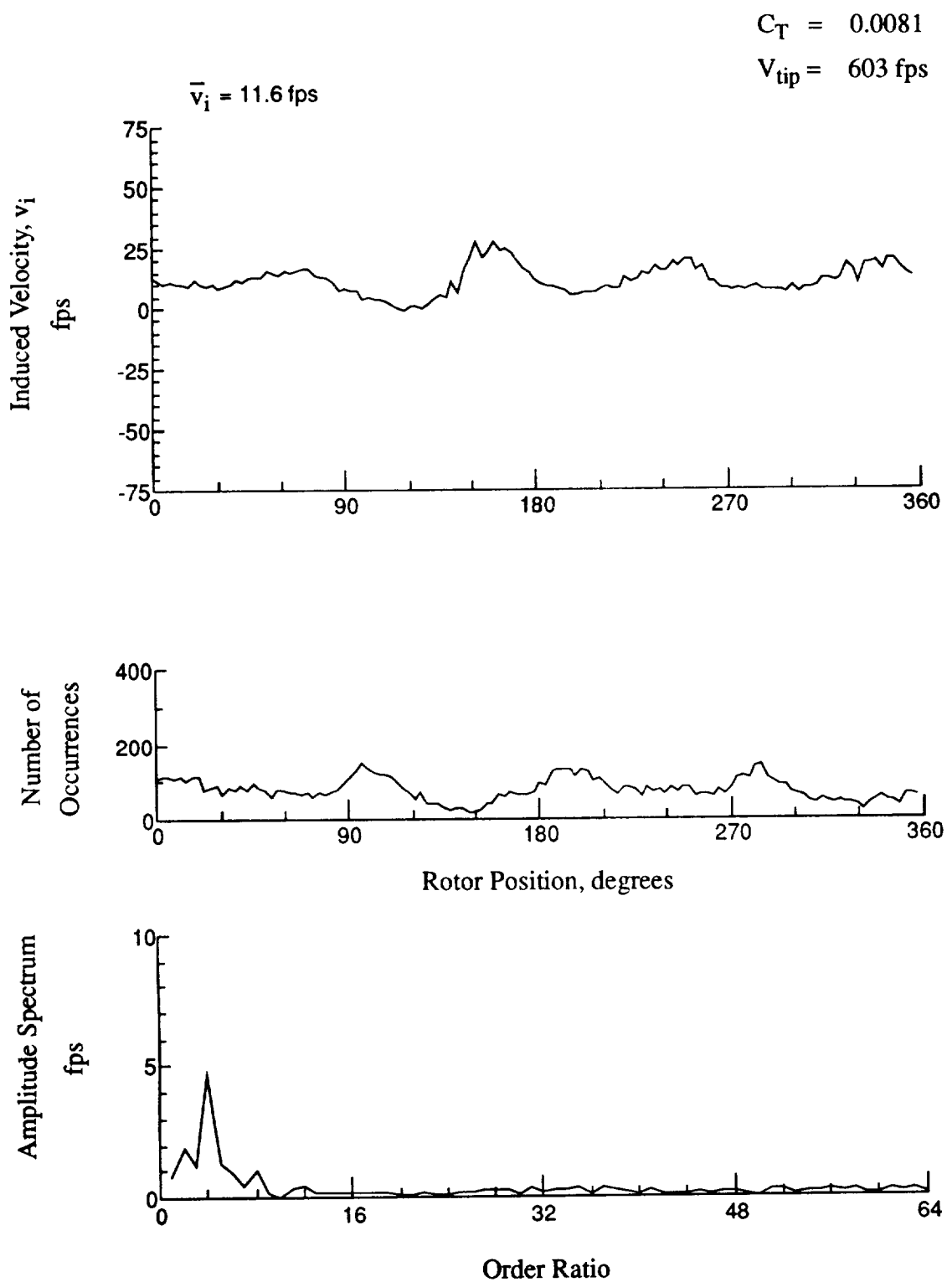


Figure 106.- Concluded.
 $x/R = 0.90$, $y/R = -0.20$, $z = -3.36 \text{ in.}$

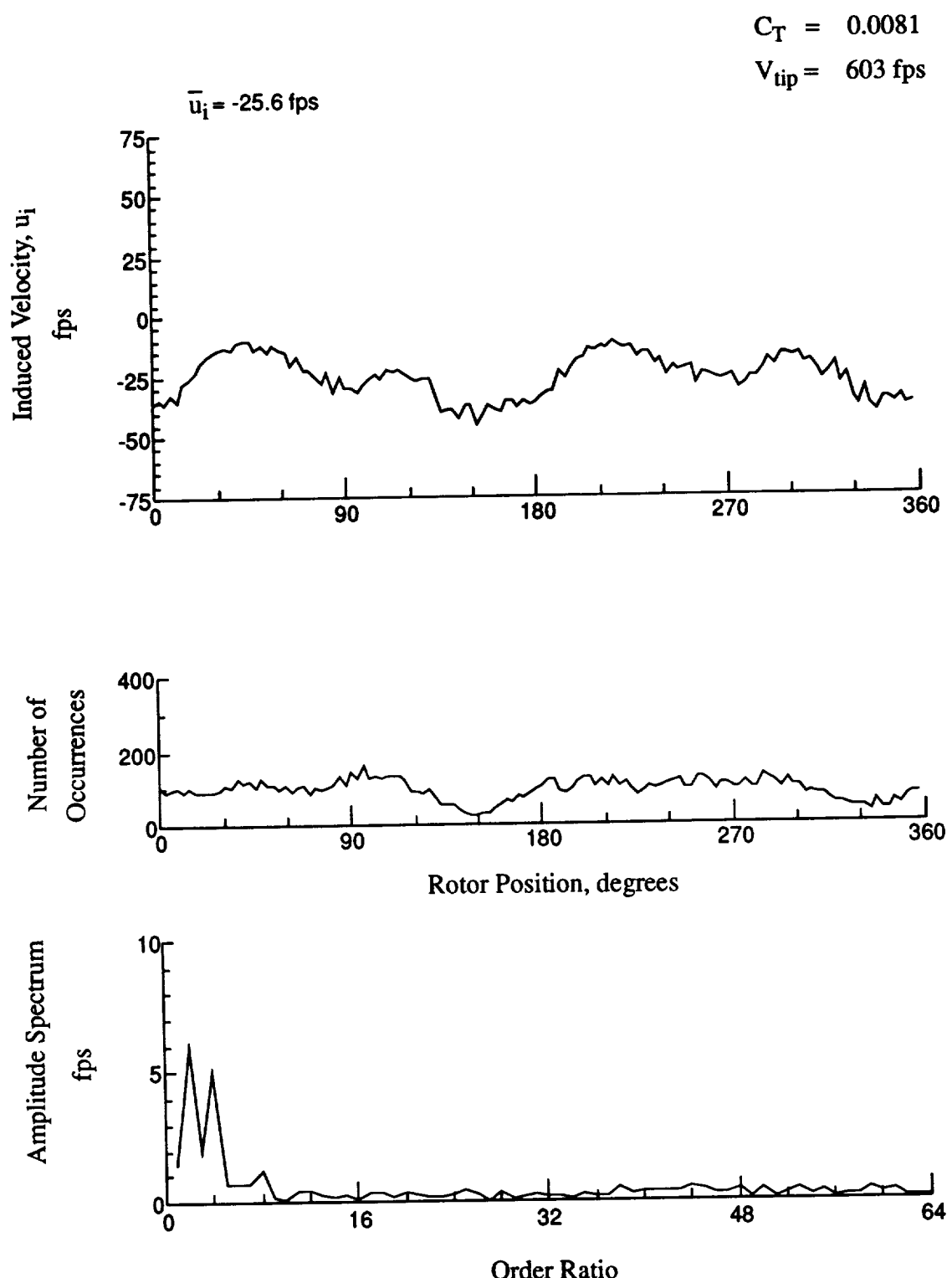


Figure 107.- Wake Measurements at
 $x/R = 0.90$, $y/R = -0.20$, $z = -4.39$ in.

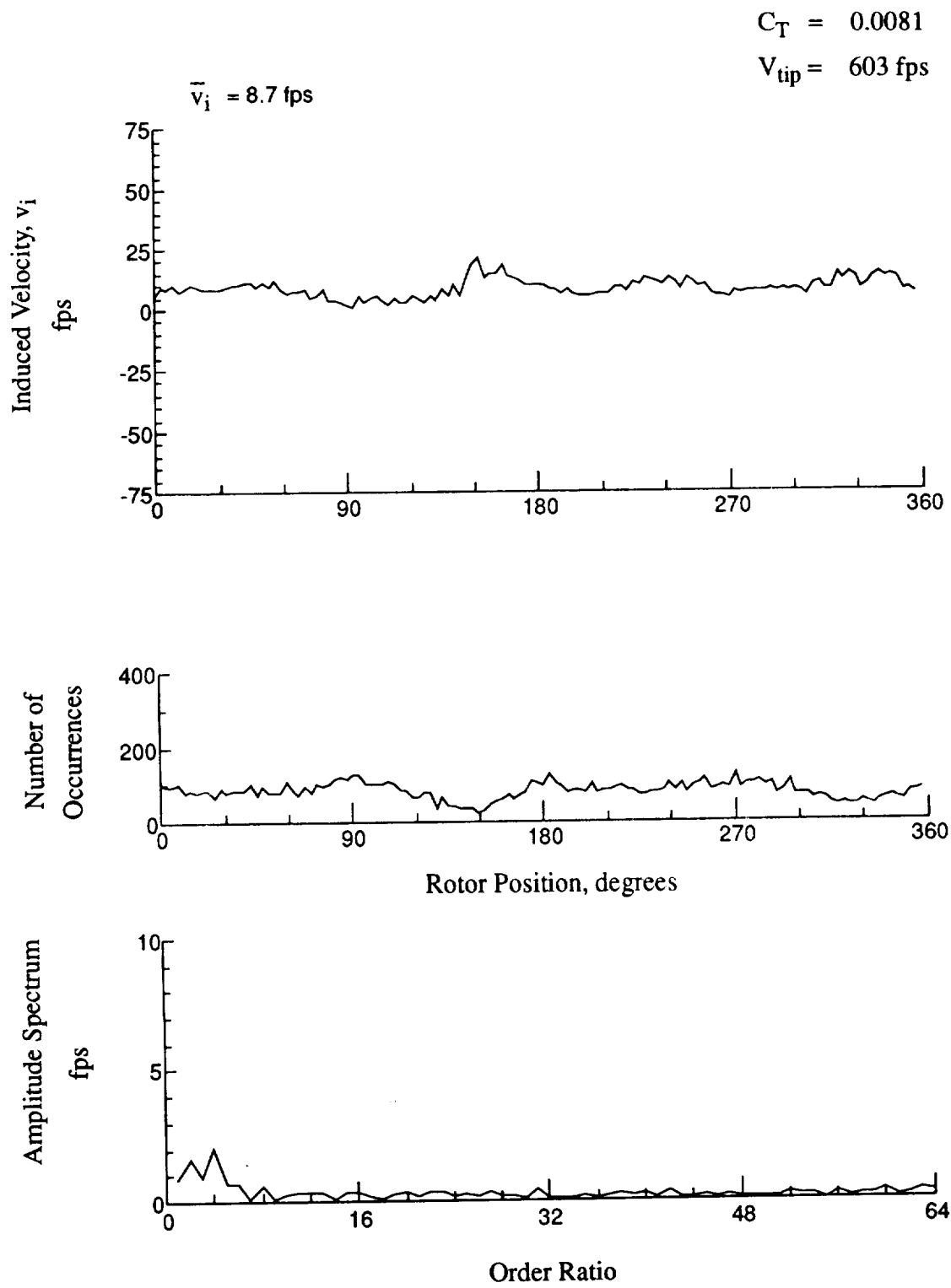


Figure 107.- Concluded.
 $x/R = 0.90$, $y/R = -0.20$, $z = -4.39 \text{ in.}$

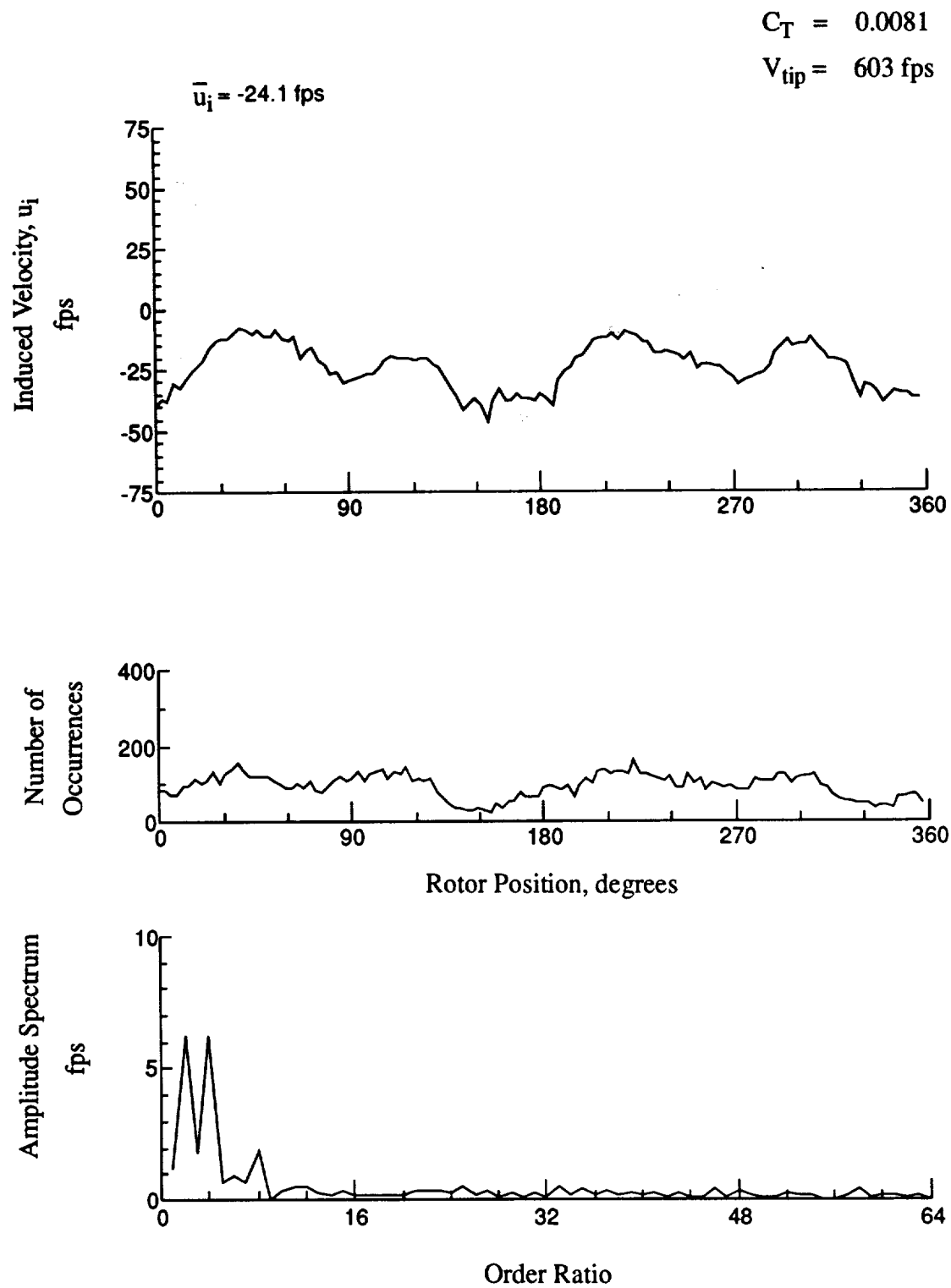


Figure 108.- Wake Measurements at
 $x/R = 0.90$, $y/R = -0.20$, $z = -5.42$ in.

$$C_T = 0.0081$$

$$V_{tip} = 603 \text{ fps}$$

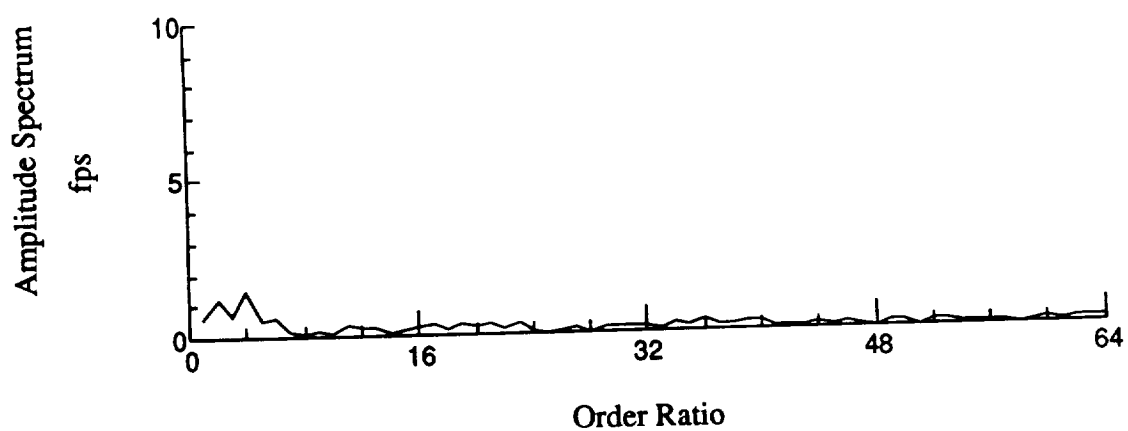
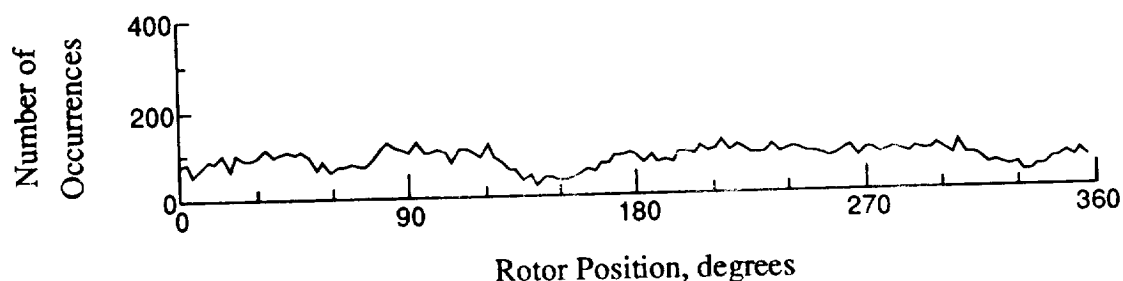
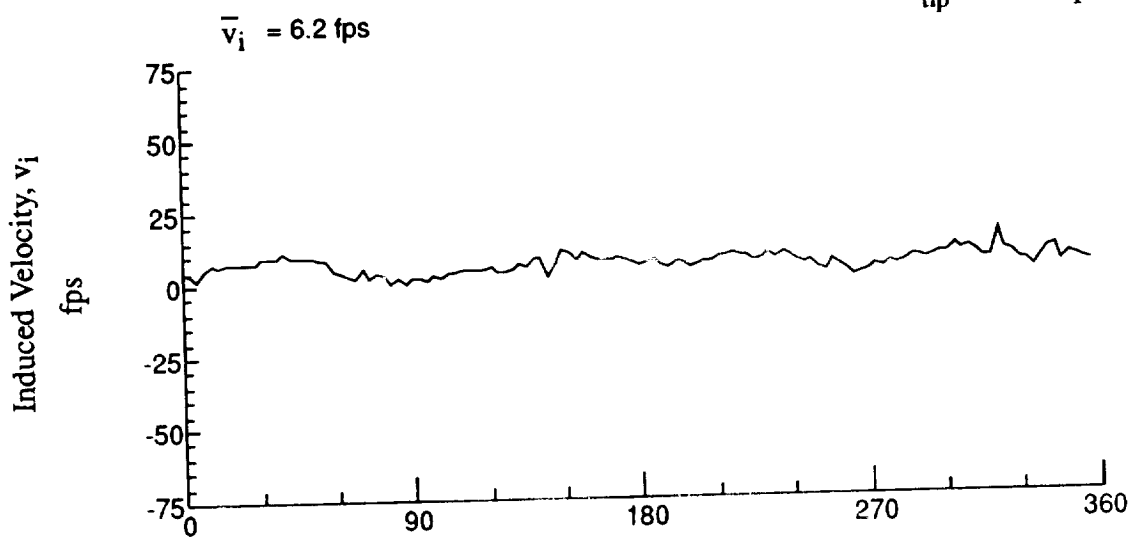


Figure 108.- Concluded.
 $x/R = 0.90$, $y/R = -0.20$, $z = -5.42$ in.

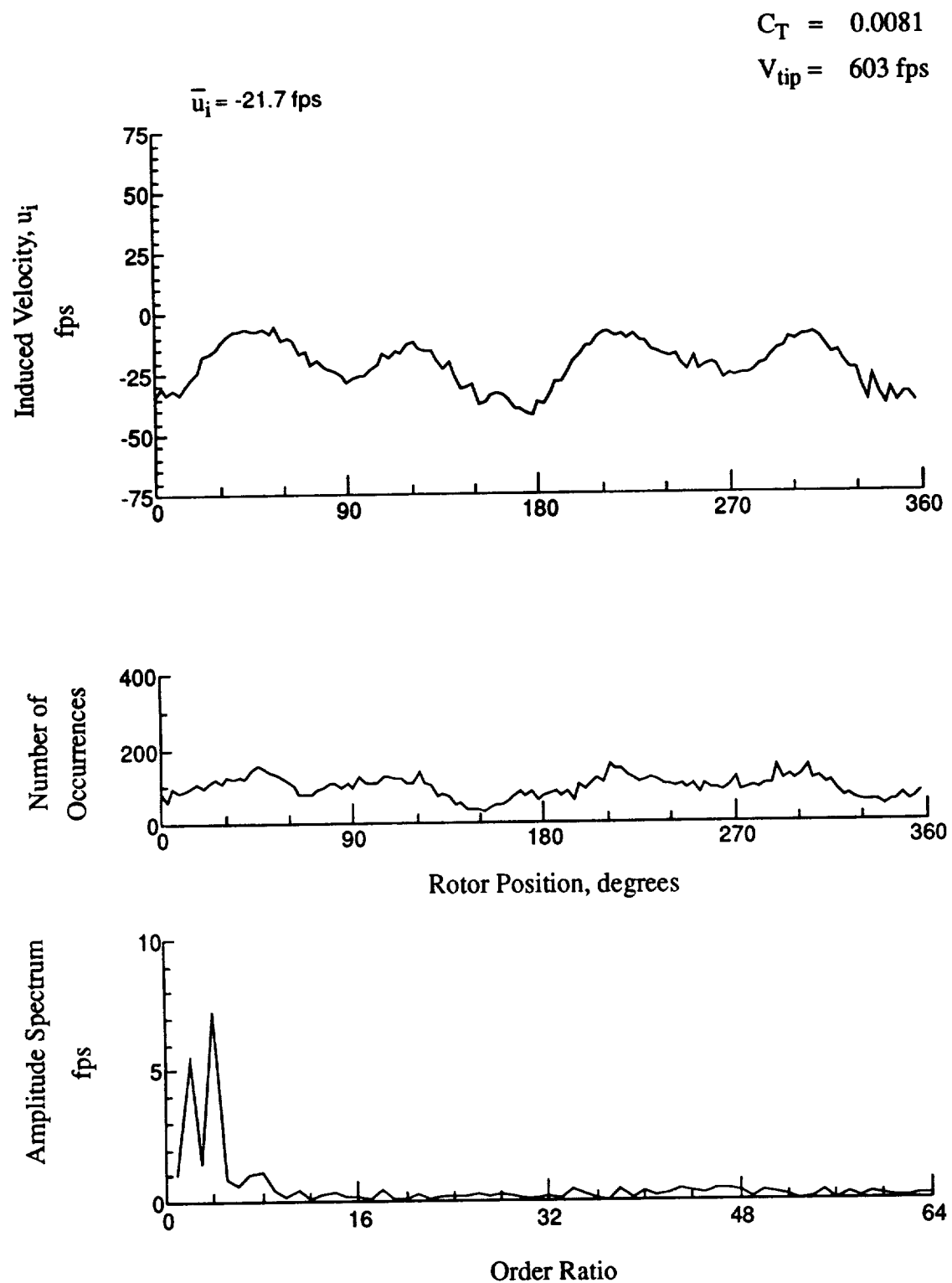


Figure 109.- Wake Measurements at
 $x/R = 0.90$, $y/R = -0.20$, $z = -6.45 \text{ in.}$

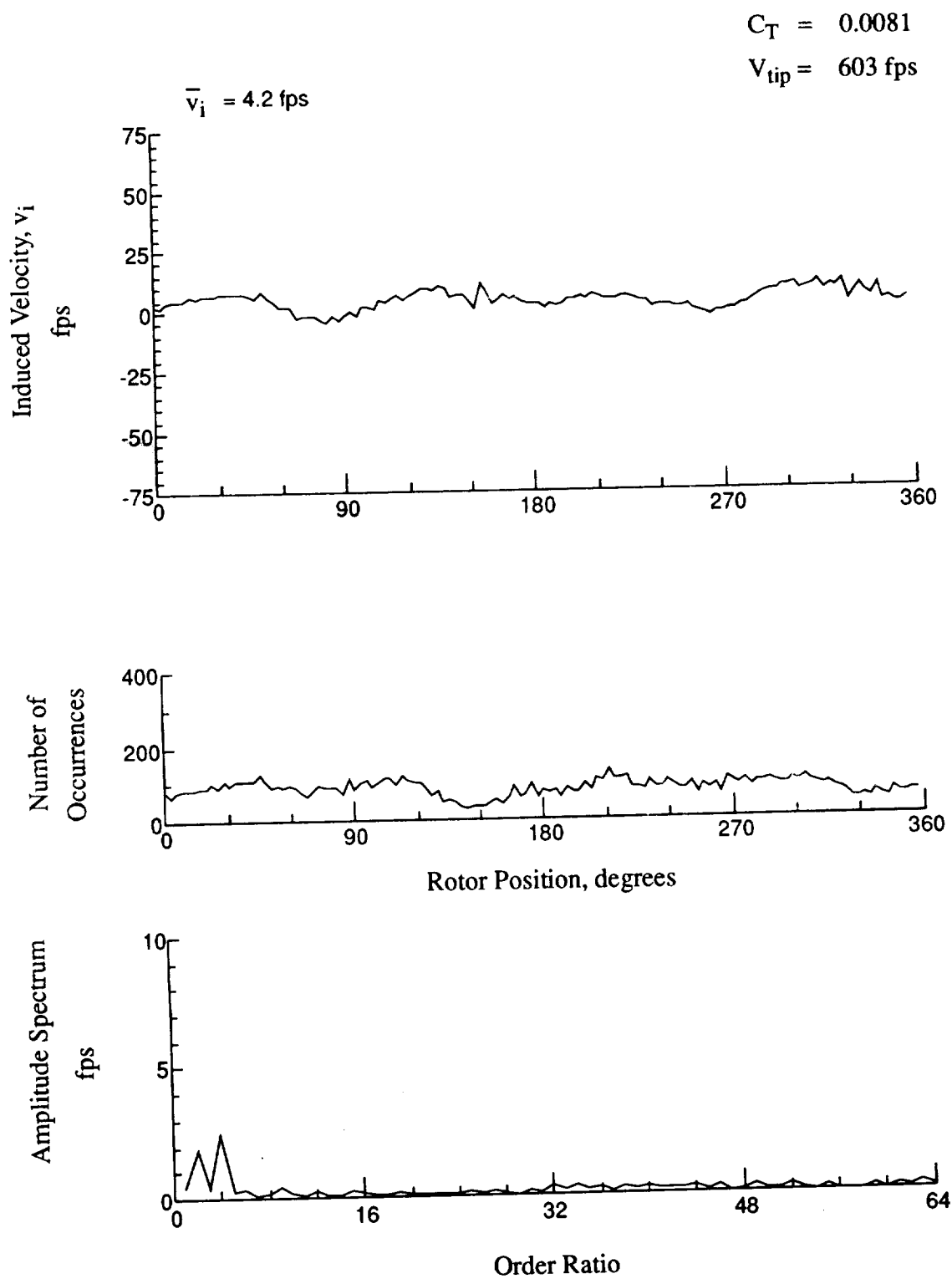
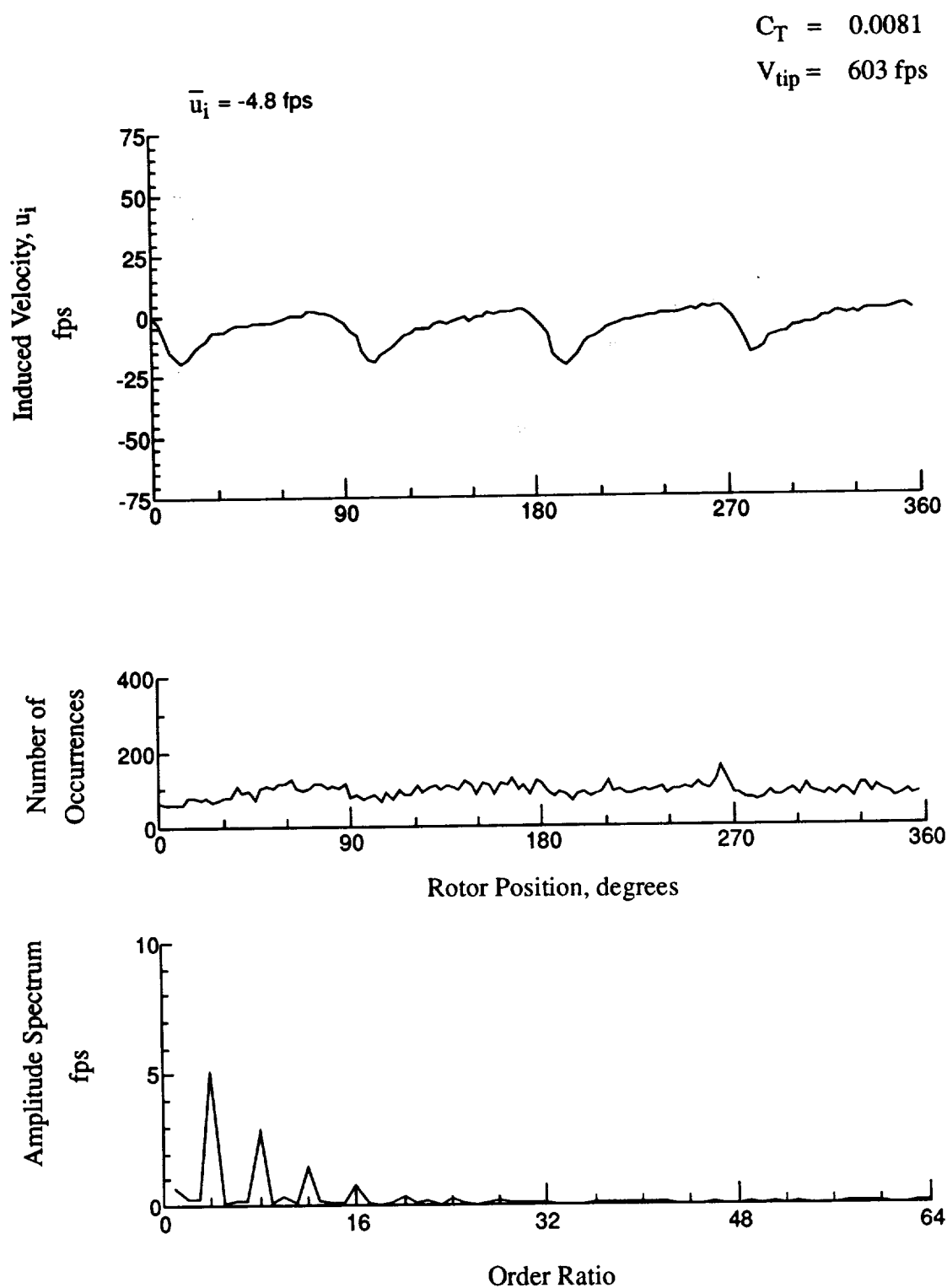


Figure 109.- Concluded.
 $x/R = 0.90$, $y/R = -0.20$, $z = -6.45 \text{ in.}$



**Figure 110.- Wake Measurements at
 $x/R = 1.10$, $y/R = -0.20$, $z = 8.85 \text{ in.}$**

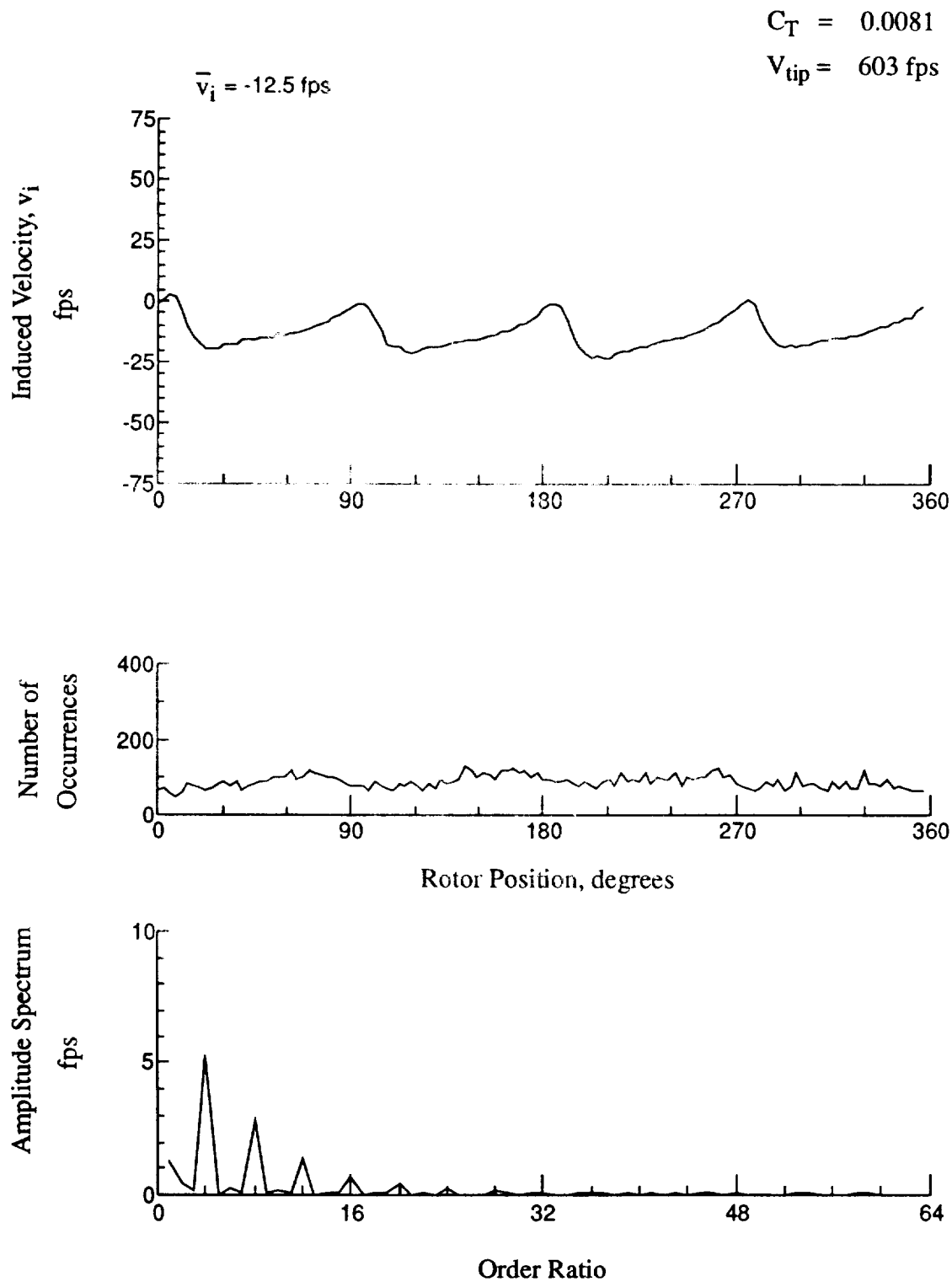
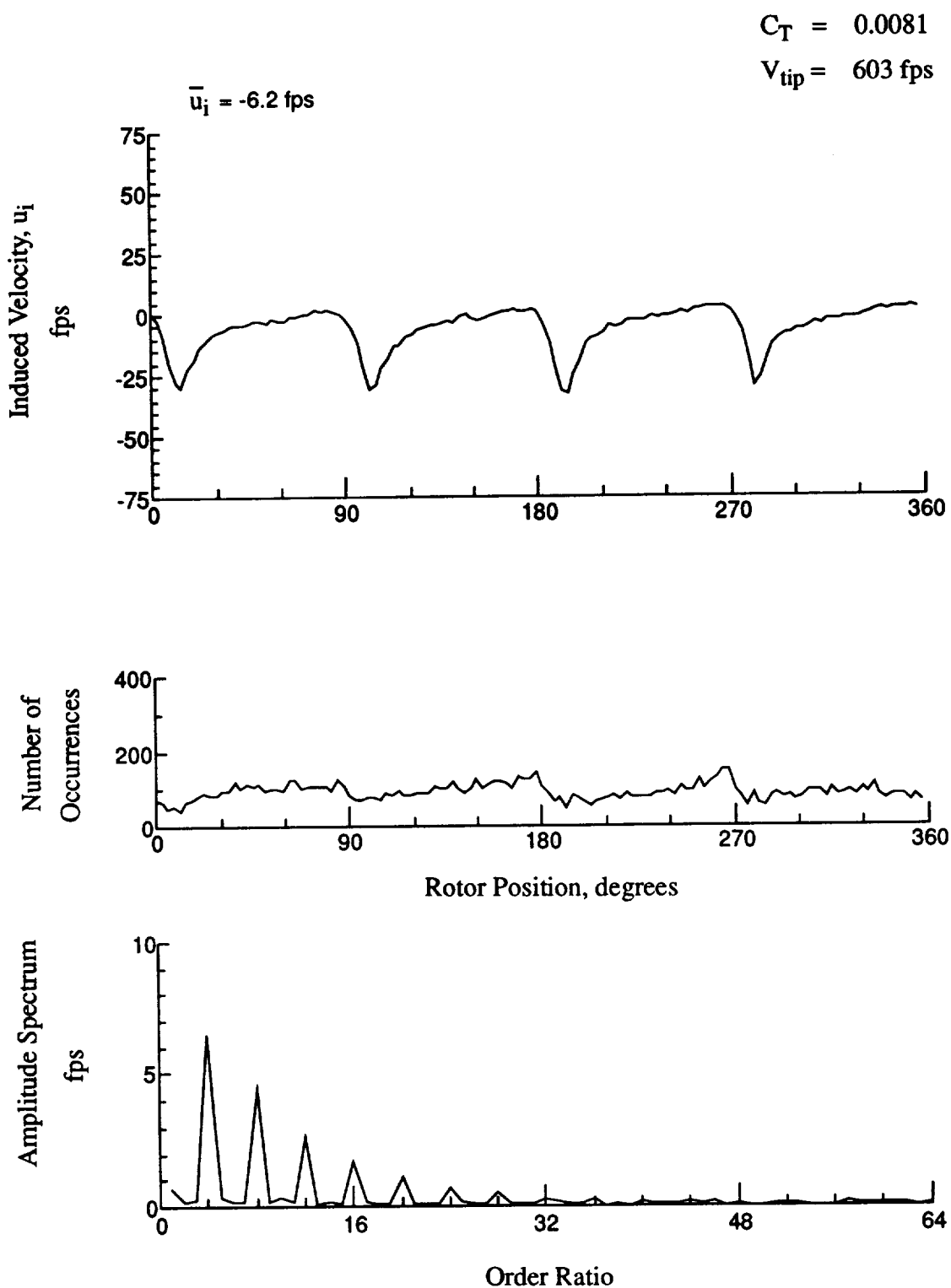


Figure 110.- Concluded.
 $x/R = 1.10$, $y/R = -0.20$, $z = 8.85 \text{ in.}$



**Figure 111.- Wake Measurements at
 $x/R = 1.10$, $y/R = -0.20$, $z = 7.82 \text{ in.}$**

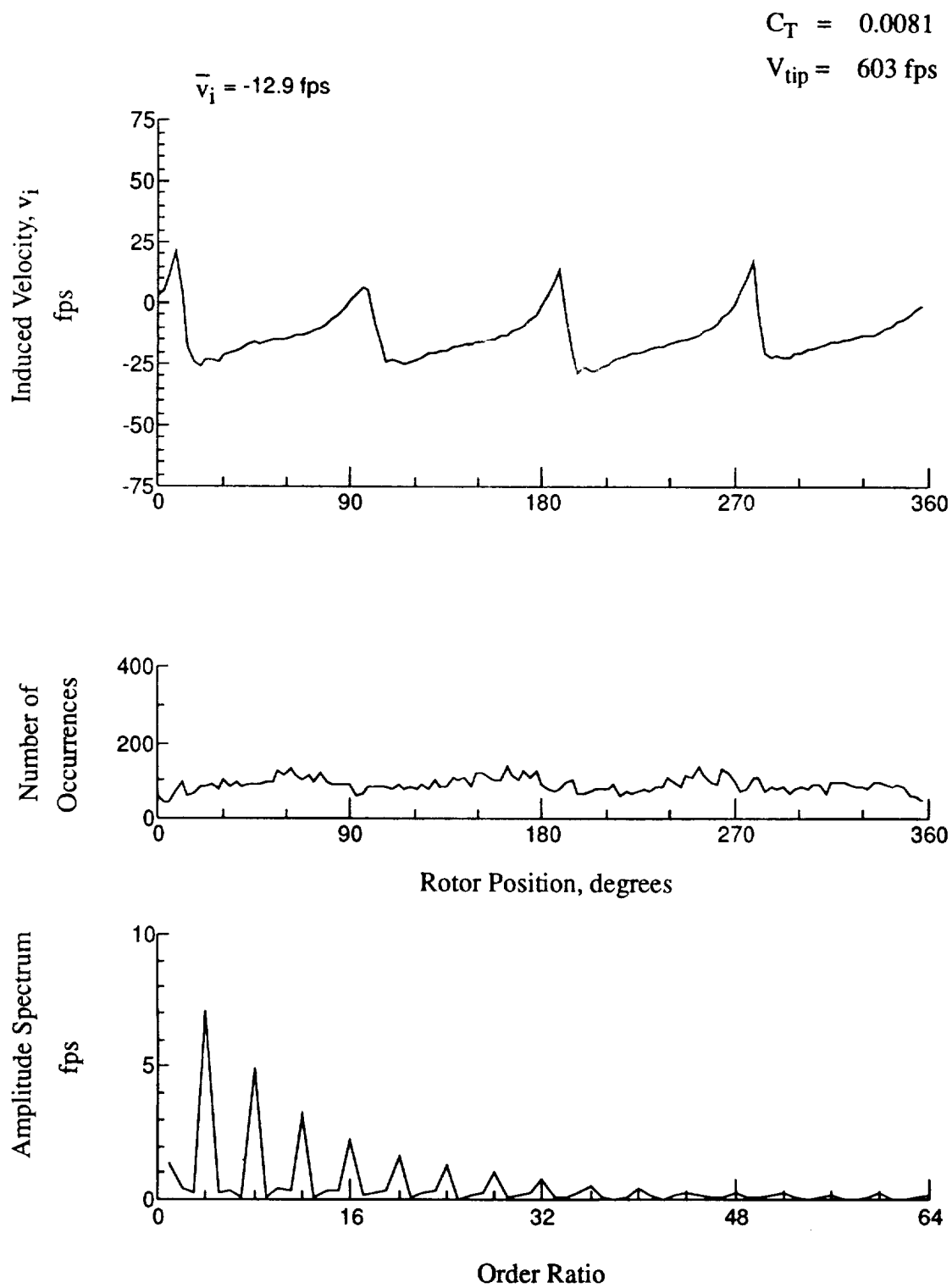


Figure 111.- Concluded.
 $x/R = 1.10$, $y/R = -0.20$, $z = 7.82 \text{ in.}$

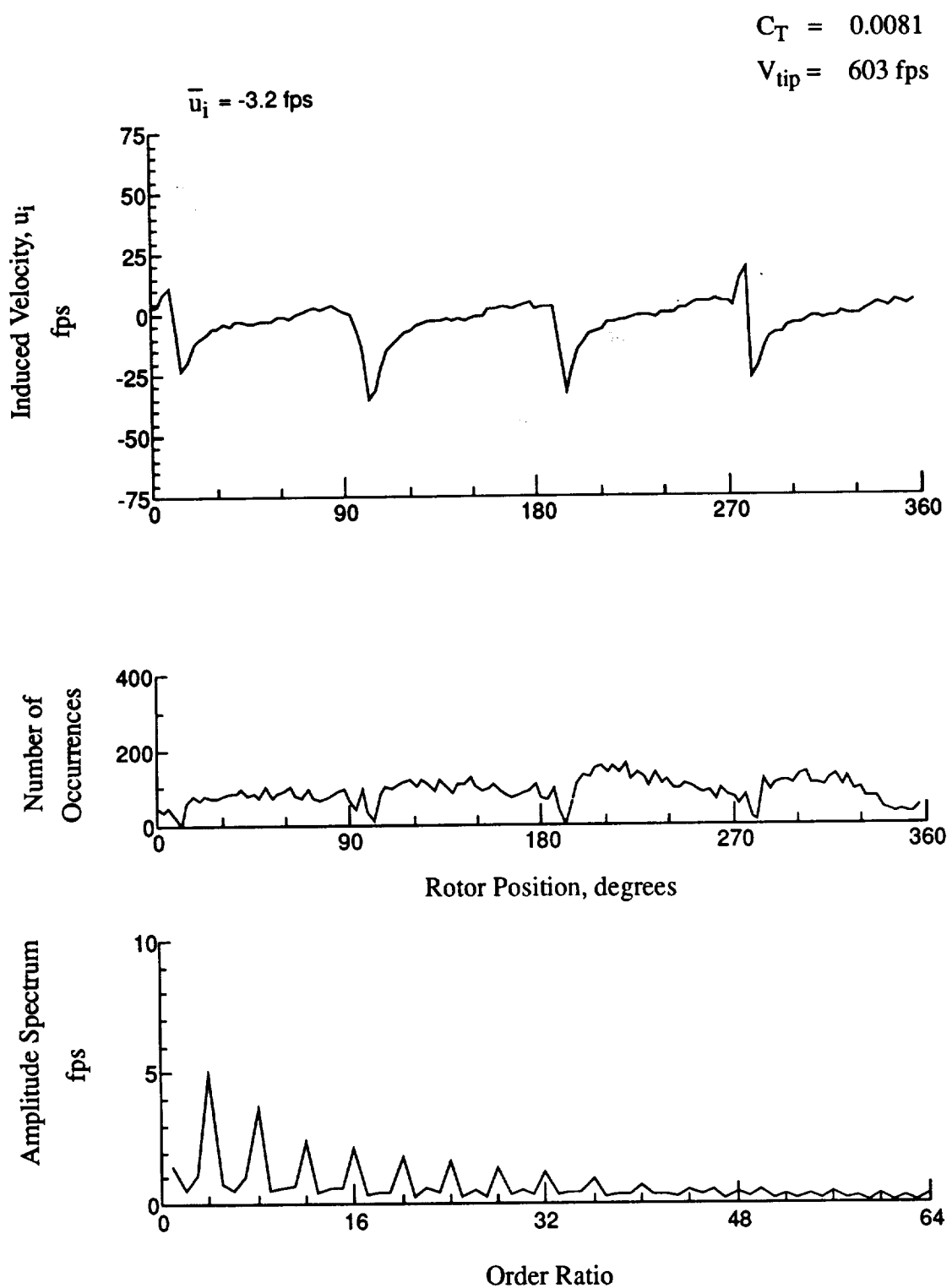


Figure 112.- Wake Measurements at
 $x/R = 1.10$, $y/R = -0.20$, $z = 6.79 \text{ in.}$

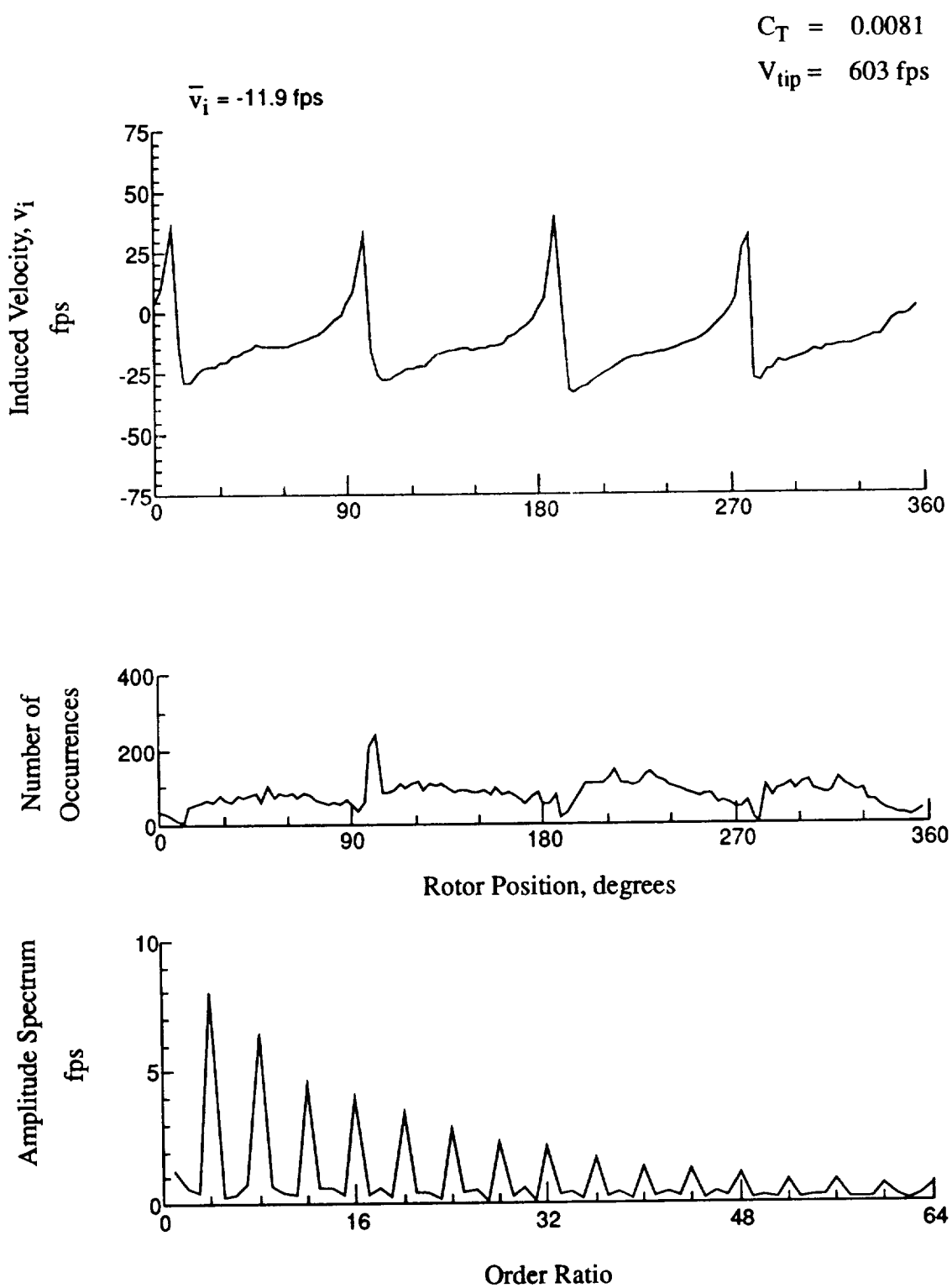
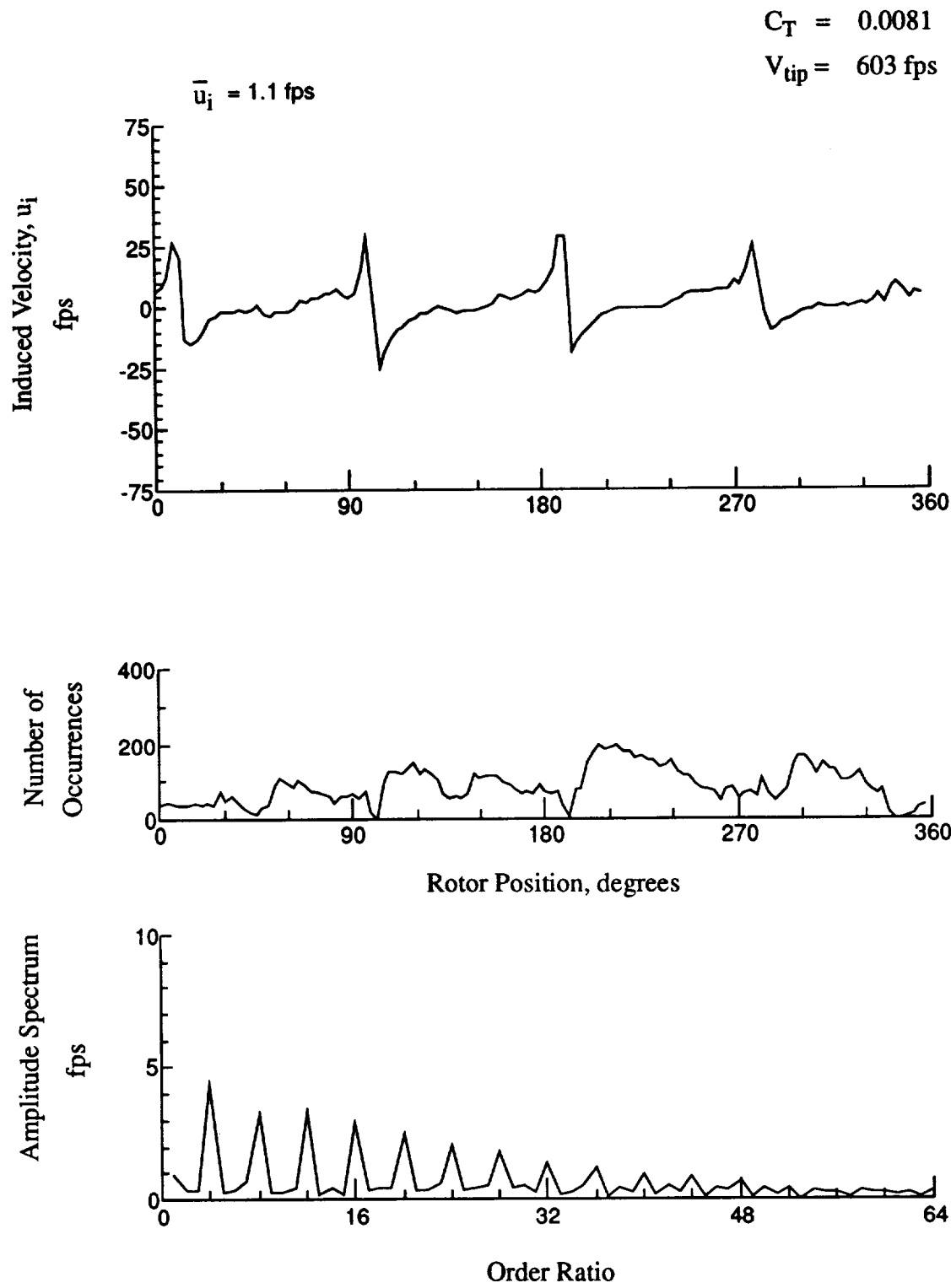


Figure 112.- Concluded.
 $x/R = 1.10$, $y/R = -0.20$, $z = 6.79 \text{ in.}$



**Figure 113.- Wake Measurements at
 $x/R = 1.10$, $y/R = -0.20$, $z = 5.76 \text{ in.}$**

$$C_T = 0.0081$$

$$V_{tip} = 603 \text{ fps}$$

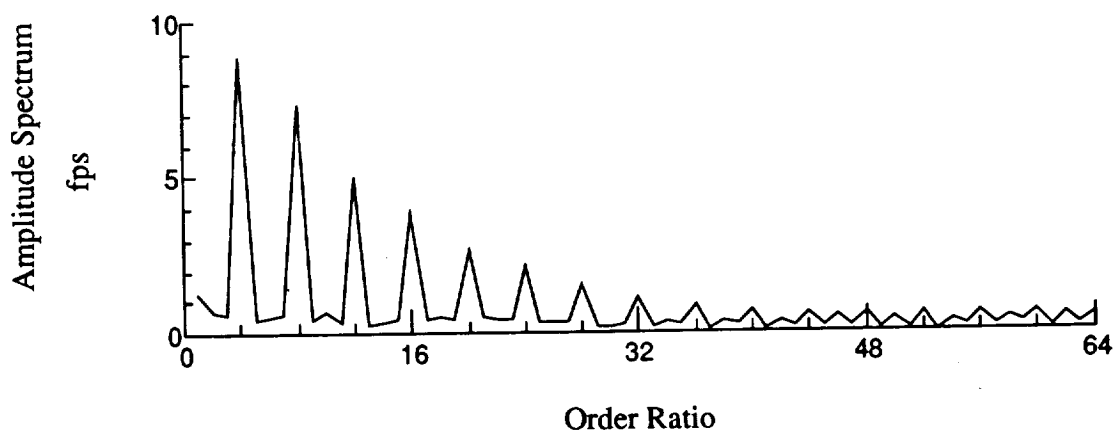
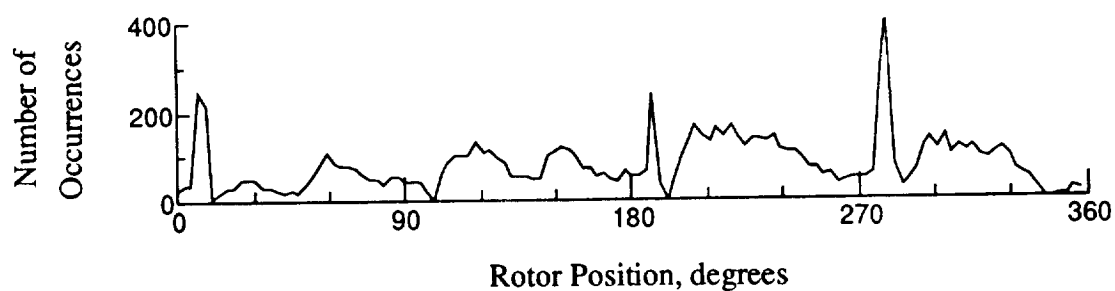
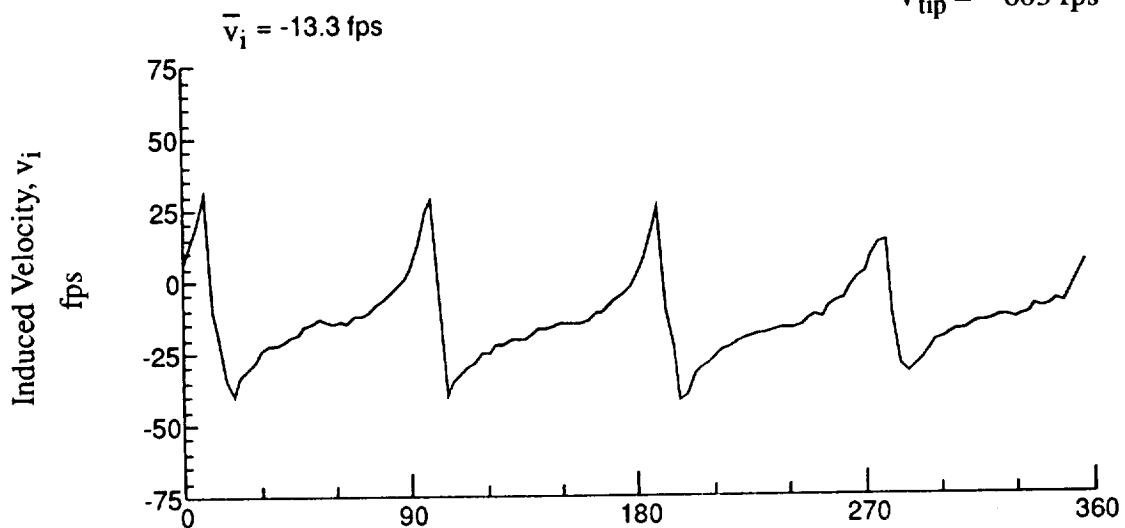


Figure 113.- Concluded.
 $x/R = 1.10$, $y/R = -0.20$, $z = 5.76 \text{ in.}$

$$C_T = 0.0081$$

$$V_{tip} = 603 \text{ fps}$$

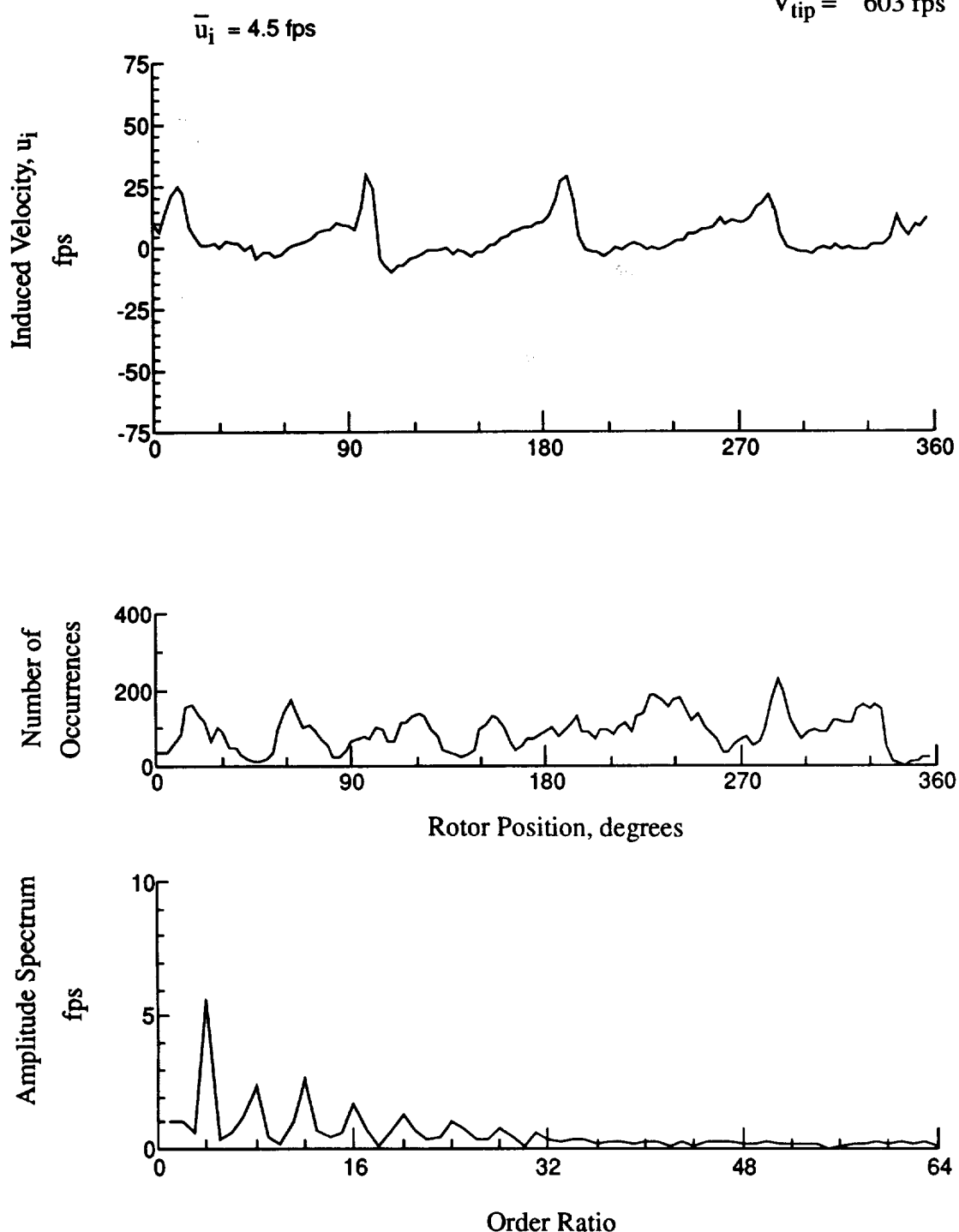


Figure 114.- Wake Measurements at
 $x/R = 1.10$, $y/R = -0.20$, $z = 4.73$ in.

$$C_T = 0.0081$$

$$V_{tip} = 603 \text{ fps}$$

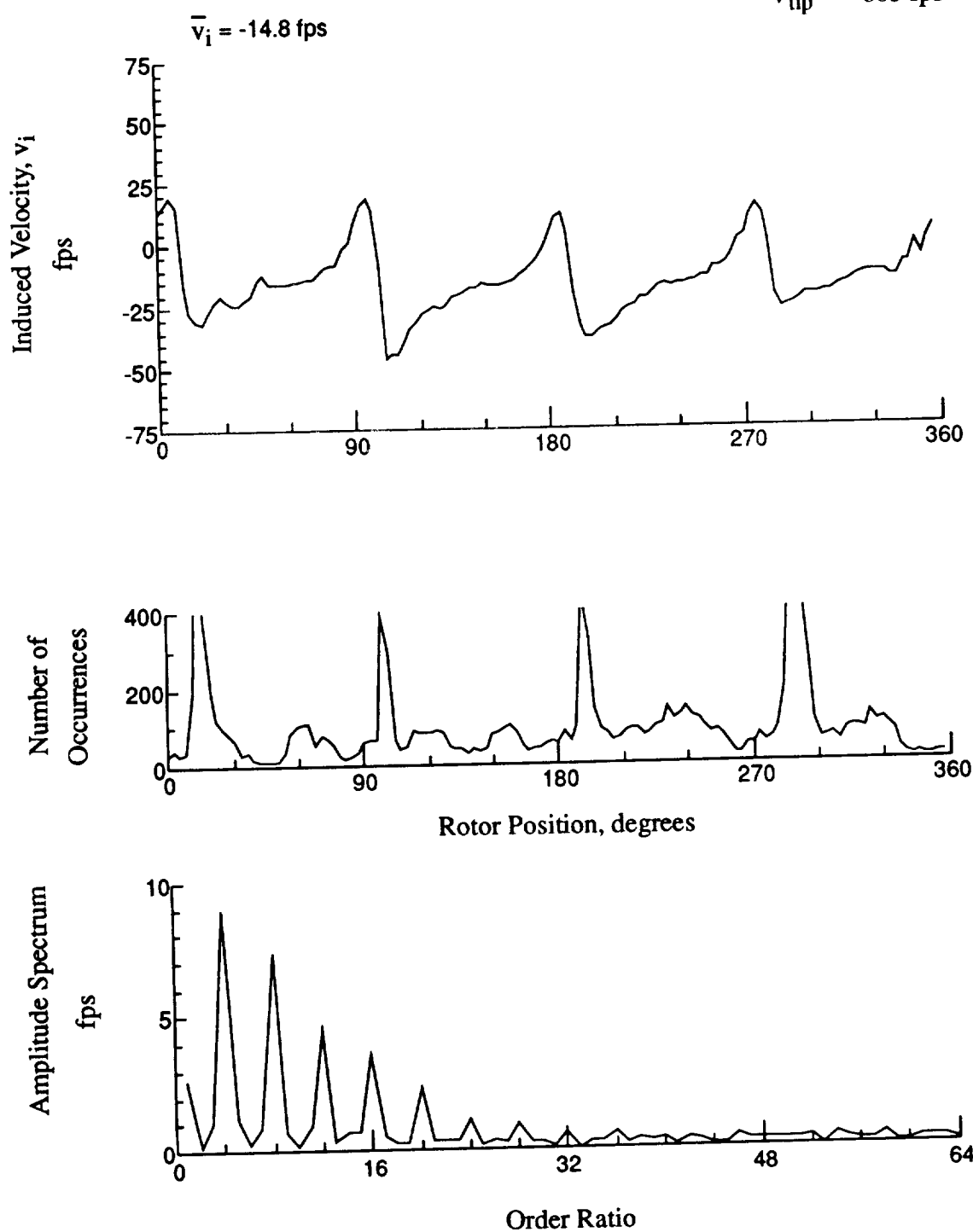
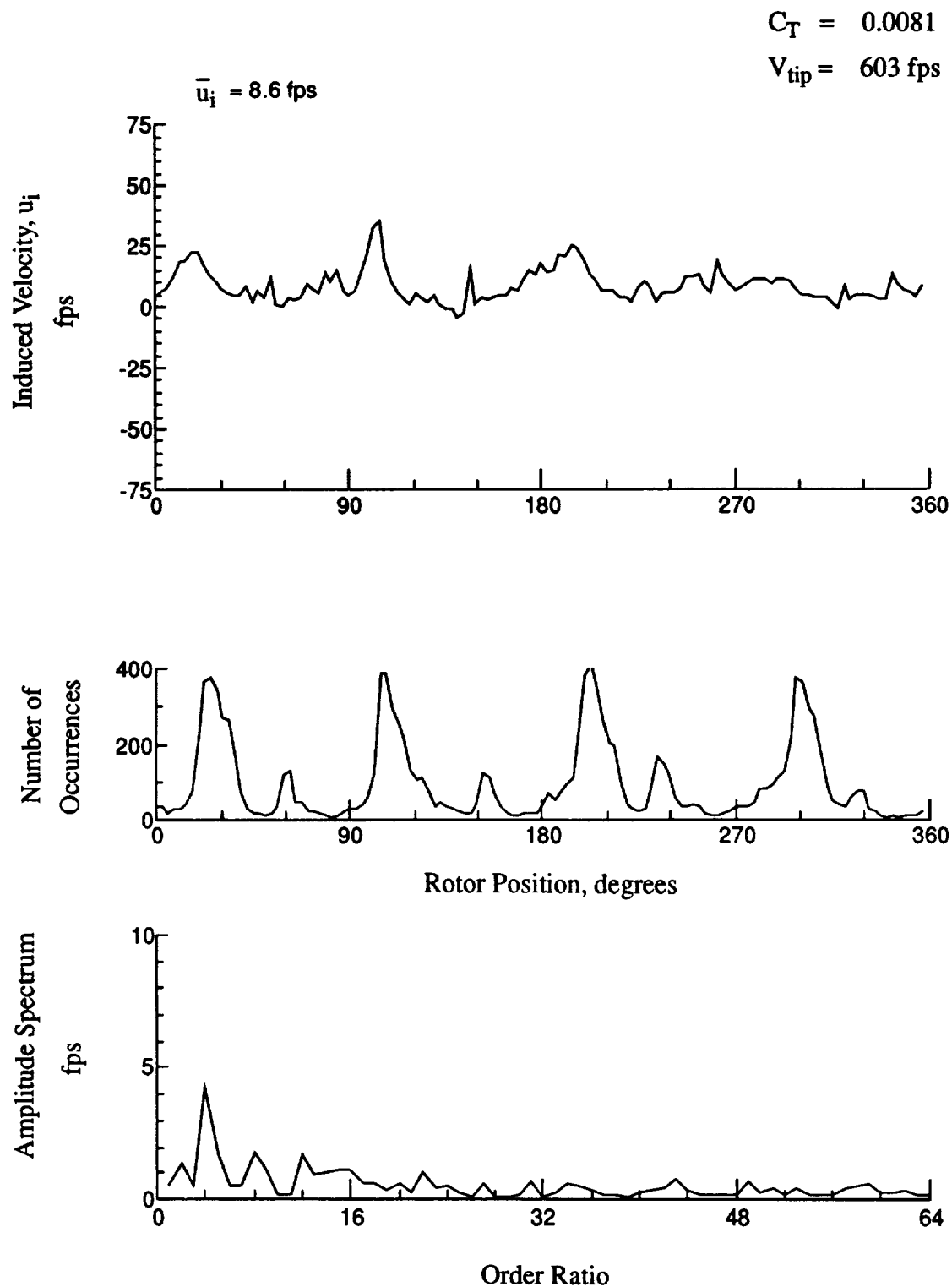


Figure 114.- Concluded.

$x/R = 1.10$, $y/R = -0.20$, $z = 4.73 \text{ in.}$



**Figure 115.- Wake Measurements at
 $x/R = 1.10$, $y/R = -0.20$, $z = 3.70 \text{ in.}$**

$$C_T = 0.0081$$

$$V_{tip} = 603 \text{ fps}$$

$$\bar{v}_i = -13.1 \text{ fps}$$

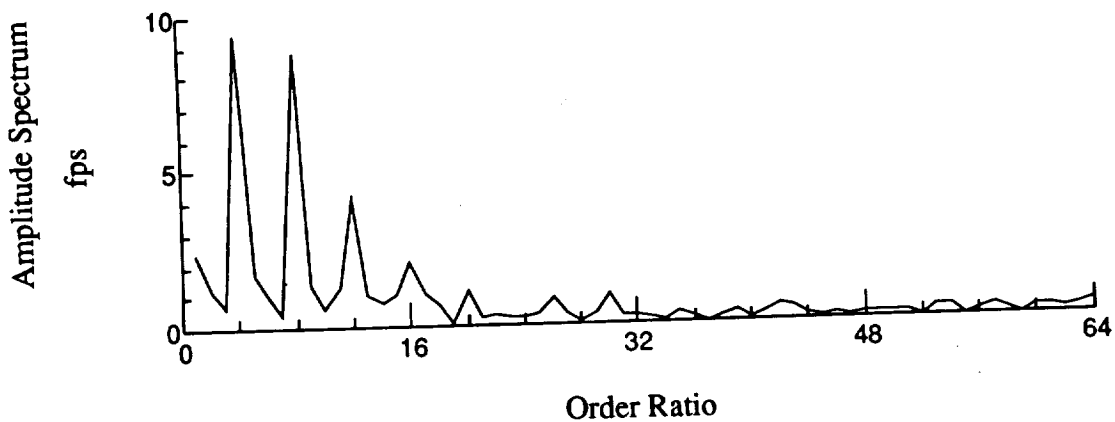
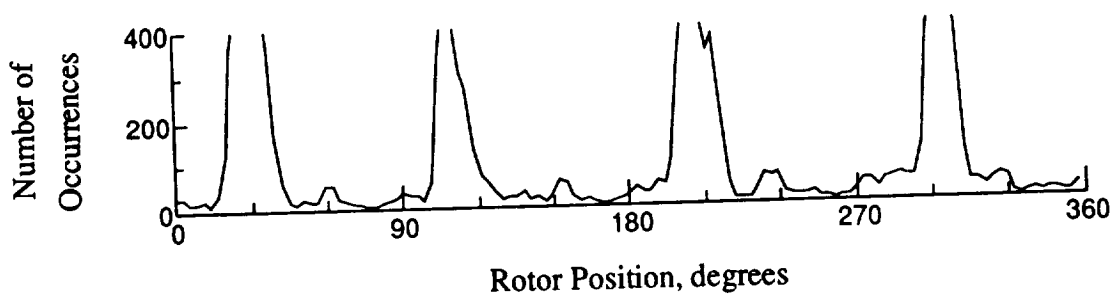
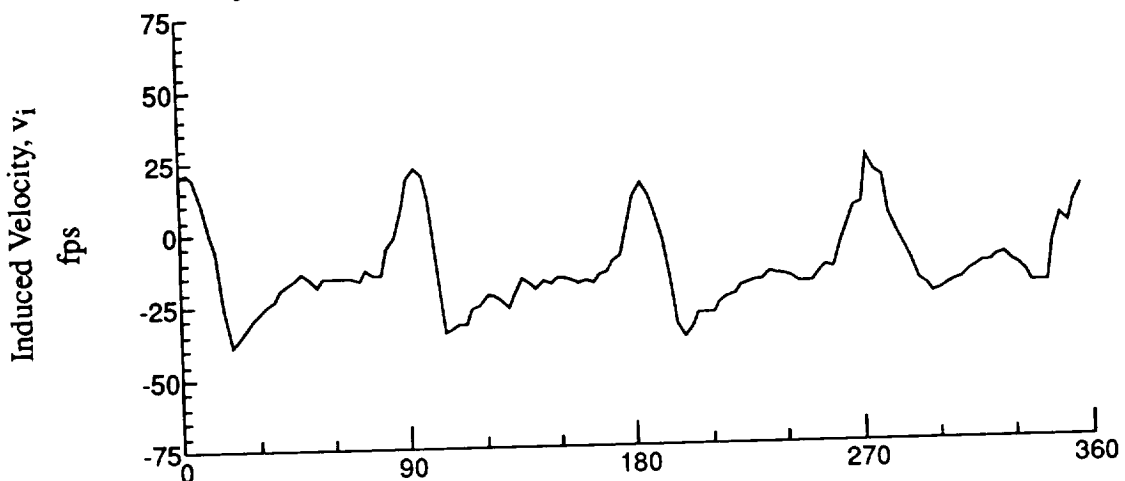


Figure 115.- Concluded.
 $x/R = 1.10$, $y/R = -0.20$, $z = 3.70 \text{ in.}$

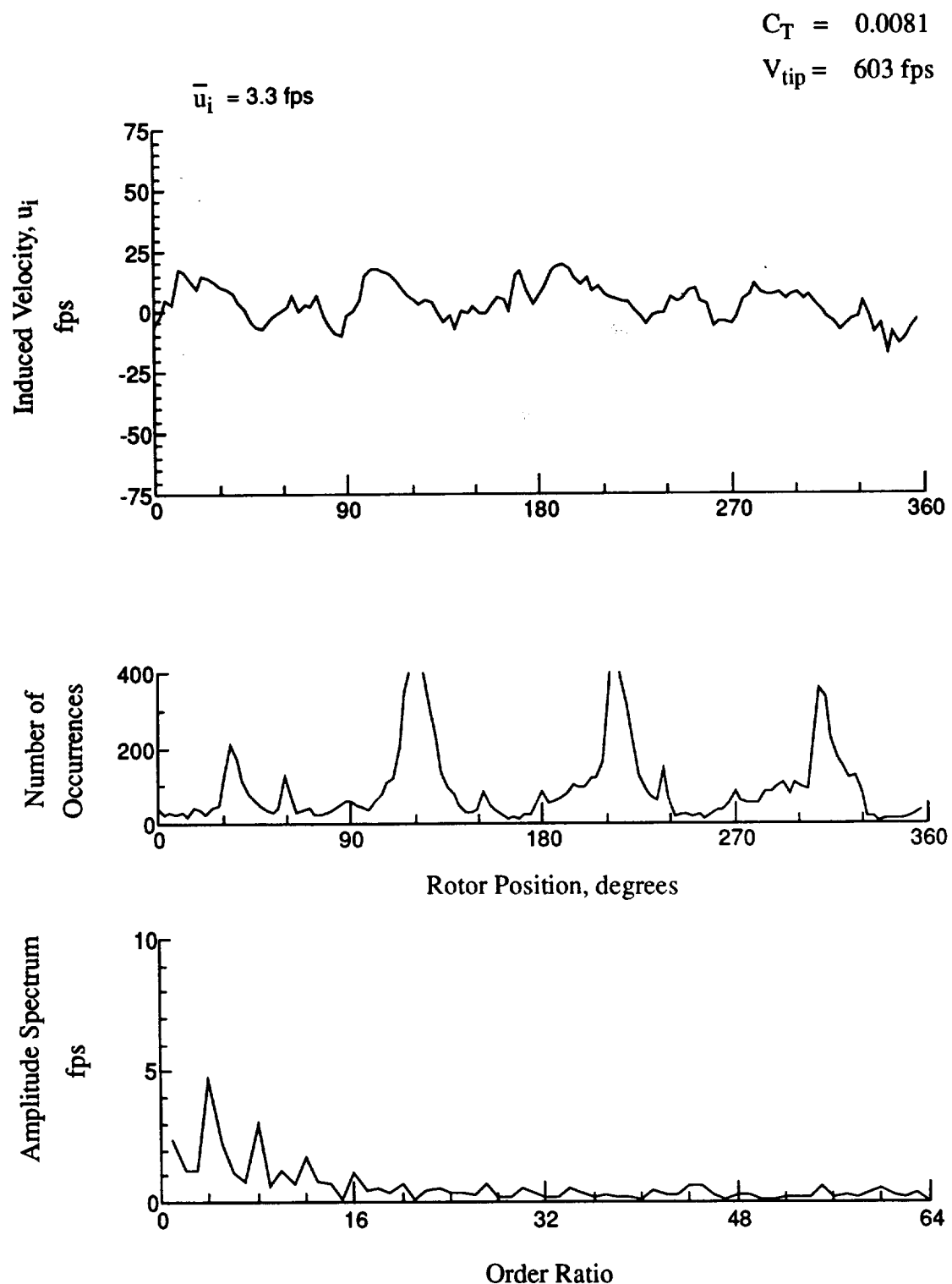


Figure 116.- Wake Measurements at
 $x/R = 1.10$, $y/R = -0.20$, $z = 2.67$ in.

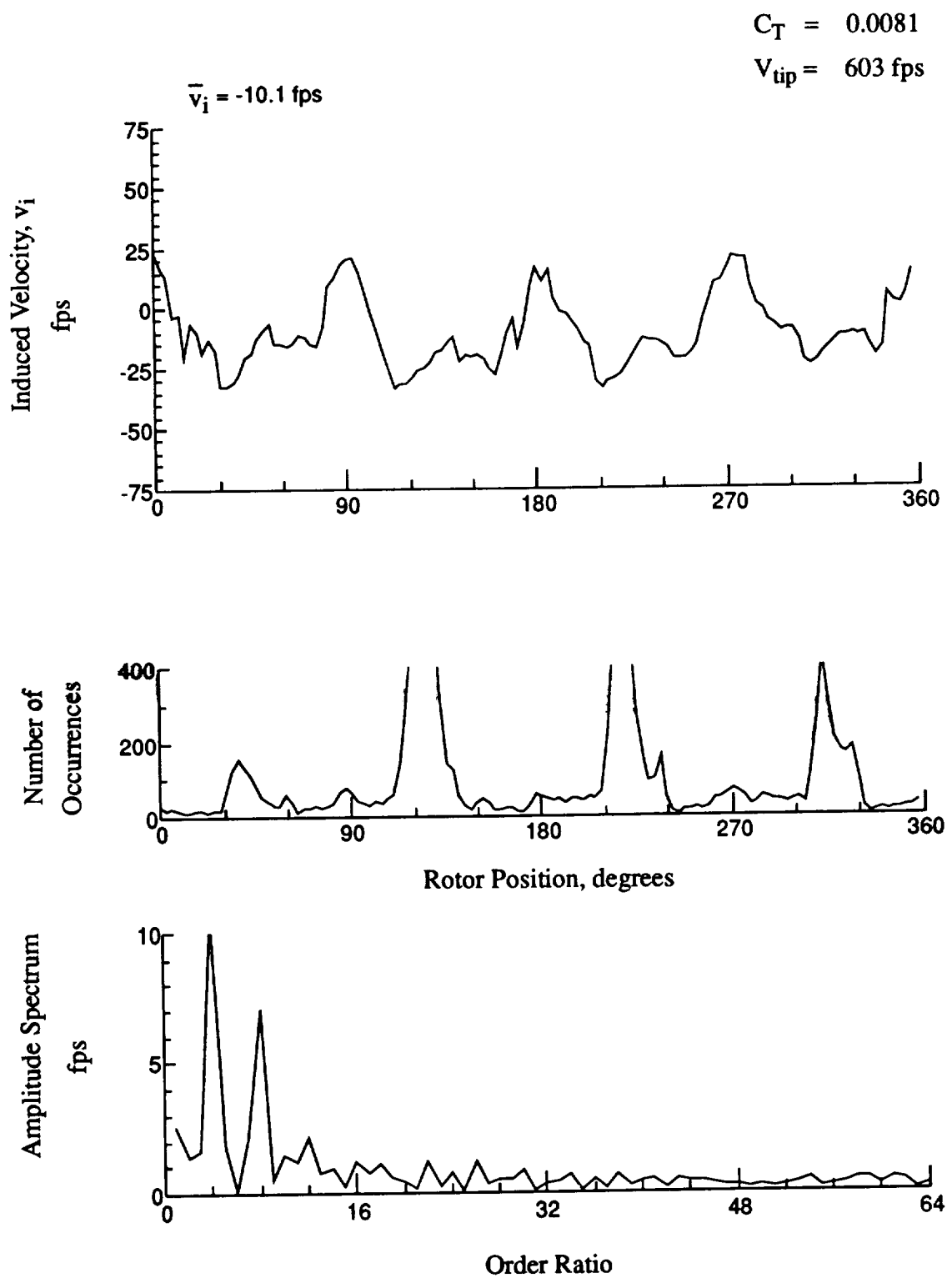
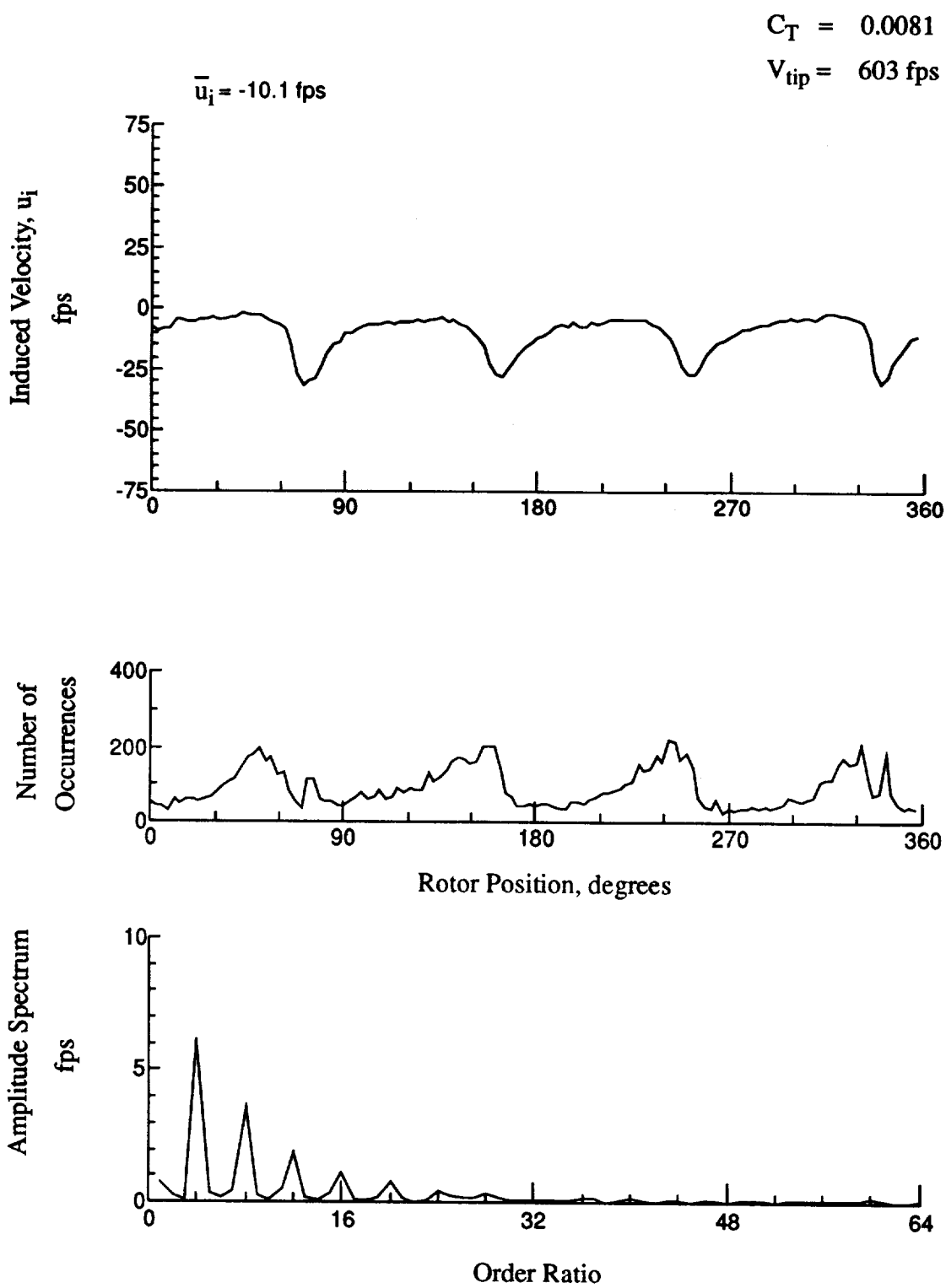


Figure 116.- Concluded.
 $x/R = 1.10$, $y/R = -0.20$, $z = 2.67 \text{ in.}$



**Figure 117.- Wake Measurements at
 $x/R = 1.50$, $y/R = -0.20$, $z = 8.37 \text{ in.}$**

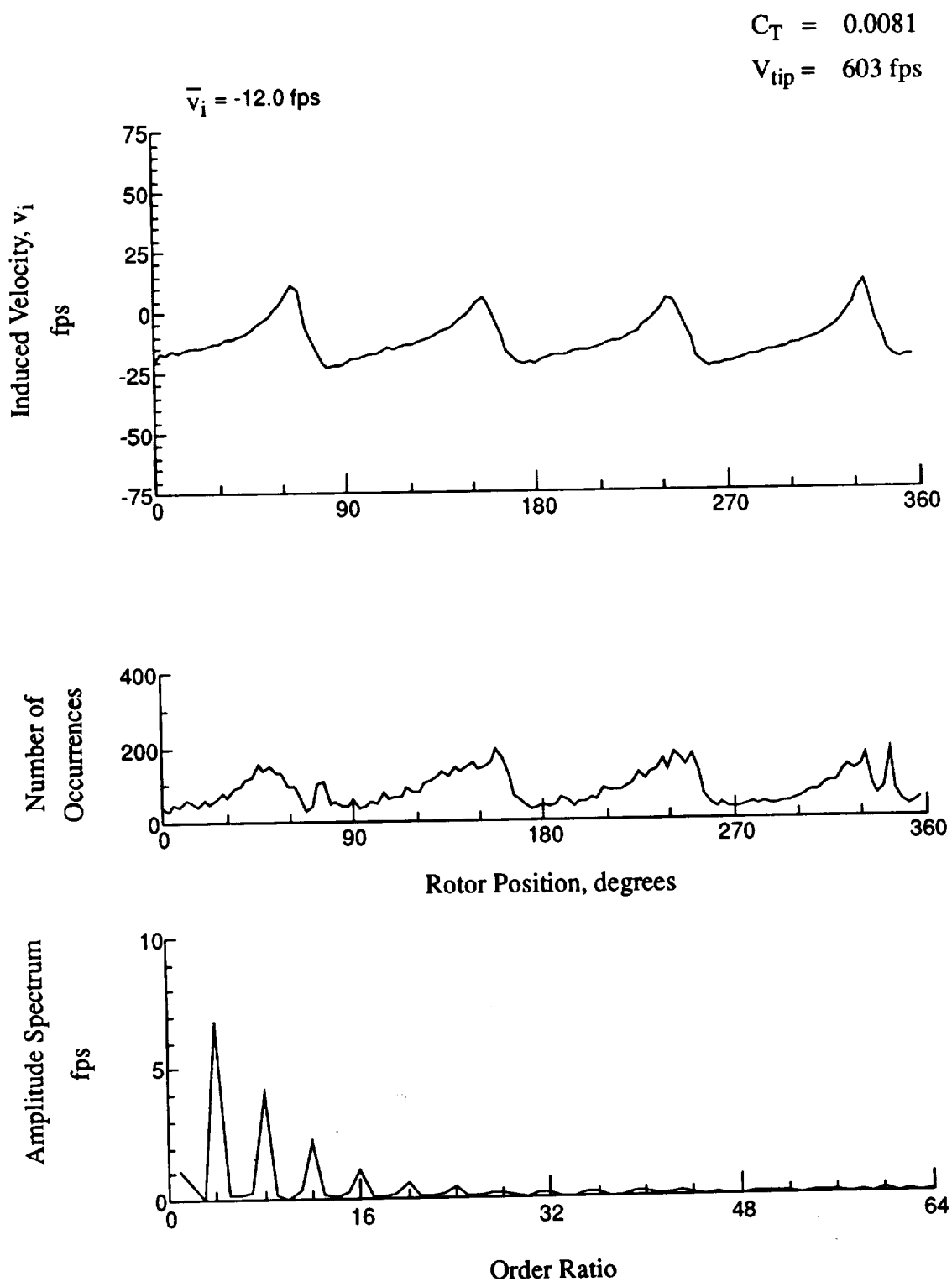


Figure 117.- Concluded.
 $x/R = 1.50$, $y/R = -0.20$, $z = 8.37 \text{ in.}$

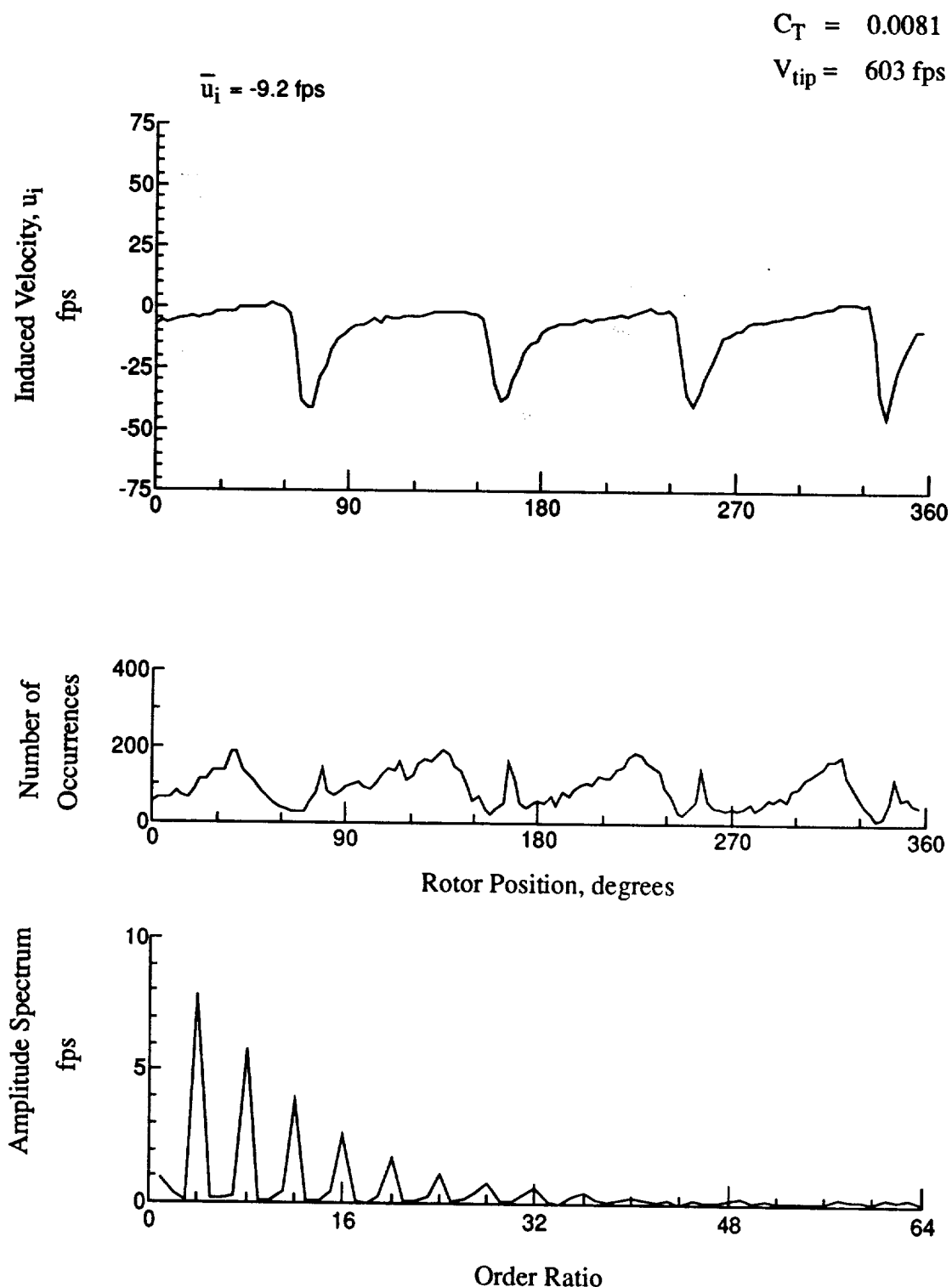


Figure 118.- Wake Measurements at
 $x/R = 1.50$, $y/R = -0.20$, $z = 7.34 \text{ in.}$

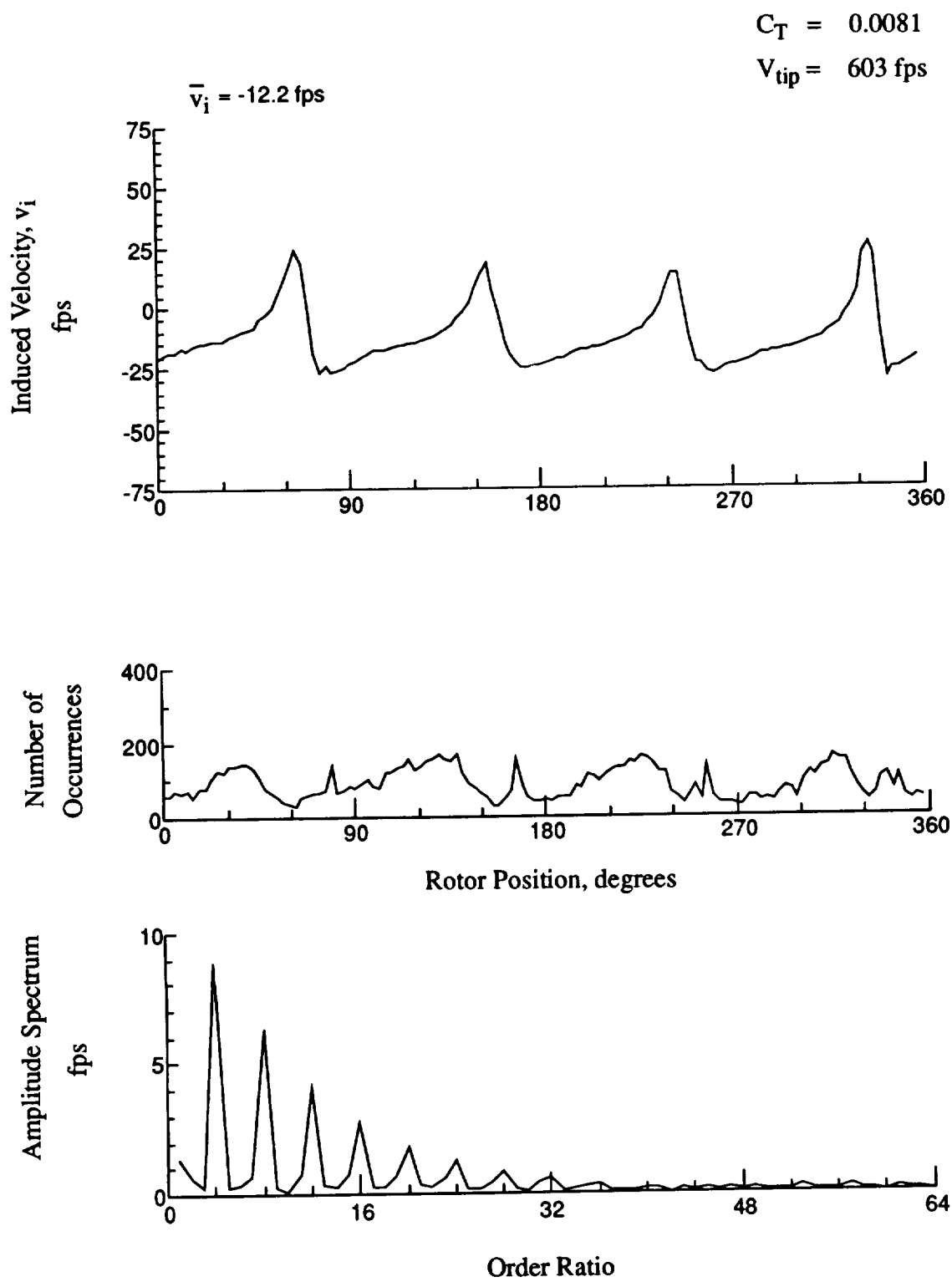


Figure 118.- Concluded.
 $x/R = 1.50$, $y/R = -0.20$, $z = 7.34 \text{ in.}$

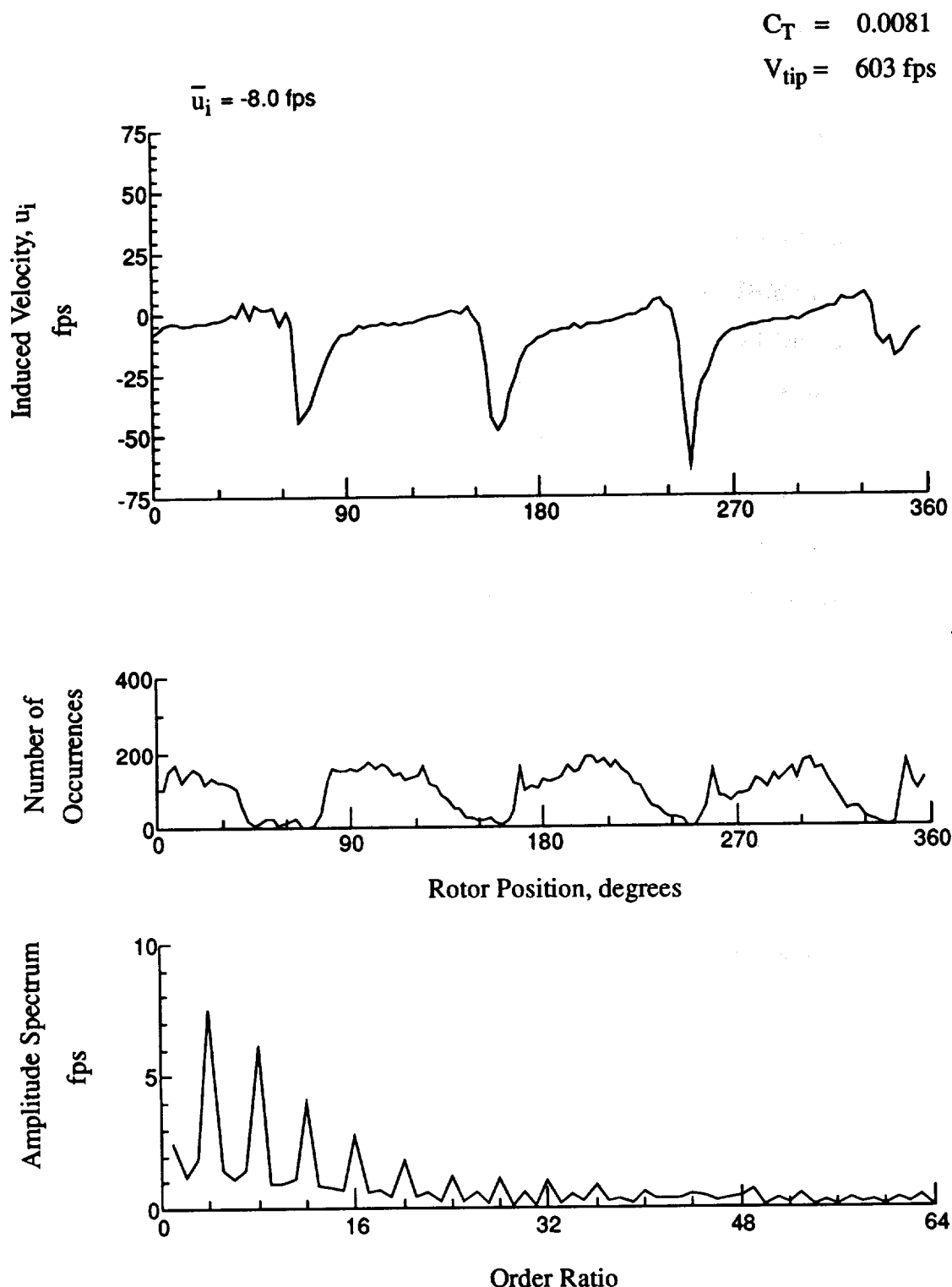


Figure 119.- Wake Measurements at
 $x/R = 1.50$, $y/R = -0.20$, $z = 6.31$ in.

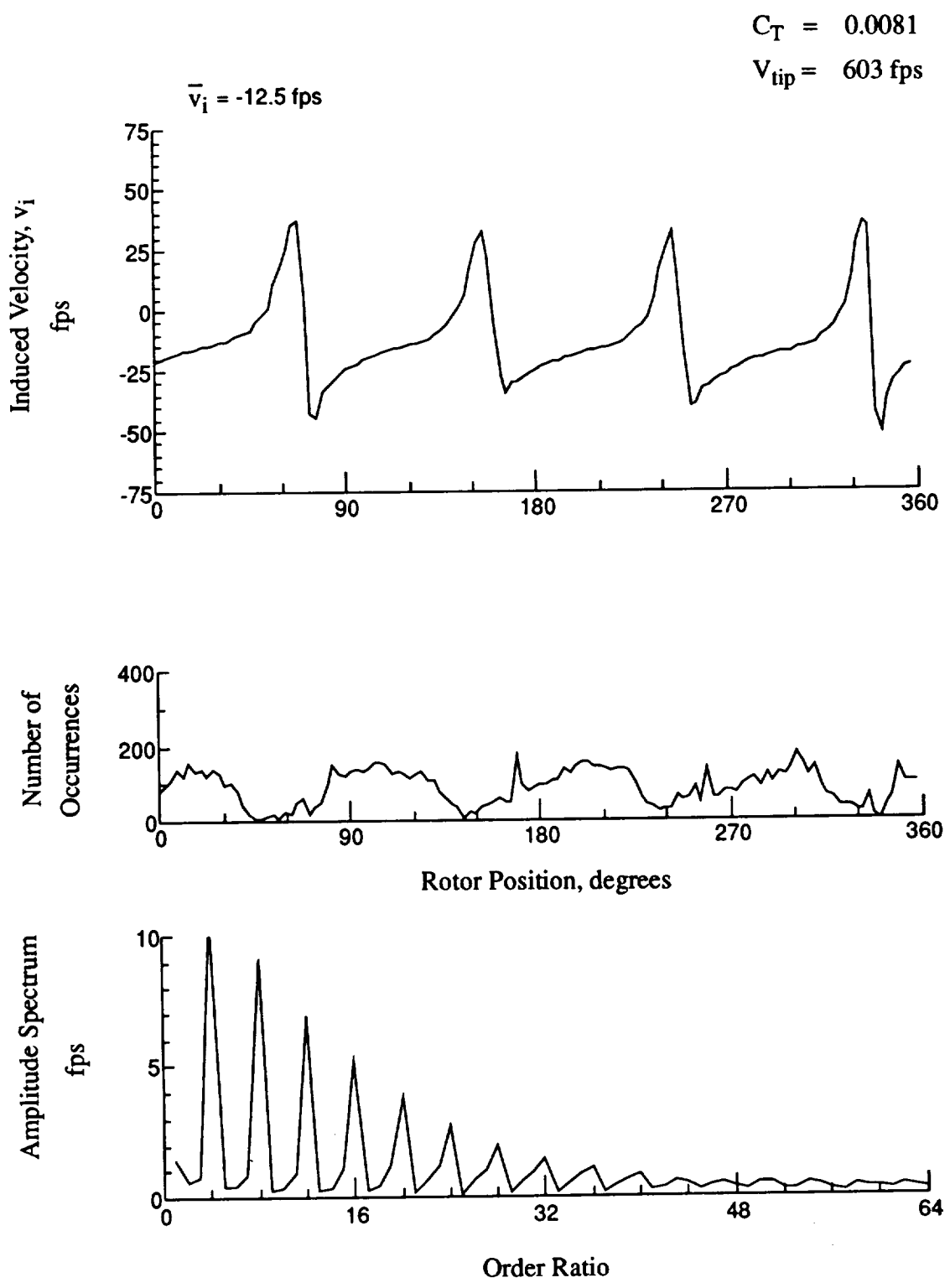


Figure 119.- Concluded.
 $x/R = 1.50$, $y/R = -0.20$, $z = 6.31 \text{ in.}$

$$C_T = 0.0081$$

$$V_{tip} = 603 \text{ fps}$$

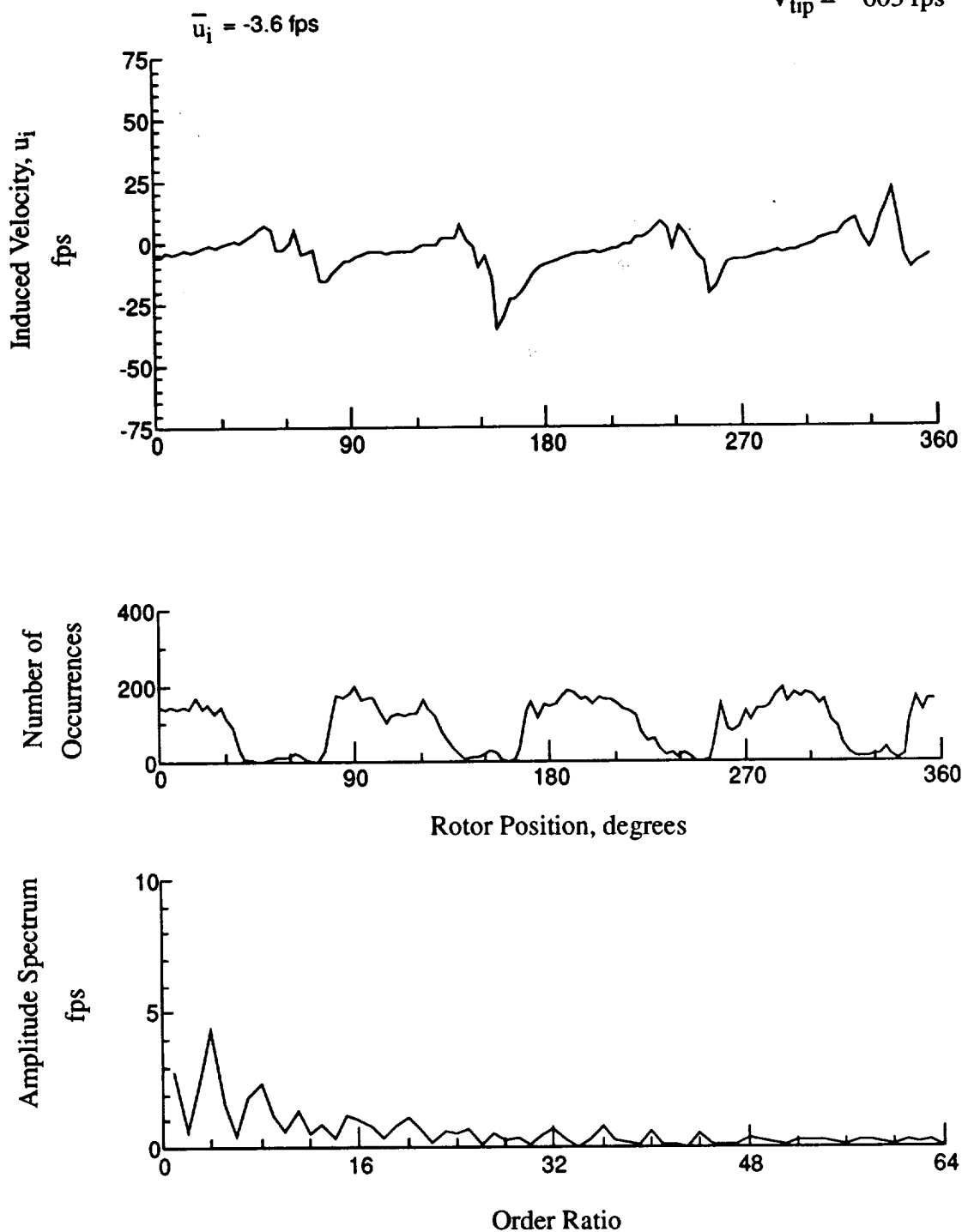


Figure 120.- Wake Measurements at
 $x/R = 1.50$, $y/R = -0.20$, $z = 5.28 \text{ in.}$

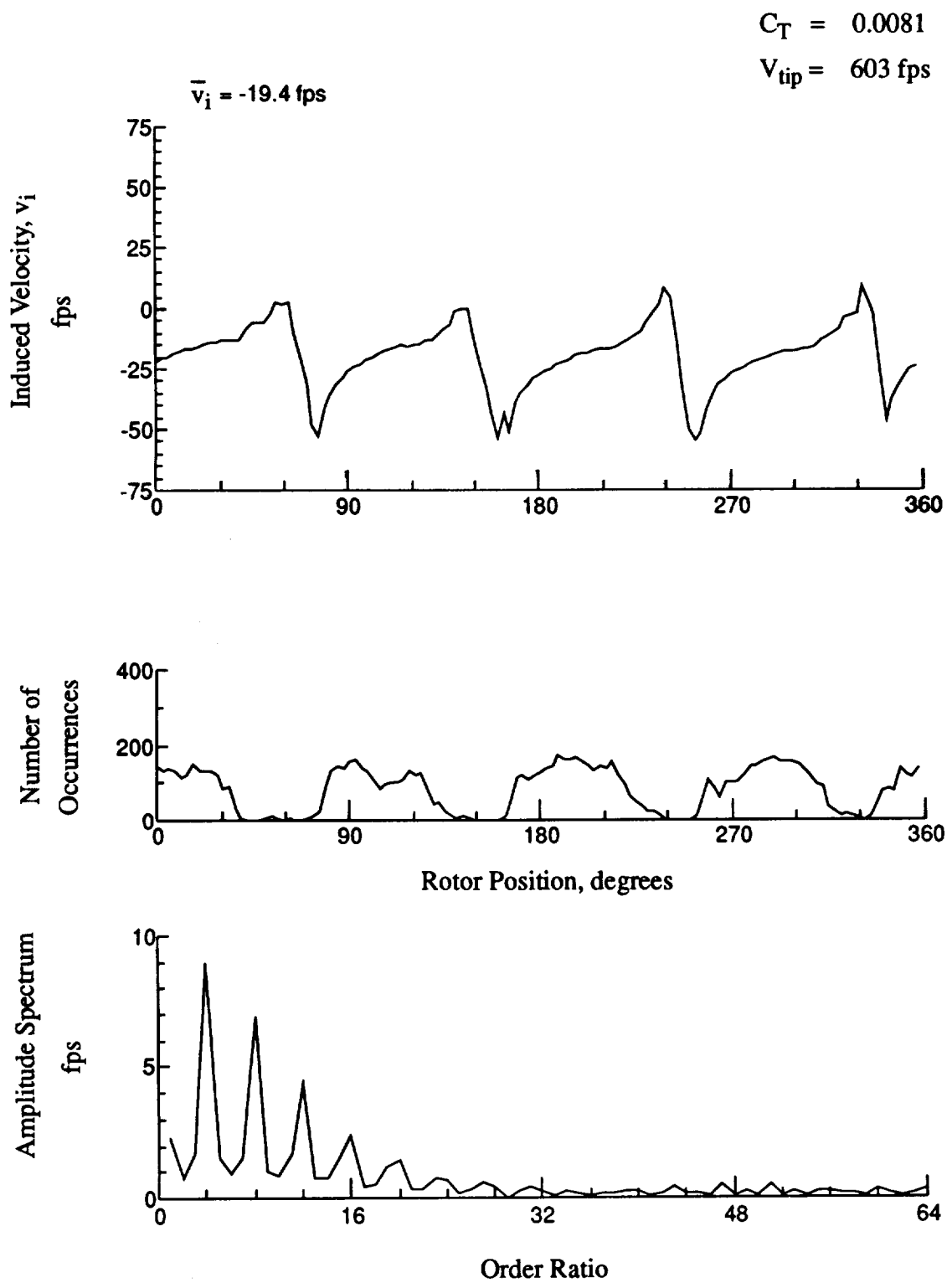


Figure 120.- Concluded.
 $x/R = 1.50$, $y/R = -0.20$, $z = 5.28 \text{ in.}$

$$C_T = 0.0081$$

$$V_{tip} = 603 \text{ fps}$$

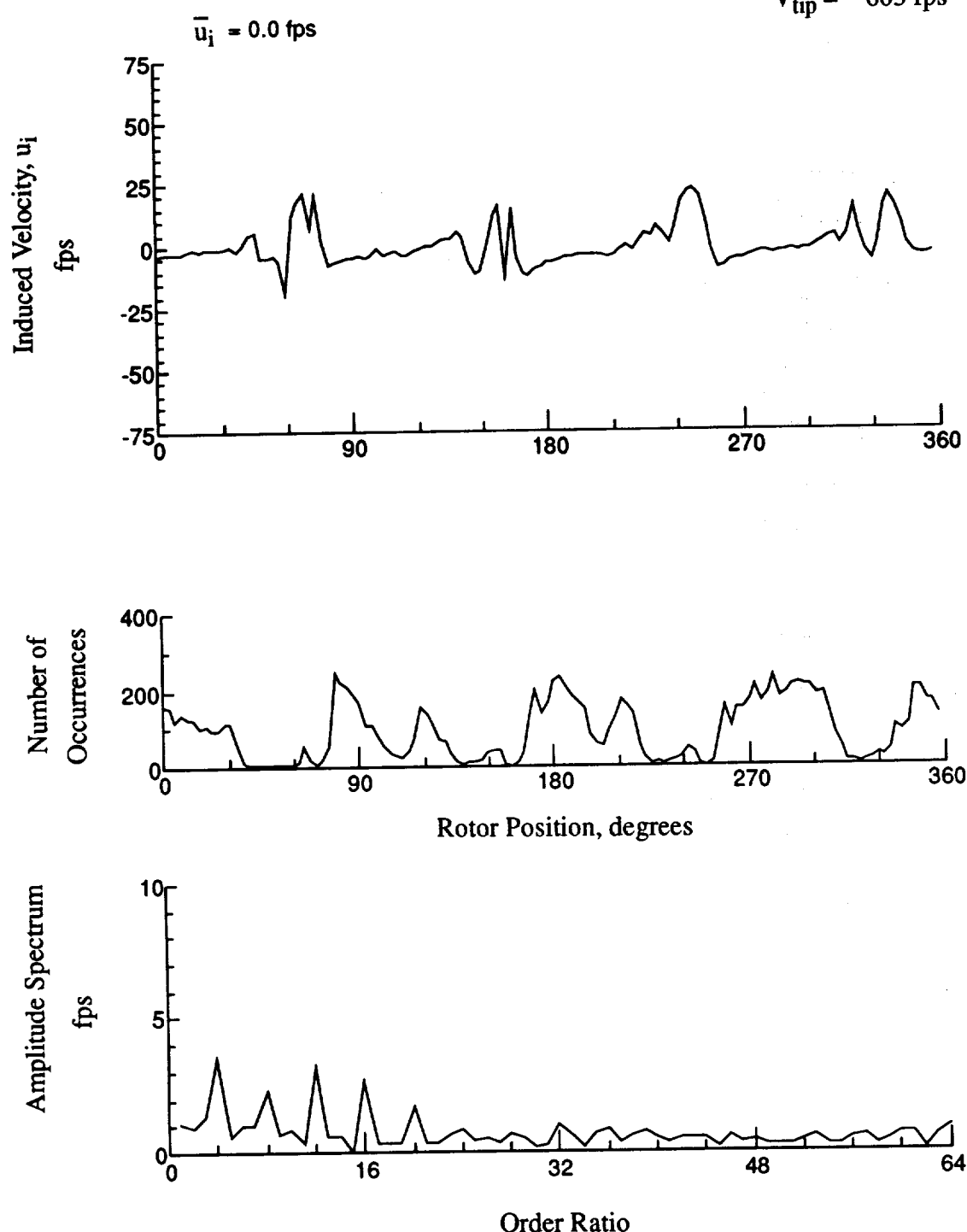


Figure 121.- Wake Measurements at
 $x/R = 1.50$, $y/R = -0.20$, $z = 4.25$ in.

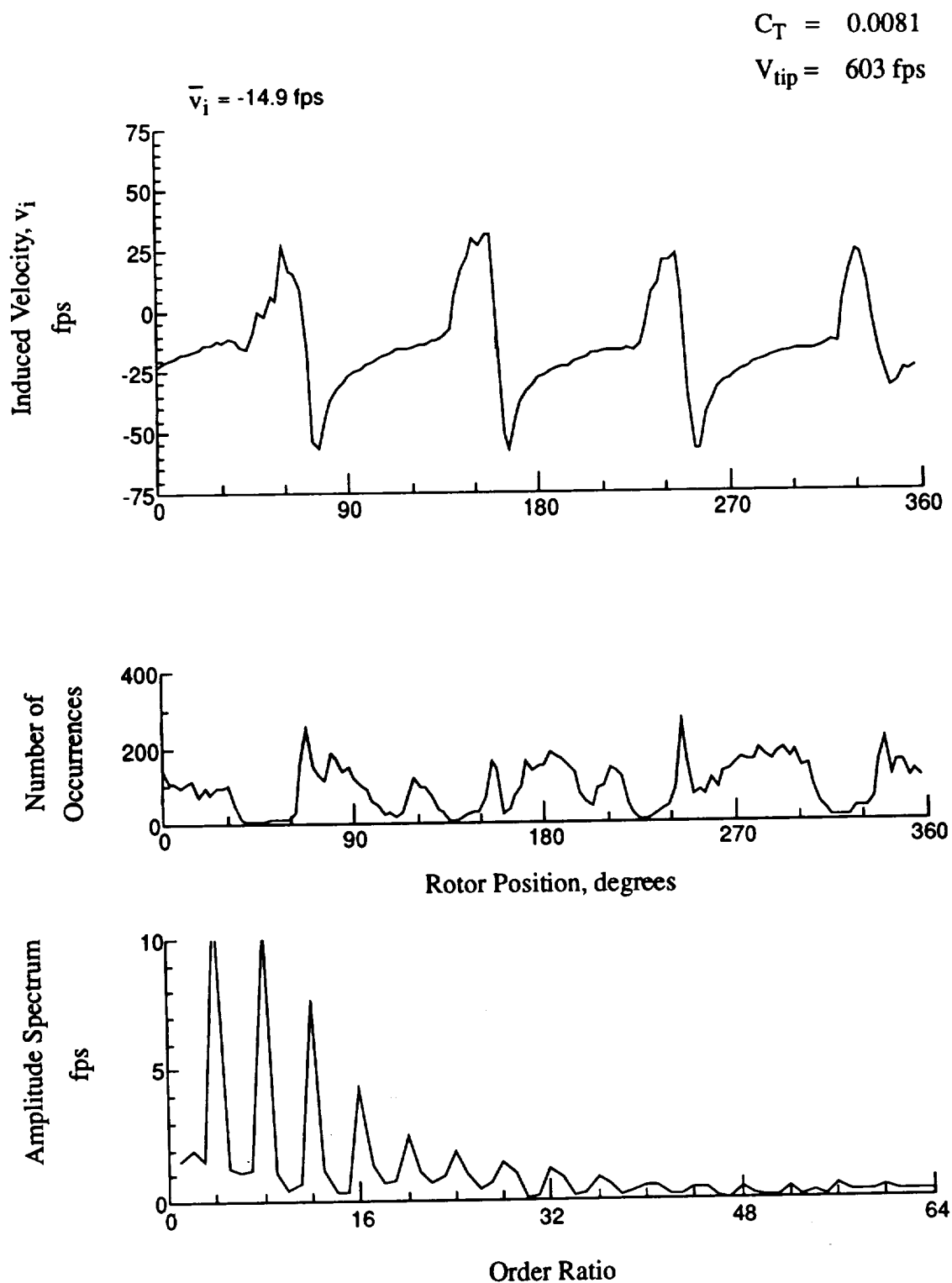


Figure 121.- Concluded.
 $x/R = 1.50$, $y/R = -0.20$, $z = 4.25 \text{ in.}$

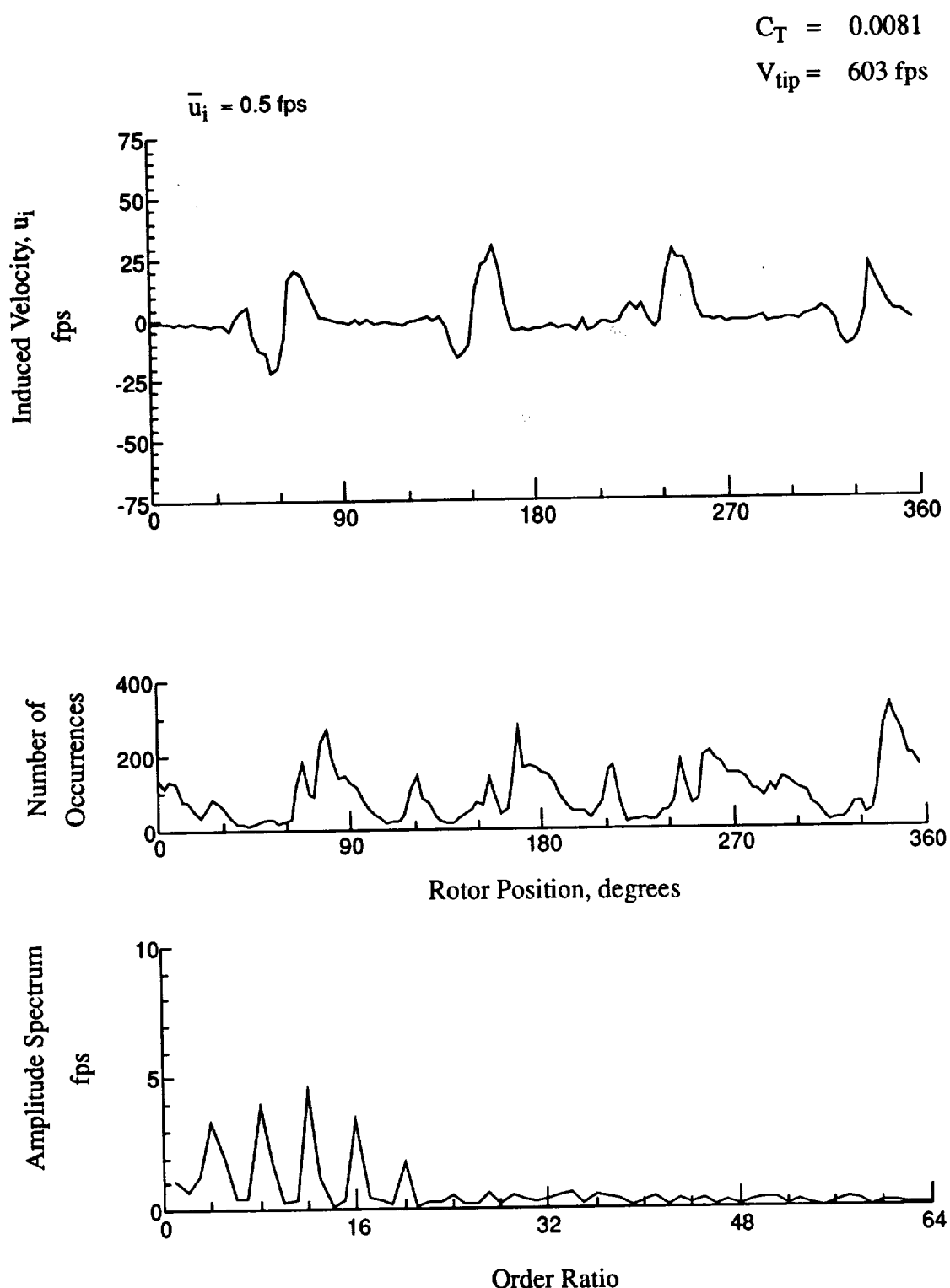


Figure 122.- Wake Measurements at
 $x/R = 1.50$, $y/R = -0.20$, $z = 3.22 \text{ in.}$

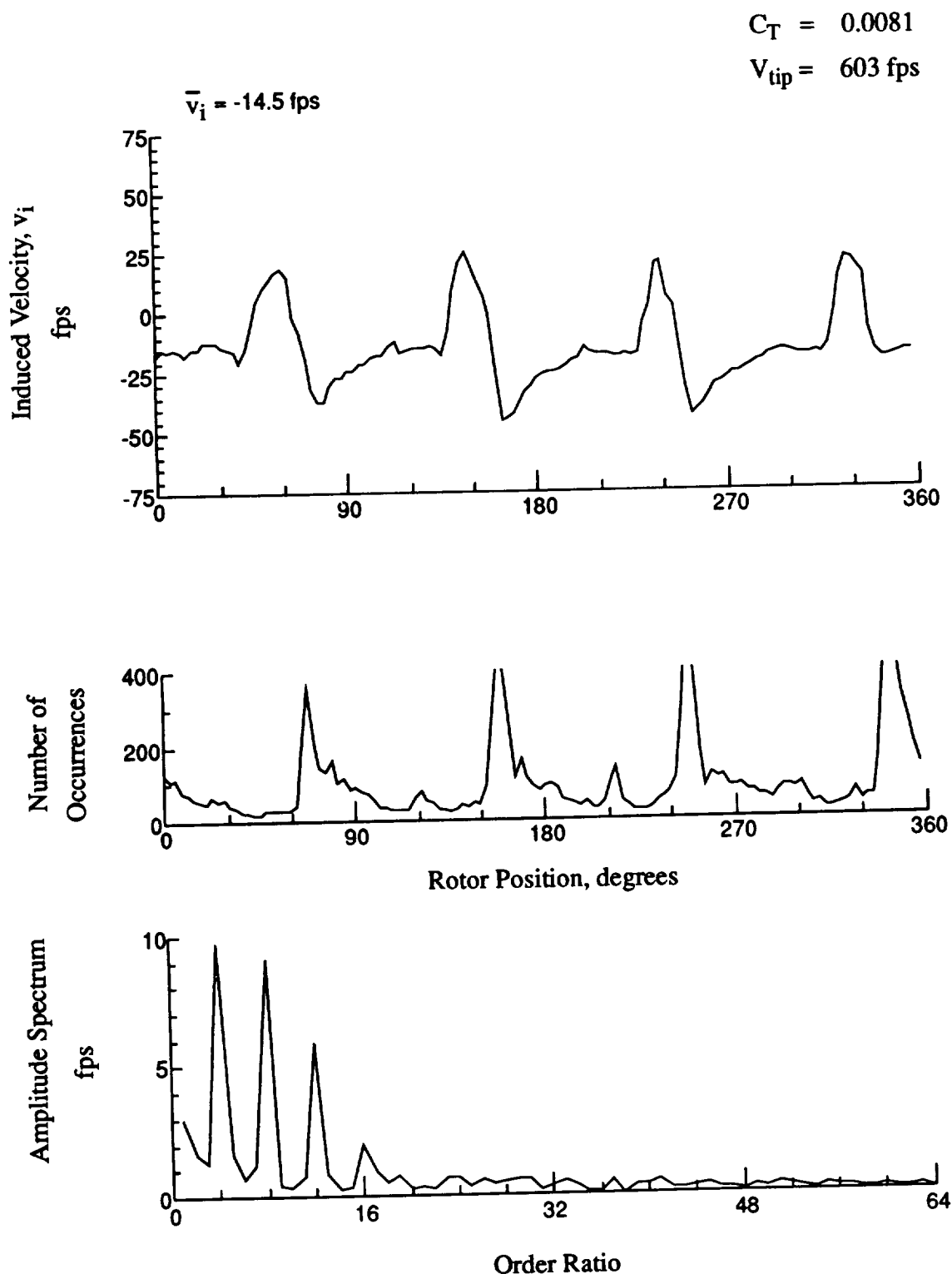


Figure 122.- Concluded.
 $x/R = 1.50$, $y/R = -0.20$, $z = 3.22 \text{ in.}$

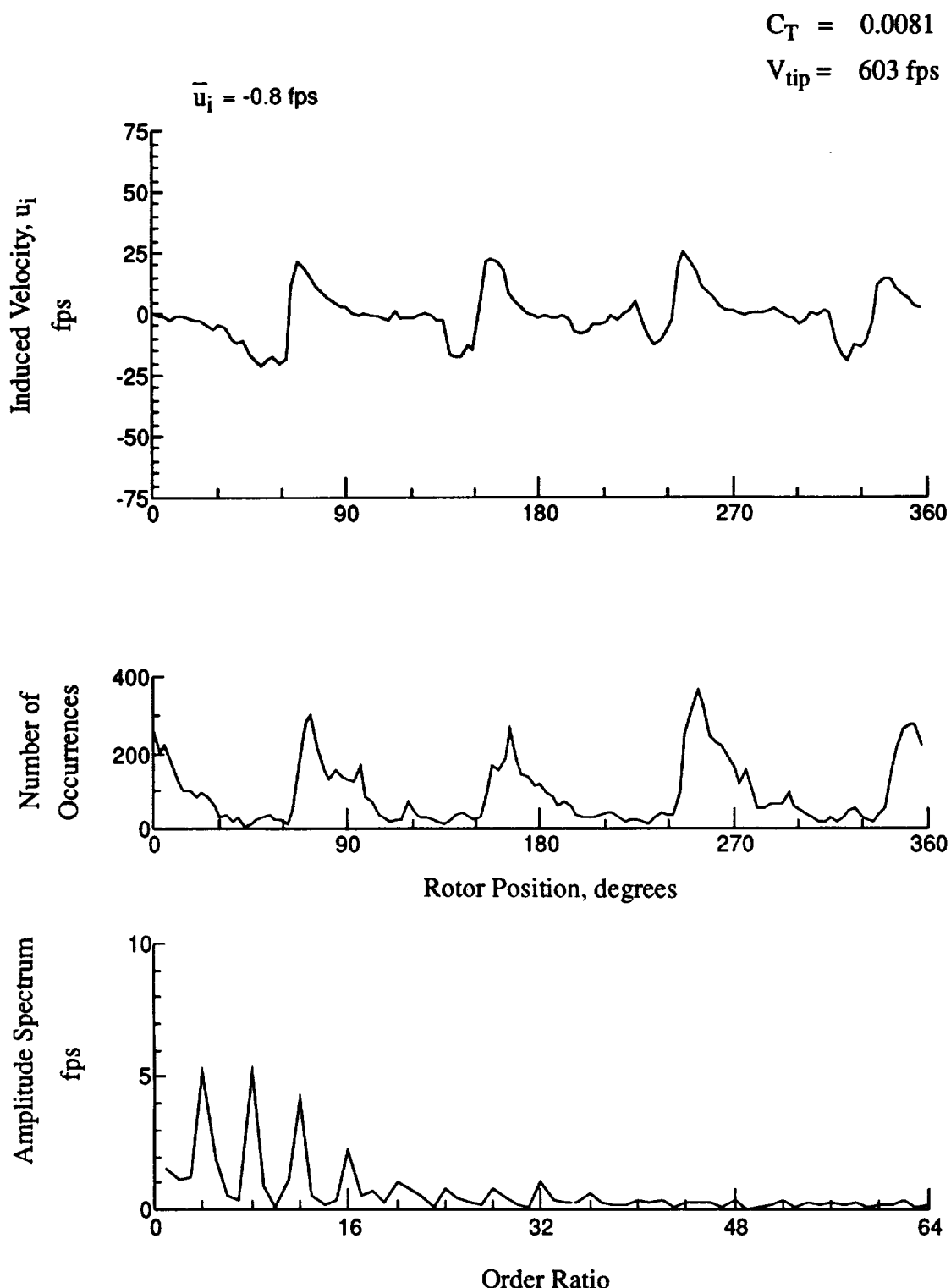


Figure 123.- Wake Measurements at
 $x/R = 1.50$, $y/R = -0.20$, $z = 2.19$ in.

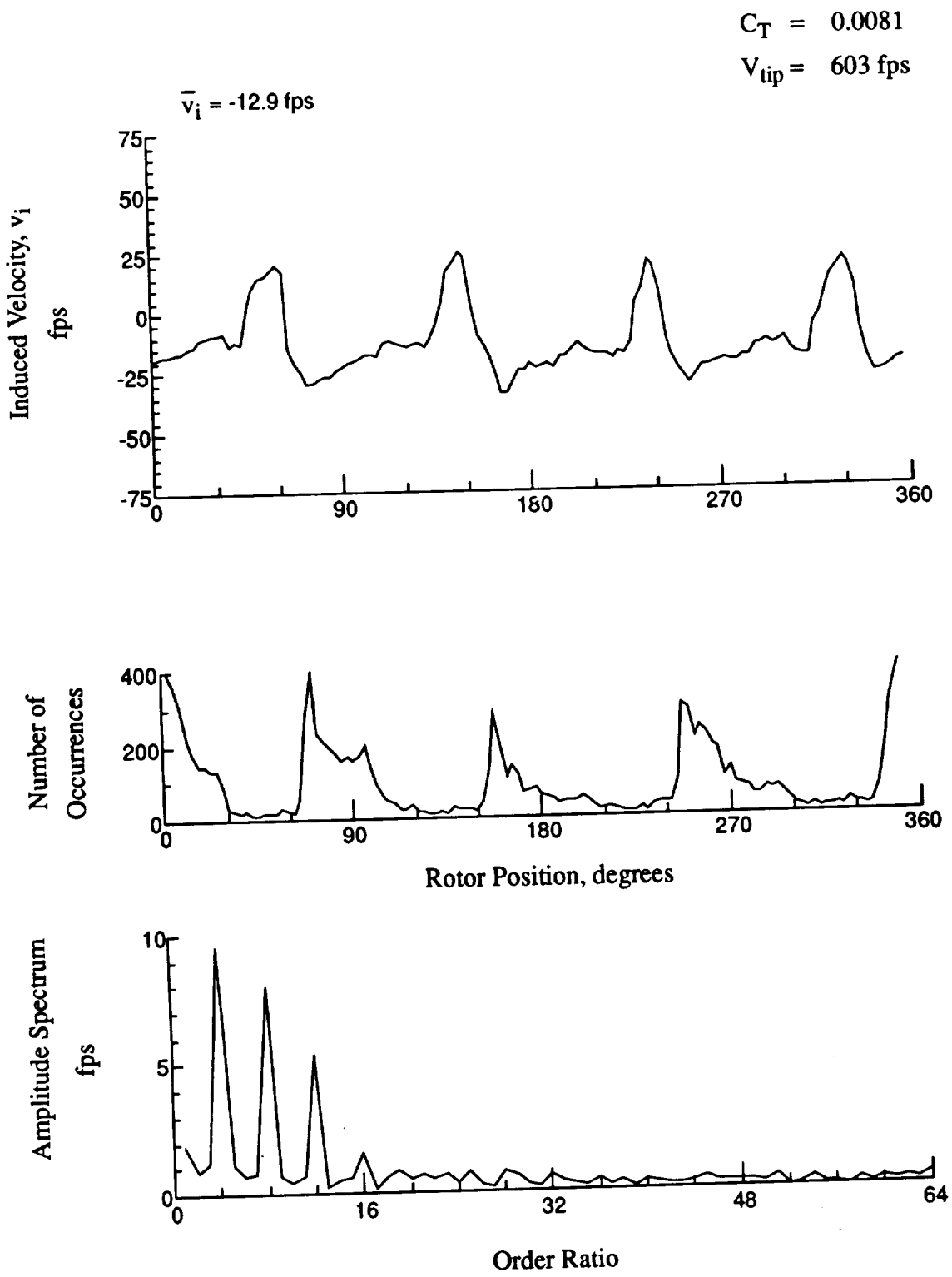


Figure 123.- Concluded.
 $x/R = 1.50$, $y/R = -0.20$, $z = 2.19 \text{ in.}$

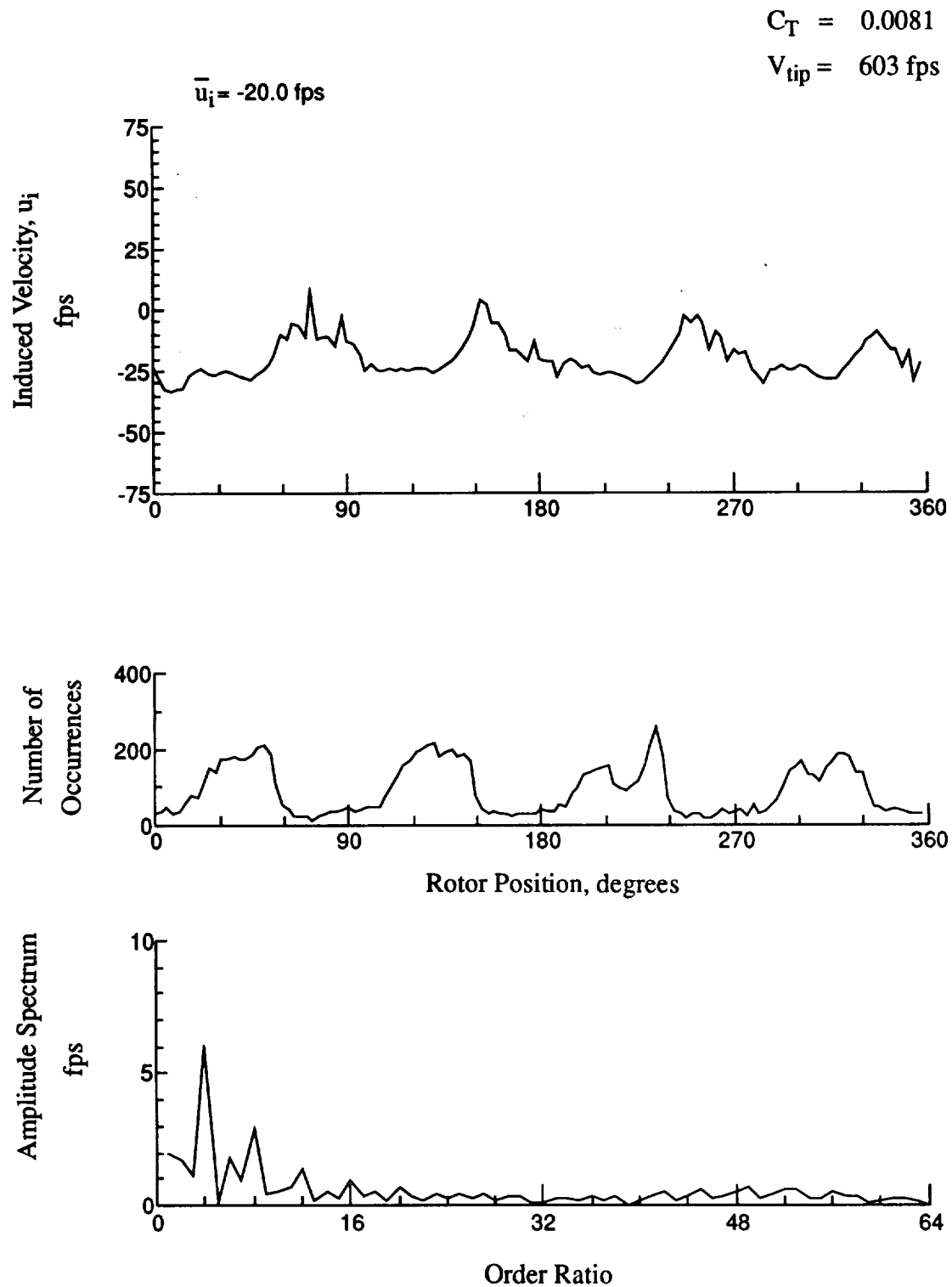


Figure 124.- Wake Measurements at
 $x/R = 1.50$, $y/R = -0.20$, $z = -1.23$ in.

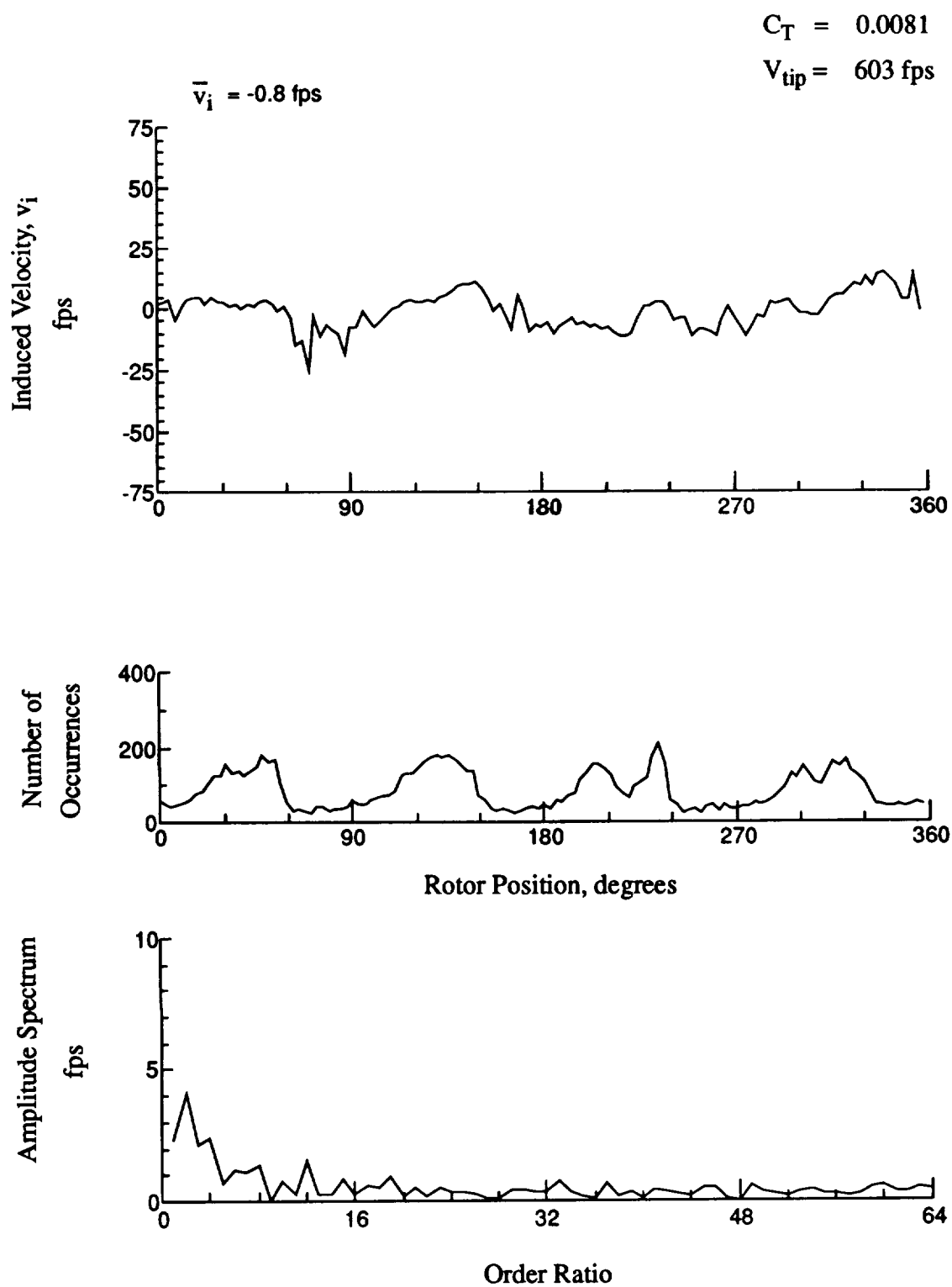


Figure 124.- Concluded.
 $x/R = 1.50$, $y/R = -0.20$, $z = -1.23 \text{ in.}$

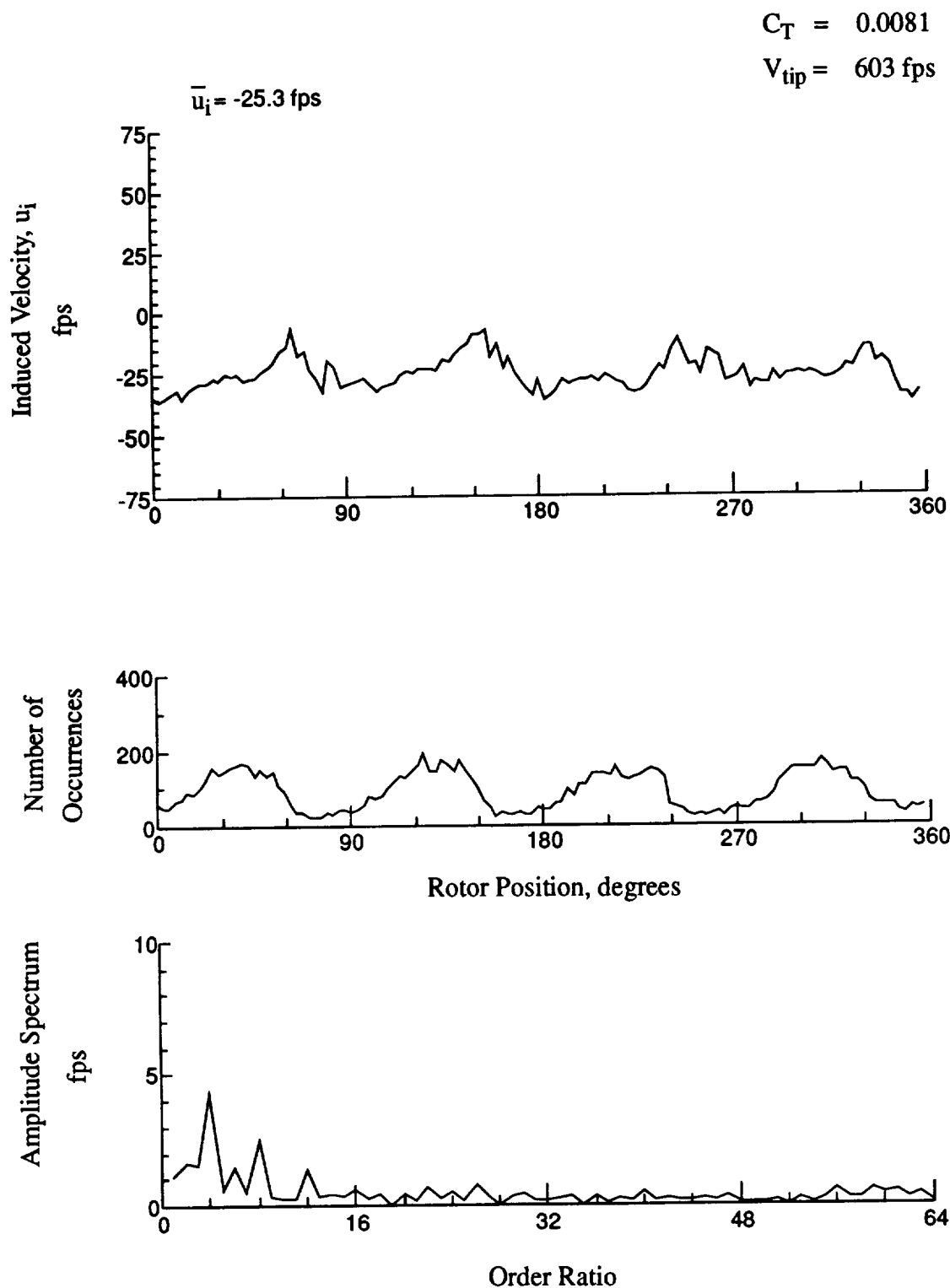


Figure 125.- Wake Measurements at
 $x/R = 1.50$, $y/R = -0.20$, $z = -2.26 \text{ in.}$

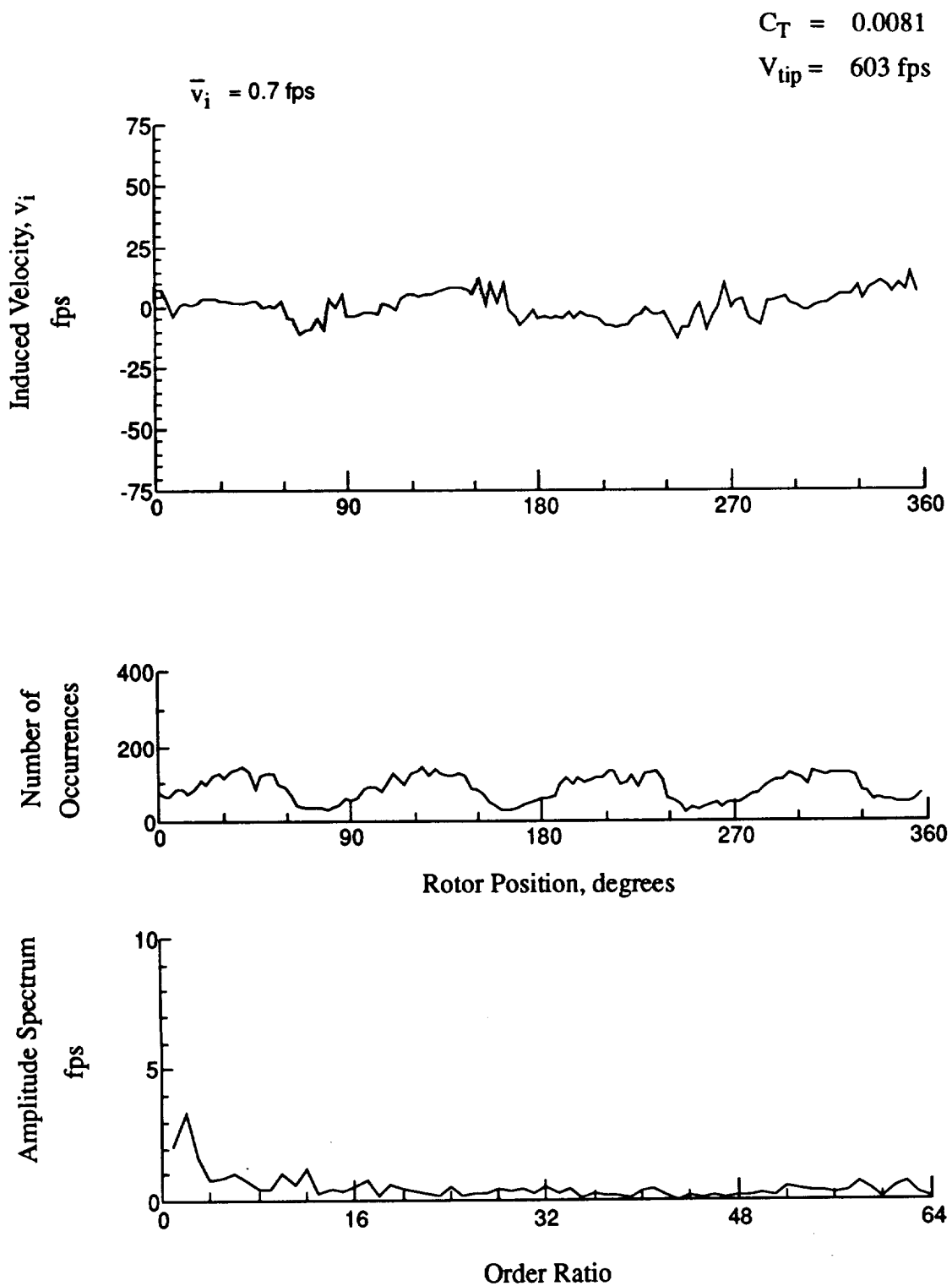


Figure 125.- Concluded.
 $x/R = 1.50$, $y/R = -0.20$, $z = -2.26 \text{ in.}$

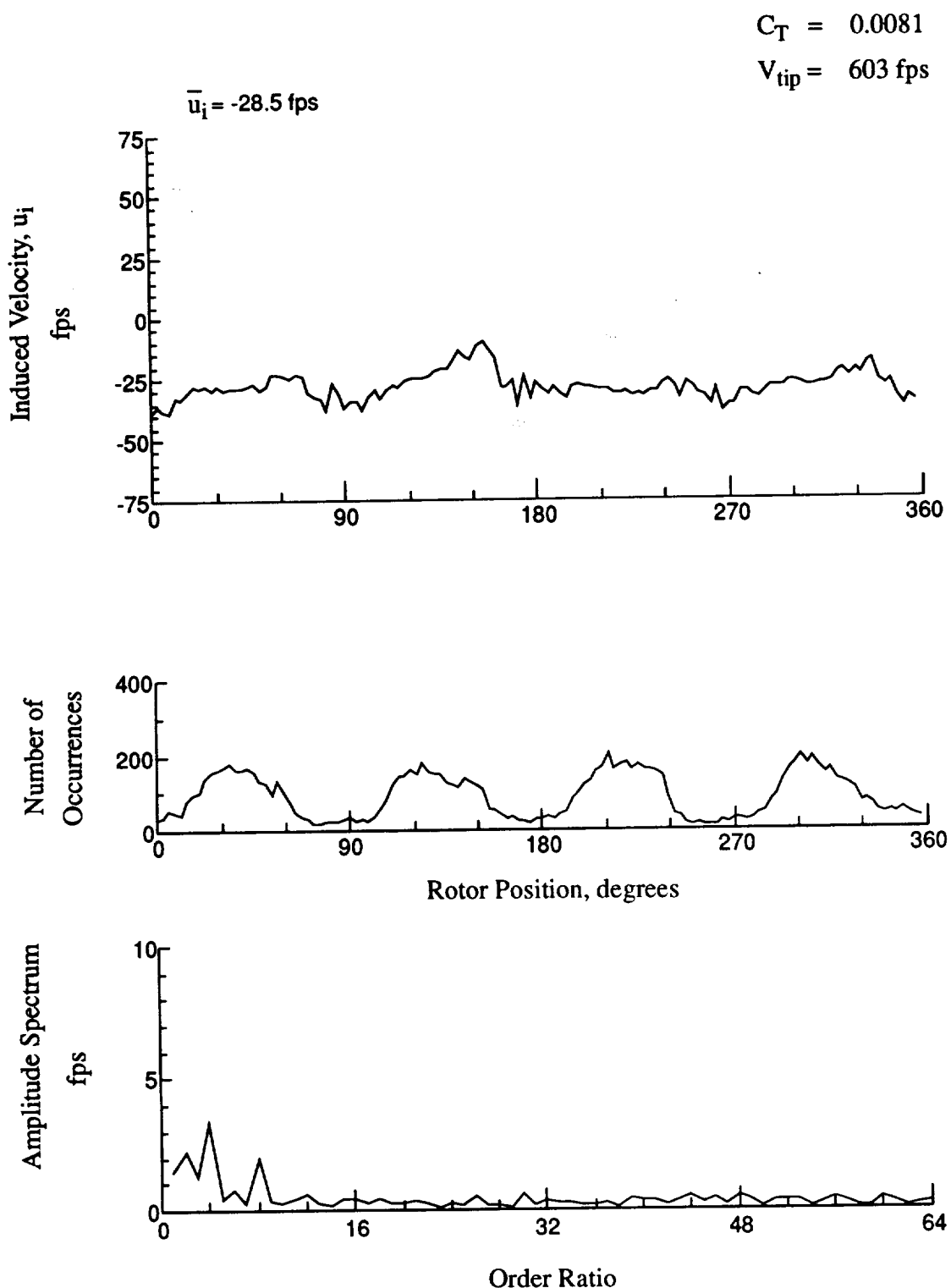


Figure 126.- Wake Measurements at
 $x/R = 1.50$, $y/R = -0.20$, $z = -3.29$ in.

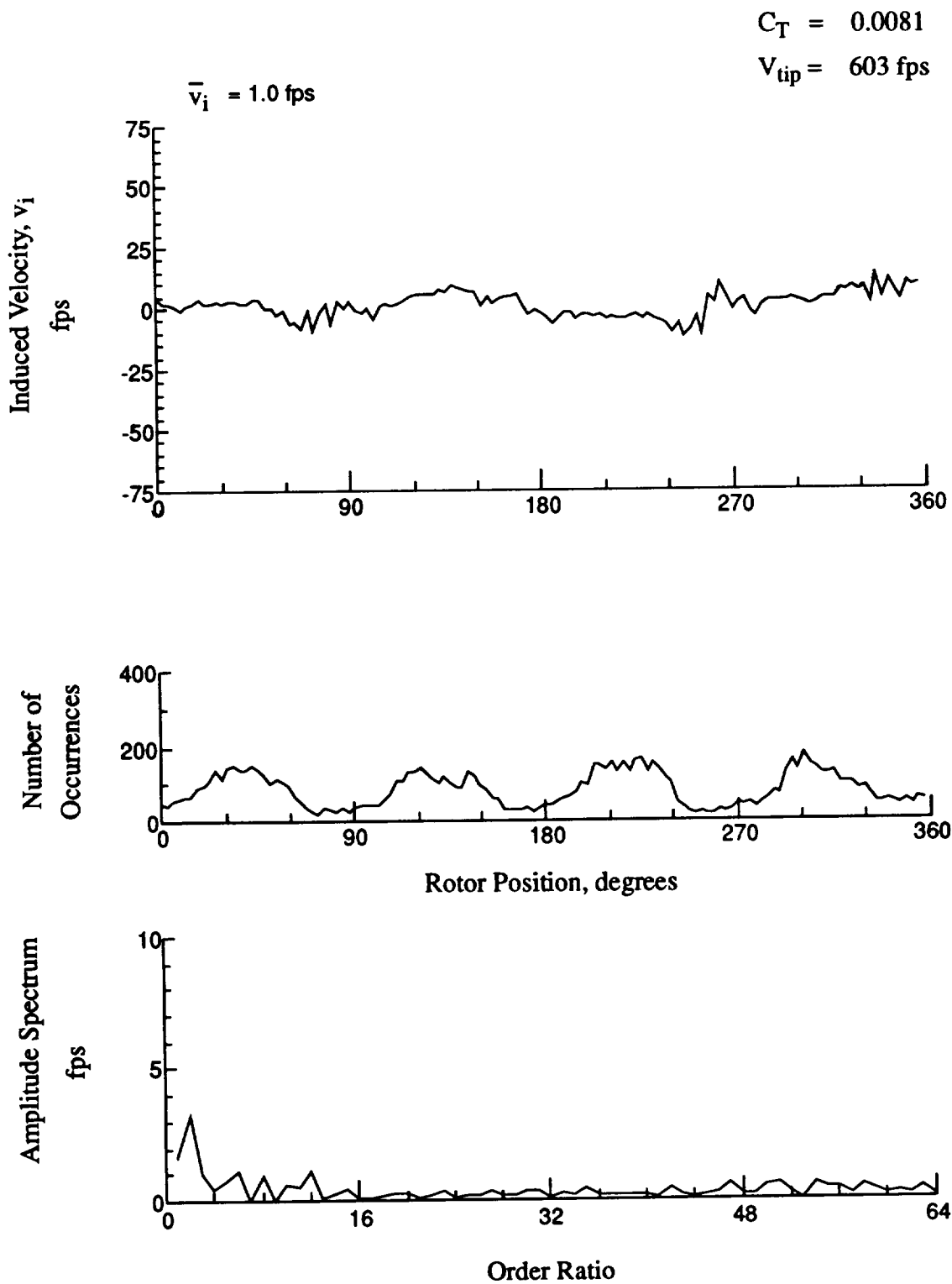


Figure 126.- Concluded.
 $x/R = 1.50$, $y/R = -0.20$, $z = -3.29 \text{ in.}$

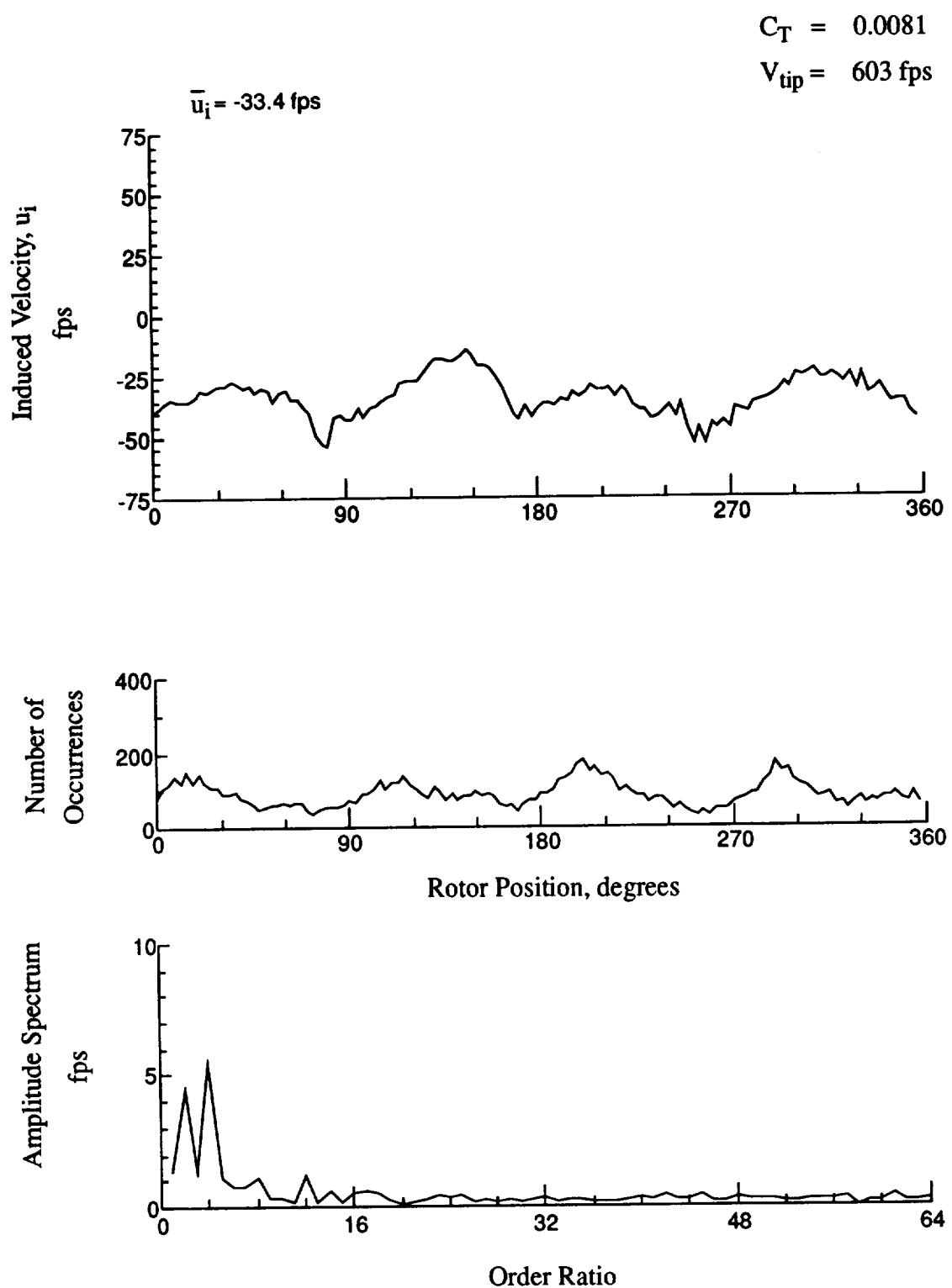


Figure 127.- Wake Measurements at
 $x/R = 1.50$, $y/R = -0.20$, $z = -4.32 \text{ in.}$

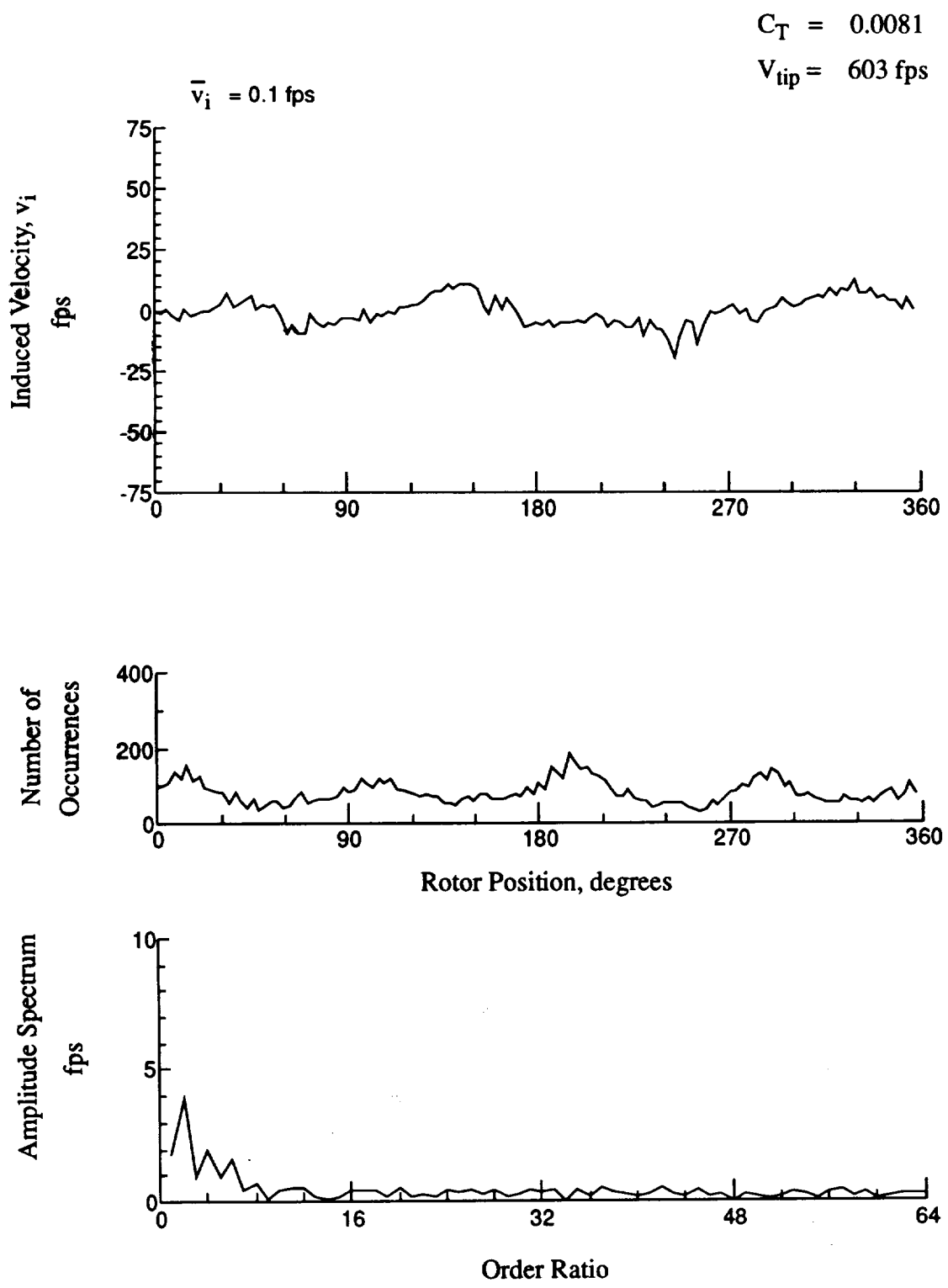


Figure 127.- Concluded.
 $x/R = 1.50$, $y/R = -0.20$, $z = -4.32 \text{ in.}$

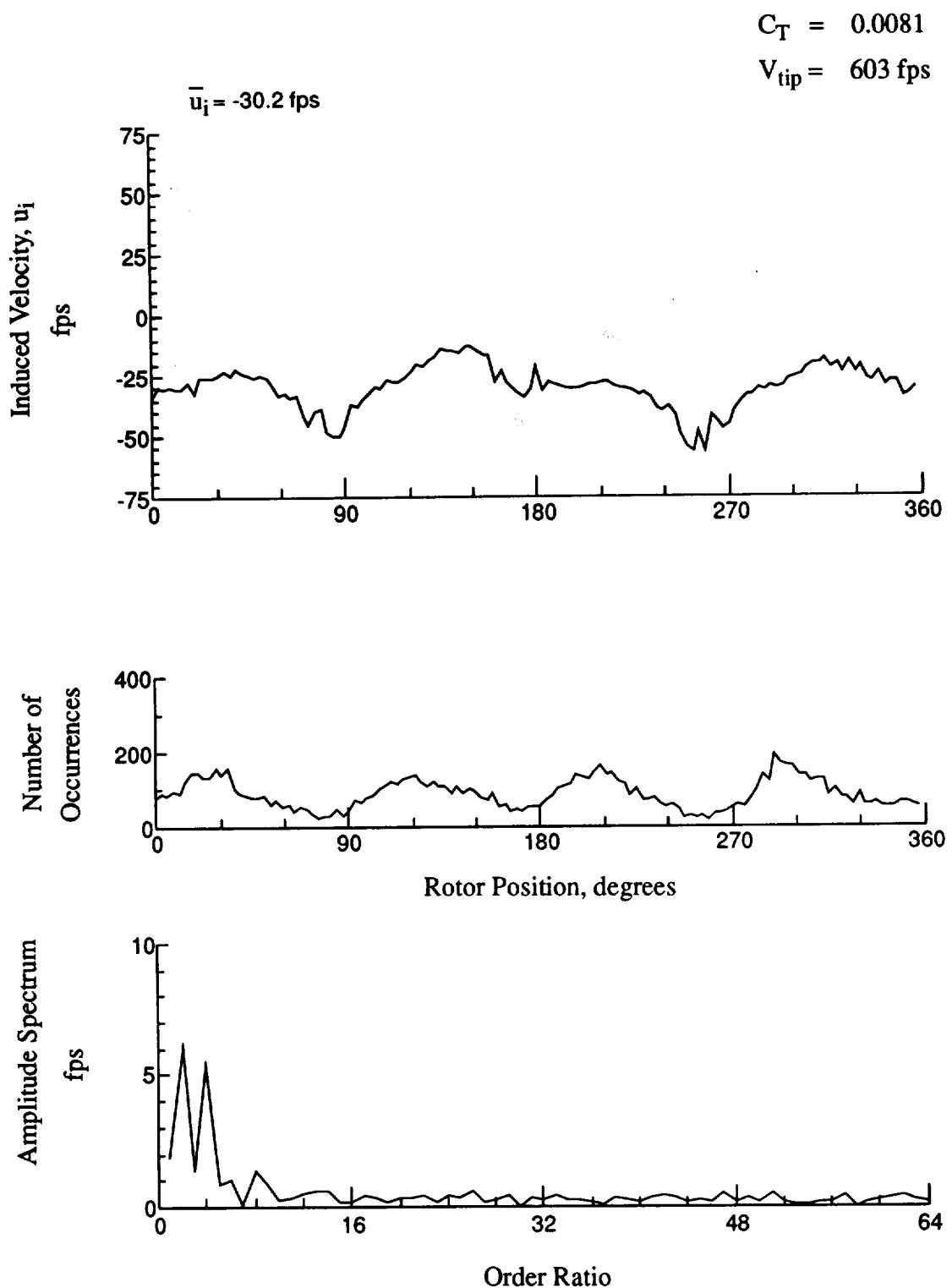


Figure 128.- Wake Measurements at
 $x/R = 1.50$, $y/R = -0.20$, $z = -5.35 \text{ in.}$

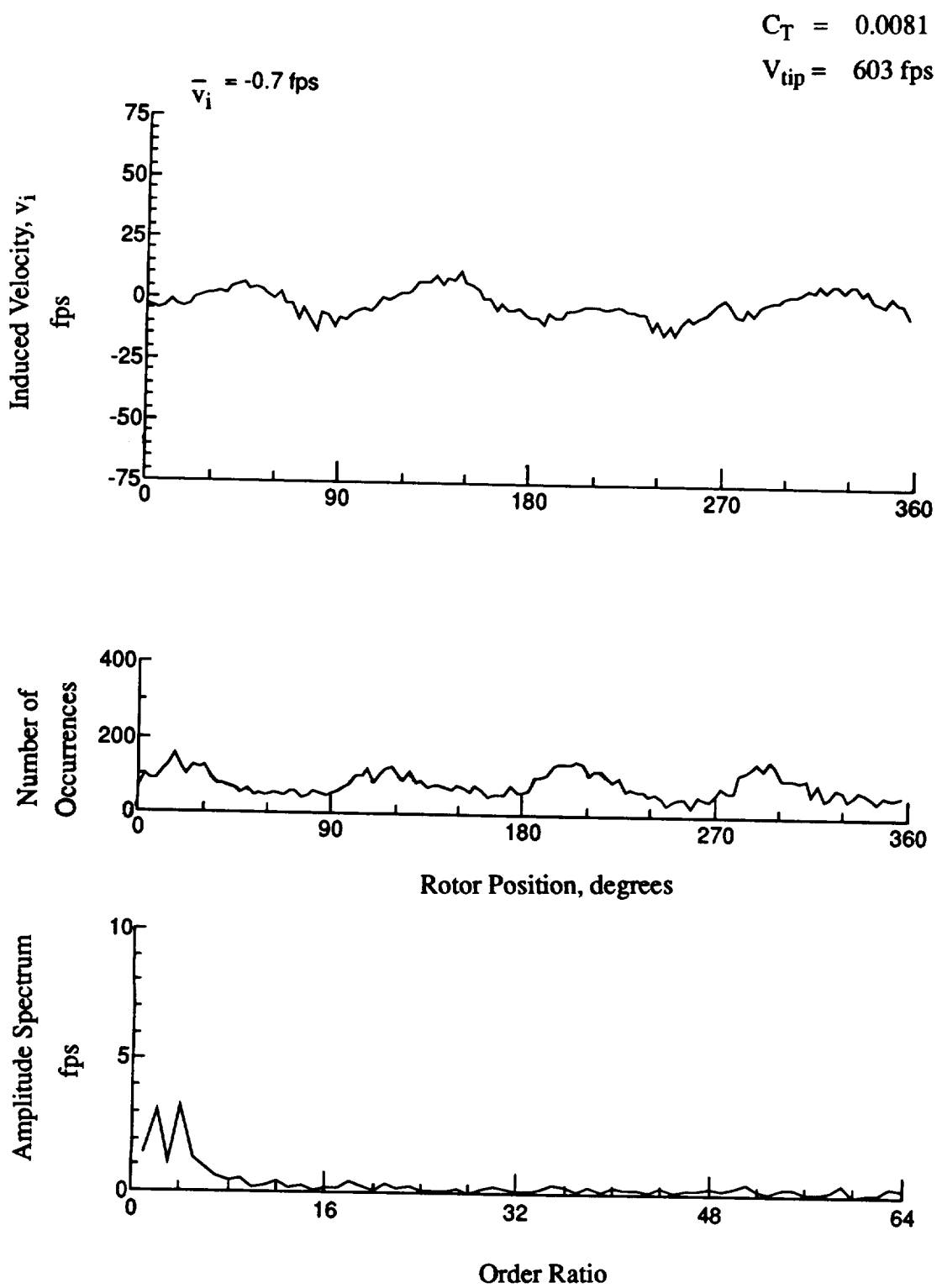
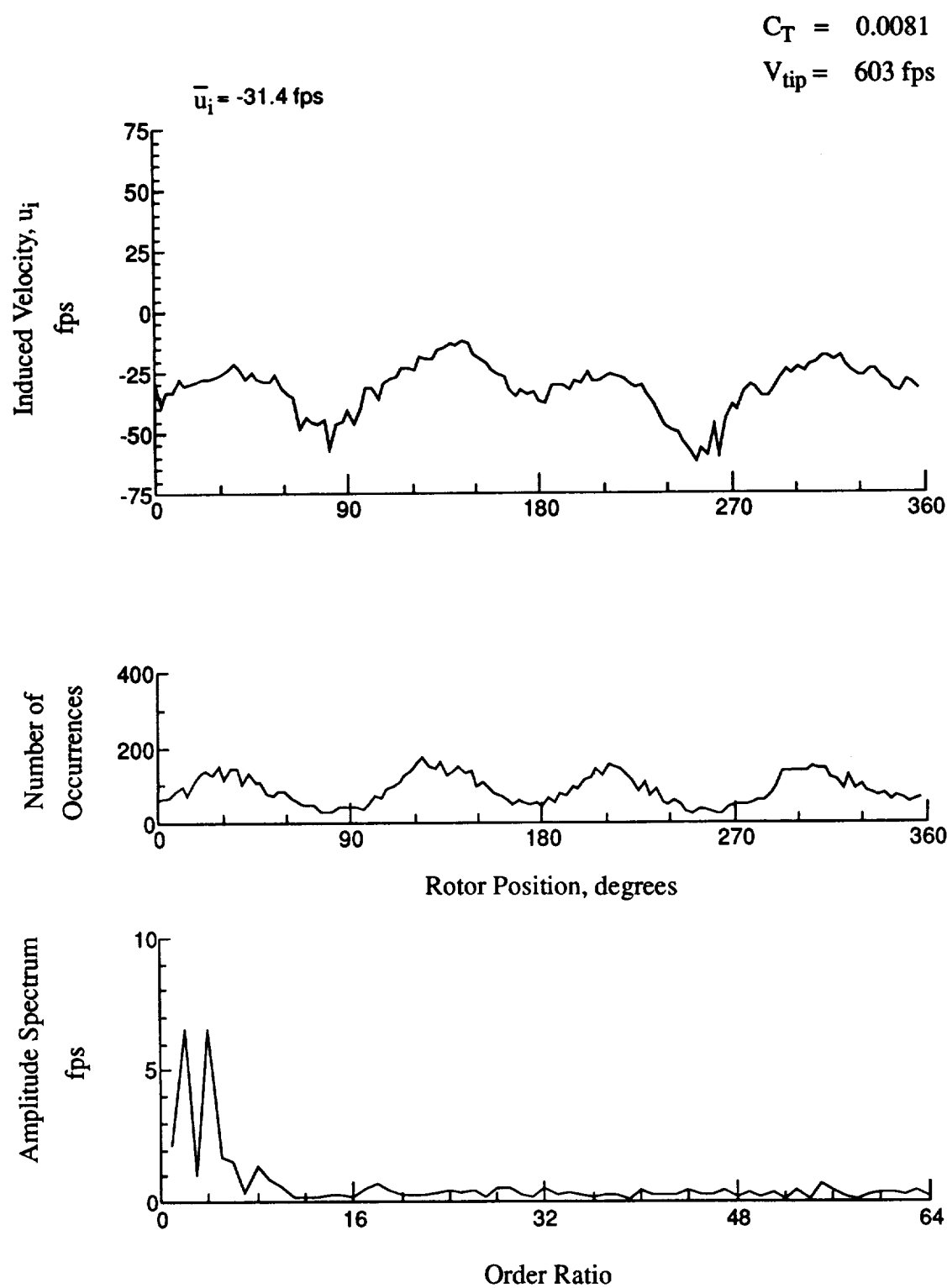


Figure 128.- Concluded.
 $x/R = 1.50$, $y/R = -0.20$, $z = -5.35 \text{ in.}$



**Figure 129.- Wake Measurements at
 $x/R = 1.50$, $y/R = -0.20$, $z = -6.38 \text{ in.}$**

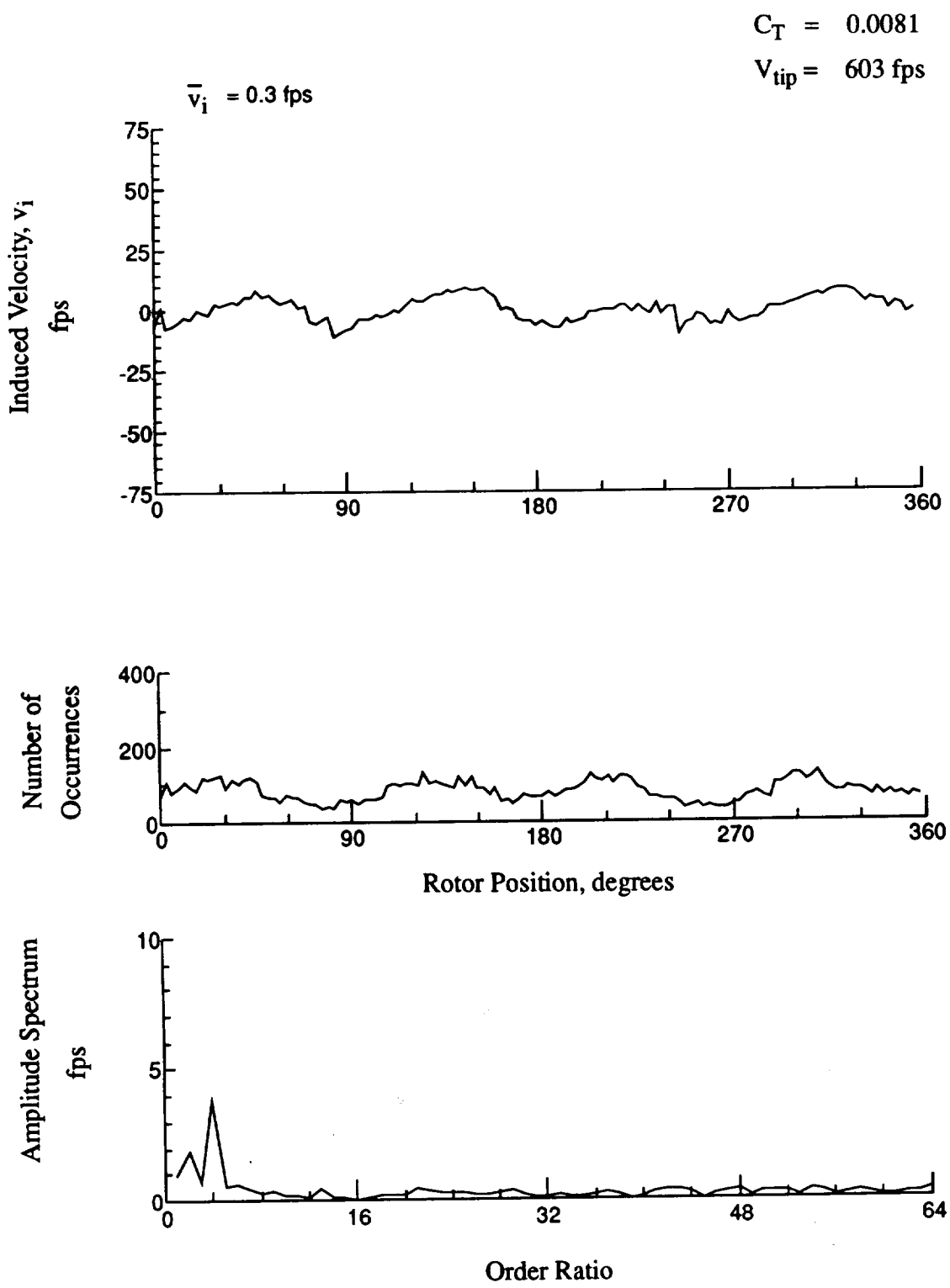


Figure 129.- Concluded.
 $x/R = 1.50$, $y/R = -0.20$, $z = -6.38 \text{ in.}$

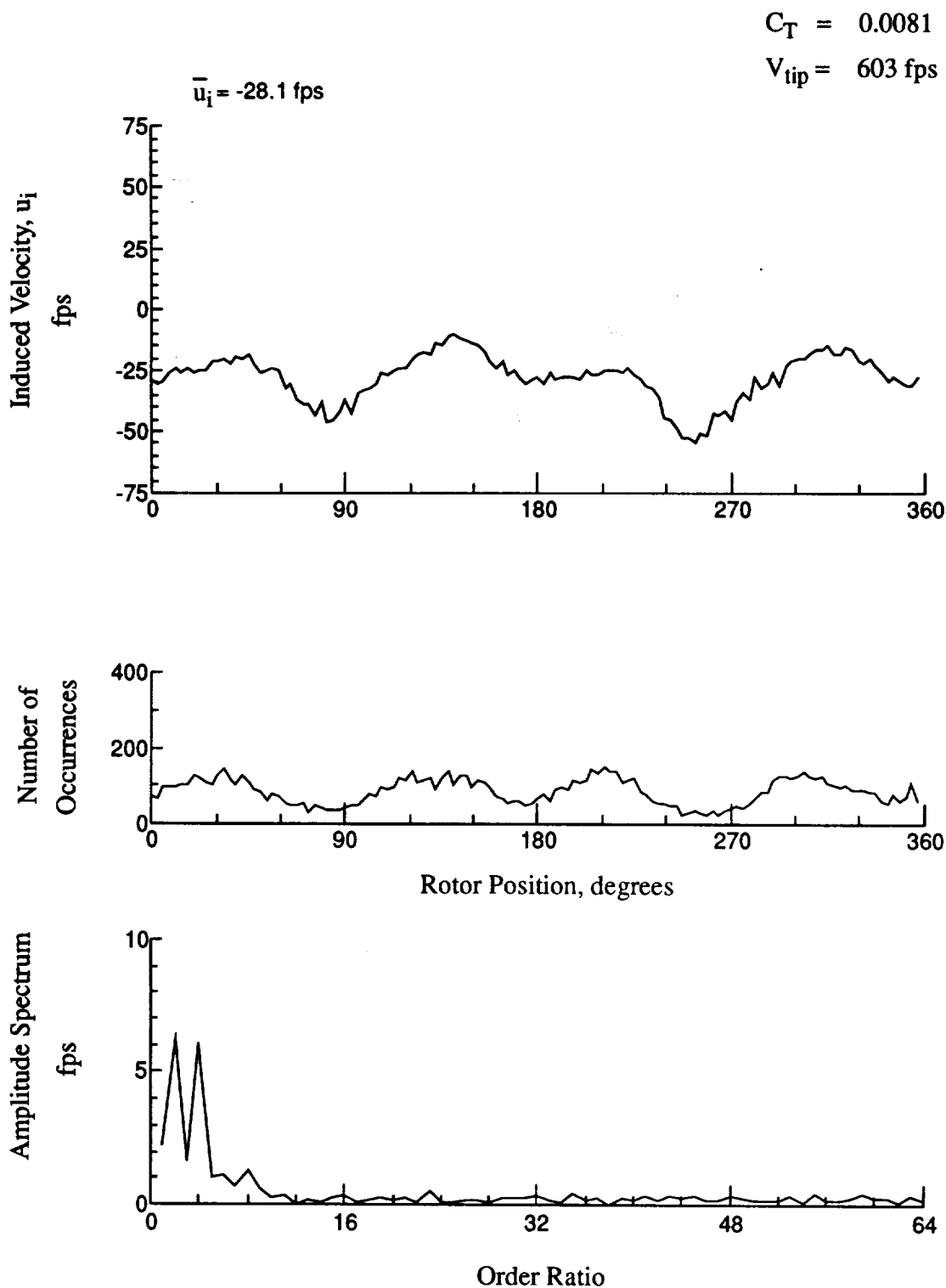


Figure 130.- Wake Measurements at
 $x/R = 1.50$, $y/R = -0.20$, $z = -7.41 \text{ in.}$

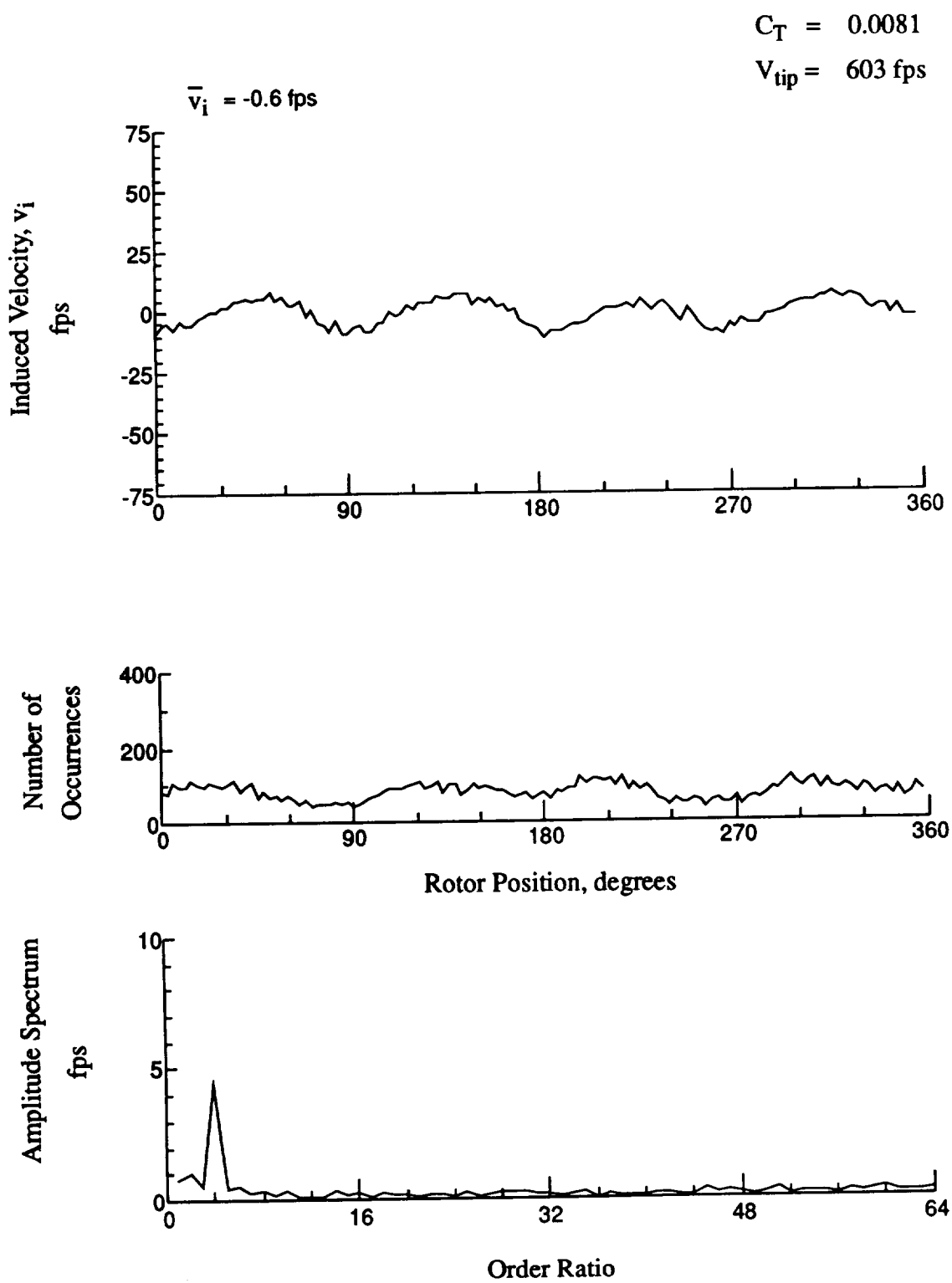


Figure 130.- Concluded.
 $x/R = 1.50$, $y/R = -0.20$, $z = -7.41 \text{ in.}$

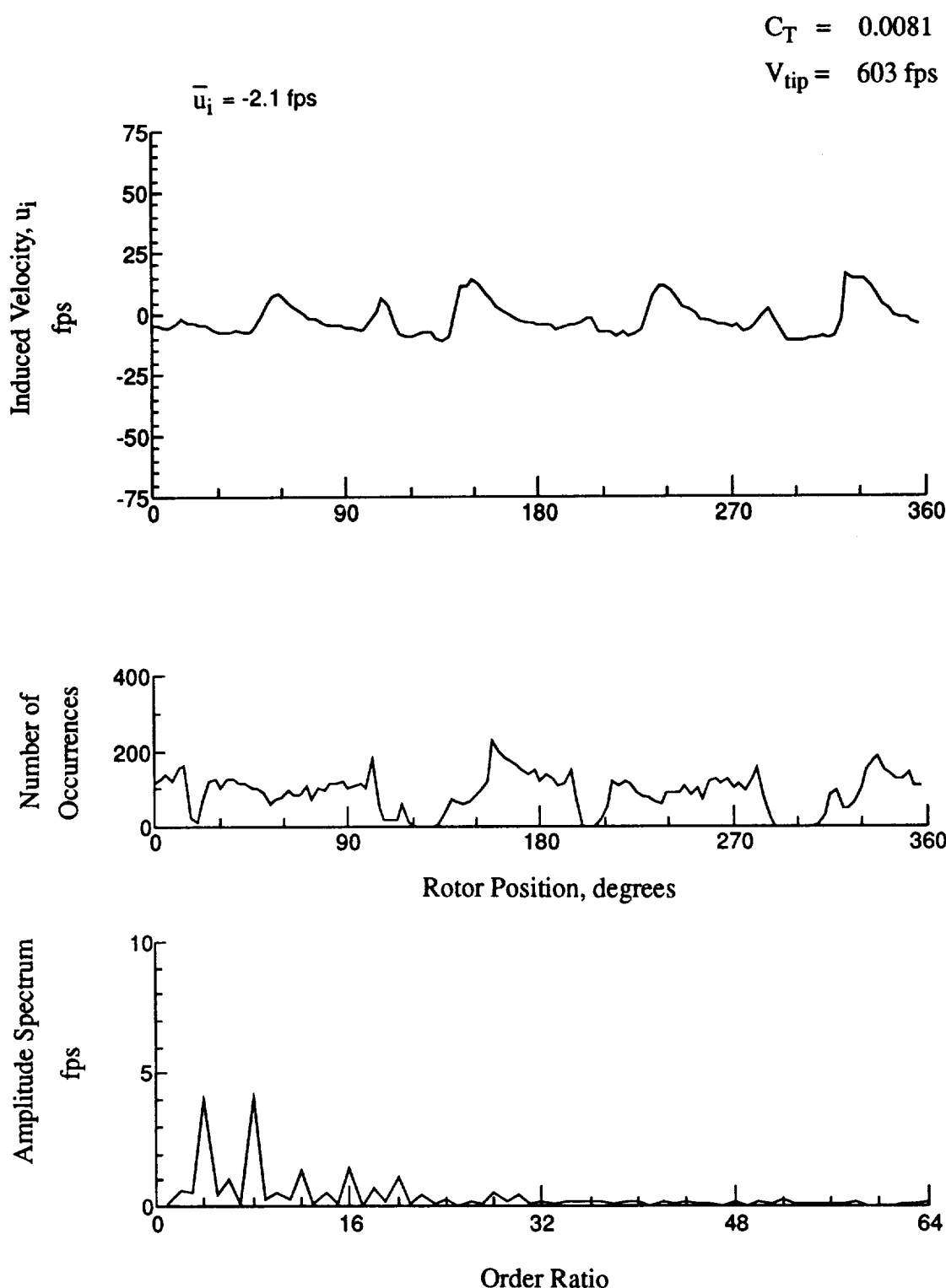


Figure 131.- Wake Measurements at
 $x/R = -0.27$, $y/R = 0.20$, $z = 0.21$ in.

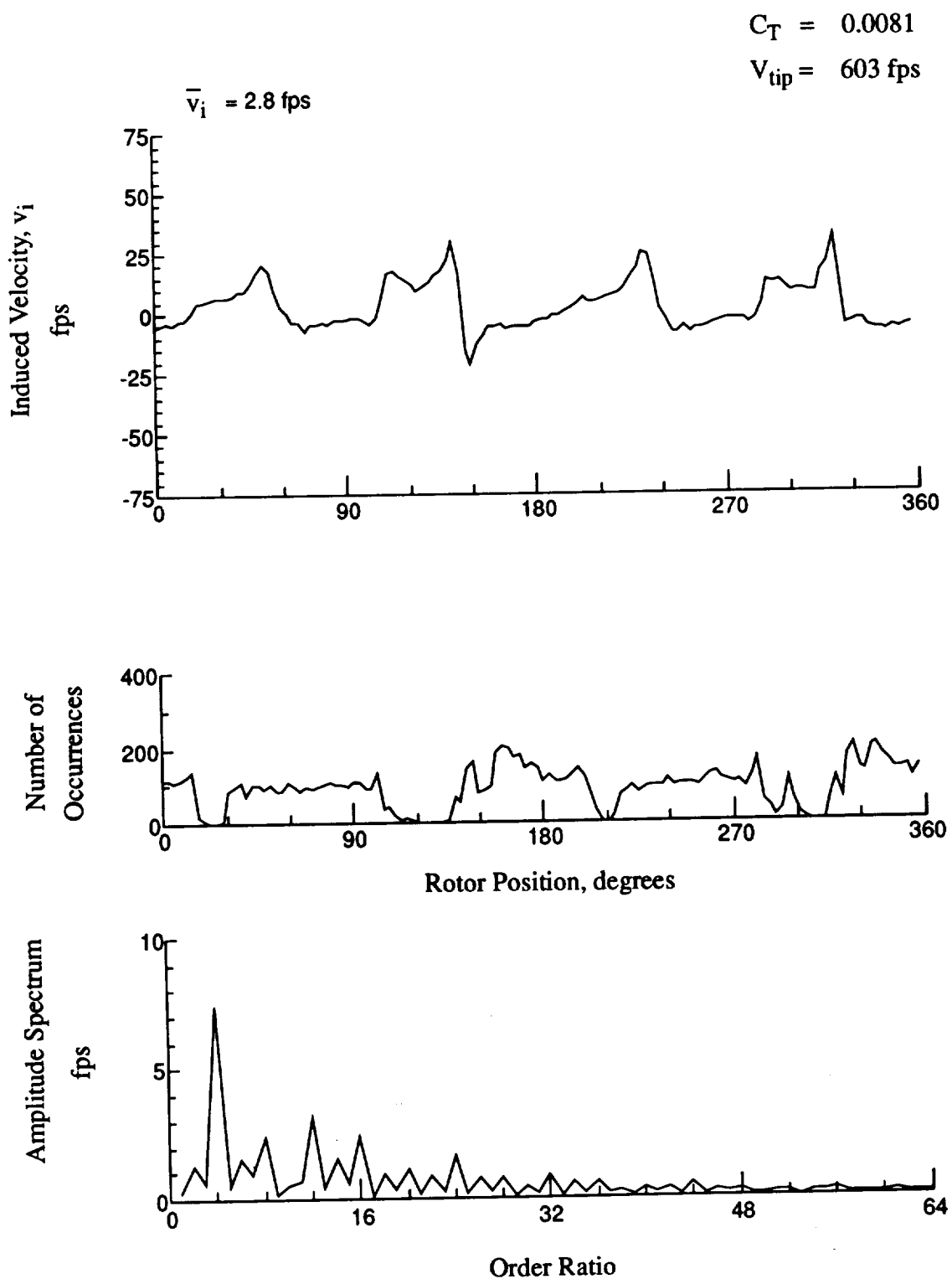


Figure 131.- Concluded.
 $x/R = -0.27$, $y/R = 0.20$, $z = 0.21 \text{ in.}$

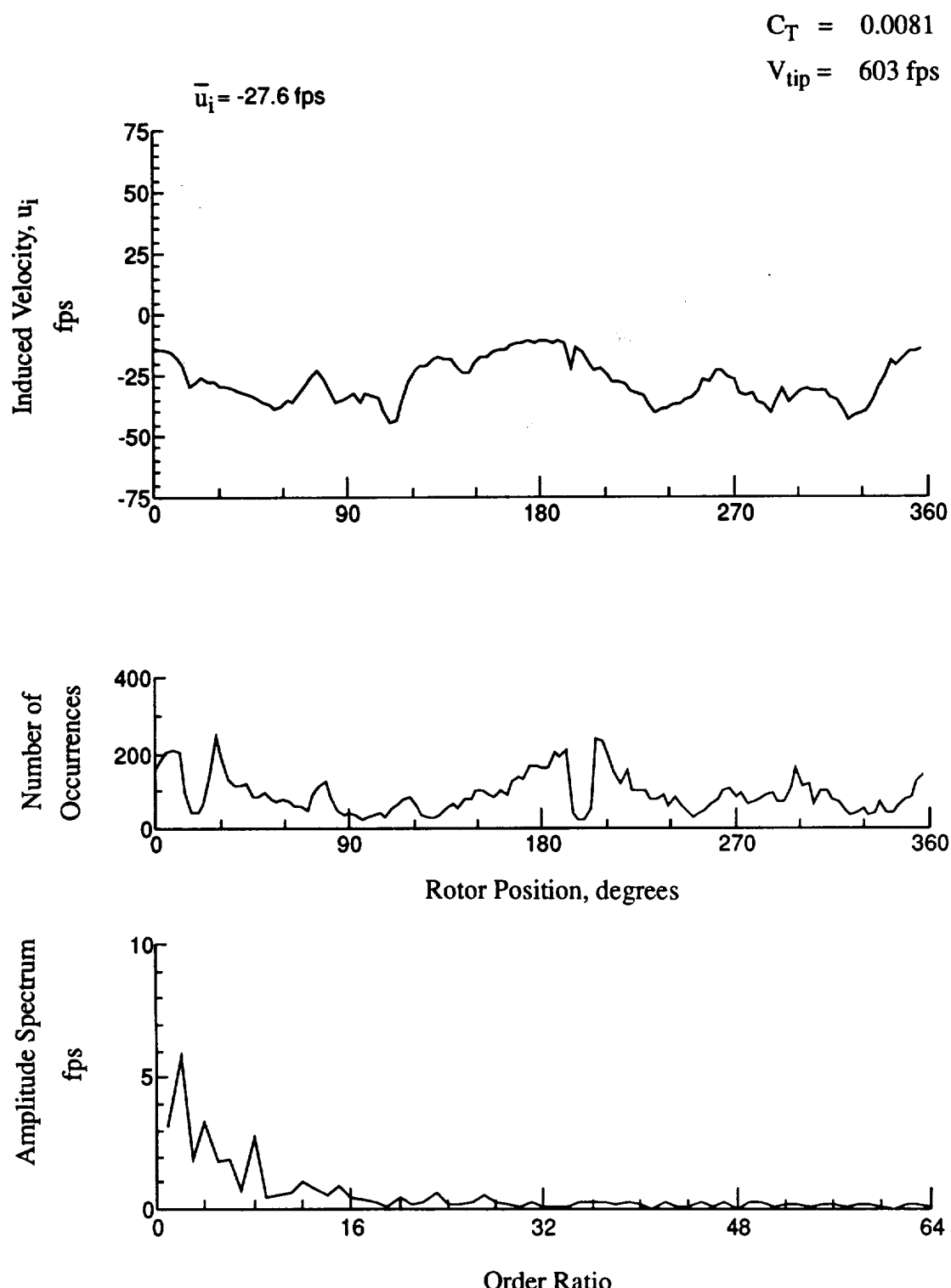


Figure 132.- Wake Measurements at
 $x/R = -0.27$, $y/R = 0.20$, $z = -1.85$ in.

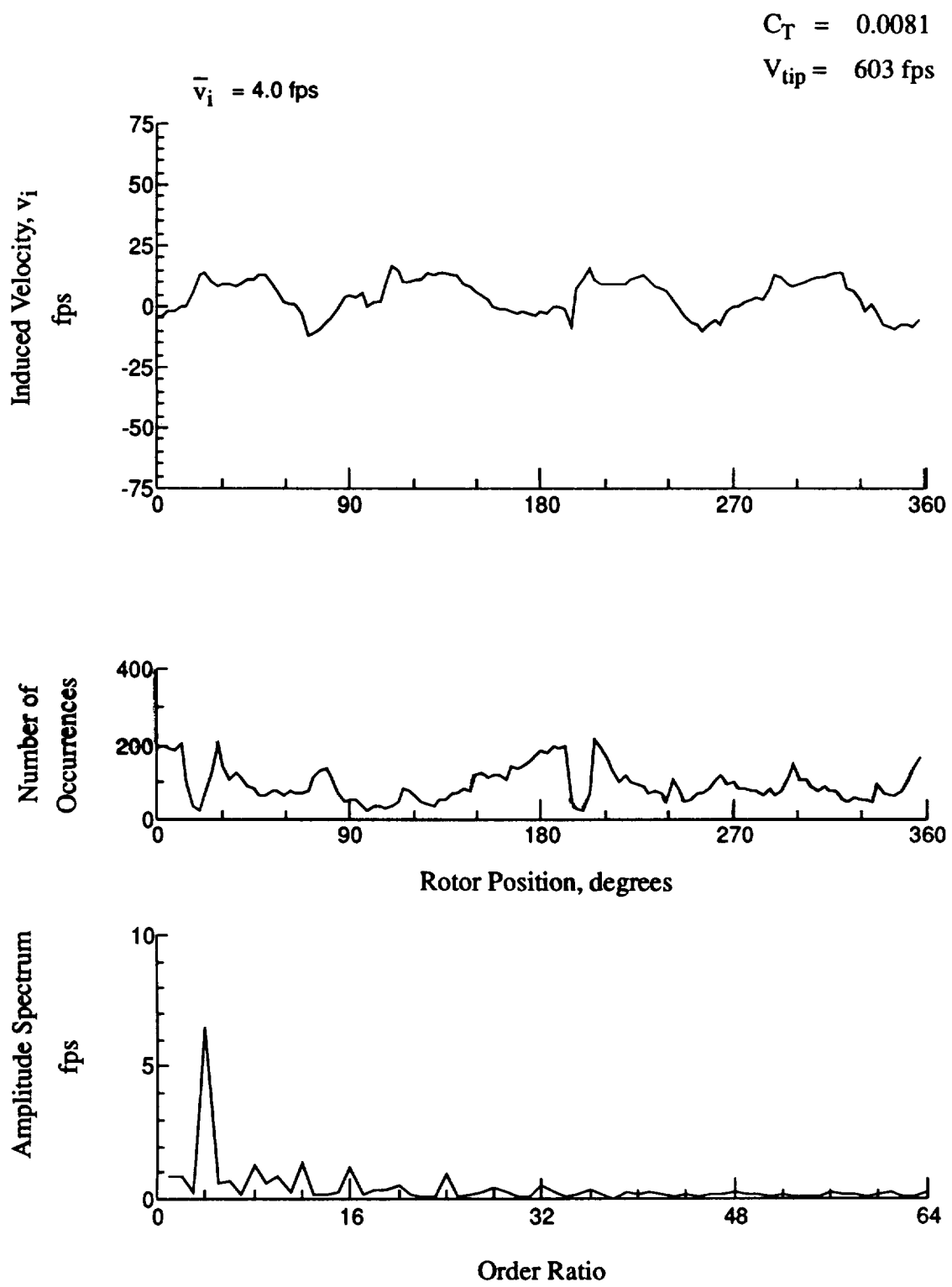


Figure 132.- Concluded.
 $x/R = -0.27$, $y/R = 0.20$, $z = -1.85 \text{ in.}$

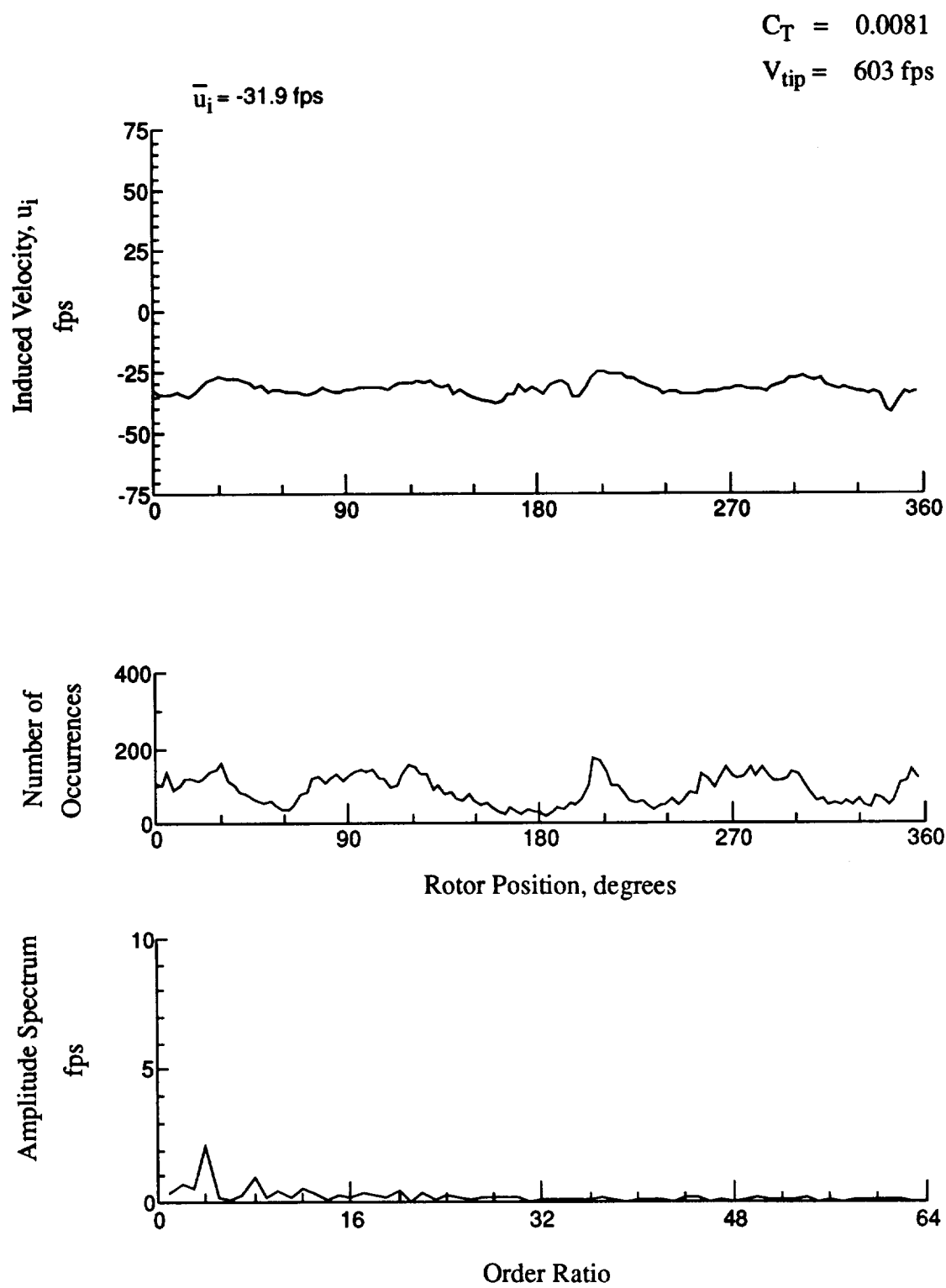


Figure 133.- Wake Measurements at
 $x/R = -0.27$, $y/R = 0.20$, $z = -2.88 \text{ in.}$

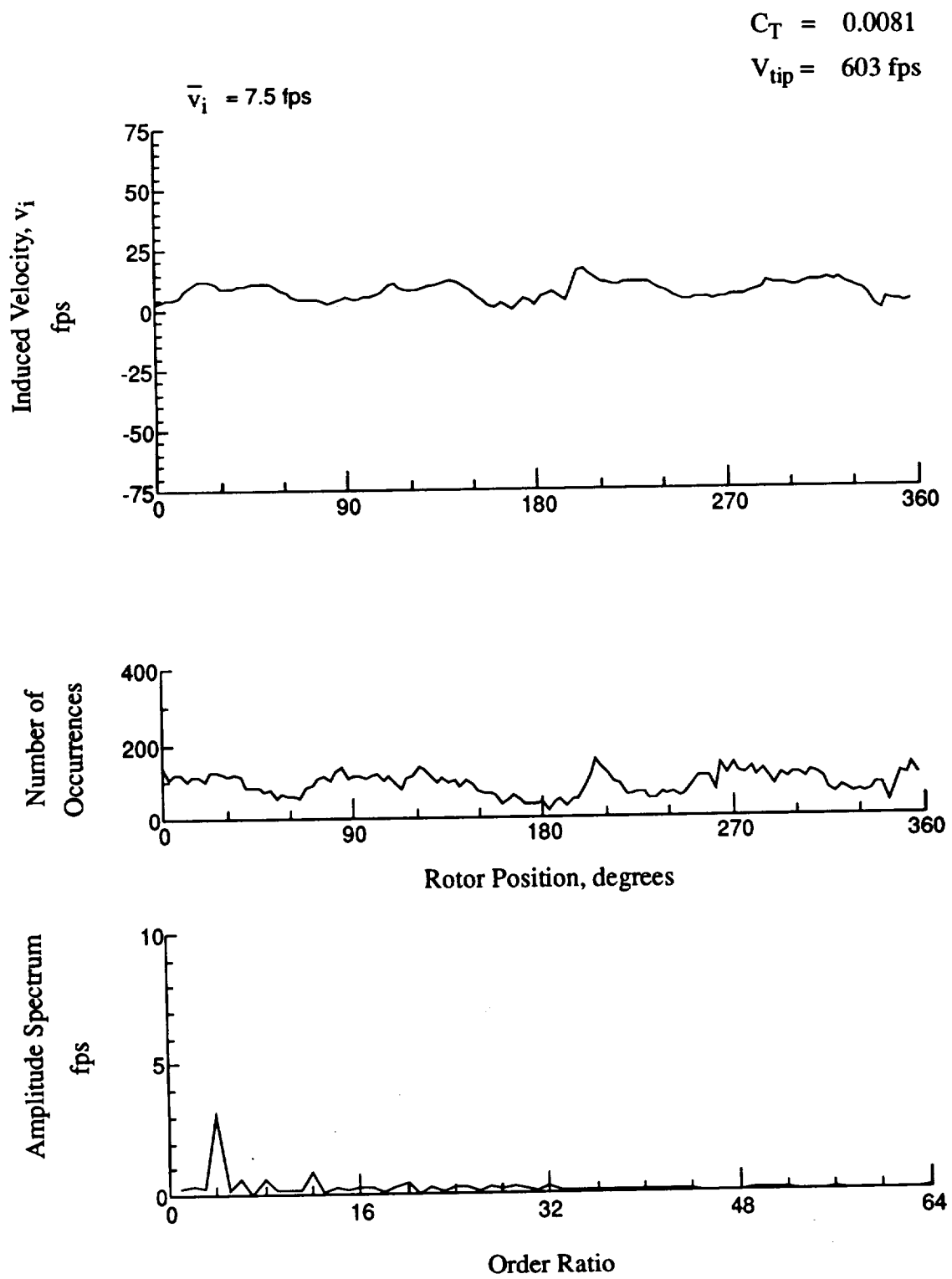


Figure 133.- Concluded.
 $x/R = -0.27$, $y/R = 0.20$, $z = -2.88 \text{ in.}$

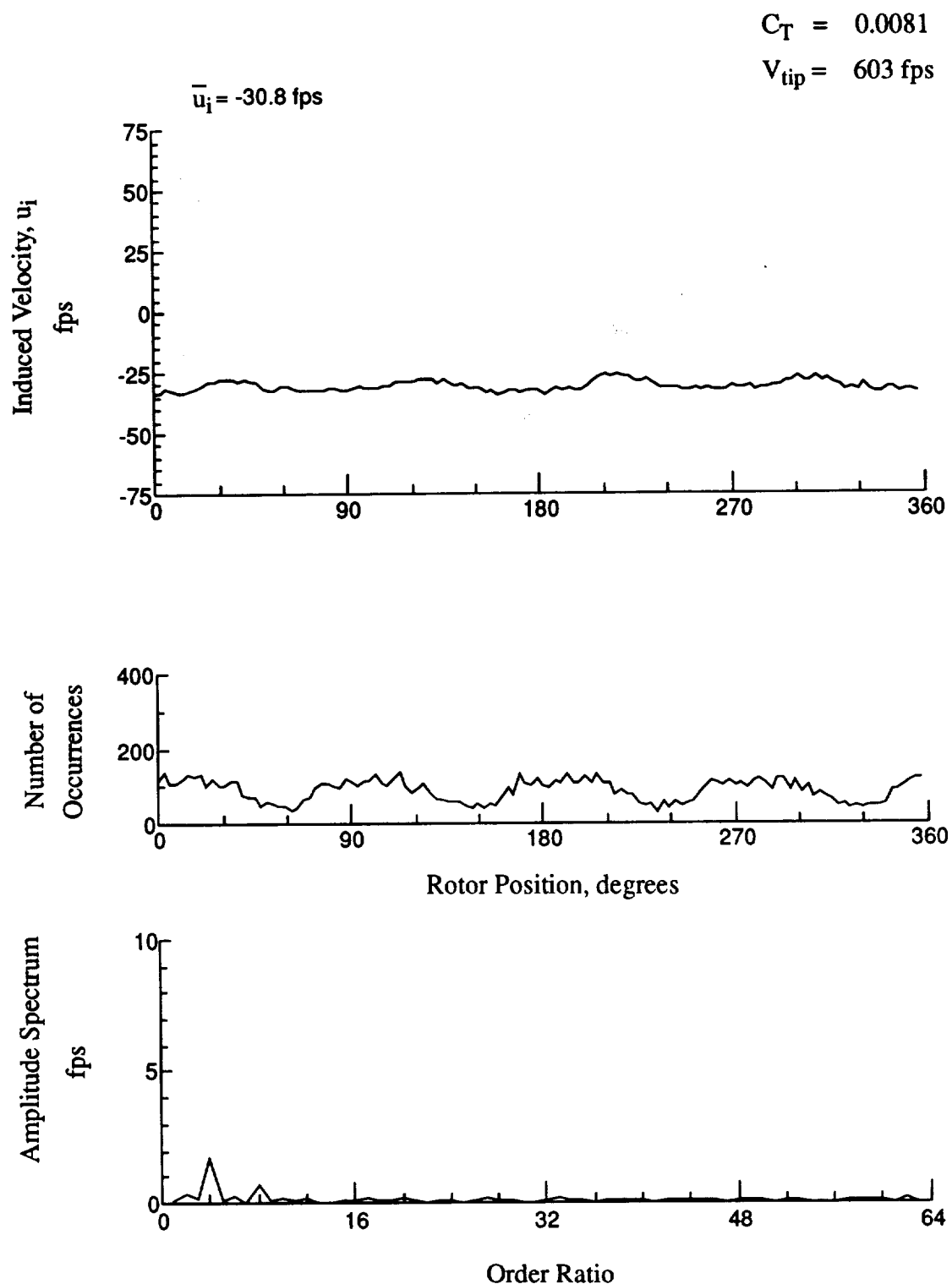


Figure 134.- Wake Measurements at
 $x/R = -0.27$, $y/R = 0.20$, $z = -3.91$ in.

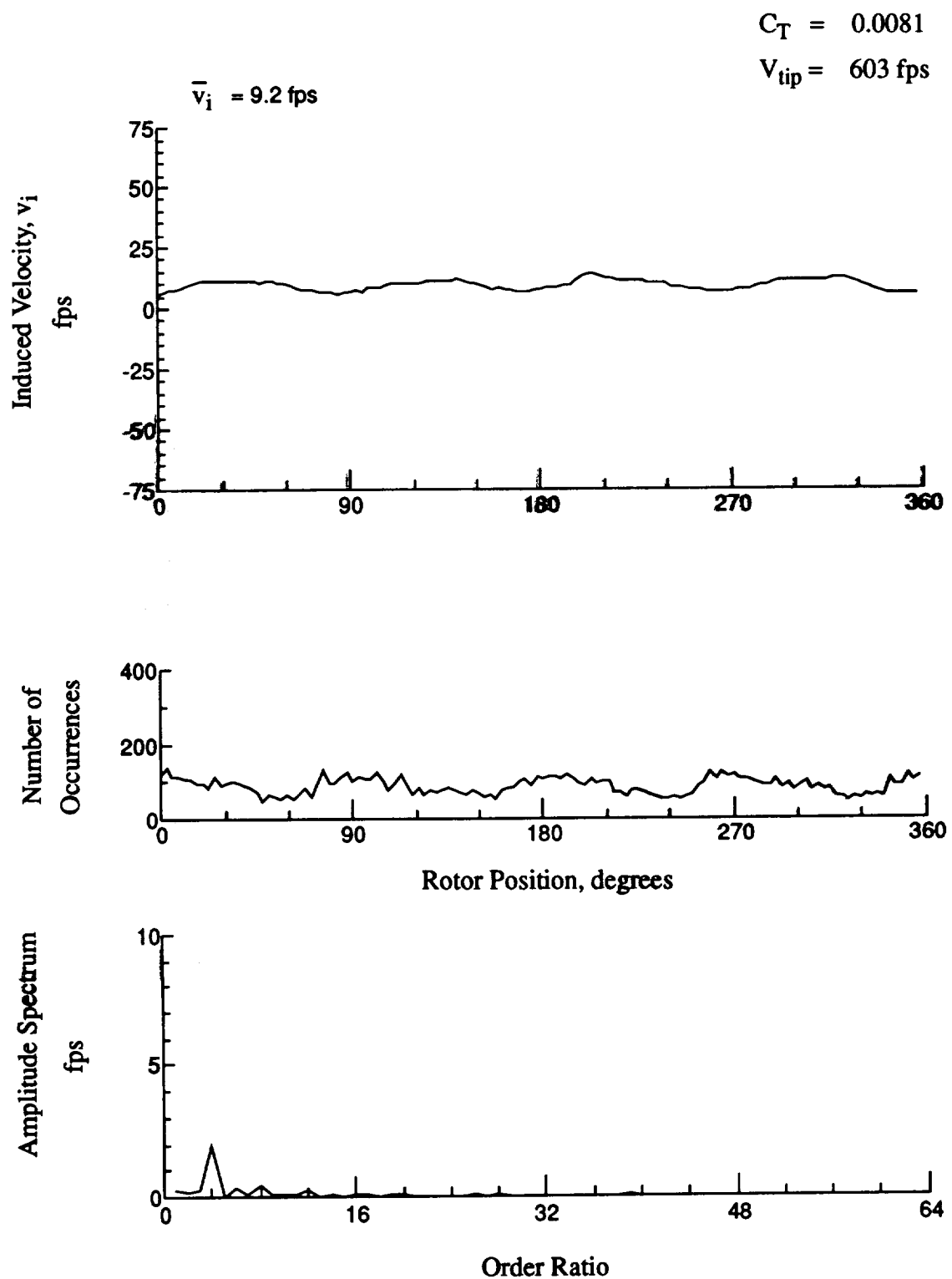


Figure 134.- Concluded.
 $x/R = -0.27$, $y/R = 0.20$, $z = -3.91 \text{ in.}$

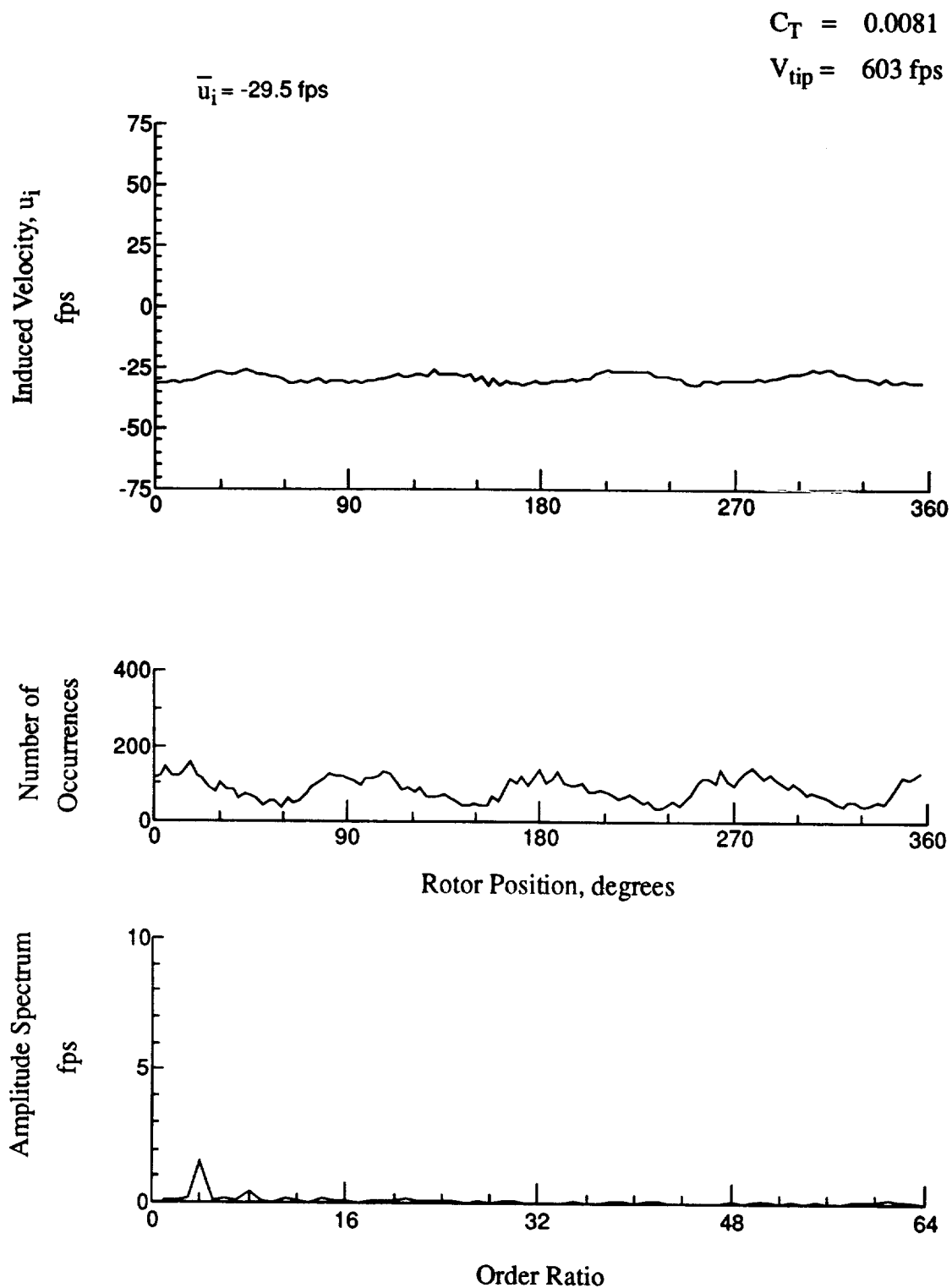


Figure 135.- Wake Measurements at
 $x/R = -0.27$, $y/R = 0.20$, $z = -4.94 \text{ in.}$

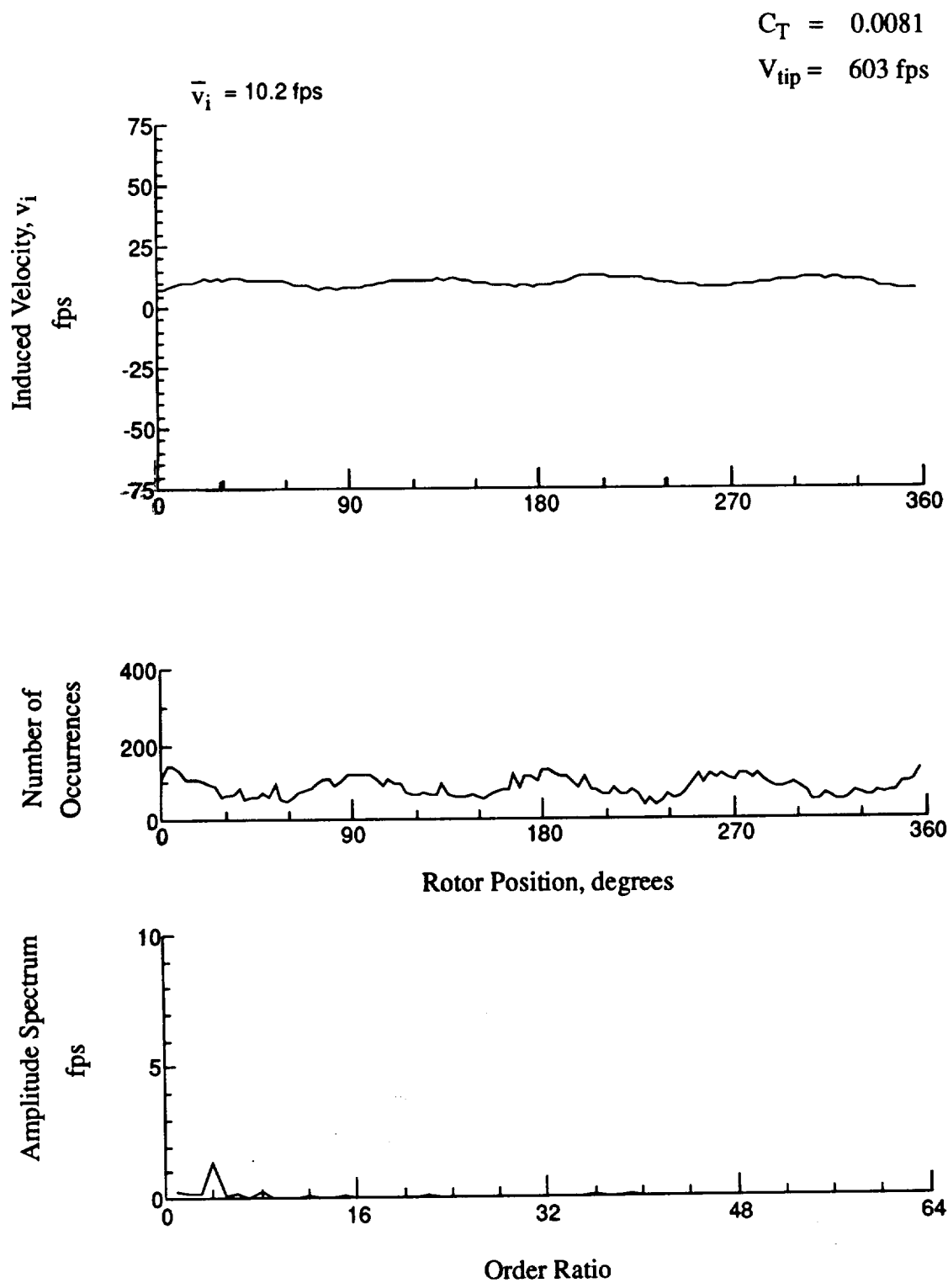


Figure 135.- Concluded.
 $x/R = -0.27$, $y/R = 0.20$, $z = -4.94 \text{ in.}$

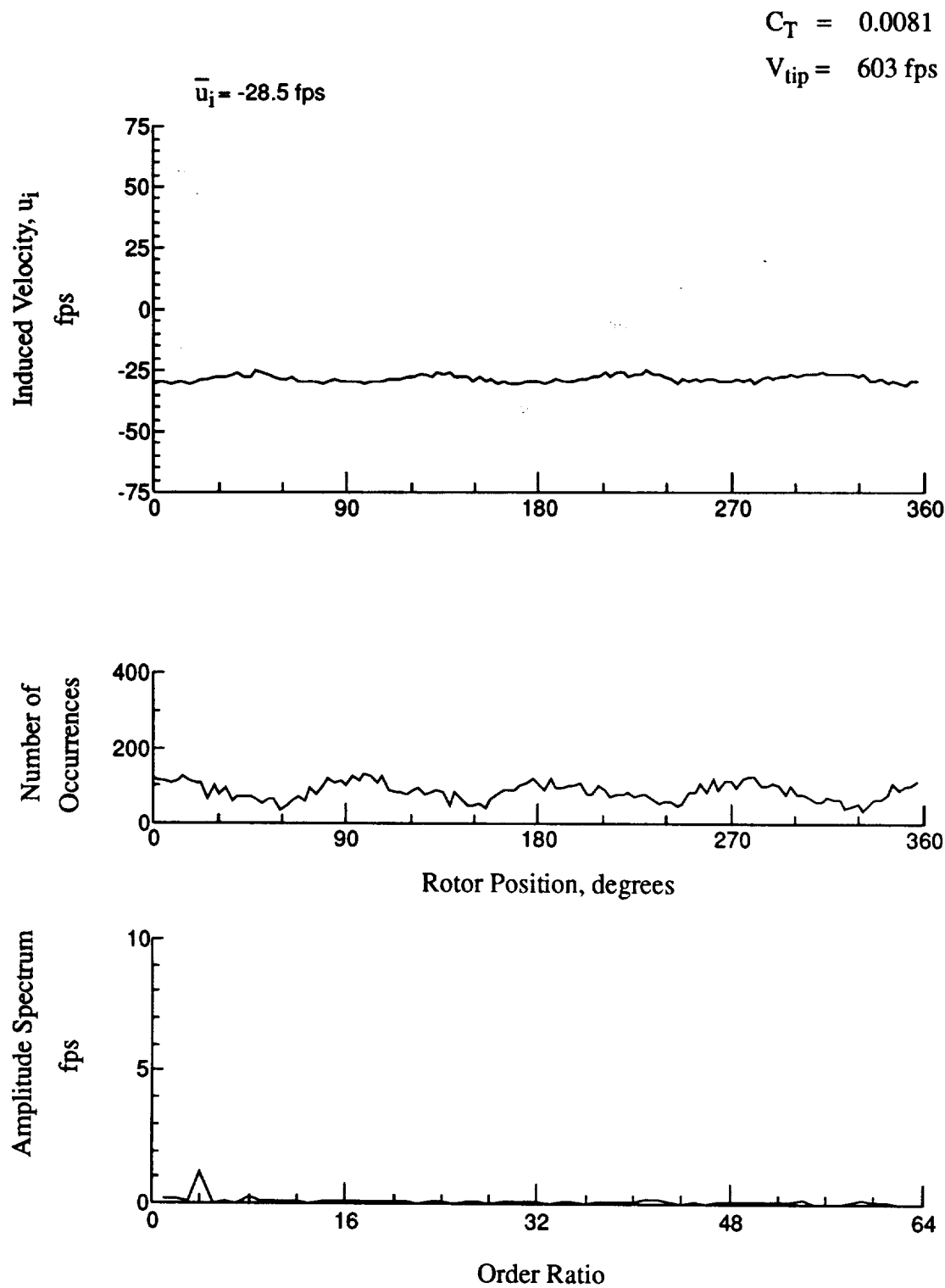


Figure 136.- Wake Measurements at
 $x/R = -0.27$, $y/R = 0.20$, $z = -5.97 \text{ in.}$

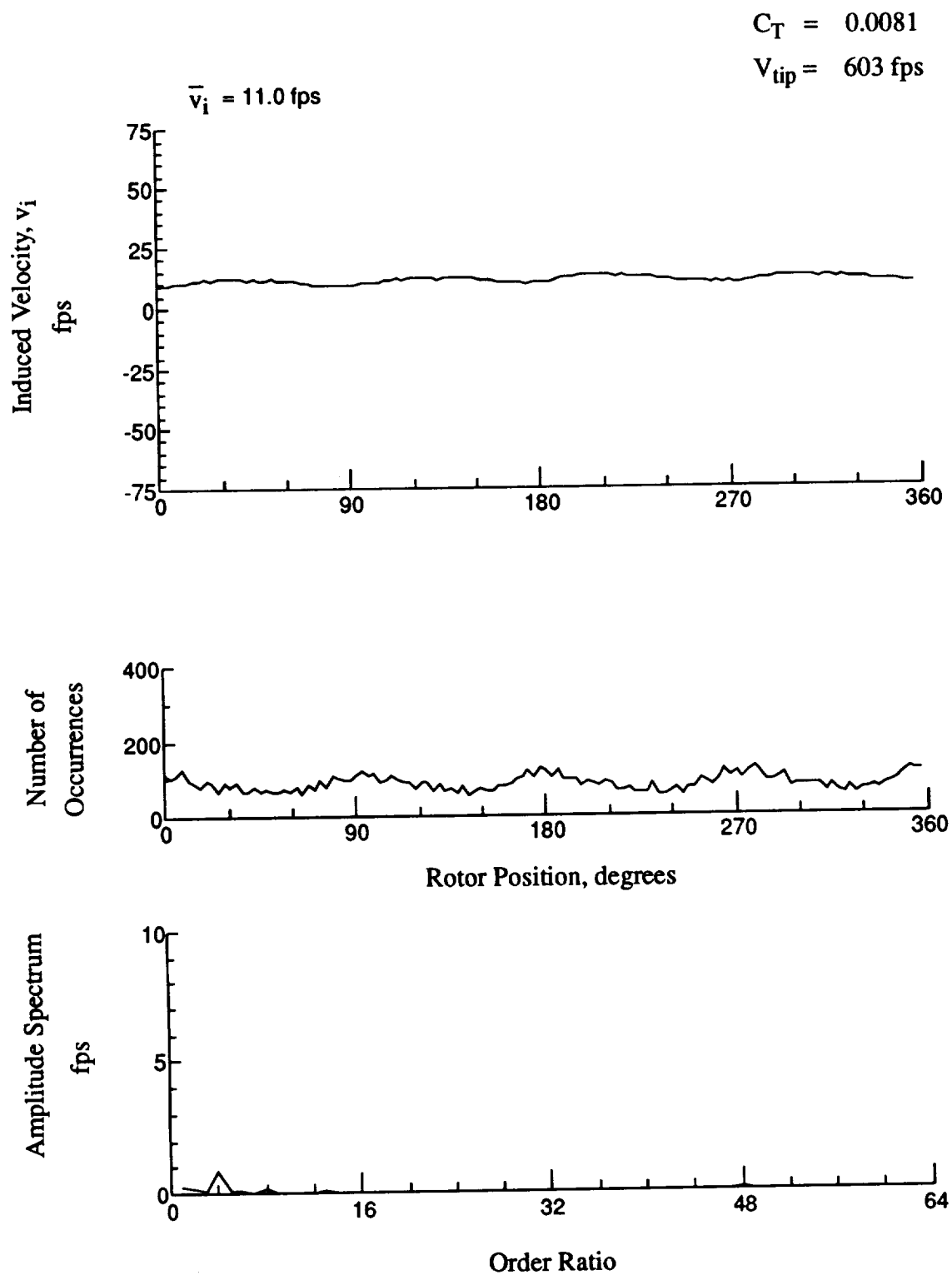


Figure 136.- Concluded.
 $x/R = -0.27$, $y/R = 0.20$, $z = -5.97 \text{ in.}$

$$C_T = 0.0081$$

$$V_{tip} = 603 \text{ fps}$$

$$\bar{u}_i = -11.5 \text{ fps}$$

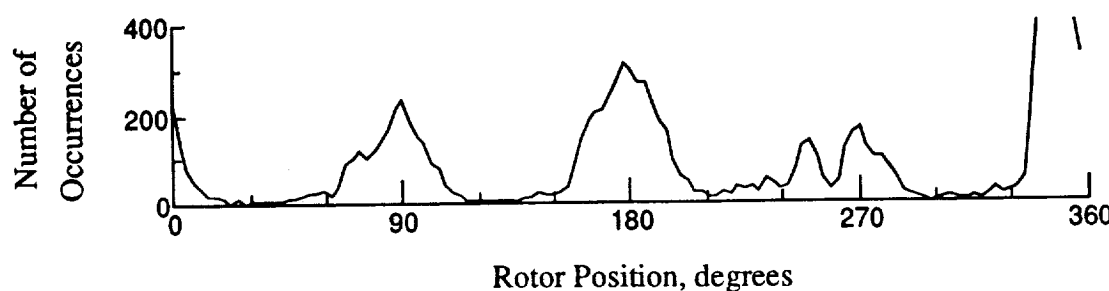
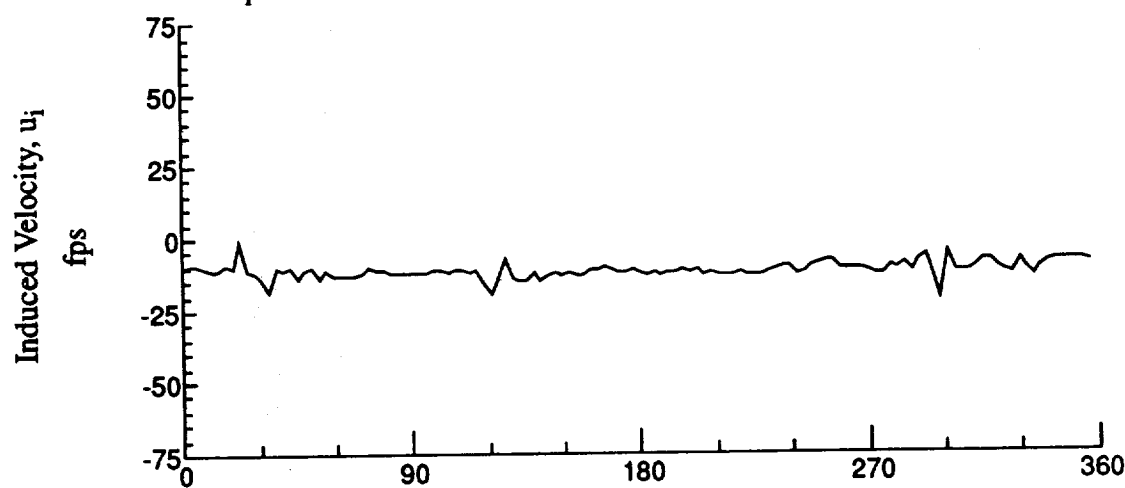


Figure 137.- Wake Measurements at
 $x/R = 0.70$, $y/R = 0.20$, $z = -6.17$ in.

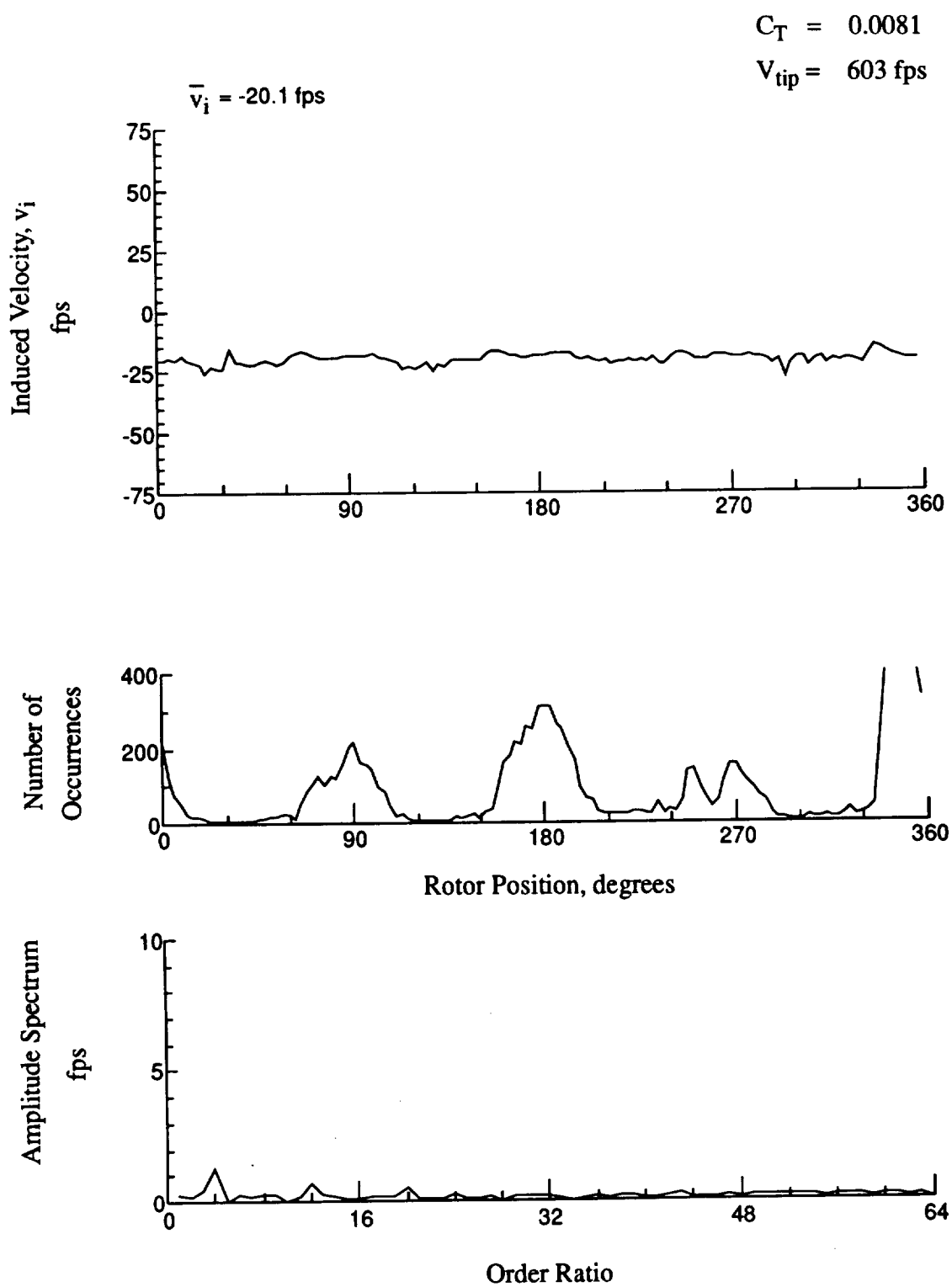


Figure 137.- Concluded.
 $x/R = 0.70$, $y/R = 0.20$, $z = -6.17 \text{ in.}$

$$C_T = 0.0081$$

$$V_{tip} = 603 \text{ fps}$$

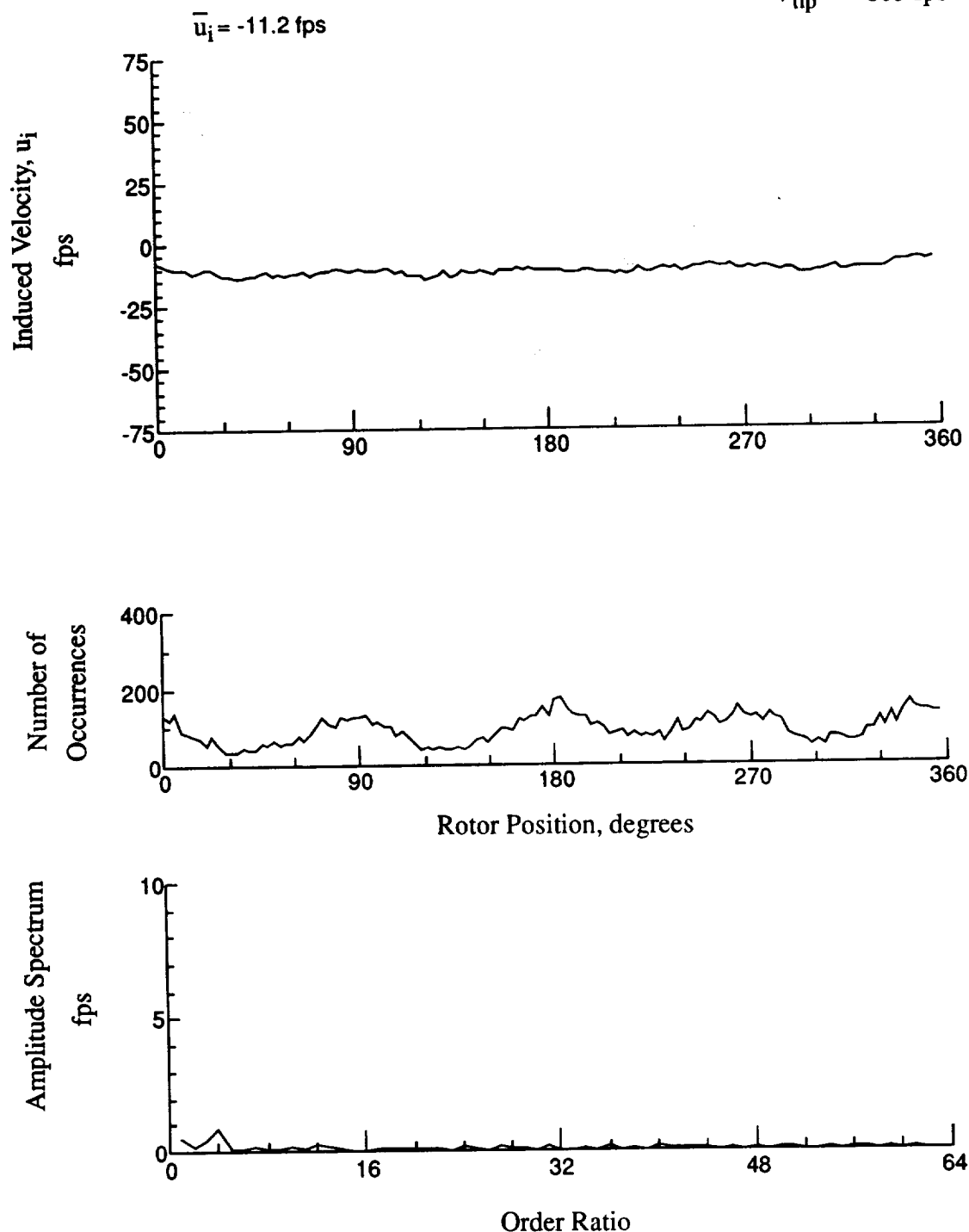


Figure 138.- Wake Measurements at
 $x/R = 0.70$, $y/R = 0.20$, $z = -7.20$ in.

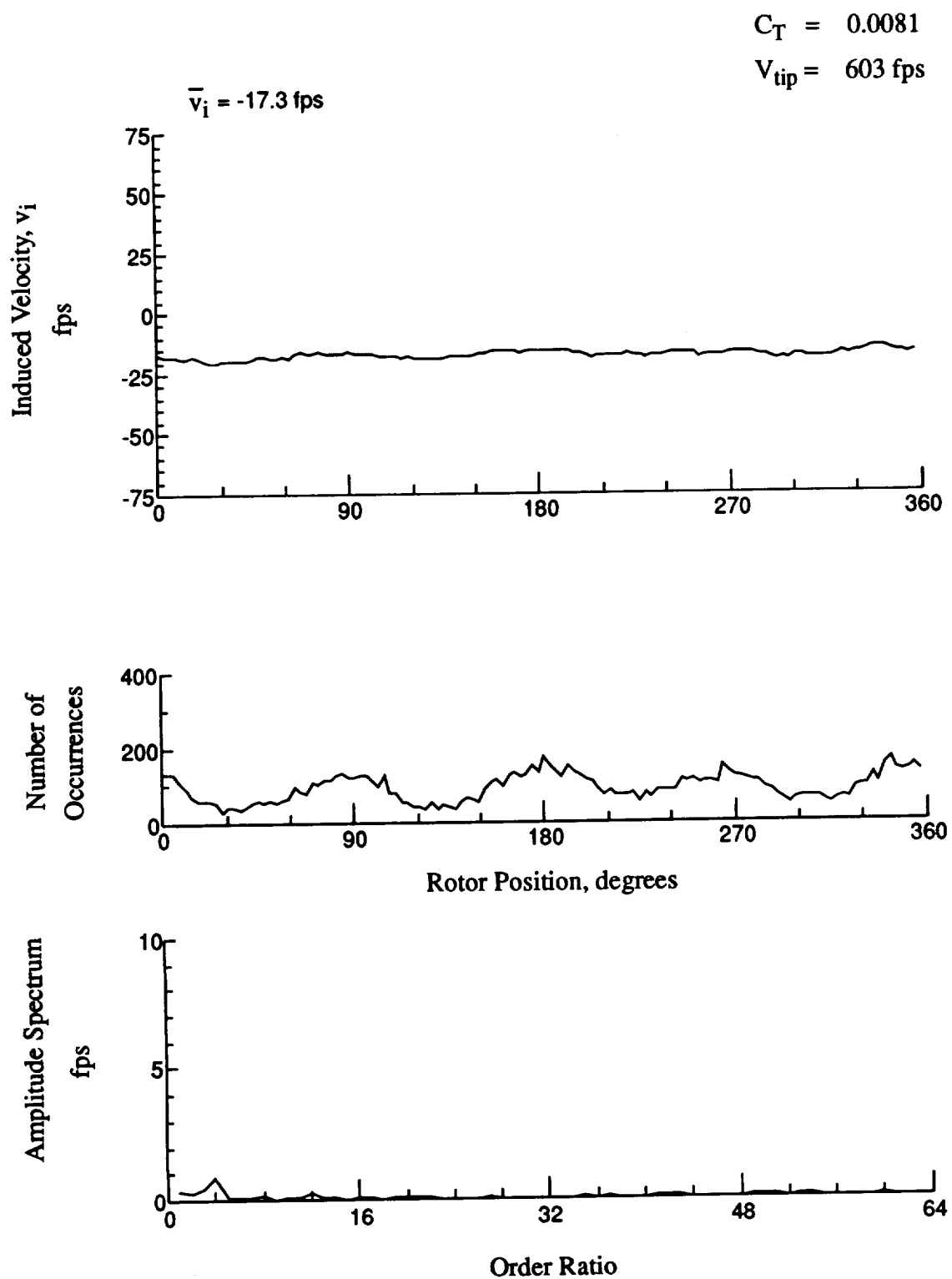


Figure 138.- Concluded.
 $x/R = 0.70$, $y/R = 0.20$, $z = -7.20 \text{ in.}$

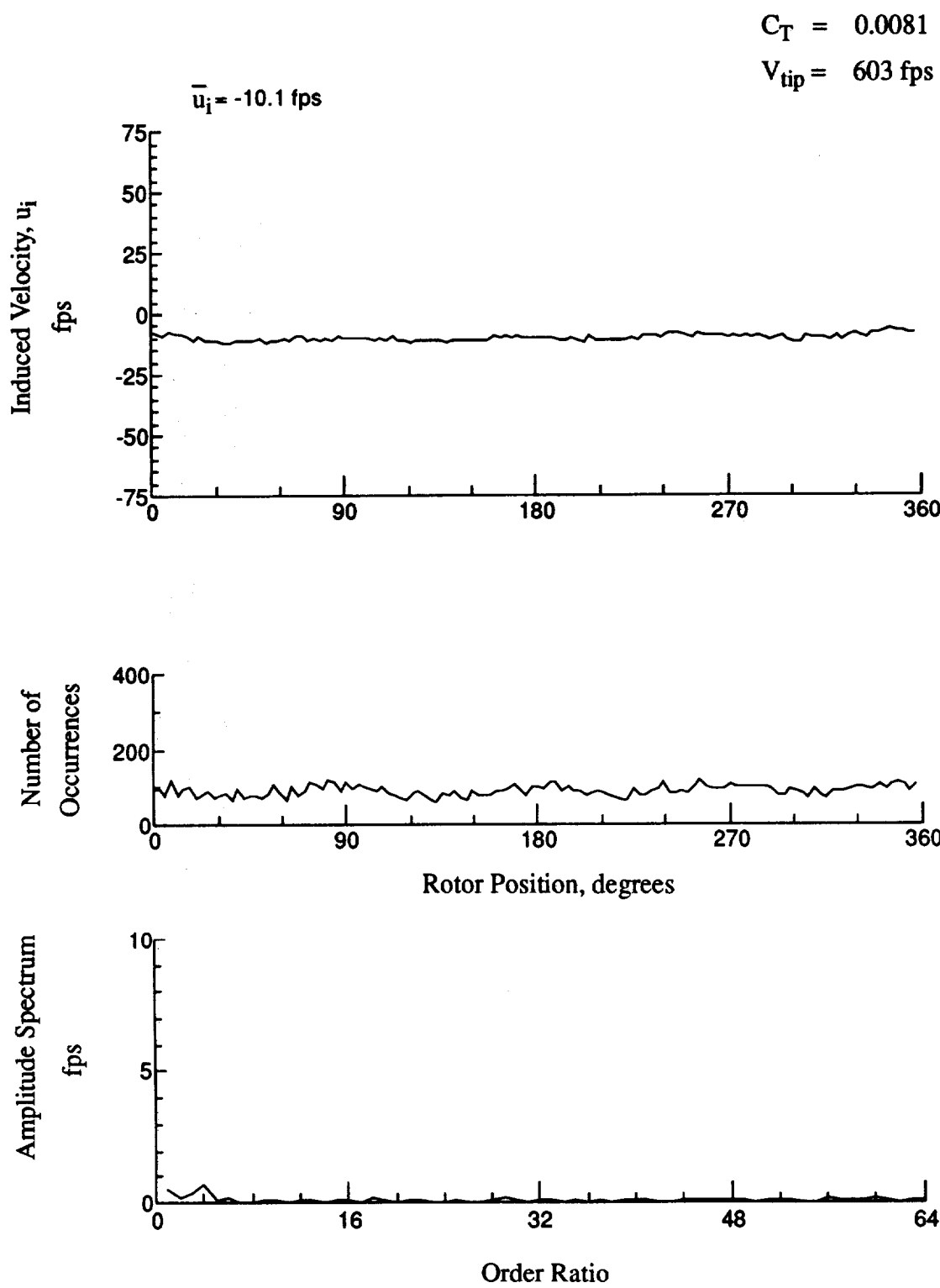


Figure 139.- Wake Measurements at
 $x/R = 0.70$, $y/R = 0.20$, $z = -8.23 \text{ in.}$

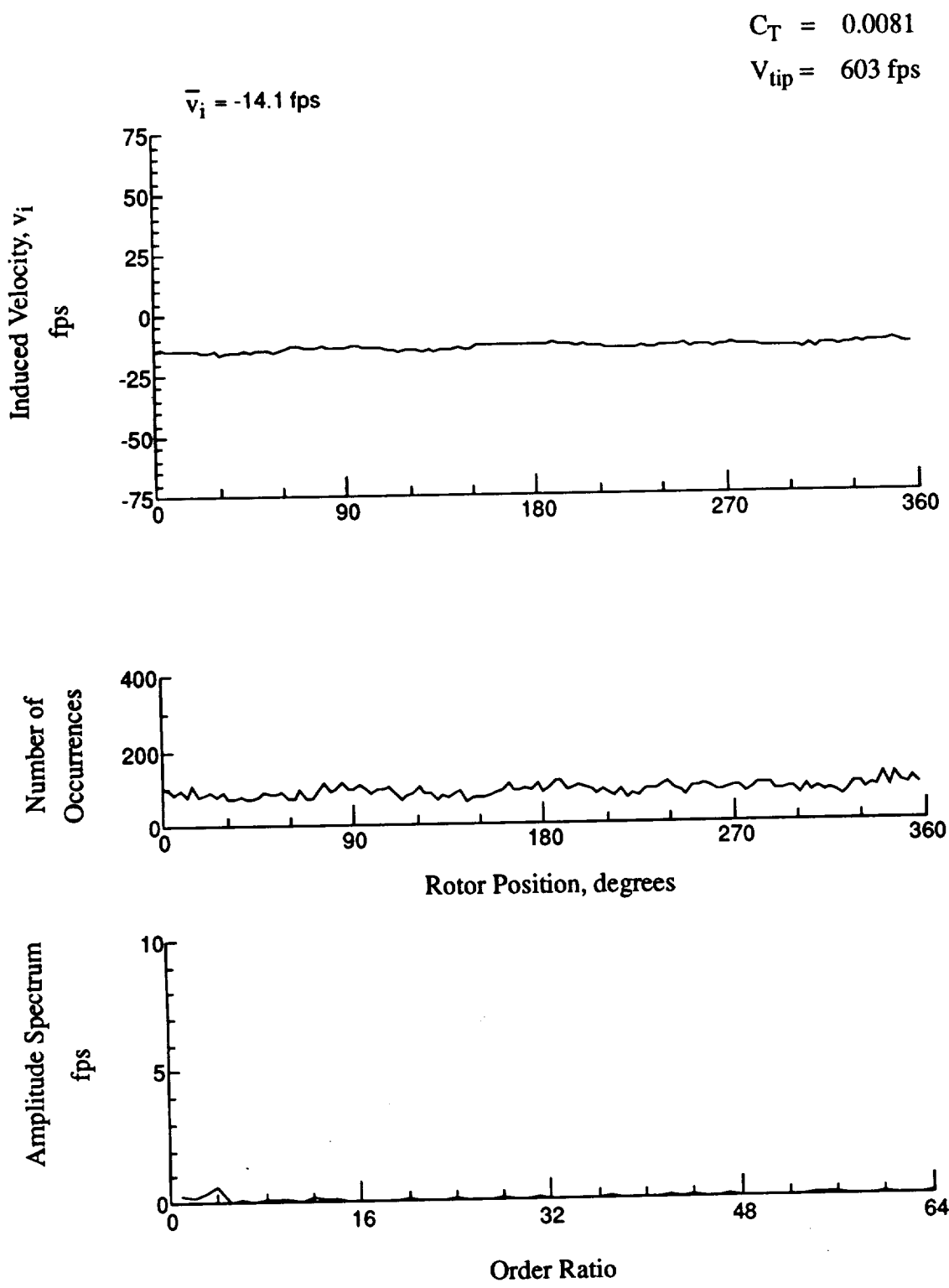


Figure 139.- Concluded.
 $x/R = 0.70$, $y/R = 0.20$, $z = -8.23 \text{ in.}$

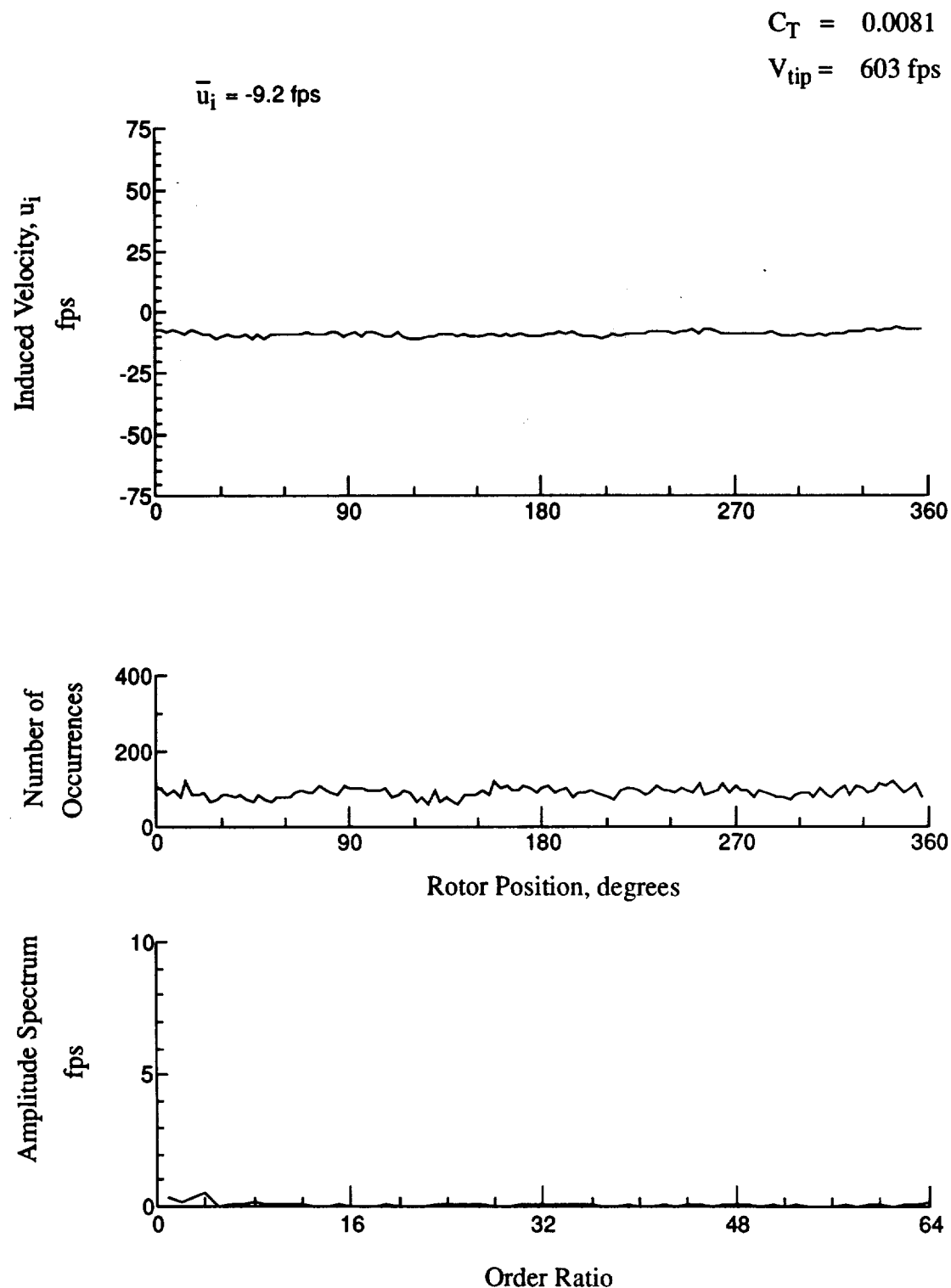


Figure 140.- Wake Measurements at
 $x/R = 0.70$, $y/R = 0.20$, $z = -9.26 \text{ in.}$

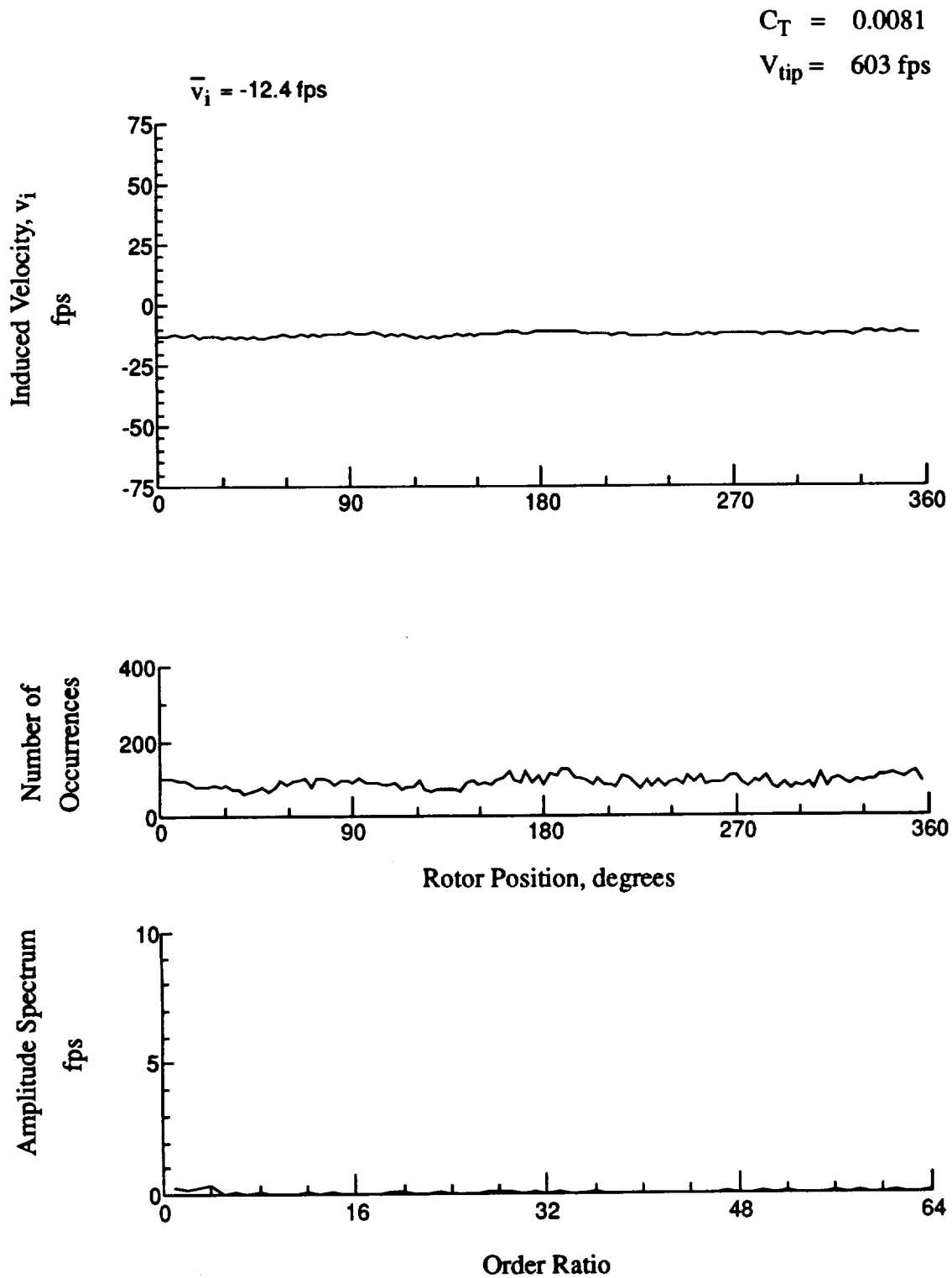


Figure 140.- Concluded.
 $x/R = 0.70$, $y/R = 0.20$, $z = -9.26 \text{ in.}$

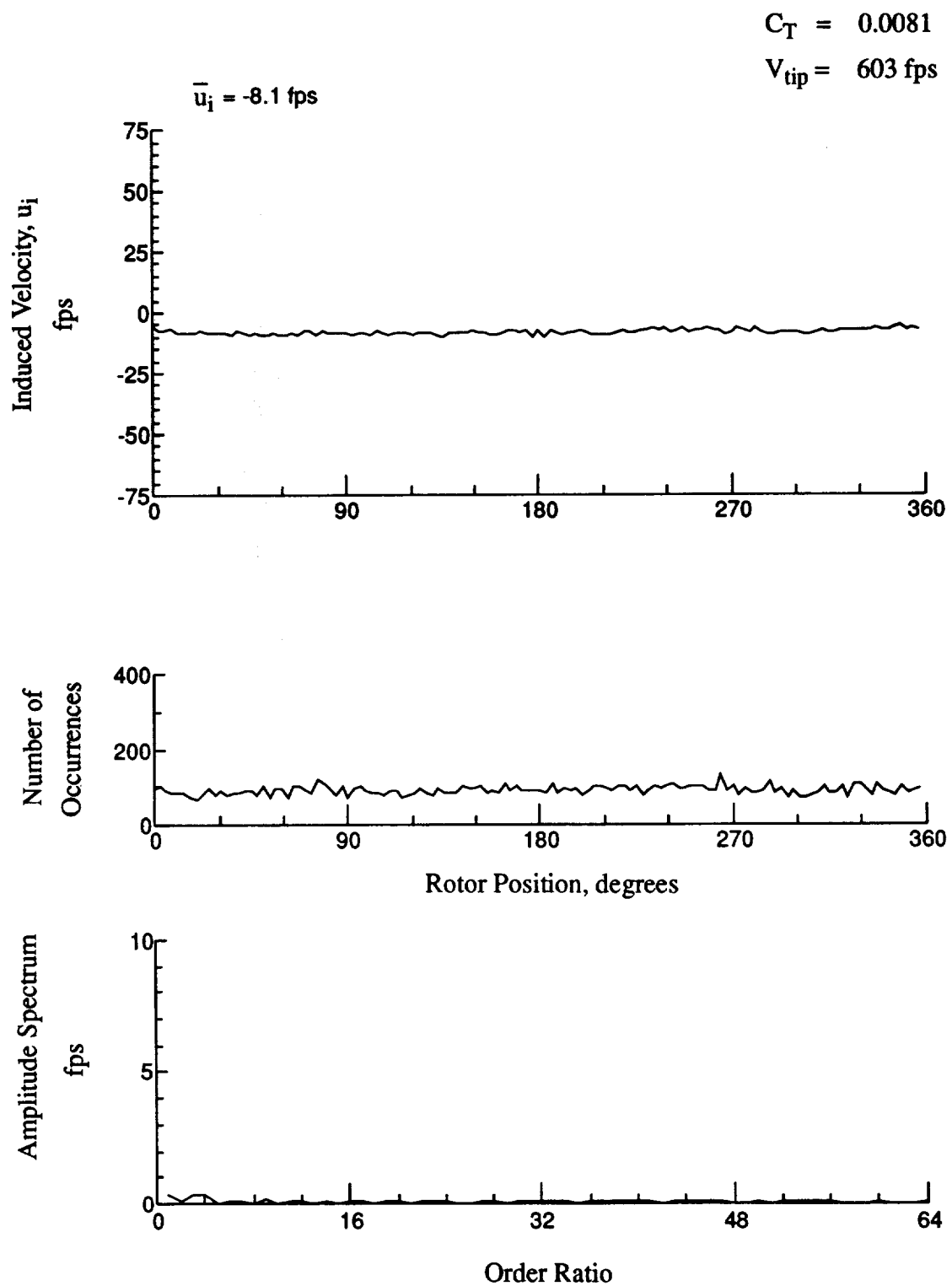


Figure 141.- Wake Measurements at
 $x/R = 0.70$, $y/R = 0.20$, $z = -10.29 \text{ in.}$

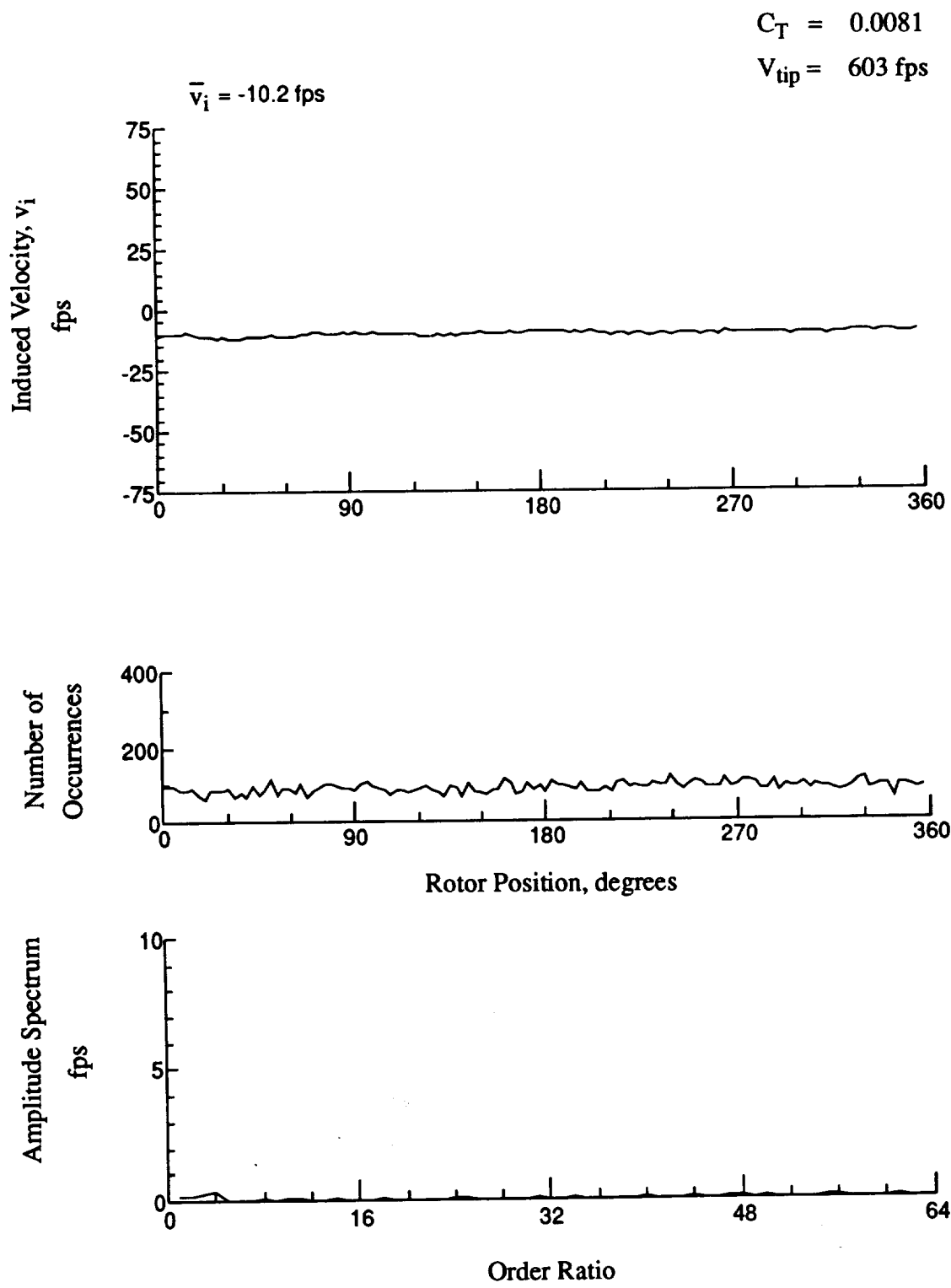


Figure 141.- Concluded.
 $x/R = 0.70$, $y/R = 0.20$, $z = -10.29 \text{ in.}$

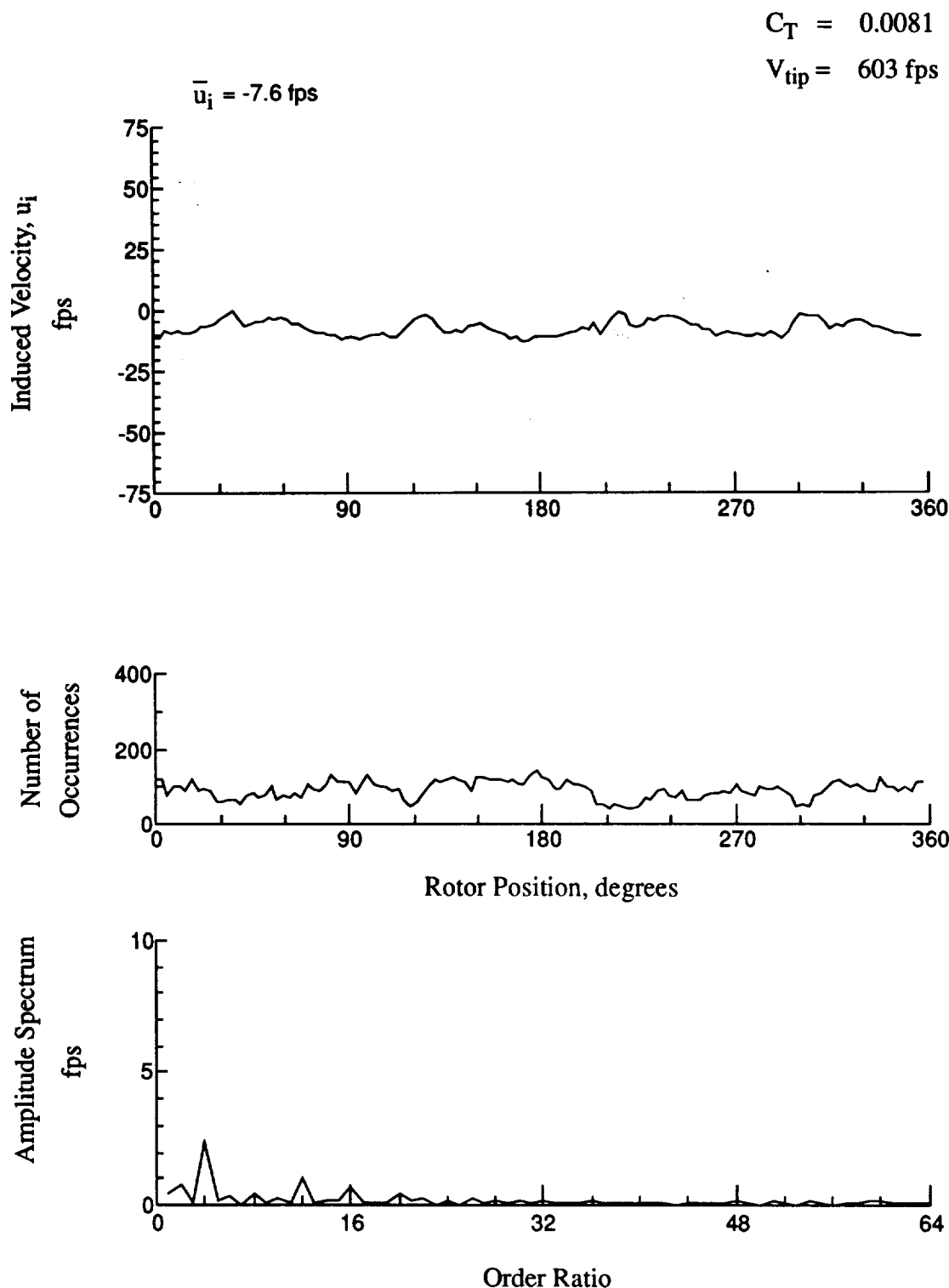


Figure 142.- Wake Measurements at
 $x/R = 1.10$, $y/R = 0.20$, $z = -6.51 \text{ in.}$

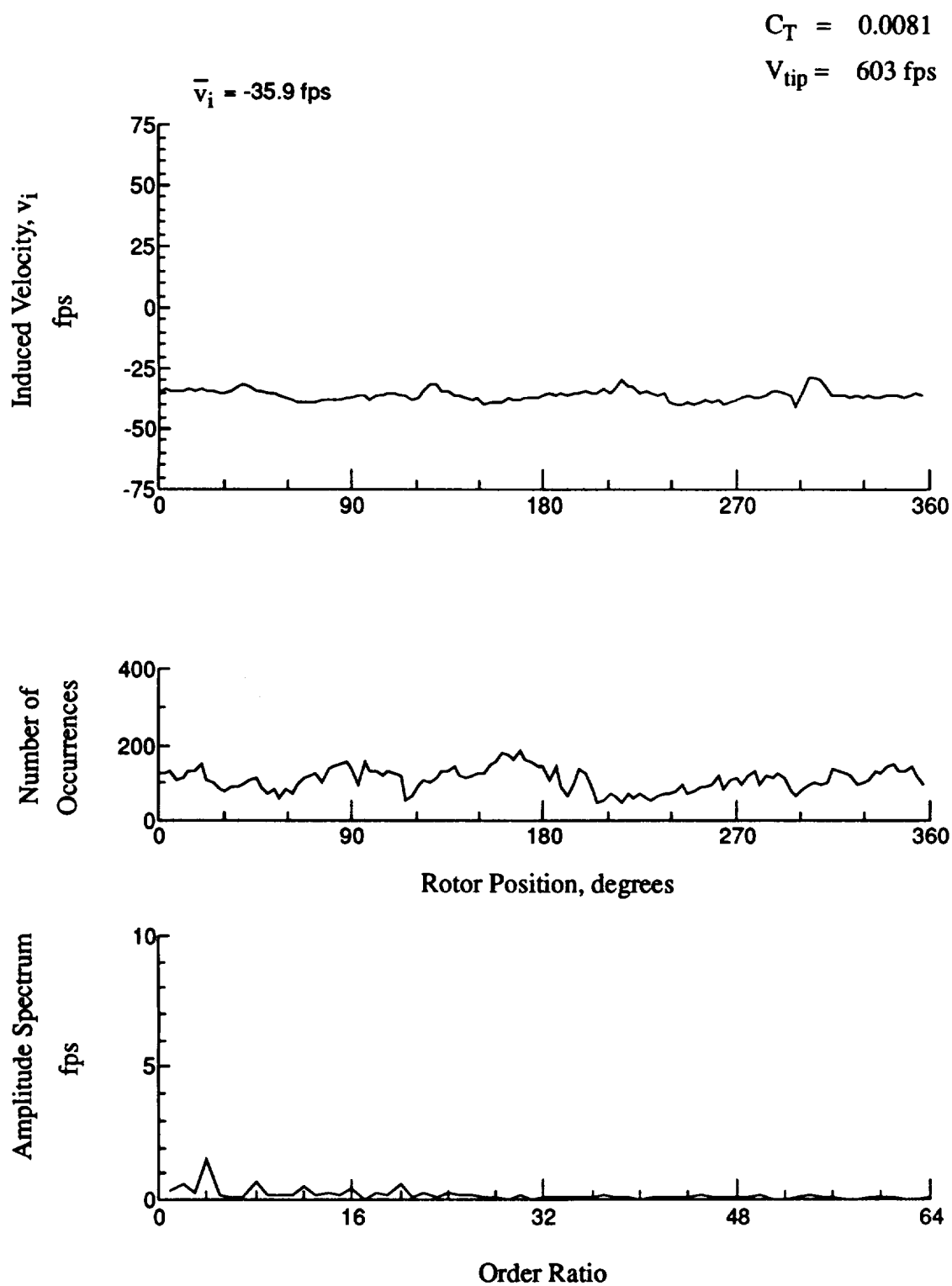


Figure 142.- Concluded.

$x/R = 1.10$, $y/R = 0.20$, $z = -6.51 \text{ in.}$

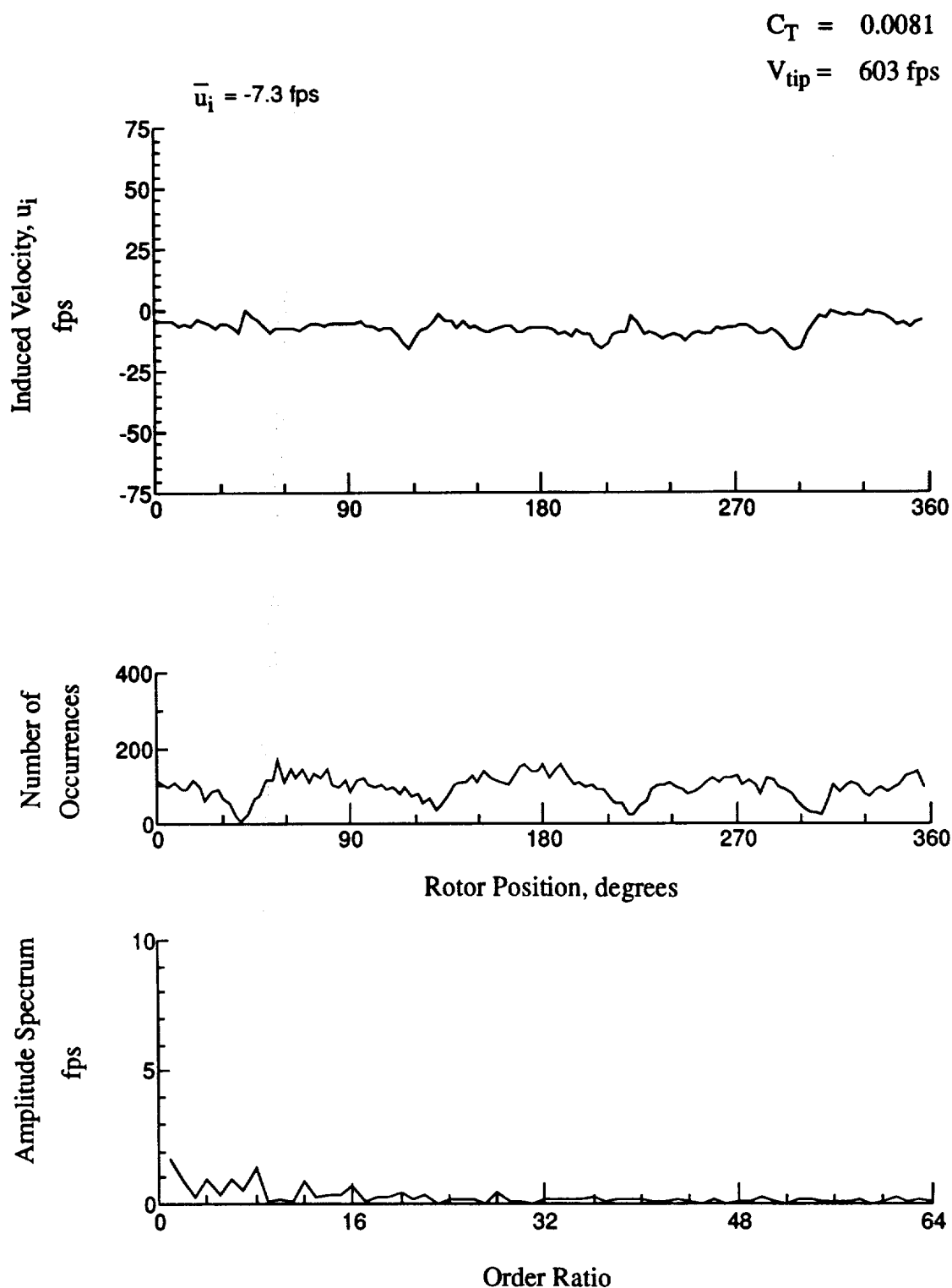


Figure 143.- Wake Measurements at
 $x/R = 1.10$, $y/R = 0.20$, $z = -7.54 \text{ in.}$

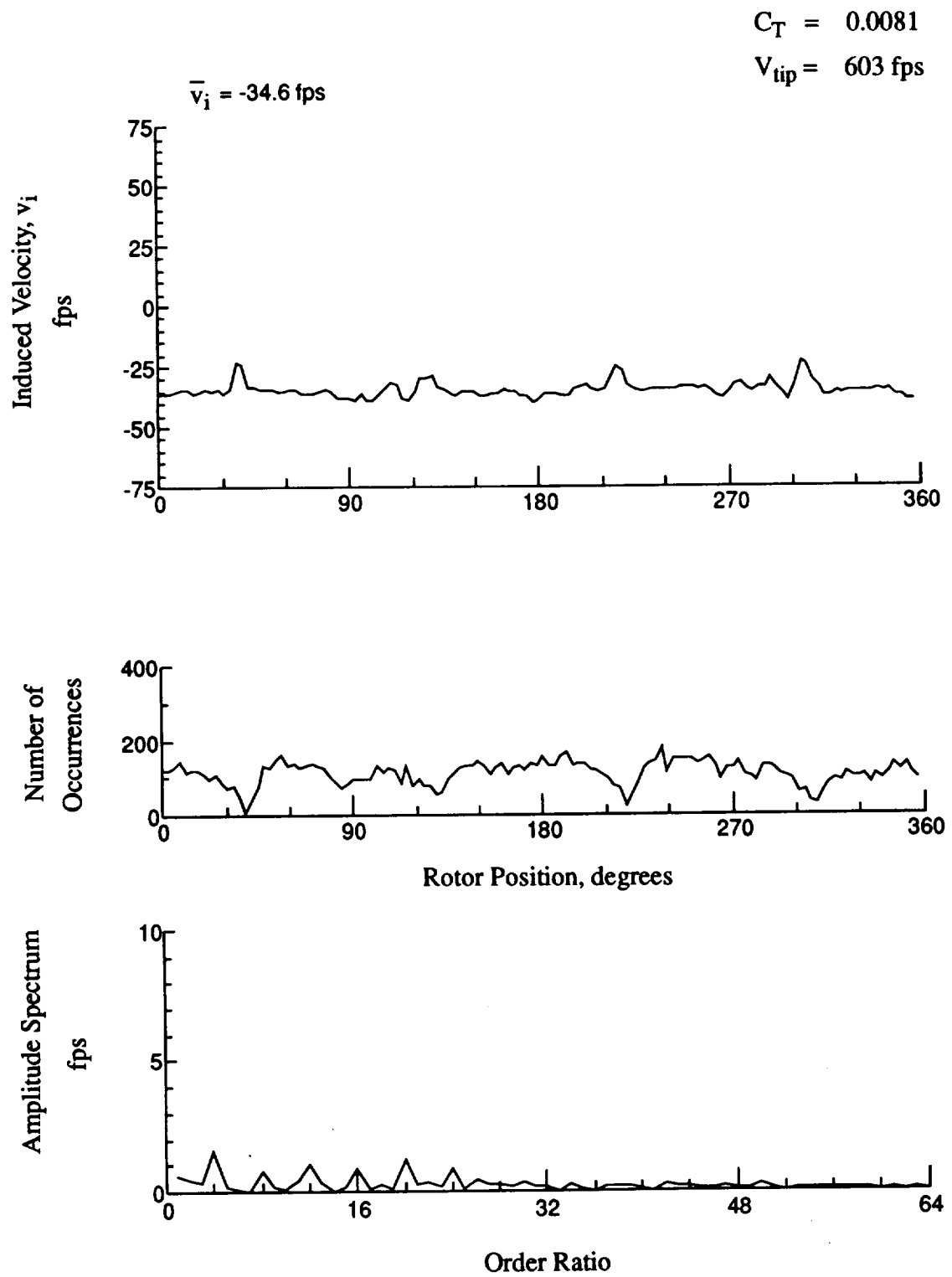


Figure 143.- Concluded.
 $x/R = 1.10$, $y/R = 0.20$, $z = -7.54 \text{ in.}$

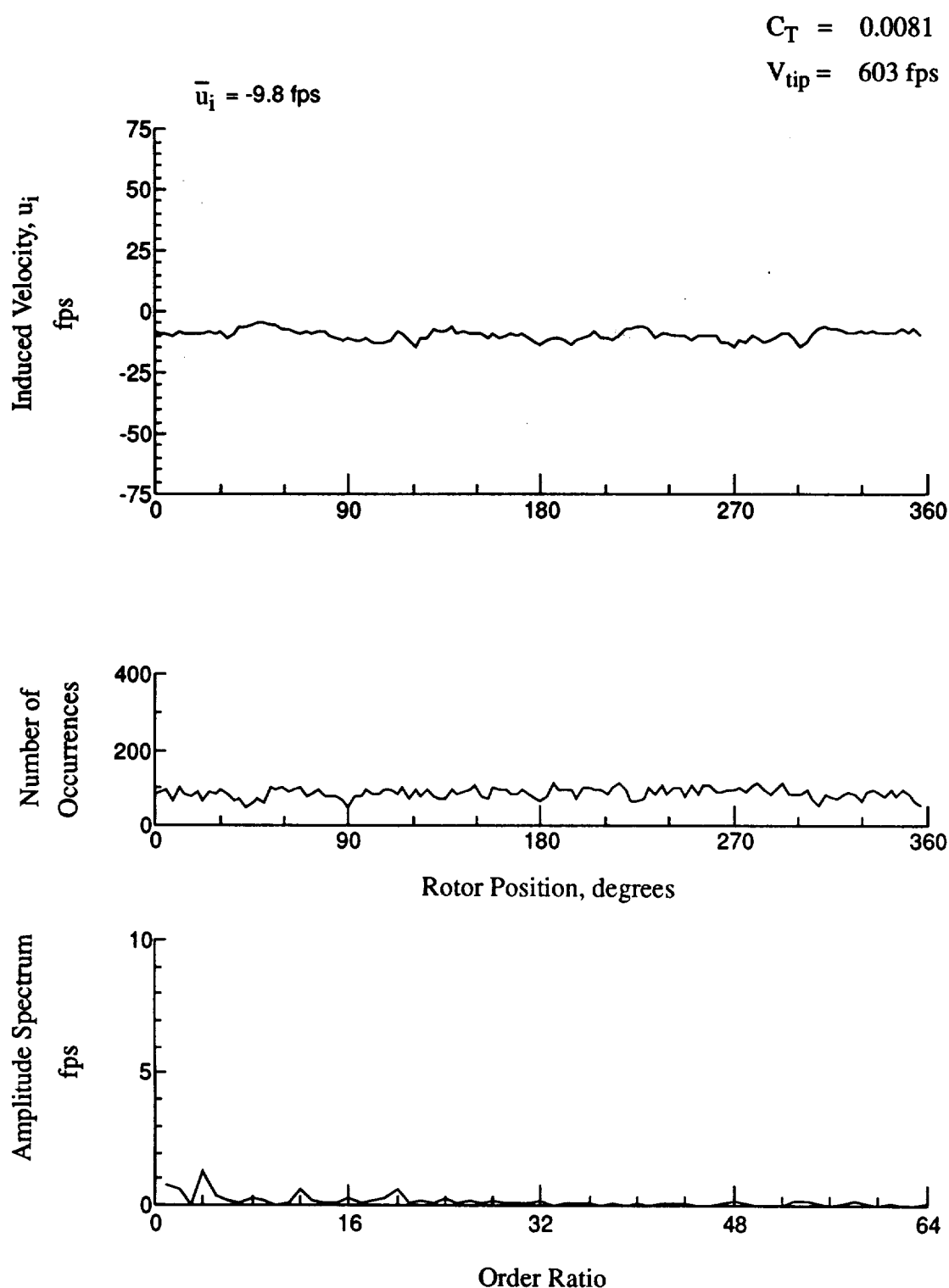


Figure 144.- Wake Measurements at
 $x/R = 1.10$, $y/R = 0.20$, $z = -8.57 \text{ in.}$

$$C_T = 0.0081$$

$$V_{tip} = 603 \text{ fps}$$

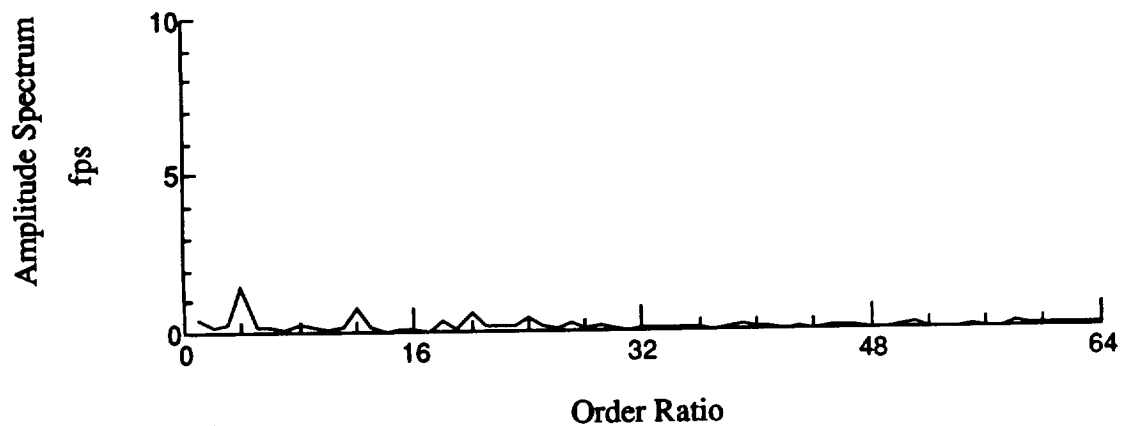
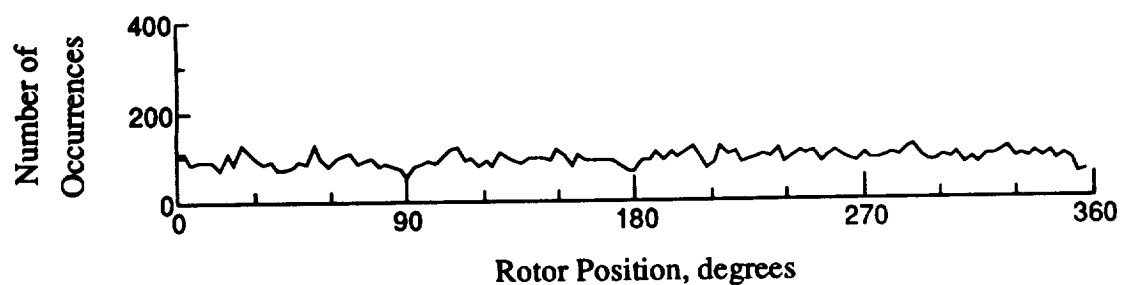
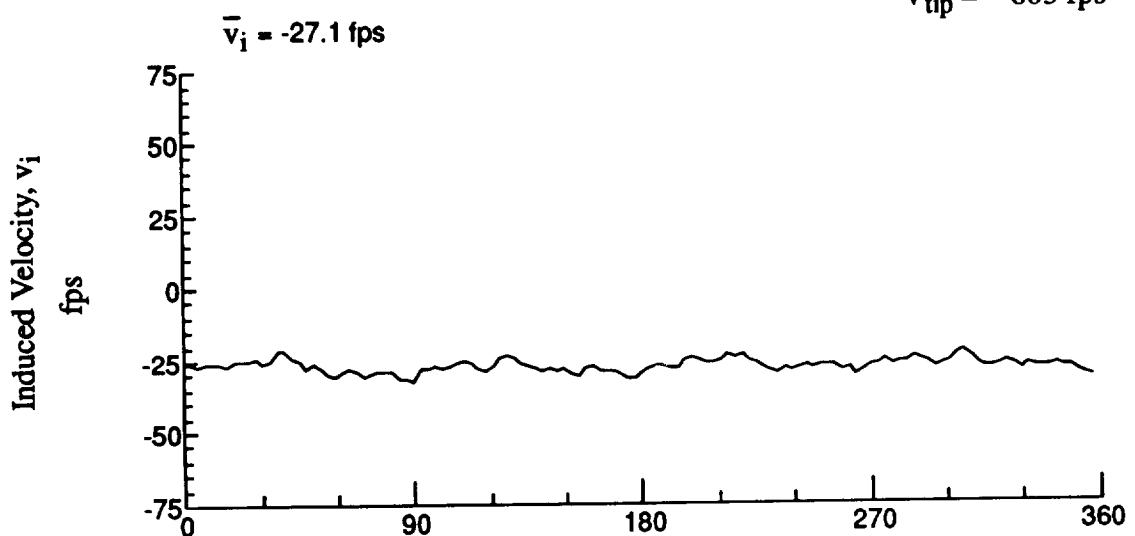
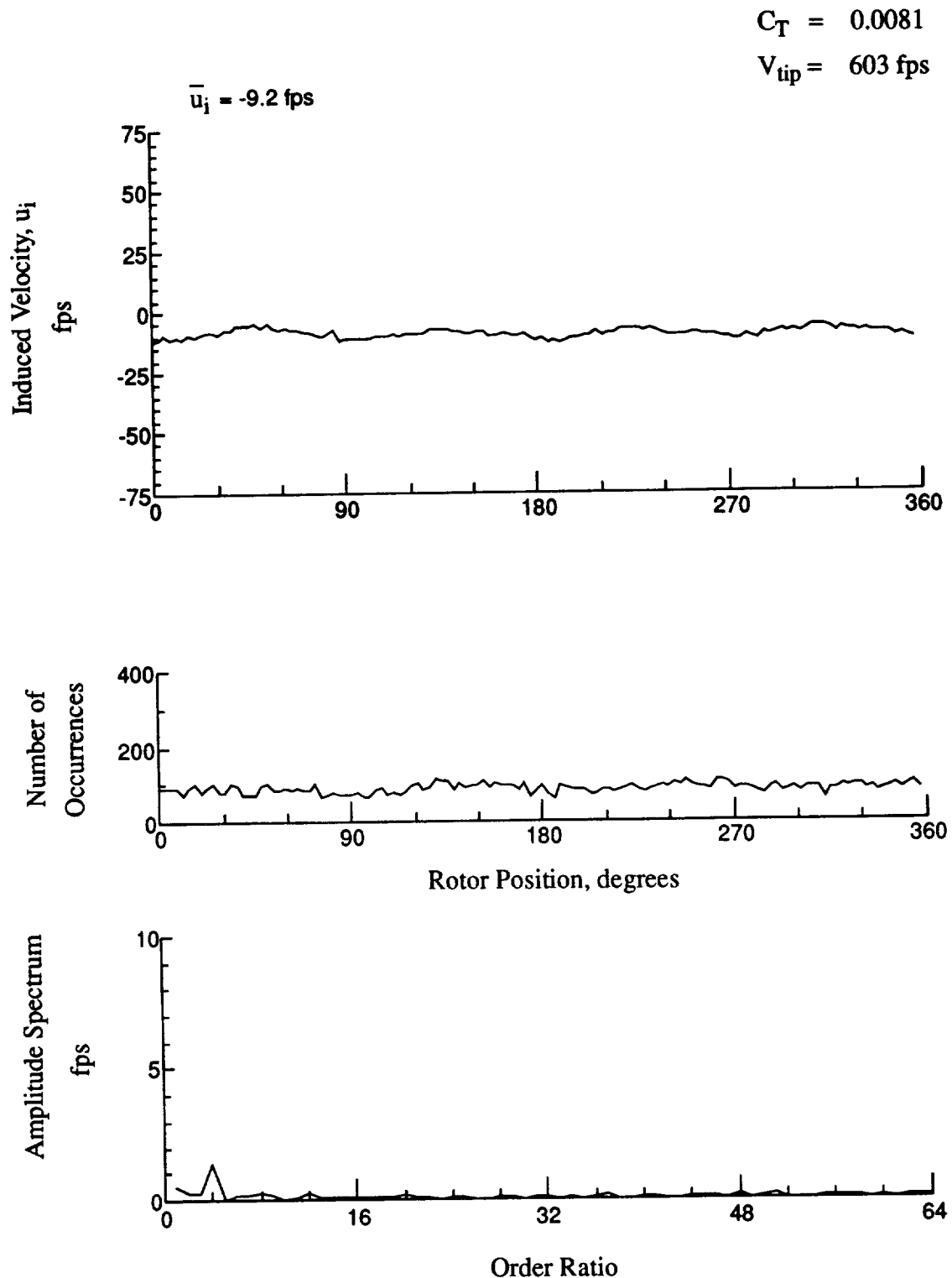


Figure 144.- Concluded.
 $x/R = 1.10$, $y/R = 0.20$, $z = -8.57 \text{ in.}$



**Figure 145.- Wake Measurements at
 $x/R = 1.10$, $y/R = 0.20$, $z = -9.60 \text{ in.}$**

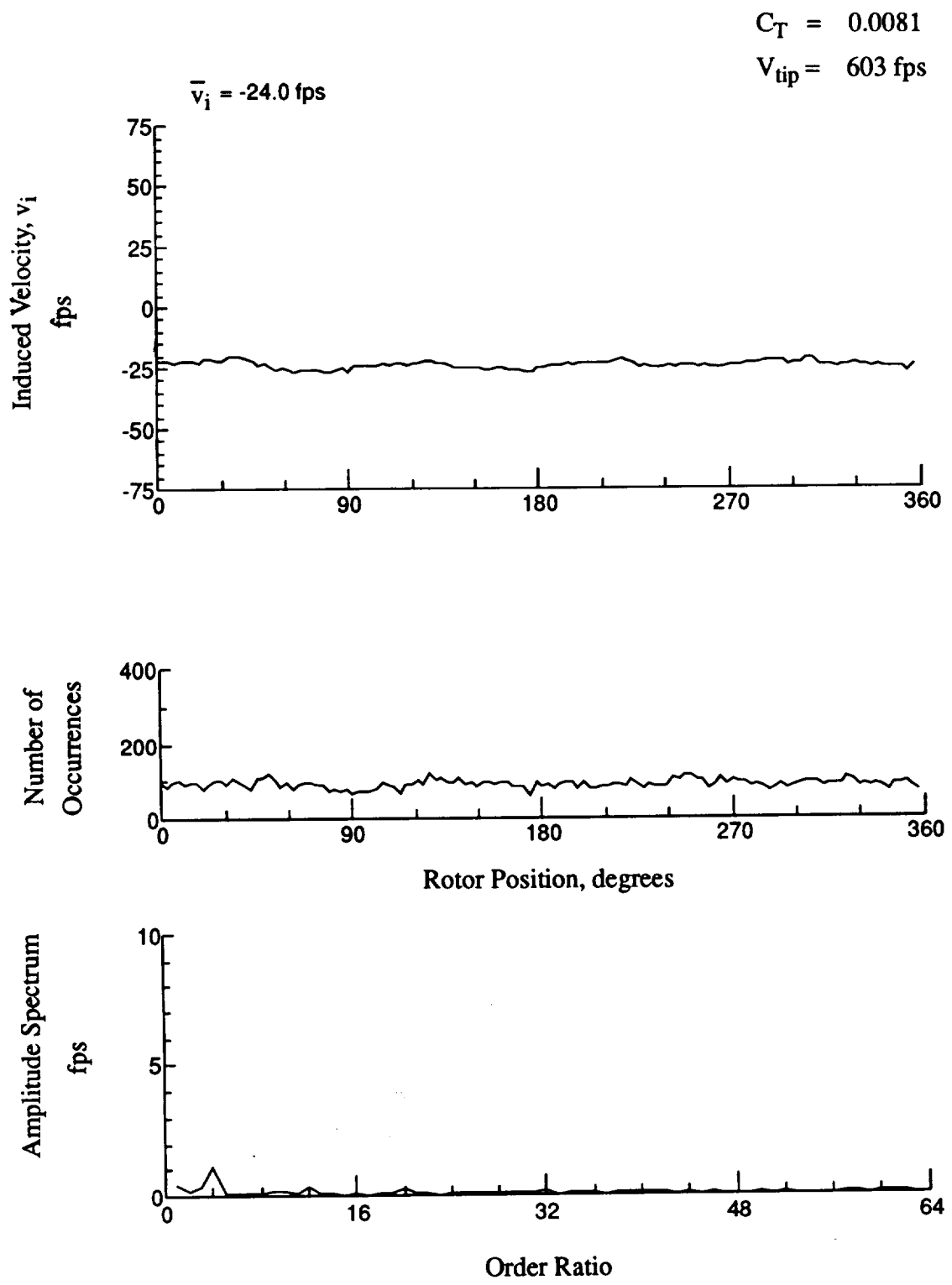


Figure 145.- Concluded.
 $x/R = 1.10$, $y/R = 0.20$, $z = -9.60 \text{ in.}$

$$C_T = 0.0081$$

$$V_{tip} = 603 \text{ fps}$$

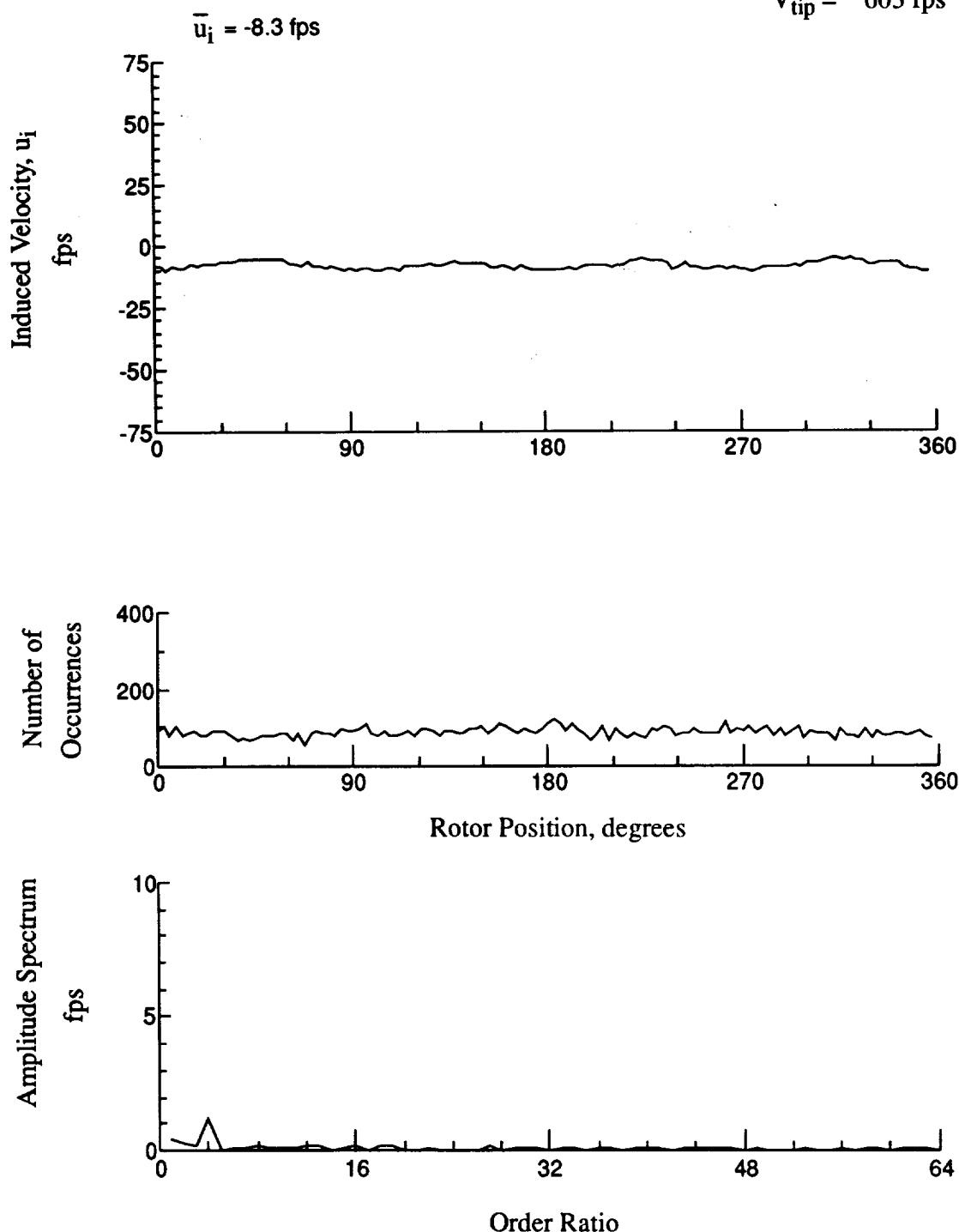


Figure 146.- Wake Measurements at
 $x/R = 1.10$, $y/R = 0.20$, $z = -10.63 \text{ in.}$

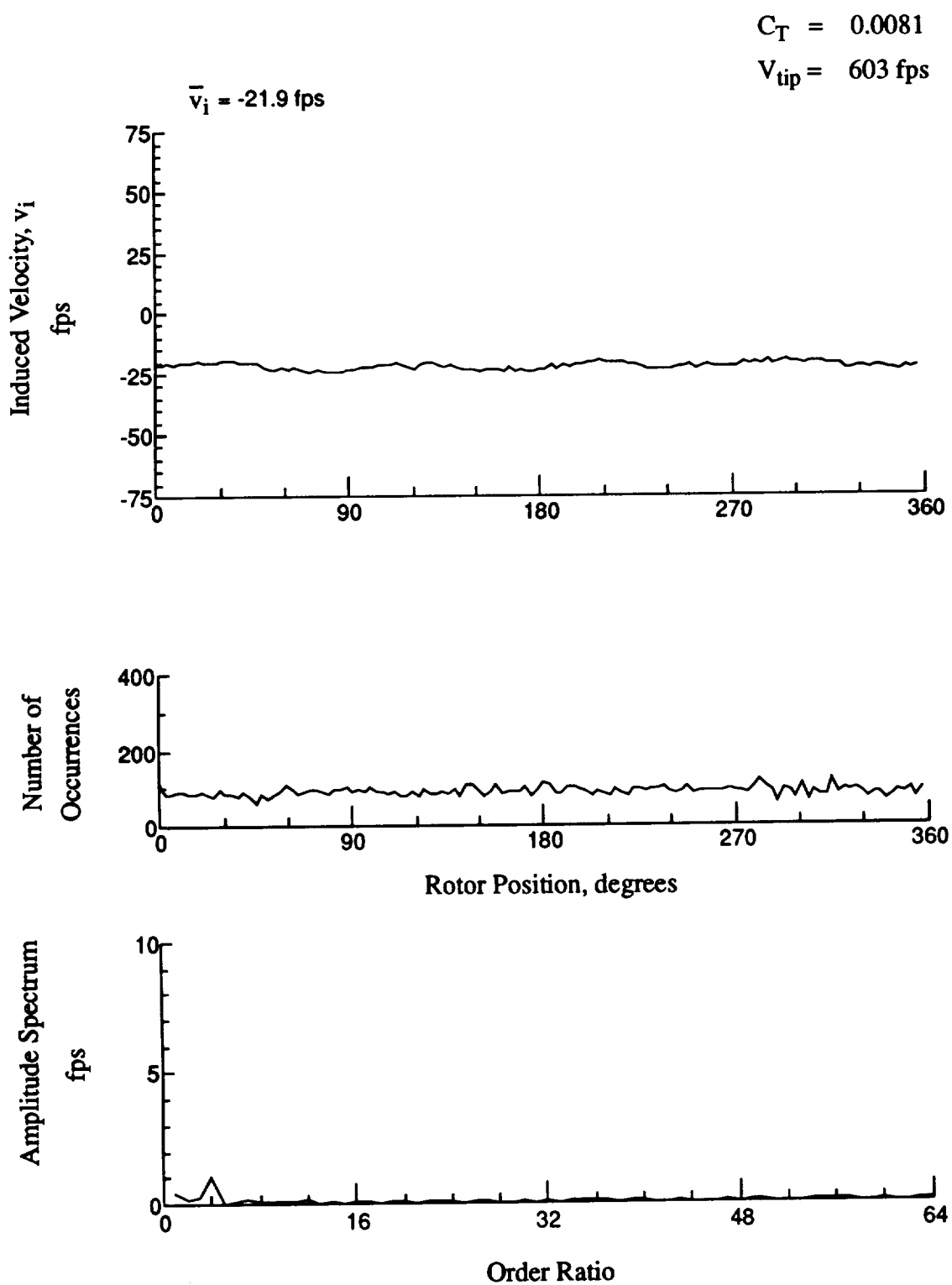
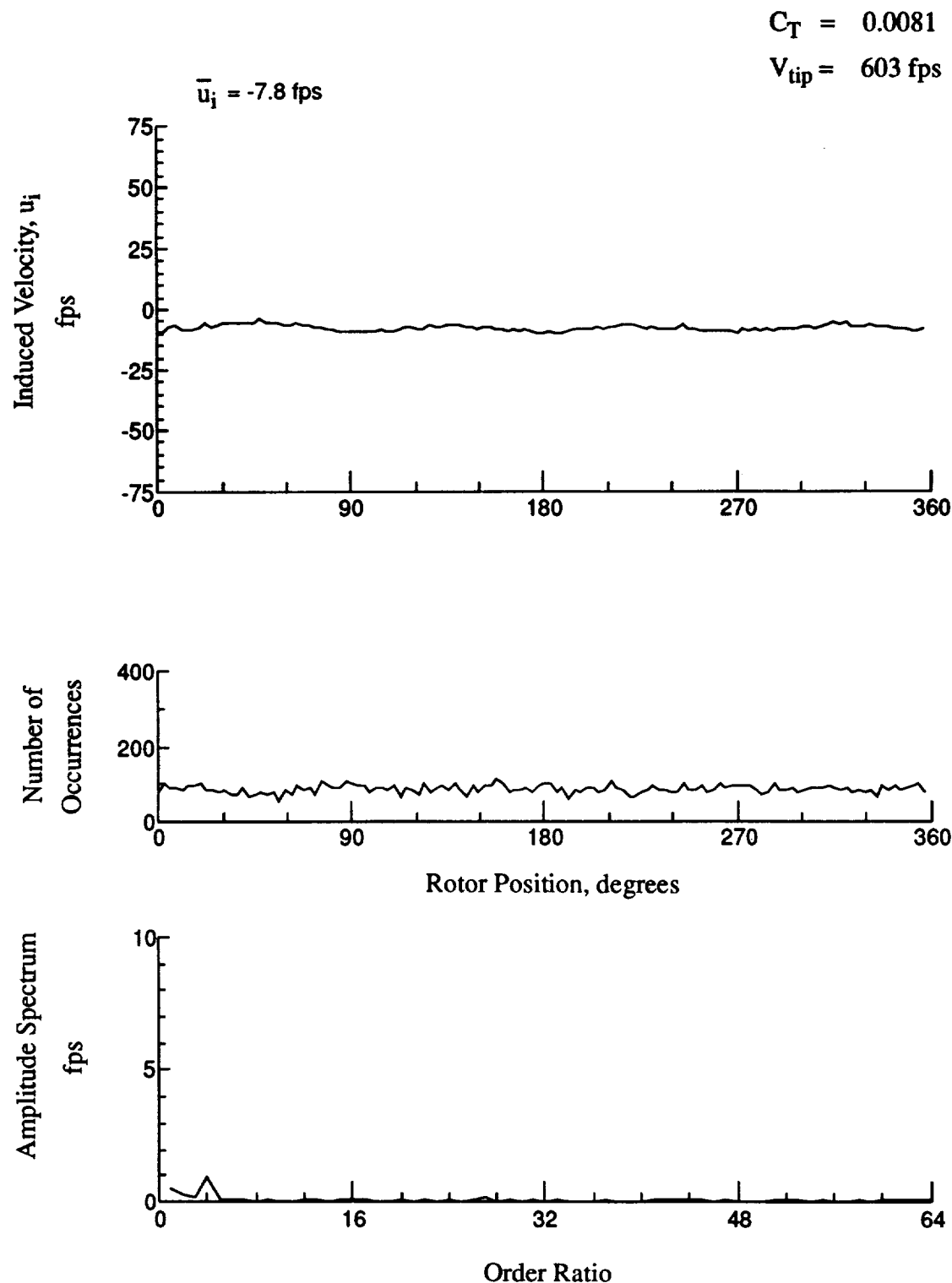


Figure 146.- Concluded.
 $x/R = 1.10$, $y/R = 0.20$, $z = -10.63 \text{ in.}$



**Figure 147.- Wake Measurements at
 $x/R = 1.10$, $y/R = 0.20$, $z = -11.66 \text{ in.}$**

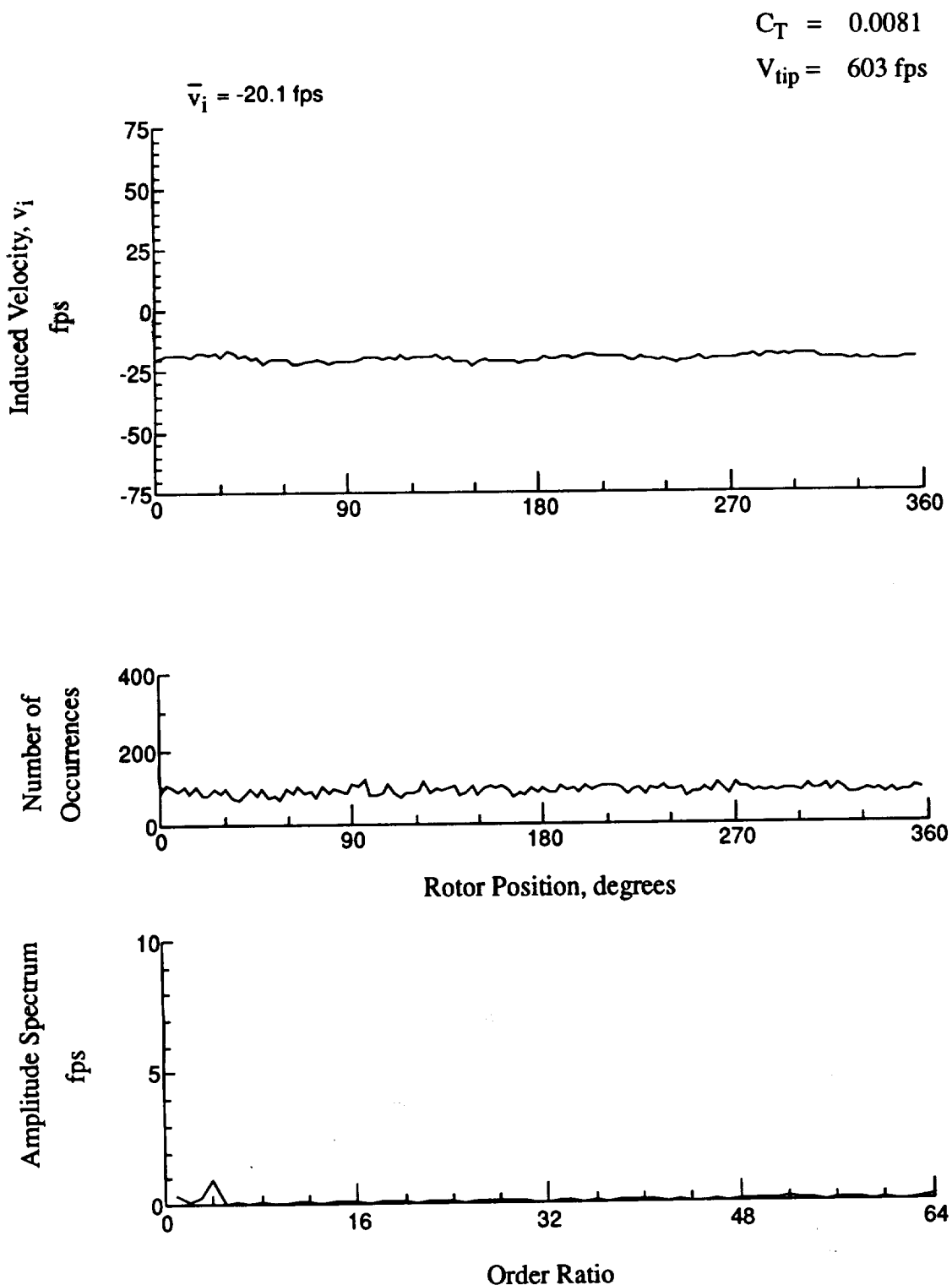


Figure 147.- Concluded.
 $x/R = 1.10$, $y/R = 0.20$, $z = -11.66 \text{ in.}$

$$C_T = 0.0081$$

$$V_{tip} = 603 \text{ fps}$$

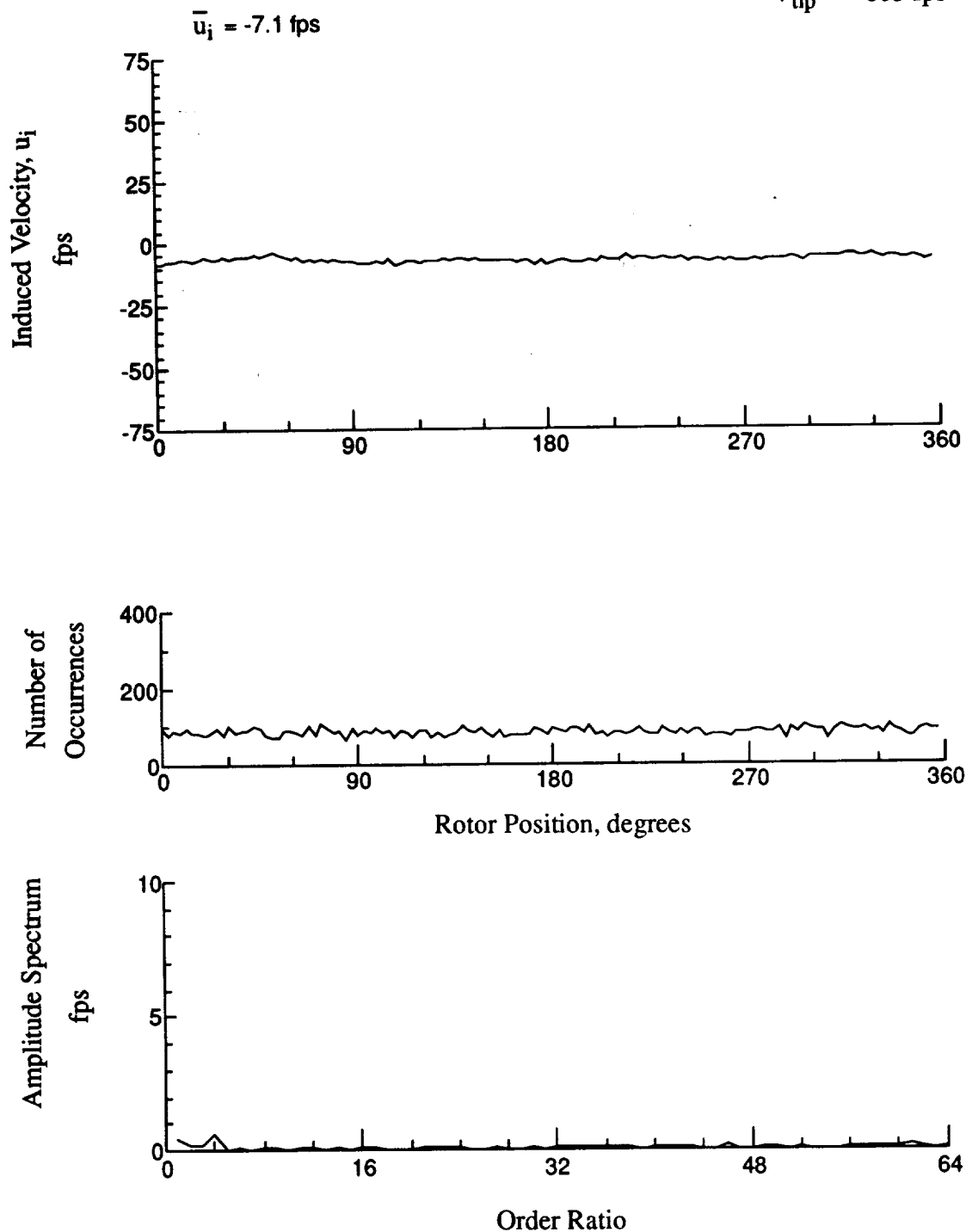


Figure 148.- Wake Measurements at
 $x/R = 1.10$, $y/R = 0.20$, $z = -12.64$ in.

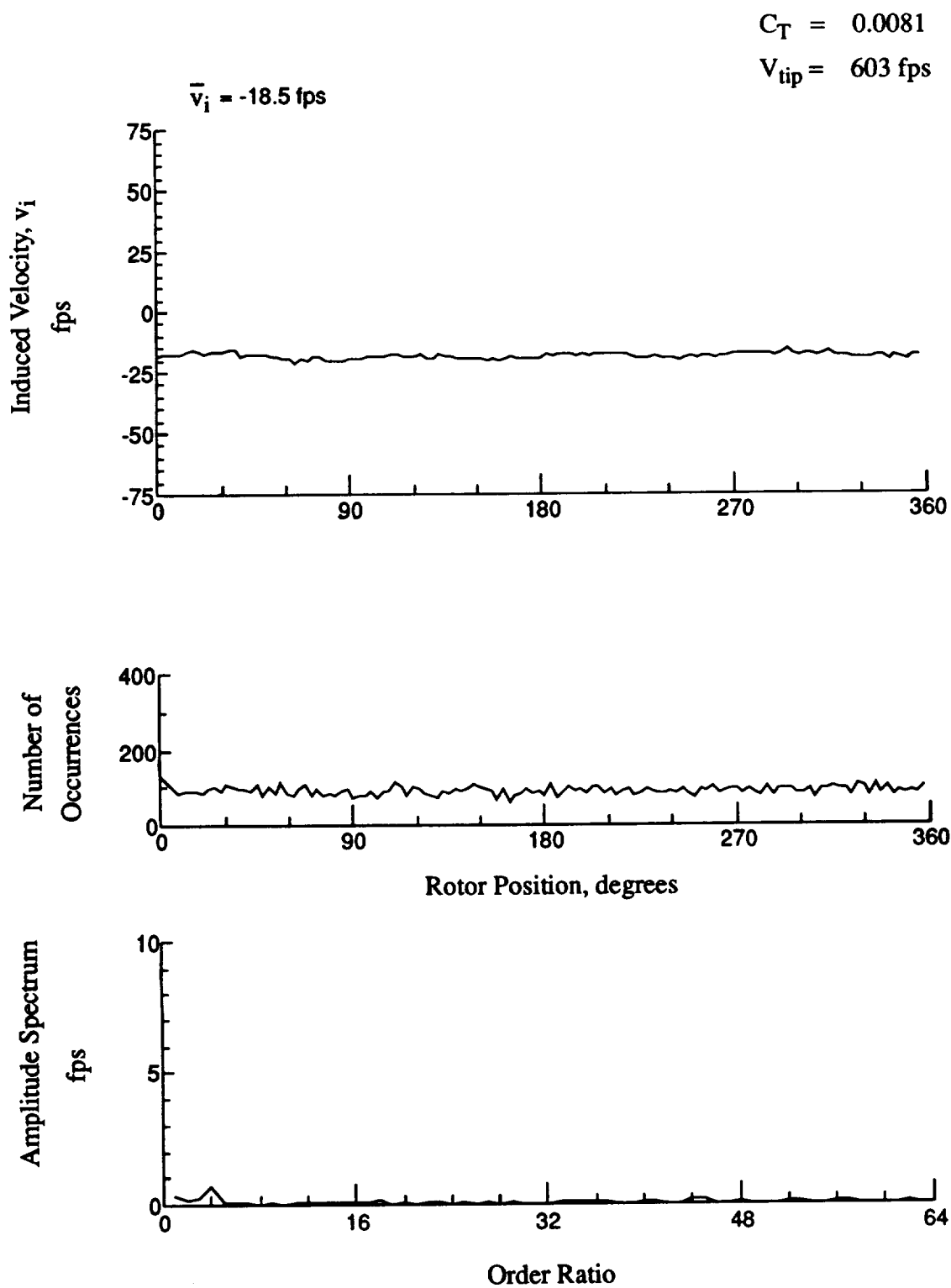


Figure 148.- Concluded.
 $x/R = 1.10$, $y/R = 0.20$, $z = -12.64 \text{ in.}$

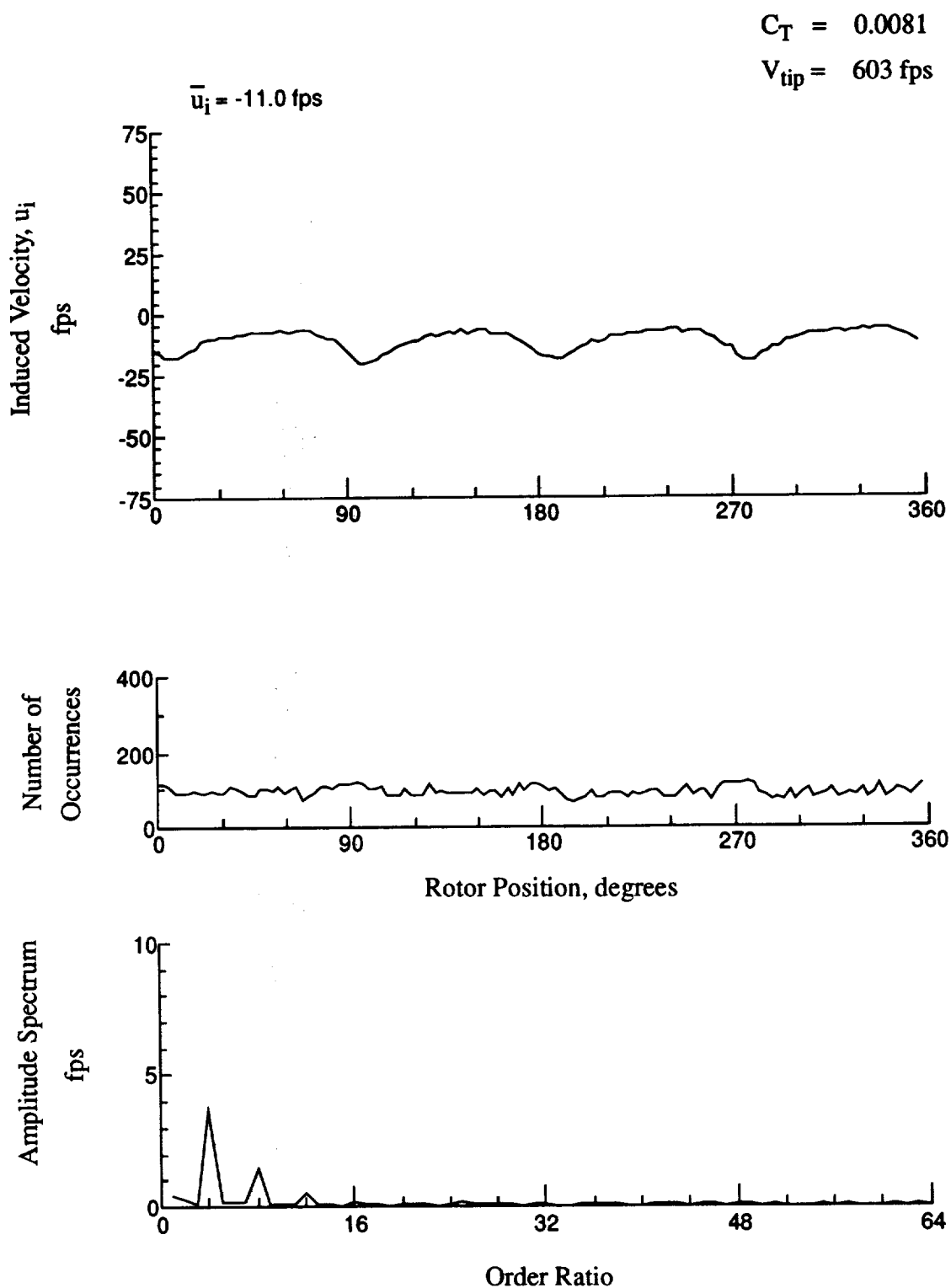


Figure 149.- Wake Measurements at
 $x/R = 1.50$, $y/R = 0.20$, $z = 6.93 \text{ in.}$

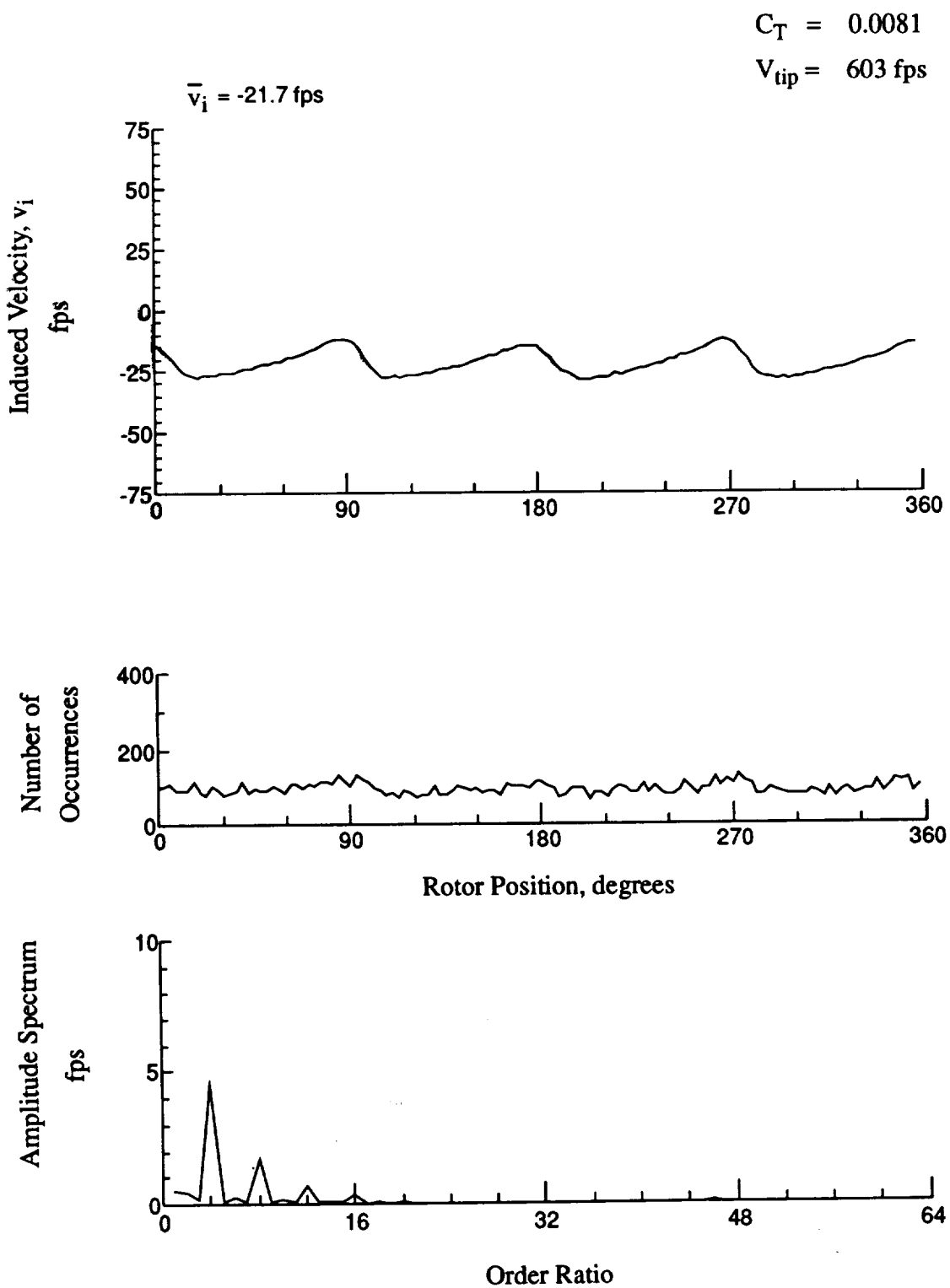


Figure 149.- Concluded.
 $x/R = 1.50$, $y/R = 0.20$, $z = 6.93 \text{ in.}$

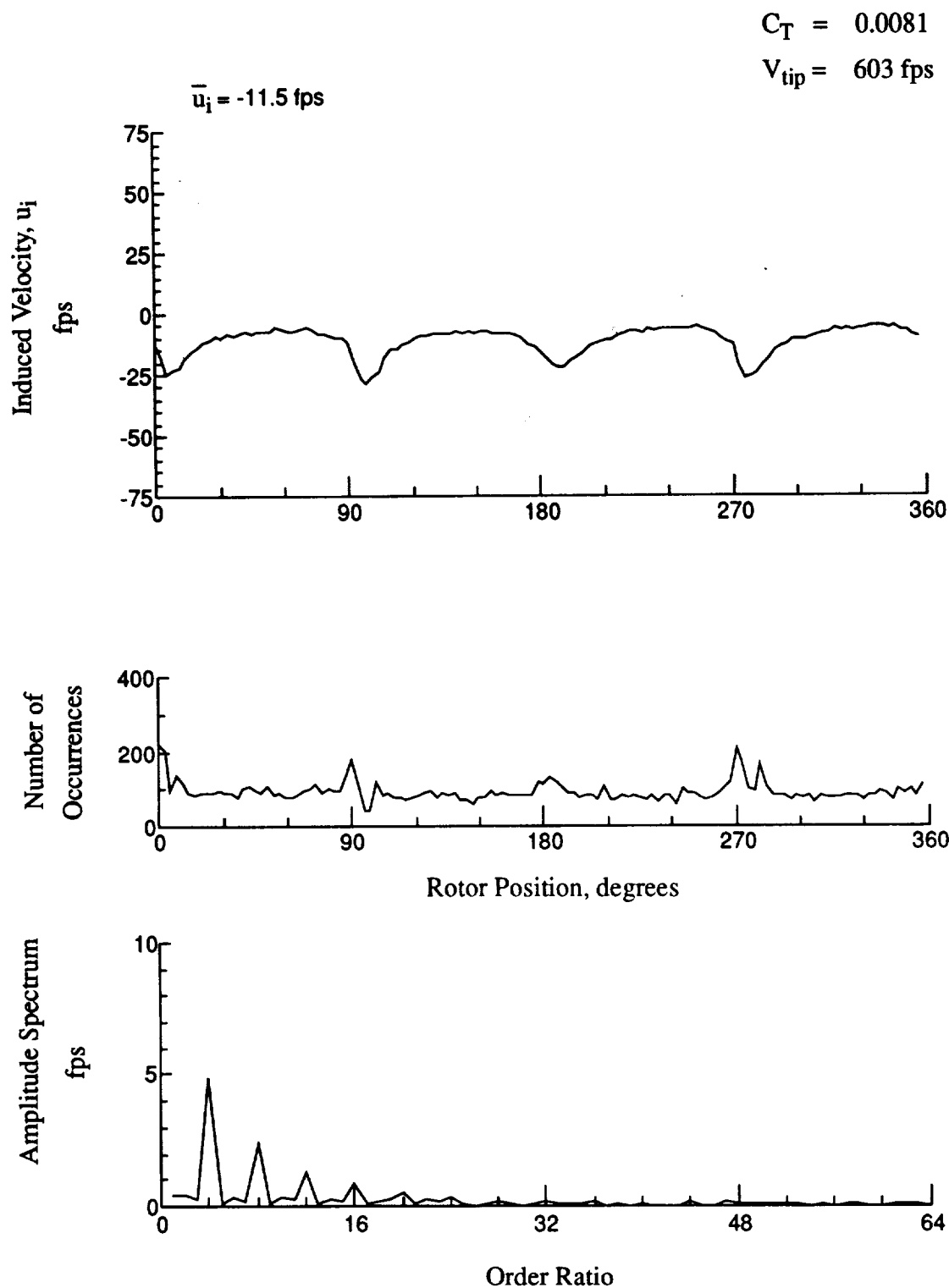


Figure 150.- Wake Measurements at
 $x/R = 1.50$, $y/R = 0.20$, $z = 5.90 \text{ in.}$

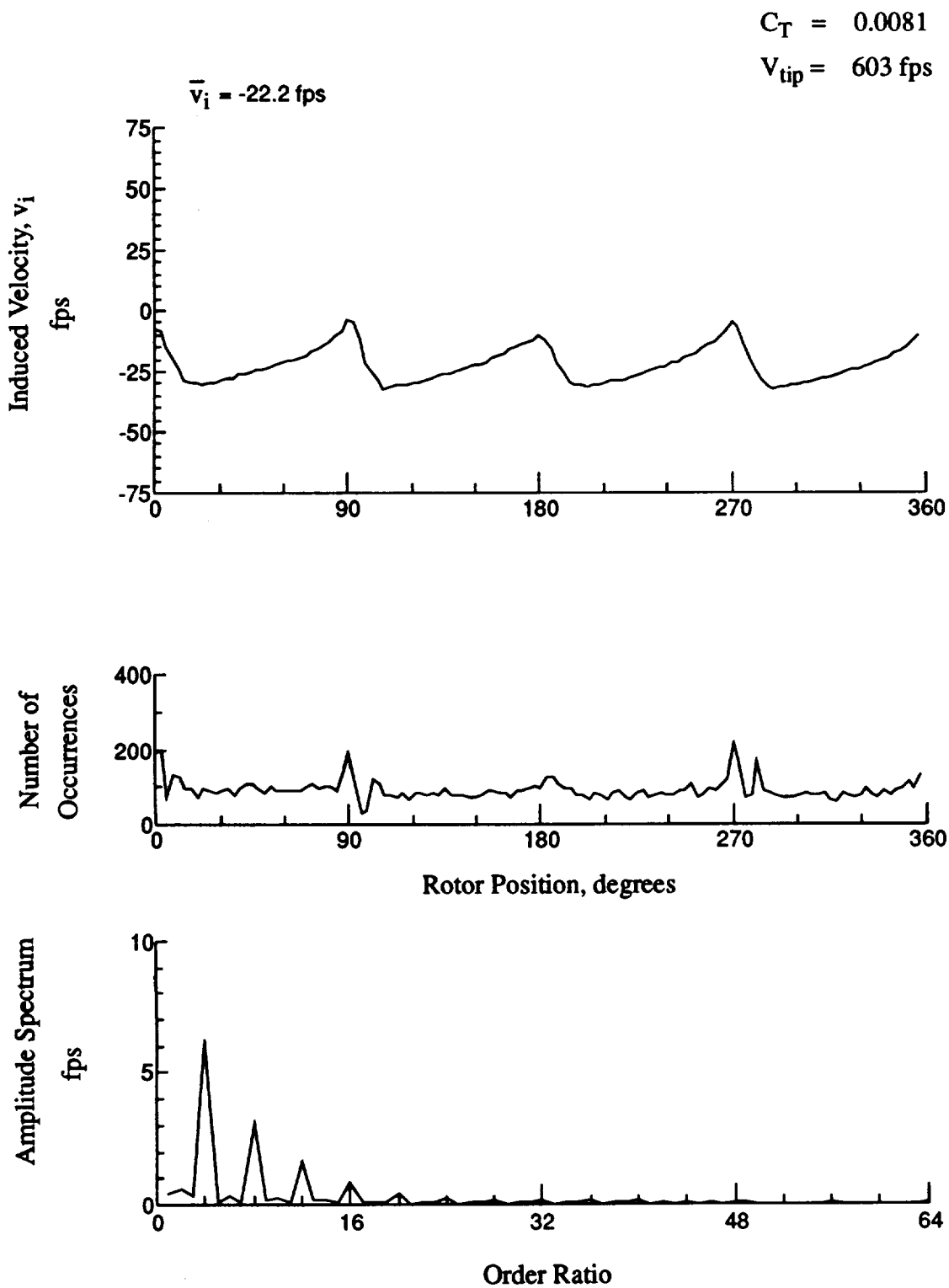


Figure 150.- Concluded.
 $x/R = 1.50$, $y/R = 0.20$, $z = 5.90 \text{ in.}$

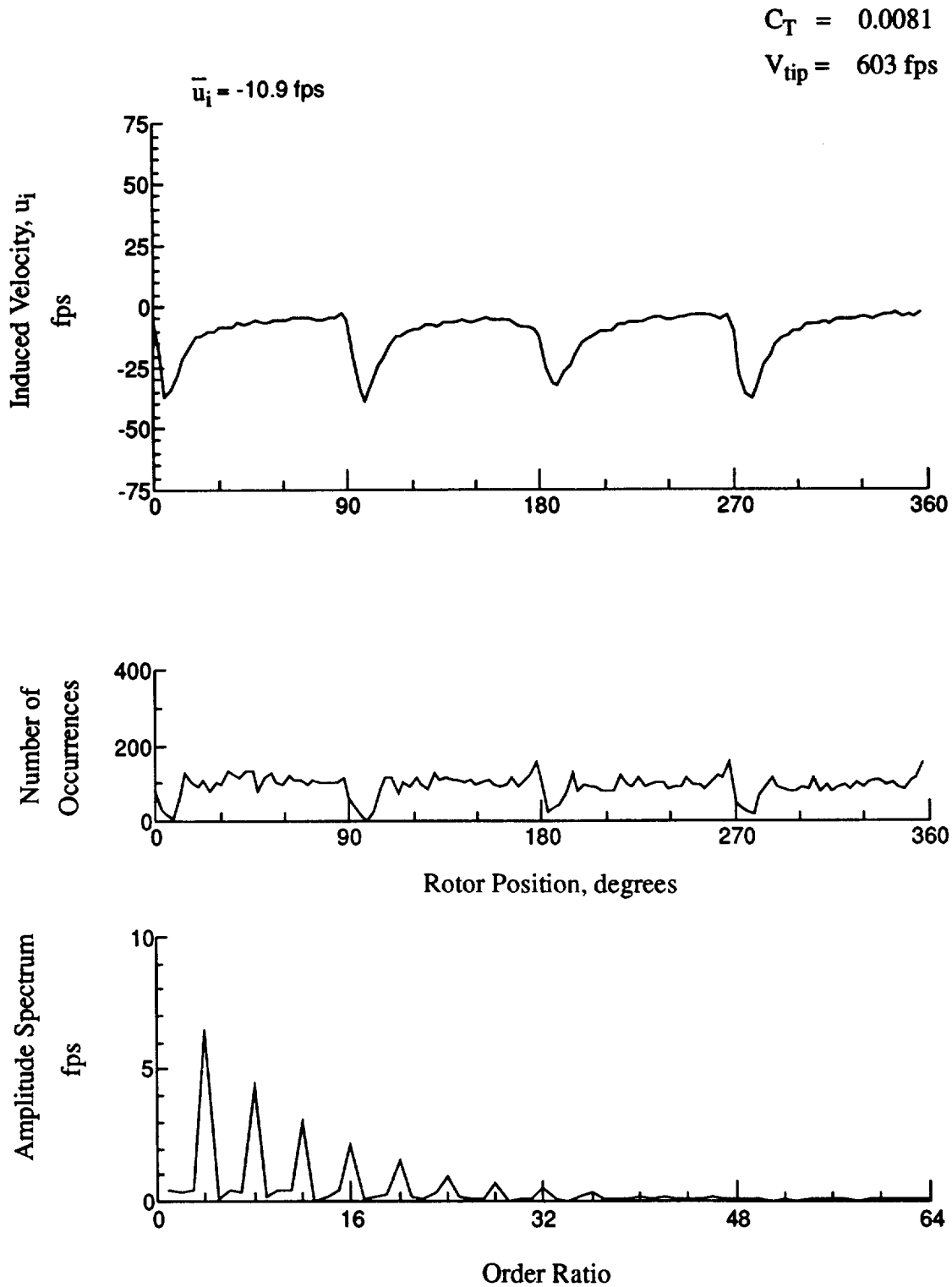


Figure 151.- Wake Measurements at
 $x/R = 1.50$, $y/R = 0.20$, $z = 4.87 \text{ in.}$

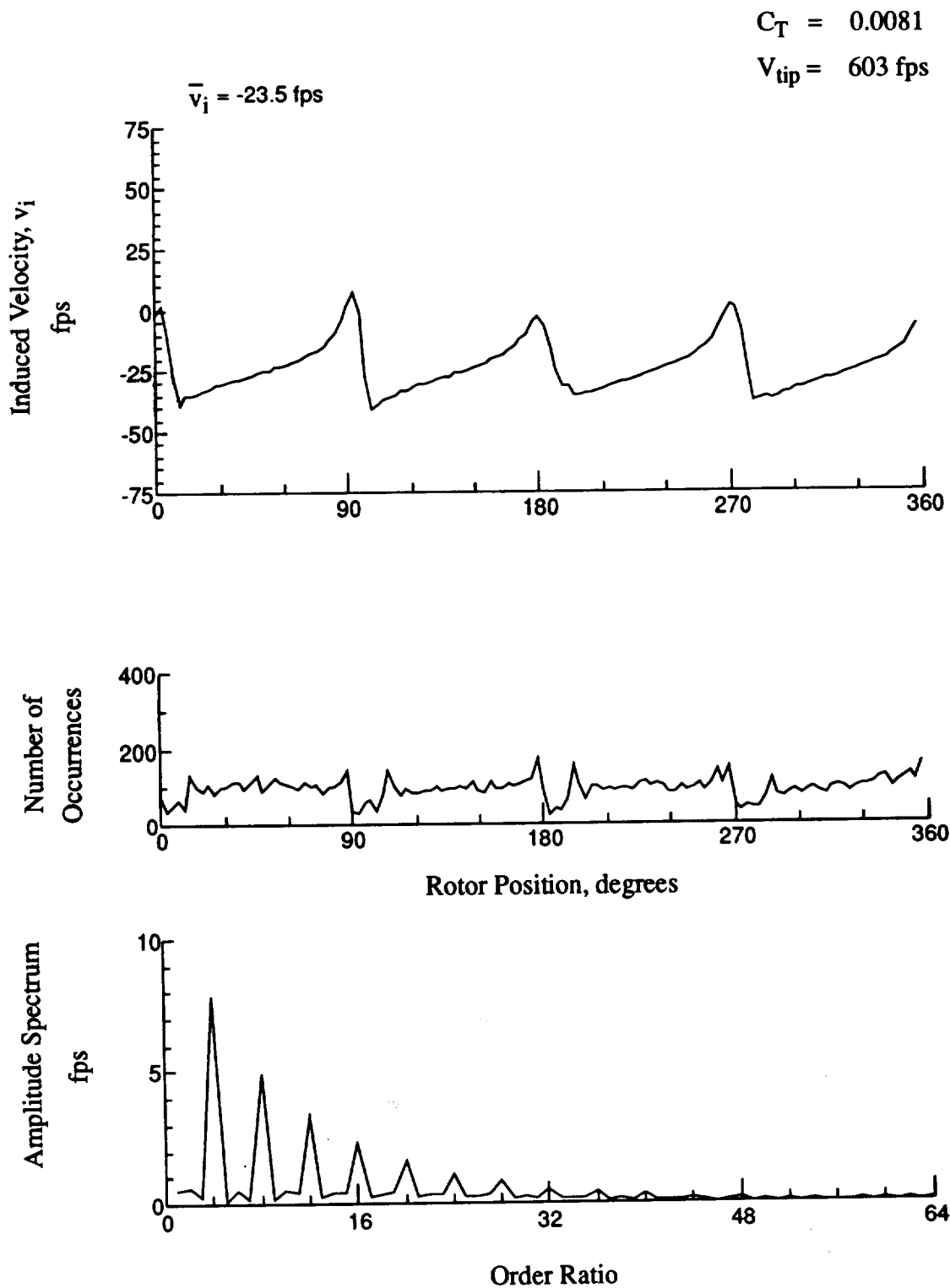


Figure 151.- Concluded.
 $x/R = 1.50$, $y/R = 0.20$, $z = 4.87 \text{ in.}$

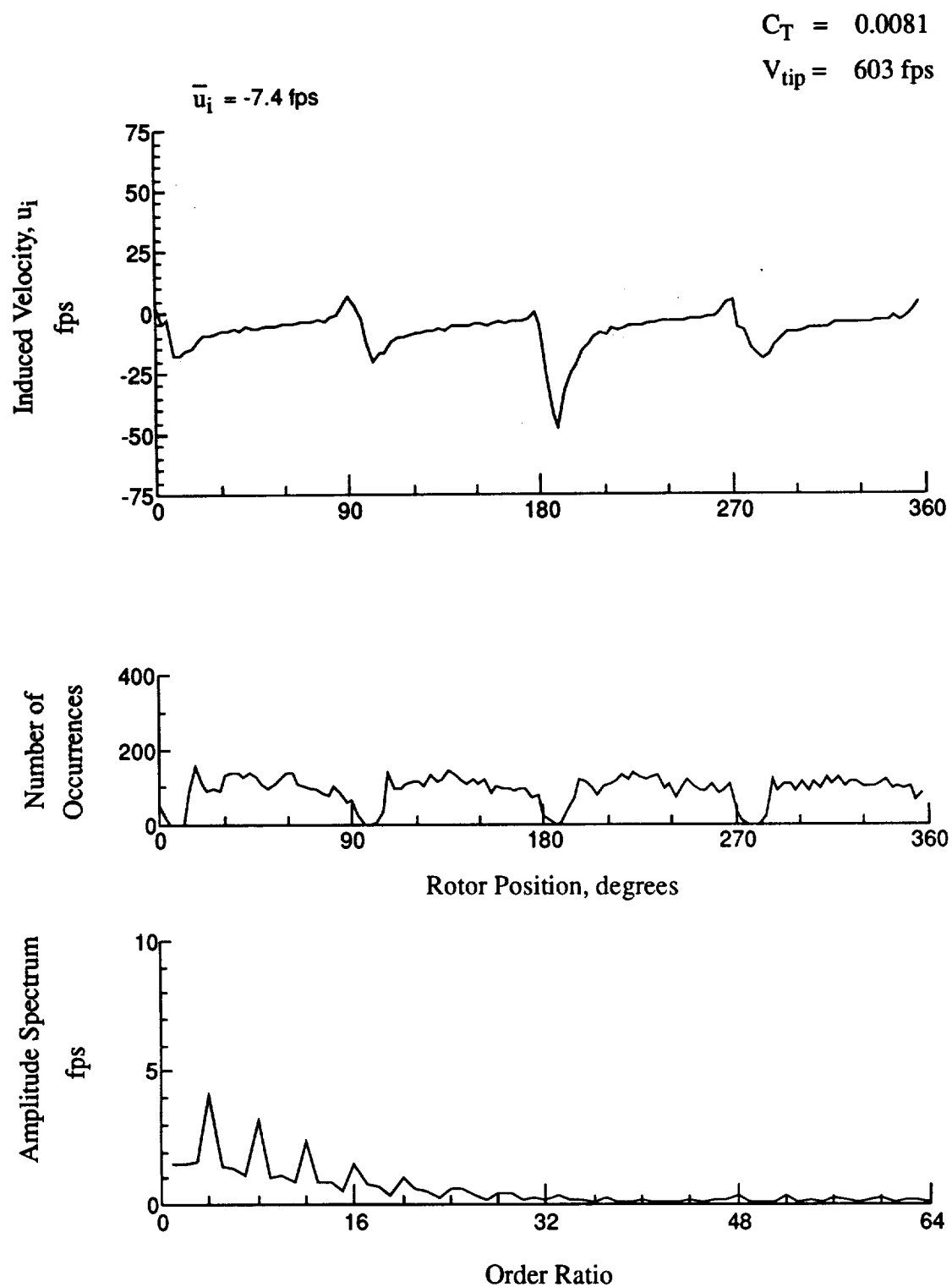


Figure 152.- Wake Measurements at
 $x/R = 1.50$, $y/R = 0.20$, $z = 3.84 \text{ in.}$

$$C_T = 0.0081$$

$$V_{tip} = 603 \text{ fps}$$

$$\bar{v}_i = -23.6 \text{ fps}$$

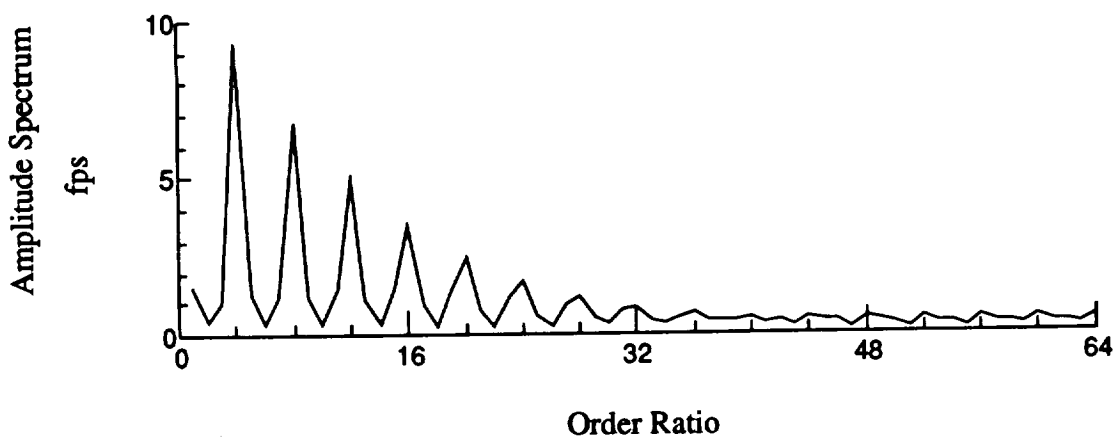
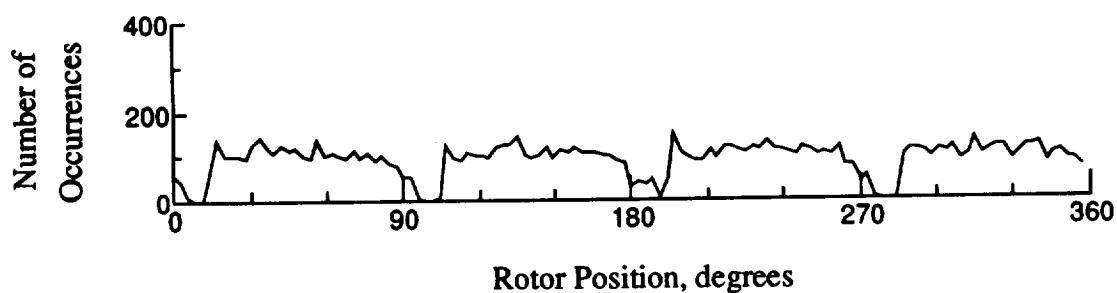
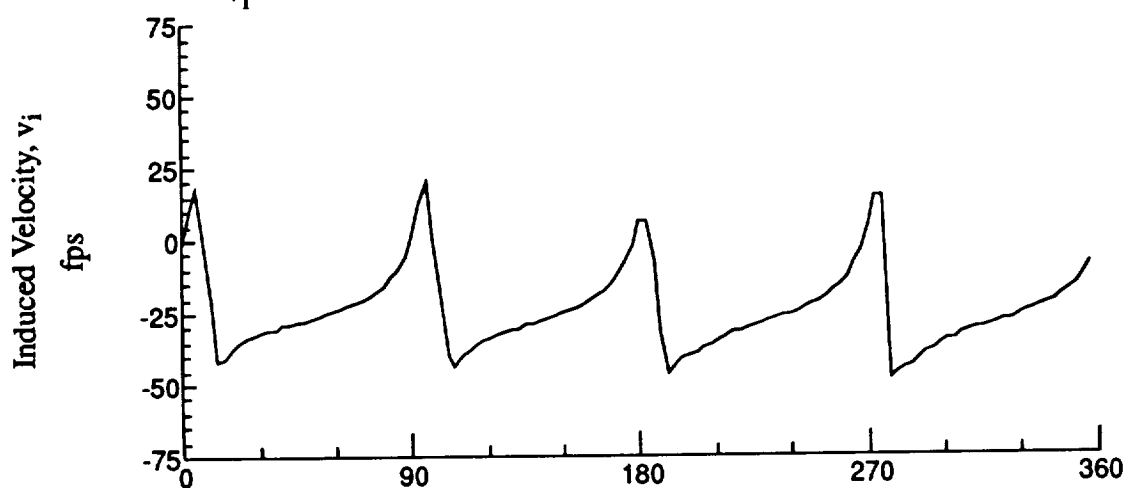


Figure 152.- Concluded.

$x/R = 1.50$, $y/R = 0.20$, $z = 3.84$ in.

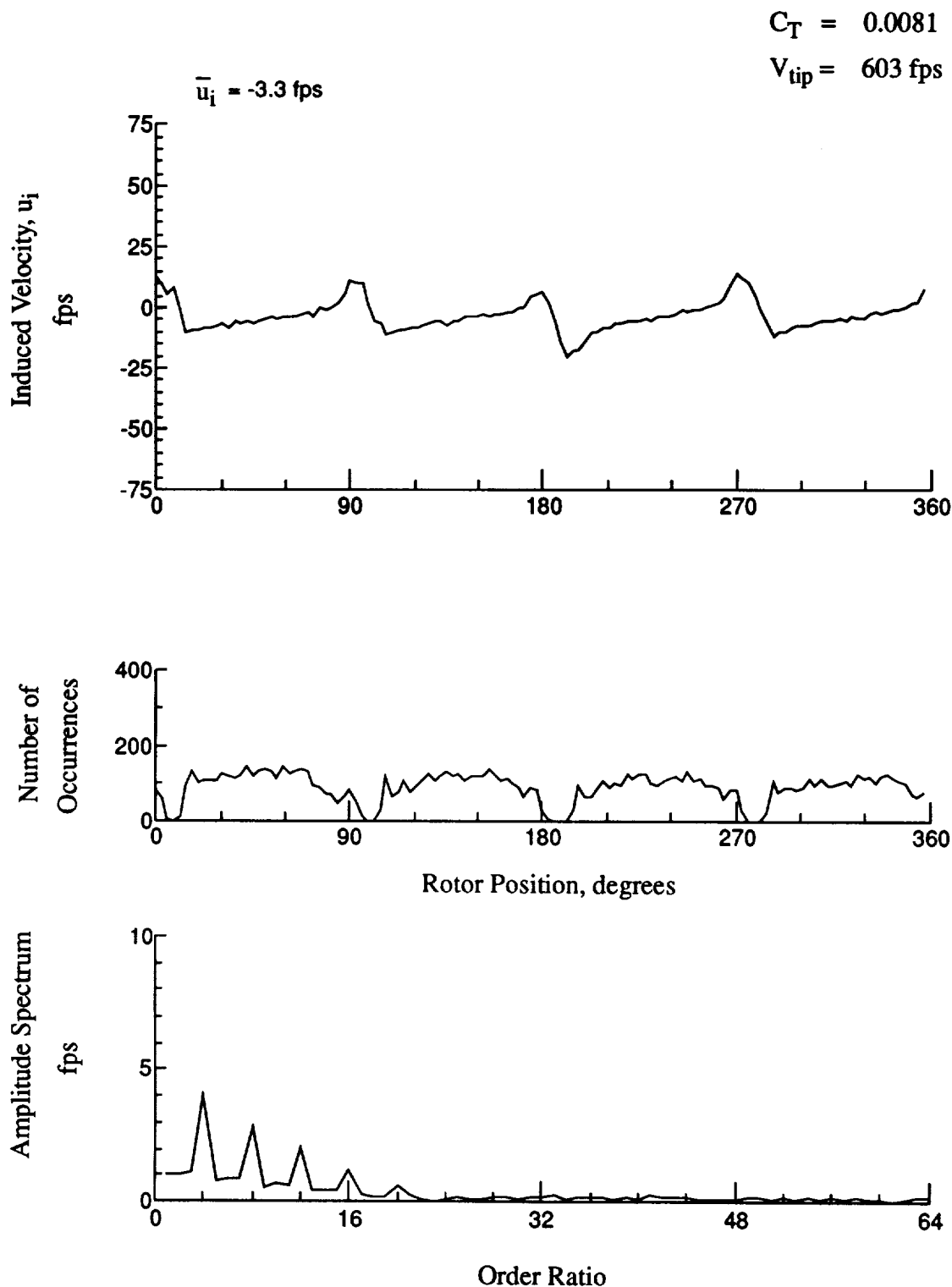


Figure 153.- Wake Measurements at
 $x/R = 1.50$, $y/R = 0.20$, $z = 2.81 \text{ in.}$

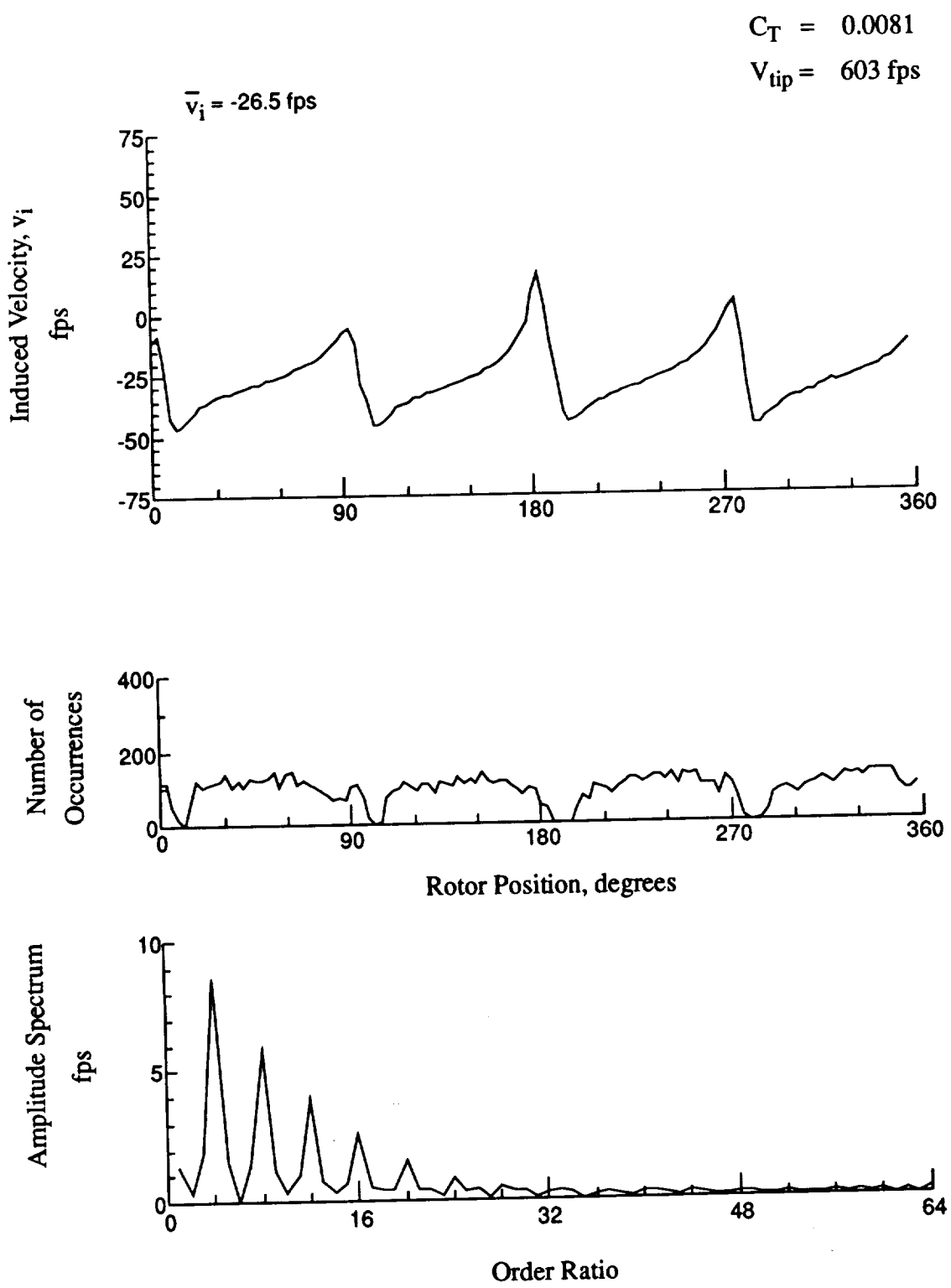


Figure 153.- Concluded.
 $x/R = 1.50$, $y/R = 0.20$, $z = 2.81 \text{ in.}$

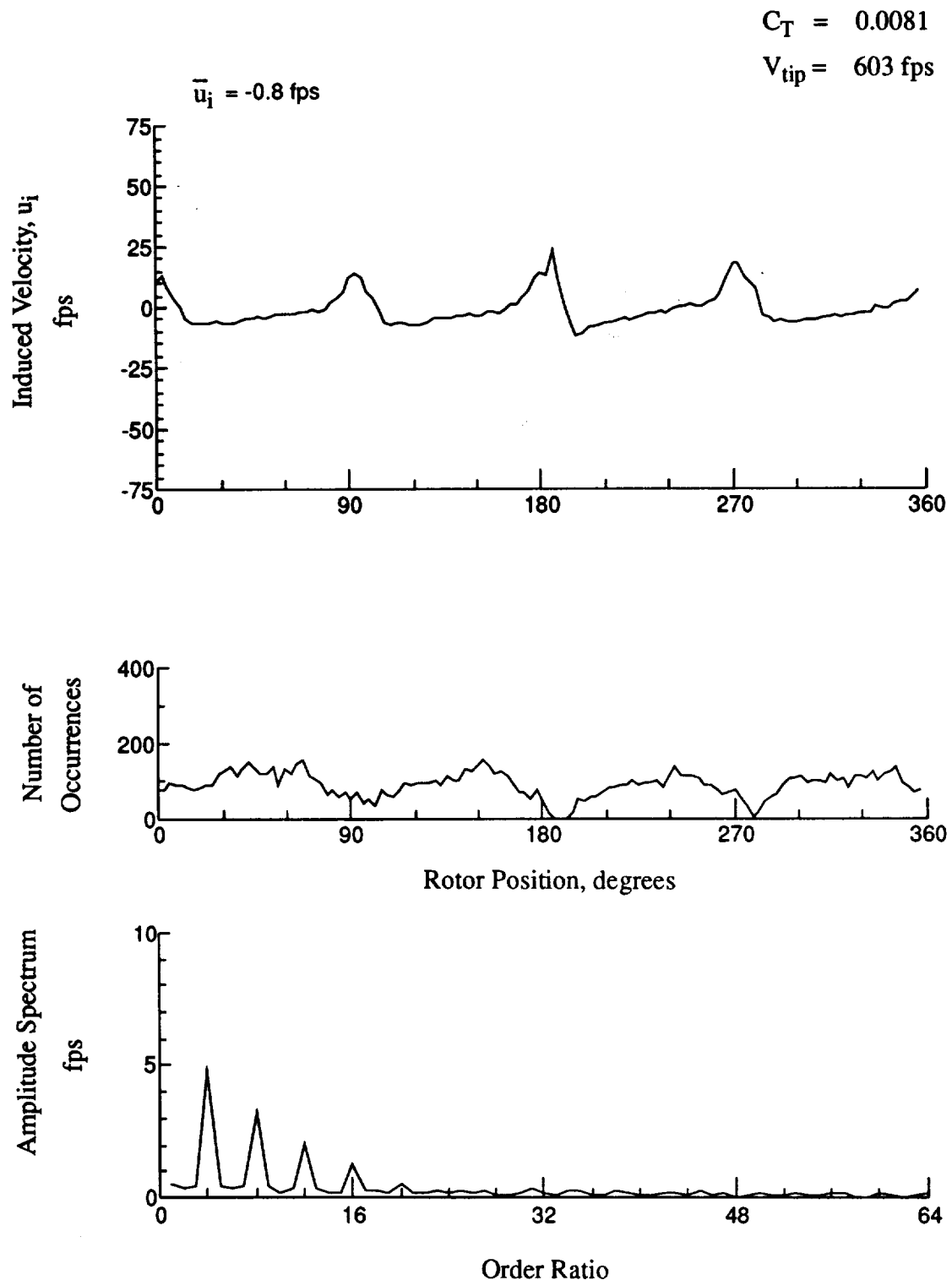


Figure 154.- Wake Measurements at
 $x/R = 1.50$, $y/R = 0.20$, $z = 1.78$ in.

$$C_T = 0.0081$$

$$V_{tip} = 603 \text{ fps}$$

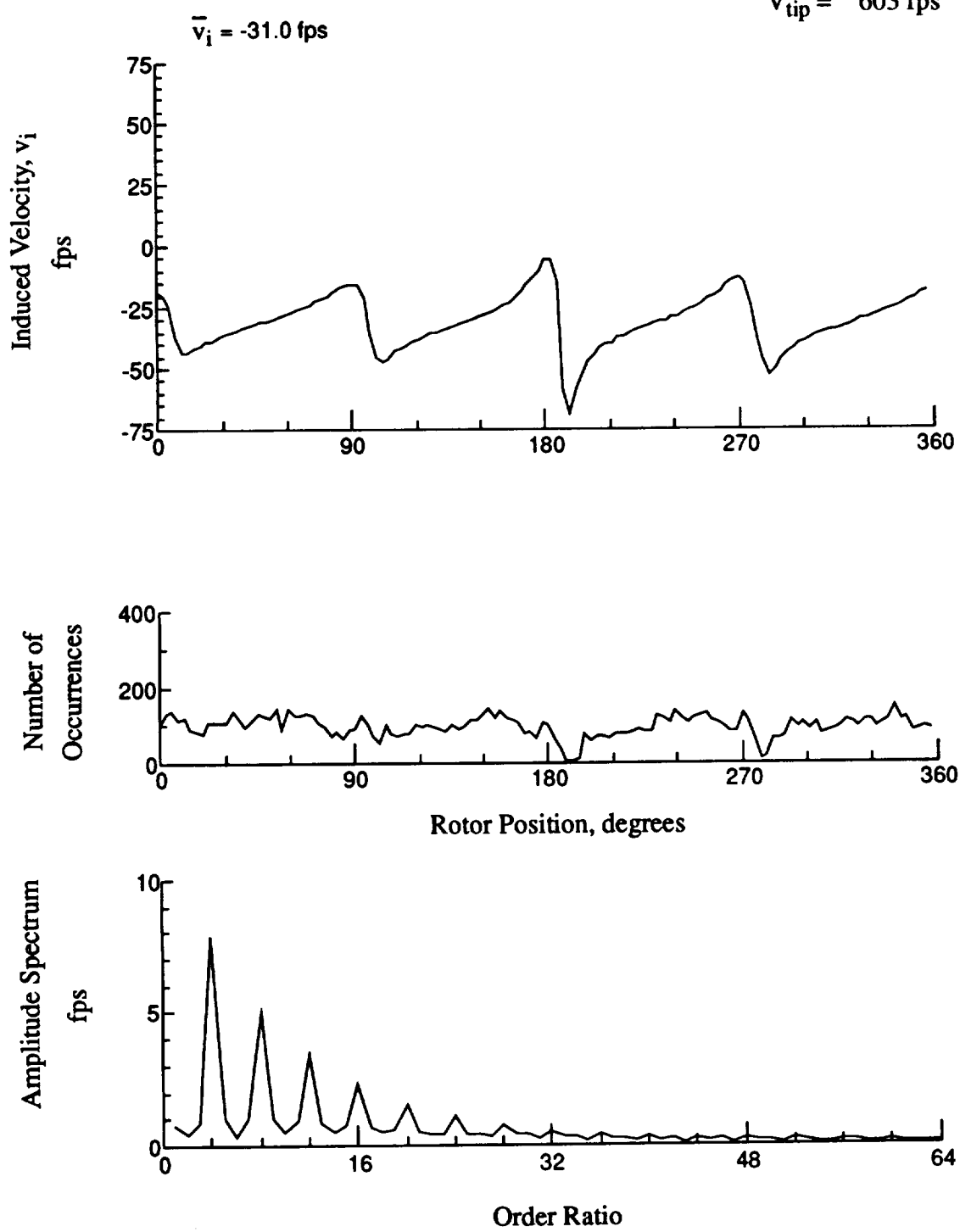


Figure 154.- Concluded.

$x/R = 1.50$, $y/R = 0.20$, $z = 1.78$ in.

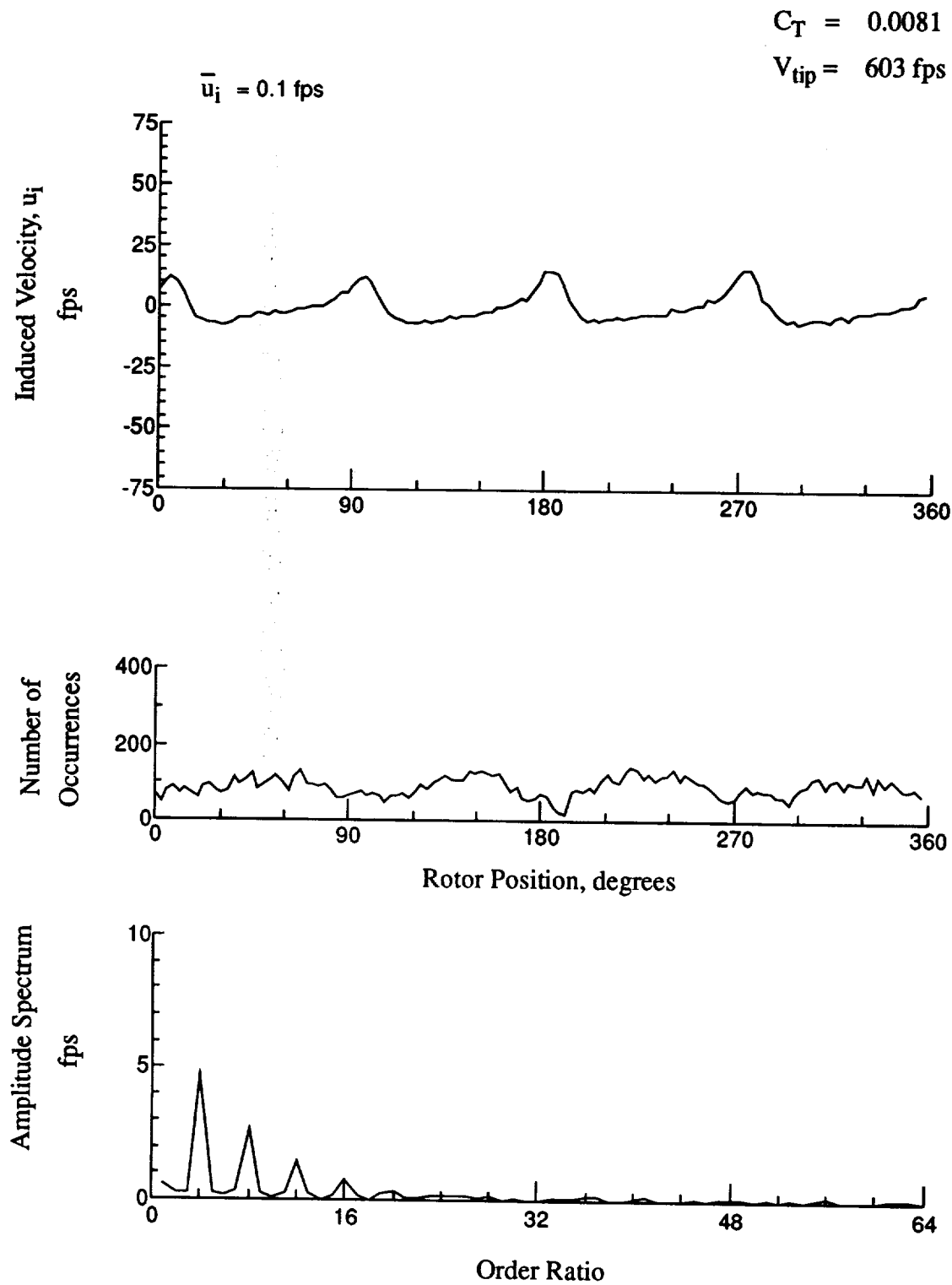


Figure 155.- Wake Measurements at
 $x/R = 1.50$, $y/R = 0.20$, $z = 0.75 \text{ in.}$

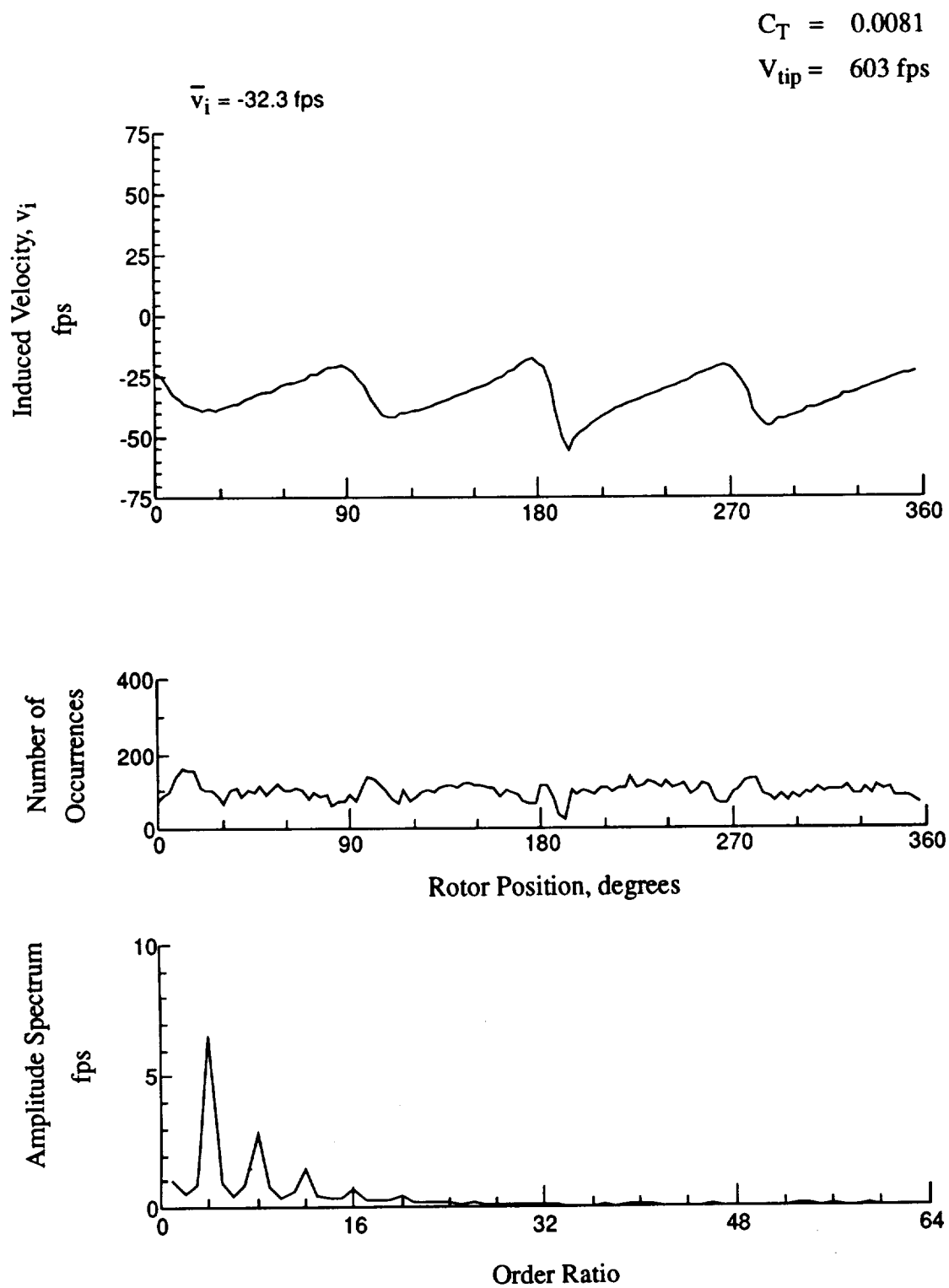


Figure 155.- Concluded.
 $x/R = 1.50$, $y/R = 0.20$, $z = 0.75 \text{ in.}$

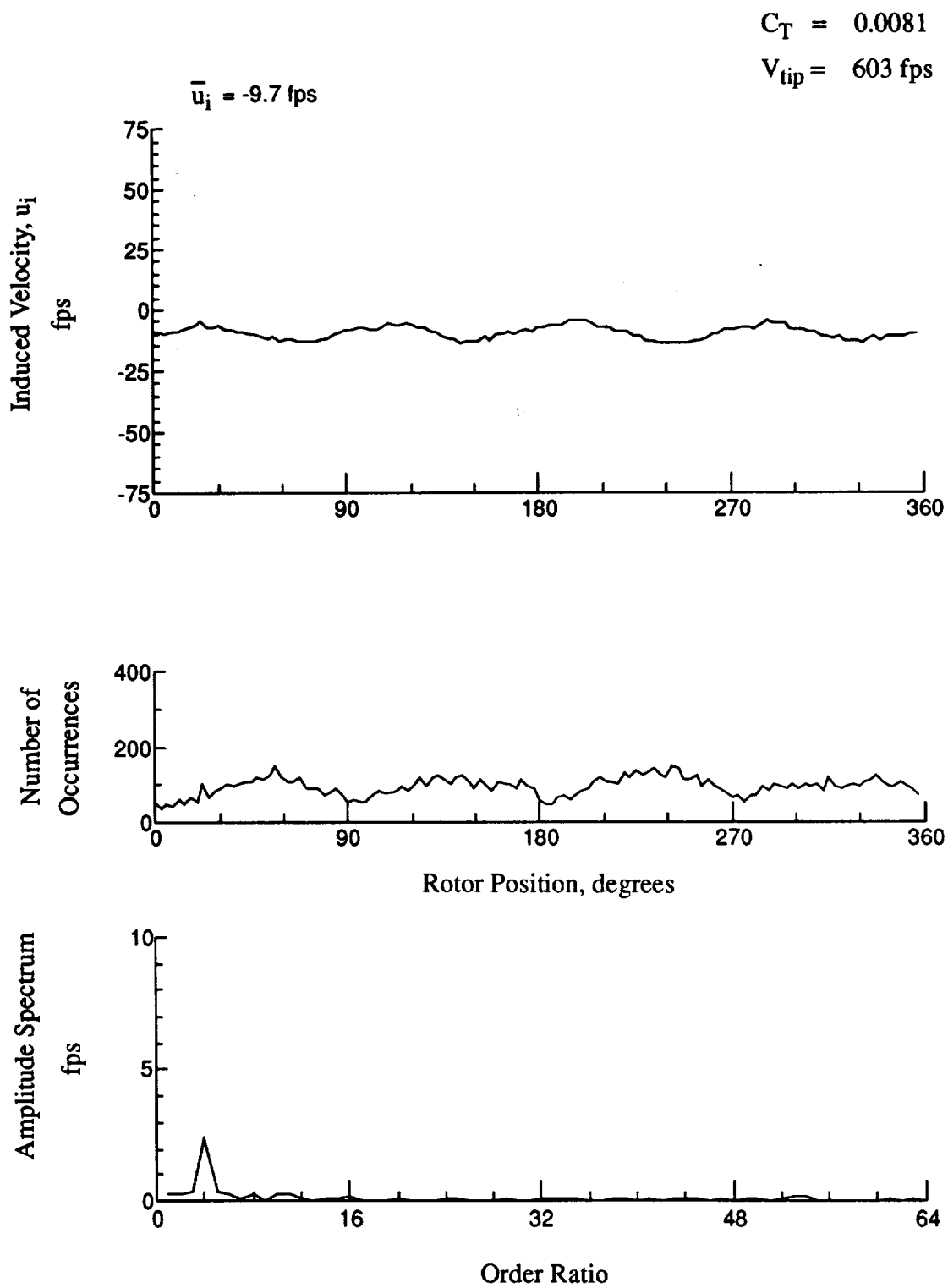


Figure 156.- Wake Measurements at
 $x/R = 1.50$, $y/R = 0.20$, $z = -7.47 \text{ in.}$

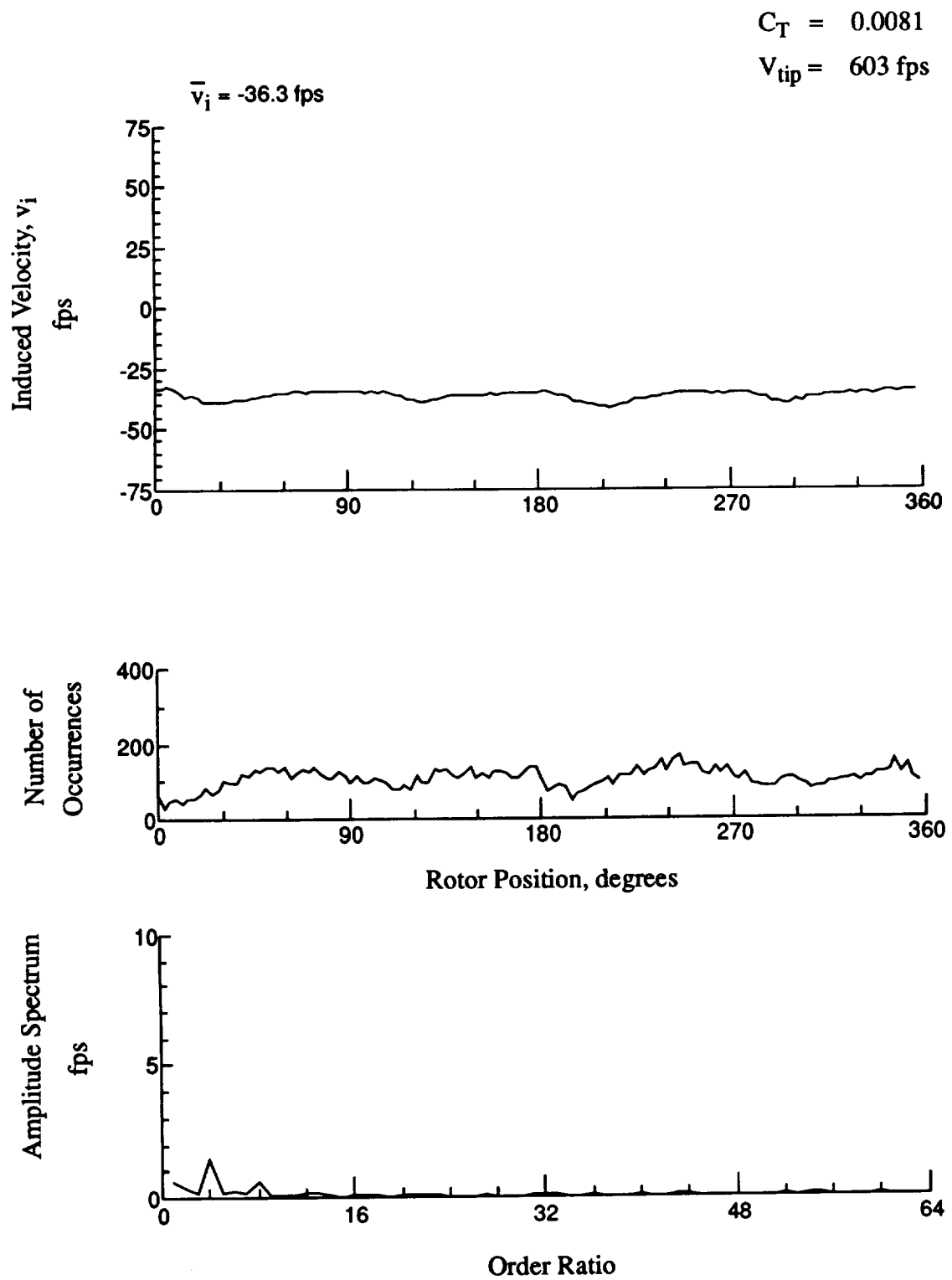


Figure 156.- Concluded.
 $x/R = 1.50$, $y/R = 0.20$, $z = -7.47 \text{ in.}$

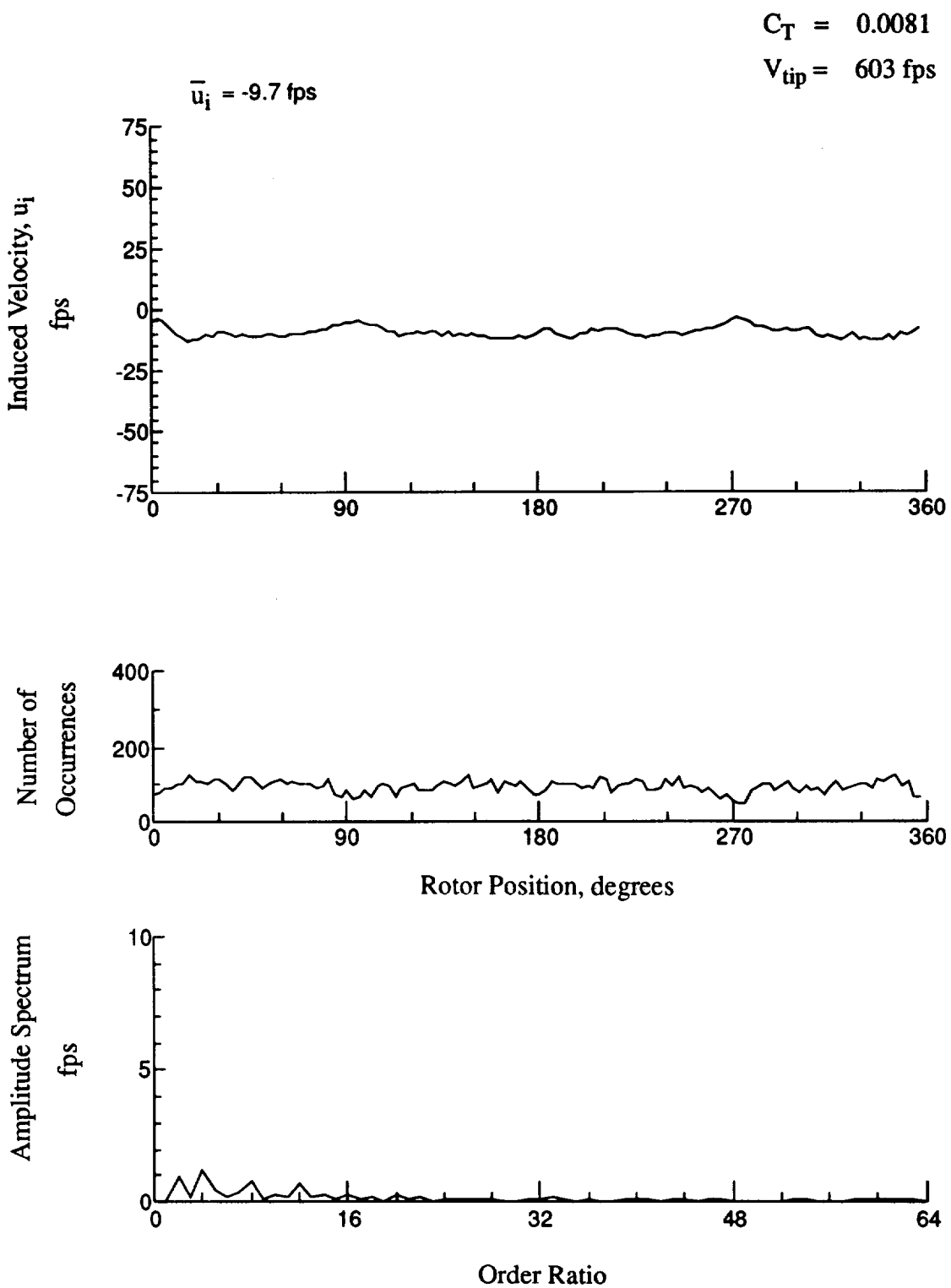


Figure 157.- Wake Measurements at
 $x/R = 1.50$, $y/R = 0.20$, $z = -8.50 \text{ in.}$

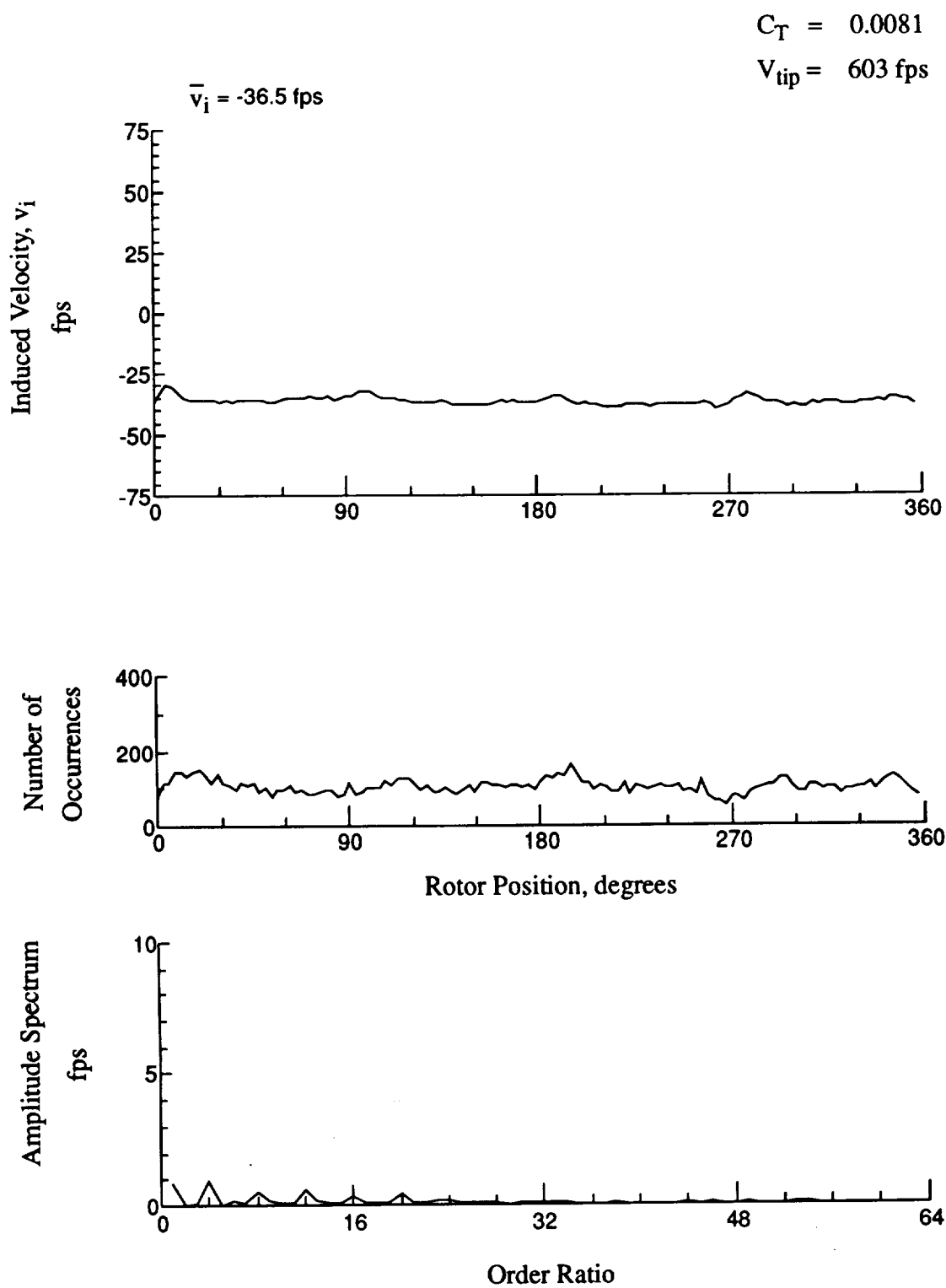


Figure 157.- Concluded.
 $x/R = 1.50$, $y/R = 0.20$, $z = -8.50 \text{ in.}$

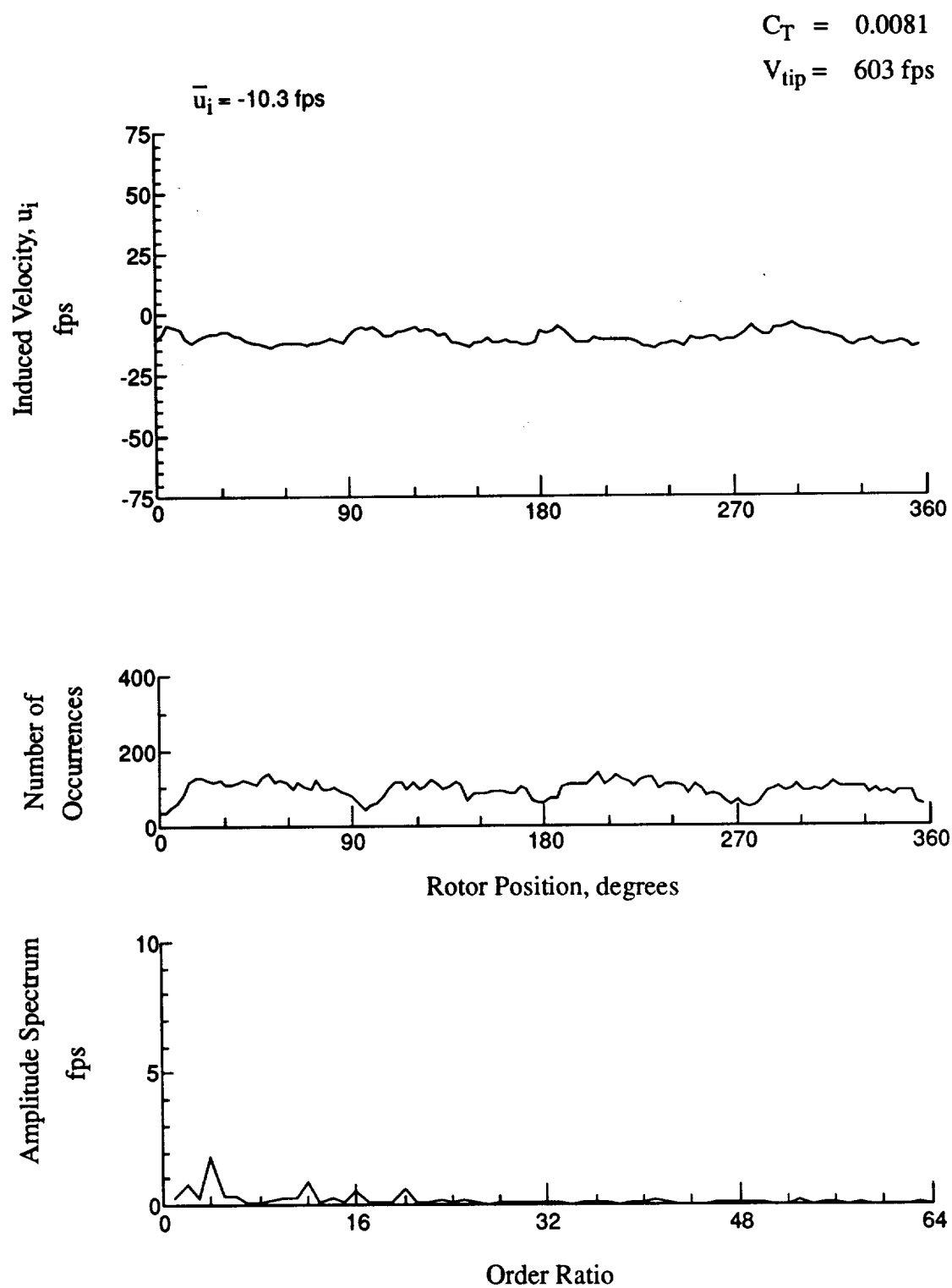


Figure 158.- Wake Measurements at
 $x/R = 1.50$, $y/R = 0.20$, $z = -9.53 \text{ in.}$

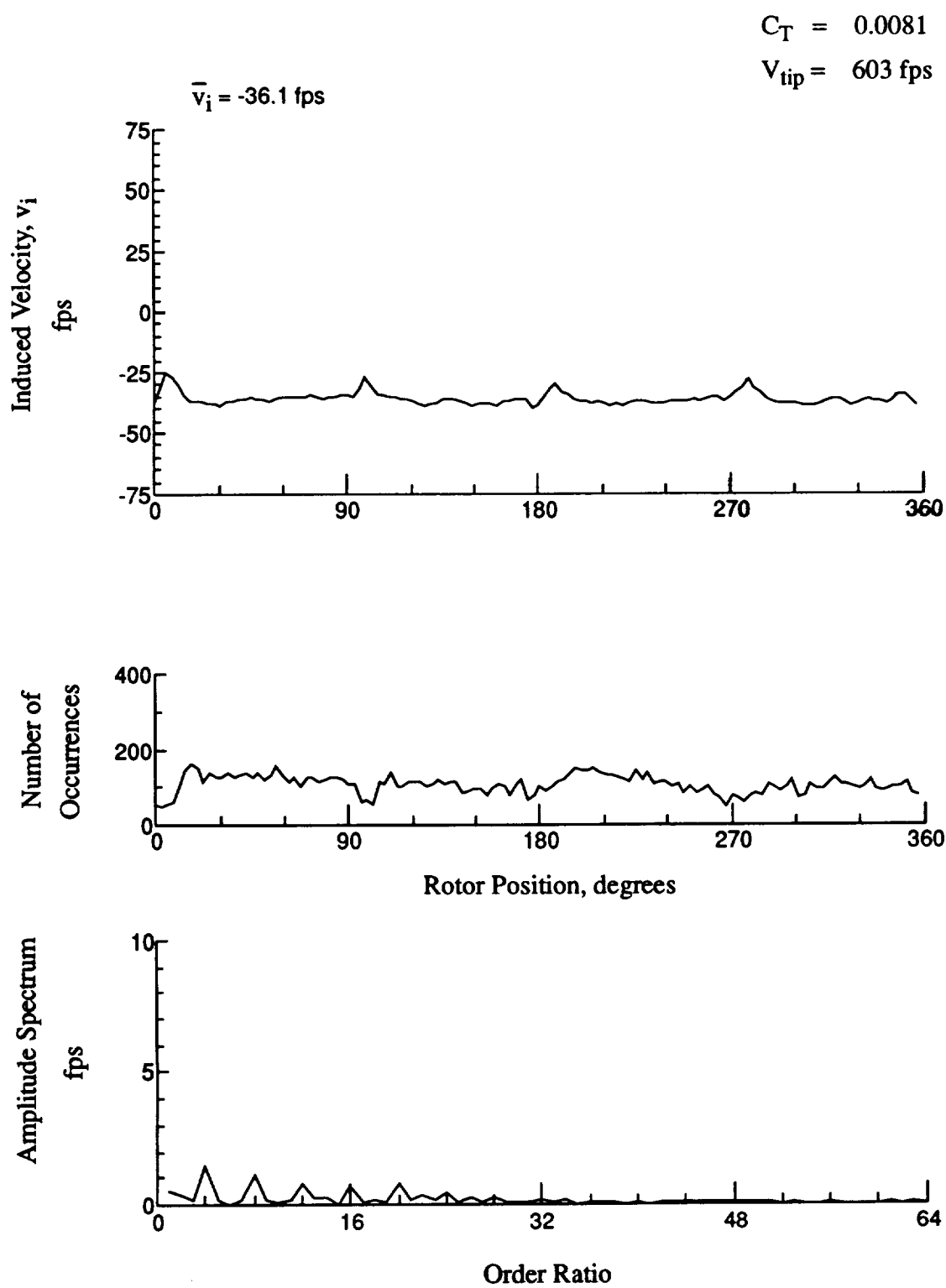


Figure 158.- Concluded.
 $x/R = 1.50$, $y/R = 0.20$, $z = -9.53 \text{ in.}$

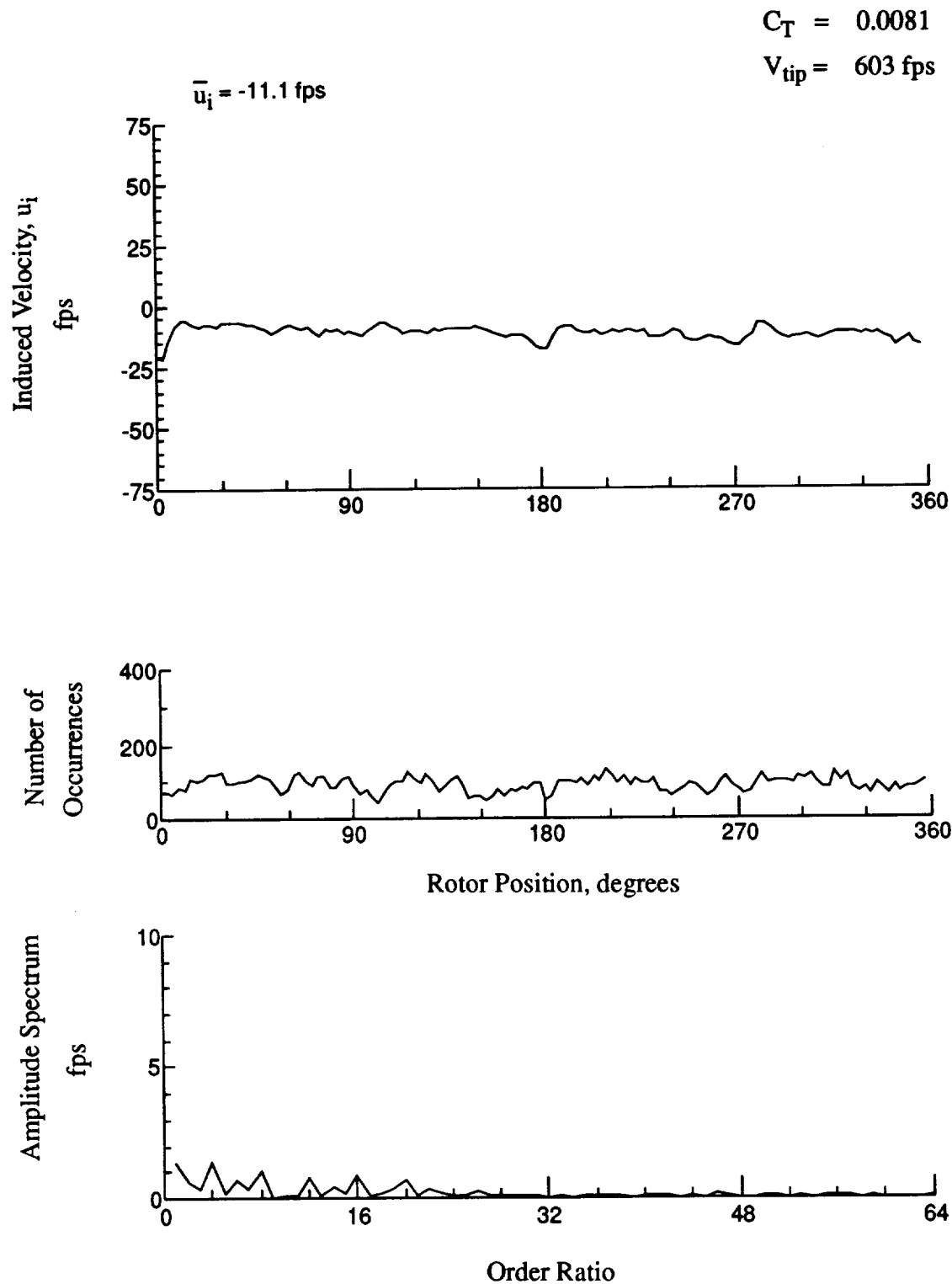


Figure 159.- Wake Measurements at
 $x/R = 1.50$, $y/R = 0.20$, $z = -10.56 \text{ in.}$

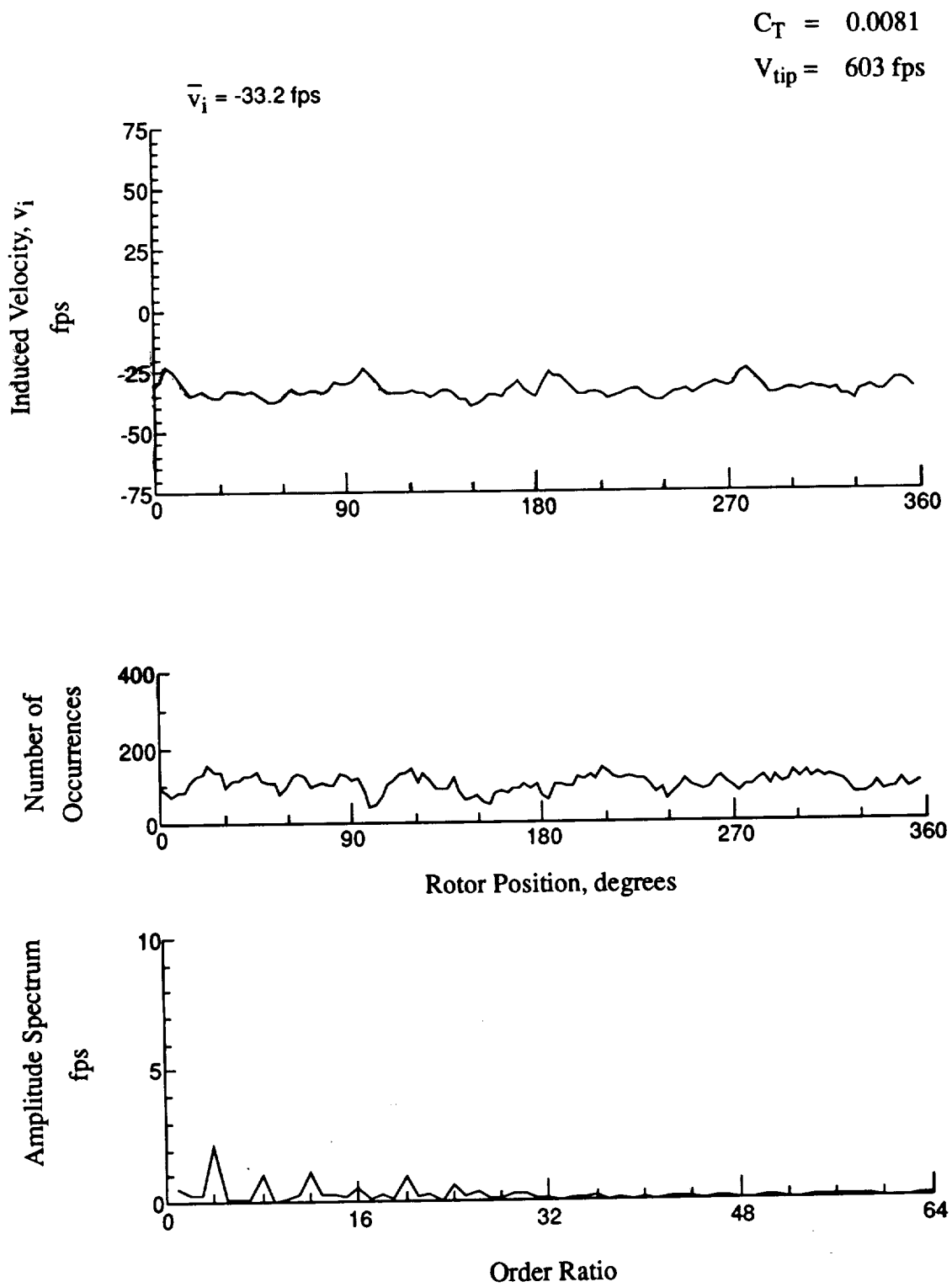


Figure 159.- Concluded.
 $x/R = 1.50$, $y/R = 0.20$, $z = -10.56 \text{ in.}$

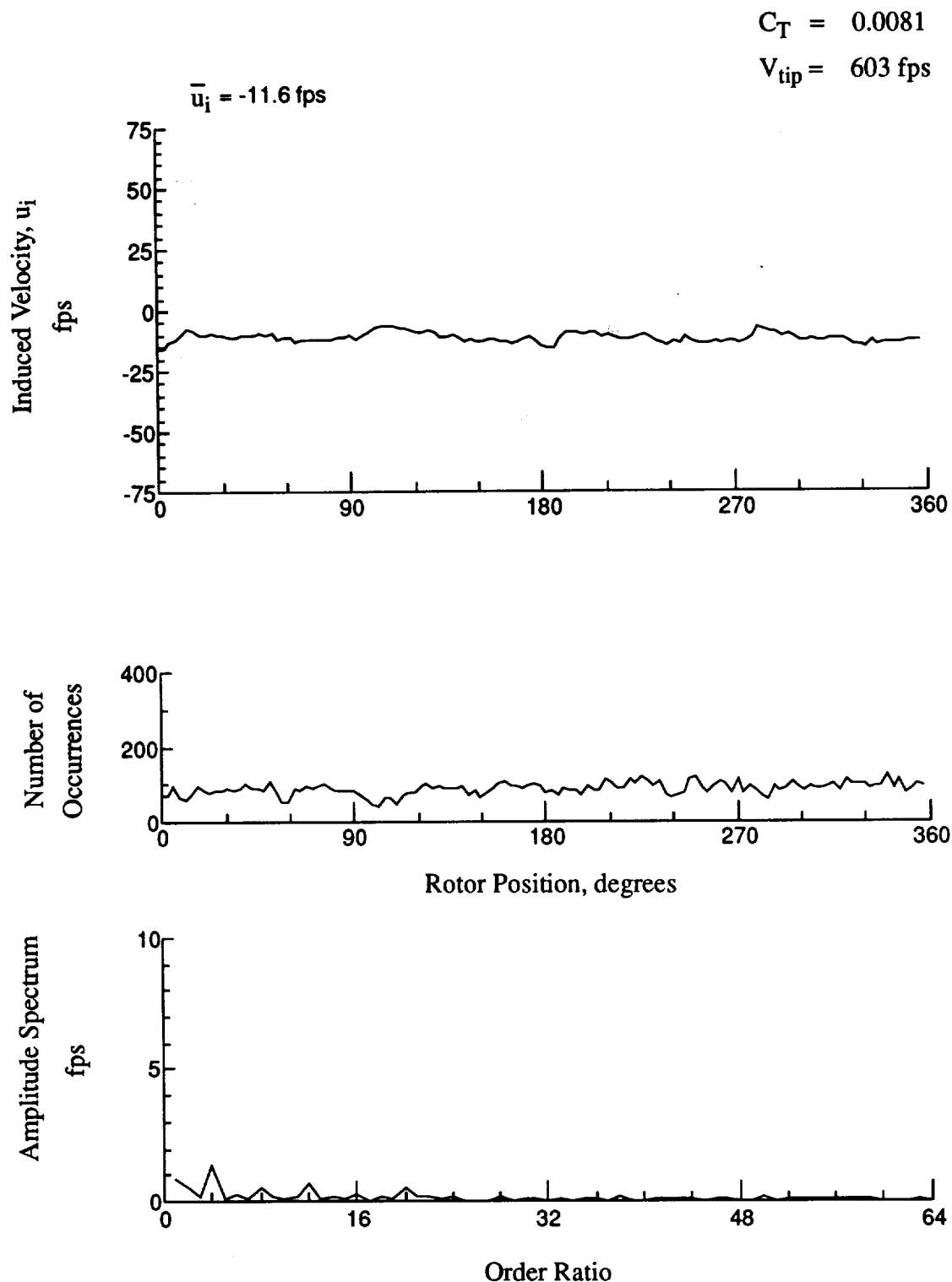


Figure 160.- Wake Measurements at
 $x/R = 1.50$, $y/R = 0.20$, $z = -11.59 \text{ in.}$

$$C_T = 0.0081$$

$$V_{tip} = 603 \text{ fps}$$

$$\bar{v}_i = -28.8 \text{ fps}$$

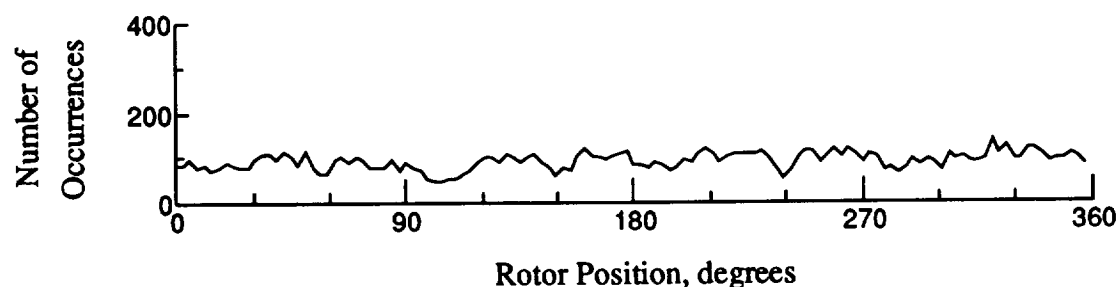
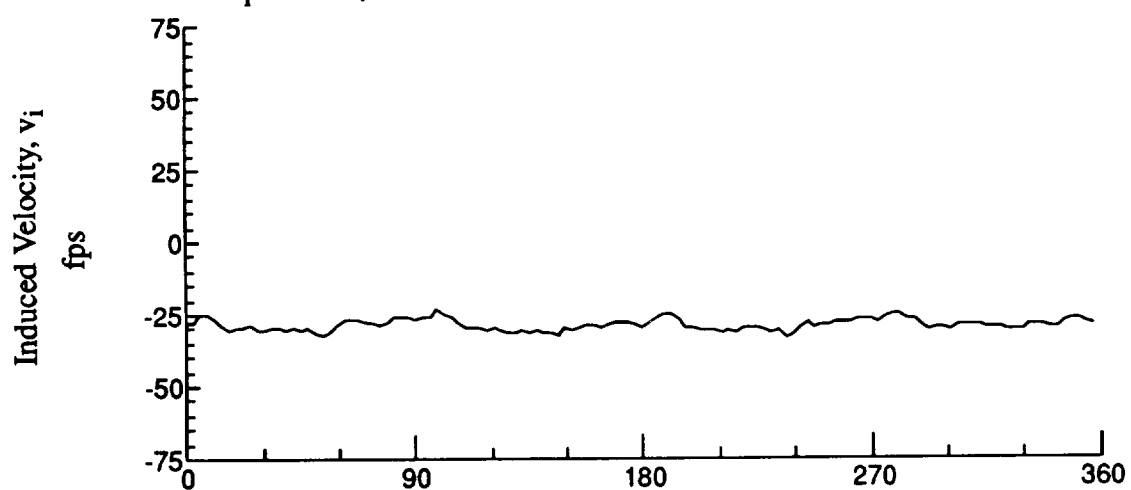


Figure 160.- Concluded.

$x/R = 1.50$, $y/R = 0.20$, $z = -11.59$ in.

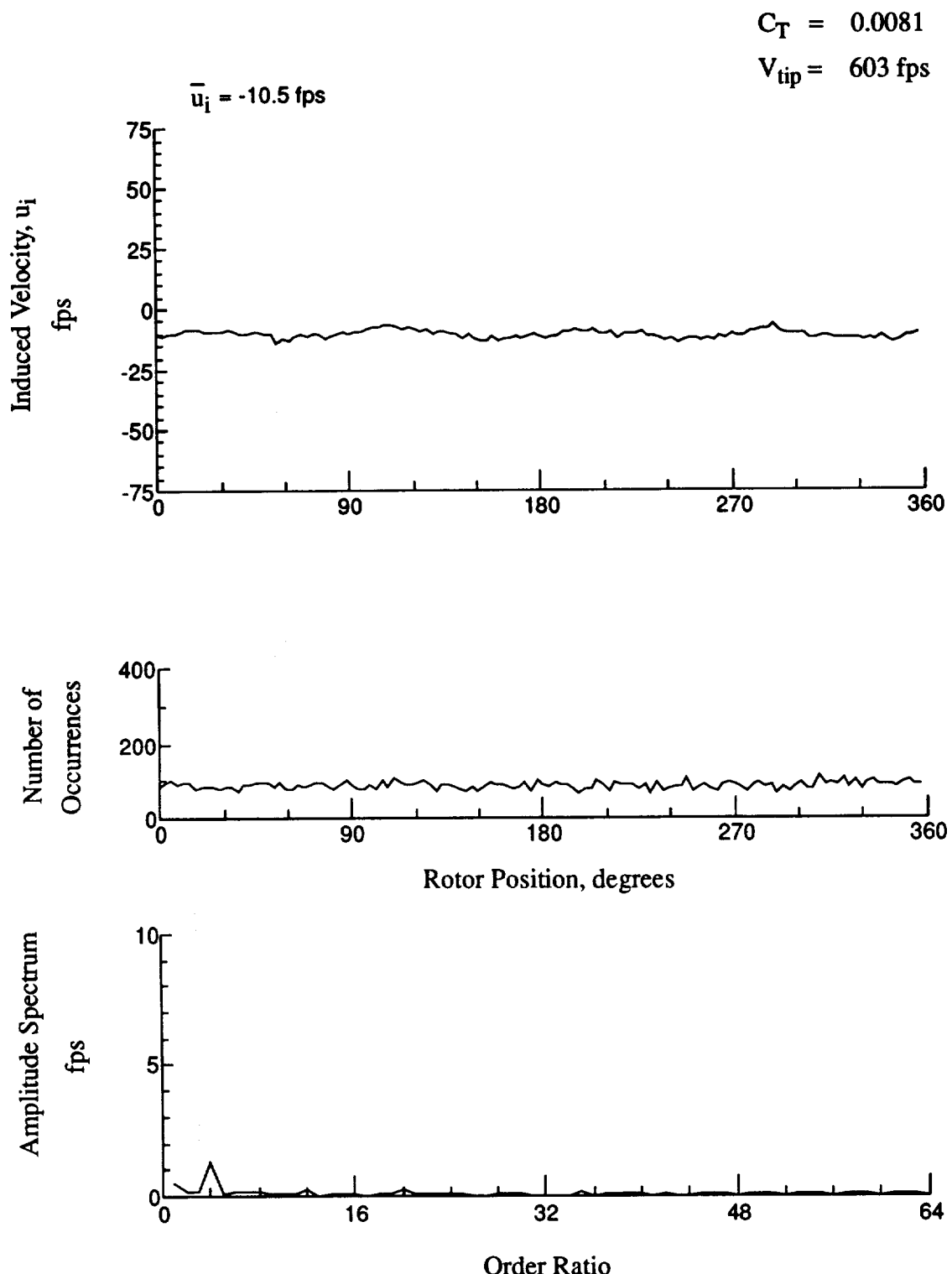


Figure 161.- Wake Measurements at
 $x/R = 1.50$, $y/R = 0.20$, $z = -12.62 \text{ in.}$

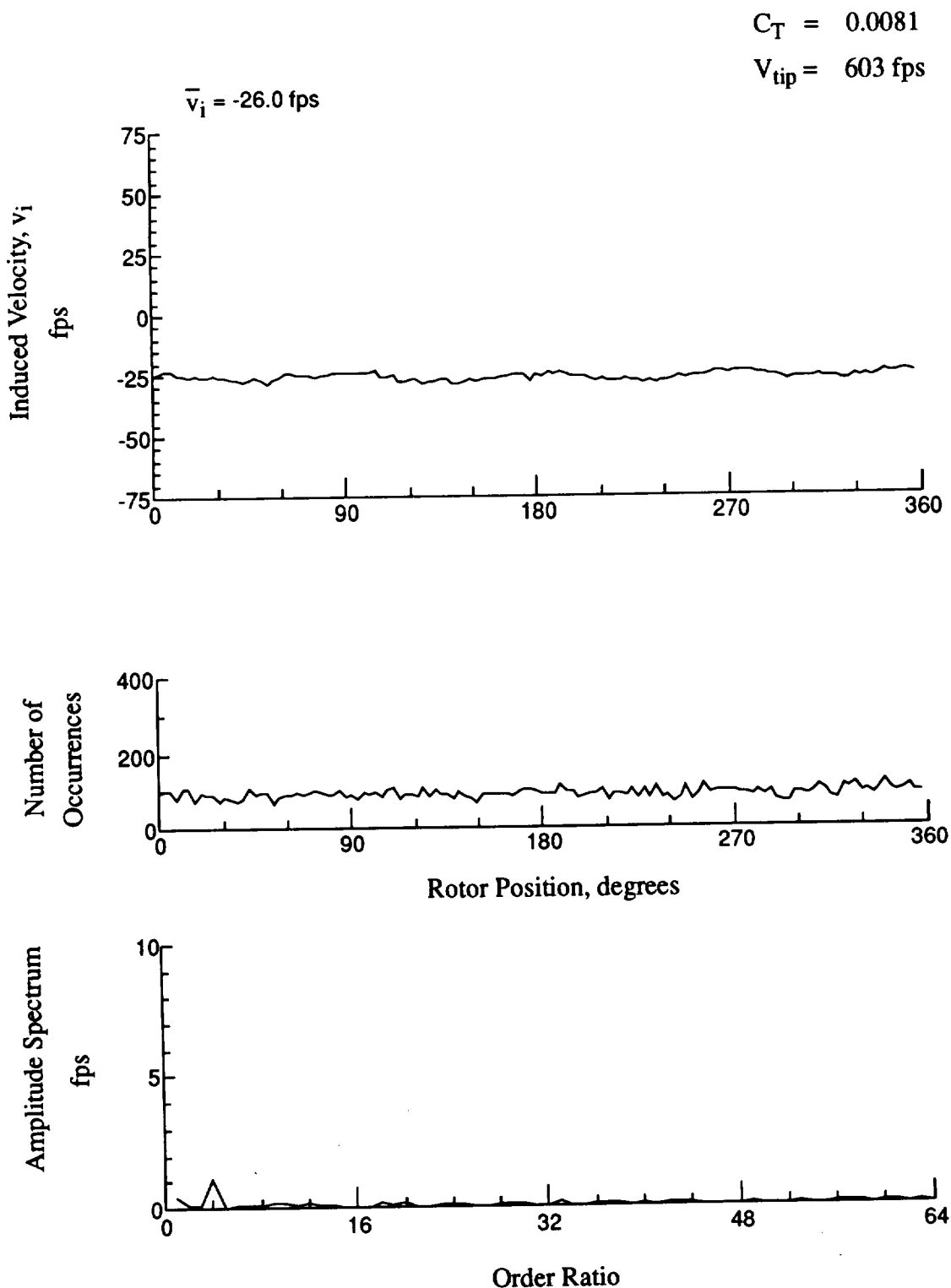


Figure 161.- Concluded.
 $x/R = 1.50$, $y/R = 0.20$, $z = -12.62 \text{ in.}$

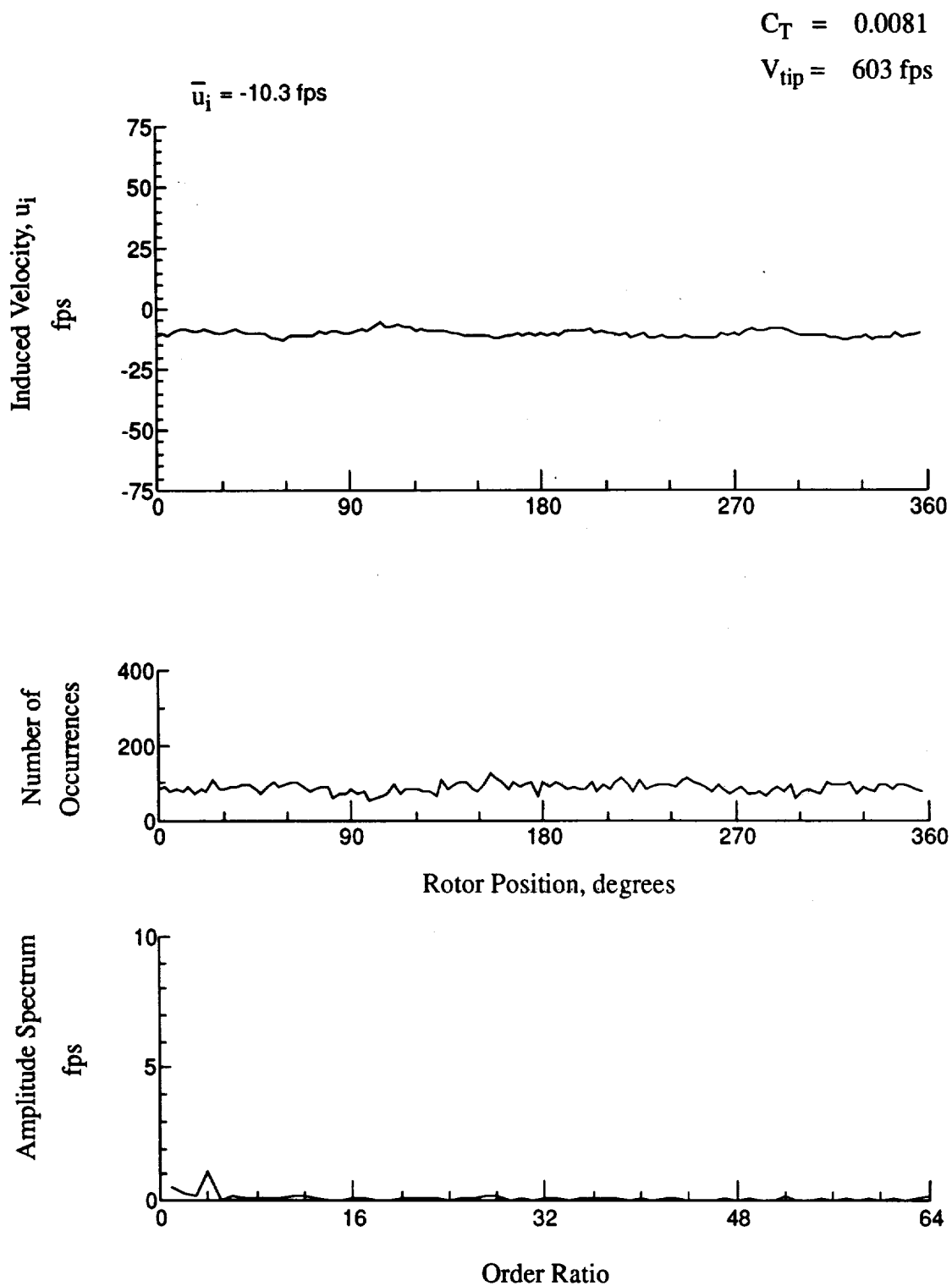


Figure 162.- Wake Measurements at
 $x/R = 1.50$, $y/R = 0.20$, $z = -13.56 \text{ in.}$

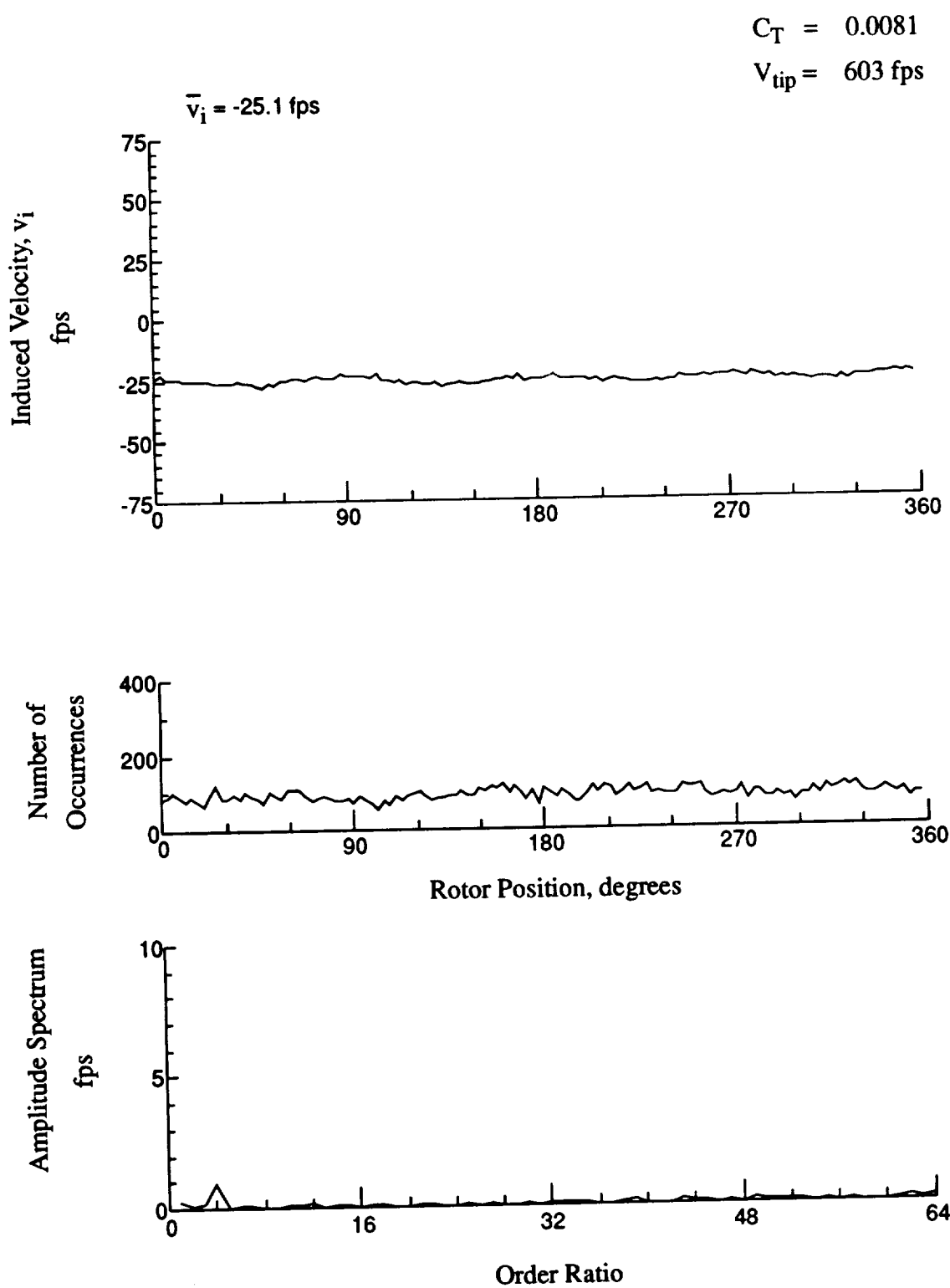


Figure 162.- Concluded.
 $x/R = 1.50$, $y/R = 0.20$, $z = -13.56 \text{ in.}$

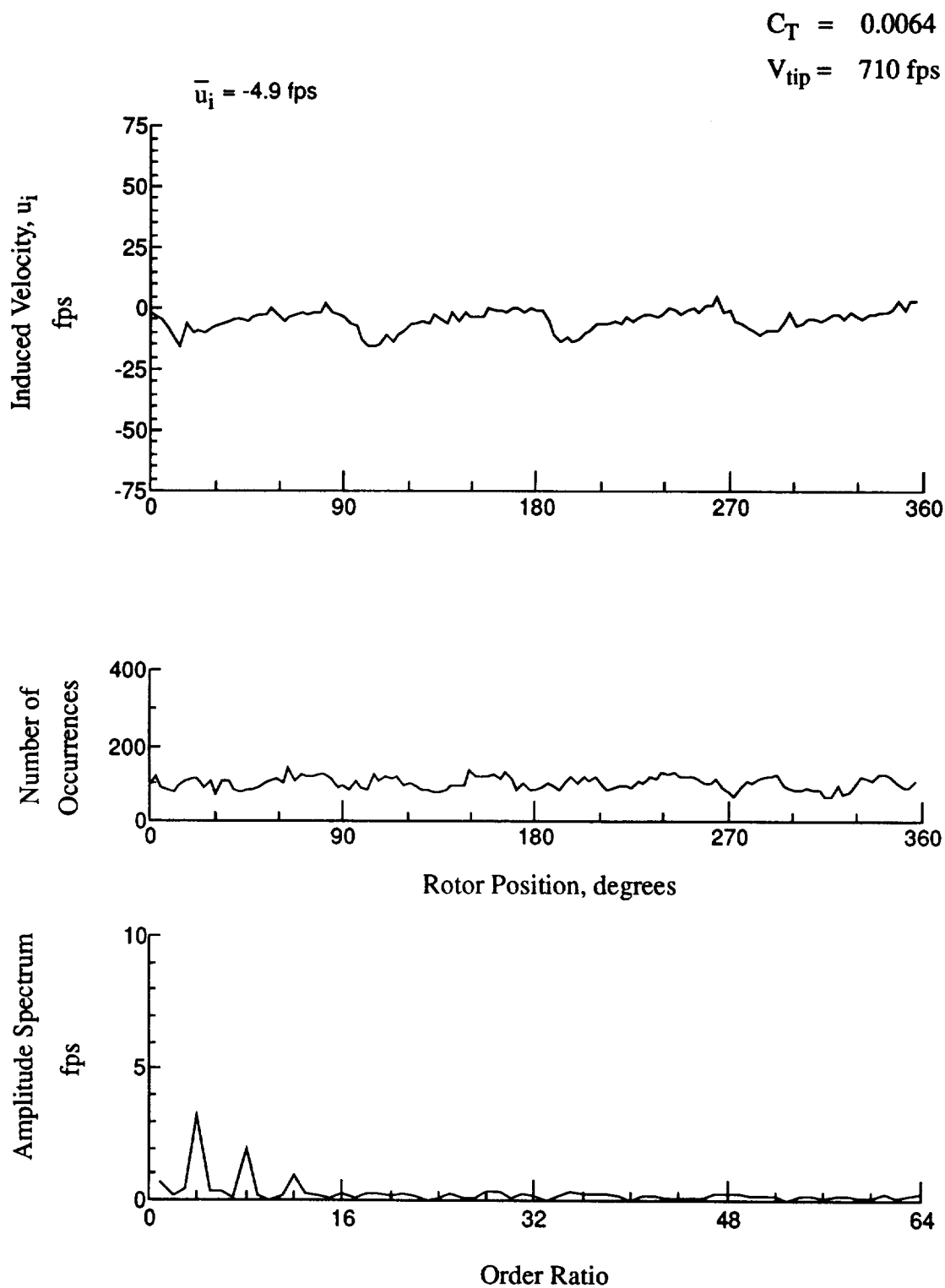


Figure 163.- Wake Measurements at
 $x/R = 1.10$, $y/R = -0.20$, $z = 8.85 \text{ in.}$

$$C_T = 0.0064$$

$$V_{tip} = 710 \text{ fps}$$

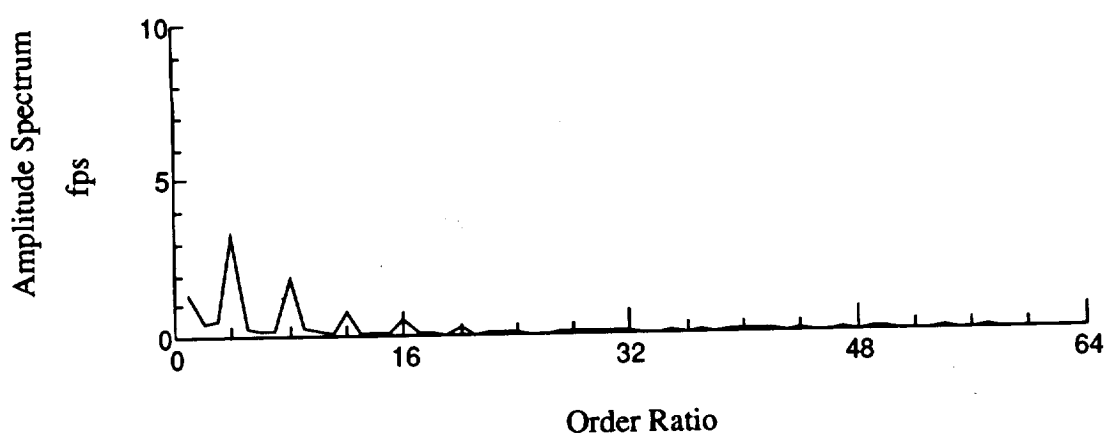
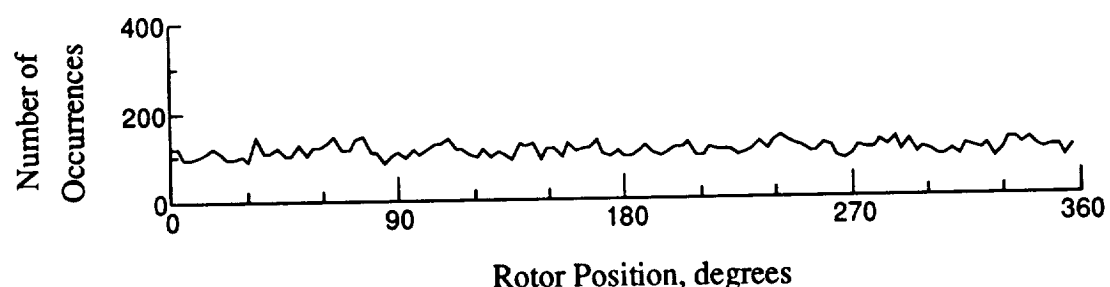
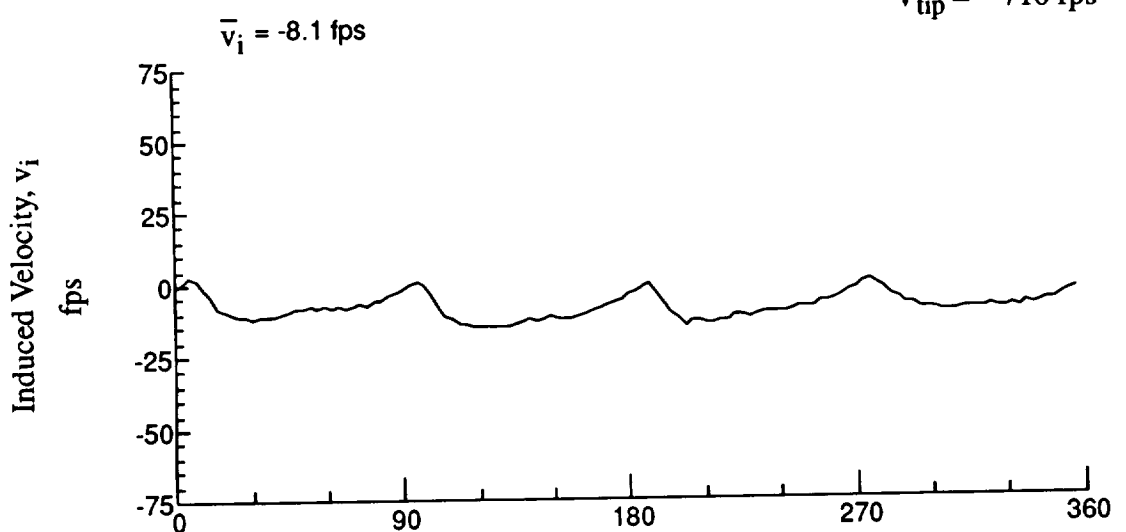


Figure 163.- Concluded.

$x/R = 1.10$, $y/R = -0.20$, $z = 8.85 \text{ in.}$

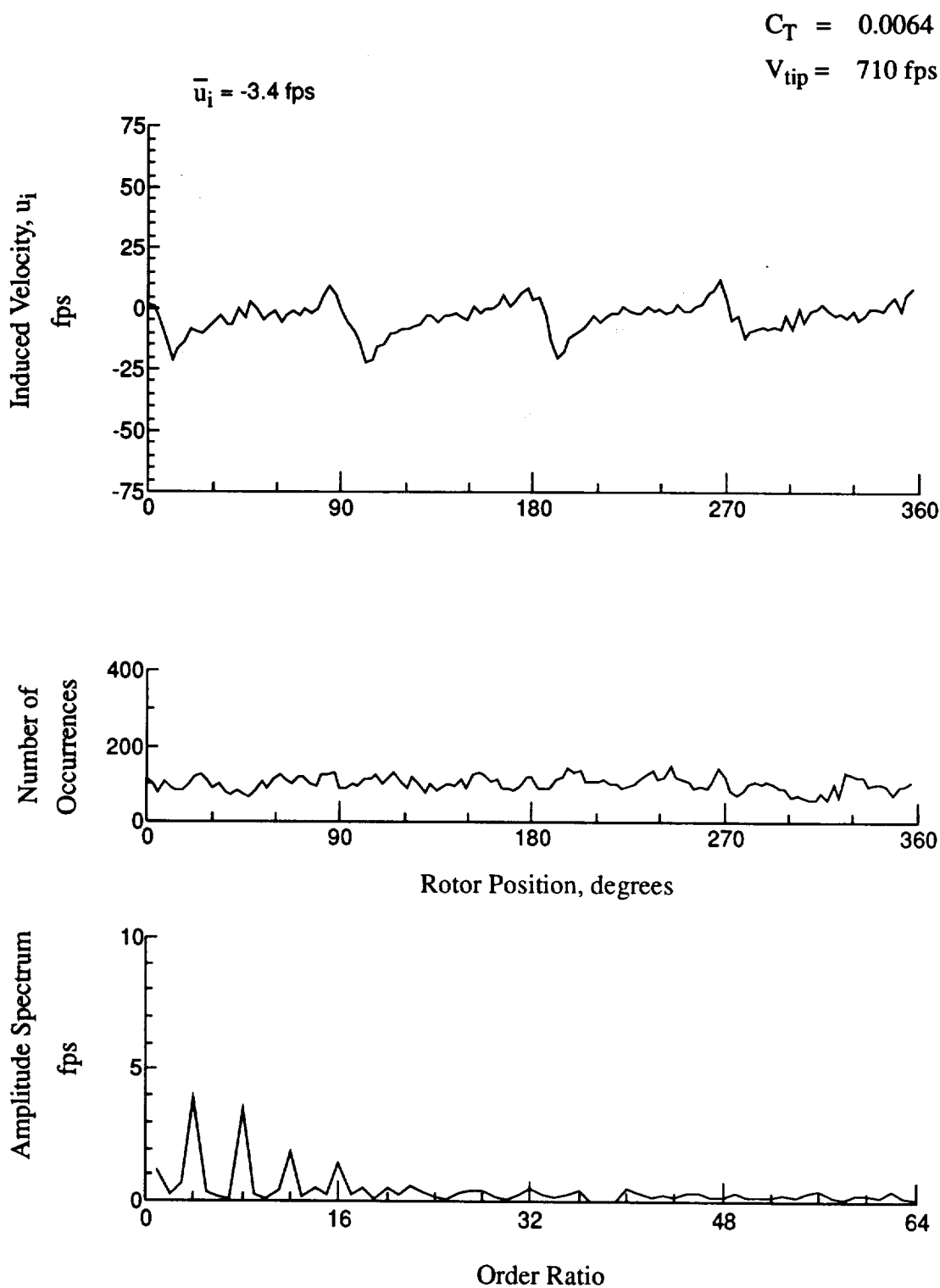


Figure 164.- Wake Measurements at
 $x/R = 1.10$, $y/R = -0.20$, $z = 7.82 \text{ in.}$

$$C_T = 0.0064$$

$$V_{tip} = 710 \text{ fps}$$

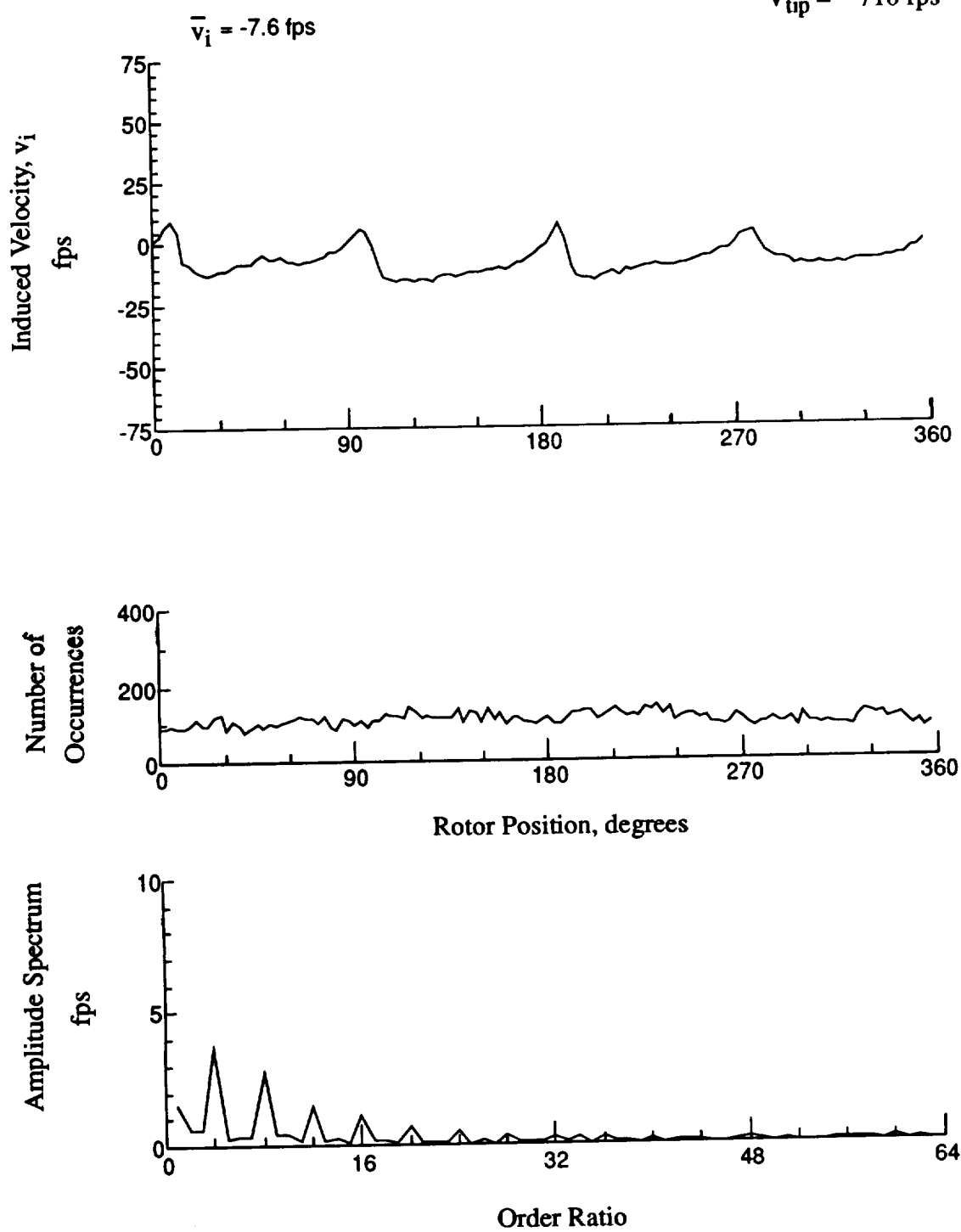


Figure 164.- Concluded.
 $x/R = 1.10$, $y/R = -0.20$, $z = 7.82 \text{ in.}$

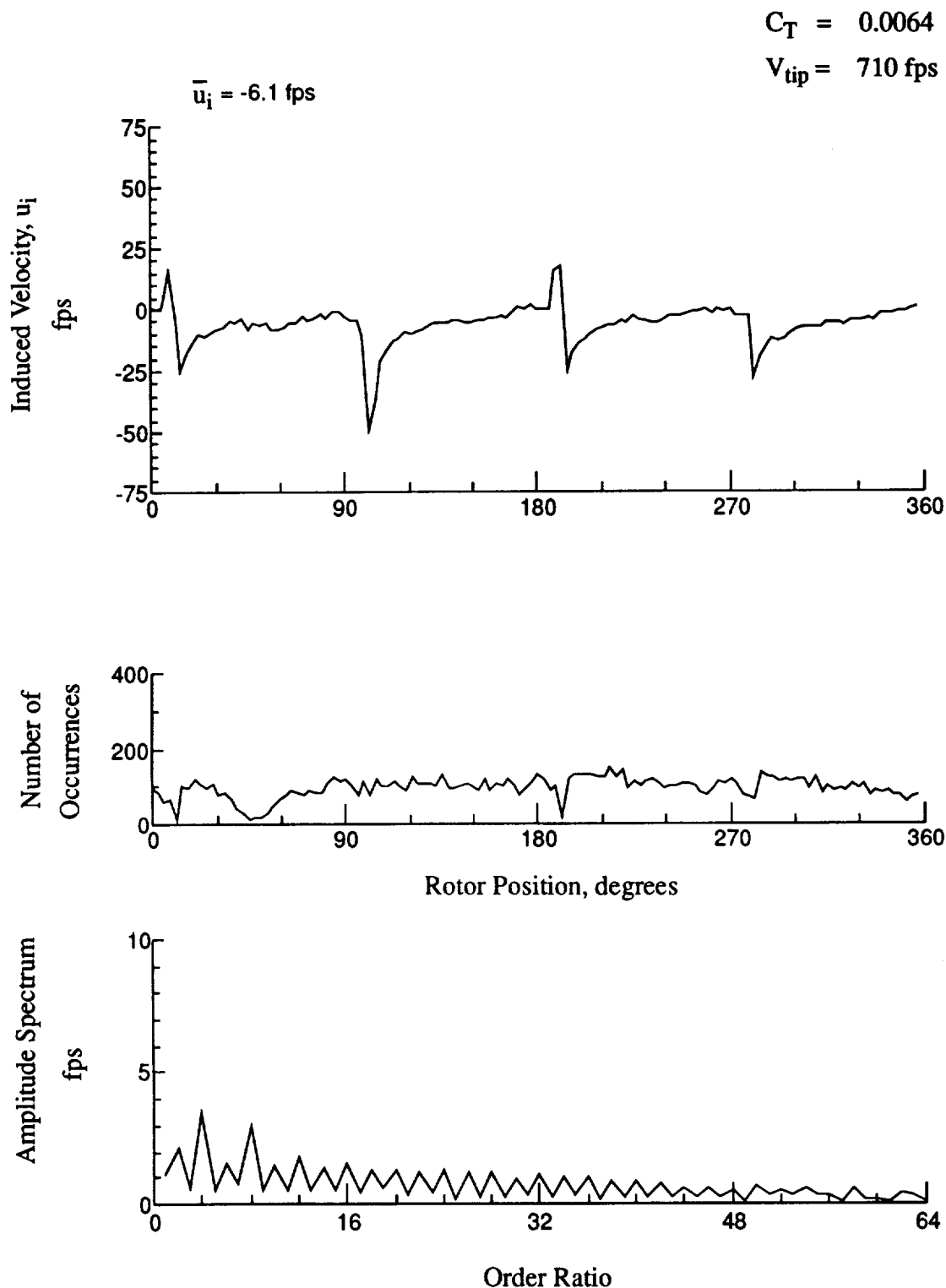


Figure 165.- Wake Measurements at
 $x/R = 1.10$, $y/R = -0.20$, $z = 6.79 \text{ in.}$

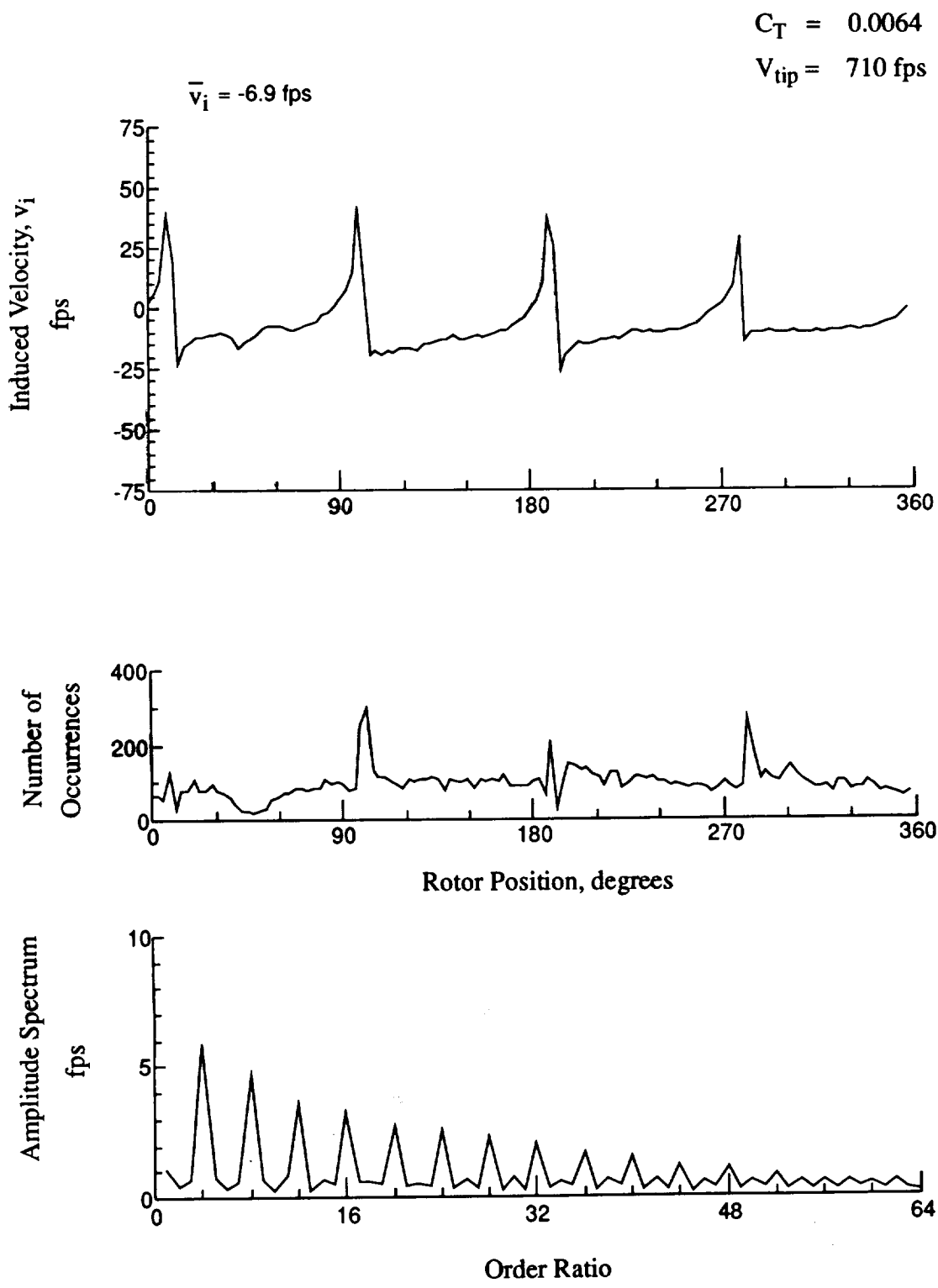


Figure 165.- Concluded.
 $x/R = 1.10$, $y/R = -0.20$, $z = 6.79 \text{ in.}$

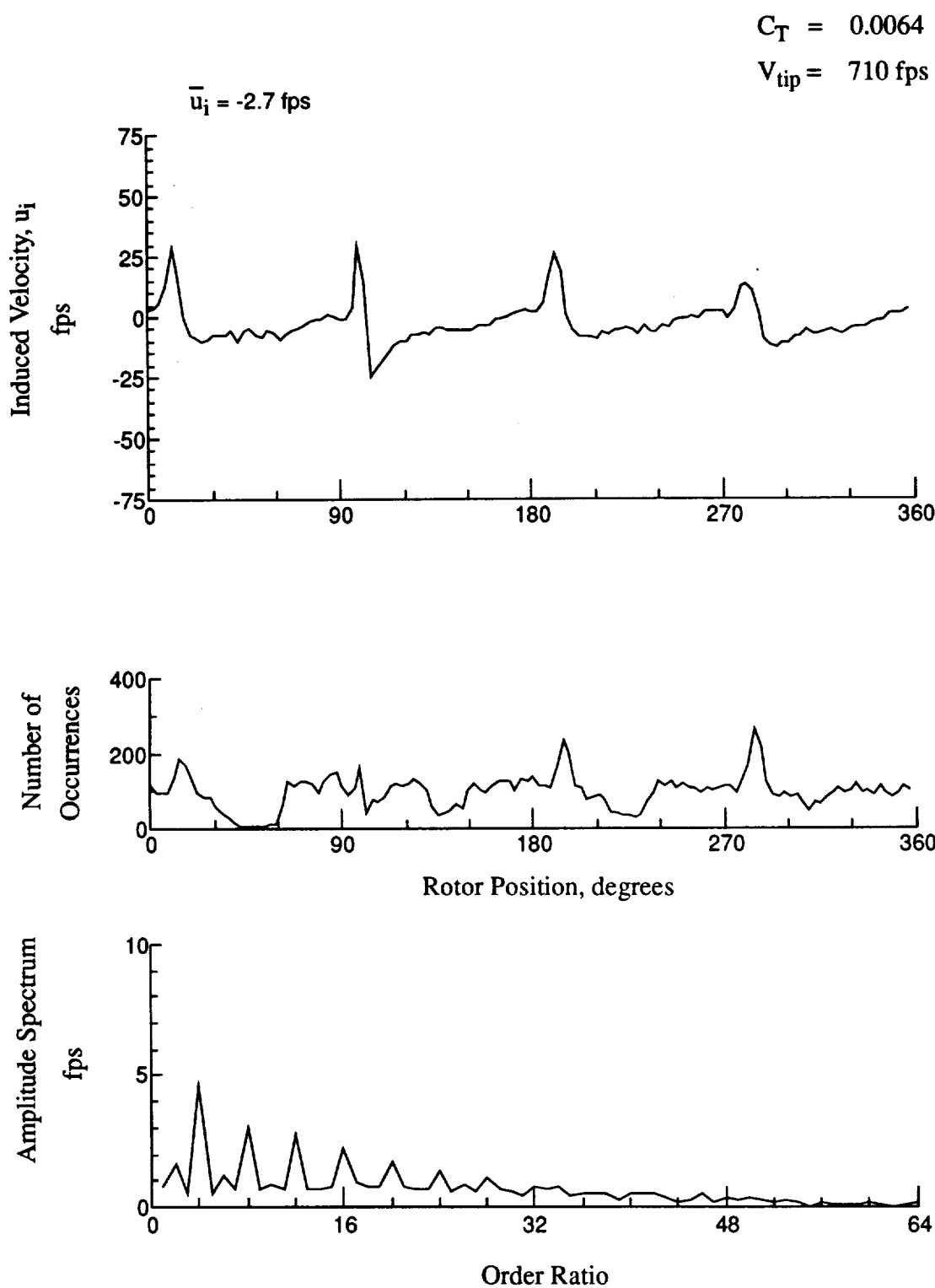


Figure 166.- Wake Measurements at
 $x/R = 1.10$, $y/R = -0.20$, $z = 5.76 \text{ in.}$

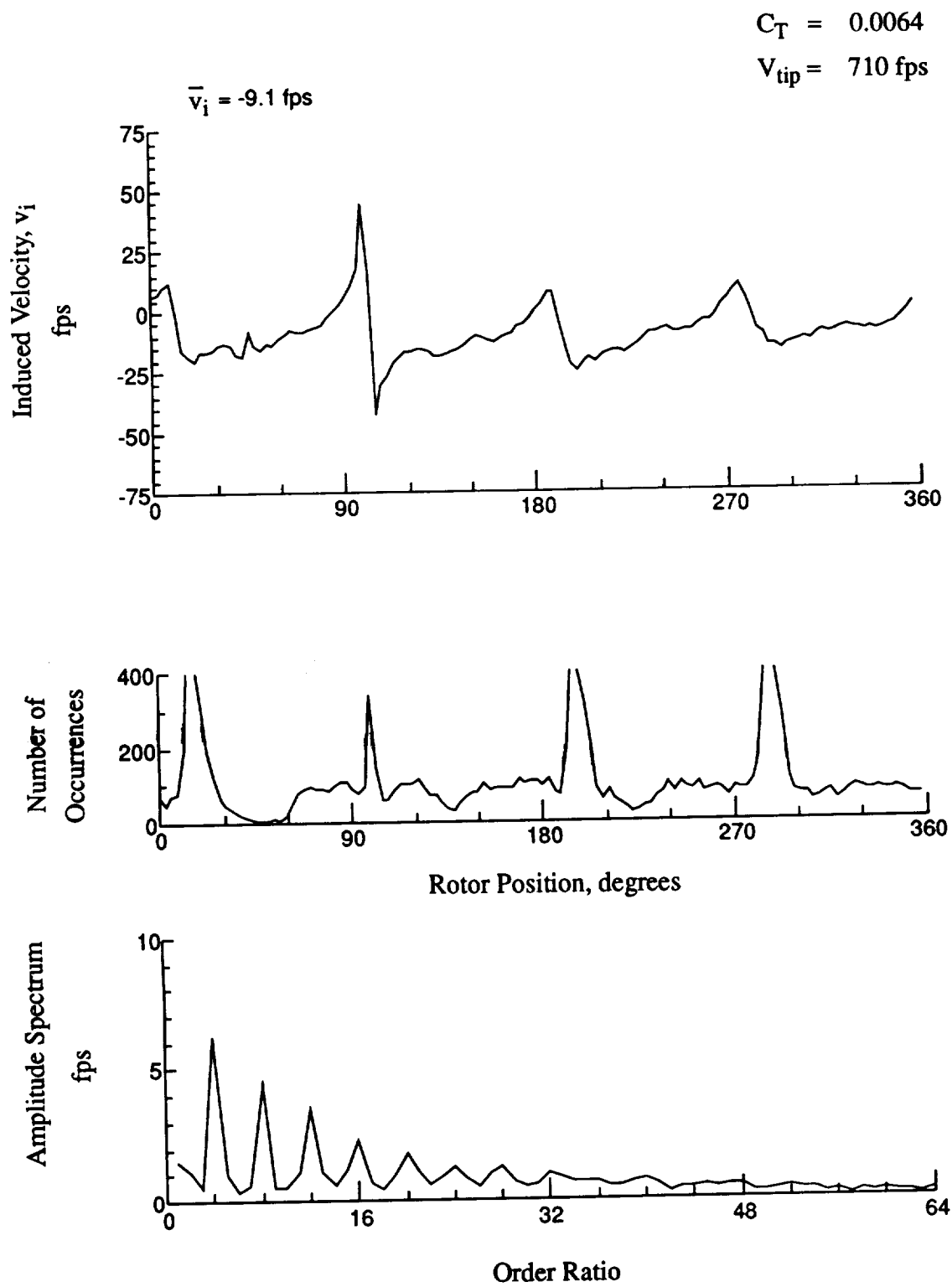


Figure 166.- Concluded.
 $x/R = 1.10$, $y/R = -0.20$, $z = 5.76 \text{ in.}$

$$C_T = 0.0064$$

$$V_{tip} = 710 \text{ fps}$$

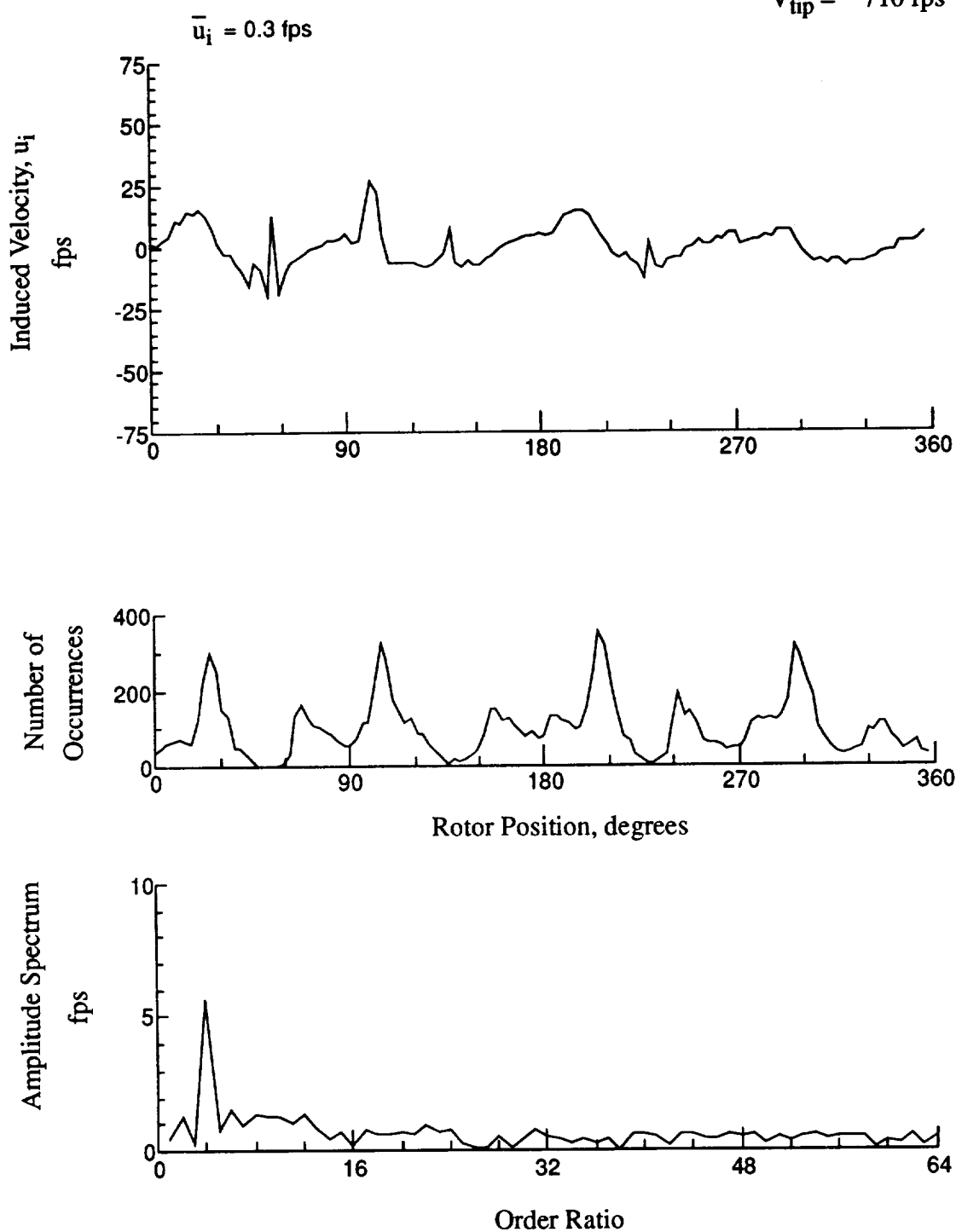


Figure 167.- Wake Measurements at
 $x/R = 1.10$, $y/R = -0.20$, $z = 4.73 \text{ in.}$

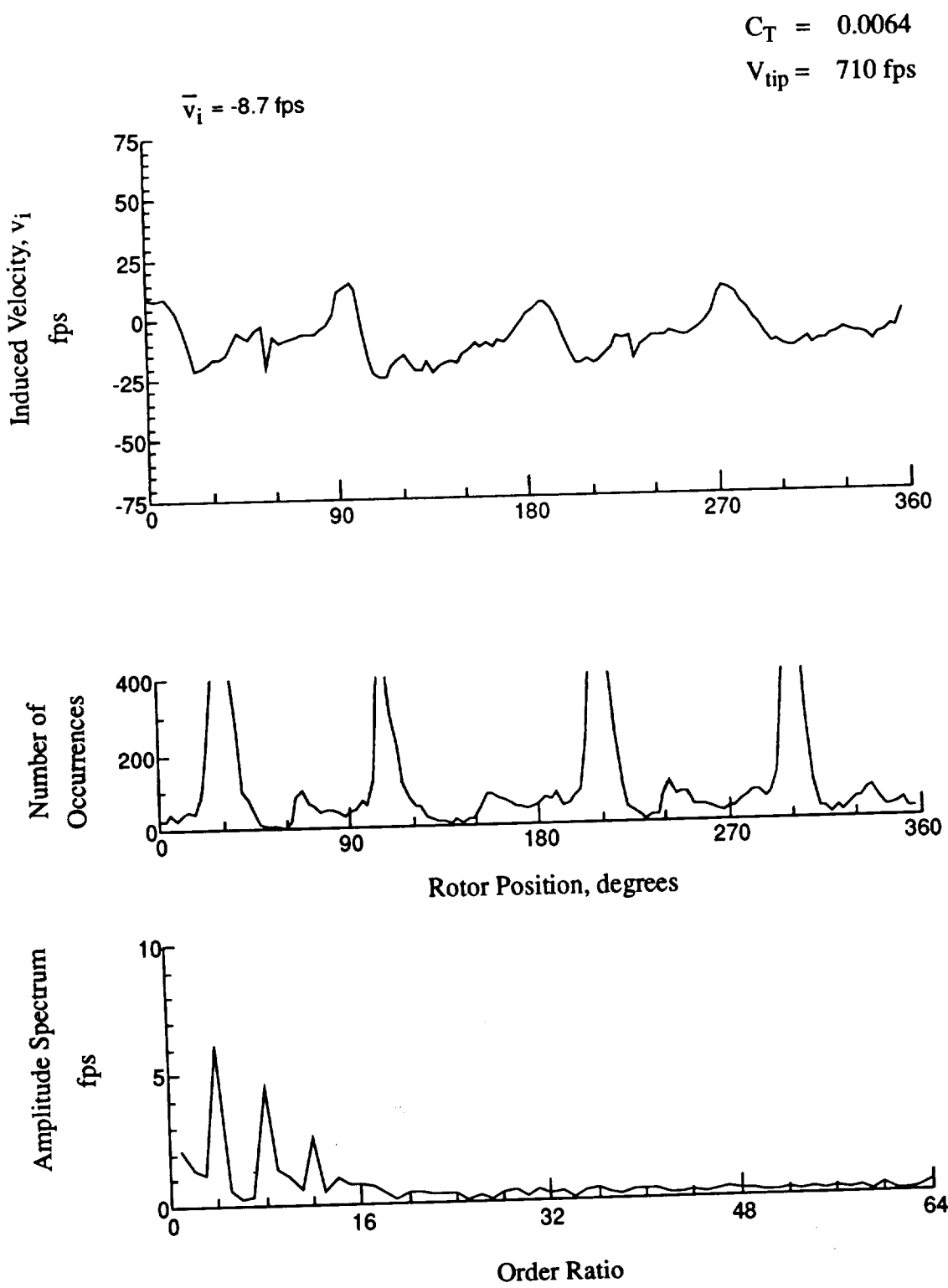


Figure 167.- Concluded.
 $x/R = 1.10$, $y/R = -0.20$, $z = 4.73 \text{ in.}$

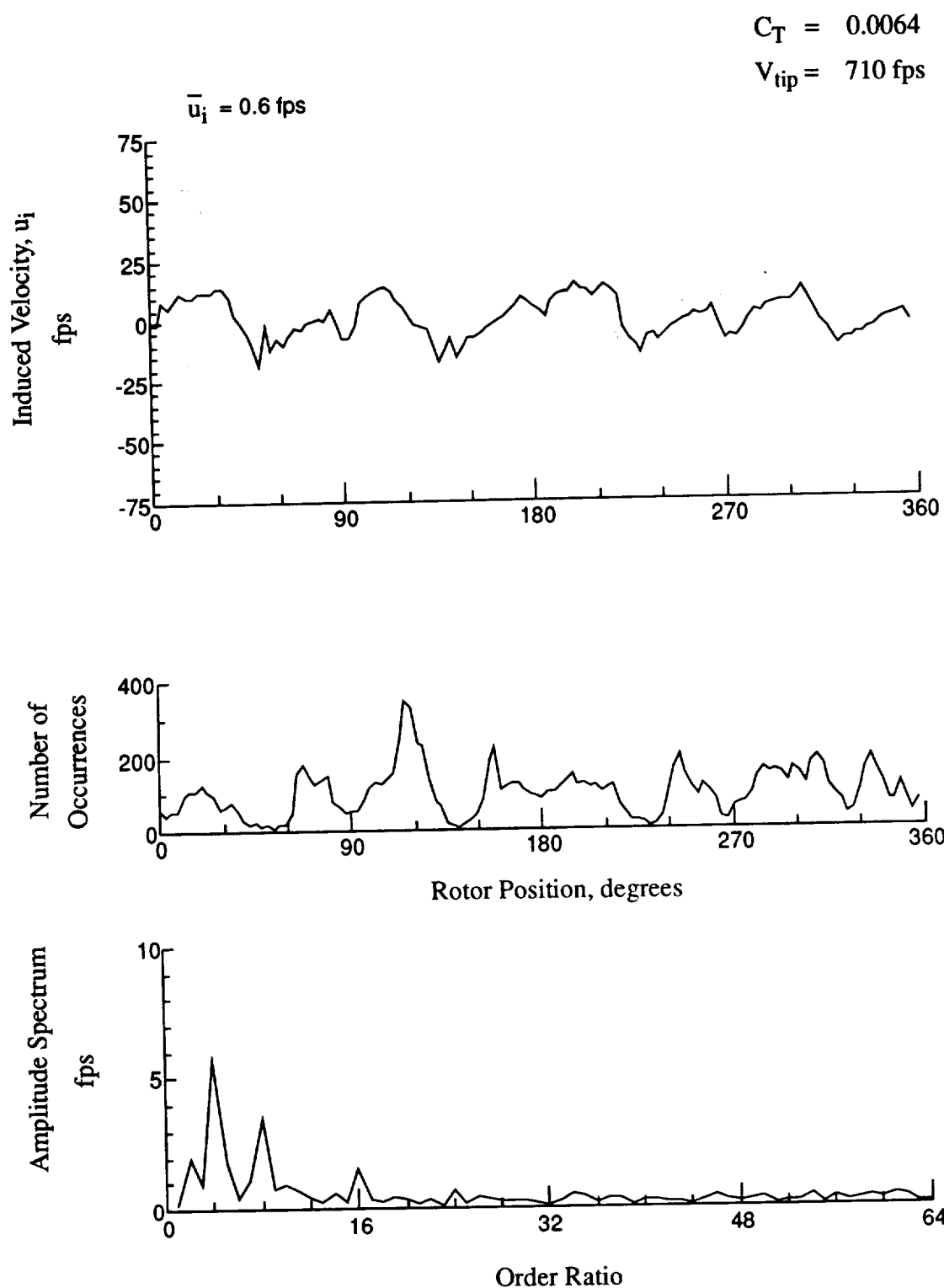


Figure 168.- Wake Measurements at
 $x/R = 1.10$, $y/R = -0.20$, $z = 3.70 \text{ in.}$

$$C_T = 0.0064$$

$$V_{tip} = 710 \text{ fps}$$

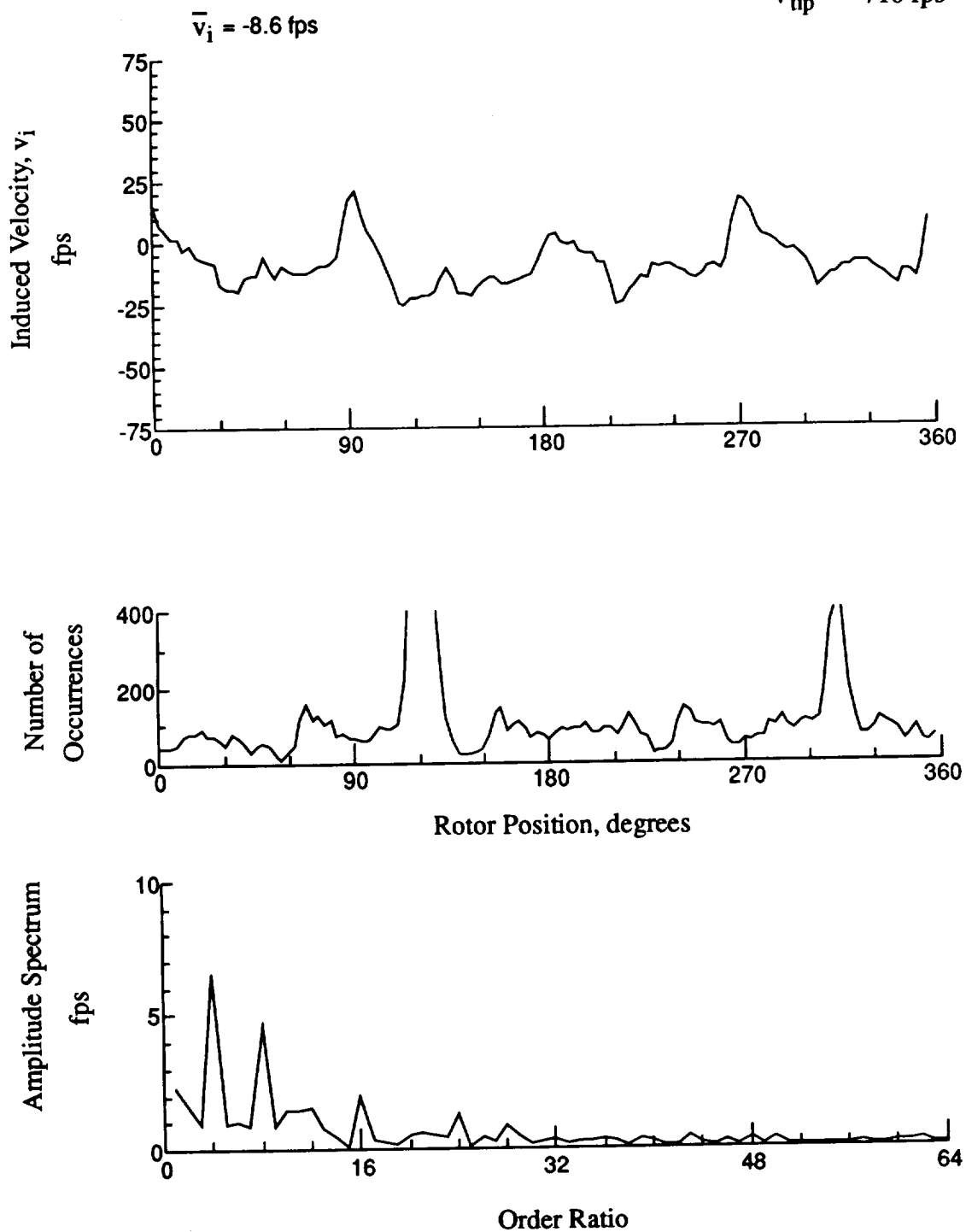


Figure 168.- Concluded.
 $x/R = 1.10$, $y/R = -0.20$, $z = 3.70 \text{ in.}$

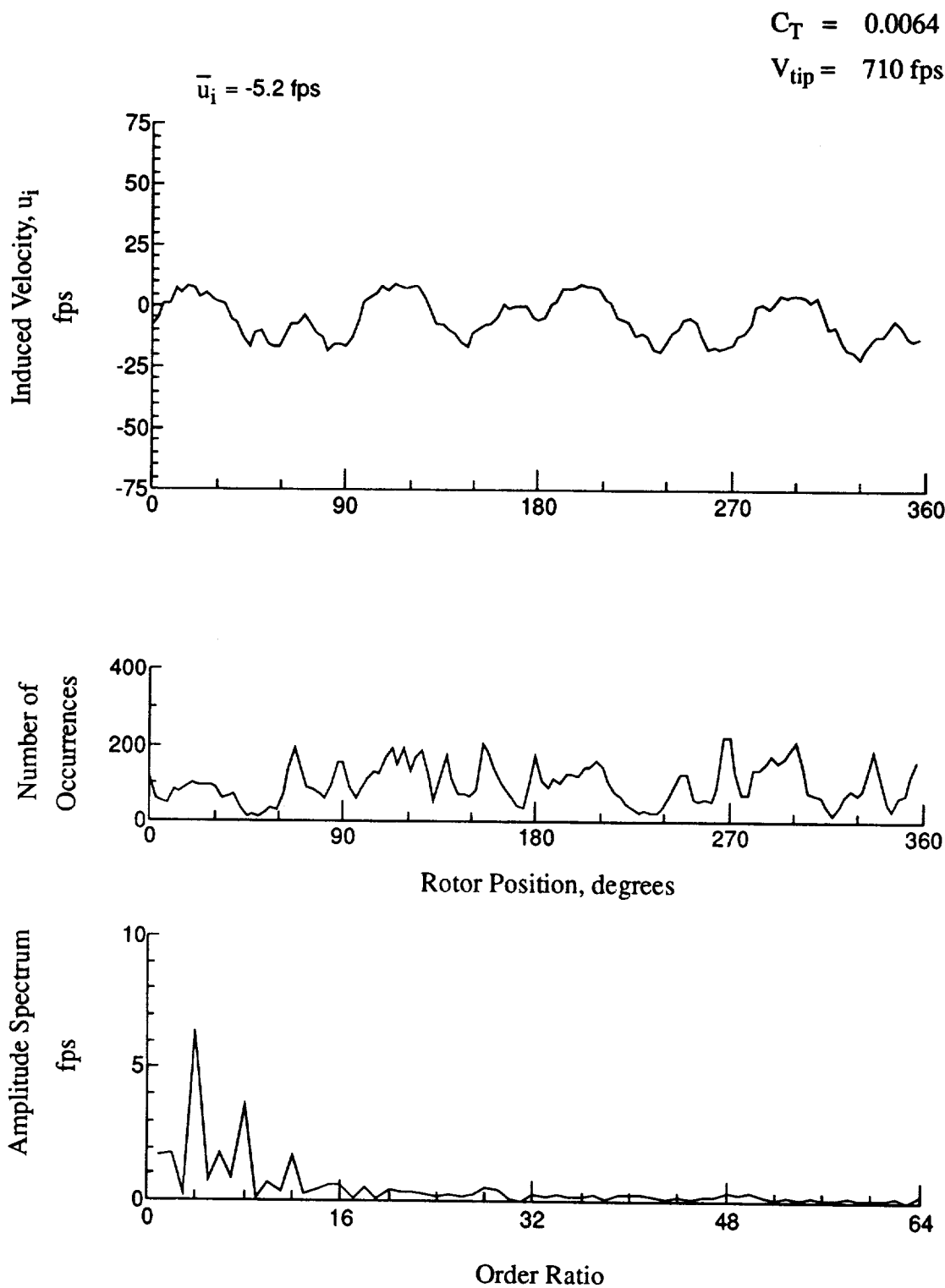


Figure 169.- Wake Measurements at
 $x/R = 1.10$, $y/R = -0.20$, $z = 2.67 \text{ in.}$

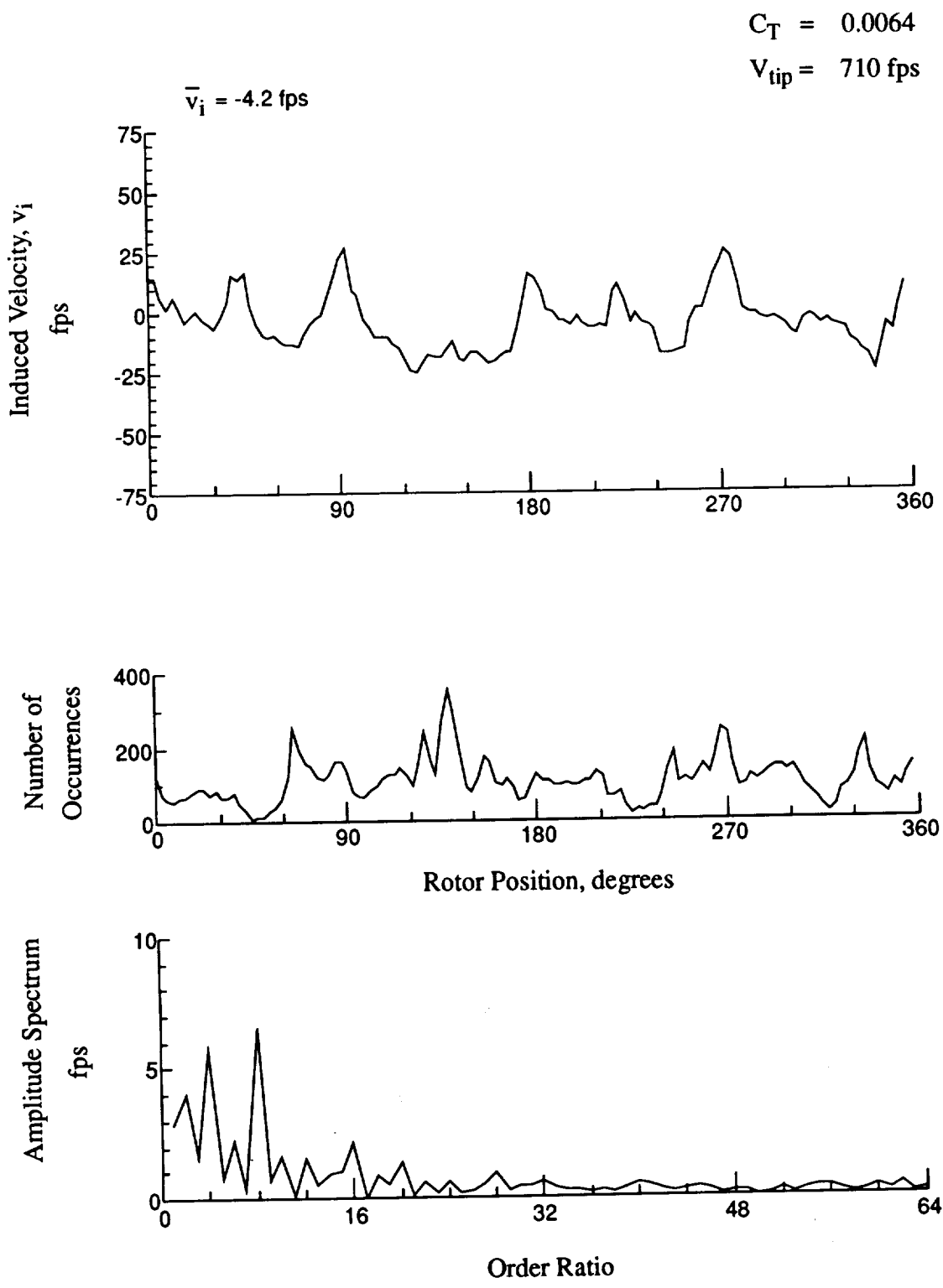


Figure 169.- Concluded.
 $x/R = 1.10$, $y/R = -0.20$, $z = 2.67 \text{ in.}$

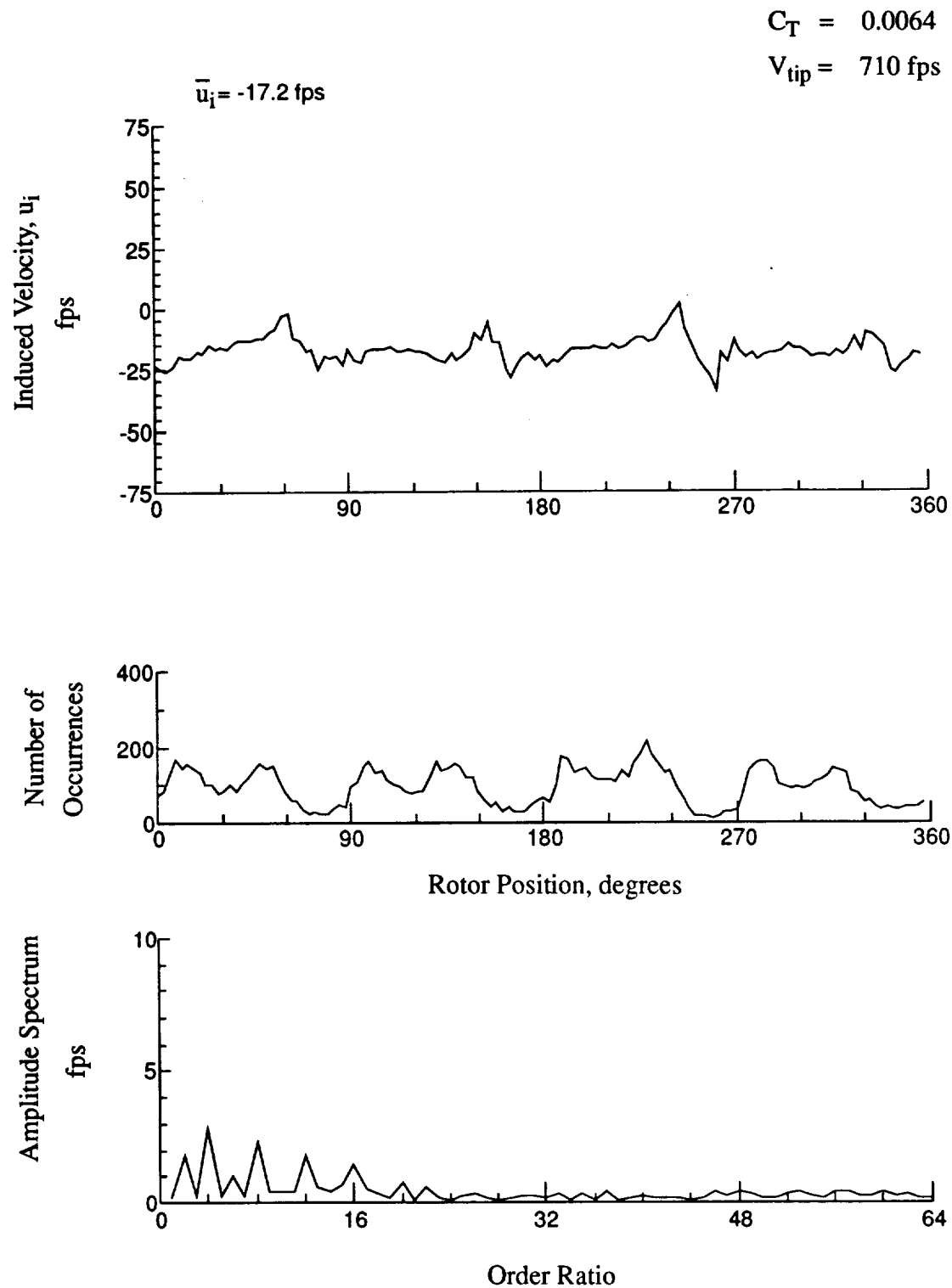


Figure 170.- Wake Measurements at
 $x/R = 0.90$, $y/R = -0.20$, $z = -0.27$ in.

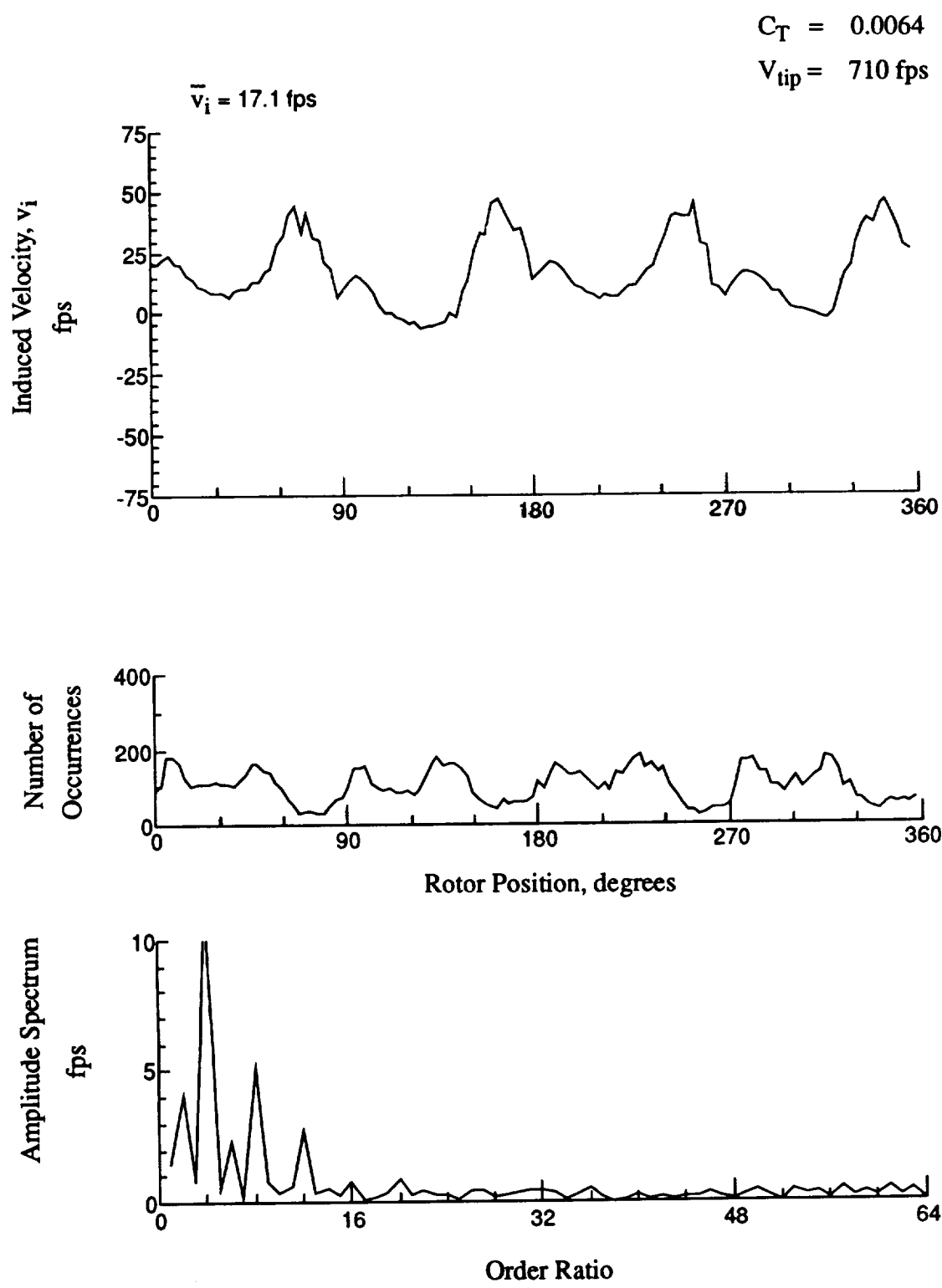


Figure 170.- Concluded.
 $x/R = 0.90$, $y/R = -0.20$, $z = -0.27 \text{ in.}$

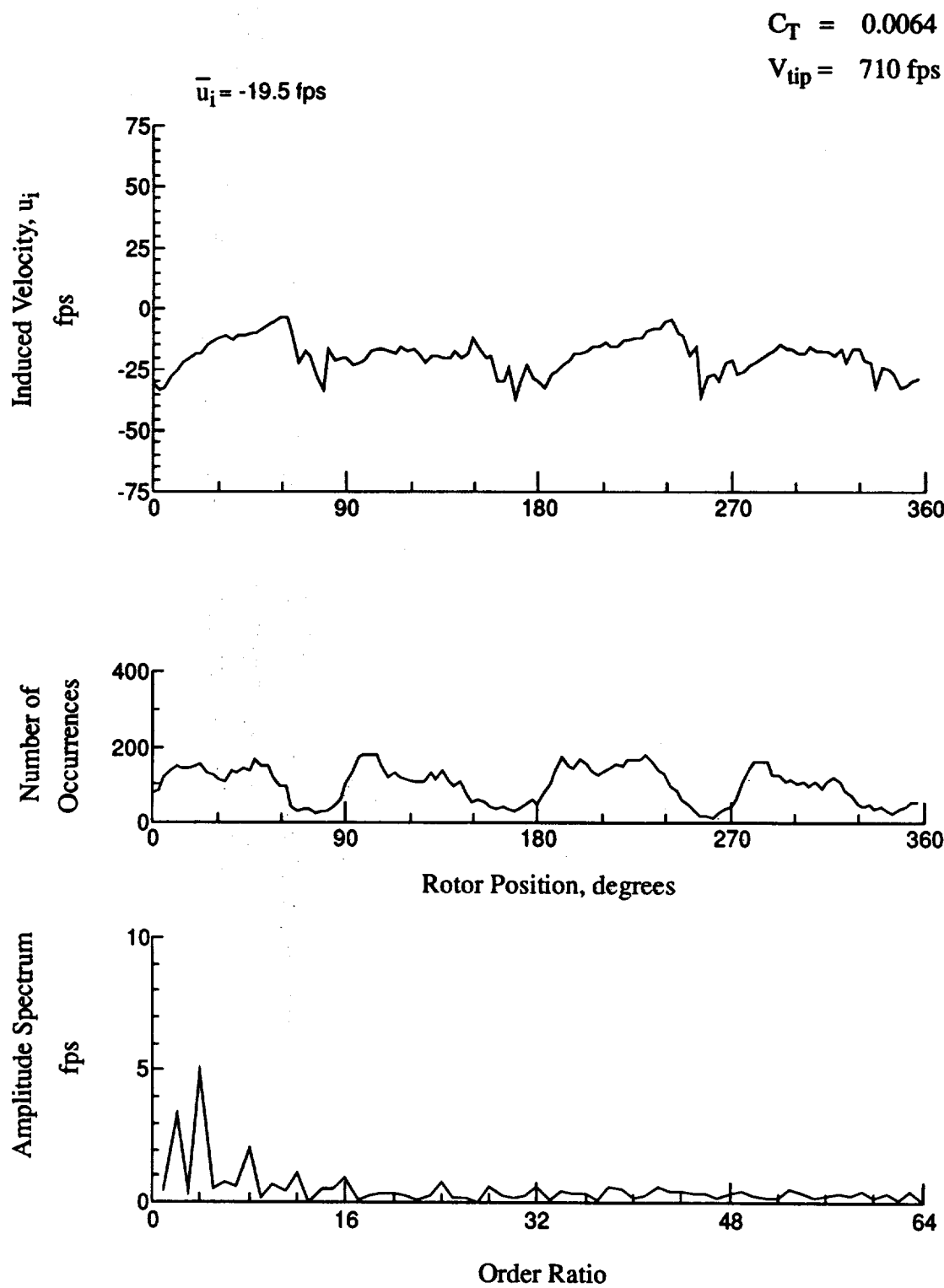


Figure 171.- Wake Measurements at
 $x/R = 0.90$, $y/R = -0.20$, $z = -1.30 \text{ in.}$

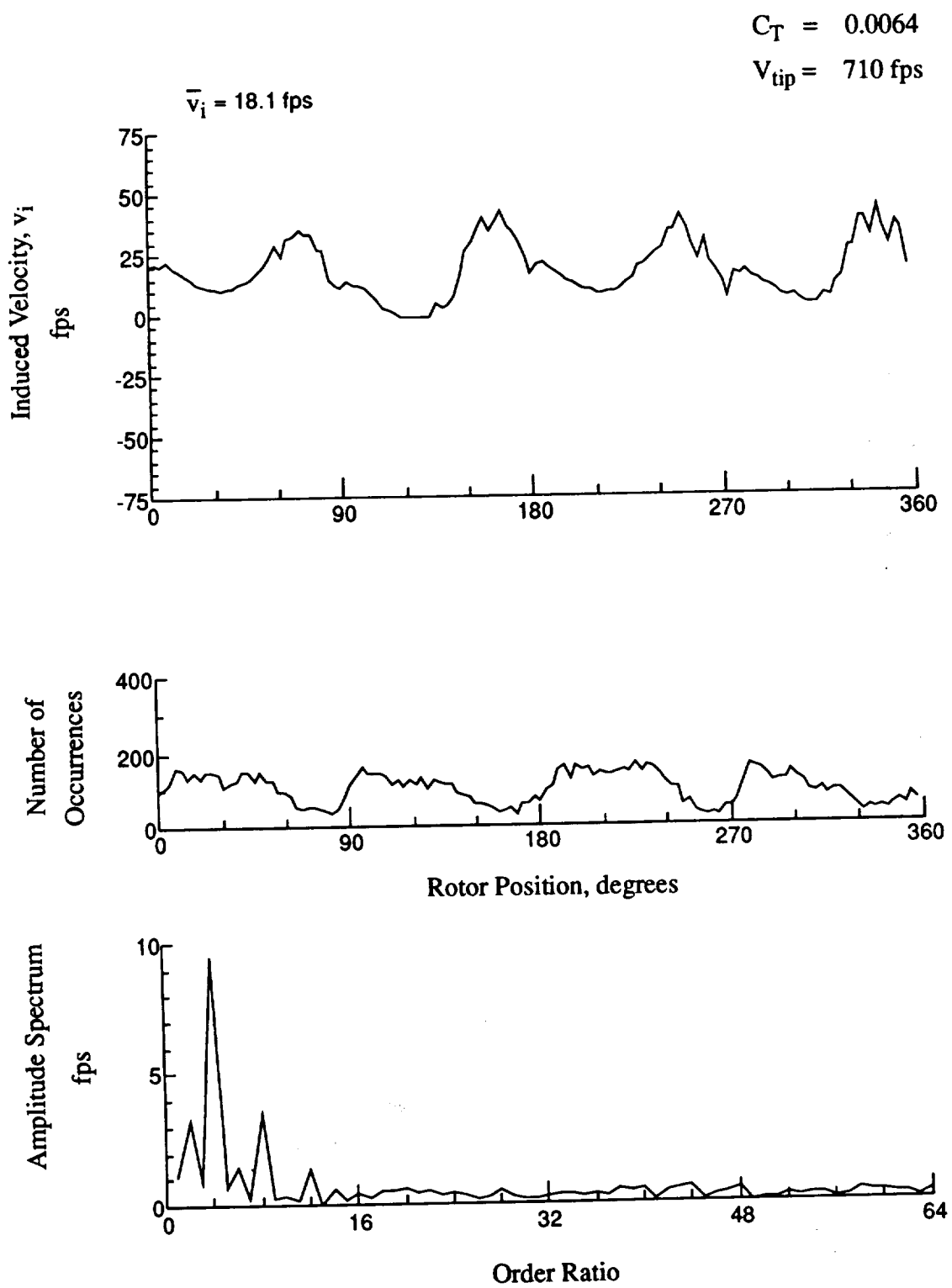


Figure 171.- Concluded.
 $x/R = 0.90$, $y/R = -0.20$, $z = -1.30 \text{ in.}$

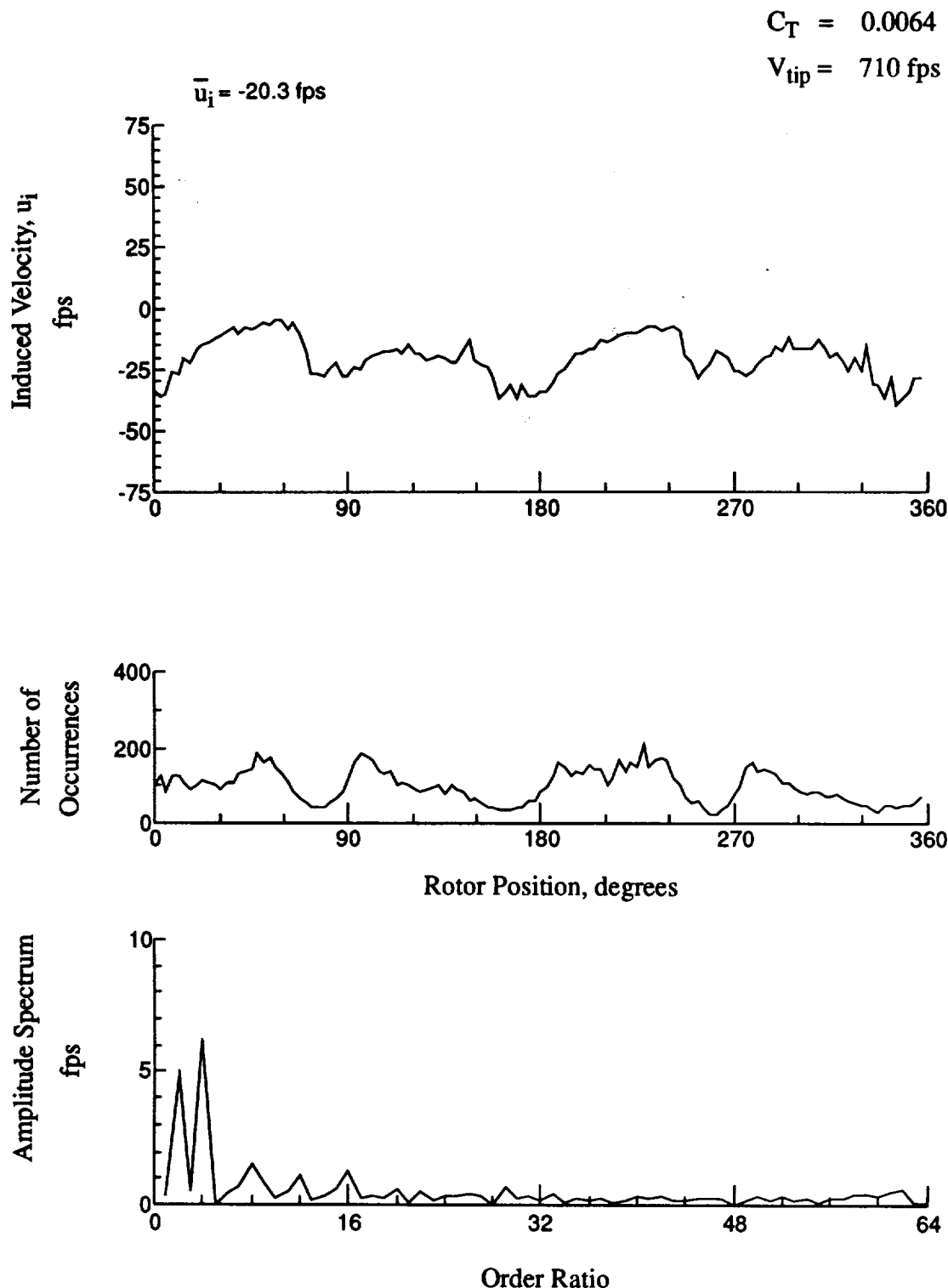


Figure 172.- Wake Measurements at
 $x/R = 0.90$, $y/R = -0.20$, $z = -2.36 \text{ in.}$

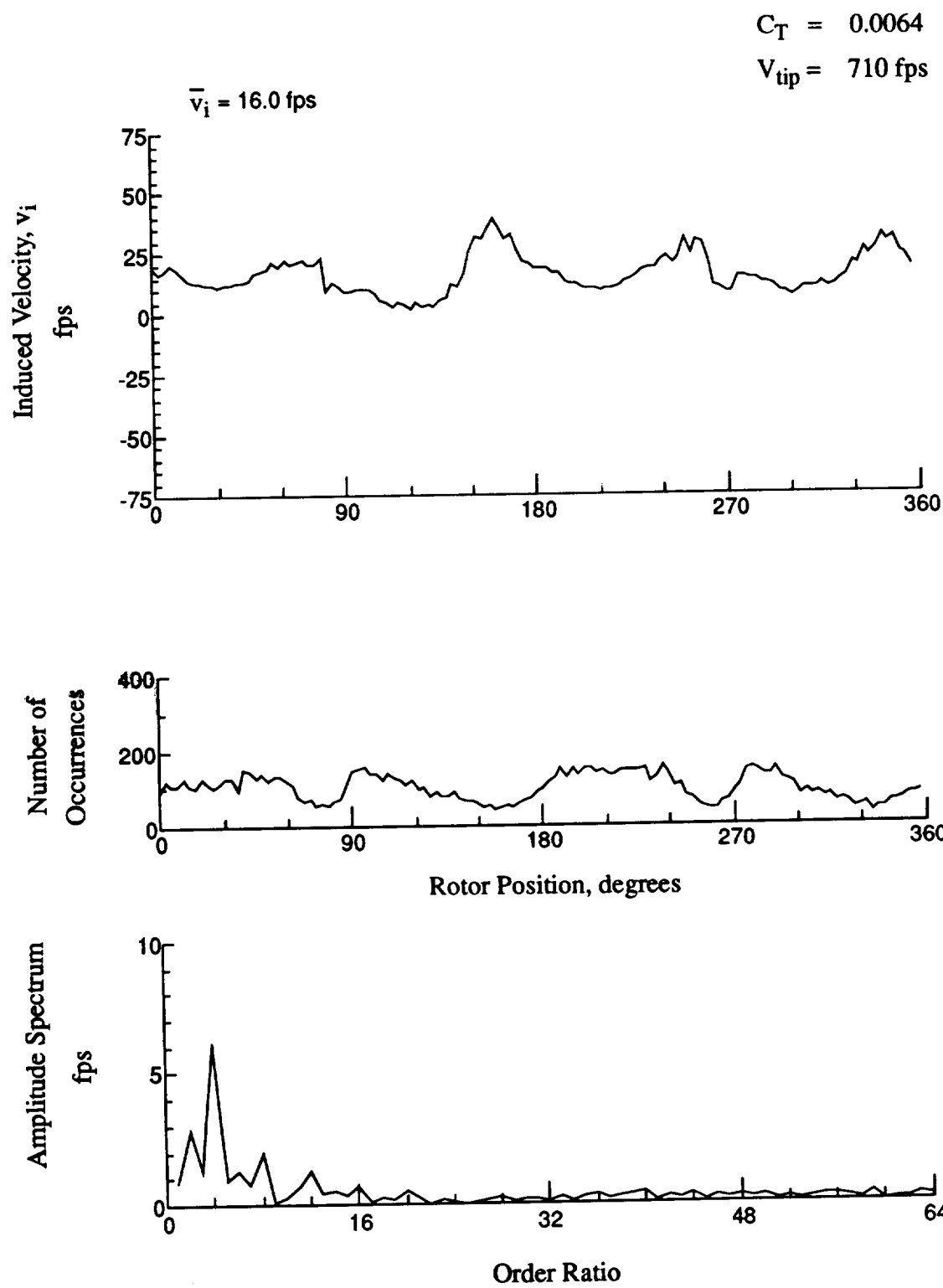


Figure 172.- Concluded.
 $x/R = 0.90$, $y/R = -0.20$, $z = -2.36 \text{ in.}$

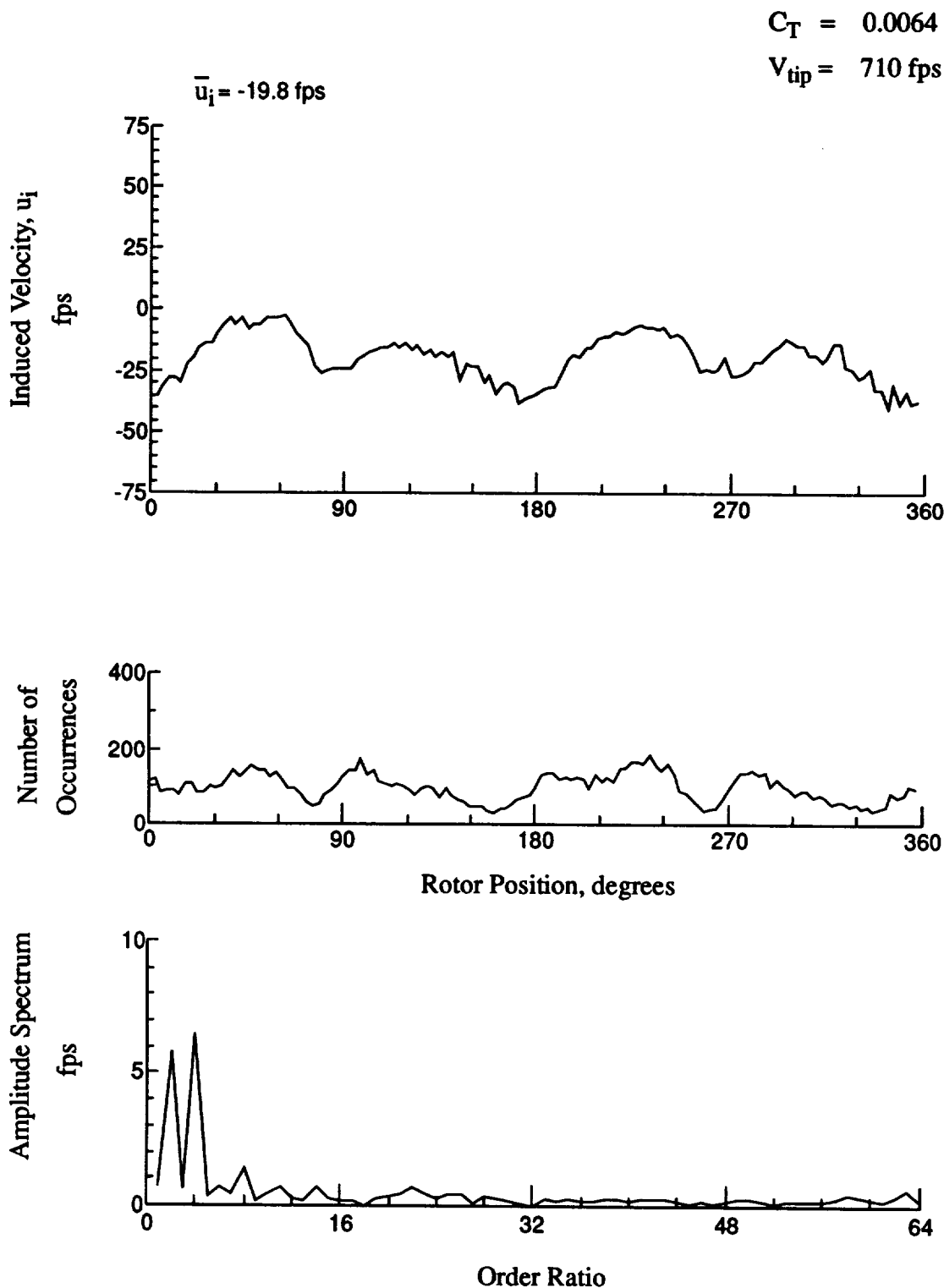


Figure 173.- Wake Measurements at
 $x/R = 0.90$, $y/R = -0.20$, $z = -3.36 \text{ in.}$

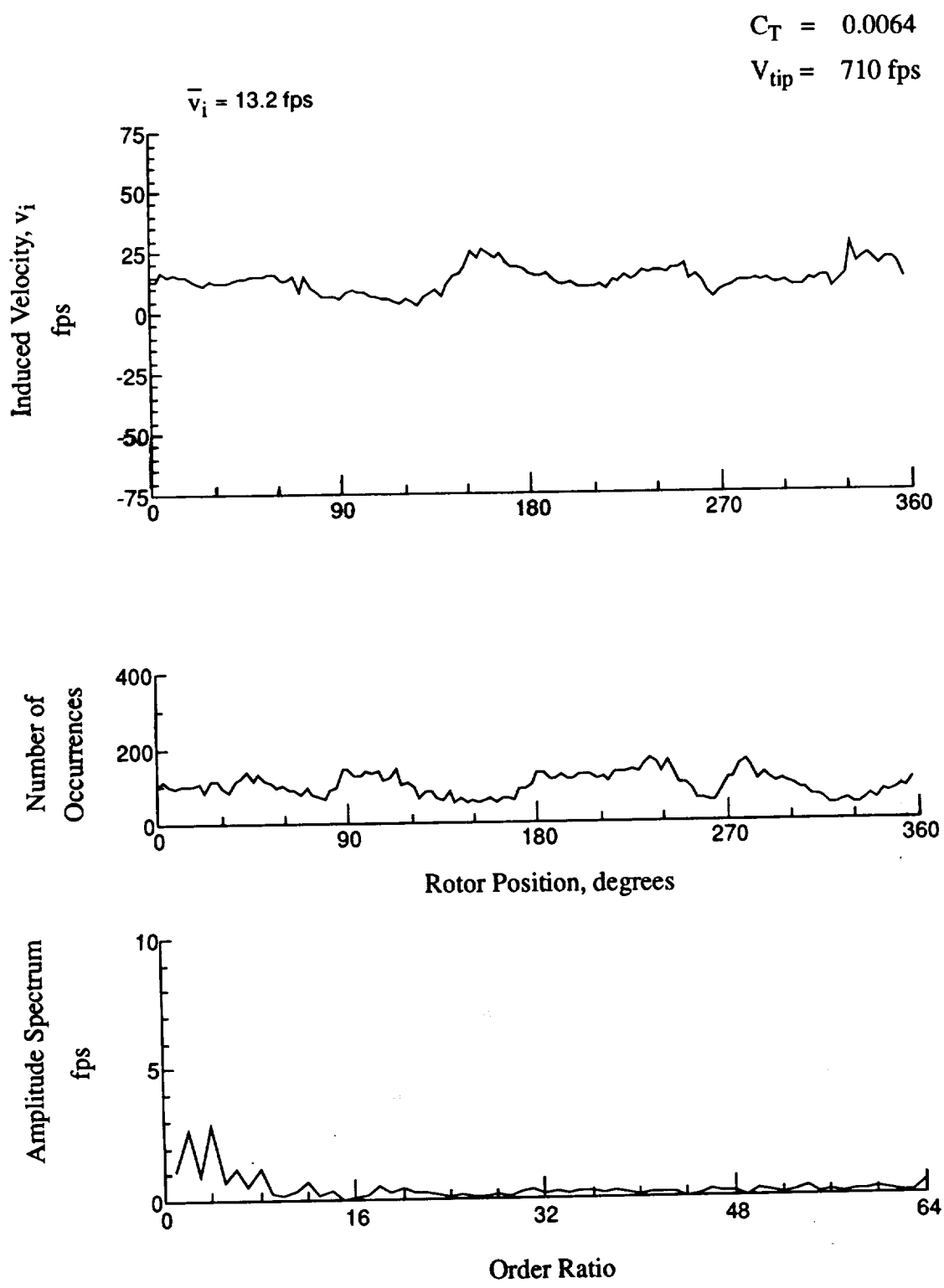


Figure 173.- Concluded.
 $x/R = 0.90$, $y/R = -0.20$, $z = -3.36 \text{ in.}$

$C_T = 0.0064$

$V_{tip} = 710 \text{ fps}$

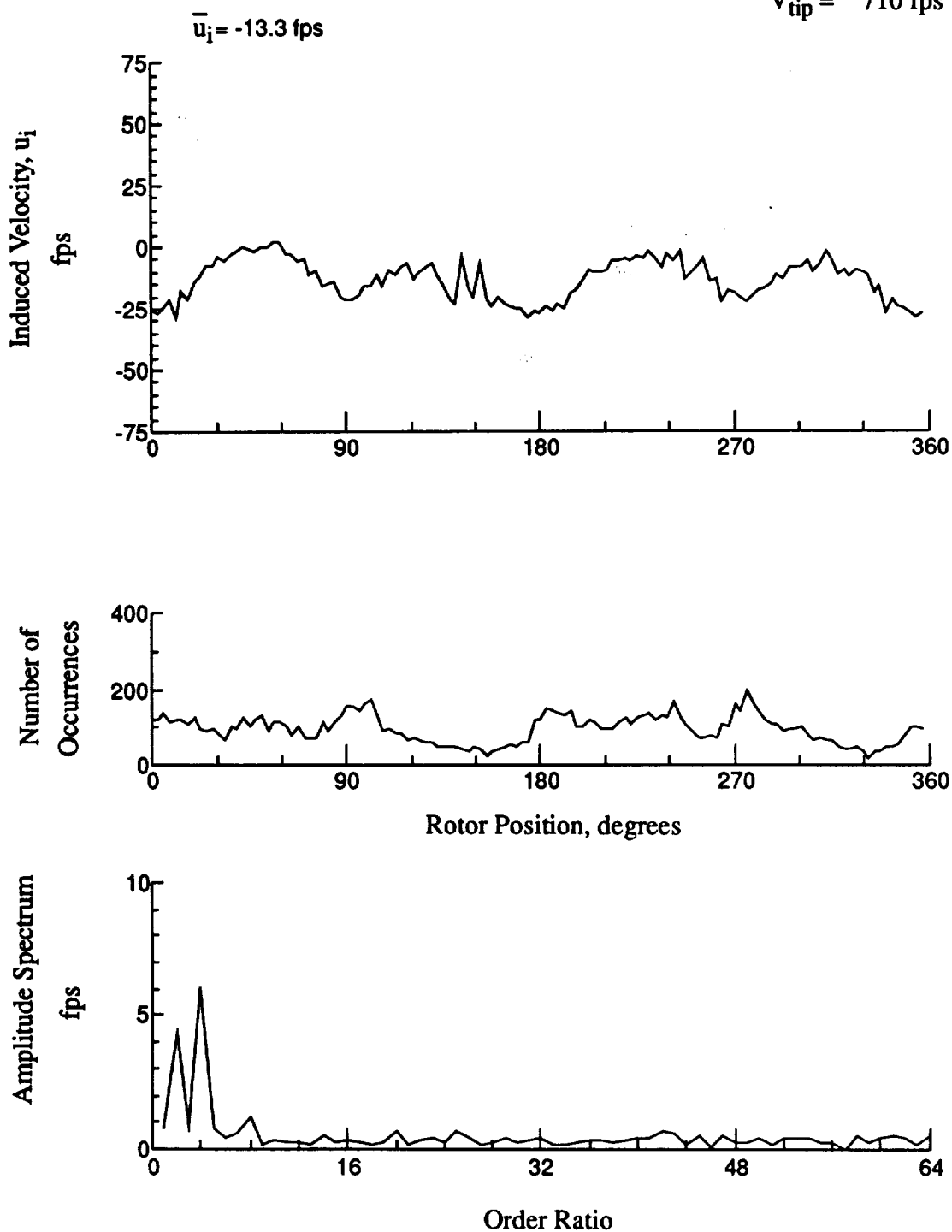


Figure 174.- Wake Measurements at
 $x/R = 0.90$, $y/R = -0.20$, $z = -4.39$ in.

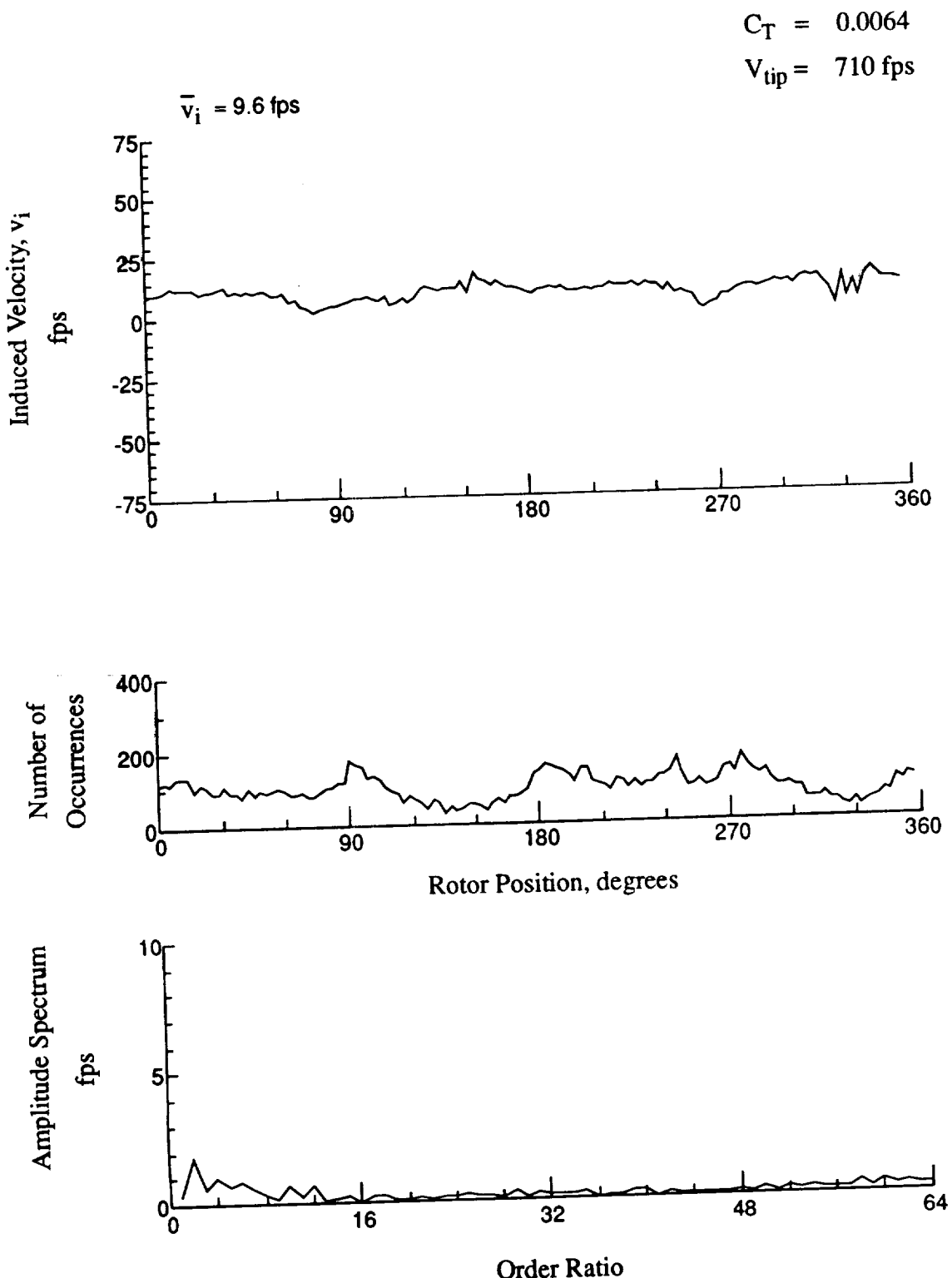


Figure 174.- Concluded.
 $x/R = 0.90$, $y/R = -0.20$, $z = -4.39 \text{ in.}$

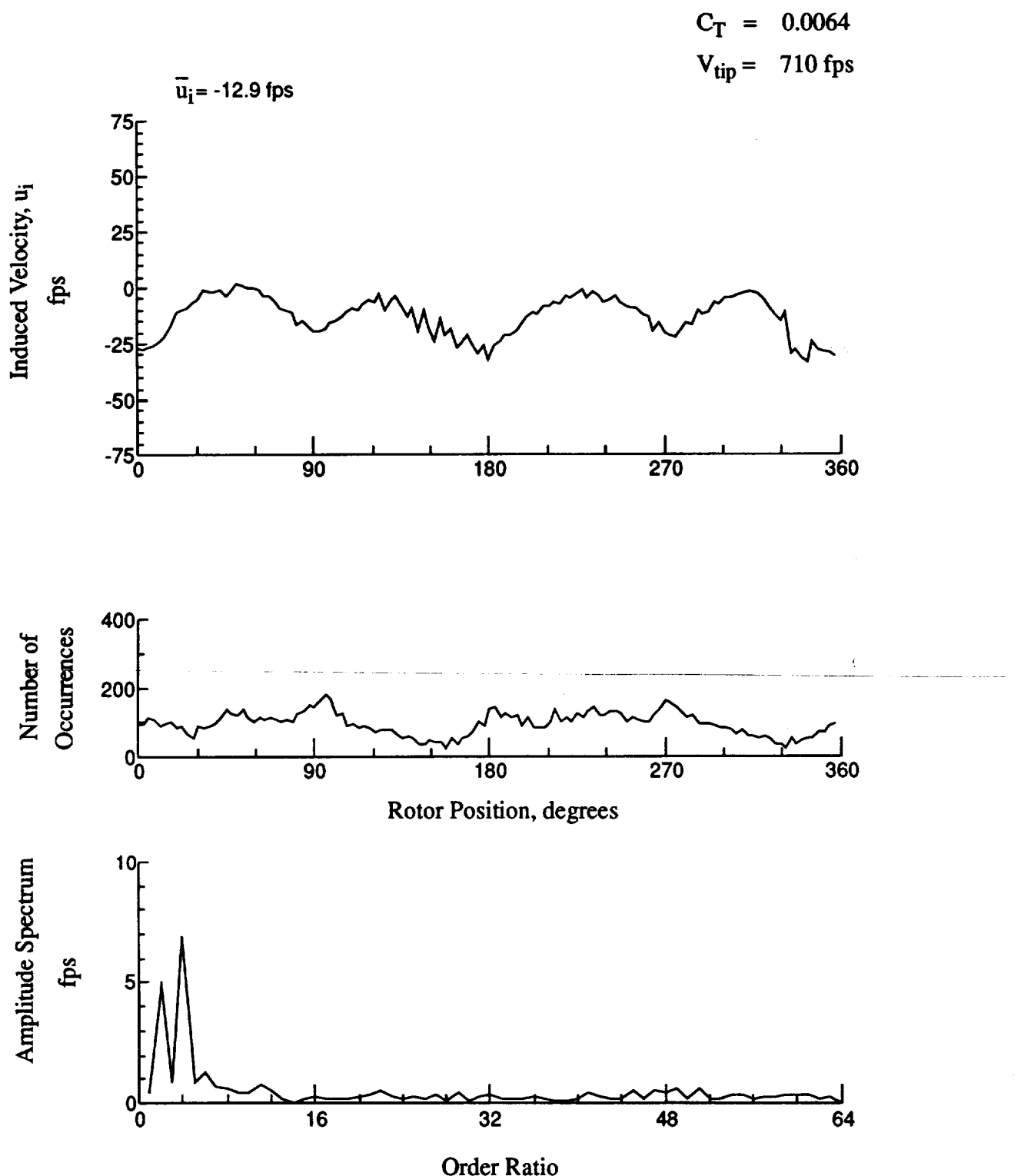


Figure 175.- Wake Measurements at
 $x/R = 0.90$, $y/R = -0.20$, $z = -5.42 \text{ in.}$

$$C_T = 0.0064$$

$$V_{tip} = 710 \text{ fps}$$

$$\bar{v}_i = 7.3 \text{ fps}$$

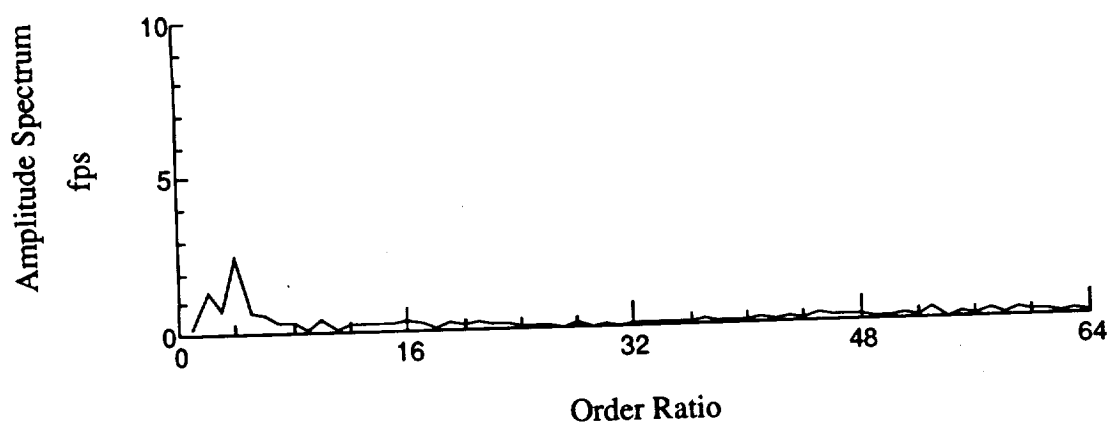
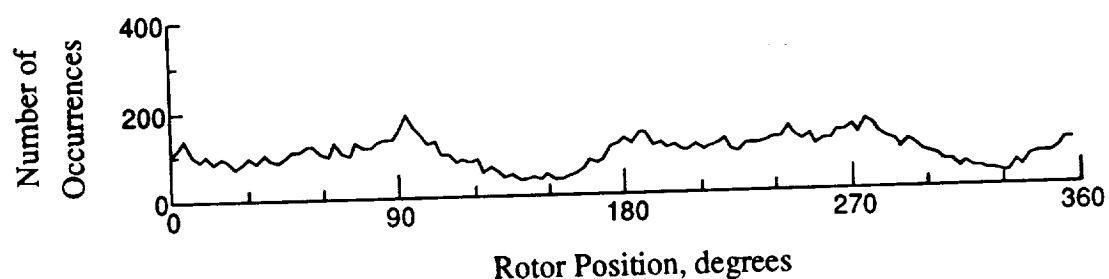
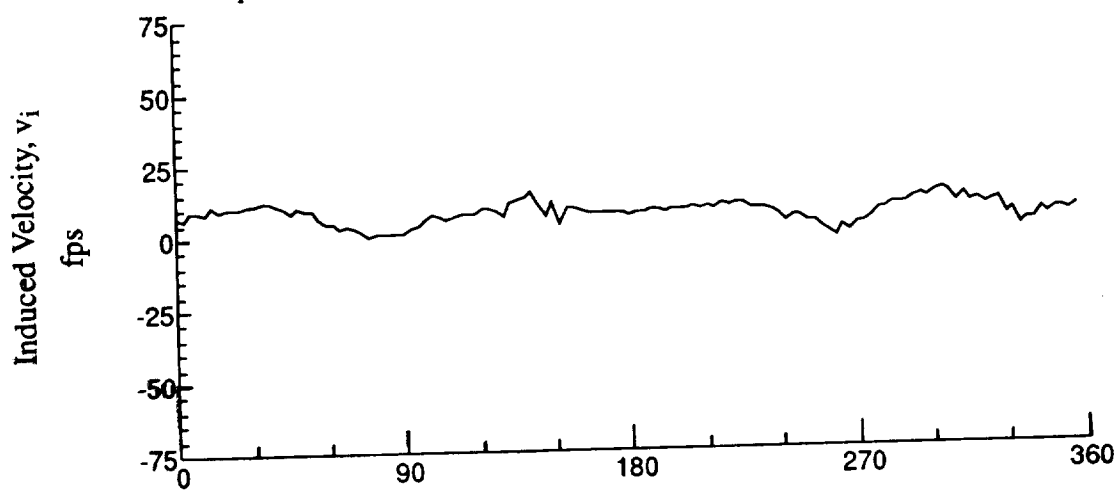


Figure 175.- Concluded.

$x/R = 0.90$, $y/R = -0.20$, $z = -5.42$ in.

$$C_T = 0.0064$$

$$V_{tip} = 710 \text{ fps}$$

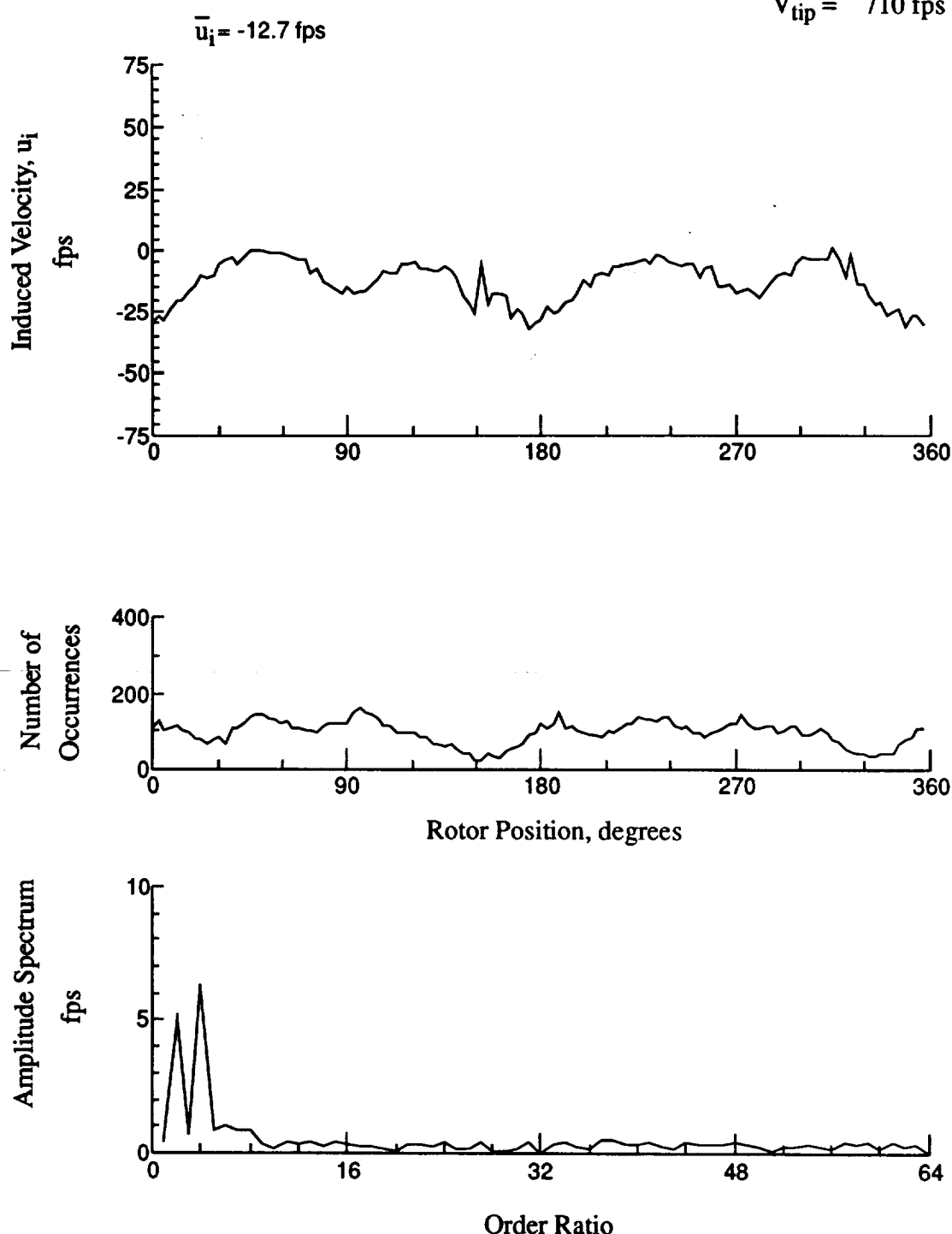


Figure 176.- Wake Measurements at
 $x/R = 0.90$, $y/R = -0.20$, $z = -6.45$ in.

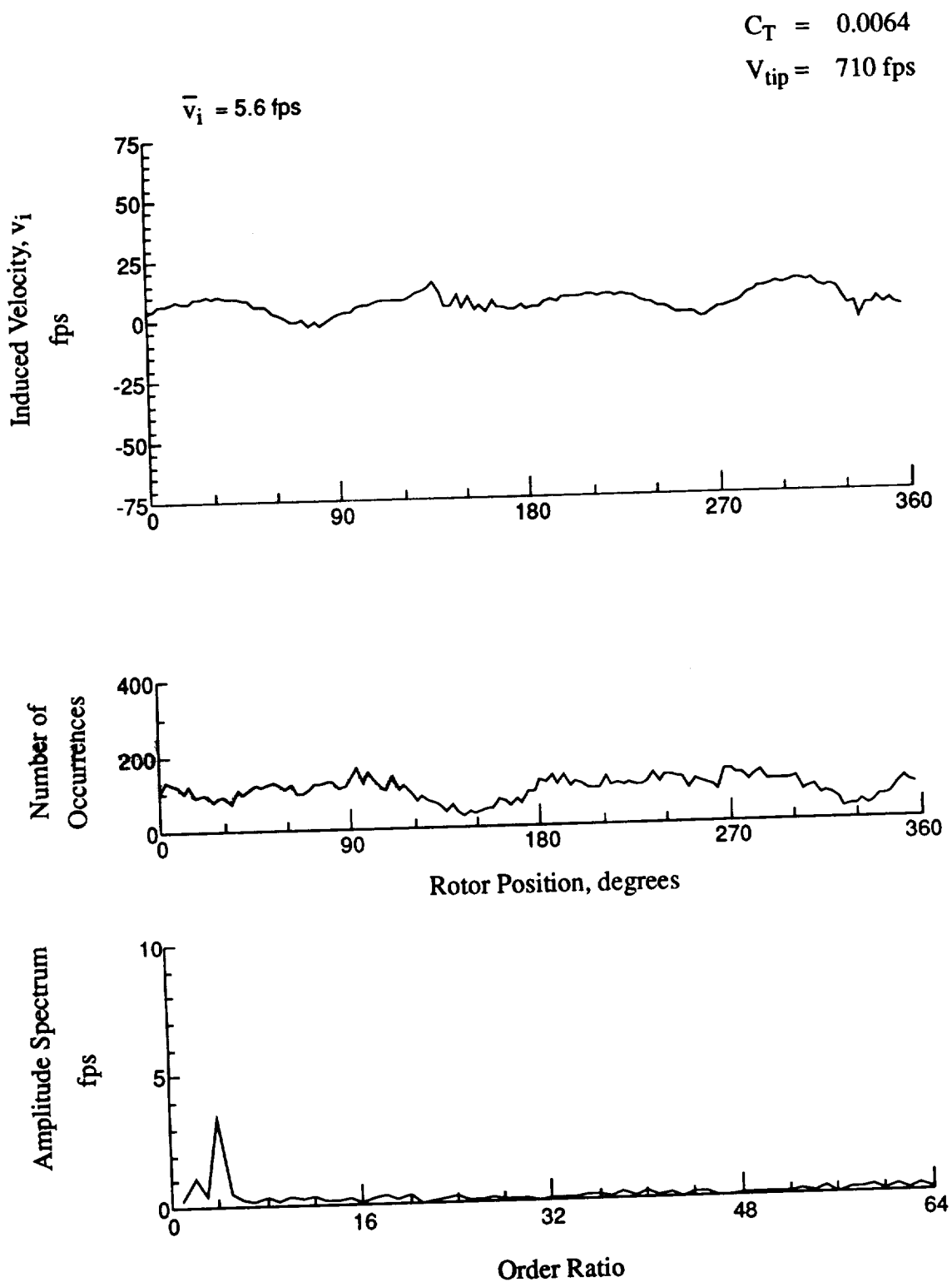


Figure 176.- Concluded.
 $x/R = 0.90$, $y/R = -0.20$, $z = -6.45 \text{ in.}$

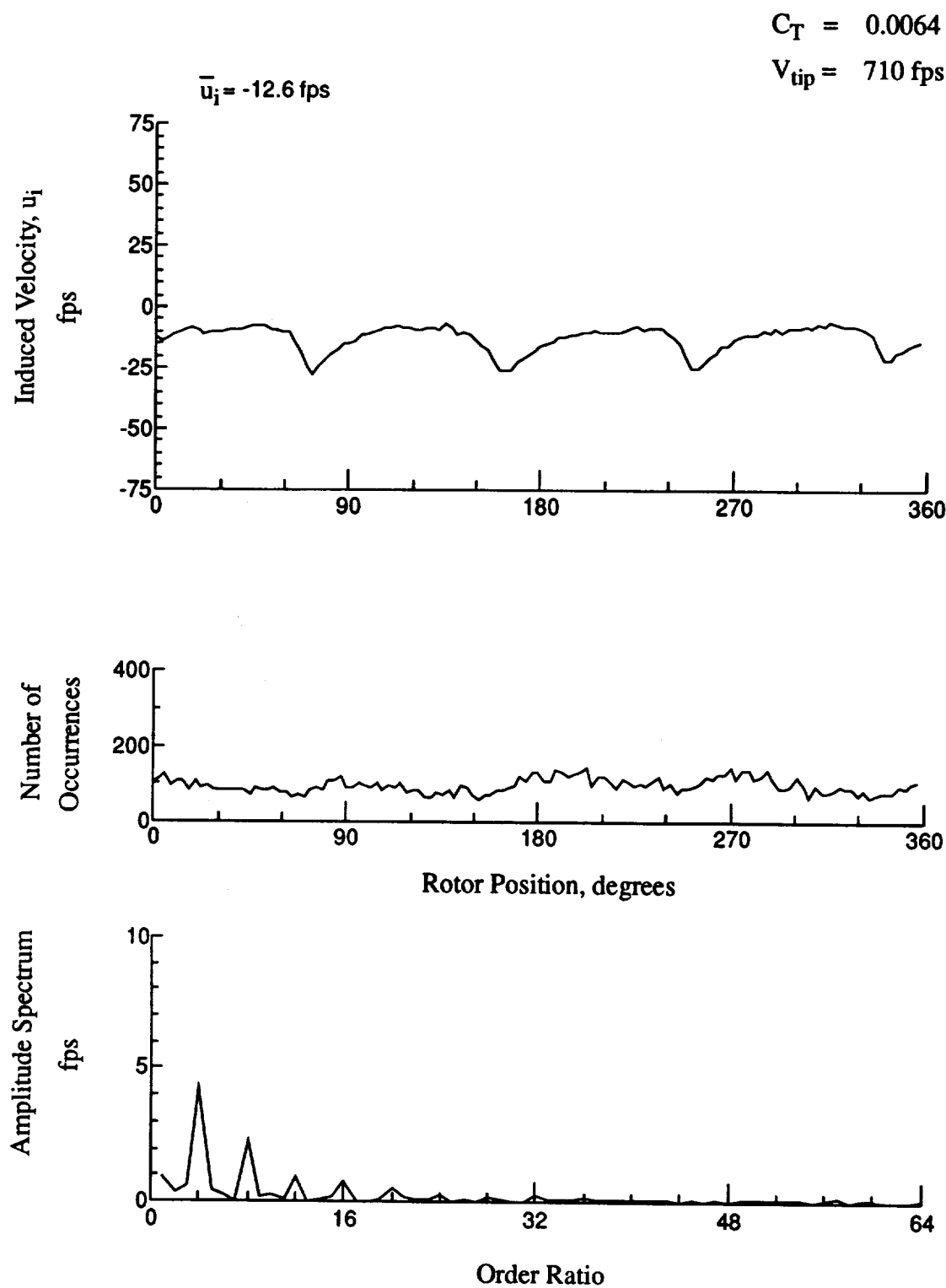


Figure 177.- Wake Measurements at
 $x/R = 1.50$, $y/R = -0.20$, $z = 8.37 \text{ in.}$

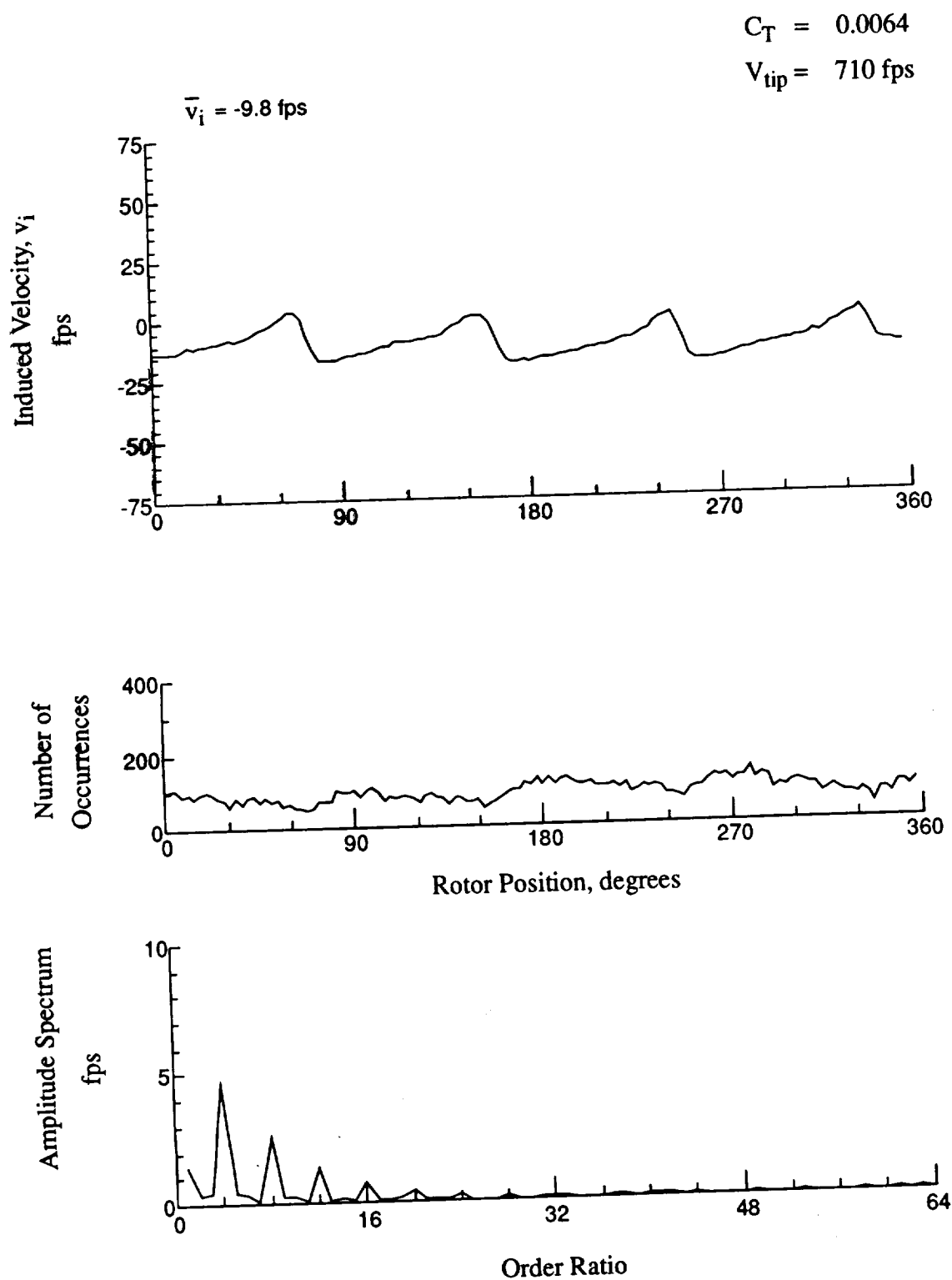


Figure 177.- Concluded.
 $x/R = 1.50$, $y/R = -0.20$, $z = 8.37 \text{ in.}$

$C_T = 0.0064$

$V_{tip} = 710 \text{ fps}$

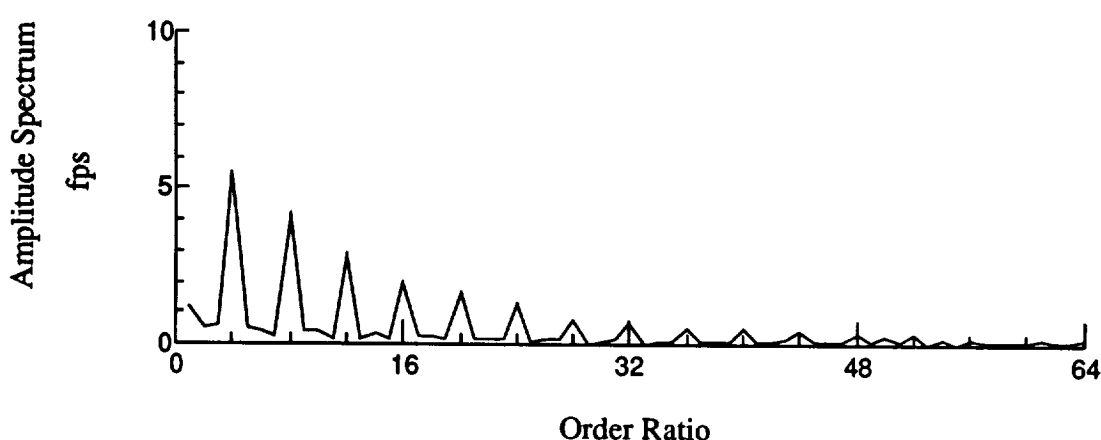
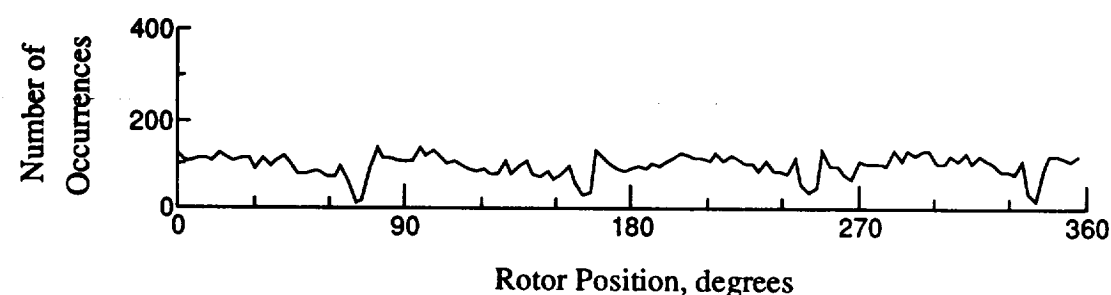
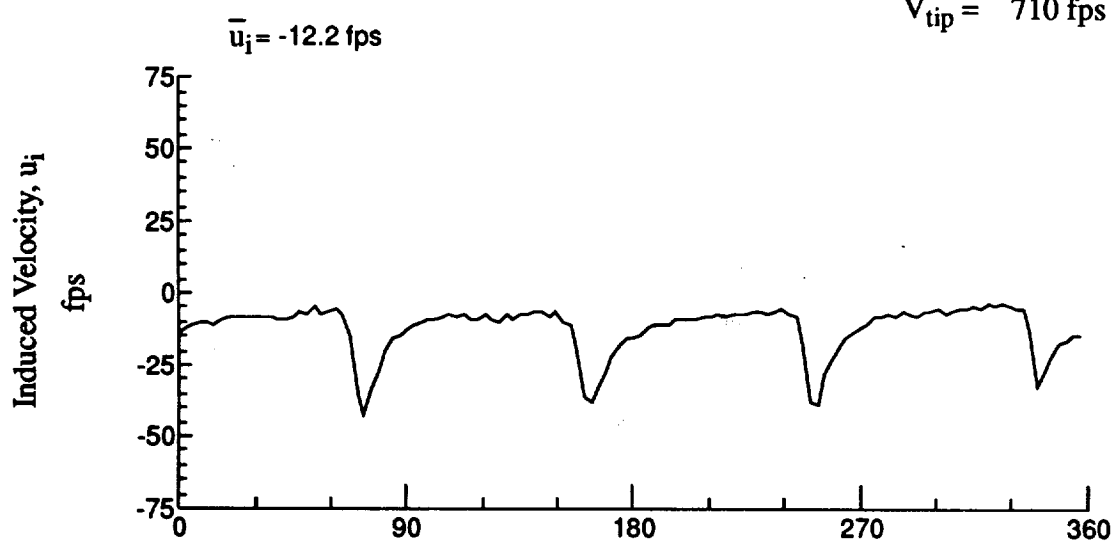


Figure 178.- Wake Measurements at
 $x/R = 1.50$, $y/R = -0.20$, $z = 7.34 \text{ in.}$

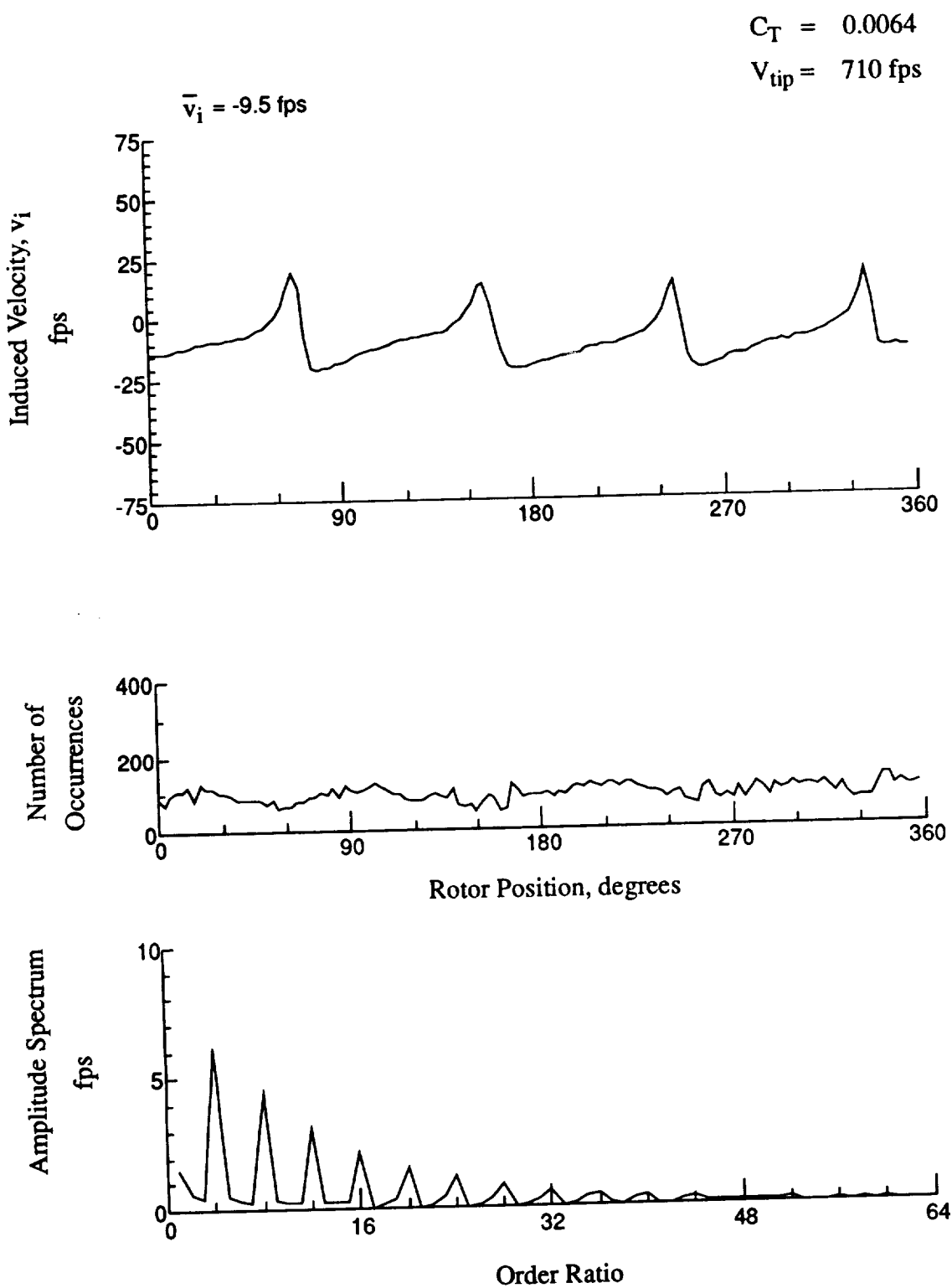


Figure 178.- Concluded.
 $x/R = 1.50$, $y/R = -0.20$, $z = 7.34 \text{ in.}$

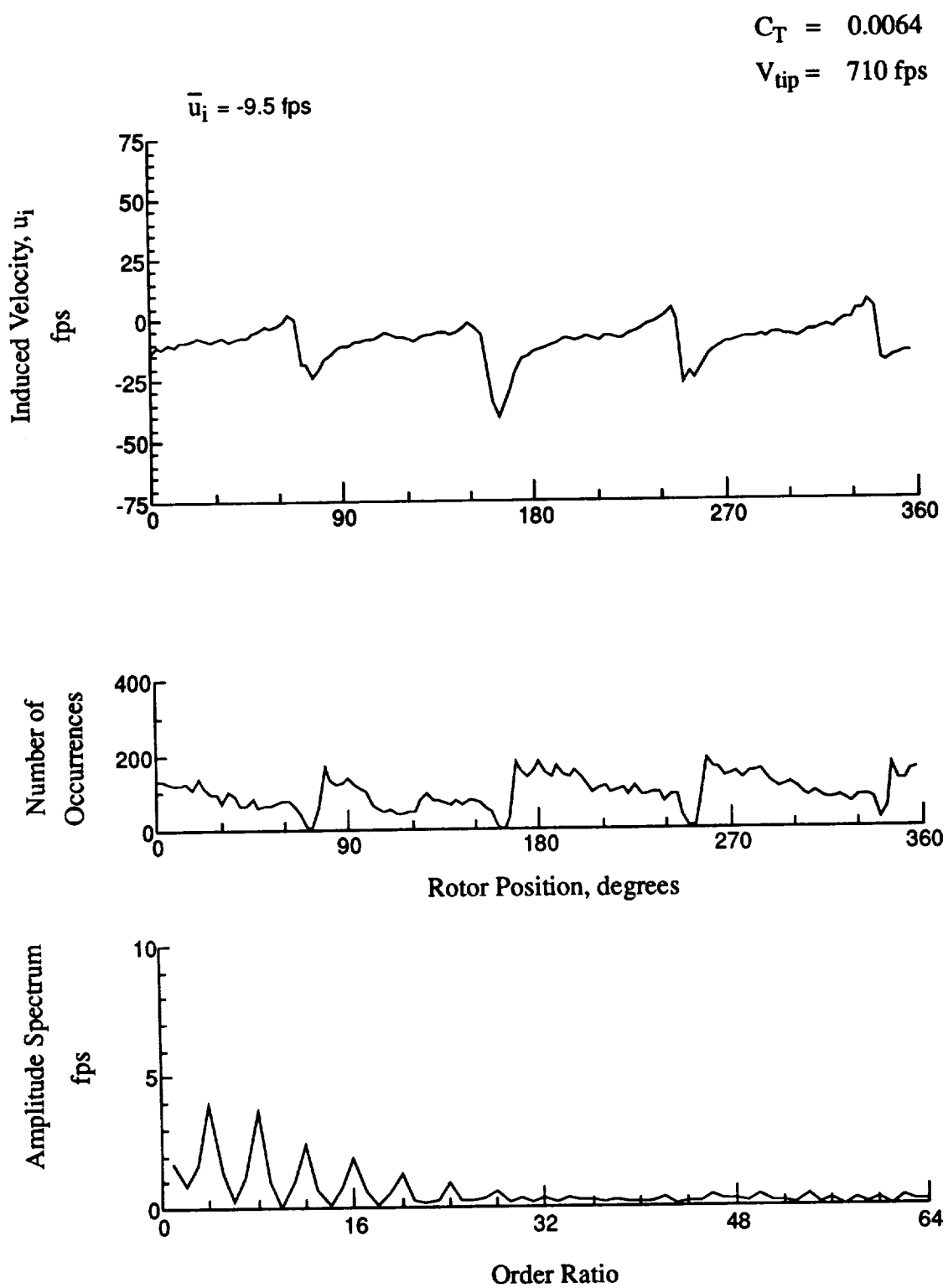


Figure 179.- Wake Measurements at
 $x/R = 1.50$, $y/R = -0.20$, $z = 6.31$ in.

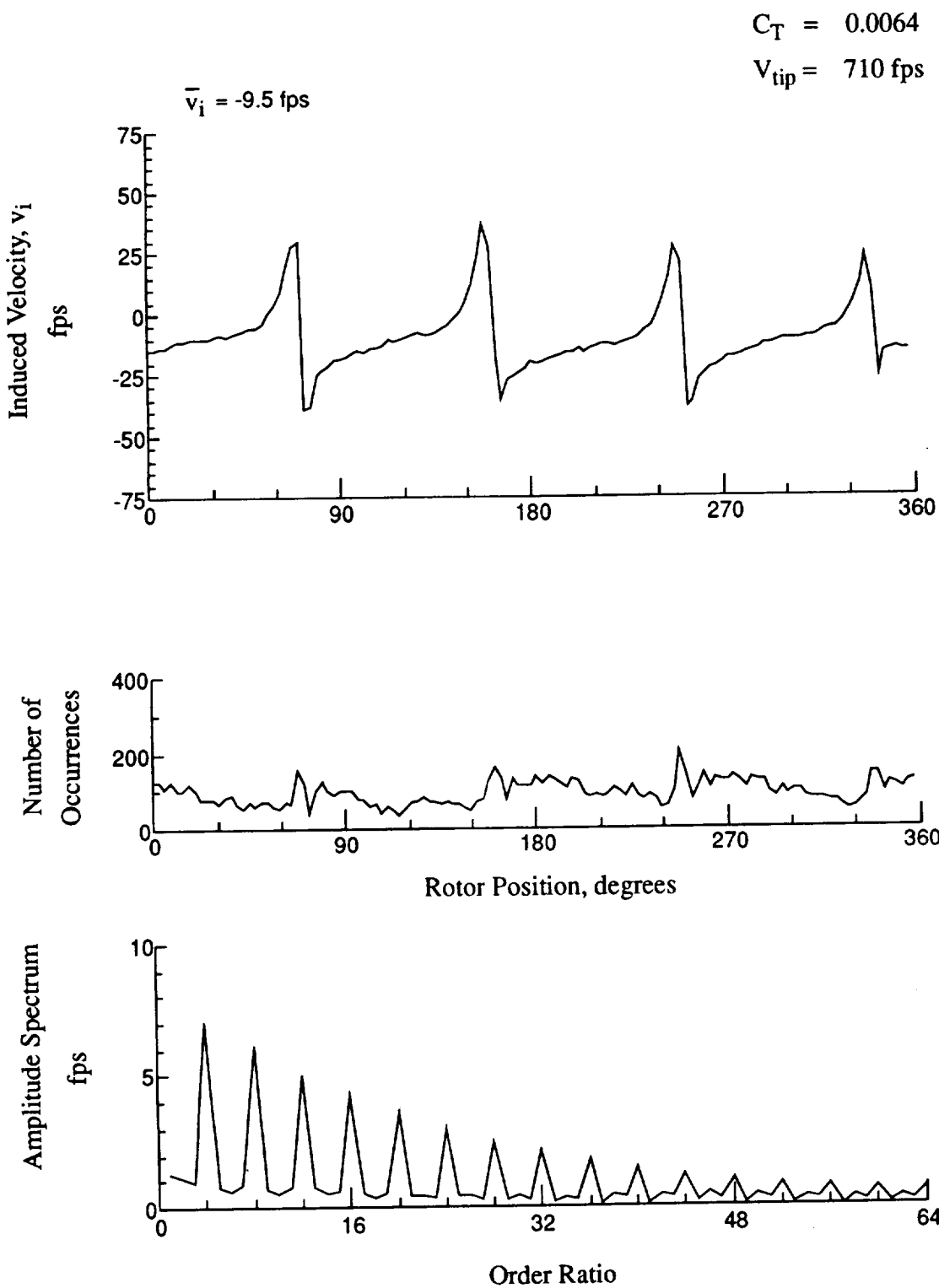


Figure 179.- Concluded.
 $x/R = 1.50$, $y/R = -0.20$, $z = 6.31 \text{ in.}$

$$C_T = 0.0064$$

$$V_{tip} = 710 \text{ fps}$$

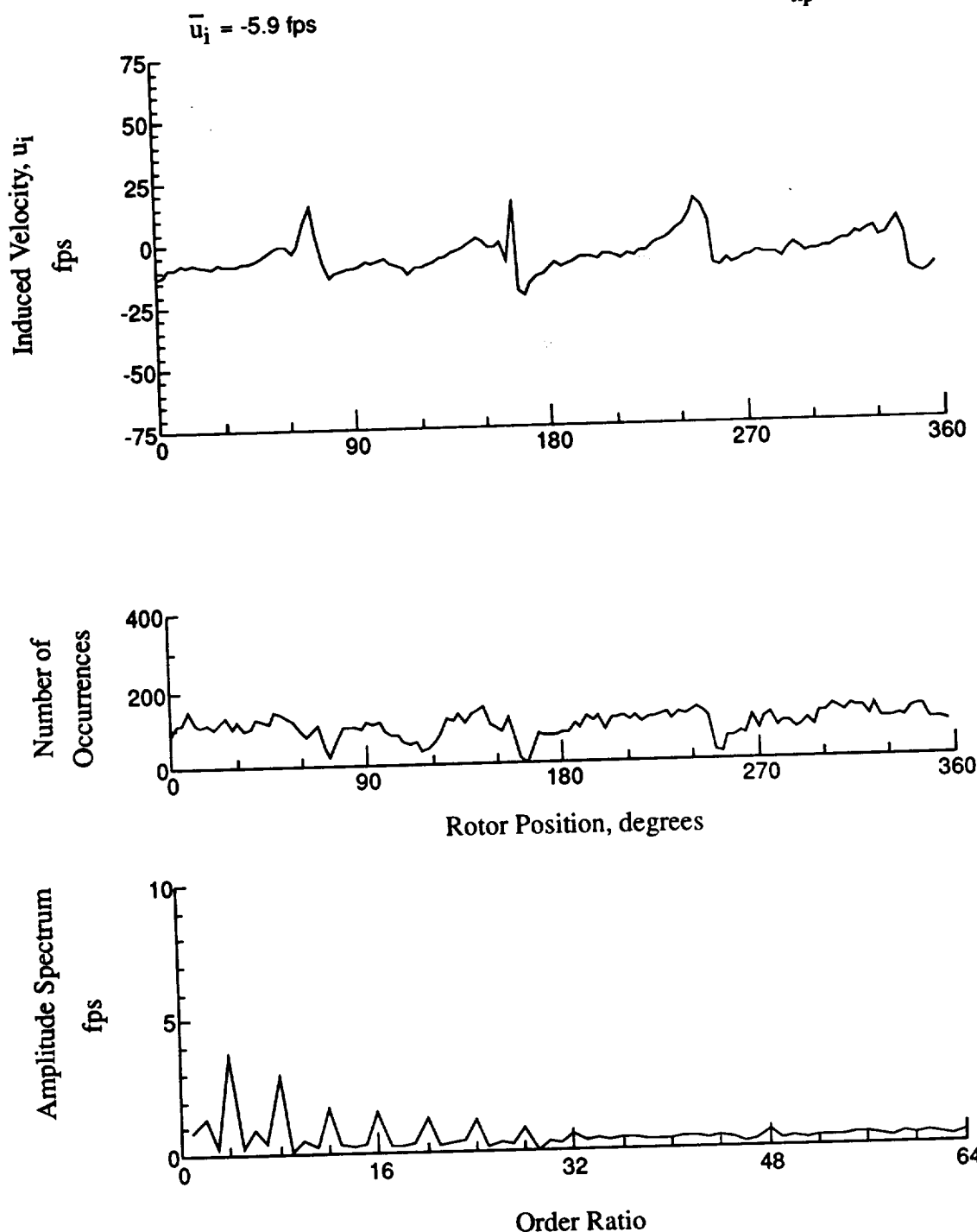


Figure 180.- Wake Measurements at
 $x/R = 1.50$, $y/R = -0.20$, $z = 5.28$ in.

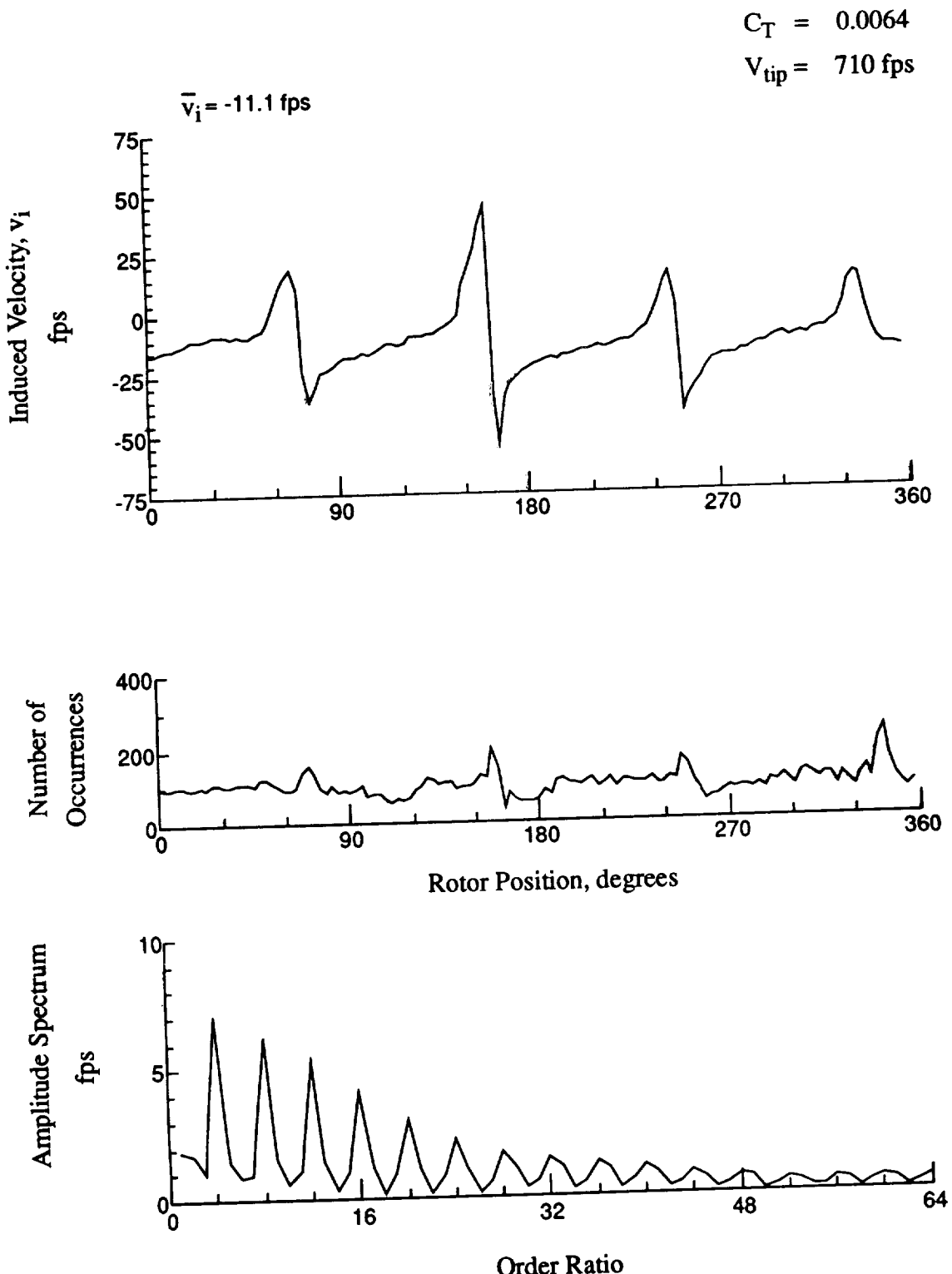


Figure 180.- Concluded.
 $x/R = 1.50$, $y/R = -0.20$, $z = 5.28 \text{ in.}$

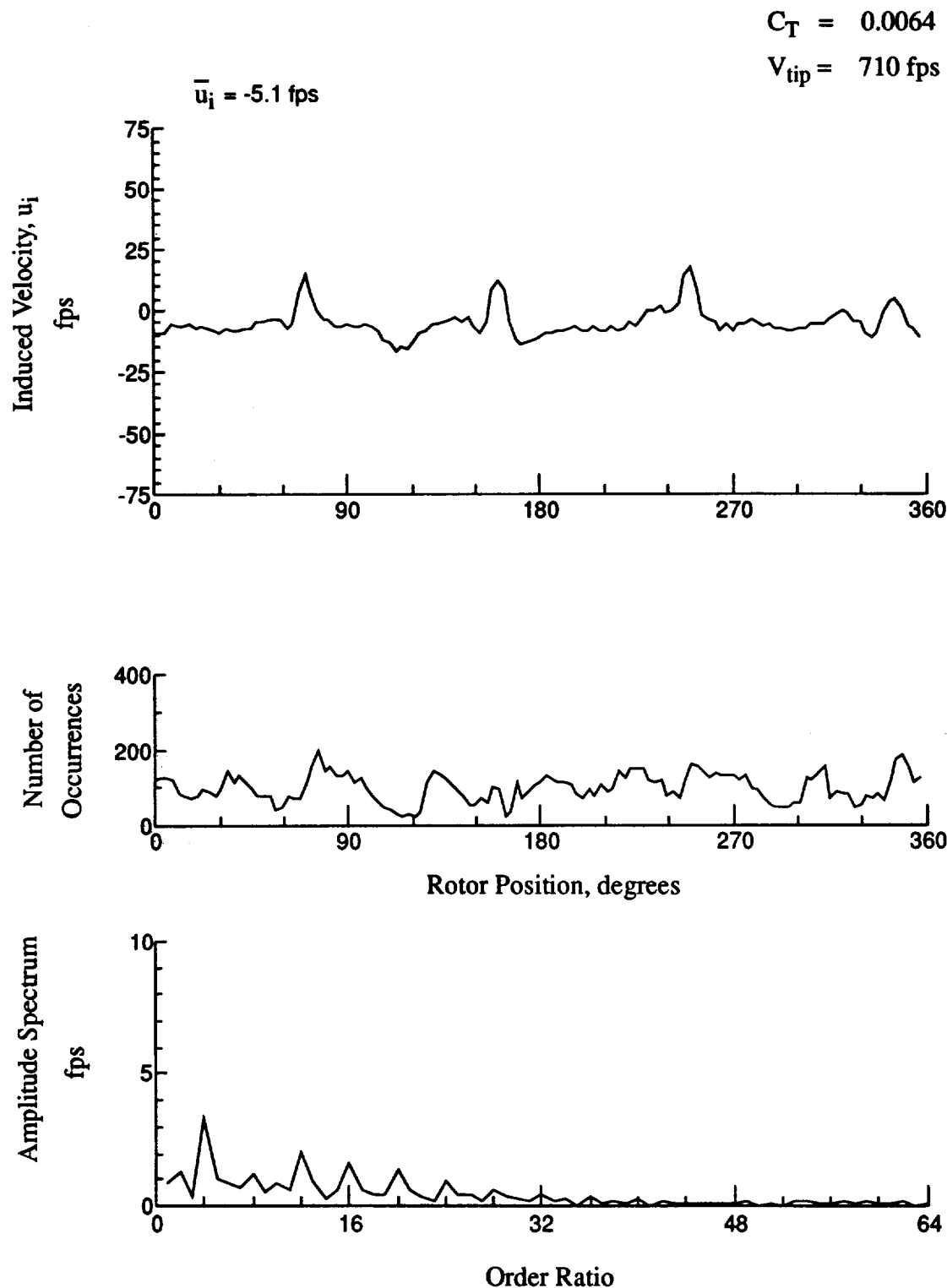


Figure 181.- Wake Measurements at
 $x/R = 1.50$, $y/R = -0.20$, $z = 4.25 \text{ in.}$

$$C_T = 0.0064$$

$$V_{tip} = 710 \text{ fps}$$

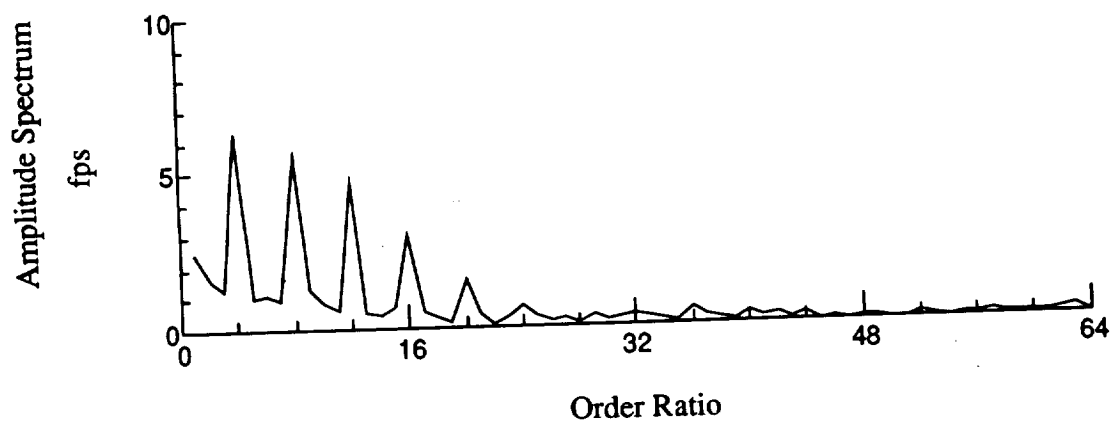
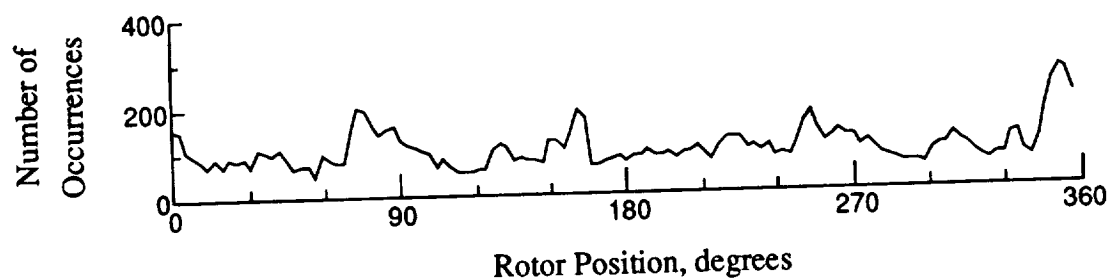
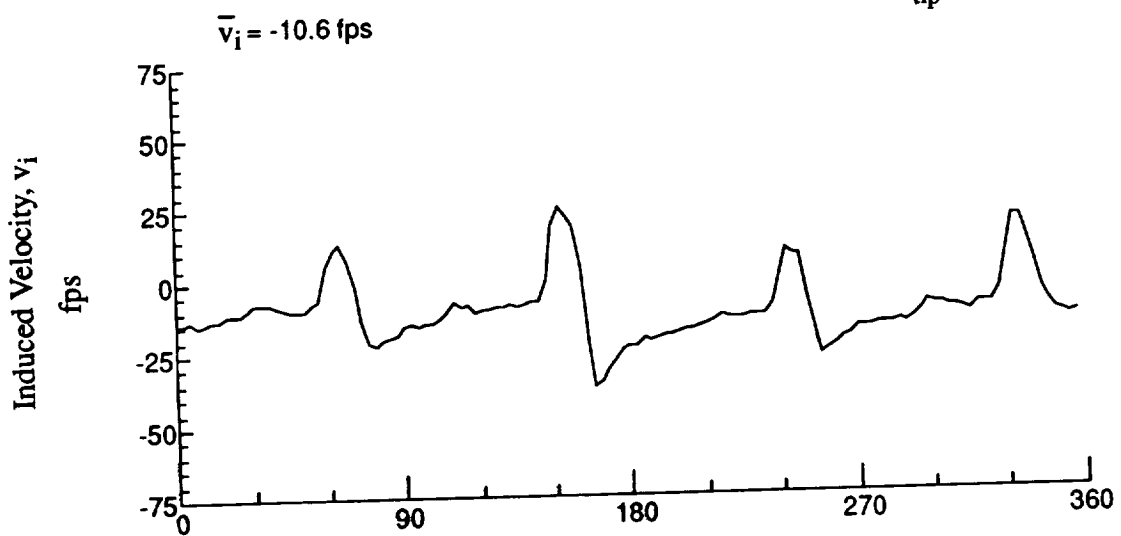


Figure 181.- Concluded.
 $x/R = 1.50$, $y/R = -0.20$, $z = 4.25 \text{ in.}$

$$C_T = 0.0064$$

$$V_{tip} = 710 \text{ fps}$$

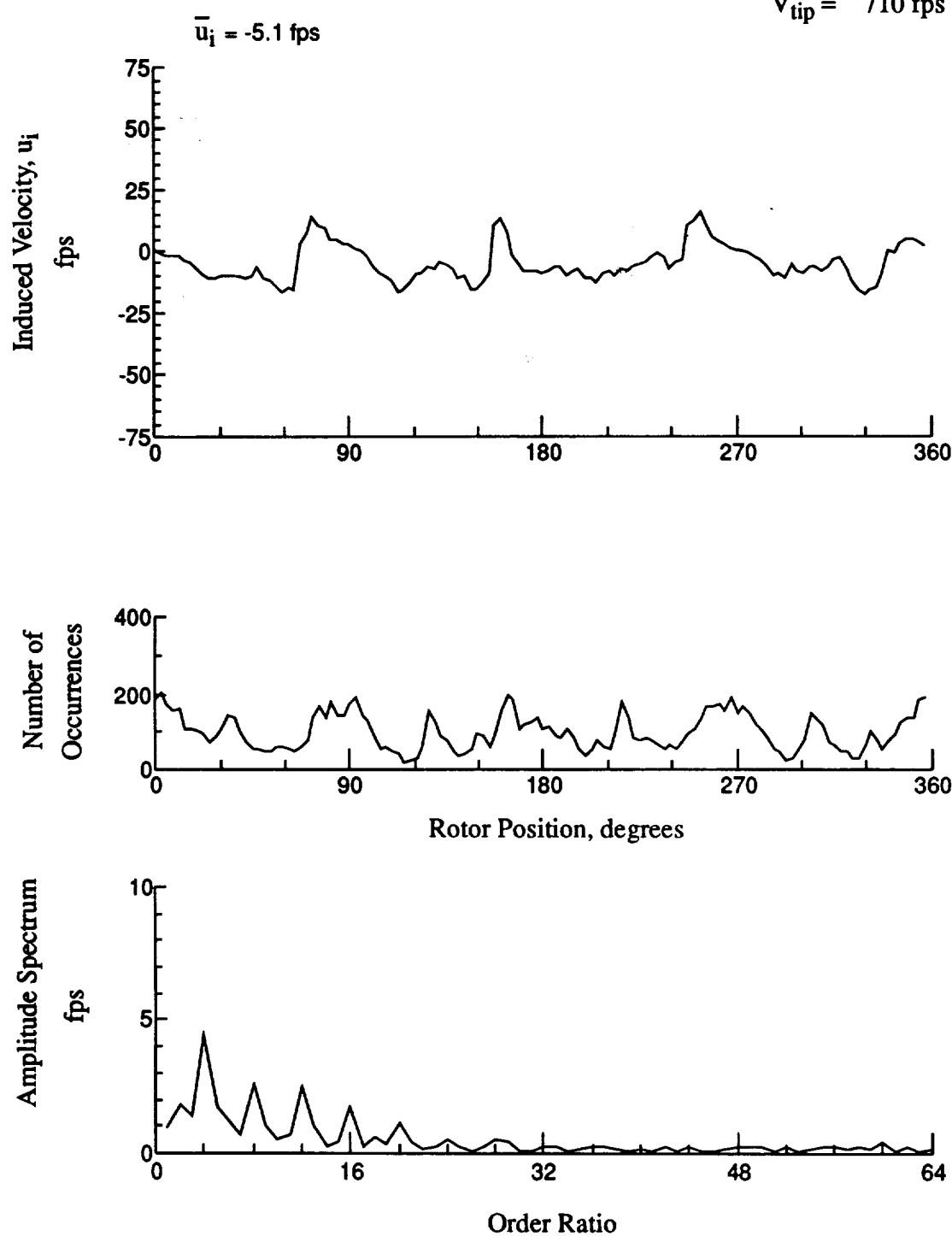


Figure 182.- Wake Measurements at
 $x/R = 1.50$, $y/R = -0.20$, $z = 3.22 \text{ in.}$

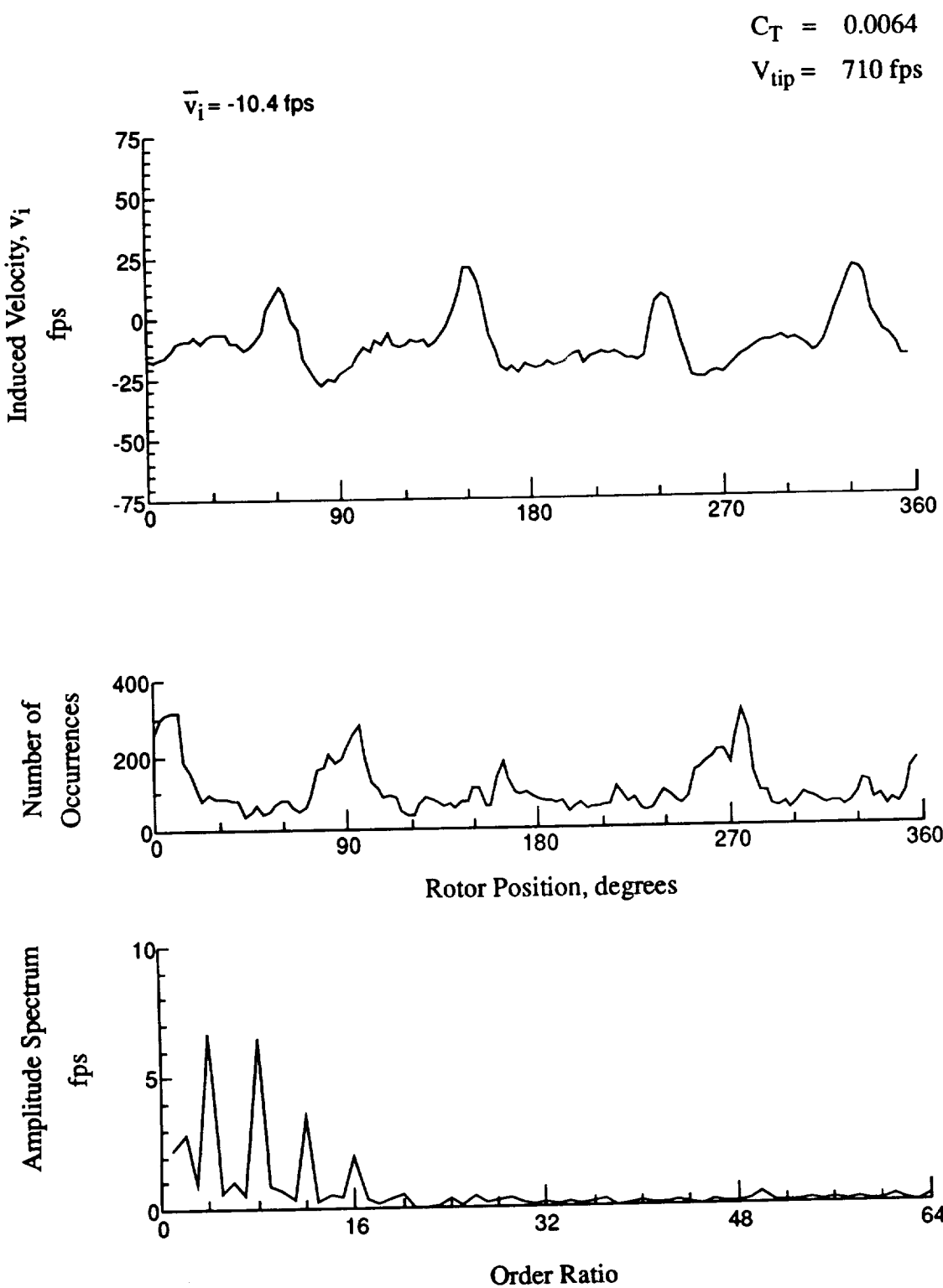


Figure 182.- Concluded.
 $x/R = 1.50$, $y/R = -0.20$, $z = 3.22 \text{ in.}$

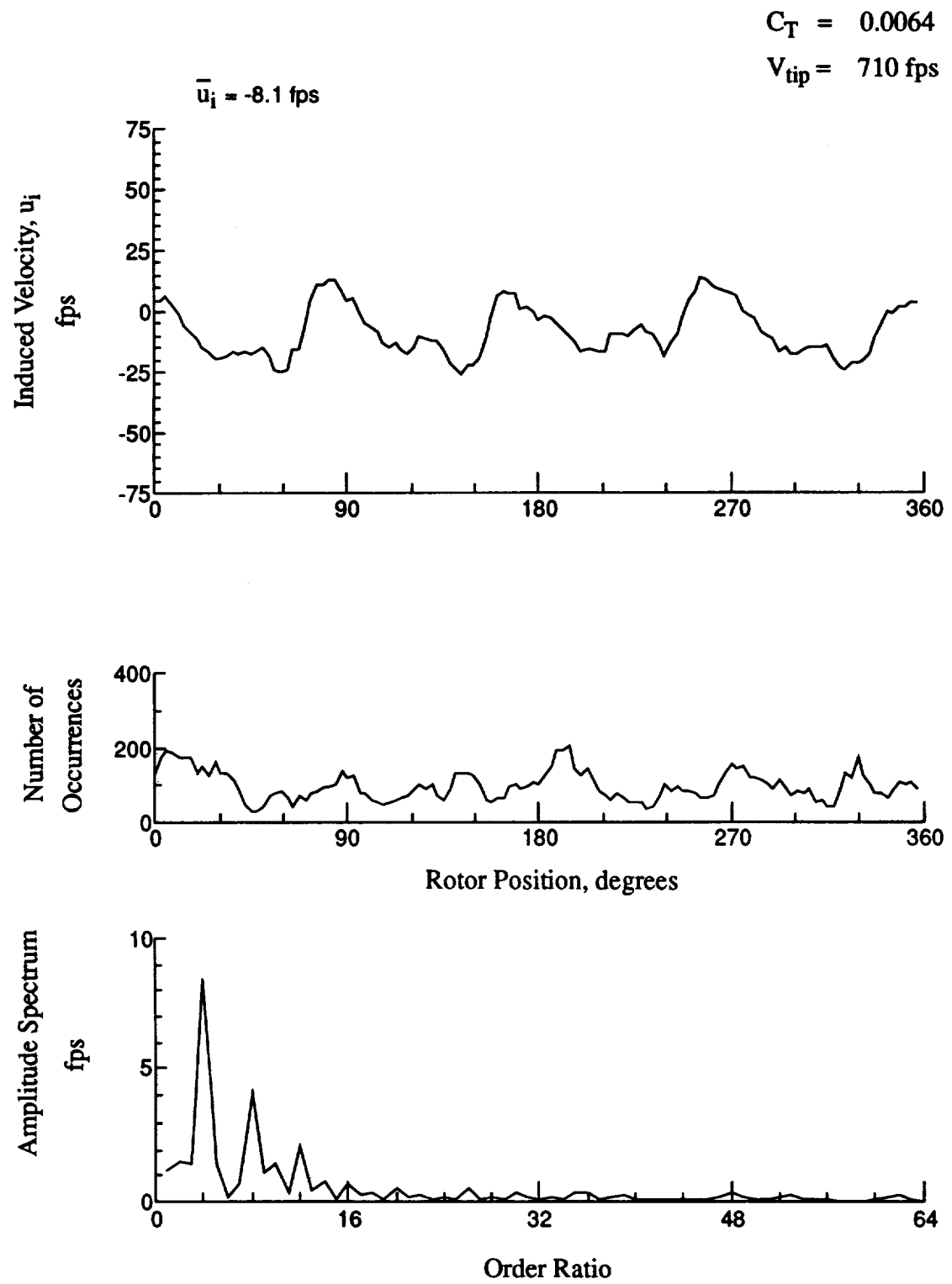


Figure 183.- Wake Measurements at
 $x/R = 1.50$, $y/R = -0.20$, $z = 2.19 \text{ in.}$

$$C_T = 0.0064$$

$$V_{tip} = 710 \text{ fps}$$

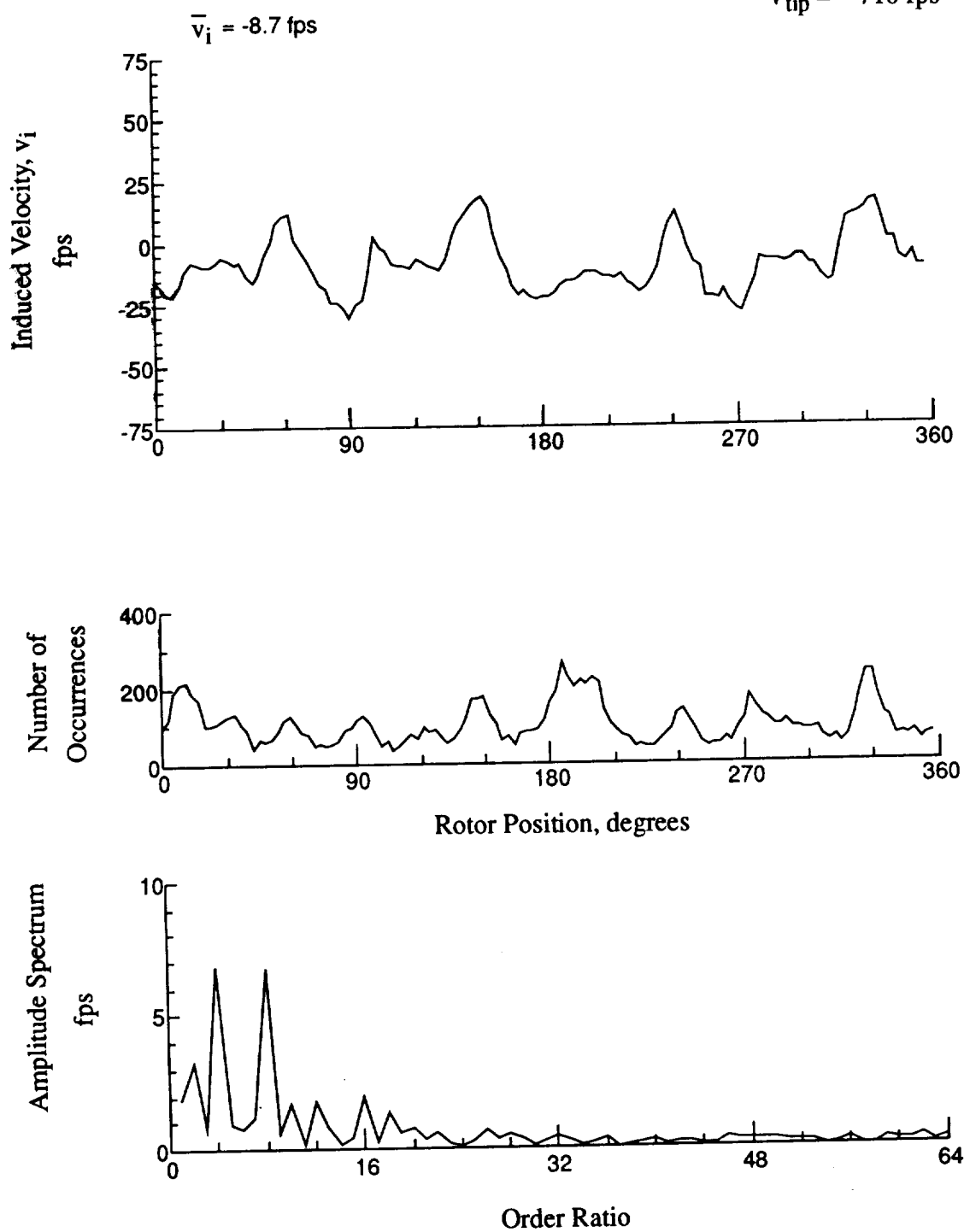


Figure 183.- Concluded.
 $x/R = 1.50$, $y/R = -0.20$, $z = 2.19 \text{ in.}$

$$C_T = 0.0064$$

$$V_{tip} = 710 \text{ fps}$$

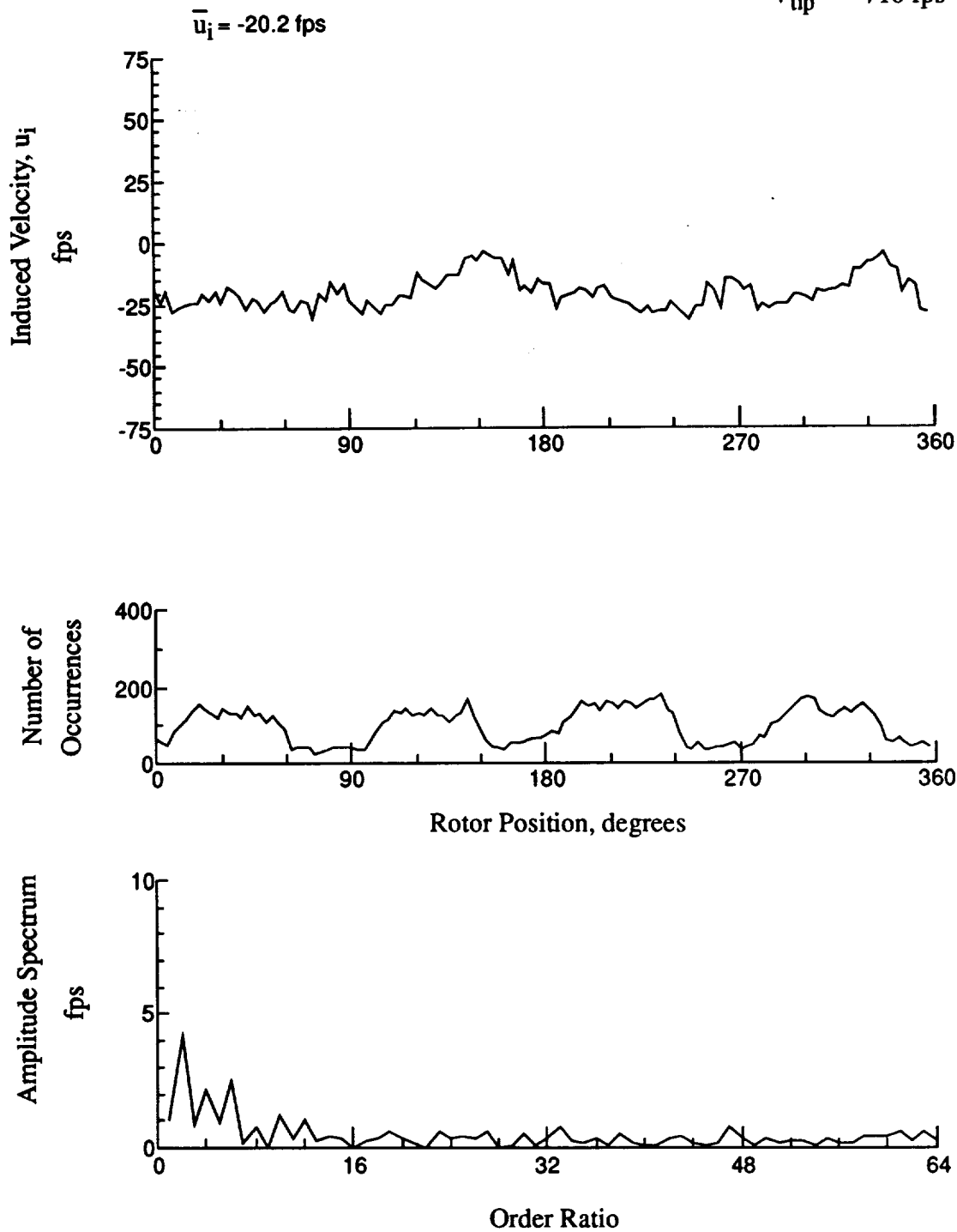


Figure 184.- Wake Measurements at
 $x/R = 1.50$, $y/R = -0.20$, $z = -1.23$ in.

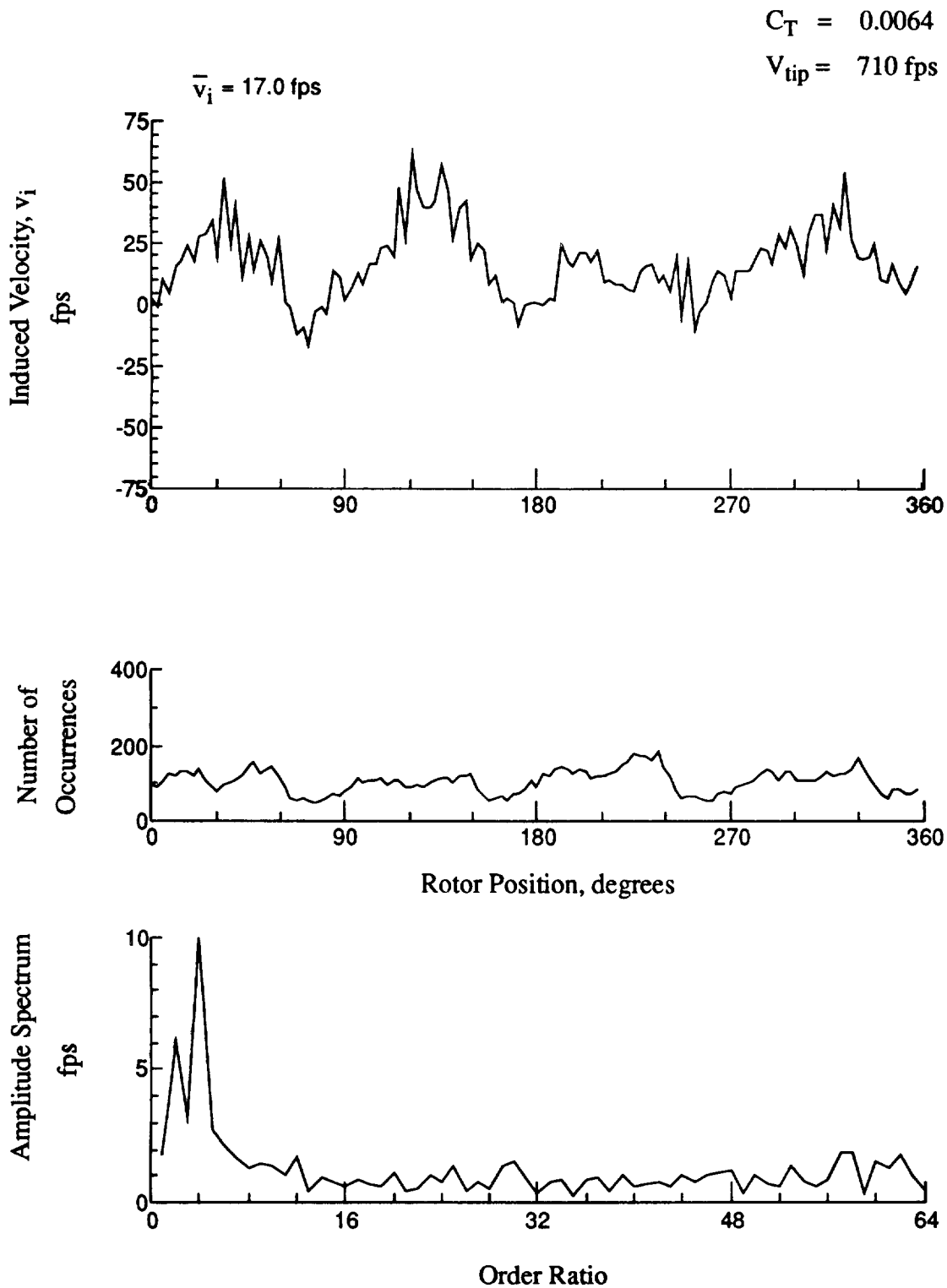


Figure 184.- Concluded.
 $x/R = 1.50$, $y/R = -0.20$, $z = -1.23 \text{ in.}$

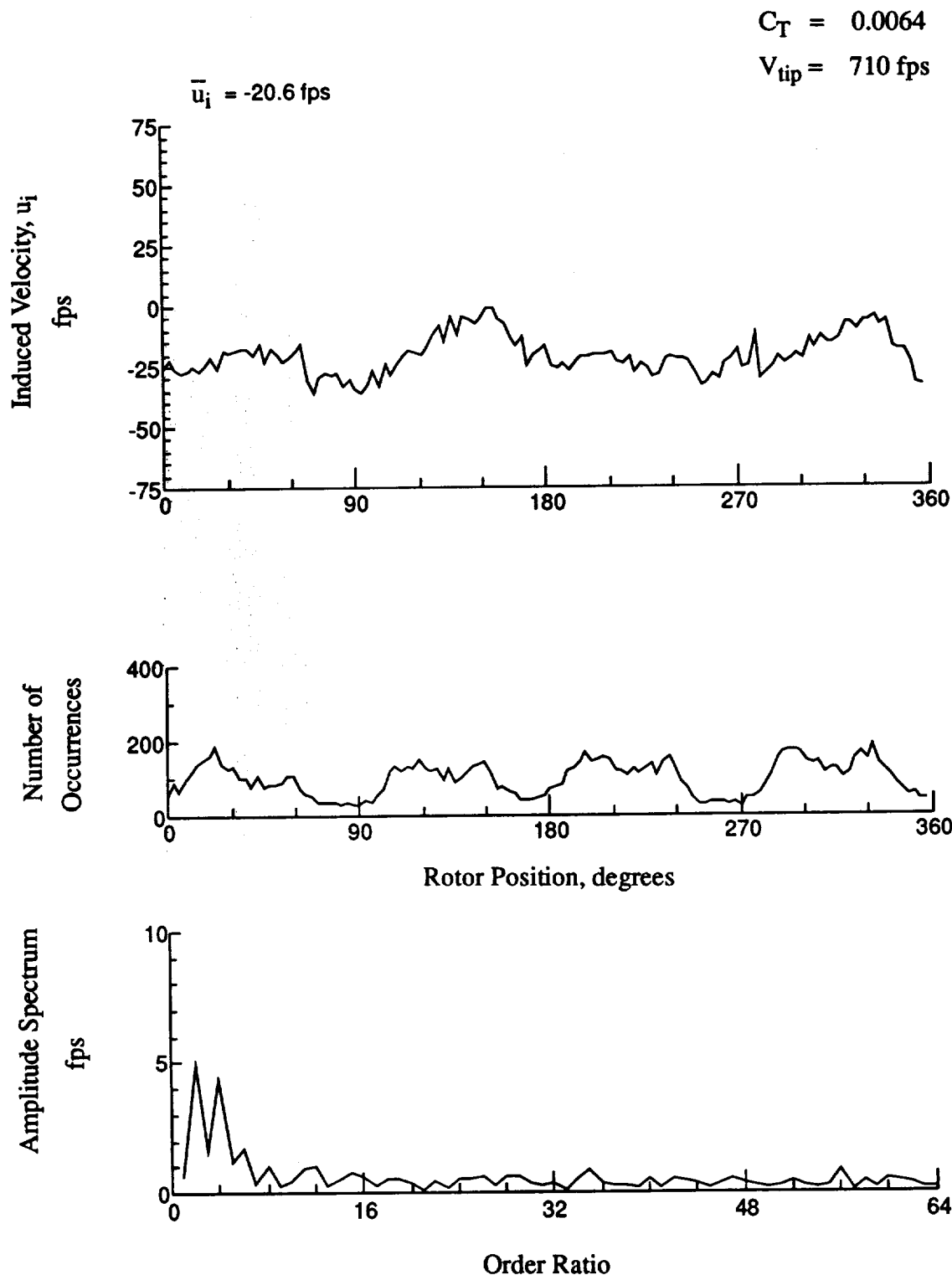


Figure 185.- Wake Measurements at
 $x/R = 1.50$, $y/R = -0.20$, $z = -2.26 \text{ in.}$

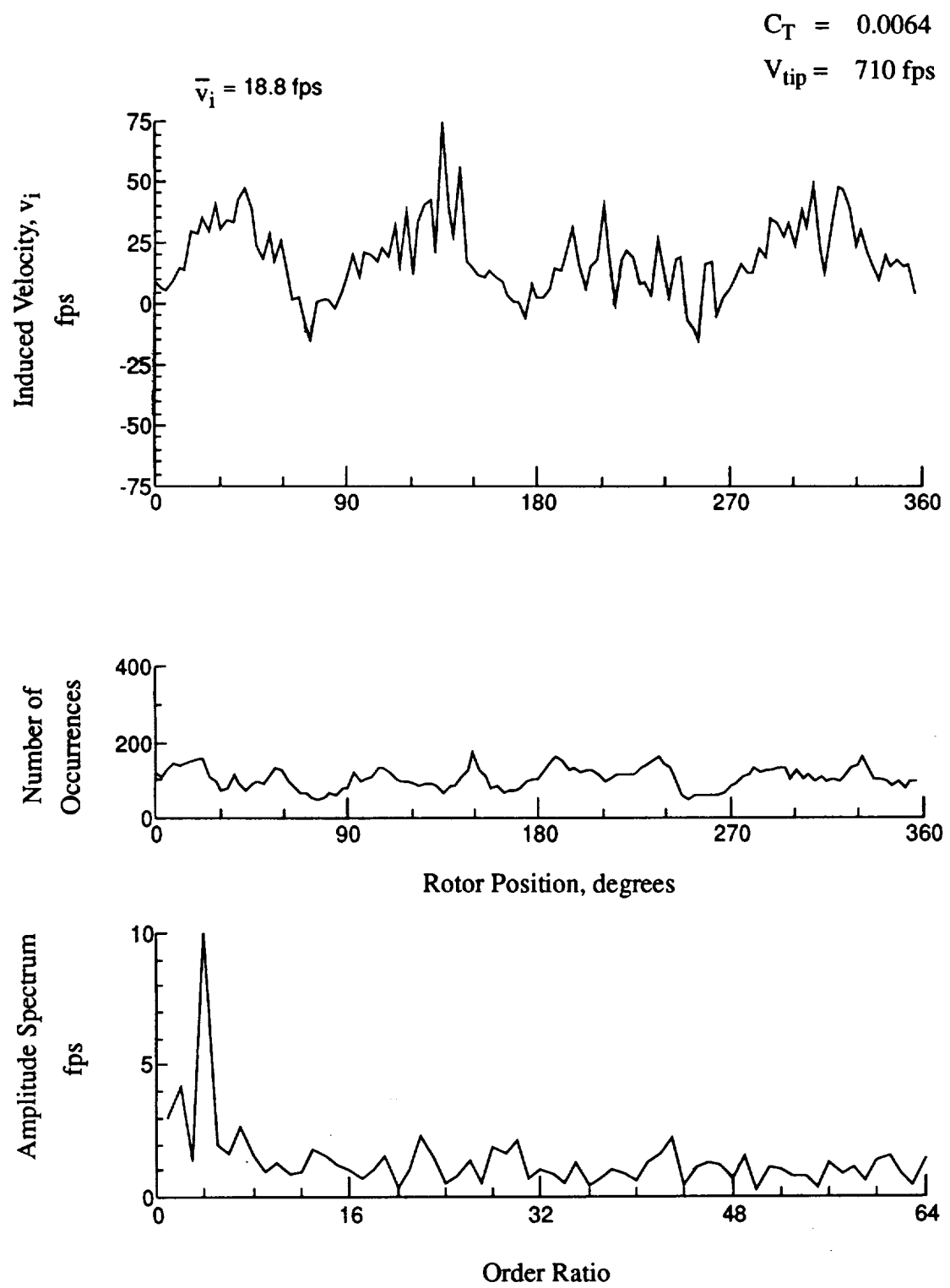


Figure 185.- Concluded.

$x/R = 1.50$, $y/R = -0.20$, $z = -2.26 \text{ in.}$

$$C_T = 0.0064$$

$$V_{tip} = 710 \text{ fps}$$

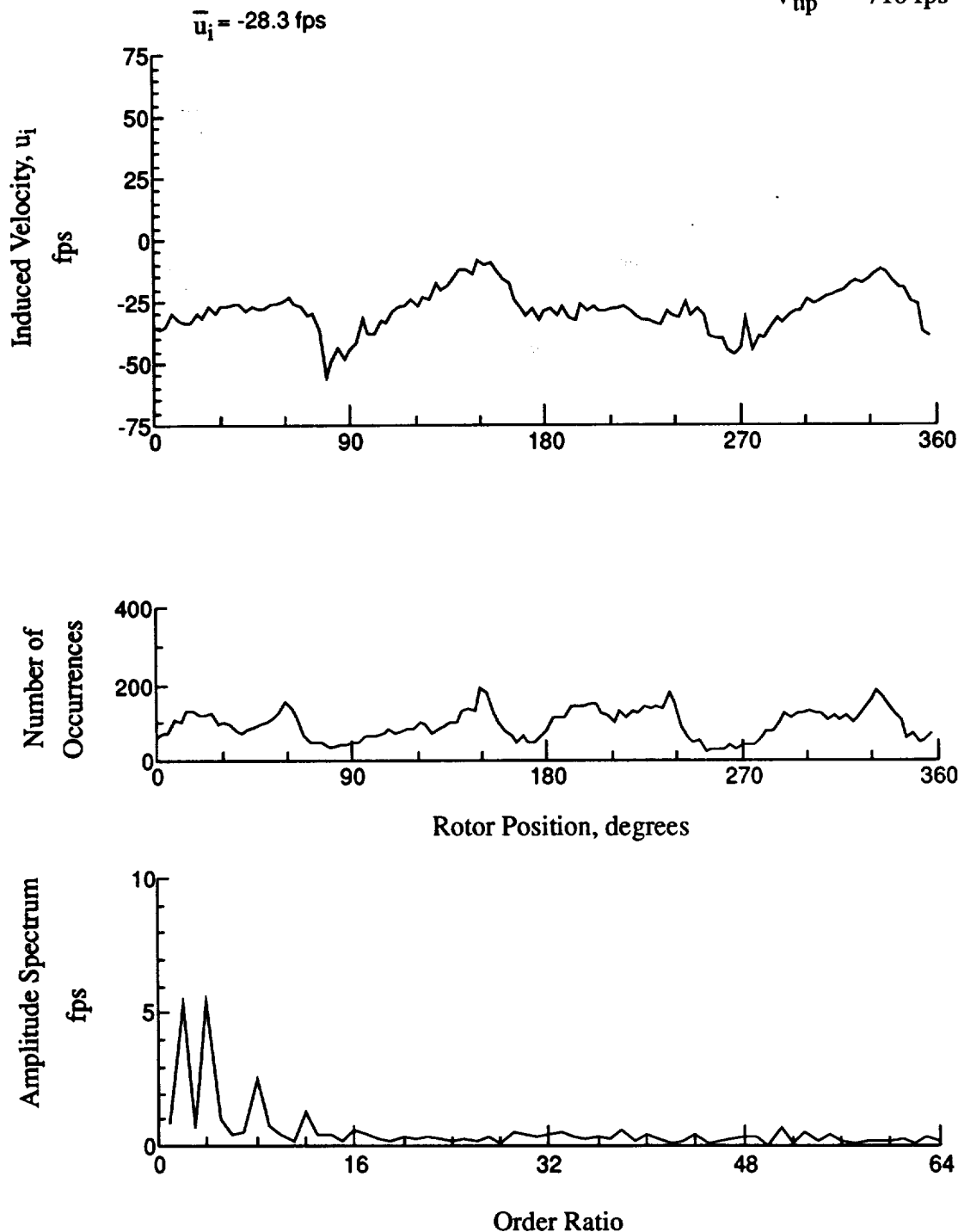


Figure 186.- Wake Measurements at
 $x/R = 1.50$, $y/R = -0.20$, $z = -3.29$ in.

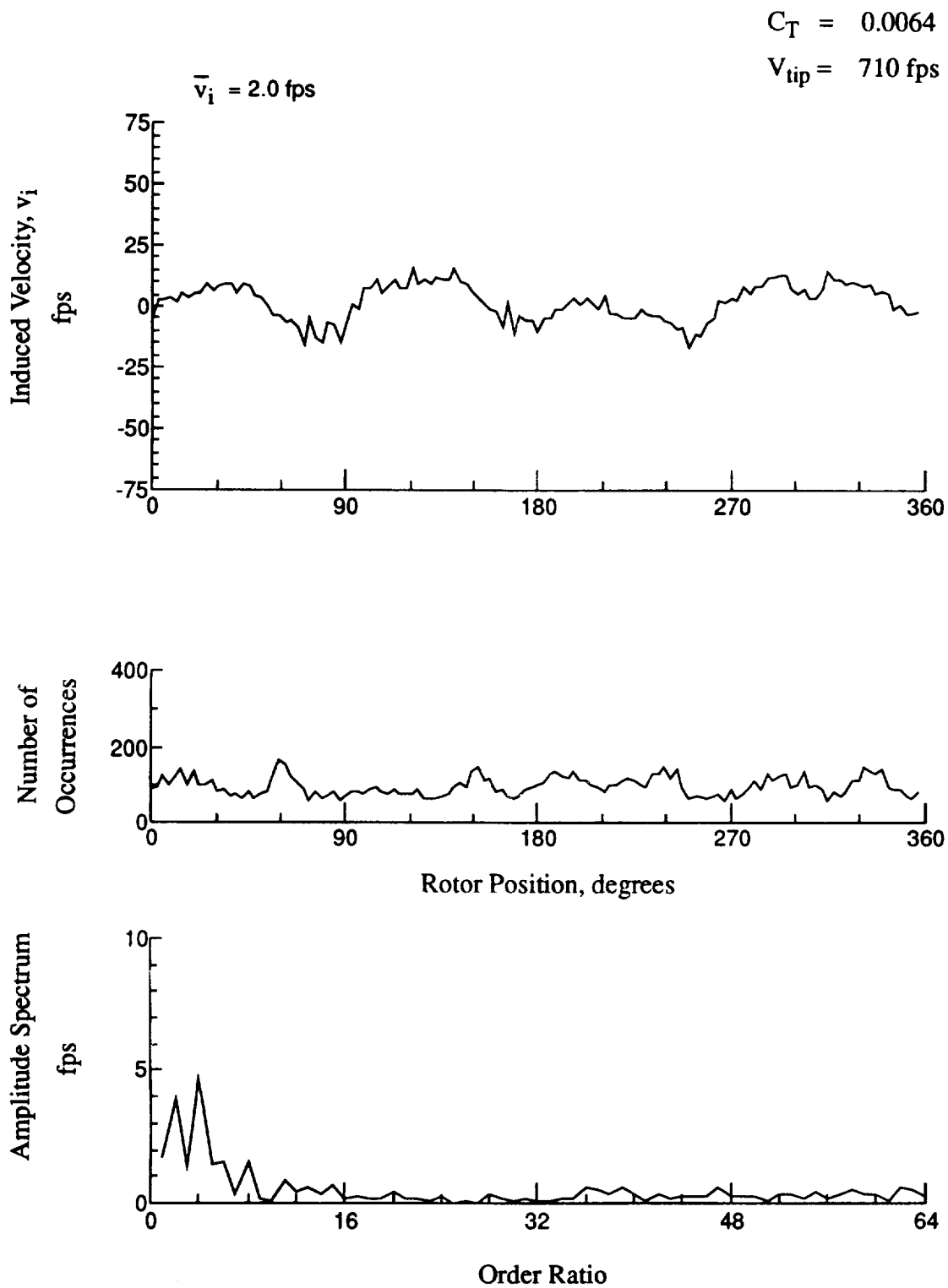


Figure 186.- Concluded.
 $x/R = 1.50$, $y/R = -0.20$, $z = -3.29 \text{ in.}$

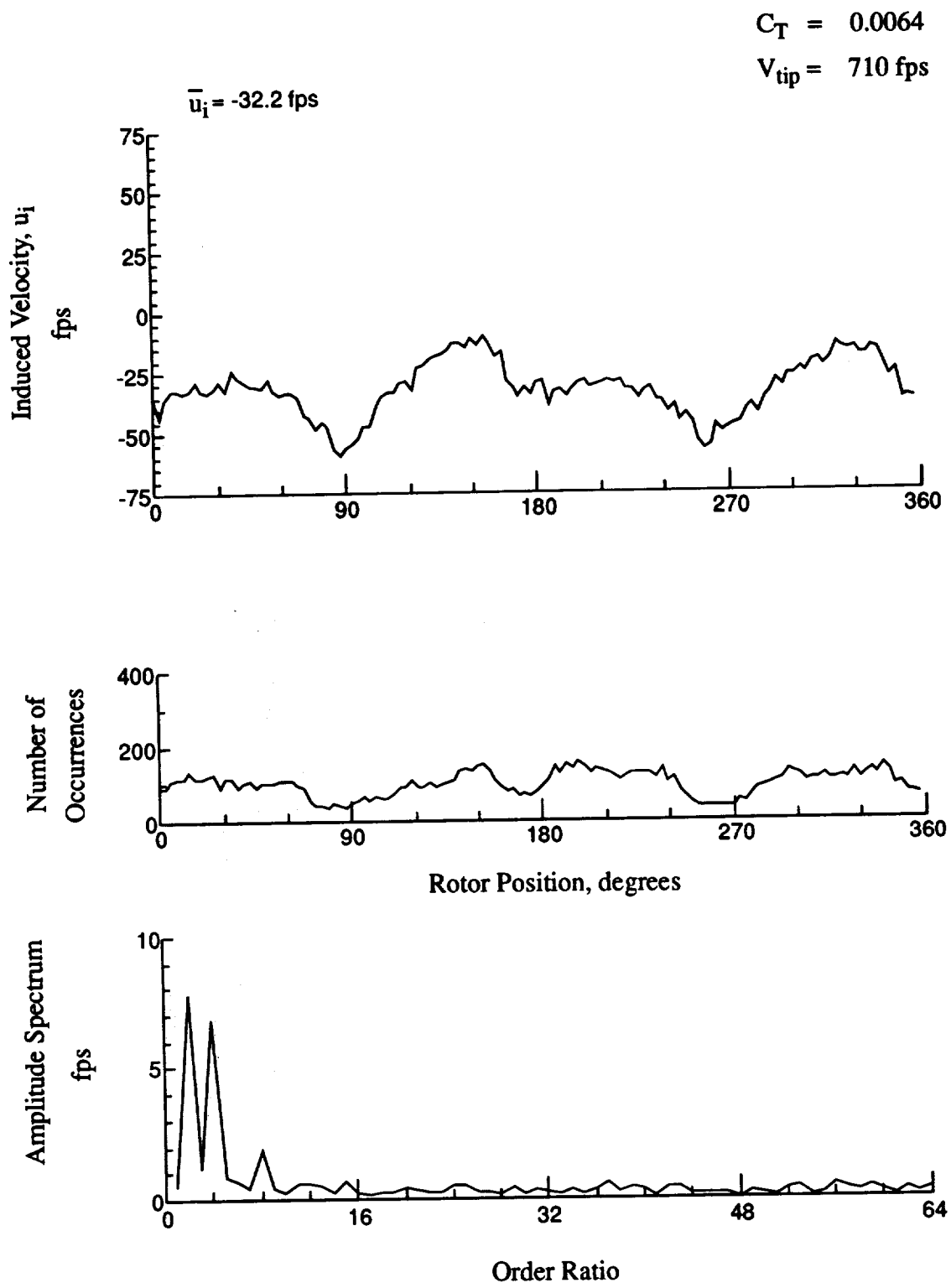


Figure 187.- Wake Measurements at
 $x/R = 1.50$, $y/R = -0.20$, $z = -4.32 \text{ in.}$

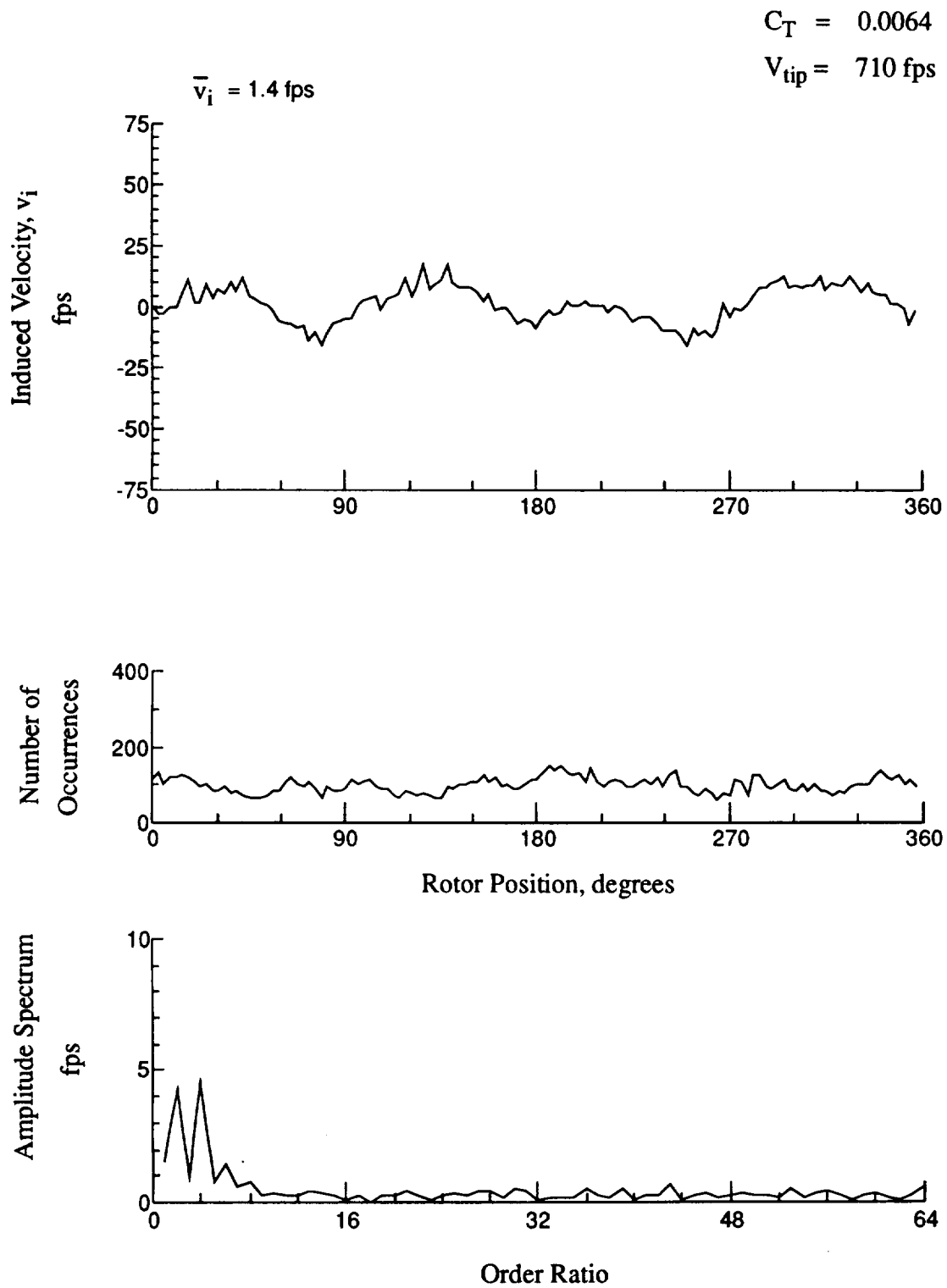


Figure 187.- Concluded.

$x/R = 1.50$, $y/R = -0.20$, $z = -4.32 \text{ in.}$

$$C_T = 0.0064$$

$$V_{tip} = 710 \text{ fps}$$

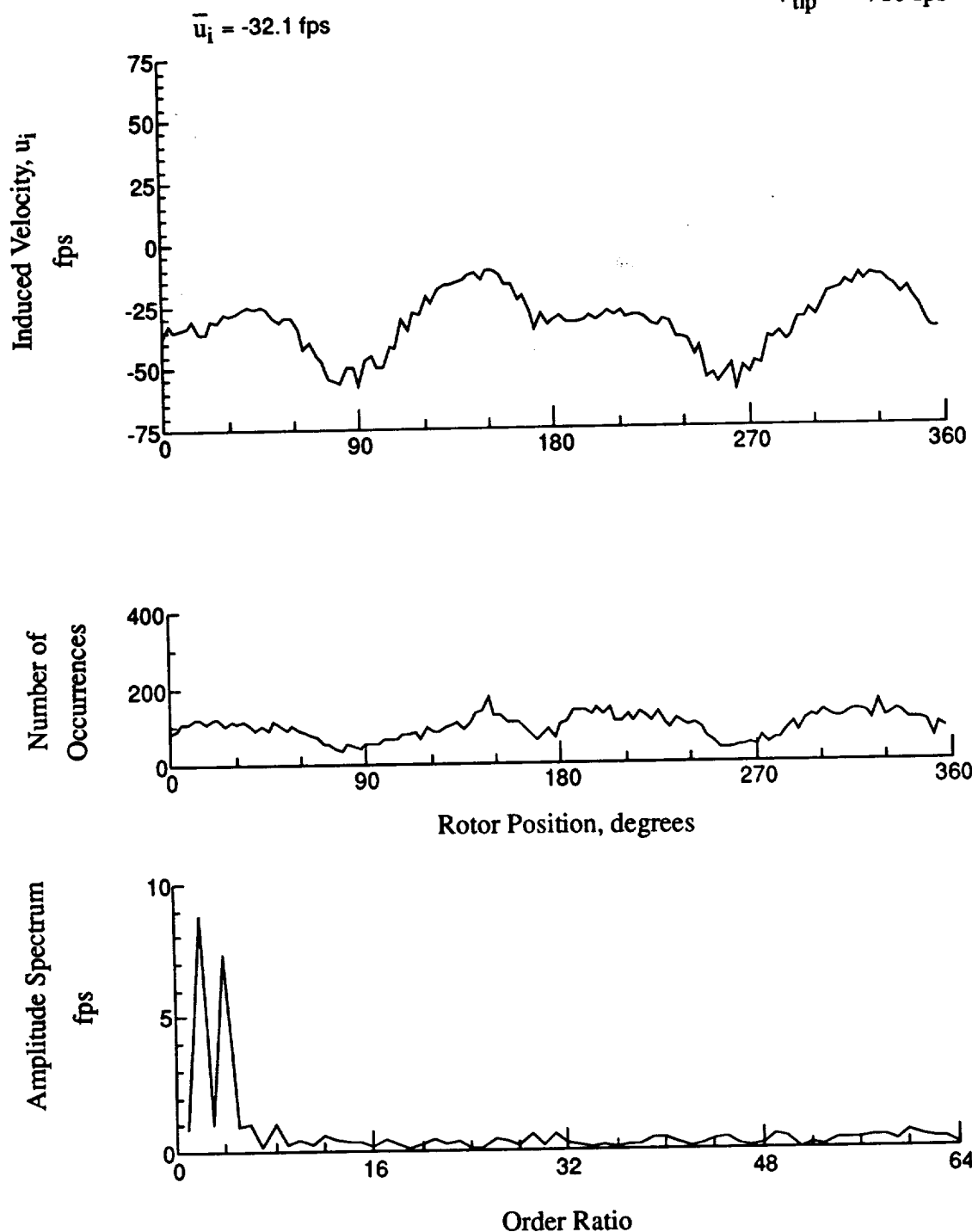


Figure 188.- Wake Measurements at
 $x/R = 1.50$, $y/R = -0.20$, $z = -5.35$ in.

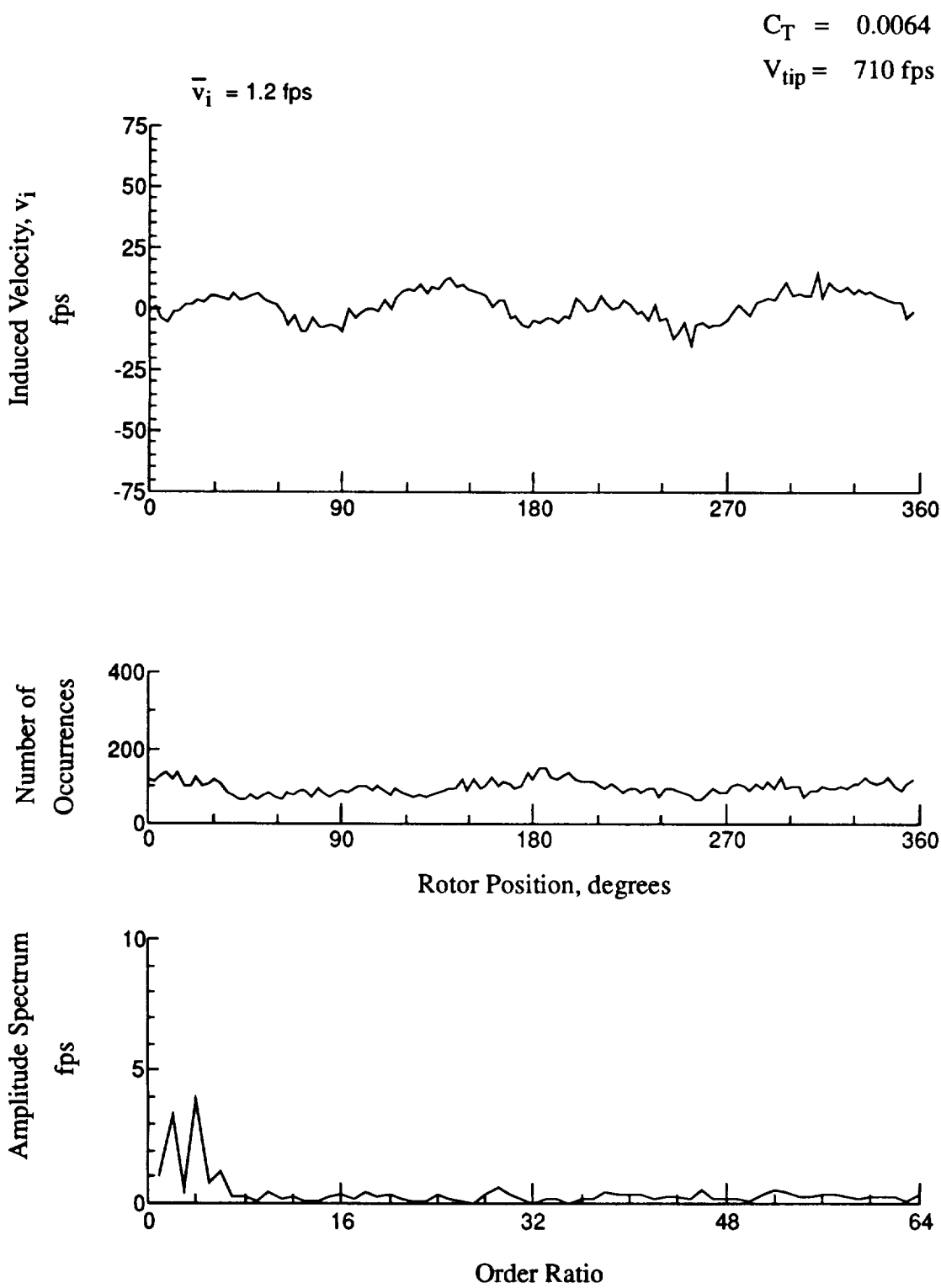


Figure 188.- Concluded.

$x/R = 1.50$, $y/R = -0.20$, $z = -5.35 \text{ in.}$

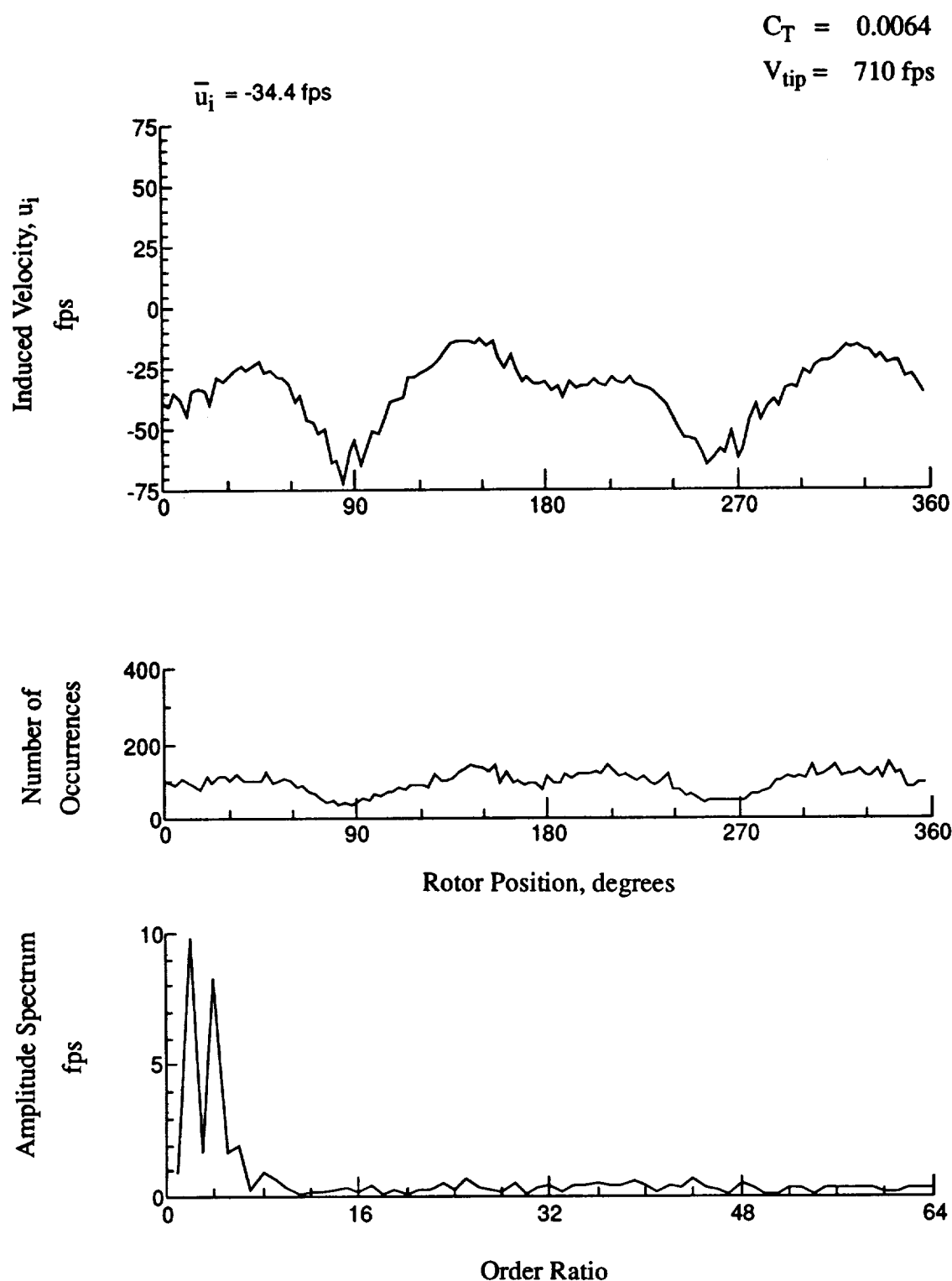


Figure 189.- Wake Measurements at
 $x/R = 1.50$, $y/R = -0.20$, $z = -6.38 \text{ in.}$

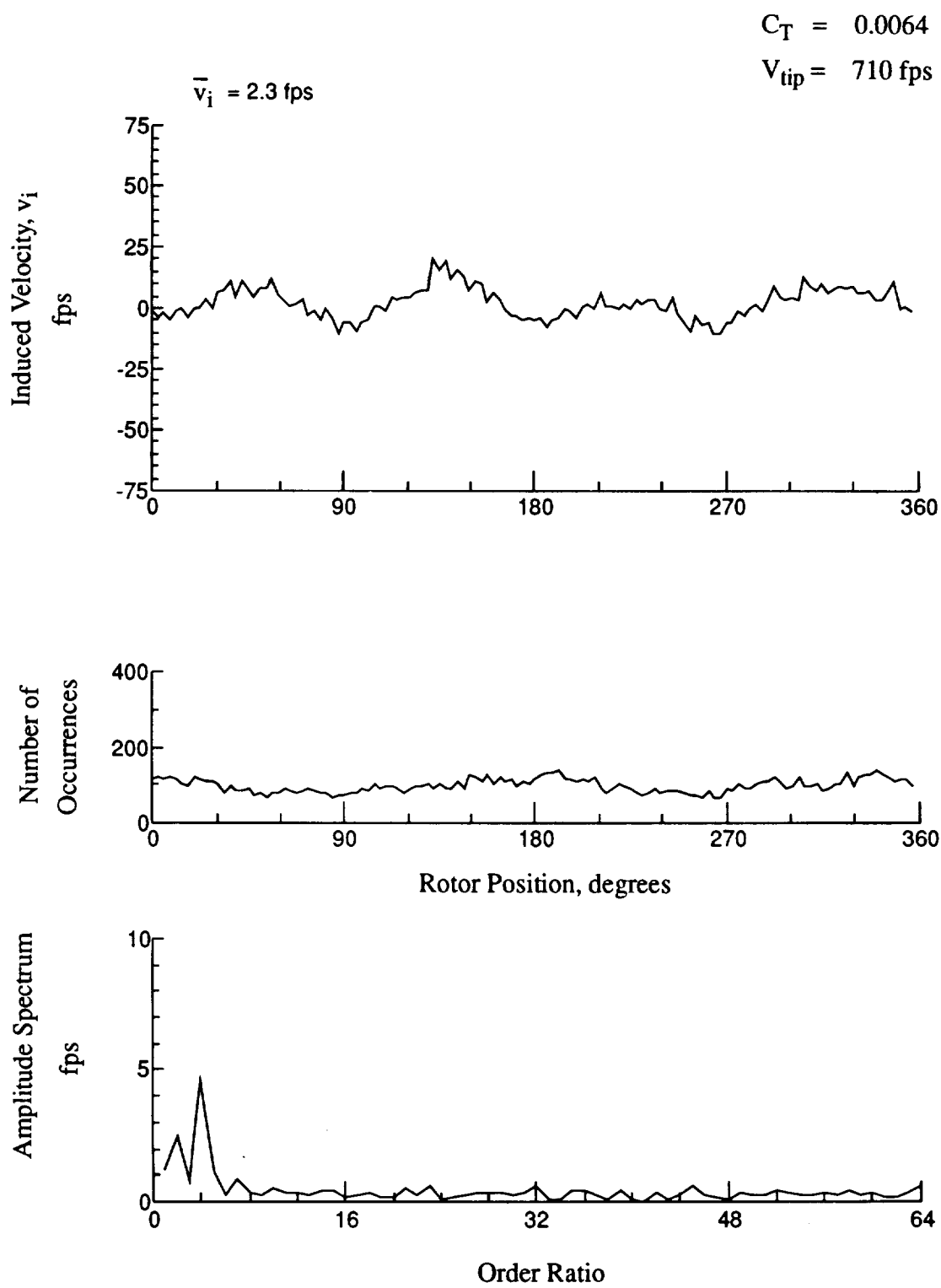


Figure 189.- Concluded.
 $x/R = 1.50$, $y/R = -0.20$, $z = -6.38 \text{ in.}$

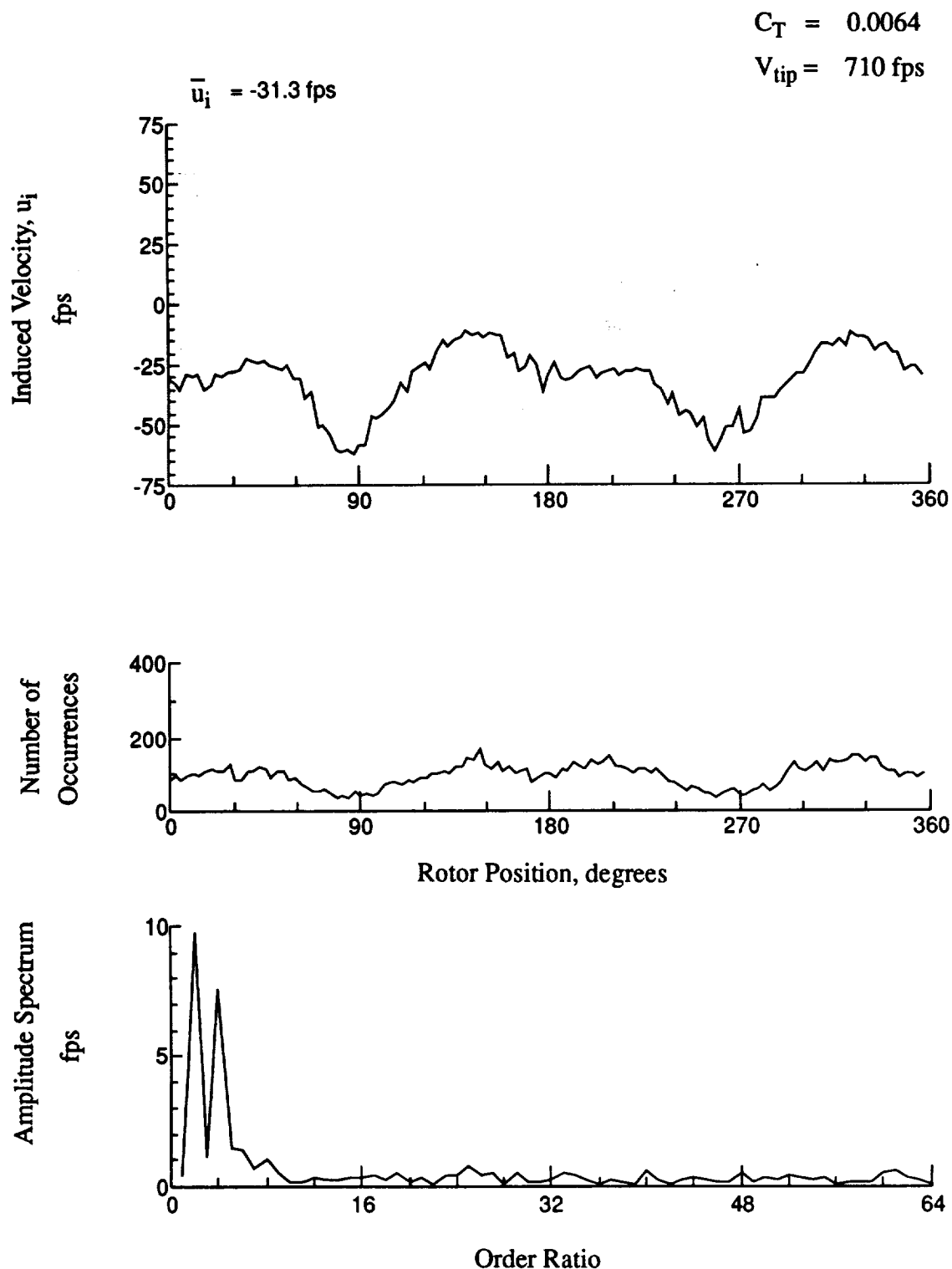


Figure 190.- Wake Measurements at
 $x/R = 1.50$, $y/R = -0.20$, $z = -7.41 \text{ in.}$

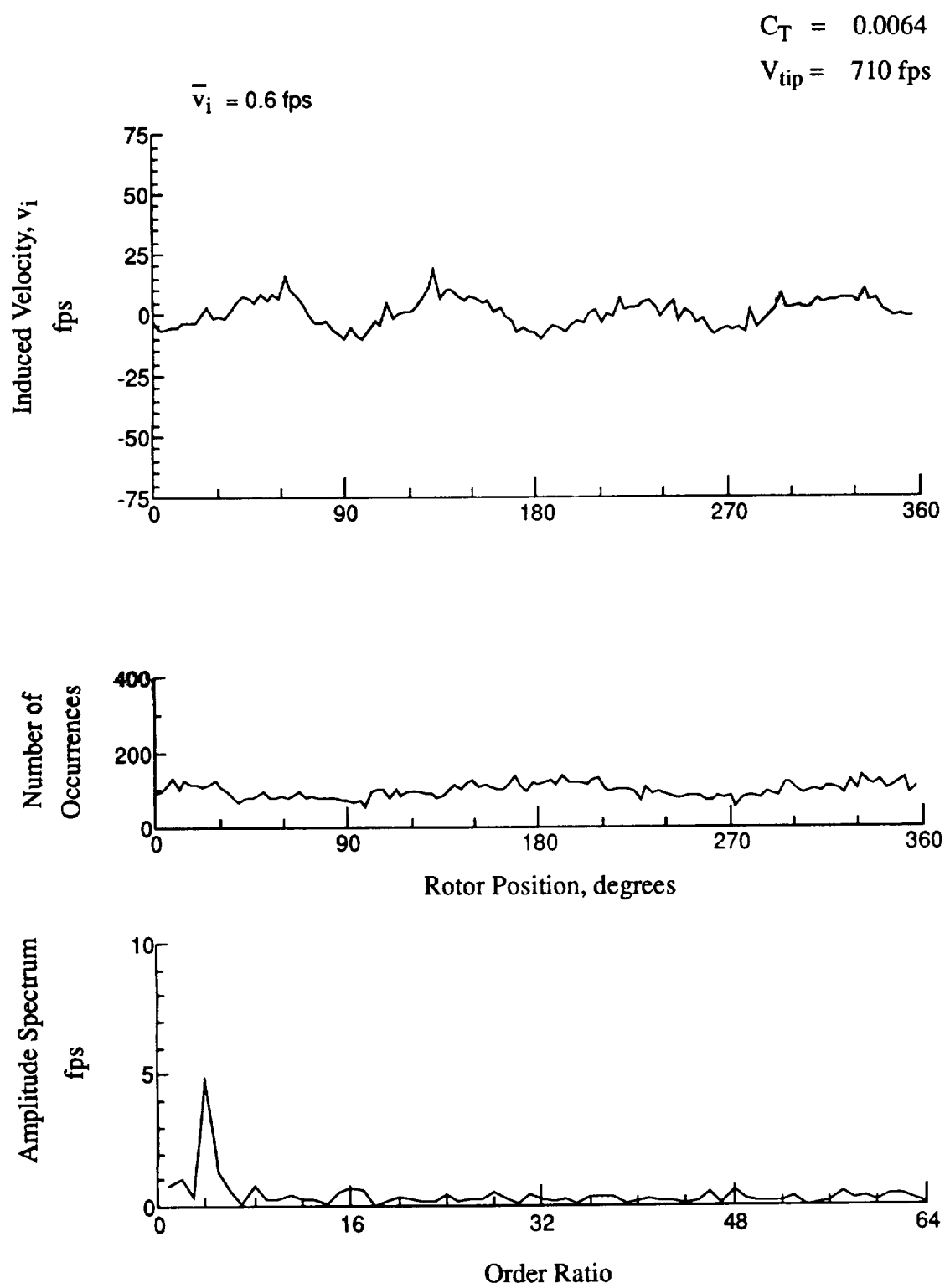


Figure 190.- Concluded.
 $x/R = 1.50$, $y/R = -0.20$, $z = -7.41$ in.

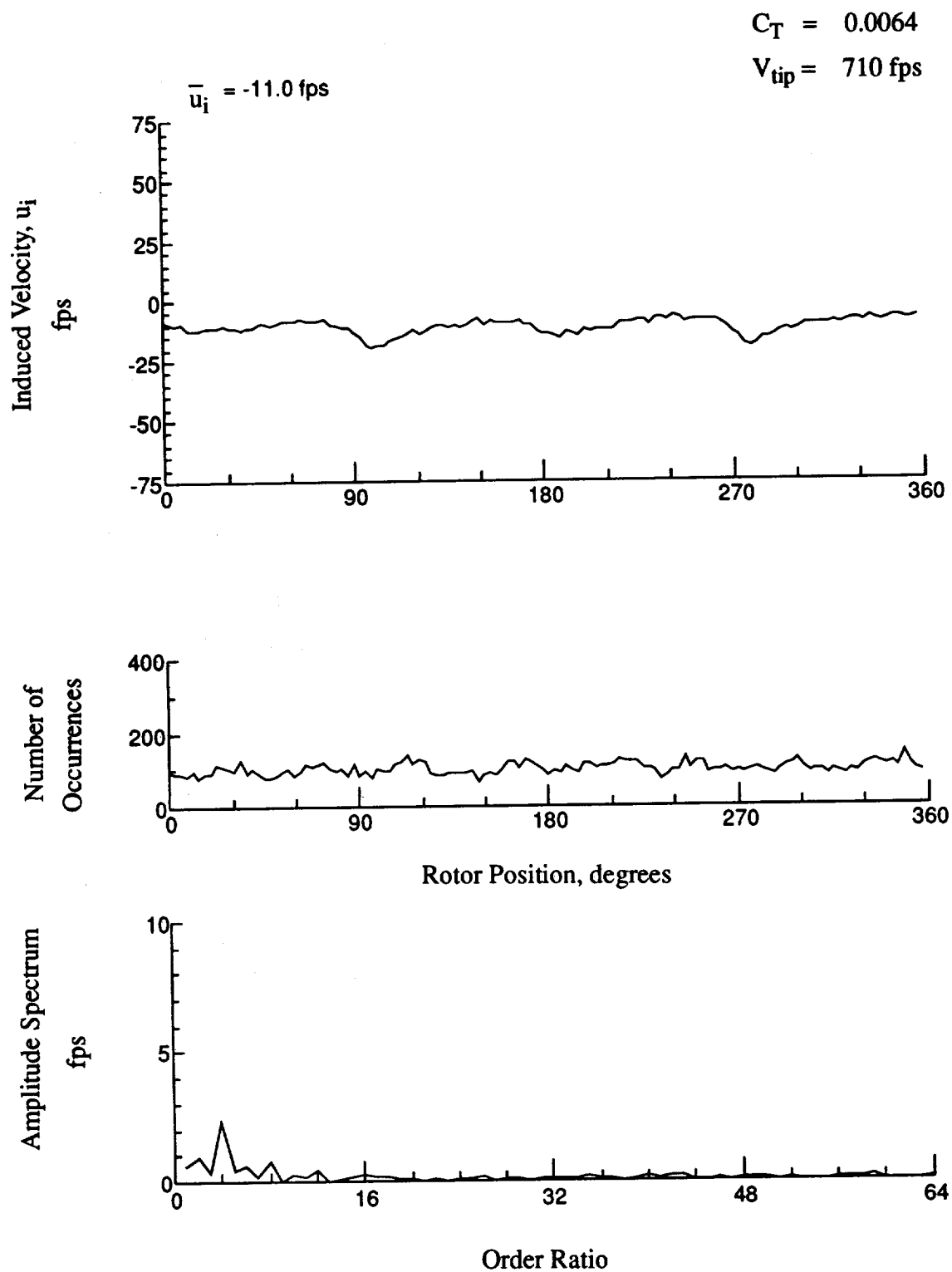


Figure 191.- Wake Measurements at
 $x/R = 1.50$, $y/R = 0.20$, $z = 6.93 \text{ in.}$

$$C_T = 0.0064$$

$$V_{tip} = 710 \text{ fps}$$

$$\bar{v}_i = -19.7 \text{ fps}$$

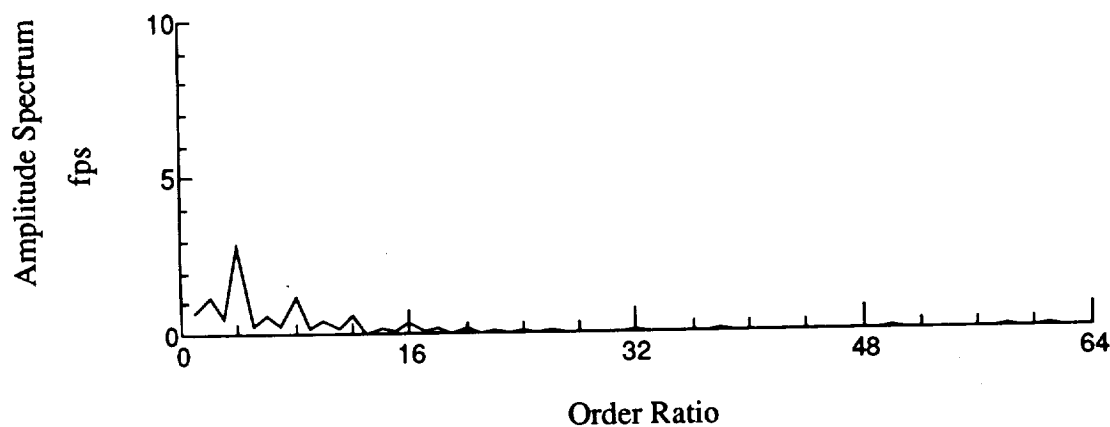
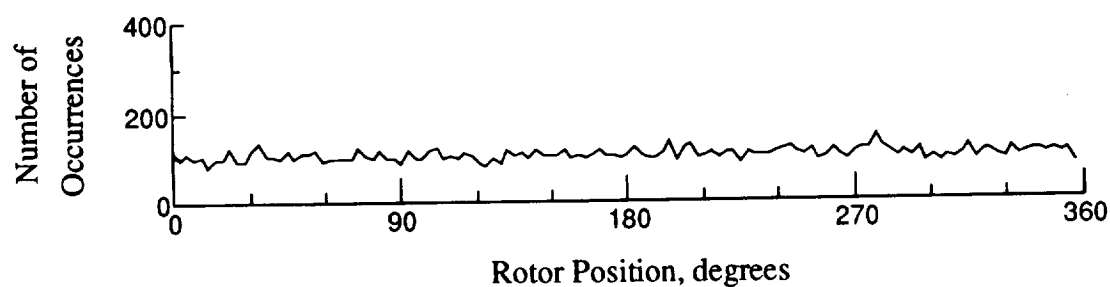
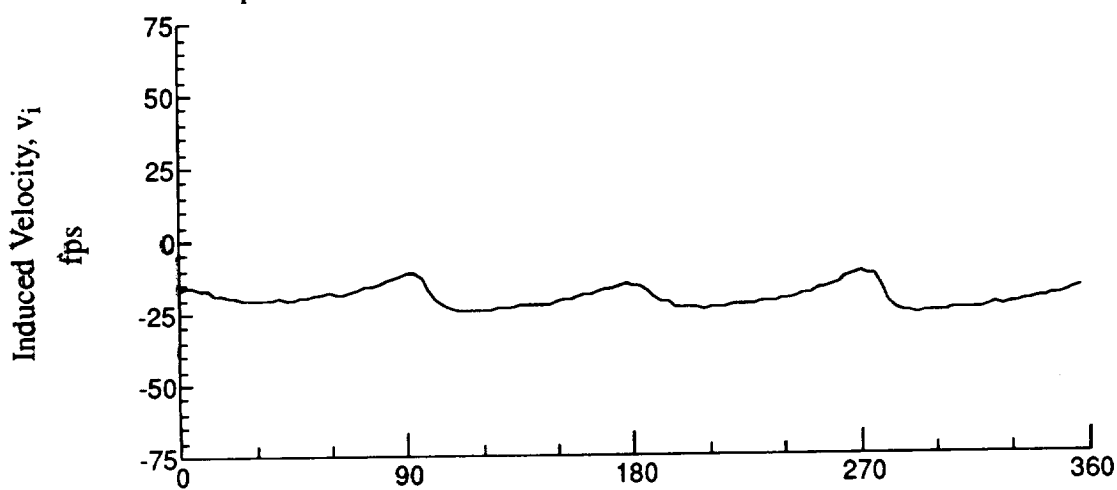


Figure 191.- Concluded.
 $x/R = 1.50$, $y/R = 0.20$, $z = 6.93$ in.

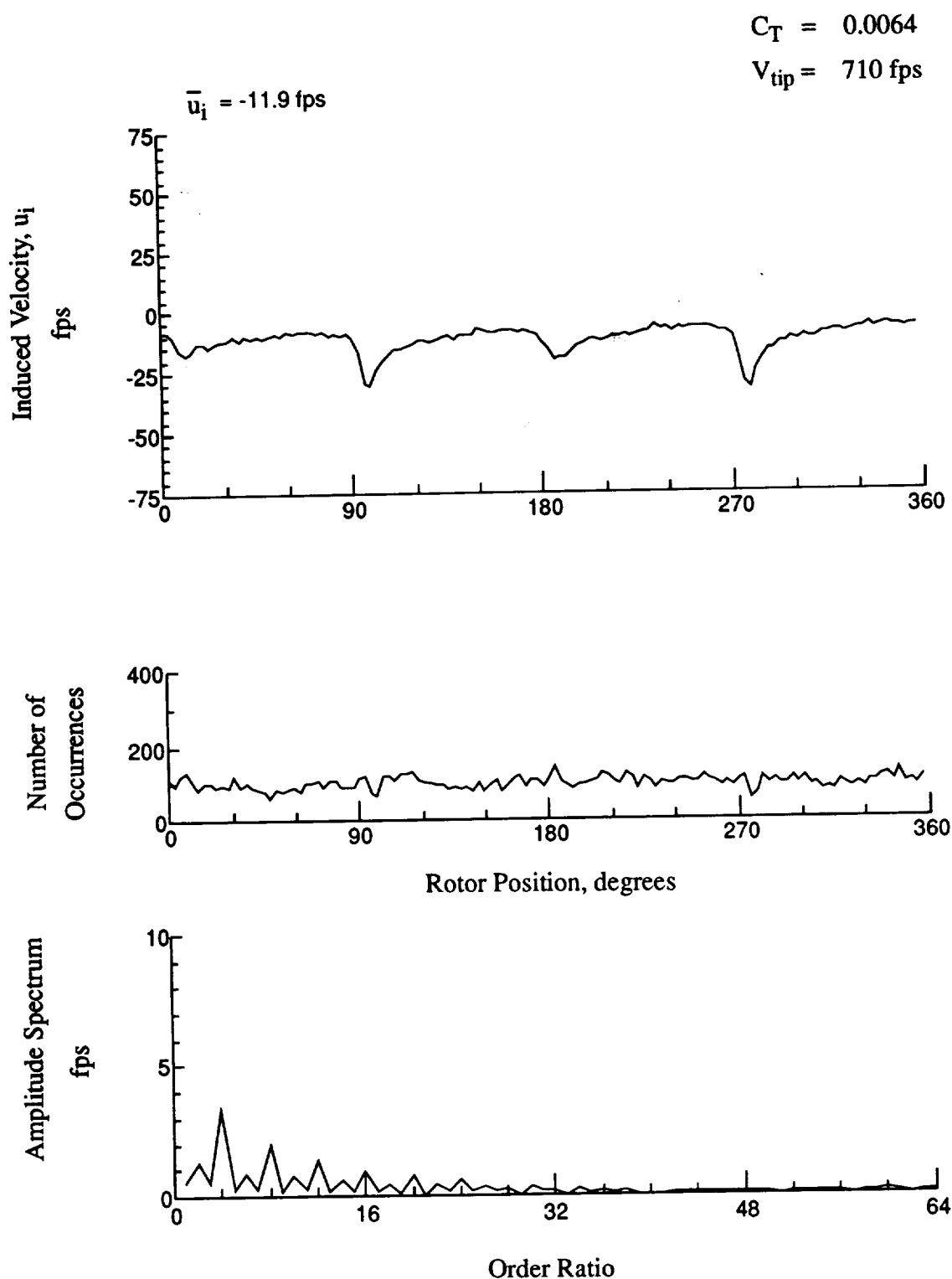


Figure 192.- Wake Measurements at
 $x/R = 1.50$, $y/R = 0.20$, $z = 5.90 \text{ in.}$

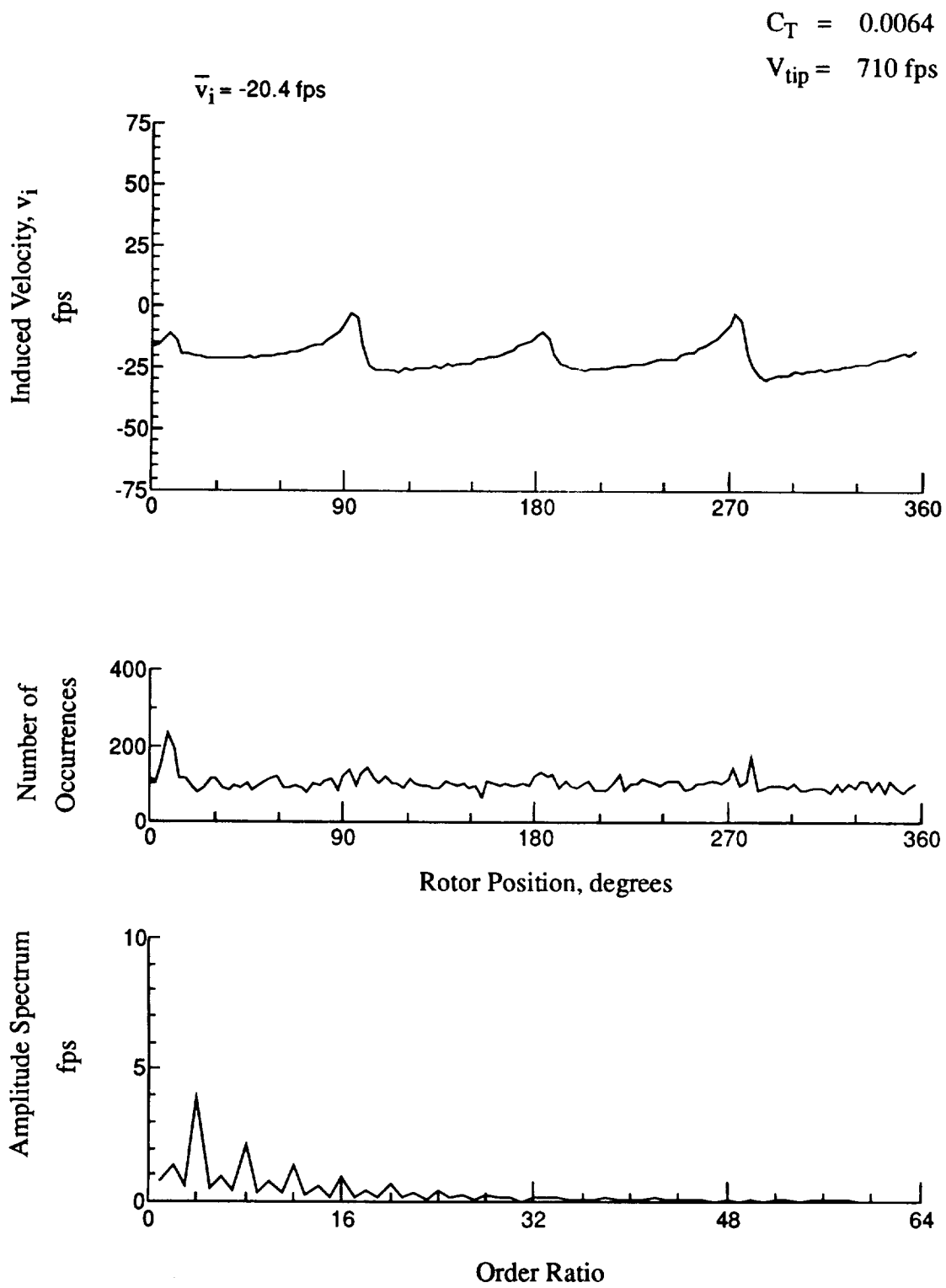


Figure 192.- Concluded.
 $x/R = 1.50$, $y/R = 0.20$, $z = 5.90 \text{ in.}$

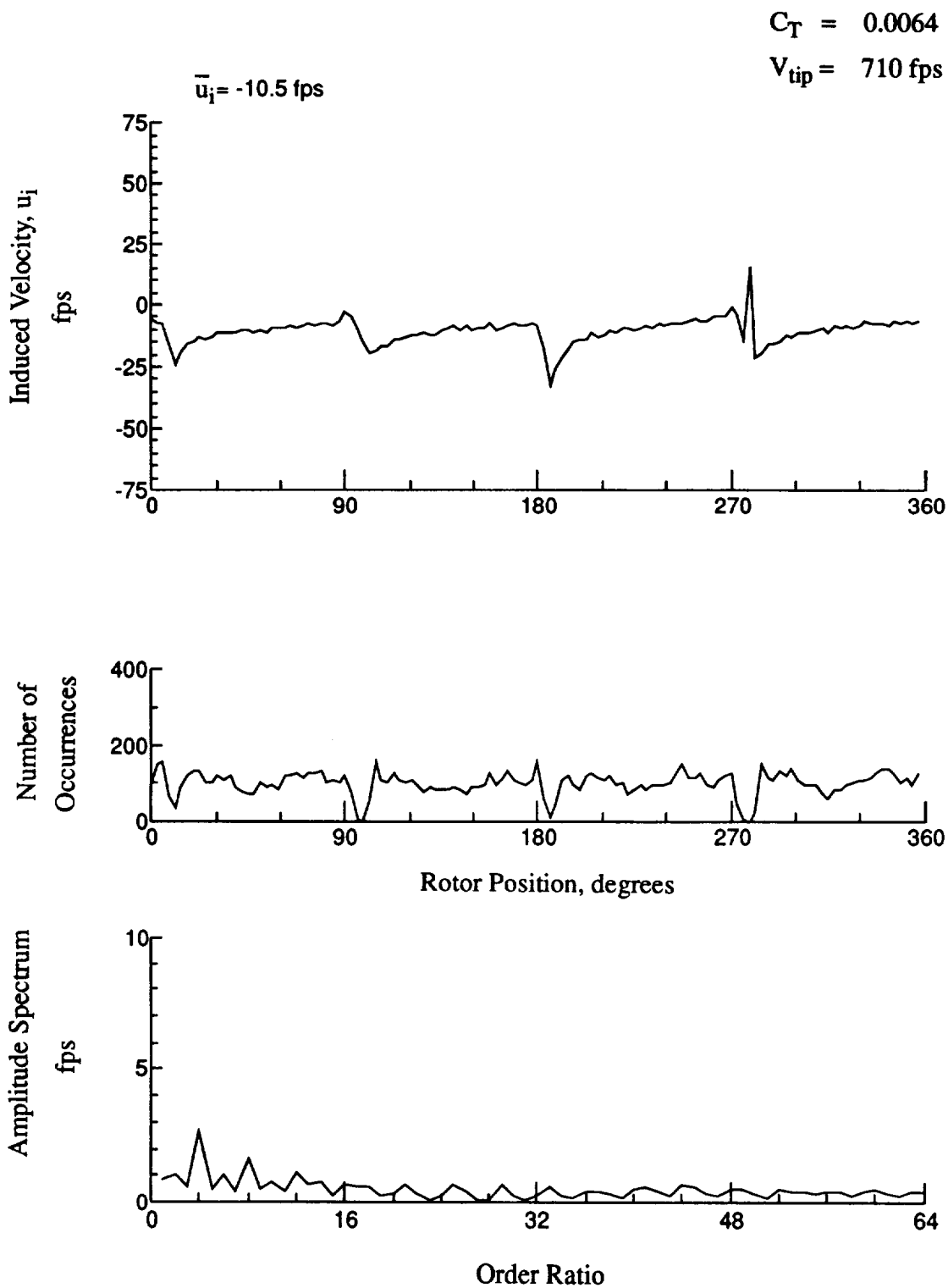


Figure 193.- Wake Measurements at
 $x/R = 1.50$, $y/R = 0.20$, $z = 4.87 \text{ in.}$

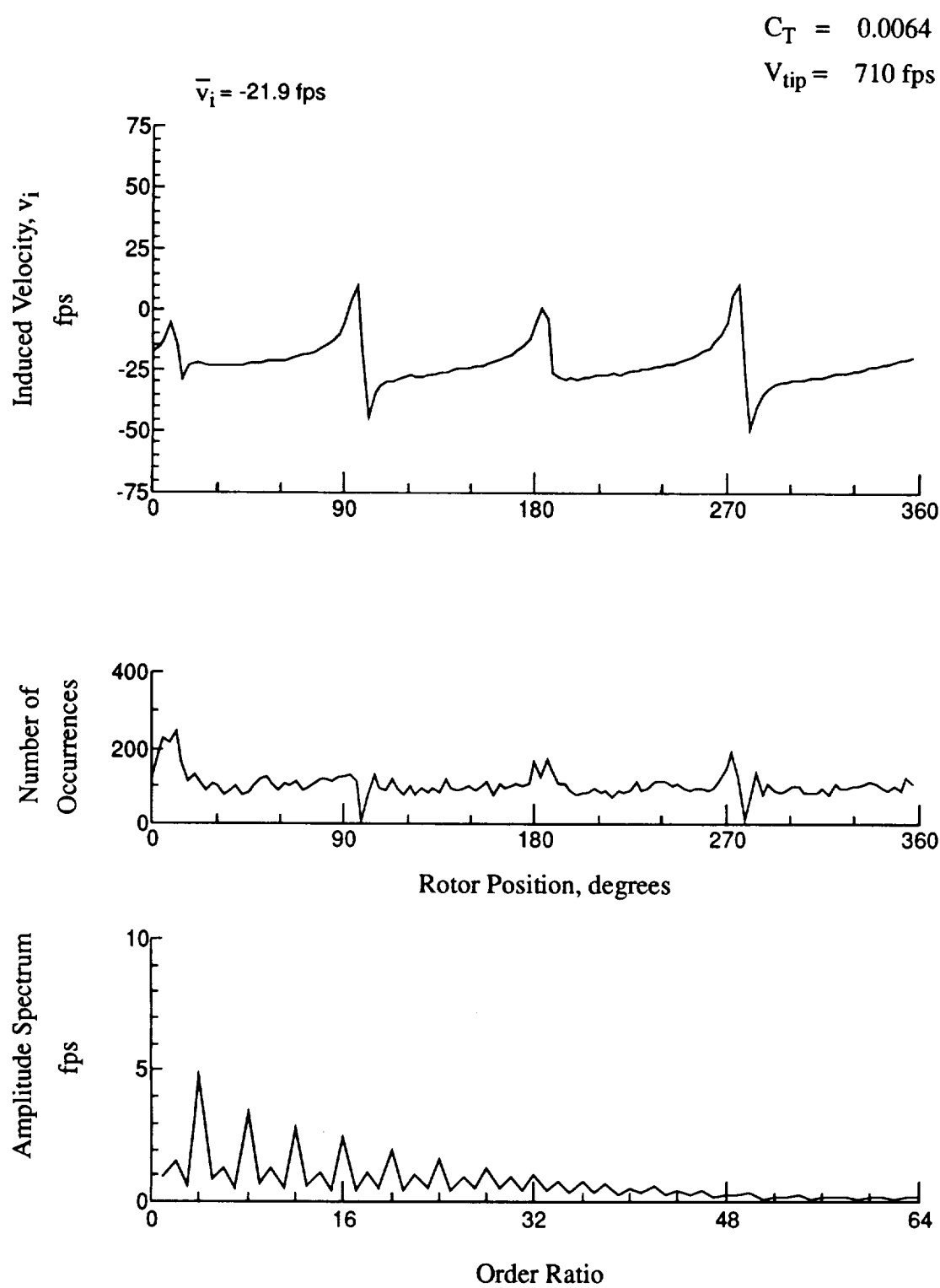


Figure 193.- Concluded.
 $x/R = 1.50$, $y/R = 0.20$, $z = 4.87 \text{ in.}$

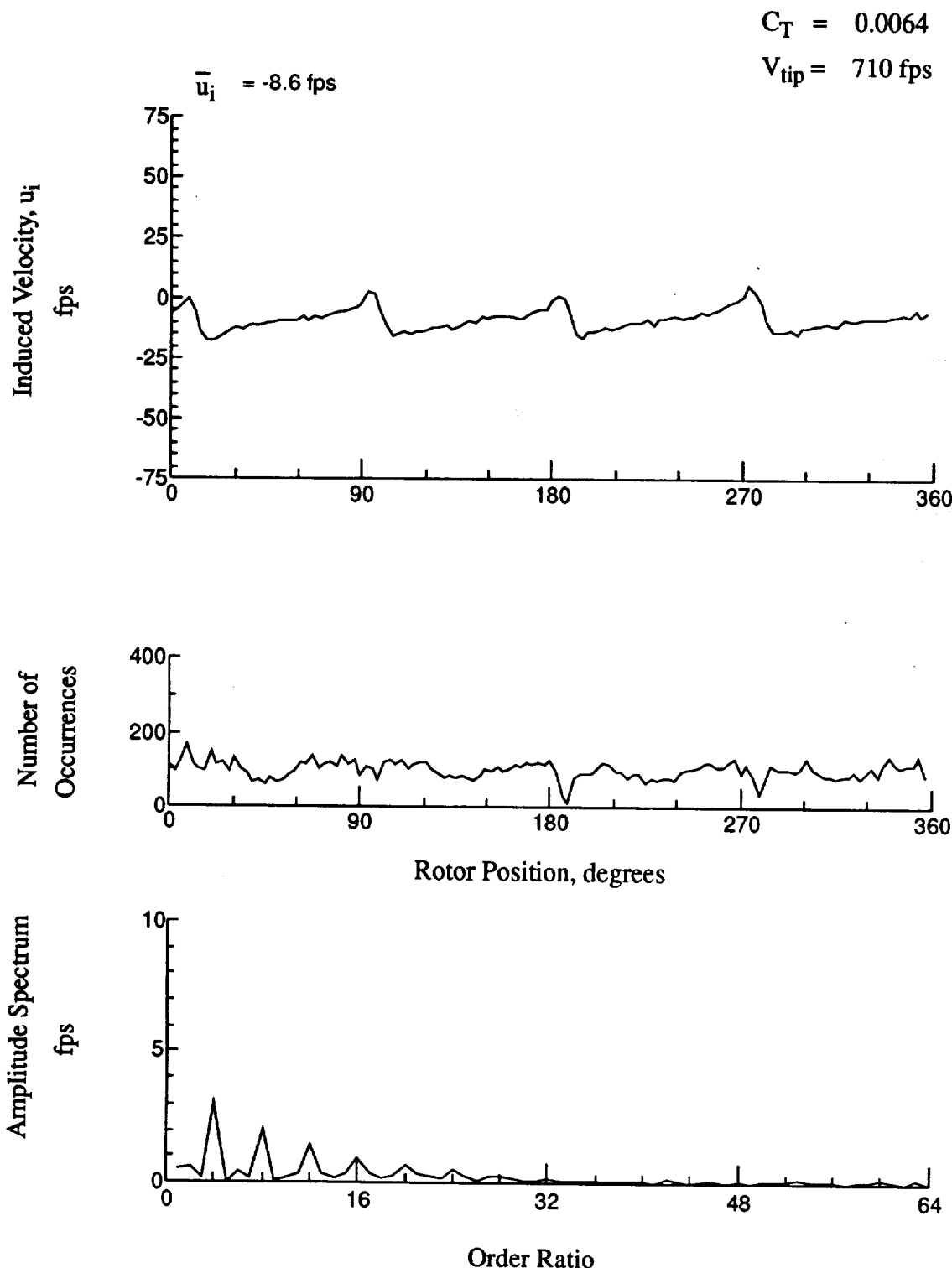


Figure 194.- Wake Measurements at
 $x/R = 1.50$, $y/R = 0.20$, $z = 3.84 \text{ in.}$

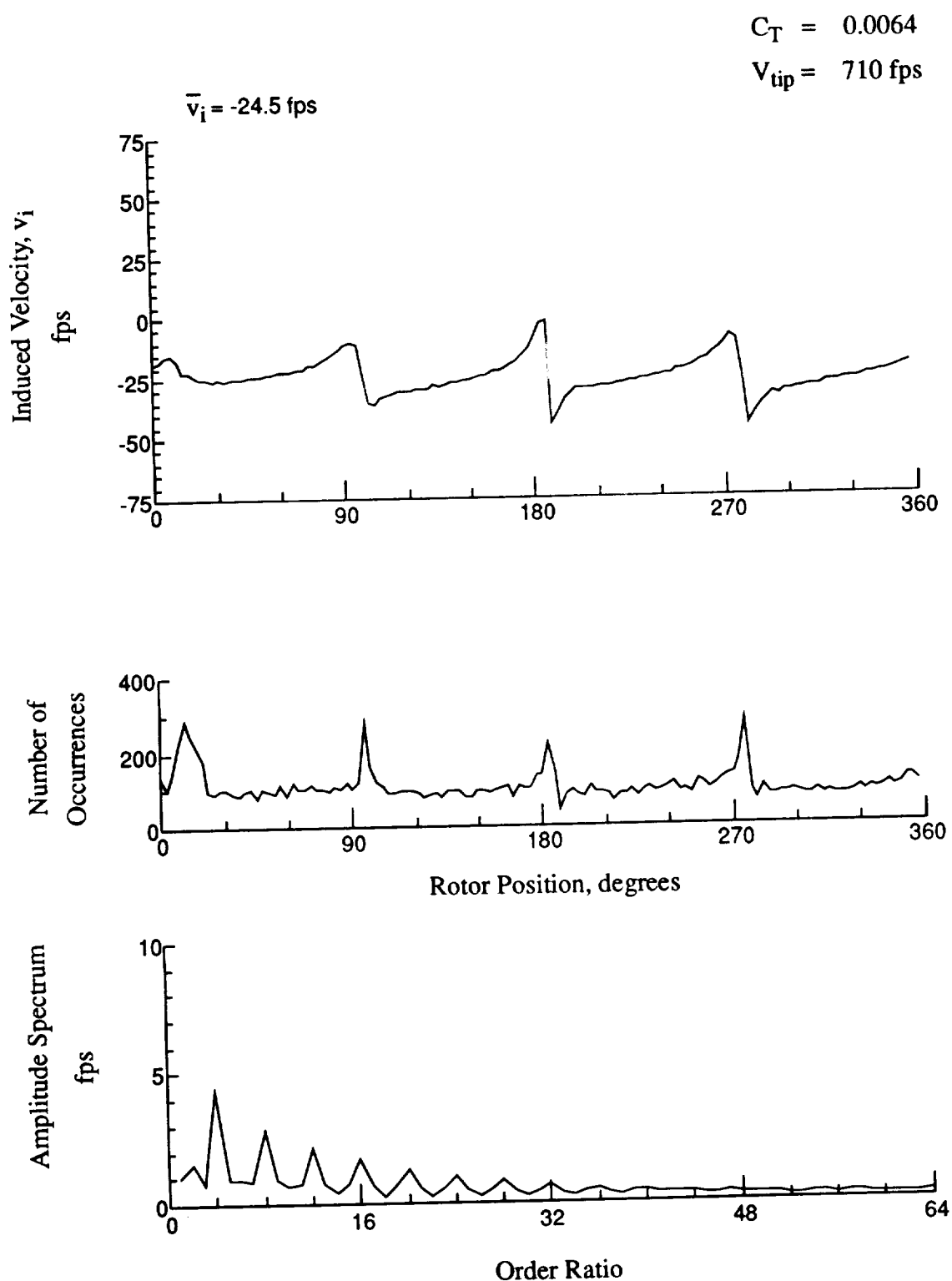


Figure 194.- Concluded.
 $x/R = 1.50$, $y/R = 0.20$, $z = 3.84 \text{ in.}$

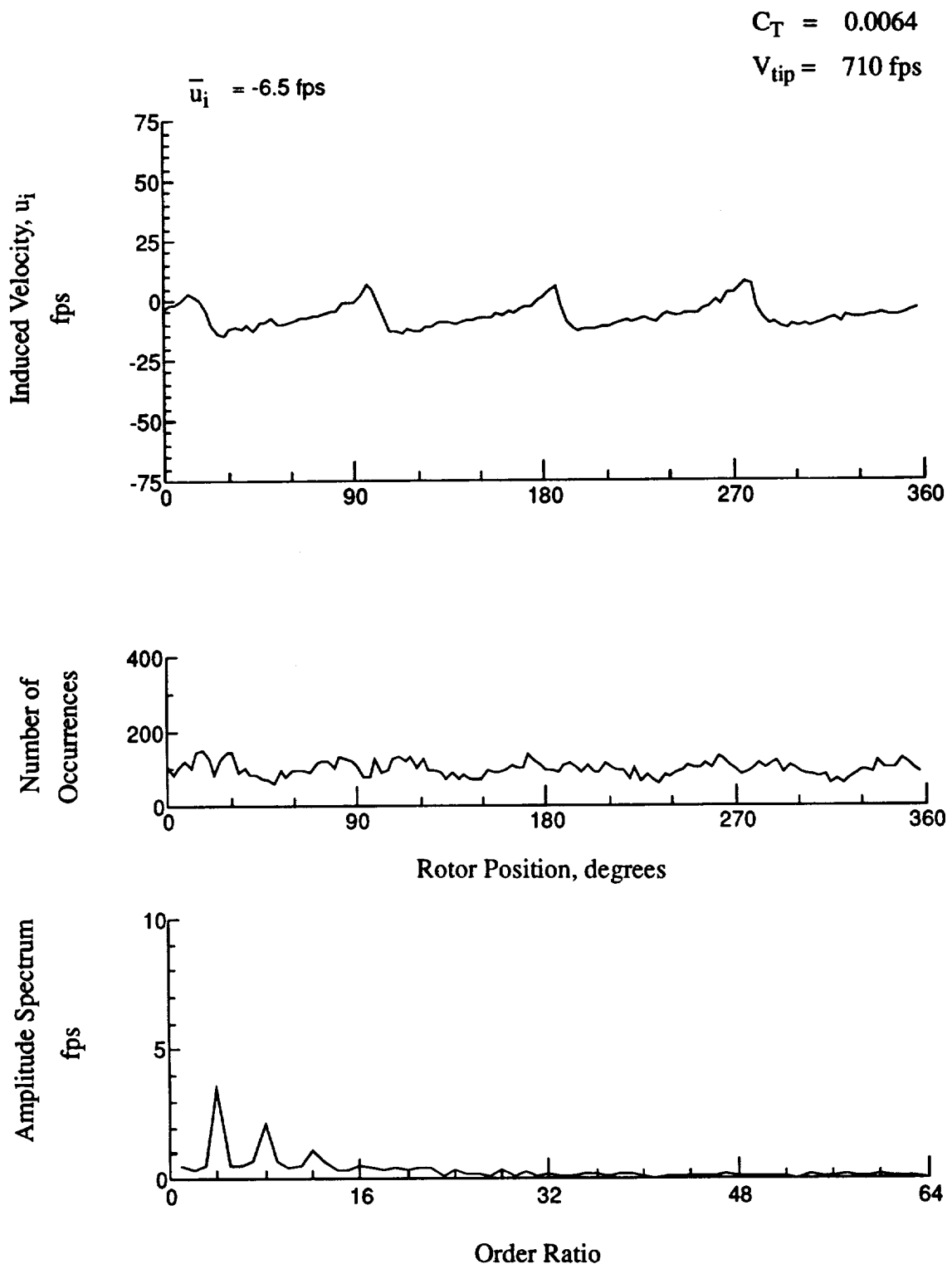


Figure 195.- Wake Measurements at
 $x/R = 1.50$, $y/R = 0.20$, $z = 2.81 \text{ in.}$

$$C_T = 0.0064$$

$$V_{tip} = 710 \text{ fps}$$

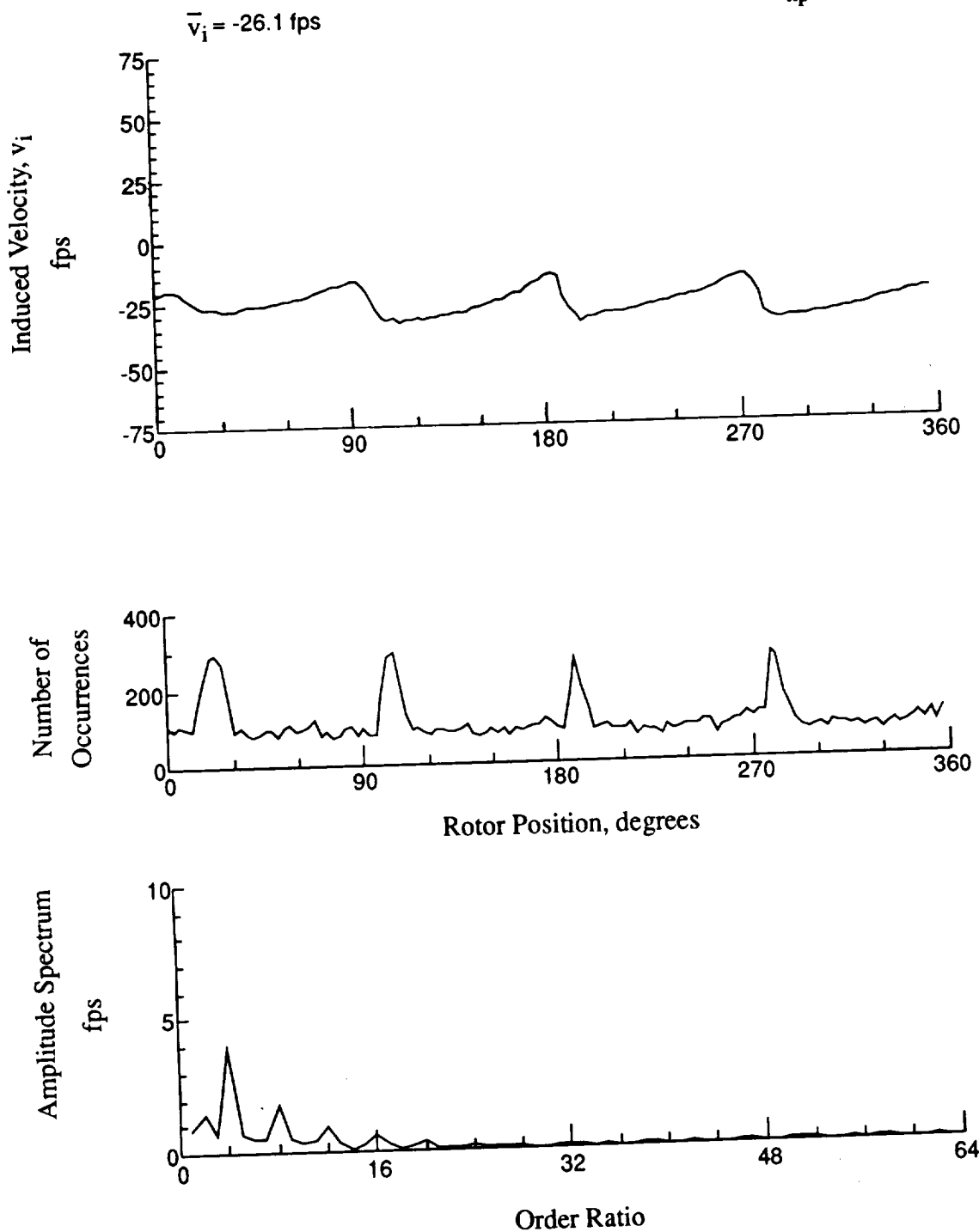


Figure 195.- Concluded.
 $x/R = 1.50$, $y/R = 0.20$, $z = 2.81 \text{ in.}$

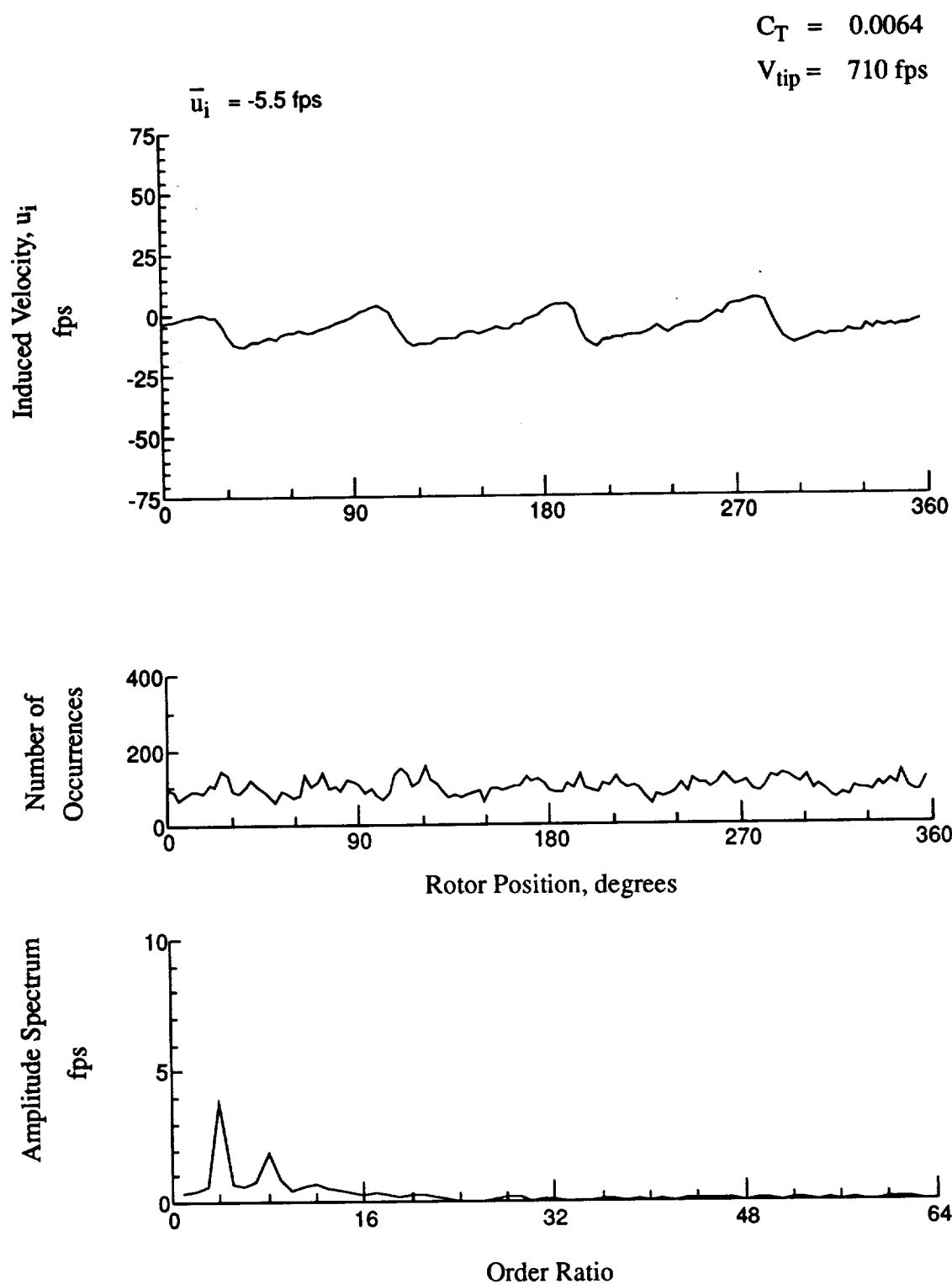


Figure 196.- Wake Measurements at
 $x/R = 1.50$, $y/R = 0.20$, $z = 1.78 \text{ in.}$

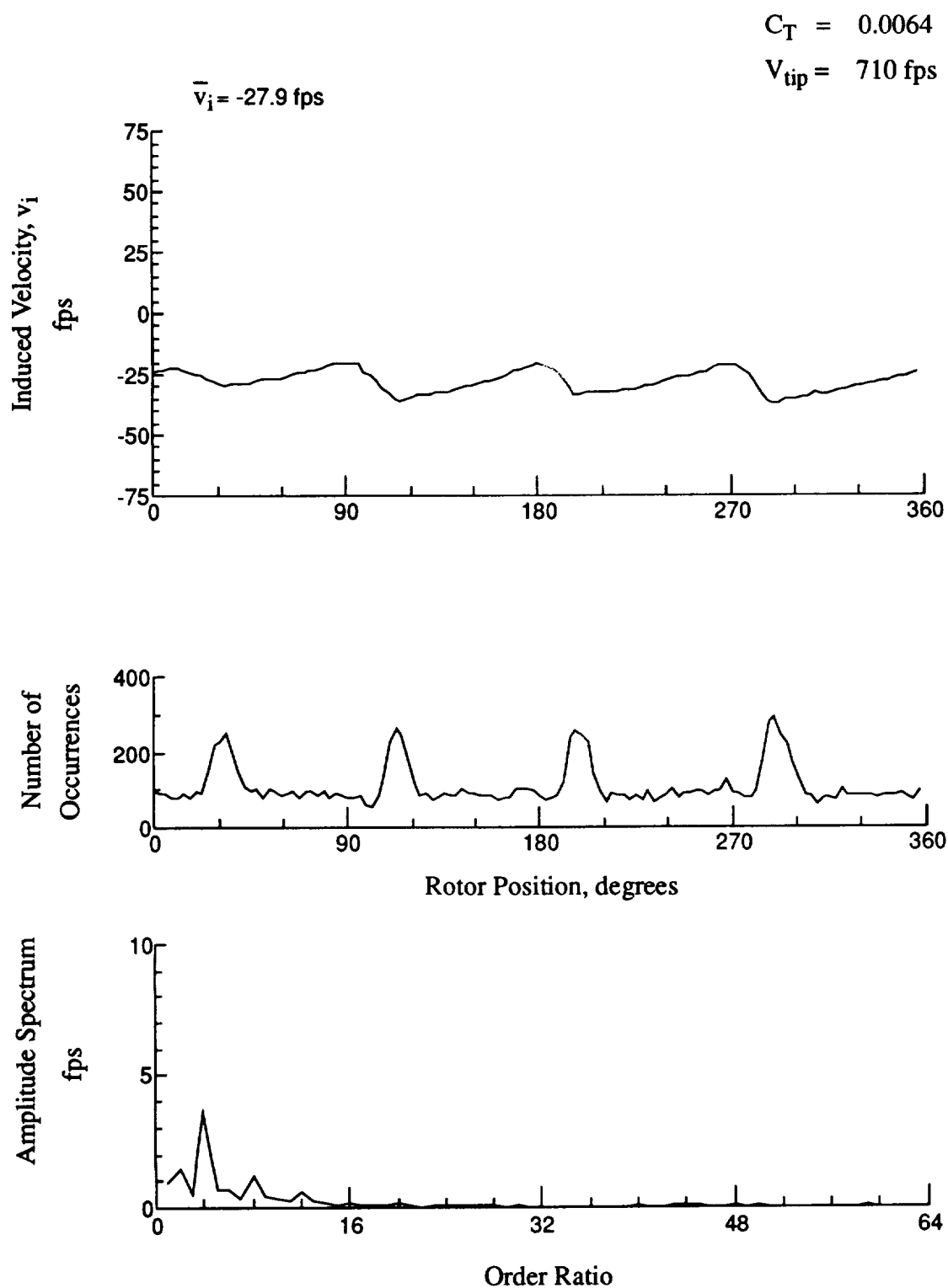


Figure 196.- Concluded.

$x/R = 1.50$, $y/R = 0.20$, $z = 1.78 \text{ in.}$

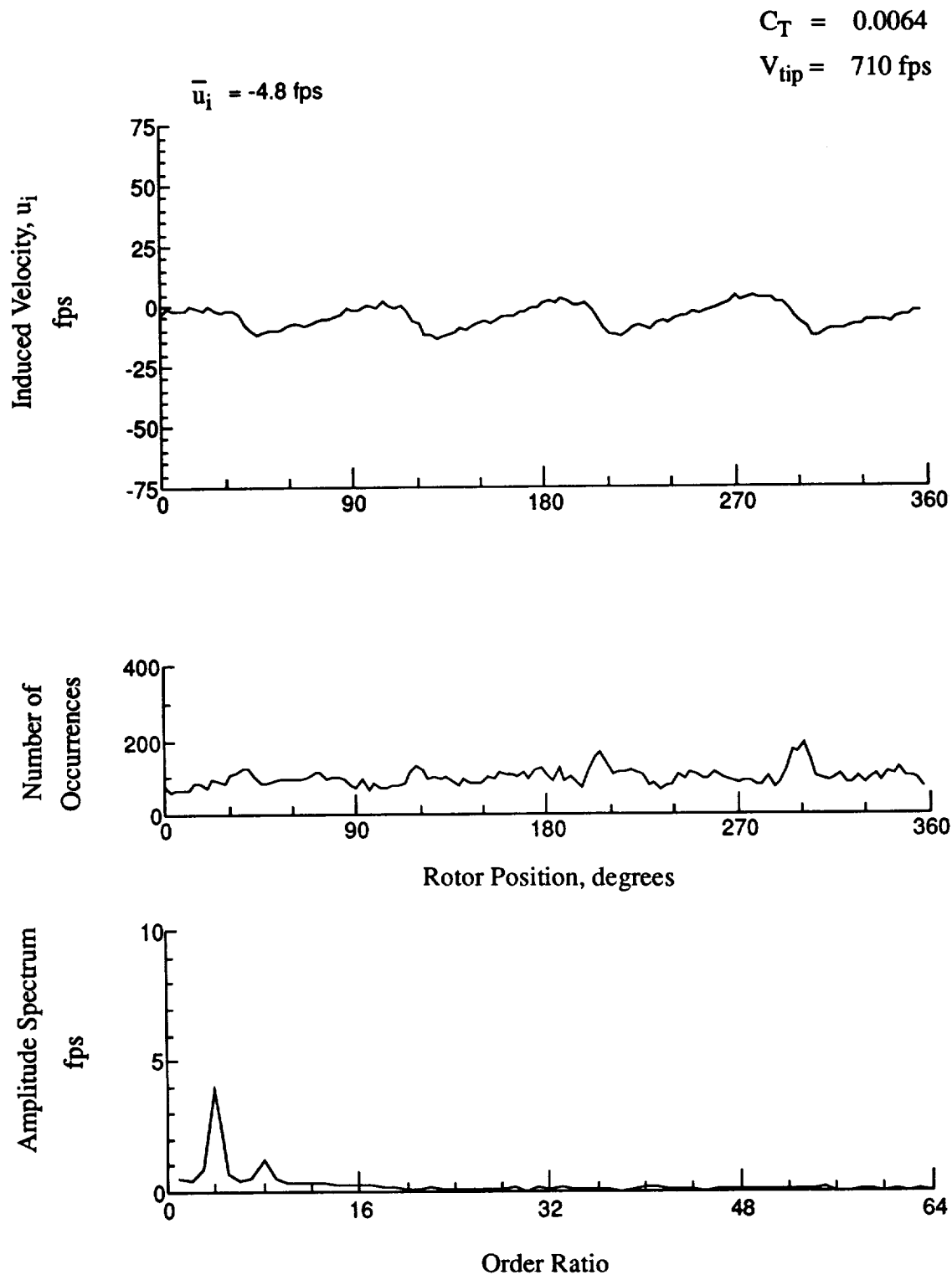


Figure 197.- Wake Measurements at
 $x/R = 1.50$, $y/R = 0.20$, $z = 0.75 \text{ in.}$

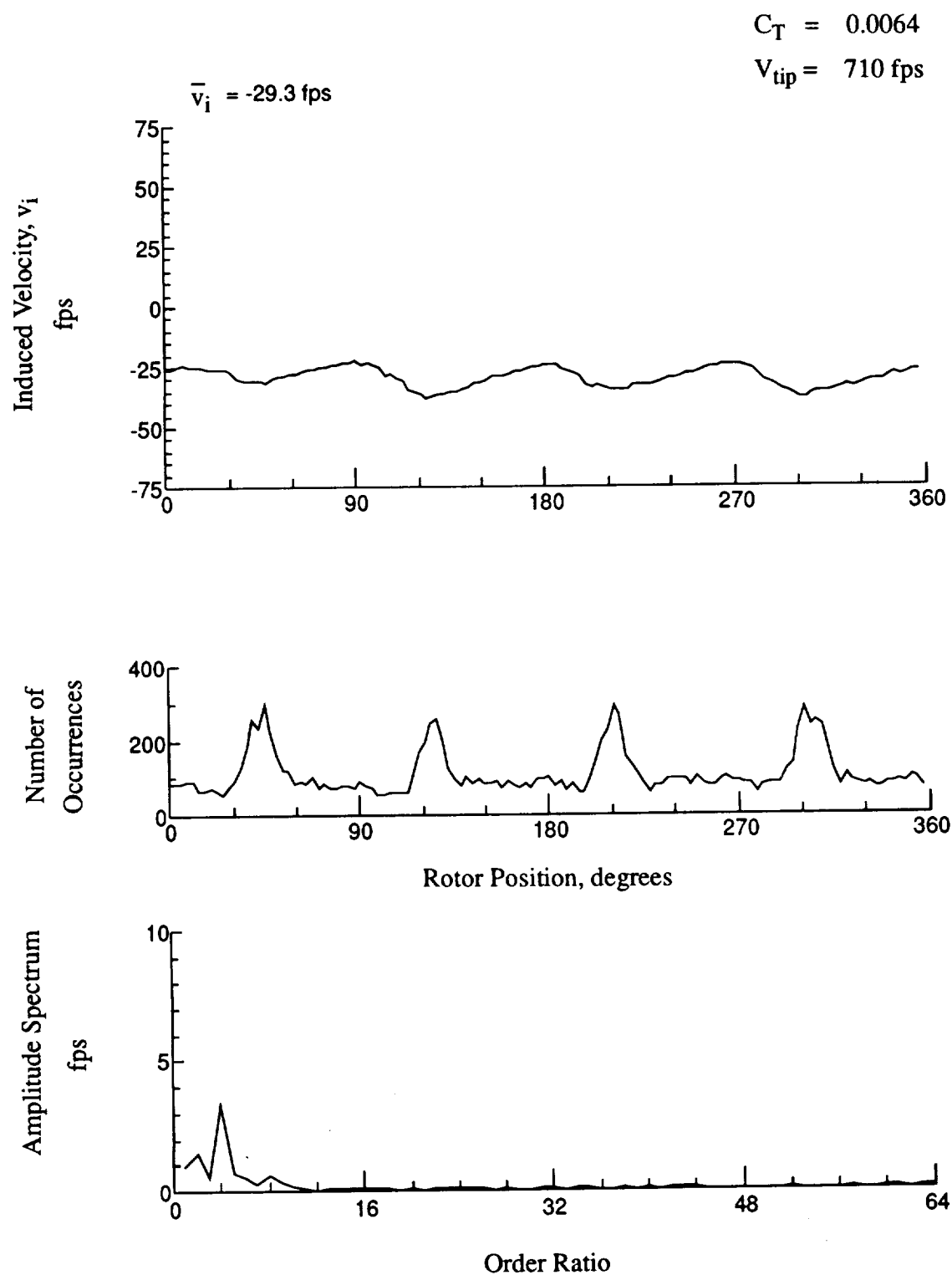


Figure 197.- Concluded.
 $x/R = 1.50$, $y/R = 0.20$, $z = 0.75 \text{ in.}$

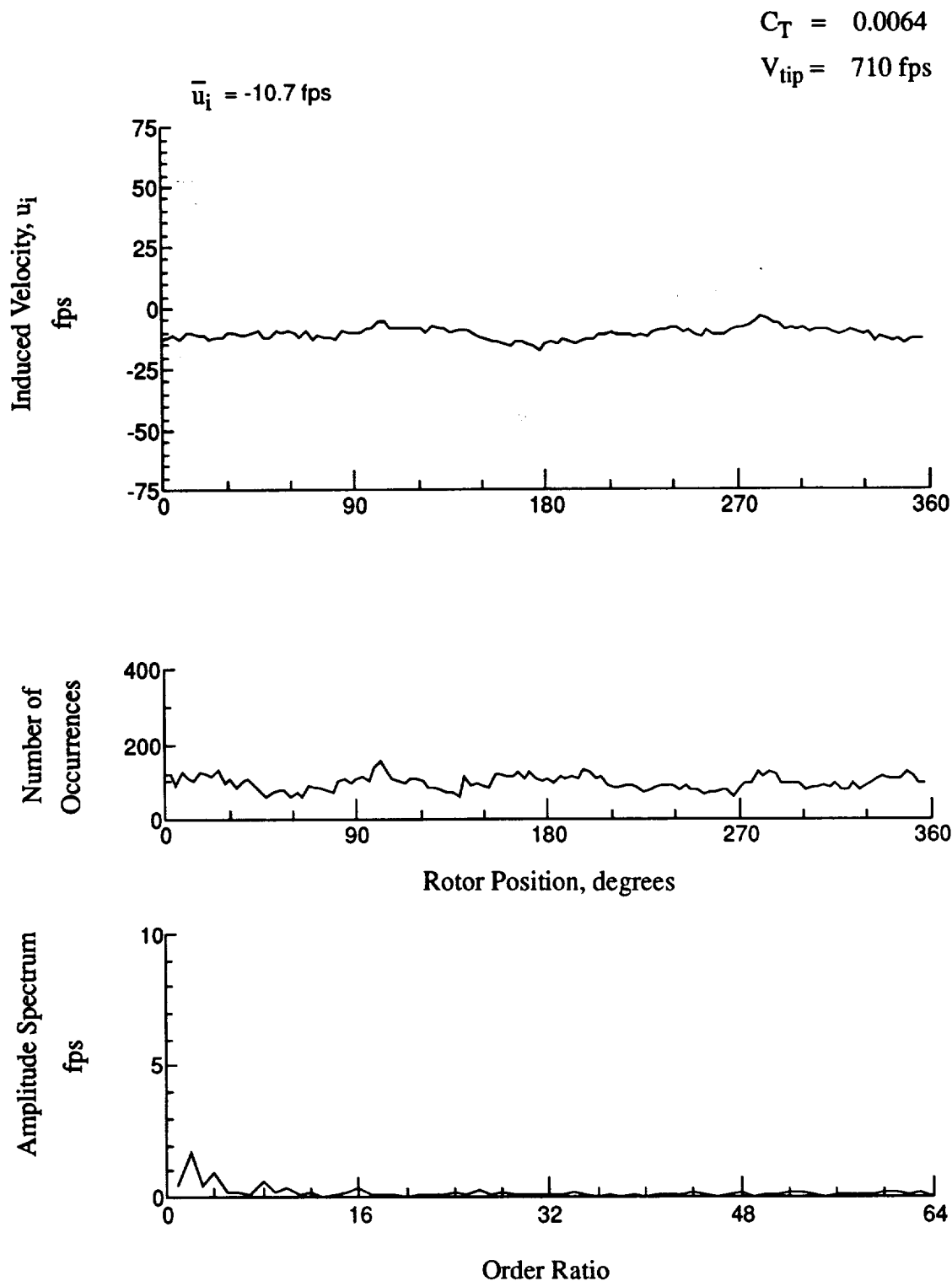


Figure 198.- Wake Measurements at
 $x/R = 1.50$, $y/R = 0.20$, $z = -7.47 \text{ in.}$

$$C_T = 0.0064$$

$$V_{tip} = 710 \text{ fps}$$

$$\bar{v}_i = -36.3 \text{ fps}$$

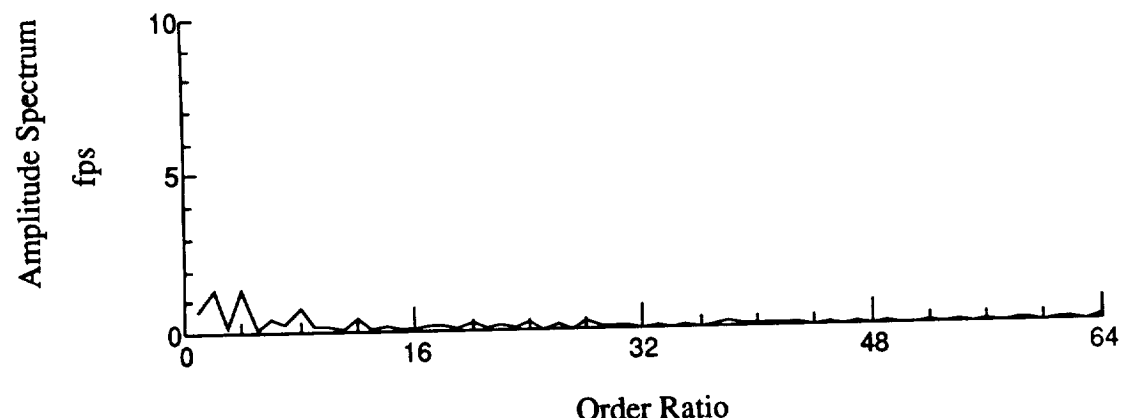
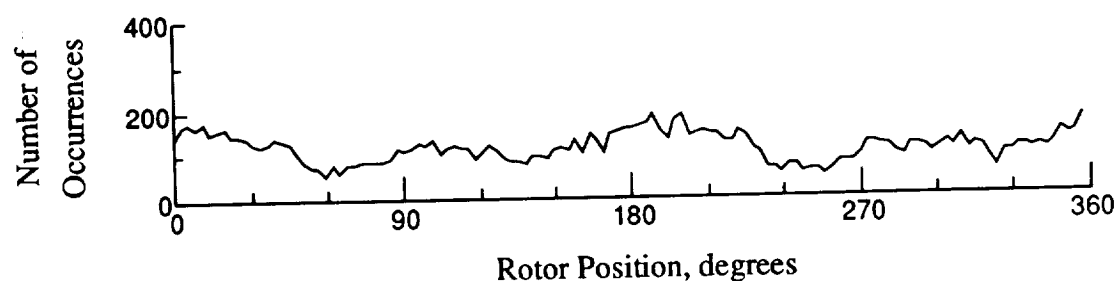
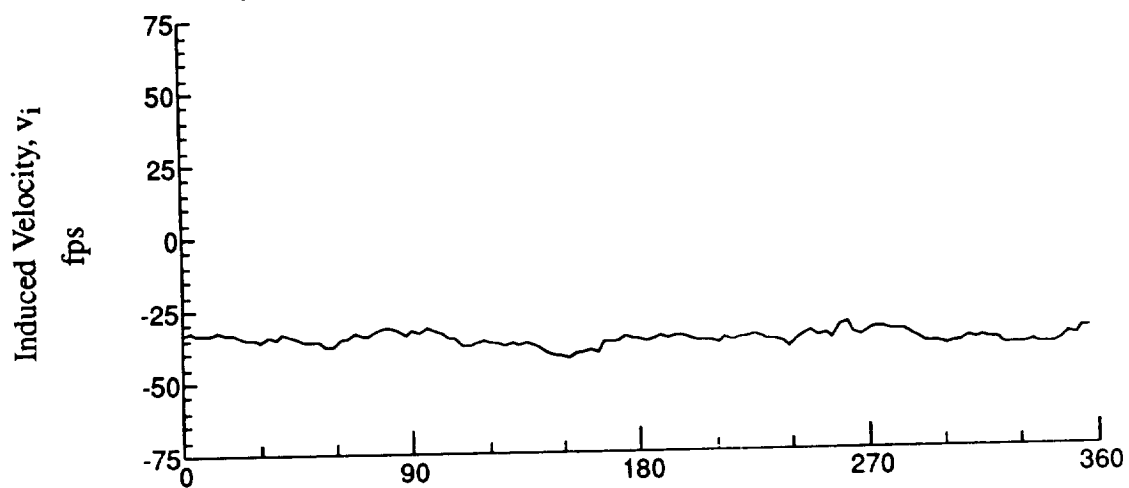


Figure 198.- Concluded.

$x/R = 1.50$, $y/R = 0.20$, $z = -7.47$ in.

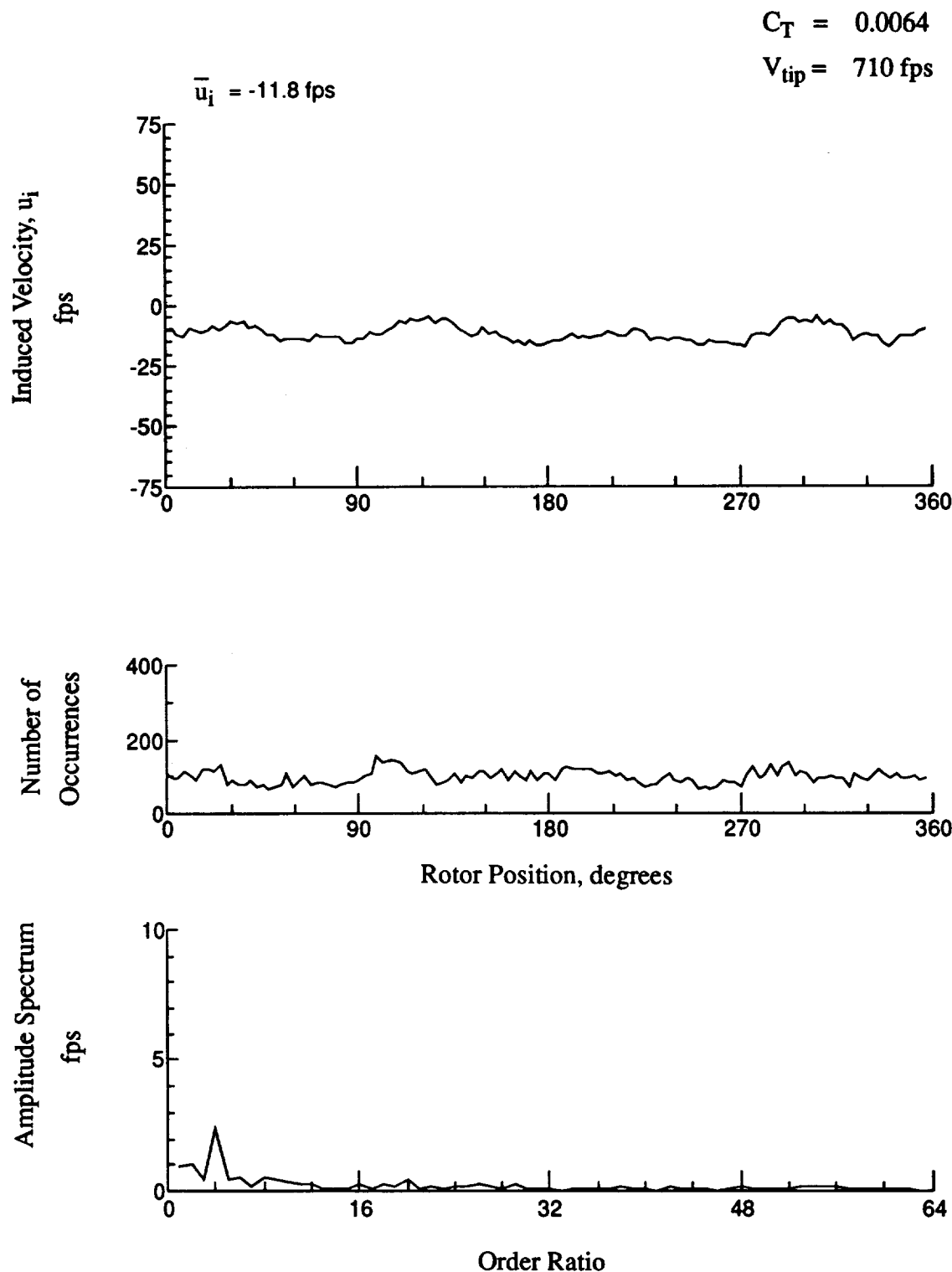


Figure 199.- Wake Measurements at
 $x/R = 1.50$, $y/R = 0.20$, $z = -8.50 \text{ in.}$

$$C_T = 0.0064$$

$$V_{tip} = 710 \text{ fps}$$

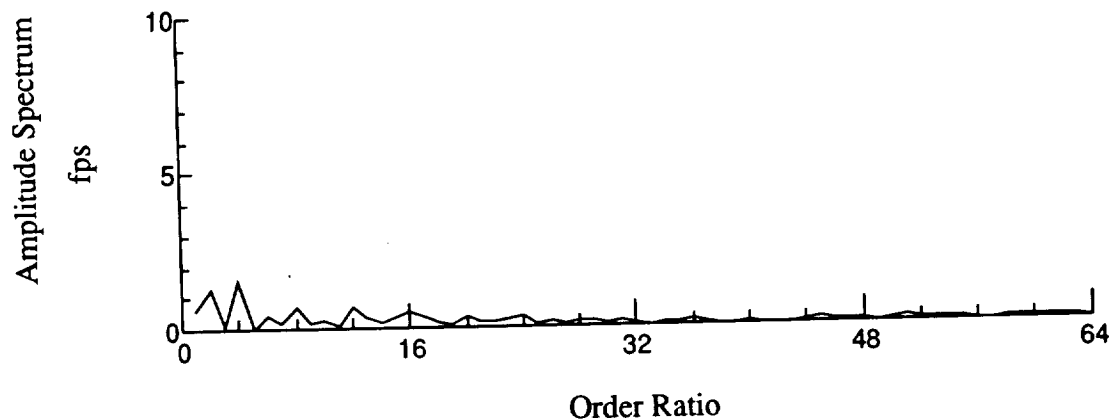
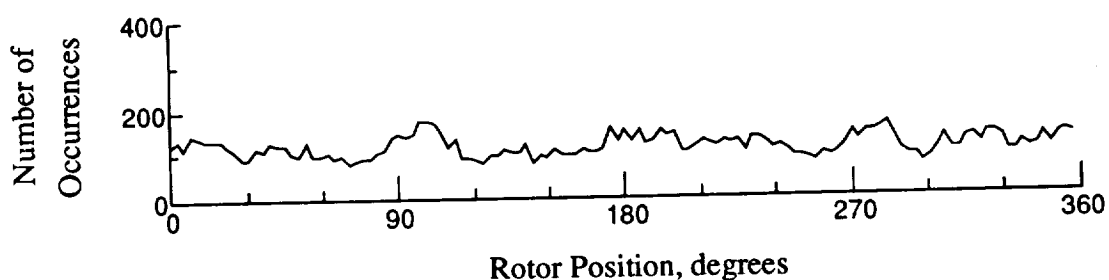
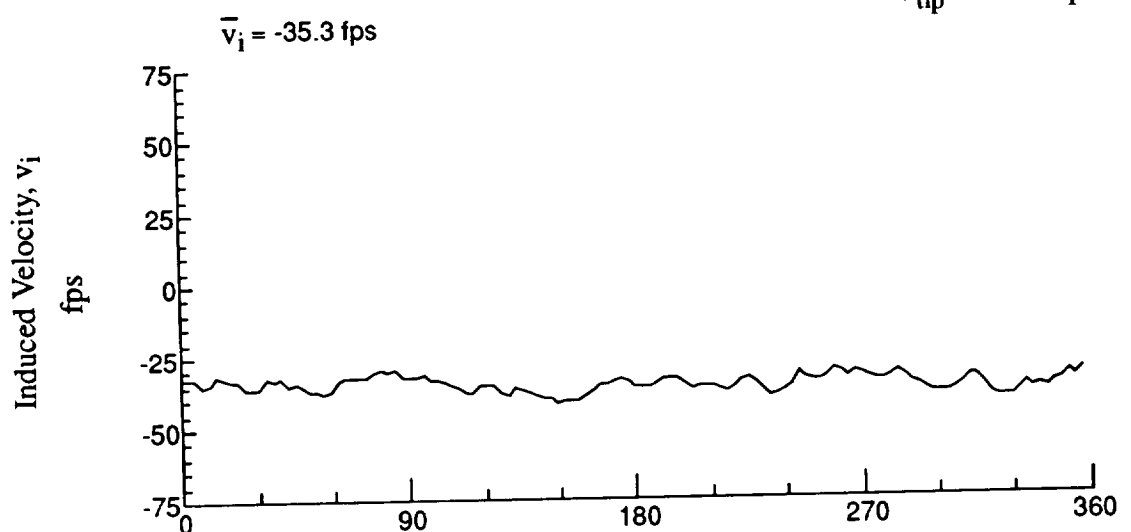


Figure 199.- Concluded.
 $x/R = 1.50$, $y/R = 0.20$, $z = -8.50 \text{ in.}$

$$C_T = 0.0064$$

$$V_{tip} = 710 \text{ fps}$$

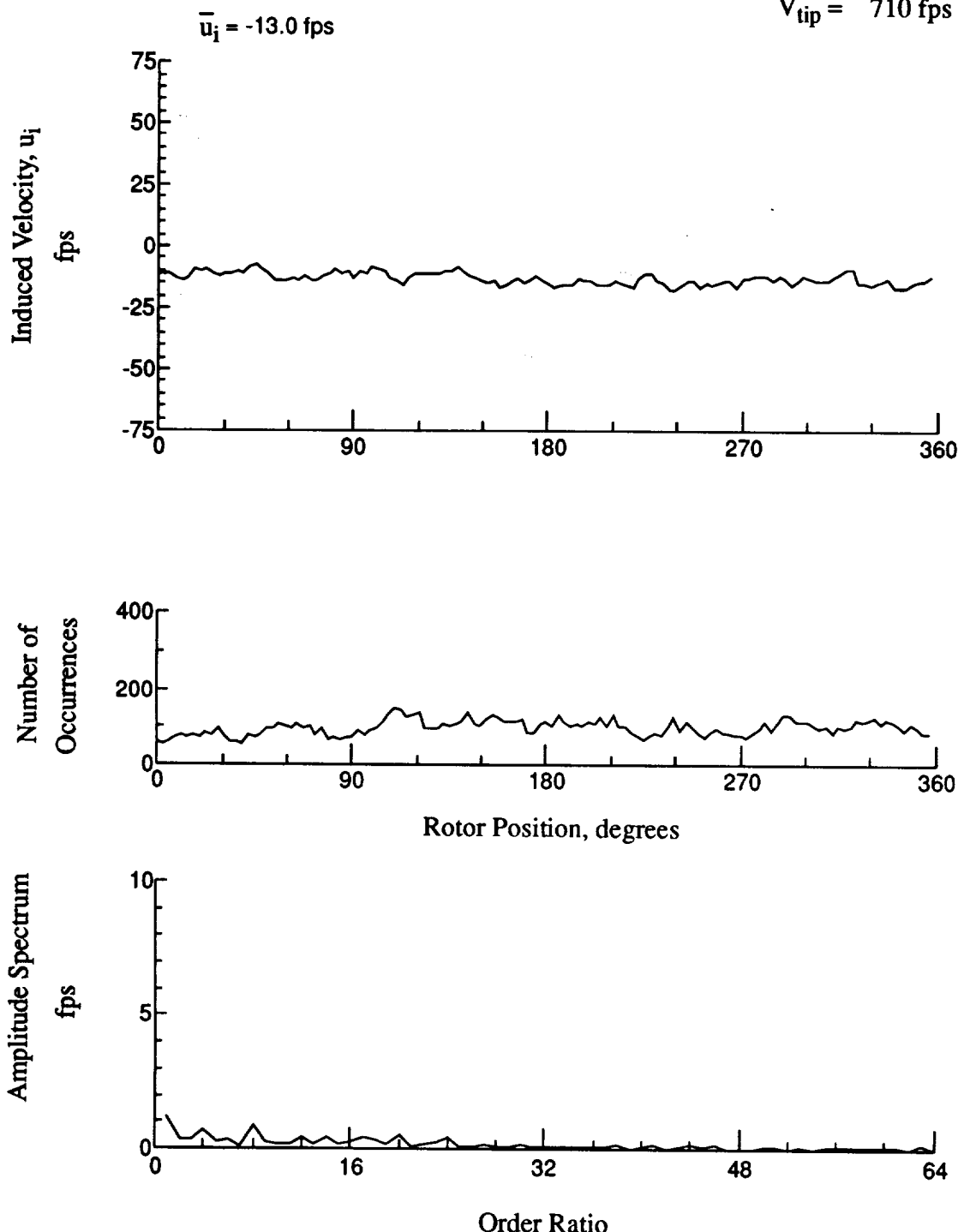


Figure 200.- Wake Measurements at
 $x/R = 1.50$, $y/R = 0.20$, $z = -9.53 \text{ in.}$

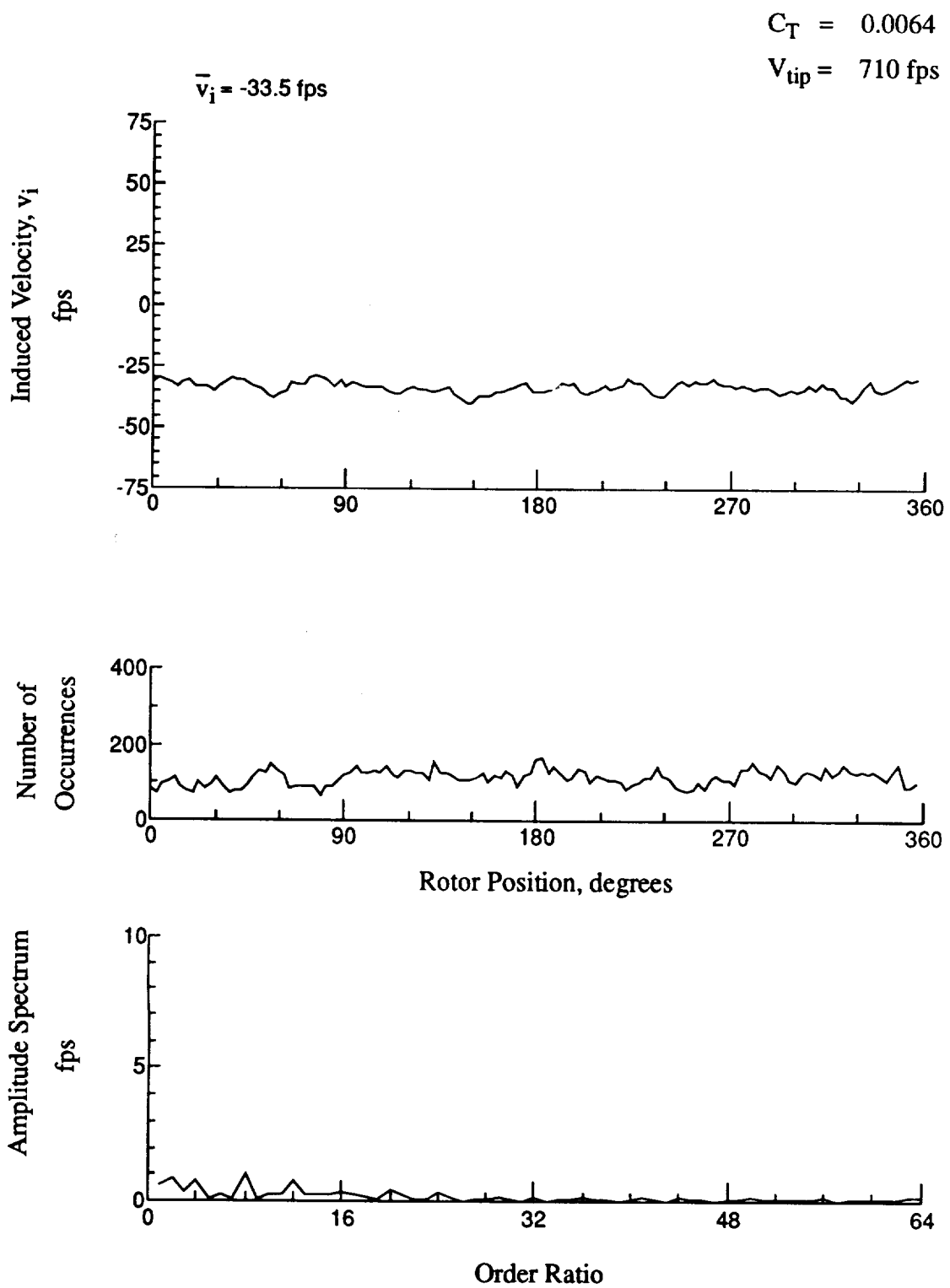


Figure 200.- Concluded.
 $x/R = 1.50$, $y/R = 0.20$, $z = -9.53 \text{ in.}$

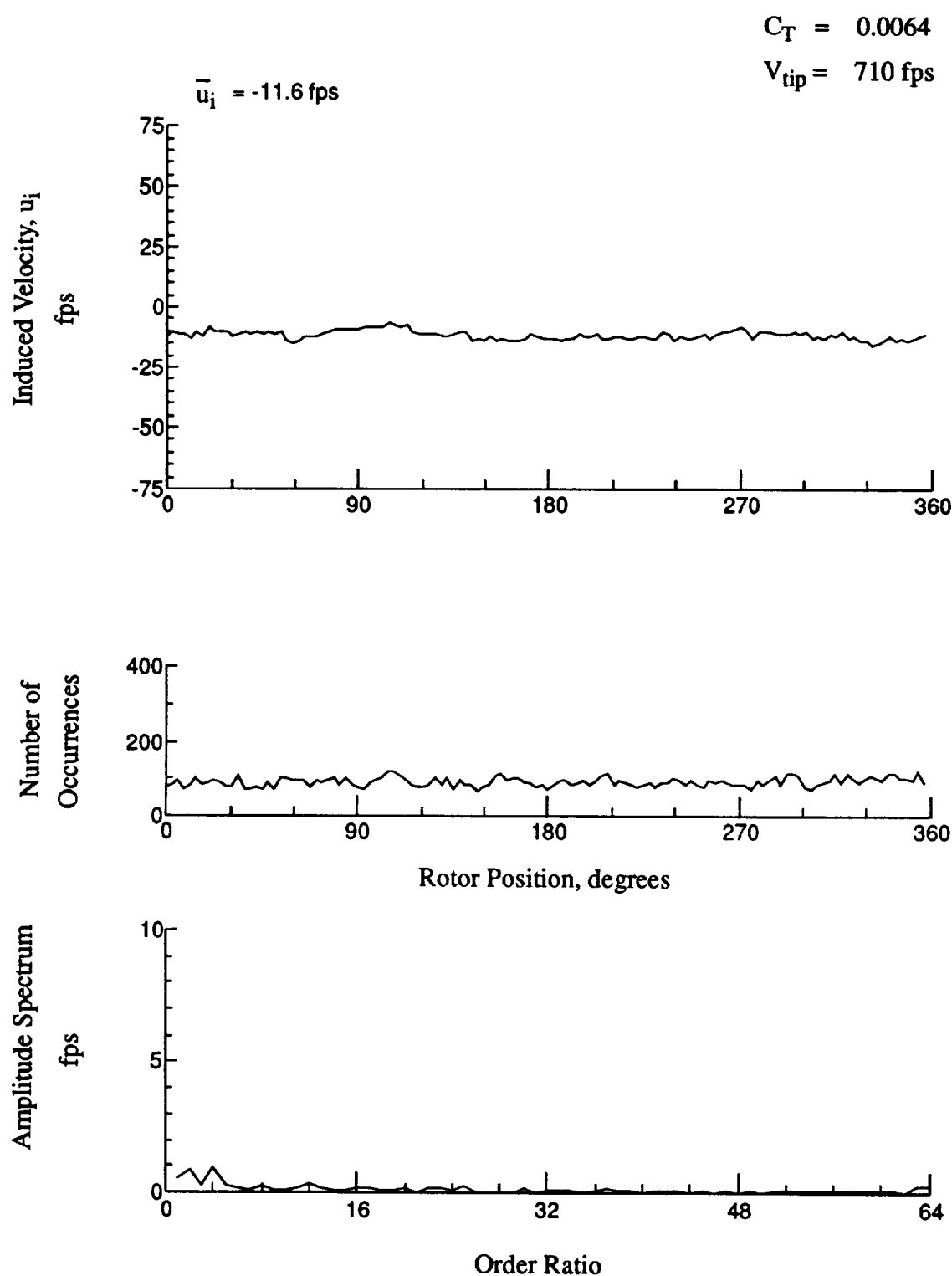


Figure 201.- Wake Measurements at
 $x/R = 1.50$, $y/R = 0.20$, $z = -10.56 \text{ in.}$

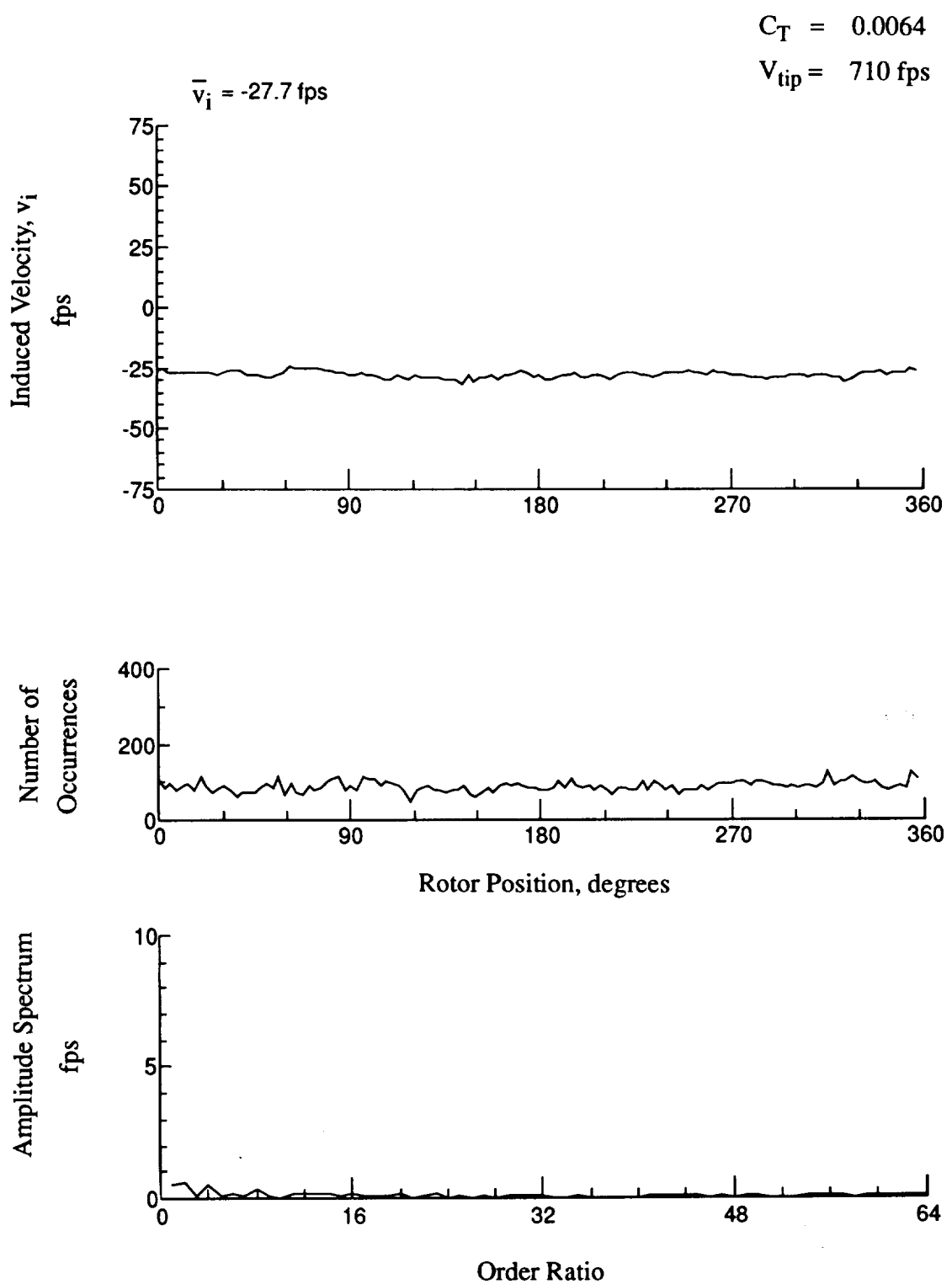


Figure 201.- Concluded.

$x/R = 1.50$, $y/R = 0.20$, $z = -10.56 \text{ in.}$

$$C_T = 0.0064$$

$$V_{tip} = 710 \text{ fps}$$

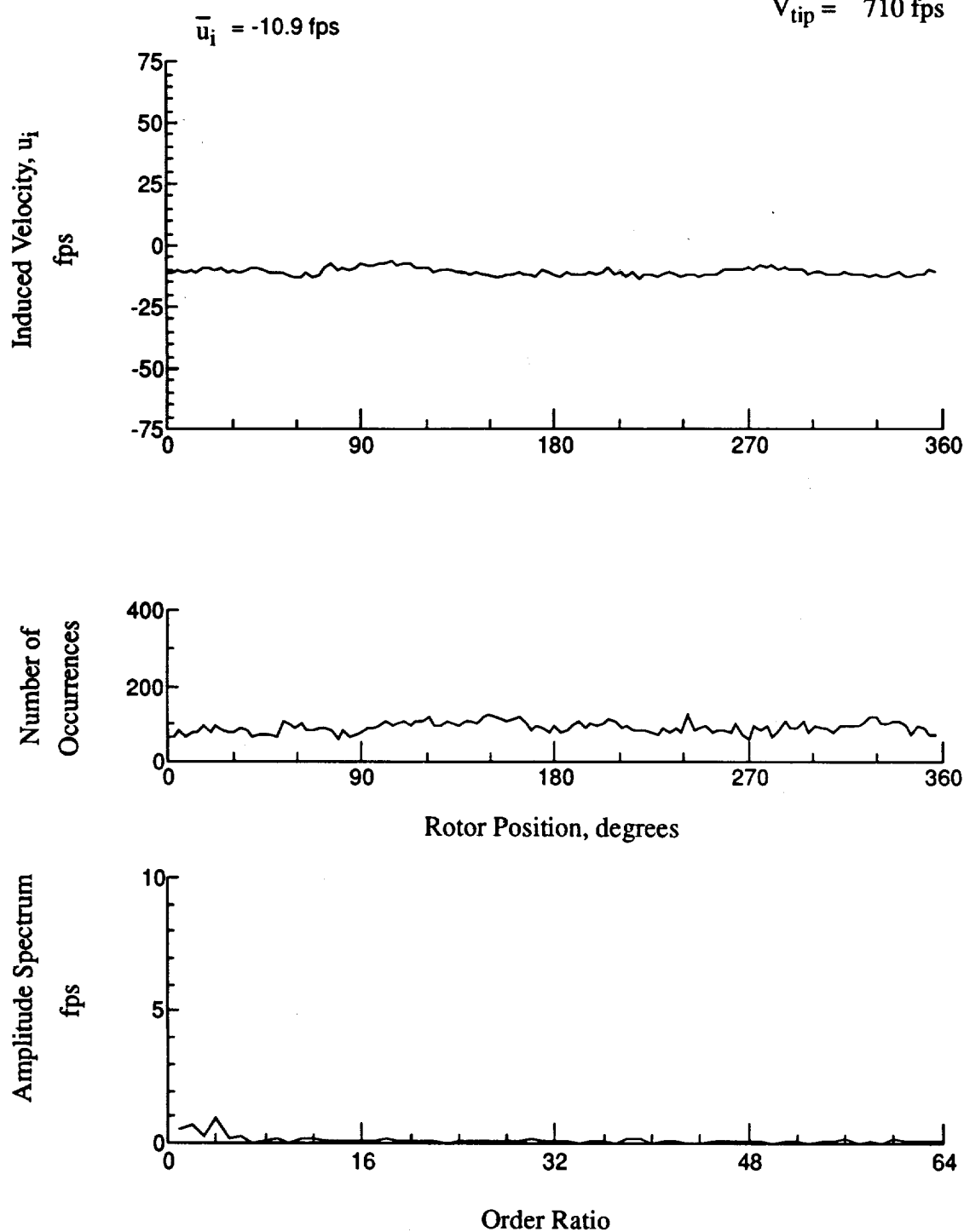


Figure 202.- Wake Measurements at
 $x/R = 1.50$, $y/R = 0.20$, $z = -11.59$ in.

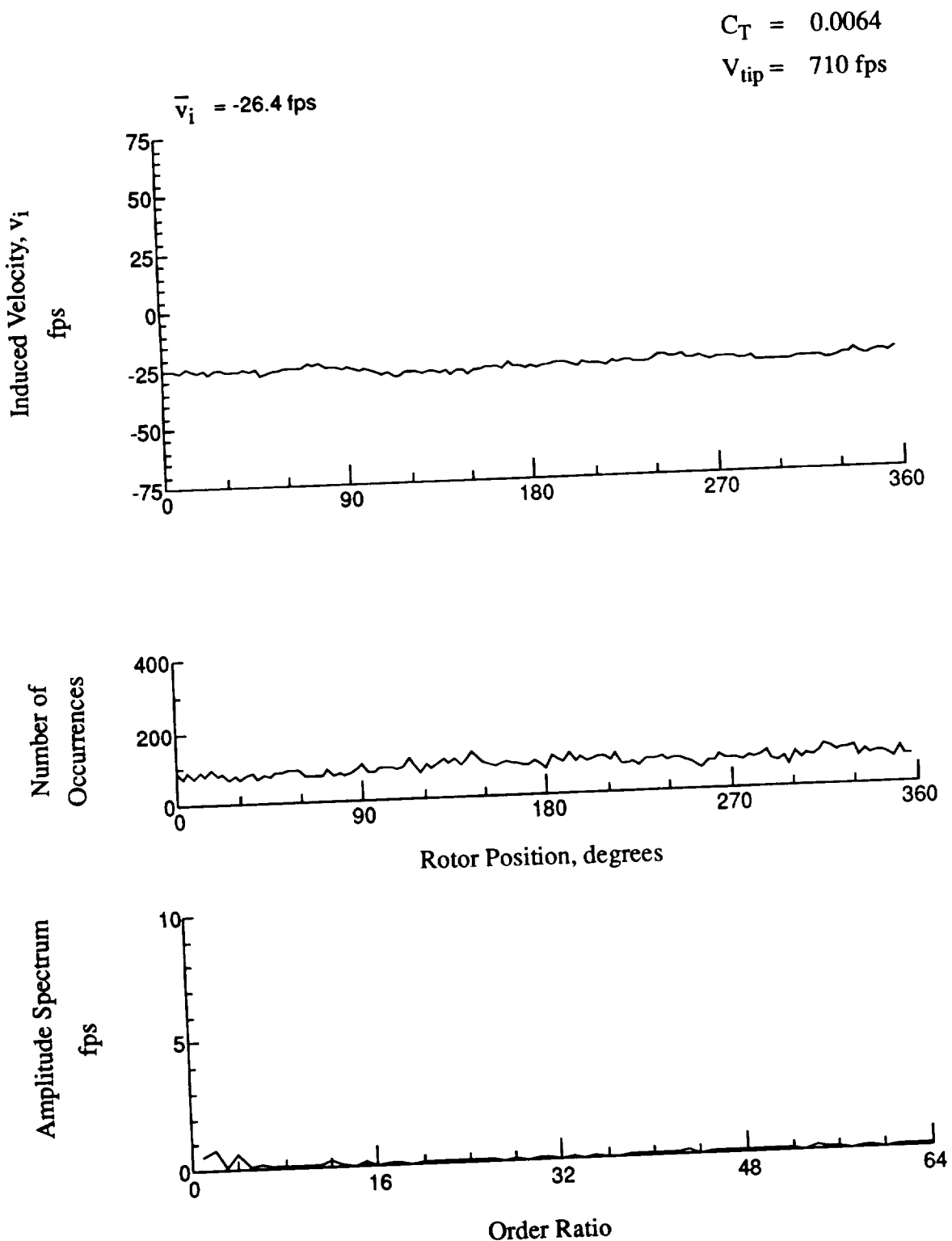


Figure 202.- Concluded.
 $x/R = 1.50$, $y/R = 0.20$, $z = -11.59 \text{ in.}$

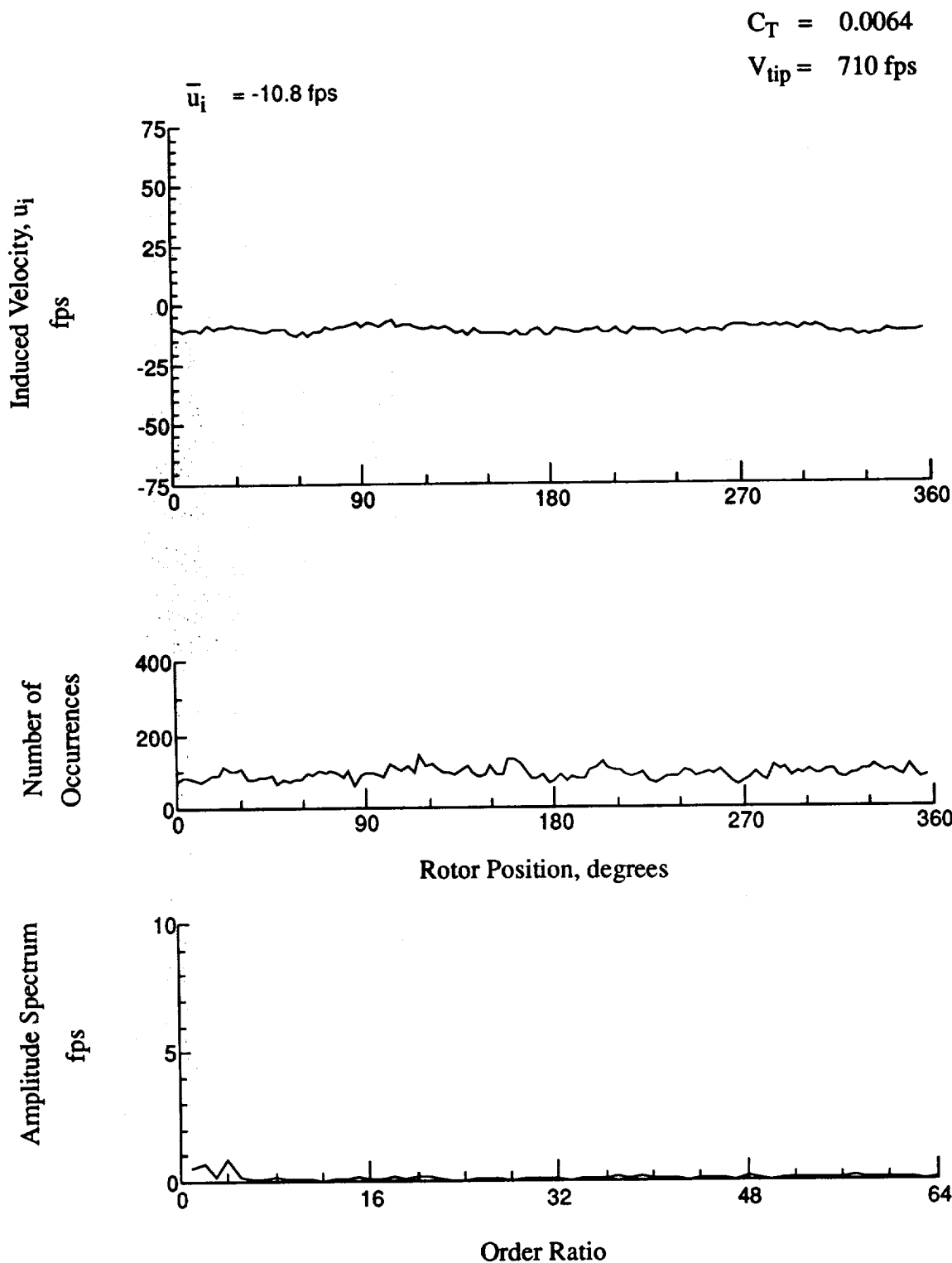


Figure 203.- Wake Measurements at
 $x/R = 1.50$, $y/R = 0.20$, $z = -12.62 \text{ in.}$

$$C_T = 0.0064$$

$$V_{tip} = 710 \text{ fps}$$

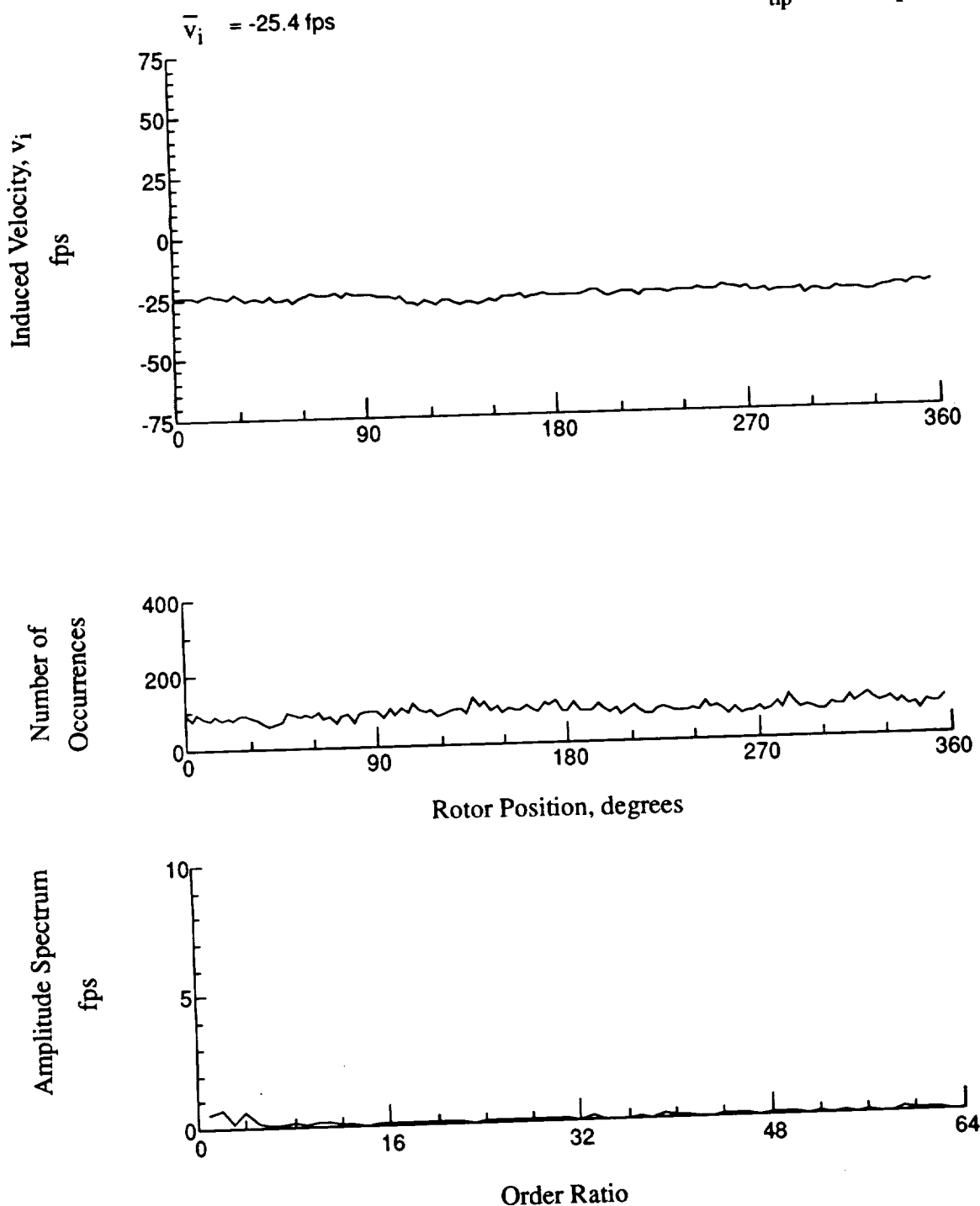


Figure 203.- Concluded.
 $x/R = 1.50$, $y/R = 0.20$, $z = -12.62 \text{ in.}$

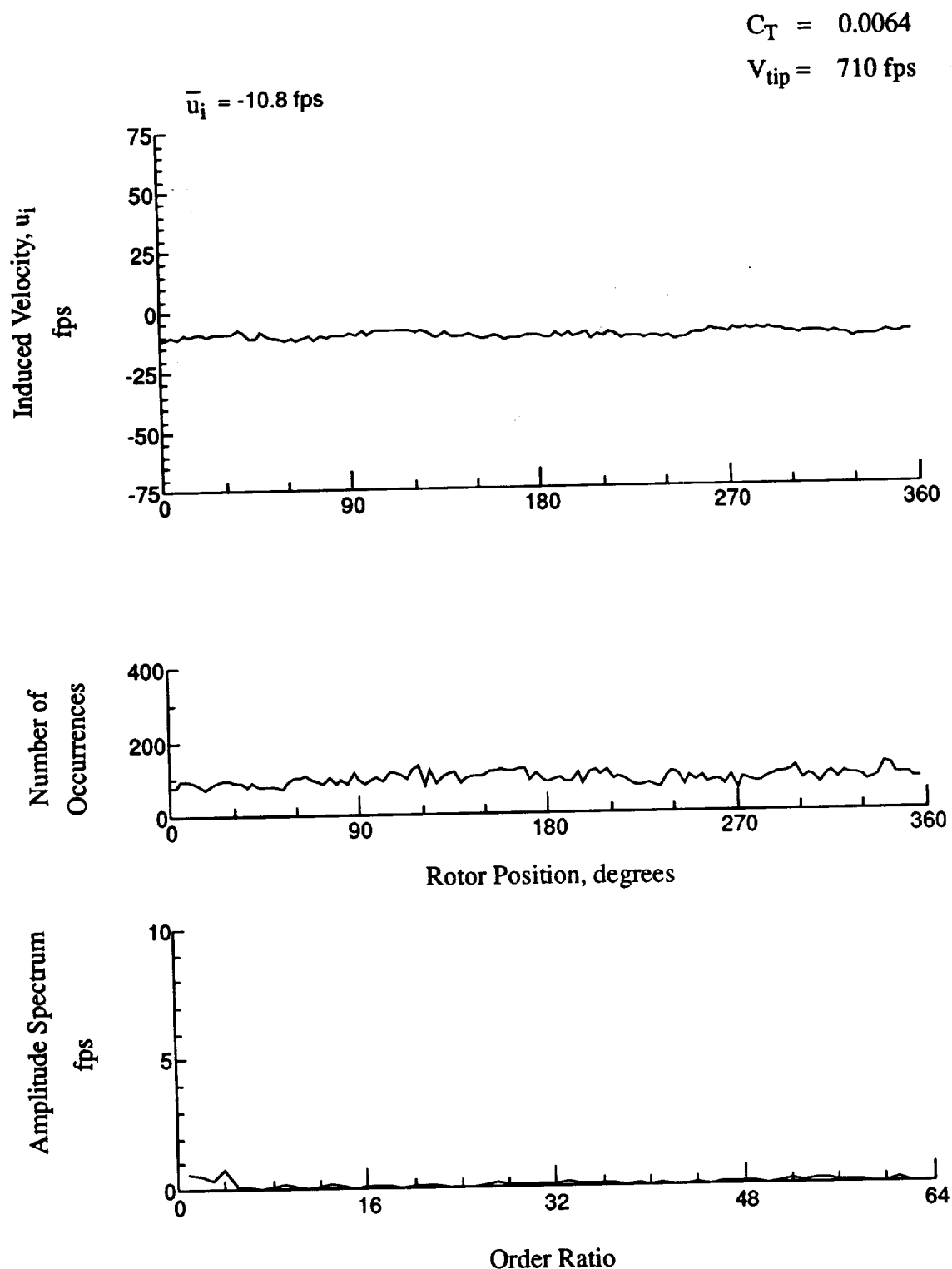


Figure 204.- Wake Measurements at
 $x/R = 1.50$, $y/R = 0.20$, $z = -13.56 \text{ in.}$

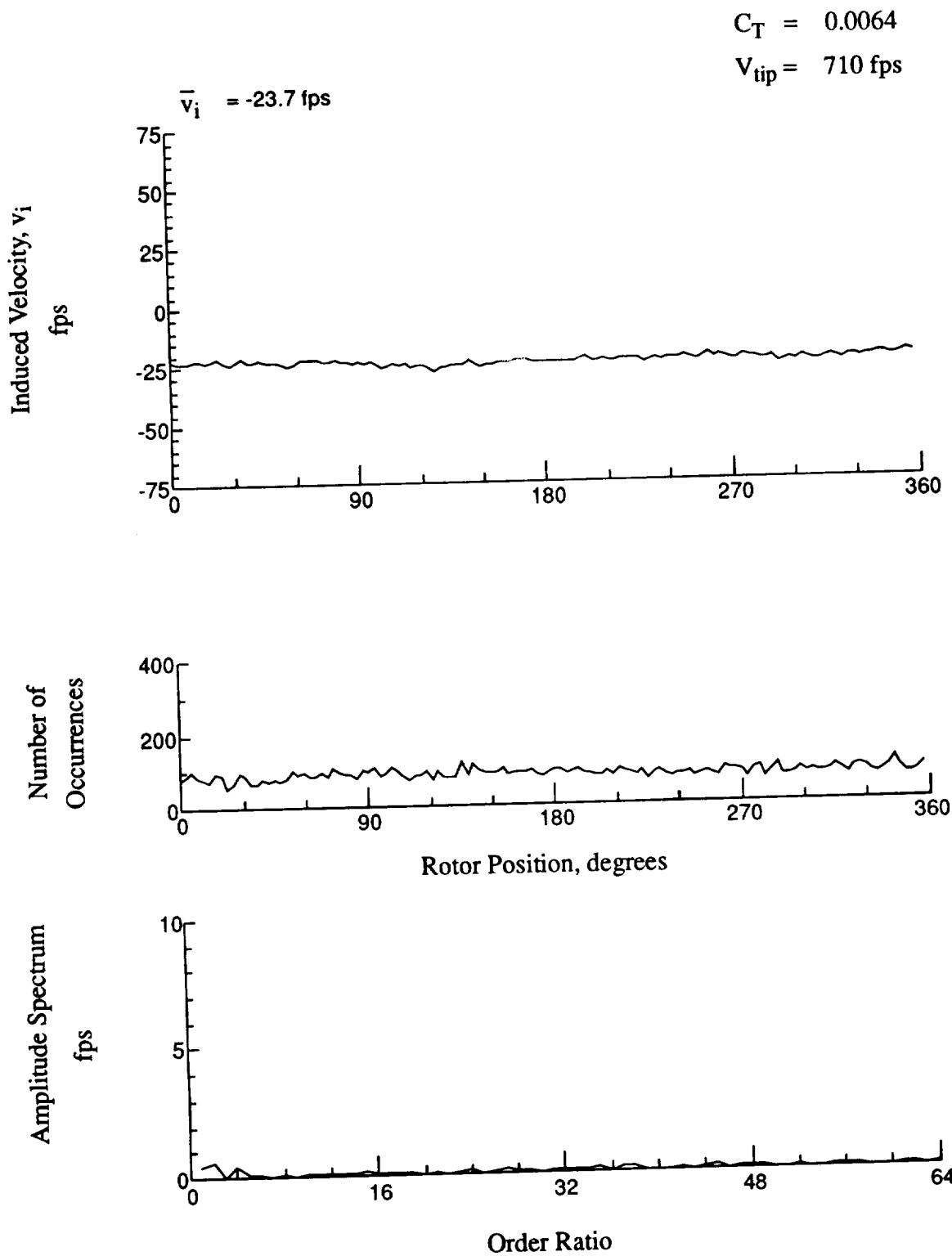


Figure 204.- Concluded.
 $x/R = 1.50$, $y/R = 0.20$, $z = -13.56 \text{ in.}$

REPORT DOCUMENTATION PAGE			Form Approved OMB No. 0704-0188
<p>Public reporting burden for this collection of information is estimated to average 1 hour per response, including the time for reviewing instructions, searching existing data sources, gathering and maintaining the data needed, and completing and reviewing the collection of information. Send comments regarding this burden estimate or any other aspect of this collection of information, including suggestions for reducing this burden, to Washington Headquarters Services, Directorate for Information Operations and Reports, 1215 Jefferson Davis Highway, Suite 1204, Arlington, VA 22202-4302, and to the Office of Management and Budget, Paperwork Reduction Project (0704-0188), Washington, DC 20503.</p>			
1. AGENCY USE ONLY (Leave blank)	2. REPORT DATE	3. REPORT TYPE AND DATES COVERED	
	November 1993	Technical Memorandum	
4. TITLE AND SUBTITLE Investigation of the Aerodynamic Environment for an Advanced Lightweight Rotor in Forward Flight. Volume 4: Laser Velocimeter Wake Data, Advance Ratio of 0.37			5. FUNDING NUMBERS WU 505-59-87-85 PR 1L161102AH45
6. AUTHOR(S) W. Derry Mace, Joe W. Elliott, Martin A. Peryea, Albert G. Brand, and Tom L. Wood			
7. PERFORMING ORGANIZATION NAME(S) AND ADDRESS(ES) NASA Langley Research Center Hampton, VA 23665-5225 and Aeroflightdynamics Directorate - JRPO NASA Langley Research Center Hampton, VA 23681-0001			8. PERFORMING ORGANIZATION REPORT NUMBER
9. SPONSORING / MONITORING AGENCY NAME(S) AND ADDRESS(ES) National Aeronautics and Space Administration Washington, DC 20546-0001 and U. S. Army Aviation and Troop Command St. Louis, MO 63120-1798			10. SPONSORING / MONITORING AGENCY REPORT NUMBER NASA TM-109040, Vol. 4 ATCOM TR-93-A-012, Vol. 4
11. SUPPLEMENTARY NOTES Floppy disks in Microsoft MS-DOS format included with report. Mace: Lockheed Engineering & Sciences Company, Hampton, VA Elliott: Aeroflightdynamics Directorate - JRPO, Langley Research Center, Hampton, VA Peryea, Brand, and Wood: Bell Helicopter Textron Inc., Fort Worth, TX			
12a. DISTRIBUTION / AVAILABILITY STATEMENT Unclassified-Unlimited Subject Category 02		12b. DISTRIBUTION CODE	
13. ABSTRACT (Maximum 200 words) An Advanced Lightweight Rotor (ALR) model was tested in high-speed forward flight, $\mu=0.37$, at the 14- by 22-Foot Subsonic Tunnel at the NASA Langley Research Center. A two-component laser velocimeter was used to obtain azimuthally dependent velocities in the inflow region and in the wake of the rotor. Data are presented here without analysis. To facilitate the use of the data sets, they are also provided on a 1.4 Mbyte 3.5 inch floppy disk in Microsoft Corporation MS-DOS format.			
14. SUBJECT TERMS Rotor model, Induced Inflow Measurements; Laser Velocimetry			15. NUMBER OF PAGES 422
			16. PRICE CODE A18
17. SECURITY CLASSIFICATION OF REPORT Unclassified	18. SECURITY CLASSIFICATION OF THIS PAGE Unclassified	19. SECURITY CLASSIFICATION OF ABSTRACT	20. LIMITATION OF ABSTRACT